UNIVERSITY OF SOUTHAMPTON

FACULTY OF SCIENCE

DEPARTMENT OF GEOLOGY

THE JIANFENGLING GRANITE COMPLEX AND THE ASSOCIATED POLYMETALLIC MINERALISATION, HUNAN PROVINCE, P. R. CHINA

A THESIS PRESENTED FOR THE DEGREE

OF DOCTOR OF PHILOSOPHY

BY

CAN SHENG WANG

NOVEMBER 1993

UNIVERSITY OF SOUTHAMPTON

ABSTRACT

FACULTY OF SCIENCE

GEOLOGY

Doctor of Philosophy

THE JIANFENGLING GRANITE COMPLEX AND THE ASSOCIATED POLYMETALLIC MINERALISATION, HUNAN PROVINCE, P. R. CHINA

by

Can Sheng Wang

The Jianfengling granite (previously known as the "430 granite") is a small, well-exposed stock approximately 4.4 km^2 in area. It was emplaced into a sequence of Devonian and Carboniferous limestones and dolomites during the Yanshan orogeny (Jurassic-Cretaceous) and has a K-Ar age of 160-170 Ma. Evidence from sharp intrusive contacts indicate the stock to be a polystage complex comprising five distinct intrusions which can be divided into two groups on the basis of petrographic and chemical characteristics: the "zinnwaldite granites" (intrusions of stages 2 and 3) which contain zinnwaldite and abundant albite; and the "biotite granites" (intrusions of stages 1, 4 and 5) which contain biotite and abundant K-feldspar. These granites are fine- to medium-grained, equigranular to slightly porphyritic textured, with essential quartz, alkali-feldspars (albitic plagioclase and K-feldspar), biotite, zinnwaldite, and topaz. Chemically, all the granites are weakly peraluminous with a molar ratio $Al_2O_3/(CaO+Na_2O+K_2O)$ ranging from 1.10 to 1.58, (normative corundum contents from 1.6-3.5 mol.%). Quartz and feldspar account for more than 95% of the normative compositions. The granites are fluorine-rich (F=0.55-2.75 wt.%), high silica (SiO_2=72.50-76.40 wt.%) types with extremely elevated contents of Li, Rb, Cs, Y, Nb, Ta, W, Sn, and U, and depletion of TiO_2, MgO, CaO, P_2O_5, Ba, and Sr. These granites are analogous to the "low-P" subtype of topaz granites of Taylor (1992). Pegmatites and pegmatitic pods were formed at a temperature range of 480-540°C and are considered to be the results of "liquid segregation" during the late stages of the evolution of the granites. Fluids in equilibrium with the pegmatitic rocks have $\delta^{18}O$ values of 8.1-10.7‰ and δD values of -70 to -88‰.

Various types of mineralisation, including Nb, Ta, W, Sn, Be, Pb, Zn, Ag and F, are spatially and genetically associated with the Jianfengling granites. They can be categorised into two main groups: granite-type and lode-type. The granite-type hosted in greisens and pegmatites is syn-magmatic and/or late-magmatic in origin and includes Nb, Ta, Pb, Zn, and rarely W, Sn mineralisation. The lode-type occurring along fractures is late- and post-magmatic in origin and consists of W, Sn, Be, F, Pb, and Zn mineralisation. The mineralisation in the Xianghuapu area occurs as four main associations: Nb-Ta, Sn (W, Be, Pb, Zn), W-F, and Pb-Zn.

Nb-Ta mineralisation occurs in the greisenised apex of intrusion B (zinnwaldite granite). Ore minerals of microlite, niobite and tantalite disseminate throughout the upper portion of the intrusion.

Sn (W, Be, Pb, Zn) mineralisation is spatially and genetically associated with both intrusions C and E. Mineralisation related to intrusion C is associated with the NW-trending quartz veins within the granite with cassiterite, wolframite, galena, sphalerite and beryl being the main ore minerals. That related to intrusion E occurs in fractures within the F_{101} fault zone and has a association of oxides, sulphides and skarn minerals.

W-F mineralisation is exclusively related to intrusion D and has a mineral assemblage of quartz, fluorite, scheelite and calcite. Orebodies occur along the NNE-trending faults and are confined to the fractured footwalls and the selvage. Fluids responsible for the mineralisation were of low to moderate temperature (Tt=180°-400°C) and salinity (S=1-19 wt.% NaCl eq.) with NaCl and $CaCl_2$ being the main solutes and had isotopic compositions of $\delta^{18}O$=-2.3 to 4.9‰, δD=-82 to -88‰, $\delta^{34}S$=+1.6 to +4.0‰ and $\delta^{13}C$=-1.3 to +0.8‰. These fluids are considered to represent a diluted, chemically exchanged successor to the predominantly magmatic fluid derived from the evolutions of intrusion D.

Pb-Zn mineralisation occurs both within the granites and in the carbonate country rocks. Most of the mineable orebodies are associated with intrusions D and E. Three types of occurrence are noted: in zones of greisenisation; with the W-F ore; and massive sulphide lodes in the carbonate host rocks. The massive lode-type deposits are the most important Pb-Zn sources in the area. The orbbodies are hosted by the gently dipping (20°-40°E), NNE-trending faults and comprise massive galena, sphalerite, pyrrhotite, arsenopyrite and cassiterite. Sulphides from these orebodies have $\delta^{34}S$ values of -9.6 to -1.9‰ indicating a mixture of magmatic sulphur and sulphur from the sedimentary country rocks.

ACKNOWLEDGEMENTS

The completion of this thesis would not be possible without the assistance of various institutions and people. I am indebted to the China University of Geoscience, Wuhan for providing me a opportunity to pursue a higher education and training. In particular I would like to thank Professors Xia, W.H. and Zhang, J.T., who initiated this project, for their supervision during my M.Sc. course and securing the fund for the field work which forms the basis of this research. I would also like to thank Xu, Q.D., Que, M.D. and a team of undergraduate students with a special mention to Bai, T., Shao, P.J., and Wang, H.Y. for their numerous forms of assistance during the field work and fruitful discussions.

I am grateful to the authorities of the Xianghualing Mine and its Xianghuapu branch, and the Dongshan, Baojinshan, and Meishi Mines, for allowing me to take access into their mining area and providing necessary information. The help and friendship of the staff of these mines and local community are greatly appreciated, in particular, Mr. Zhou, X.L. and Mr. Wu, J.H. are thanked sincerely for their guiding and accompanying me on the first few days of first field season and uncountable assistance throughout the whole field work periods. I also wish to express my sincere gratitude to Sir Y.K. Bao, who died during the course of this study and will be remembered for his long-time generous support to China's education, the British Council and the Education Commission of China for setting up the SBFSS (Sino-British Friendship Scholarship Scheme) through which this study has been funded. I am very grateful to the help and support I received throughout this study from Mrs Sandra Bance, officer in charge at the British Council Southampton Branch.

To Drs. R.P. Foster and I.W. Croudace, my supervisors, I would like to say a big THANK YOU for their guidance, encouragement and patience through the last four years or so. Thanks are also extended to Prof. J.W. Murray and Dr. D.A.V. Stow for being members of my advisory group. Uncountable assistance and advice from all the staff of the Geology Department are greatly appreciated. In particular, I would like to thank Dr. Ian Croudace once more for his help with the XRF, INAA and AAS analyses, Dr. Steve Roberts for his advice on fluid inclusion study. Thanks are due to Bob Jones and John Ford for preparing my polished and thin sections, to Posy for her assistance on sample preparation, to Dave Spanner for helping me out in use of computers. Dr. Anthony Fallick of SURRC, Glasgow is thanked for the stable isotope analyses. I am grateful to Dr. K. Randle of the Department of Chemistry, Birmingham University for analysing fluorine (through Ian Croudace). The company of the present and past postgraduate community who made my stay at the University not to be an unhappy one is acknowledged.

Finally my thanks and love must go to Yan-yan my wife for her accompany and continuous moral and financial support throughout the past few years, for looking after our newborn daughter when I have to put my every minute into this thesis.

LIST OF CONTENTS

Abstract i

Acknowledgement ii

List of contents ..... iii-v

Chapter one Introduction 1

1.1 Rationale 1

1.2 Location 2

1.3 Mining history and previous geological work 2

1.4 Objectives 3

1.5 Layout of the thesis 4

Chapter two Regional geology and local setting 5

2.1 Regional geology 5

2.1.1 The geology of Southeast China 5

2.1.2 Granitoids in Southeast China 13

2.1.3 Mineralisation associated with the granitoids 21

2.2 Geology of the Xianghualing orefield 27

2.2.1 Introduction 27

2.2.2 Lithostratigraphy 27

2.2.3 Structural evolution 30

2.2.4 Granitic intrusions 33

Chapter three Petrology of the Jianfengling granites 37

3.1 Introduction 37

3.2 Field relationships and general petrography of the granites of the Jianfengling stock 39

3.2.1 Intrusion A: medium-grained biotite granite 39

3.2.2 Intrusion B & C: medium-grained zinnwaldite albite granite 42

3.2.3 Intrusion D: medium-grained biotite granite 43

3.2.4 Intrusion E: Medium- to fine-grained biotite granite 45

3.3 Petrography and mineralogy of the Jianfengling granites 50

3.3.1 Introduction 50

3.3.2 Quartz 55

3.3.3 Plagioclase (albite) 55

3.3.4 K-feldspar 59

3.3.5 Other minerals 60

Chapter four Geochemistry of the Jianfengling granites 69

4.1 Introduction 69

4.2 Major and trace element geochemistry 76

4.3 Rare earth element geochemistry 96

4.4 Discussion 101

Chapter five Mineralisation 114

5.1 General aspects of mineralisation in the Xianghuapu area 114

5.1.1 Types of mineralisation 114

5.1.2 Nb-Ta mineralisation 115

5.1.3 Sn-W (Pb, Zn) mineralisation 116

5.1.4 W-F (fluorite-scheelite) mineralisation 117

5.1.5 Pb-Zn mineralisation 117

5.2 Typical deposits 121

5.2.1 Meishi Pb-Zn deposit 121

5.2.2 Xianghuapu W-F (fluorite-scheelite) deposit 127

5.3 Summary 131

Chapter six Fluid inclusion and stable isotope studies 132

6.1 Fluid Inclusion Microthermometry 132

6.1.1 Introduction 133

6.1.2 Microthermometry 134

6.1.2.1 Fluid inclusions of the Pegmatitic rocks 134

6.1.2.2 Fluid inclusions of the fluorite-scheelite ores 140

6.1.2.3 Estimation of pressure and pressure corrections 144

6.1.3 Summary 146

6.2 Stable Isotope Studies 147

6.2.1 Samples studied and analytical methods 147

6.2.2 Isotopic compositions of the granite-related rocks 147

6.2.3 Isotopic compositions of the W-F mineralisation 150

6.2.4 Sulphur isotope composition of Pb-Zn mineralisation 152

6.2.5 Discussion 157

Chapter seven Discussion 162

7.1 Introduction 162

7.2 Petrogenesis of the Jianfengling granites 162
7.3 Origin of the pegmatitic rocks 168
7.4 The roles of volatile components 170
7.5 Fluid evolution 181
7.5.1 Extraction and transport of ore-forming metals 181
7.5.2 Segregation and concentration of mineralising fluids 187
7.6 Mineralisation 189
7.6.1 Origin of fluids 189
7.6.2 Deposition of ore-metals and formation of various types of deposits in the Xianghuapu area 190
7.7 Petrogenetic-metallogenetic model 197

Chapter eight Conclusions 199

References 203
Appendices 221
I. Geological map of Xianghuapu, Hunan Province, P. R. China. 222
II. List of samples used in this study. 223
III. Sample preparation procedures for the geochemical analyses. 226
IV. Data set of SEM analyses 228
V. Data set of XRF and INAA analyses. 235
VI. Rare-earth element geochemistry of the Jianfengling granite stock. 240
VII. Major-element geochemistry of the Jianfengling granite stock (wet-chemical analyses). 241
VIII. Chondrite-normalised REE patterns of individual samples analyzed. 242
IX. Data set of fluid inclusion study. 247

CHAPTER ONE

INTRODUCTION

CHAPTER ONE

INTRODUCTION

Contents

1.1 Rationale
1.2 Location
1.3 Mining history and previous geological work
1.4 Objectives
1.5 Layout of the thesis

1.1 RATIONALE

There is abundant evidence that many polymetallic ore deposits are genetically related to granitic intrusions. Hydrothermal fluids associated with the granitic intrusions play an important role in element mobilisation, transport and deposition, and eventually forming economic deposits.

A large number of detailed geologic, mineralogical, fluid inclusion, and stable isotope studies of granite-related polymetallic deposits (W, Sn, Nb, Ta, Mo, Bi, Pb, Zn, REE etc.) have been published in the last two decades (Kelly and Turneaure, 1970; Landis and Rye, 1974; Jackson *et al.*, 1974, 1982; Kelly and Rye, 1979; Alderton *et al.*, 1980; Tu *et al.*, 1980; Yan *et al.*, 1980; Collins, 1981; Naumov and Ivanova, 1981; Patterson *et al.*, 1981; Pollard, 1983; Chen, 1983; Candela and Holland, 1986; Campbell, 1987; Witt, 1988; Xia *et al.*, 1989; Heinrich, 1990; Lehmann *et al.*, 1990; Salvi and Williams-Jones, 1990; Layne *et al.*, 1991a,b; and many others). Several important tin-tungsten polymetallic provinces have been identified, such as those of Bolivia, Thailand, the Nanling area of China, and Cornwall in England. Relatively few studies have been carried out concerning specific individual granites and their mineralisation in South China.

As a continuing programme of research on the relationships of polymetallic mineralisation and granitic intrusions in the Nanling (Southern Mountains) area of South China, this project represents one part of a national research programme which was initiated in 1985 to determine the mineralising conditions

of W, Sn, Pb, Zn and to identify hidden deposits in the Xianghualing ore field, Hunan Province (series no. 75-55-01-03-A). The current project was established to investigate the relationship between the Jianfengling granite stock and the various types of mineralisation, and hence to predict new potentially important areas in the Xianghuapu ore district.

1.2 LOCATION

The Xianghualing ore field, which covers an area of more than 100 km^2, is situated (112°34'E, 25°24'N) approximately 310 km SSW of Changsha and 270 km NNW of Guangzhou, within Lingwu county of Hunan Province, Southern District of China. This area is served by regular buses, which link the Xianghualing town with the county town --- Lingwu (20km to the south) and Chenzhou (70 km to the northeast), a major commercial centre in South Hunan Province. The closest rail link is located at Jiahuo (25 km to the northwest of Xianghualing).

The Jianfengling granite stock, which comprises the main part of the Xianghuapu ore district, occurs in the southern part of the Xianghualing ore field.

1.3 MINING HISTORY AND PREVIOUS GEOLOGICAL WORK

There is a long mining history in the Xianghualing area with silver being mined and smelted about 400 years ago, but reconnaissance geological studies were not started until 1915. The earliest recorded survey was carried out by Wei (1915), who uncovered several localities of tin mineralization. On the basis of Wei's research, Wang, X.C. (1945) conducted a more detailed investigation on tin and arsenic mineralization in this area.

After 1949, when the Communist Party took power in China, a nationalised Xianghualing Mine was established. At the early stage of mine operation, Fei (1956-1976) conducted the major prospecting and exploration works in this area. In 1962, the Hunan Geological Survey produced a regional geological map at a scale of 1:200,000, together with a detailed geological report and a geochemical exploration report. These reports have provided basic information for detailed research in the Xianghualing ore field. As a result of the geological survey, a number of W, Sn, Pb, Zn, Nb, Ta, Be and REE mineralised locations have been identified. In the last two decades, comprehensive research on the mineralogy, petrology, geochemistry and structural geology in the Xianghualing area have been

carried out by Du and Huang (1979), Huang and Du (1979), Huang *et al.* (1979) and Luo *et al.* (1988).

In the Xianghuapu area, a detailed geological investigation, specifically focusing on the Jianfengling granite stock, was conducted by the No. 238 Geological Team, commencing in 1957. A map which covers the whole granite stock at a scale of 1:2,000 was produced and niobium-tantalum mineralisation was found and explored in the top of the stock (No. 238 Geol. Team, 1962, 1974). The granite stock was identified as a single intrusion which experienced multi-stage alteration(No. 238 Geol. Team, 1974). In the mid 1960s, a medium sized mill and processing plant was installed. It is estimated that the plant has a capacity of treating 300-400 tones per day, although no official figures have ever been released. The plant was abandoned for both political and economic reasons in the early 1970s.

Exploration for fluorite-scheelite mineralisation was started in the early 1960s and completed by the Xianghualing mine in 1981 (Luo et al., 1981). A number of orebodies have been discovered and mined for scheelite and 240-290 tonnes of concentrate containing 80-90 wt.% of scheelite have been produced each year. In addition, a significant amount of galena-sphalerite ore associated with the fluorite-scheelite ore has been mined and concentrated. Currently, a comprehensive mineral separation complex is being established and is expected to be in operation in 1993.

In the last decade, the number of private (small scale) miners has increased tremendously, most of the areas near to the granite stock having been exposed. This provides an excellent opportunity for conducting detailed field investigations.

1.4 OBJECTIVES

Although there is a long mining and exploration history in the Xianghualing area, previous investigations were limited to a few ore blocks and restricted types of mineralization. Up to the beginning of this study, no systematic research had been undertaken on the specific relationship between the various types of mineralisation and the granite stock which is believed to have provided most of the ore-forming elements in this area. Nor have the relations among the different types of mineralisation been evaluated.

The aims of the present study have been primarily to investigate the relationship between the evolution of the granite stock and the formation of the various types of mineralization, and to determine the controls of mobilisation, migration and deposition of the metals. The main areas addressed by the

research are:

i) Petrology and geochemistry of the granites

ii) Mineralogy of the mineralisation

iii) Sources of hydrothermal fluids

iv) Mobilisation, migration and deposition of metals

v) Controls of fluid compositions

1.5 LAYOUT OF THE THESIS

The thesis is consist of eight chapters and nine appendices. An introduction, which includes the location of the studied area, mining history and previous geological work and the objectives of the current study, to the thesis is made in chapter one. In chapter two, the regional and local setting are presented. The geology of China is briefly reviewed, the characteristics of the granitoids and the associated mineralisation of Southeast China are summarised. The geology of the Xianghualing orefield, where the studied area is situated in, is also introduced in this chapter. The petrology and geochemistry of the Jianfengling granites are presented in chapters three and four. Detailed field relationships, petrography and mineralogy of the granites of the Jianfengling stock are introduced, and the geochemical evolution and origin of these granites are discussed. A comparison of these granites with others of similar compositions is also made. Chapter five describes the mineralisation associated with the Jianfengling granites. Following a general description of the various types of mineralisation in this area, two of the most important deposits are presented in great detail in terms of their mineralogy and paragenesis. Fluid inclusion microthermometry and stable isotope studies are the themes of chapter six. Optical and thermometric characteristics of the fluid inclusions from samples of pegmatitic rocks and fluorite-scheelite ores are discussed. The results of oxygen, hydrogen, carbon and sulphur isotope analyses are presented and the isotopic evolution of the Jianfengling granites and associated mineralisation is discussed. In the discussion of chapter seven the results of the studies of the petrology and geochemistry of the Jianfengling granites and associated mineralisation presented in the previous chapters are summarised and evaluated. The petrogenesis of these granites is discussed and a petrogenetic and metallogenetic model for these intrusions and mineralisation is constructed. The main conclusions drawn from the results of the current study are presented in chapter eight and followed by appendices which include a geological map of the studied area, a full list of samples collected during the field work, sample preparation procedures, full reports of XRF, INAA and SEM analyses, and a complete fluid inclusion data set.

CHAPTER TWO

REGIONAL GEOLOGY AND LOCAL SETTING

CHAPTER TWO

REGIONAL GEOLOGY AND LOCAL SETTING

Contents

2.1 Regional geology
2.1.1 The geology of Southeast China
2.1.2 Granitoids in Southeast China
2.1.3 Mineralisation associated with the granitoids
2.2 Geology of the Xianghualing orefield
2.2.1 Introduction
2.2.2 Lithostratigraphy
2.2.3 Structural Evolution
2.2.4 Granitic intrusions

2.1 REGIONAL GEOLOGY

2.1.1 The Geology of Southeast China

Stratigraphy

China is a country with a great expanse of hills, mountains and plateaux. It is marked by great changes in relief: highest in the west (Tibetan Plateau), becoming lower and lower to the east (the Coastal Area), like a giant staircase. Over this staircase flow eastward great rivers, such as the Yangtze and the Yellow River, which empty into the Pacific (Yang et al., 1986).

Stratigraphically, China has been defined as an area consisting of five super-regions which are subdivided into fourteen regions (Fig. 2.1) (Wang, H.Z., 1978, 1986). These regions basically correspond to those tectonic units of Wang, H.Z. (1981) based on the theory of Geosyncline-Platform. Briefly, the Precambrian is widely distributed in the Northern Continental Super-region (Fig. 2.1 II), notably on the North China Platform, or Sino-Korean Craton of Zhang (1984). Rocks range from

schists, gneisses, granulites and migmatites to sandstones and limestones. Another important area for the Precambrian is the Yangtze Platform which constitutes an integral part of the Southern Continental Super-region (Fig.2.1 IV). This super-region has a basement composed mostly of the Proterozoic, but here the Sinian System is widespread and forms the first genuine cover sequence on the platform, overlying the basement rocks with a fragrant unconformity.

The Palaeozoic strata extensively occur on the stable continental super-regions in the eastern part of China. In South China, the Palaeozoic and the Triassic are almost entirely marine phases and fossiliferous throughout on the Yangtze Platform as well as in the surrounding geosynclinal regions. The Lower Palaeozoic shallow-sea facies are especially preserved on the Yangtze Platform, and pass eastwards into the geosynclinal facies of southeast China, the continental margin of that time. The Cambrian and Ordovician on the Platform are abundant in carbonates, but the Silurian contains more argillaceous and clastic rocks (Wang, H.Z., 1986). Compared with the Lower Palaeozoic, the Upper Palaeozoic is less widespread on the Yangtze Platform. The Devonian and Carboniferous are usually confined to the border areas, and are in general lack in the interior of the Platform. It was not until Permian times that transgressive shallow sea once more covered the whole Yangtze region and brought about the extensive deposition of carbonates. In southeast China, the Upper Palaeozoic, unlike the Lower, has not been metamorphosed, although facies change is much more pronounced than on the Platform.

The Indosinian orogeny brought a basic reform of the geotectonic framework and a consequent change in the stratigraphic development of China. The main part of China was incorporated in the Eurasian continent. In southeast China, the Mesozoic is characterized by Triassic shallow-seas deposits, Jurassic volcanic and sedimentary rocks, and Cretaceous downwarped- and faulted-basin deposits of various types. Volcanic eruptions began in the early Jurassic and became prevalent in Late Jurassic times, when volcanic activity became general throughout the circum-Pacific belt of East Asia (Wang, H.Z., 1986). Further to the east, marine Cretaceous rocks are known in Taiwan, the region representing the continental margin at that time.

The distribution and development of the Cenozoic of China closely resemble those of the Mesozoic. In east China Cenozoic continental deposits usually occupy rifted basins in the huge subsiding belt that extends from the Bohai Bay in the north to Leizhou Peninsula (Guangdong Province) in the south, which contains important oil-producing horizons in the middle and upper part of the sequence. Small faulted basins of graben or semi-graben type are common in southeast China. Cenozoic deposits in these basins may reach a hugh thickness.

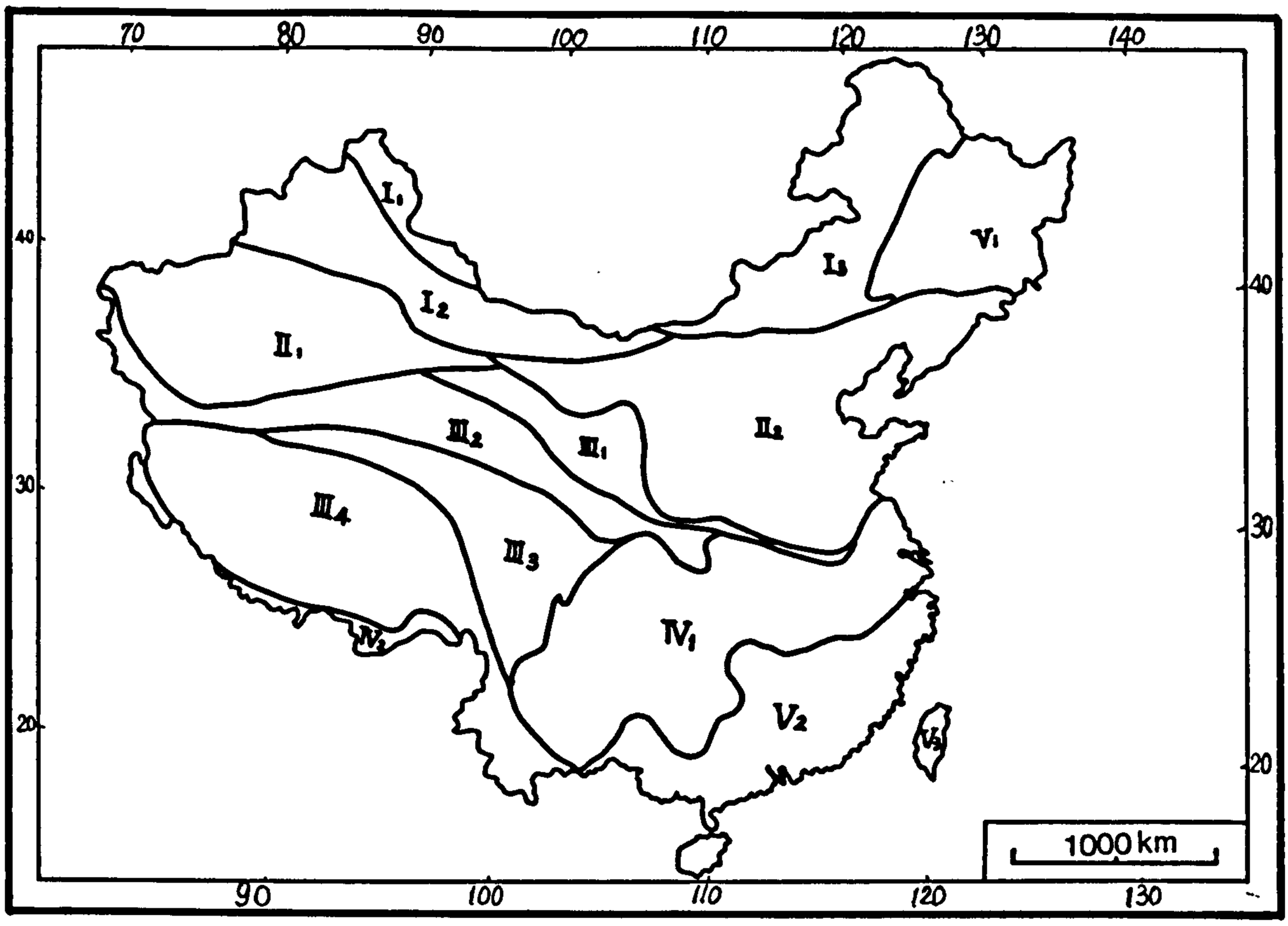

Fig 2.1 Stratigraphic Provinces of China (simplified from Wang, H. (1986)

I. Northern Intercontinential Super-region:

I_1, Altai-Bayitik Region;

I_2, North Tianshan-Beishan Region;

I_3, Hingan-Nei Mongol Region.

II. Northern Continental Super-region:

II_1, Tarim Region;

II_2, North China Region.

III. Central Intercontinental Super-region:

III_1, Qilian-North Qinling Region;

III_2, Kunlun-South Qinling Region;

III_3, Bayan Har-West Sichuan Region;

III_4, Xizang-West Yuannan Region.

IV. Southern Continential Super-region:

IV_1, Yangzi Region;

IV_2, Himalaya Region.

V. Eastern Continental Margin Super-region:

V_1, Songhuajiang-Yanbian Region;

V_2, Southeast Region;

V_3, Taiwan Region.

Magmatic rocks

Igneous rocks occur in great variety in China and are widely distributed outside the Mesozoic and Cenozoic basins and the regions of dominant late Proterozoic and Palaeozoic sedimentation.

Basic and ultrabasic rocks in China were formed at frequent intervals in time but limited distributions. They occur especially in Palaeozoic fold belts and fracture zones of many geological ages (Cheng, 1986).

Granitoids are the most widely distributed igneous rocks in China, with exposures covering an area close to 9 per cent of the whole country (Cheng, 1986). They have came into being during crustal movements at almost every stage of the geological history. Permo-Carboniferous rocks of the Hercynian orogeny and those of Jurassic-Cretaceous age related to the Yanshanian are far the most developed and widespread, are frequently connected with migration and enrichment of various mineral substances and formation of many polymetallic deposits.

Extrusive rocks are extensively developed both in time and space throughout the country. They may be submarine or continental origin. Rocks of the first category constitute the dominant group, and were mostly formed in geosynclinal, especially eugeosynclinal, belts. The continental type became dominant only from the Jurassic onwards and are exposed mainly in the eastern part of the country (the circum-Pacific region, Cheng, 1986).

Tectonics

China contains one of the tectonically most important and complicated terrains in the world. The two major Mesozoic-Cenozoic tectonic zones --- the Circum-Pacific zone and the Tethys-Himalayas zone --- extend along the eastern coast and the southwestern border respectively, and conjoin and interfere with each other. China is principally a part of the Eurasian plate, but margins of the Indian and Philippine Sea plate are involved in the Himalayas and in the Coastal Region of Taiwan, respectively (Zhang et al., 1984). Profound interactions among the Eurasian, Pacific, and Indian plates have resulted in many mountain belts (including the latest collision belt to the north of the Himalayas, and the Chinghai-Tibet plateau where the thickest continental crust exits in the world), many neotectonic activities , and a frequency of interplate and introplate earthquakes. Based on the plate tectonic theory, China has been divided into thirty three tectonic units, including three Precambrian Cratons,

Table 2.1 Tectonic stages and orogenic movements of China (after Wang, 1986)

Geologic time scale			Tectonic stages		Orogenic movements	Main geologic events	Orogenic movements of Laurasia		
								Europe	N. America
Cainozoic		2.0	Megastage of Pangaea (Gondwana) disintegration	Himalayan stage	Himalayan 2	Upheaval of Qinghai Tibet Plateau	Young Alpedic	Rodanian	
		24.6			Himalayan 1	Collision of Himalayan and Gangdise		Savian	
		65			Yanshanian 3	Opening of South China Sea		Pyrenean	Laramidian
Mesozoic		144		Yanshanian stage	Yanshanian 2	Collision of Gangdise and Qiangtang		Late Cimmerian	Nevadian
					Yanshanian 1	Activation of East China continental margin	Old Alpedic		
		213			Indosinian 2	Covergence of Yangtze and N. China to form Palasia		Early Cimmerian	
		248	Megastage of Pangaea (Laurasia) formation	Indosinian stage	Indosinian 1			Pfalzian	
Late Palaeozoic		286			Yinningian	Covergence of N. China and Siberian-Mongolia	Hercynian	Sudetian	Alleghenian
		360		Hercynian (Variscan) stage	Tianshanian	Disruption of W. border of Yangtze Platform		Bretonian	Acadian
		408			Qilianian	Formation of S. China Caledonides and close of Qilian troughs		Erian	
Early Palaeozoic		438		Caledonian stage	Gulangian		Caledonian		Taconian
		505			Xingkaian	Formation of Junggar and other median massifs		Salairian	
		600			Chengjiangian			Assyntian	
Late Proterozoic		850			Jinningian (Xuefengian)	Formation of Yangzi Platform and Qaidam Massif etc.			
		1050	Megastage of Platform formation	Jinningian stage	Sibaoan			Gothian	Grenvillian
Middle Proterozoic		1400			Zhangyuean			Karelian	Hudsinian
		1850			Luliangian (Zhongtianoan)	Formation of N. China and Tarim Protoplatforms			
Early Proterozoic		2200-2300		Luliangian stage	Wutaian			Belomorian	Kenoran
		2500-2600			Fupingian	Formation of Ordos and Jilu Nuclei			
Archean		2900-3000	Megastage of continental nuclei formation	Fupingian stage					
		3800							
Hadean		4500							

fourteen Phanerozoic accretionary fold belts (A-M), and sixteen microcontinents (1-16) (Fig. 2.2, Table 2.2; Zhang et al., 1984).

The study area is situated in the South China accretionary fold belt (G) which was a passive continental margin along the southeastern rim of the Yangtze Craton during the late Proterozoic and early Palaeozoic, and in which thick flysch, greywacke, carbonates, and minor volcanic rocks accumulated. In part of the fold belt, metamorphosed basaltic rocks are closely associated with dismembered serpentinized harzburgite, pyroxenite, pyroxenite and gabbro. All of the strata were folded at the end of the early Palaeozoic and were unconformably overlain by terrestrial Devonian clastic sediments. Widespread granitic intrusions occur throughout geological history and are commonly accompanied by regional low P/T metamorphism with andalusite and sillimanite as index minerals (Zhang et al., 1984). The fold belt became a stable terrane after the Caledonian Orogeny, great thicknesses of shallow marine sediments, mainly carbonates, were deposited throughout the whole late Palaeozoic Era (Hsü et al. 1988, 1989). The Mesozoic Indosinian and Yanshanian Orogenies strongly affected the terrane and left a complicated fracture system and numerous granitic intrusions (Structural Research Group, Nanling Programmme, 1988).

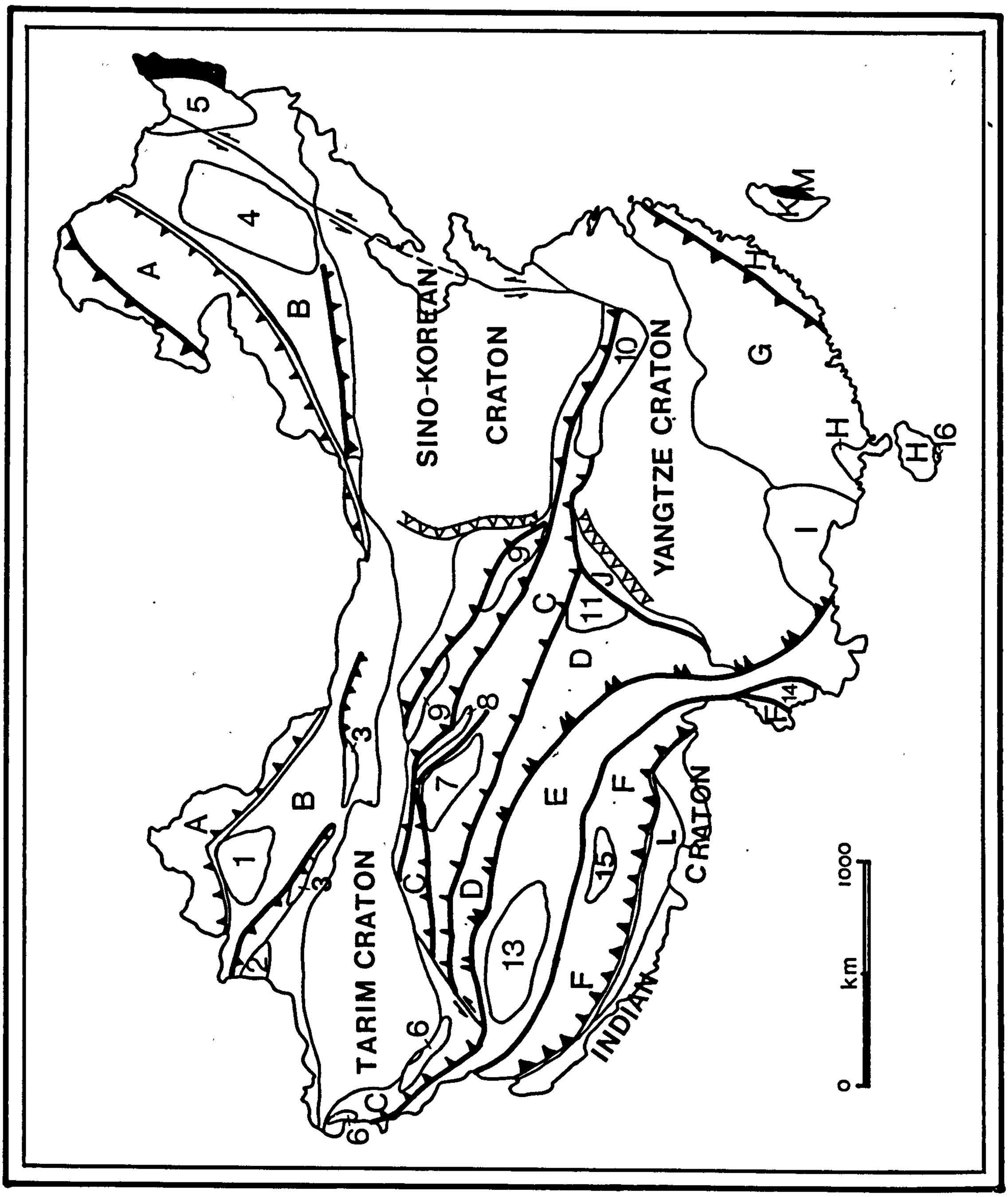

Fig. 2.2 Tectonic units of China, names of the units are listed in Table 2.2 (after Zhang et al., 1984)

Table 2.2 Tectonic units of China (after Zhang, 1984)

Name of plate, palaeoplate, and fold belt	Designation in figure	
EURASIAN PLATE		
Angaraian palaeoplate		
Junggar-Xingan accretionary fold belt	A	
Cathaysian palaeoplate		
(1) Tarim-Sino-Korean microplate		
Tarim craton		
Sino-Korean craton		
Tisenshan-Tumen accretionary belt	B	
Junggar microcontinent		1
Yili microcontinent		2
Central Tienshan microcontinent		3
Sonhliao microcontinent		4
Jiamusi microcontinent		5
Kunlun-Qinling accretionary fold belt	C	
Central Kunlun microcontinent		6
Chaidam microcontinent		7
Oulungbruk microcontinent		8
Central Qinling microcontinent		9
Huaiyang microcontinent		10
(2) Southwest China microplate		
Kekexili-Jinsha-Ailao accretionary fold belt	D	
Songpan microcontinent		11
Zhongza microcontinent		12
North Tibet-WestYunnan accretionary fold belt	E	
Qiangtang microcontinent		13
Gangdesi-Nienching Tangla accretionary fold belt	F	
Baoshan microcontinent		14
Namu Lake microcontinent		15
(3) South China microplate		
Yangzi Craton		
South China accretionary fold belt	G	
Maritime accretoinary fold belt	H	
South China Sea microcontinent		16
Youjiang back-arc basin	I	
Motianling accretionary fold belt	J	
West Taiwan inland basin	K	
INDIAN PLATE		
Indian craton		
Yarlung Zangbo Indus accretionary fold belt	L	
PHILIPPINE SEA PLATE		
East Taiwan accretionary fold belt	M	

2.1.2 Granitoids in Southeast China

Granitoids are widely distributed in southeast China and cover an area of approximately 190,000 km², 1/5 of the total area (Tu et al., 1980; Fig.2.3). Intensive investigations on the petrology, geochemistry, and related mineralization of such rocks have been carried out by a number of geoscientists in the last three decades (Dept. Geol., Nanjing Univ., 1972, 1980, 1981; Guiyang Inst. Geochem., 1979; Mo et al., 1980; Yuan et al., 1986; Xia et al., 1989; and many others). Many important mineral deposits, including W, Sn, Bi, Mo, Nb, Ta, Pb, Zn, REE, Fe, Cu, etc., have been found in this region, and they are genetically related to the granitoids.

The distribution of granitoids in southeast China geotectonically correspond to the South China (Cathaysian) (Caledonian) accretionary Fold Belt (Fig. 2.2 G), the Maritime (Hercynian) accretionary Fold Belt (Fig. 2.2 H), and the southeastern part of the Yangzi Craton. In general, it seems that many granitoids of older age often occur on the northern or northwestern side of the younger ones, and the Late Mesozoic Yanshanian granites became more and more abundant eastward or southeastward. This indicates a tendency for the locus of the granitoids to shift from the interior of the continent towards the coastal margin with time. However, more detailed investigations reveal that there is partial or local inward migration of granite formation in later tectonogenetic cycles or later phases of the same cycle (Cheng, 1986).

Geochronological groups

Six geochronological groups have been classified in terms of tectonic age and orogenic movements in southeast China. They are called Sibaoan, Xuefengian (Jinningian), Caledonian, Hercynian, Indosinian and Yanshanian (Guiyang Inst. Geochem., 1979). The Sibaoan and Xuefengian are late Proterozoic in age. The Hercynian and Indosinian granitoids are difficult to distinguish in some regions (Fujian, Guangdong, etc.), and those of Caledonian and Yanshanian are often subdivided.

Typical Sibaoan granitoids (about 1100 Ma in age) are only formed in the northern Guangxi Province, and occur as small intrusions of granodiorite with an initial $^{87}Sr/^{86}Sr$ ratio of 0.7001 (Cheng, 1986). They also occasionally appear as plagioclase-granite, often with marginal quartz-diorite rocks and intimately associated with a suite of ultra-basic and intermediate rocks. This is consistent with a mantle origin involving differentiation of a basic magma (Guiyang Inst. Geochem., 1979). Xuefengian (Jinningian) (840-900 Ma) rocks are represented by a number of granitic intrusions with peraluminous

Distribution of granitic rocks in Southeast China (modified from Tu, 1980)

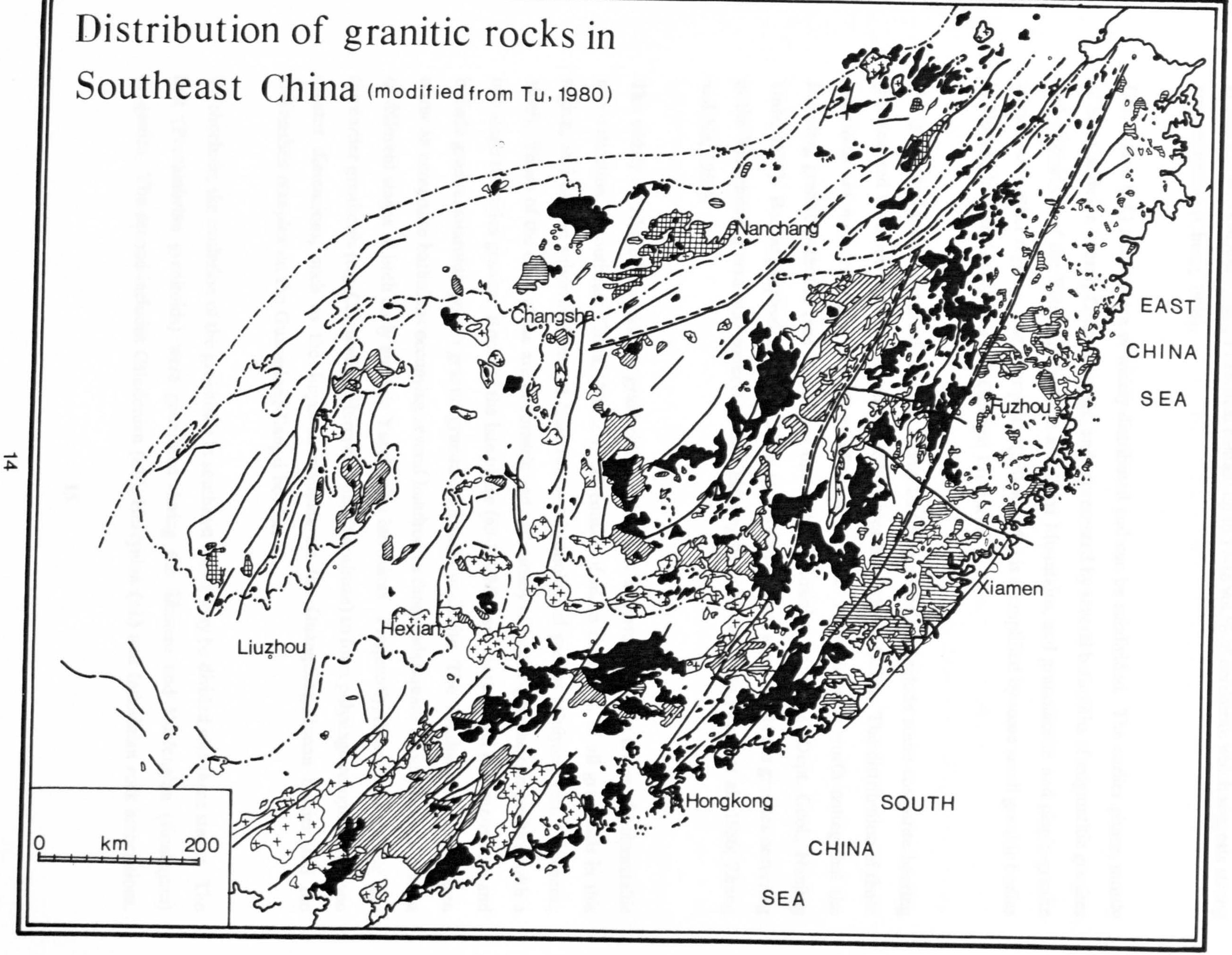

Xuefengian granits

Caledonian granits

Hercynian granits

Early Yanshanian granits

Late Yanshanian granits

Regional and conjectured faults

Boudary of tectonic units

Fig. 2.3

compositions, often accompanied by marginal migmatisation. The high initial $^{87}Sr/^{86}Sr$ ratios of these peraluminous granites (*e.g.* 0.735 in the Motianling granitic complex of Jiangxi, Mo et al., 1980) probably indicate an origin through remelting of metasedimentary crustal materials. The Xuefengian granites of northwestern Jiangxi Province contain up to 17-18 vol.% of cordierite which suggests strong contamination (Cheng, 1986).

Caledonian (s.l.) granites are of widely distributed and can be subdivided. The earlier phase, mostly of late Cambrian to early Ordovician age, and represented by several batholiths of migmatitic granites and migmatites of the Yunkai Mountains and Wuyi Mountains, and granodiorite and plagio-granite intrusions in other regions. The later phase (380-400 Ma) is exemplified by some small granitic bodies in Hunan, Jiangxi, Guangdong and Guangxi Provinces.

Hercynian and Indosinian granitoids are mainly biotite-granites but include some cordierite-bearing granites, and have been found in a number of localities in southeast China. The distribution of these granitoids are more restricted than those of other periods. However, it is worth noting that the Jitianling granite batholith (see Fig. 3.1) is one of the Indosinian intrusions (Dept. Geol., Nanjing Univ., 1979). Recent geophysical investigations (gravity anomalies) suggest that the granites occurring in the Xianghualing area may connect to the Jitianling batholith at depth (Yang et al., 1986; Zhang and Xu, 1989).

The widely distributed Yanshanian granitoids are the most important rocks in terms of polymetallic mineralization in southeast China. These rocks consist of more than 60% of all granitoids in this region, and can be subdivided into at least two geochronological groups (Guiyang Inst. Geochem., 1979). Those of the early phase are of Jurassic age and mostly of biotite-granitic composition with a late stage two-mica granite. Rocks of the late phase (69-139 Ma) are more varied in composition, and include granite, miarolitic potash granite, granodiorite and also diorite. The Yanshanian granites often occur as composite batholiths occupying several hundred to thousands square kilometres and consist of different stages of both early and late Yanshanian intrusions. Frequently, these rocks intrude into the earlier granitoids (e.g. Caledonian, Hercynian and Indosinian) to form polystage complexes of even greater dimensions, such as the Jiuyishan complex on the Guangdong-Hunan border and the Jiulianshan complex on the Guangdong-Jiangxi border.

To conclude, the evolution of the granitoids in southeast China may be divided into three stages. The first (Precambrian granitoids) were generated during the Sibaoan and Xuefengian (Jinningian) orogenies. The second includes Caledonian (s.l.), Hercynian (s.l.) and Indosinian rock associations.

Those of the early Caledonian (s.l.) are mostly of migmatitic type, the late-Caledonian are chiefly granite and granodiorite, with subordinate adamellite, while the Hercynian-Indosinian often show contamination characteristics, being frequently the regional products of the further evolution of the early Palaeozoic migmatites and migmatitic granites (Mo et al., 1980). The third Yanshanian stage is much simpler, being predominantly biotite-granite, which includes by a unique miarolitic potash granite of Late Cretaceous age.

Structural controls on granite intrusion

Granite intrusion, which was often associated with slightly earlier or later volcanism, was in general closely related to the tectonic evolution of this region, especially to the regional rifting and fracturing beginning in the late-middle Proterozoic (Cheng, 1986). The late Proterozoic intrusions are mostly intimately related to the regional fractures situated within the limit of the Yangzi Craton, especially near its southern and eastern boundaries; Caledonian granites were genetically connected to both the folding and faulting of the Caledonian accretionary fold belt located further southeast. The associated intrusions often occur at the intersection of NE-SW and E-W trending fracture systems. The Hercynian granitoids seem to be of wider distribution than those of the Caledonian, coinciding with the greater extent of the Hercynian fracturing up to the coastal islands of China. The extent of Indosinian fracturing, which controls the emplacement of Indosinian granites, may be slightly greater than that of the Hercynian fracturing, but the depth and the intensity of its influence seem to be less. The Yanshanian granitic activity coincided with the middle to late Mesozoic fracturing. It was very widely distributed and very intense in relation to both magmatism and tectonic activity, with the intensity increasing eastward and southeastward. The easternmost fracture belt along the Fujian coast on the mainland is marked not only by granitic and migmatitic activity but also by slightly earlier metamorphism, both related to the subduction of the Pacific Plate under the Eurasian Plate. The migration of the zones of granitoid activity towards the coast (especially its cumulative effect) is related to the tectonic development and the accretion of the continental crust (Mo et al., 1980).

Petrochemistry

Following an intensive study on the granitoids of different ages in the Nanling region (east of 108°E, and between 21°40'-26°40'N), Mo and his colleagues (1980) classified them into five petrographic groups, namely granodiorites, adamellites, biotite-granites, mica-granites and miarolitic potash-granites.

Table 2.3 Exposure and distribution of different types of granitoids in the Nanling region (after Mo *et al.*, 1980)

Rock types	Total area (km^2)	%
Granodiorite	3895	5.1
Admellite	5172	6.8
Biotite-granite	65141	85.7
Mica-granite*	590	0.8
Miarolitic potash-granite	1200	1.6
Total	75998	100.00

* Including muscovite-granite

Table 2.4 Average chemical composition of granitoids in the Nanling region, (weighted according to areal coverage, after Mo *et al.*, 1980)

Composition	Grano-diorite	Adamellite	Biotite-granite	Mica-granite*	Miarolitic potash-granite	Average
SiO_2	67.16	69.68	73.12	74.19	76.80	72.65
TiO_2	0.49	0.43	0.25	0.14	0.14	0.27
Al_2O_3	15.04	14.42	13.43	13.77	12.12	13.56
Fe_2O_3	1.74	1.24	0.84	1.01	0.88	0.92
FeO	2.97	2.54	1.88	1.16	0.72	1.97
MnO	0.06	0.08	0.07	0.06	0.06	0.07
MgO	1.51	1.07	0.52	0.47	0.16	0.60
CaO	3.09	2.21	1.22	0.52	0.36	1.36
Na_2O	3.22	3.19	3.08	3.35	4.12	3.11
K_2O	3.80	4.25	4.87	4.62	4.46	4.76
P_2O_5	0.24	0.13	0.11	0.23	0.01	0.11
Loss on ignition	0.68	0.76	0.61	0.57	0.17	0.62
Total	100.00	100.00	100.00	100.00	100.00	100.00
No. of samples	45	39	444	12	49	-

* Including muscovite-granite

The biotite-granites are of the most widely distributed spatially (Table 2.3) and temporally, ranging from Xuefengian to Late Yanshanian. The overall chemical composition of the five types weighted on the basis of their areal coverage is listed in table 2.4. Mo et al. also calculated the areally weighted average chemical compositions of the biotite-granites of the five groups of the Palaeozoic-Mesozoic in the Nanling region (Table 2.5) to study the petrochemical evolution of these rocks during this interval. It is interesting to note that with time progress both SiO_2 and Na_2O show a gradual increase whereas TiO_2, FeO, MgO, CaO and P_2O_5 decrease; Al_2O_3, MnO and K_2O remain almost constant or fluctuate within a small range.

The Guiyang Institute of Geochemistry computed the arithmetic average composition of the granitoids of different ages from the Sibaoan and Xuefengian (Jinningian) to the late Yanshanian in the Nanling region together with the district further north up to the Yangzi River in Jiangxi, Anhui and Jiangsu Provinces (Table 2.6). The results show an overall petrochemical evolution similar to that of Mo *et al.* (1980). The differences are the decrease in Al_2O_3, especially from the Caledonian through the Hercynian to the Yanshanian compared with the decrease of these values in the biotite-granites in the Nanling region during late Palaeozoic and Mesozoic times.

Table 2.5 Average chemical composition of biotite-granite of various ages of the Nanling region (weighted according areal coverage, after Mo *et al.*, 1980)

Composition	Early Palaeozoic	Late Palaeozoic to Triassic	Early to Middle Jurassic	Late Jurassic	Early Cretaceous
SiO_2	71.79	72.28	72.46	73.46	74.09
TiO_2	0.33	0.28	0.28	0.22	0.20
Al_2O_3	13.54	13.72	13.59	13.35	13.20
Fe_2O_3	1.42	1.05	0.94	0.72	1.02
FeO	2.47	1.71	1.99	1.88	1.35
MnO	0.07	0.06	0.07	0.07	0.06
MgO	1.00	0.65	0.48	0.40	0.39
CaO	1.42	0.84	1.16	1.23	1.06
Na_2O	2.58	2.80	3.13	3.10	3.39
K_2O	4.65	5.12	5.06	4.91	4.65
P_2O_5	0.16	0.14	0.16	0.08	0.04
Loss on ignition	0.57	1.35	0.68	0.58	0.55
Total	100.00	100.00	100.00	100.00	100.00
No. of samples	45	39	88	166	46

Table 2.6 Chemical composition of granitoids of various geological ages in South China (after Guiyang Institute of Geochemistry, 1979)

Composition	Sibaoan and Xuefengian	Caledonian	Hercynian	Early Yanshanian and Indosinian	Late Yanshanian
SiO_2	69.31	70.53	71.23	72.76	73.80
TiO_2	0.43	0.42	0.43	0.23	0.20
Al_2O_3	14.87	14.04	13.38	13.51	13.15
Fe_2O_3	0.82	0.86	1.20	0.90	0.89
FeO	3.26	3.14	3.18	1.77	1.48
MnO	0.13	0.07	0.06	0.07	0.06
MgO	1.34	1.15	1.04	0.51	0.46
CaO	1.24	1.81	1.60	1.30	0.97
Na_2O	2.83	2.78	2.23	3.27	3.36
K_2O	3.92	3.86	4.36	4.71	4.69
H_2O	-	-	0.93	0.55	0.59
P_2O_5	0.20	0.14	0.14	0.09	0.05
Loss on ignition	1.45	1.19	1.26	0.88	0.63
Total	99.80	99.99	99.98	100.00	99.74
No. of samples	61	143	62	272	91

Granite series

According to Cheng (1986), Weng Wenhao was the first (1920) to classify the Yanshanian granitoids of South China into two types. The first is a granodiorite type of deeper origin genetically related to iron and copper mineralisation, represented by the intrusions in the middle to lower Yangtze Valley. The second type is of granitic composition genetically related to tin, tungsten, niobium and tantalum mineralisation, exemplified by intrusions in the Nanling region. These two were named as Yangtze (Yangzi) and Hongkong types respectively by Xie Jaron in 1936. The related mineralogenetic problems have been discussed further by a number of geoscientists since the 1950s (Wang et al., 1982), especially since the middle 1970s by geoscientists from the Nanjing University, China University of Geosciences, Guiyang Institute of Geochemistry, Jiangxi Geological Institute, Guangdong Bureau of Geology, and Yichang Institute of Geology and Mineral Resources.

On the bases of the probable source materials from which the rocks might have been derived, and the geological setting in which the rocks occur, Xu et al. (1980, 1982) have divided the Mesozoic granitoids in South China into two genetic series, namely the *Transformation Series* and the *Syntaxis Series*. The former occurs mainly to the west of the Zhenghe-Dapu Fault (extending from 120°E, 30°N to 115.5°E, 22.6°N), "*in a well developed crust inside the continental plate*". This series is mainly derived from crustal materials through transformations, including metasomatism (migmatisation and granitisation), partial anatexis, etc. The syntaxis series appears chiefly to the southeast of the same fault, "*in the active continental margin along some deep fault zones and fault depressions inside the continental plate*". It is mainly derived from syntaxis of crustal materials admixed with others origining from the mantle. The transformation series consists of normal granites and is genetically related to deposits of tungsten, tin, tantalum, niobium and beryllium. The syntaxis series is mainly intermediate in composition, which usually varies from diorite, granodiorite, quartz-diorite through monzodiorite to potash granite, and is noted for its close connection with iron, copper and molybdenum mineralisation. Some of the other differences between them are briefly listed below:

	Syntaxis Series	**Transformation Series**
K_2O-SiO_2:	linear relation	no linear relation
K_2O/Na_2O:	small, increasing inland (0.77-1.70; 0.90-1.77)	larger (0.82-2.41; 0.85 -2.55)
accessories:	mt. 5214 ppm; ilm. 171 ppm; sph. 966 ppm	mt. 345 ppm; ilm. 25 ppm; sph. 84.7 ppm
evolution:	Na-rich to K-rich high Ca, low Al	K-rich to Na-rich high Al, low Ca.
$^{87}Sr/^{86}Sr$:	usually 0.7005-0.7010	c. 0.710 or more

At about the same time, geoscientists from the Guiyang Institute of Geochemistry (Guiyang Inst. Geochem., 1979; Wang et al., 1982) proposed two petrogenetic and metallogenetic series for the granitoids of South China which are broadly similar to those defined by Nanjing University. Series I, or the Nanling Series, is formed mainly through anatexis of crustal materials, whereas Series II, or The Yangzi Series, is derived chiefly from the mantle or lower part of the crust. The Nanling Series shows the following sequences of petrogenesis and mineralisation: monzonitic granite or granodiorite -- biotite granite -- leucocratic granite -- granoporphyry or quartz porphyry -- intermediate-basic dykes; REE -- Nb, Ta (Li, Rb, Cs), Be, Sn, W, Mo, Bi, As -- Cu, Pb, Zn -- Sb, Hg, U. The Yangzi Series

exhibits different sequences: pyroxene diorite (or gabbro) -- diorite -- granodiorite (quartz monzonite) or monzonitic granite -- granite -- K-feldspar granite -- granoporphyry or quartz porphyry (syenitic porphyry or quartz-syenitic porphyry) -- intermediate-basic dykes; Fe -- Cu (Au) -- Mo (W) -- Pb, Zn - Pb (Ag). Other differences between them may be briefly tabulated as follow:

	Nanling Series	**Yangtze Series**
Bulk composition:	granitic, high SiO_2 & K_2O	andesitic, high MgO & CaO
Formation temp.:	600 - 800°C	900 - 1140°C
Biotite:	high in Mg	high in Fe
Accessories:	mt. sph. apat. or mt. il. REE-rich zir.	complicated, mt. il. zir. or monaz. xenot. zir.
Trace elements:	dominated by F, Li, Rb (Cs), and Be, with $\Sigma Y > \Sigma Ce$, relatively low δEu with distinct depletion	dominated by Cl and Sr, with $\Sigma Ce > \Sigma Y$ in rocks and accessories, relatively high δEu (0.74-0.99) without depletion
Other features:	$\delta^{18}O > 10‰$, greater varying $\delta^{34}S$; low in Pt-group elements; high $^{87}Sr/^{86}Sr$ (0.7112-0.7360)	$\delta^{18}O < 10‰$, $\delta^{34}S$ close to meteoritic sulphur; relatively high in Pt-group elem.; low $^{87}Sr/^{86}Sr$ (0.7036-0.7085)

Wang, L. K. *et al.* (1982) pointed out that the granitoids of these two series show considerable dissimilarities from those of Australia (Chappell and White, 1974) and Japan (Ishihara, 1977) in $^{87}Sr/^{86}Sr$, $\delta^{18}O$ and $\delta^{34}S$ values.

2.1.3 Mineralisation associated with the granitoids

The Nanling region is well known as the most important tungsten metallogenetic province of the world and is also one of the most significant polymetallic provinces in China. A wide variety of metallic mineral deposits (W, Sn, Nb, Ta, Be, Mo, REE, Cu, Fe, etc.) in this region have close genetic relations to the granitic rocks, especially the Yanshanian anatectic granitoids (*e.g.* Tu *et al.*, 1980). The various types of mineralisation can be broadly categorised into four groups: rare granitophile element (W, Sn, Nb, Ta, Be, Li, REE) mineralisation, base metal (Pb, Zn, Ag, Sb) mineralisation, porphyry copper (± molybdenum) mineralisation, and iron (± copper) mineralisation.

Rare granitophile element mineralisation

The complex nature of the rare granitophile element mineralisation preclude a detailed discussion. However, a number of general isotones may be made which hold for the bulk of the deposits.

The important W, Sn, Nb, Ta ore deposits are genetically related to granites almost exclusively generated during the Yanshanian period. The older granites are generally barren in mineralisation of economic significance except for rare-earth elements (REE). The contents of W, Sn, Nb, Ta and REE are much higher than those of older granites and the average of common granites (Table 2.7). Among the Yanshanian granites which consist of two substages and five phases (see section 2.1.2), wolframite is most abundant in the second phase of the early substage, niobium- and tantalum-bearing minerals are rich in the third phase of the early substage, and cassiterite reaches its maximum in the first phase of the late substage (Yan *et al.*, 1980).

Granite type ores, which are synchronous with granite intrusion, commonly contain niobium, tantalum and rare-earth elements. They are related to potash feldspathisation and albitisation in the upper parts of the intrusive body, such as the Limu deposit in Guangxi (Xu, 1989) and the 414 deposit in Jiangxi (Xia *et al.*, 1989). These elements are mainly concentrated in accessory minerals (microlite, niobite, tantalite, monazite, apatite, etc.)which occur as inclusions within the feldspars (Zhou, 1980; Zhang & Xia, 1988; Xu, 1989).

Much of the niobium, tantalum (tungsten, tin, beryllium) mineralisation in this province occurs in *greisens* in the roof of the major plutons and satellite stocks. Disseminated microlite, niobite, tantalite, together with cassiterite, wolframite and other Cu-Fe-As sulfides, are usually the main element-bearing minerals.

Lodes and replacement (skarn) deposits are the major source of tungsten, tin, beryllium (bismuth, lead, zinc, copper) mineralisation in the Nanling region. They occur in the top parts of the plutons and satellite intrusions. Pegmatitic pods and veins which host bunches of massive wolframite and cassiterite, are well-developed in many granites. Besides wolframite and cassiterite, these pods and veins often contain aggregates of arsenopyrite, galena, sphalerite with minor tourmaline, molybdenite, beryl and native bismuth. Disseminated wolframite, cassiterite, scheelite and Cu-Fe-As sulfides occur in skarns developed along the granite contacts. Frequently, the lodes and skarn deposits are combined in the same area to form large scale tungsten-polymetallic deposits, such as the Shizhuyuan orefield -- the largest of this kind in the world.

Table 2.7 Trace element concentrations of various granites from the Nanling ares (after Guiyang Institute of Geochemistry, 1979)

	Sibaoan-Xuefengian	Caledonian	Hercynian	Indosinian	Yanshanian	Average[a]
Nb	15	21	21	25	35	29
Ta	3	6	4	3	8	7
REE	208	209	152	195	256	229
W	2.2	2.2	-*	-	4.1	3.5
Sn	5	15	25	13	42	32
Be	1.6	2.6	2.9**		5.4	4.2
Rb	190	-	235	-	358	279
Li	67	-	-	-	96	147
F	726	792	-	-	1388	1049
Sr	381	123	157	176	147	159

a - average of Sibaoan-Yanshanian granites calculated on the base of areal coverage
* data not available ** average for Hercynian and Indiosinian granites

Sheeted vein swarms, usually hosted by small granite stocks, are also important sites of rare metal mineralisation. They comprise subparallel sets of steeply dipping quartz veins with greisen borders (quartz + muscovite / Li-mica + topaz). These quartz veins are usually a few centimetres to two meters in width and occur in both granite and adjacent country rocks. Bunches of bladed wolframite crystals and equigranular cassiterite, often nucleating on the vein walls, are common ore minerals. Polymetallic sulfides, including galena, sphalerite, pyrite, arsenopyrite, chalcopyrite, stannite, molybdenite and bismuthinite usually occur interstitial to polygranular quartz in the central part of the vein. Gangue minerals include tourmaline, feldspar, mica, fluorite and calcite.

Since the discovery of *porphyry* tungsten (+ molybdenum) deposits at Yangchuling, Jiangxi Province in the late 1970s, a new member has been accounted in the giant family of mineralisation in the Nanling area, South China. It is an explosion breccia porphyry of granodioritic composition. The mineralisation is closely related to multistage alterations of silicification, sericitisation, potash-feldspathisation and carbonatisation, and occurs as a mixture of stock-work and impregnation both inside and outside the breccia pipe. Scheelite and molybdenite are the main ore minerals. The scheelite is characterised by the high content of molybdenum, and the molybdenite is rich in WO_3 and Re (Liu & Shen, 1984)

Based on gathering a large quantity of information and intensive reviewing, a comprehensive ideal

metallogenetic model of rare-earth, rare metal and nonferrous metal ore deposits related genetically to Yanshanian granites in South China has been presented by Chen (1983) (Fig. 2.4).

Base metal mineralisation

Base metal(Pb, Zn, Cu, Ag, Sb) mineralisation in southeastern China is closely related to small hypabyssal - ultra-hypabyssal intrusives with an acidic composition (granite, granoporphyry, quartz porphyry, granodiorite). It is often accompanied by the rare metal mineralisation as a late stage product. Faults and contact zone strictly controlled the locations of mineralisation which occurs as two series. One is the Sn-bearing series which is characterised by the occurrence of cassiterite in the ore and a high content of tin in ore minerals. Marmatite, galena, cassiterite, pyrrhotite, bournonite and freibergite are the main ore minerals. Another is the Cu-bearing series which is typified by the present of a large amount of chalcopyrite and pyrite, and the high content of copper in ore minerals consisting of sphalerite, galena, chalcopyrite,pyrite, etc. (Hu *et al.*, 1985)

Porphyry Copper (+ molybdenum) mineralisation

Represented by the Dexing deposits (the largest of this kind in China), porphyry copper (molybdenum) mineralisation is one of the major copper resources of China. The deposits occur in the contact zones of small separate stocks of early Yanshanian granodiorite porphyries which are typically intermediate-acidic calc-alkaline rocks and are enriched in ore-forming elements, such as copper and molybdenum. The mineralisation is closely related to intensive alterations ---- late-magmatic autometamorphism and post-magmatic metasomatism. The principal ore body spans the contact zone of the granodiorite porphyry mass, with the portion in the outer contact zone making up 2/3 of the ore body (Yan & Hu, 1980). It occurs in the form of a hollow-pipe, which, following the contact zone, plunges downwards with a vertical depth of more than 1000m and a diameter of 400-700m. The main ore minerals are pyrite, chalcopyrite and molybdenite in a weight ratio of approximately 300:33:1, the average copper content ranges from 0.41 wt.% to 0.53 wt.%. Gangue minerals mainly consists of quartz, sericite, chlorite and anhydrite. Native gold, petzite, matildite, native silver, siegenite, millerite and rutile as well as the dispersive elements Te, Sc, Re and Os are valuable by-products (Yan & Hu, 1980).

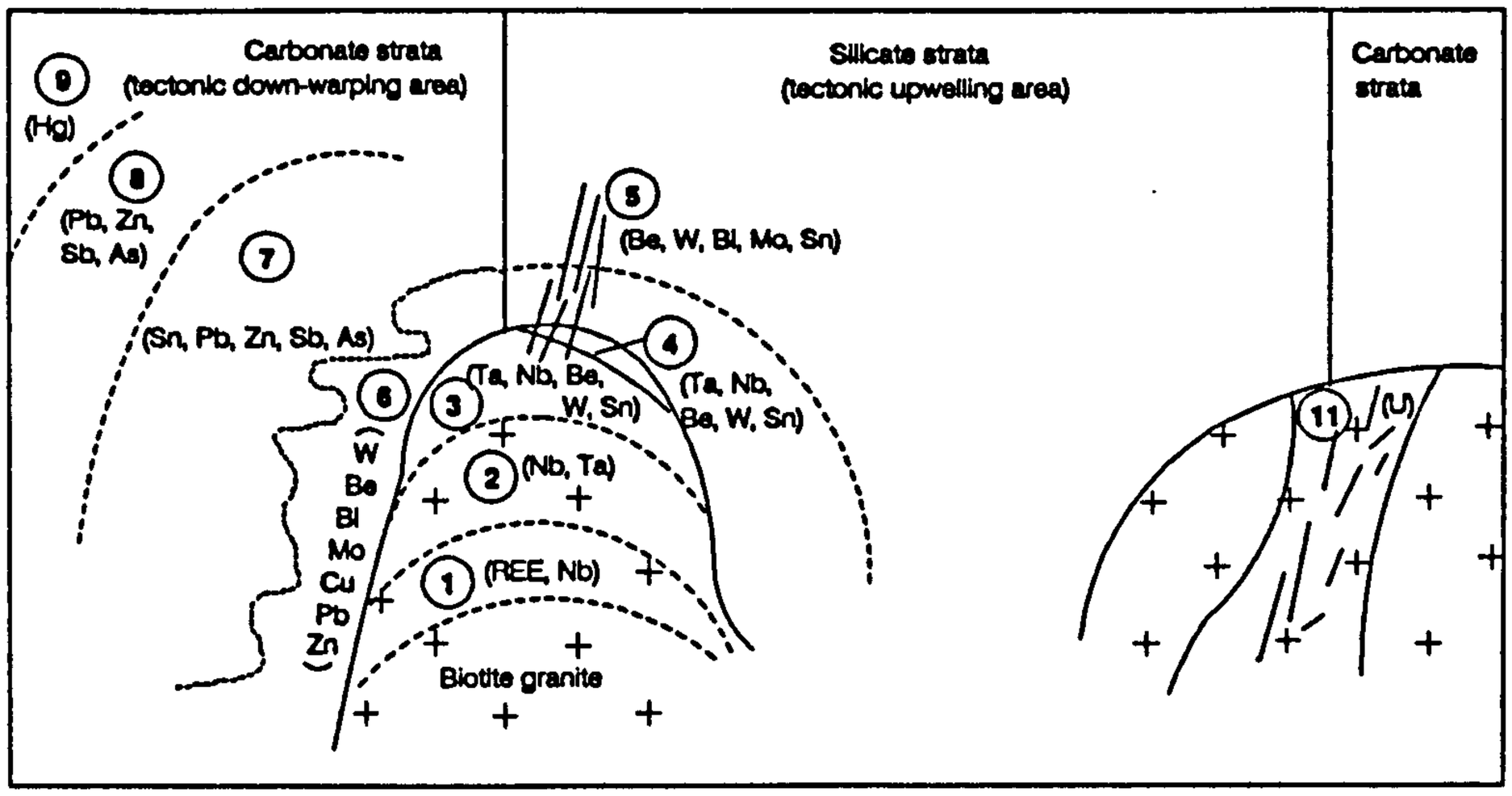

Fig 2.4 A Ideal metallogenetic model of rare-earth, rare metal and non-ferrous metal deposits related genetically to the Yanshanian granites in South China (after Chen, 1983)

1 -- Granite-type rare-earth, rare metal (Nb) deposit;

2 -- Granite-type Nb-Ta deposit;

3 -- Greisenised granite or greisen:

3-1 -- Nb, Ta, Be, W, Sn deposit;

3-2 -- Quartz-muscovite (sericite) stock-work W, Be, Bi, Mo, Sn deposit;

4 -- Pegmatite-type Ta, Nb, Be, W, Sn deposit;

5 -- Pneumatolytic hydrothermal quartz-(feldspar) vein-type W, Be, Bi, Mo, sn deposit;

6 -- Skarn-type deposits:

6-1 -- Skarn W, Bi, Be, Mo, Sn deposit (including ribbon Be deposit);

6-2 -- Skarn Cu, Zn deposit;

7 -- K-feldspar-tourmaline-marble zone:

7-1 -- High-moderate temperature hydrothermal cassiterite-tourmaline-sulphide (Pb, Zn) stock-work deposit;

7-2 -- High-moderate temperature hydrothermal cassiterite-sulphide (Pb, Zn, Sb, As) interlayer-filling and stock-work deposits;

8 -- Deposits in marble:

8-1 -- Mesothermal galena-sphalerite lode-type deposit;

8-2 -- Low-moderate temperature hydrothermal Pb, Zn, Sb, As sulphide and silicate veins;

9 -- Low-moderate hydrothermal cinnabar deposit in limestone;

10 -- Low-moderate temperature hydrothermal wolframite-antimonite-quartz veins and scheelite-fluorite-calcite veins;

11 -- Low-moderate temperature uranium deposit in fracture zone within granite intrusion.

Stage	First	Second	Third	Fourth
Mineralization	W, REE, Nb, Ta, (BE, Bi, Mo, Sn)	W, Sn, Pb, Zn, Nb, Ta, Be, (Bi, Mo)	Sn, Pb, Zn, Cu, Sb, As, Hg, (W)	U
Age	134-181 Ma (rock- and ore-formation age)	121-172 Ma (rock-formation age)	91-107 Ma (rock-formation age)	47.6-86.7 Ma (ore-formation age)
Tectonic location and country rock	Caldonian basement upwelling area silicate strata	Upper Palaeozoic down-warping area carbonate strata	Upper Palaeozoic down-warping area carbonate strata	upwelling and down-warping areas composite granitic batholith
Granite chemistry	SiO2>74%, K2O>Na2O, K2O+Na2O>8% Al2O3 = 12-13.3%	SiO2>74%, K2O>Na2O, K2O+Na2O>8% Al2O3 = 12.5-14.6%	SiO2=71-74%, K2O>Na2O, K2O+Na2O<7.5% Al2O3 = 15%	
Ideal metallogenetic model	Silicate strata 5 (W, Be, Bi, Mo, Sn) 4 (Ta, Nb, Be, W, Sn) 3-1 (Ta, Nb, W, Sn) 2 (Nb, Ta) 1 (REE, Nb) Hornstone biotite granite	carbonate strata 8-1 (Pb, Zn) 7-1 (Sn, Pb, Zn) (W, Bi, Be Mo, Sn) 5 3-2 (Ta, Nb) 2 6-1 biotite granite	Carbonate strata 9 (Hg) 8-2 (Pb, Zn, Sb, As) 7-2 (Sn, Pb, Zn, Sb, As) (Cu, Sn) 6-2 10 biotite granite	11 (U) Skarn Greisen

Fig. 2.4B Schematic diagram showing the evolution of the metallogenetic series of rare-earth, rare metal and non-ferrous metal ore deposits related genetically to the Yanshanian granites in South China (after Chen, 1983)

2.2 GEOLOGY OF THE XIANGHUALING OREFIELD

2.2.1 Introduction

The Xianghualing orefield is tectonically situated in the central part of the South China Accretionary fold belt (South China fold system of Huang, 1980; or Huanan Terrane of Hsü, 1981), which was considered to be a late Caledonian (s.l.) fold system and became a stable terrane during the late Caledonian phase. A huge thickness of shallow marine sediments was developed through the Late Palaeozoic Era. The Mesozoic Indosinian and Yanshanian Orogenies left this area with complicated fracture systems, numerous granitic intrusions and a wide variety of mineralisation.

As one of the most important tungsten-tin polymetallic orefield in South Hunan Province, the Xianghualing orefield covers an area of over 100 km^2, and consists of four ore districts and more than ten separate deposits which include various types of mineralisation (Nb, Ta, W, Sn, Be, Pb, Zn). The study area occupies the southern portion of the orefield with an area of approximately 20 km^2 and broadly corresponds to the outcrop pattern of the Jianfengling granite stock (Fig. 2.5 and Appendix I).

2.2.2 Lithostratigraghy

The rocks exposed in this region are a series of Cambrian-Lower Carboniferous marine clastics and carbonates which were deposited in the South China Accretionary fold belt (Sun *et al.*, 1989; Hsü *et al.*, 1989). The terminology adopted in this study is that defined by the Hunan Geological Survey (1962).

Cambrian System

The Cambrian rocks occupy the centre part of the orefield and are present as the core of the Tongtianmiao anticline. Although detailed research concerning the compositions of these rocks has not been carried out, three lithological units are recognised, the lower unit consists mainly of arenaceous, argillaceous and calcareous slates with locally interbedded metamorphic sandstone; the middle unit is typified by alternations of slates and metamorphosed fine- to medium-grained

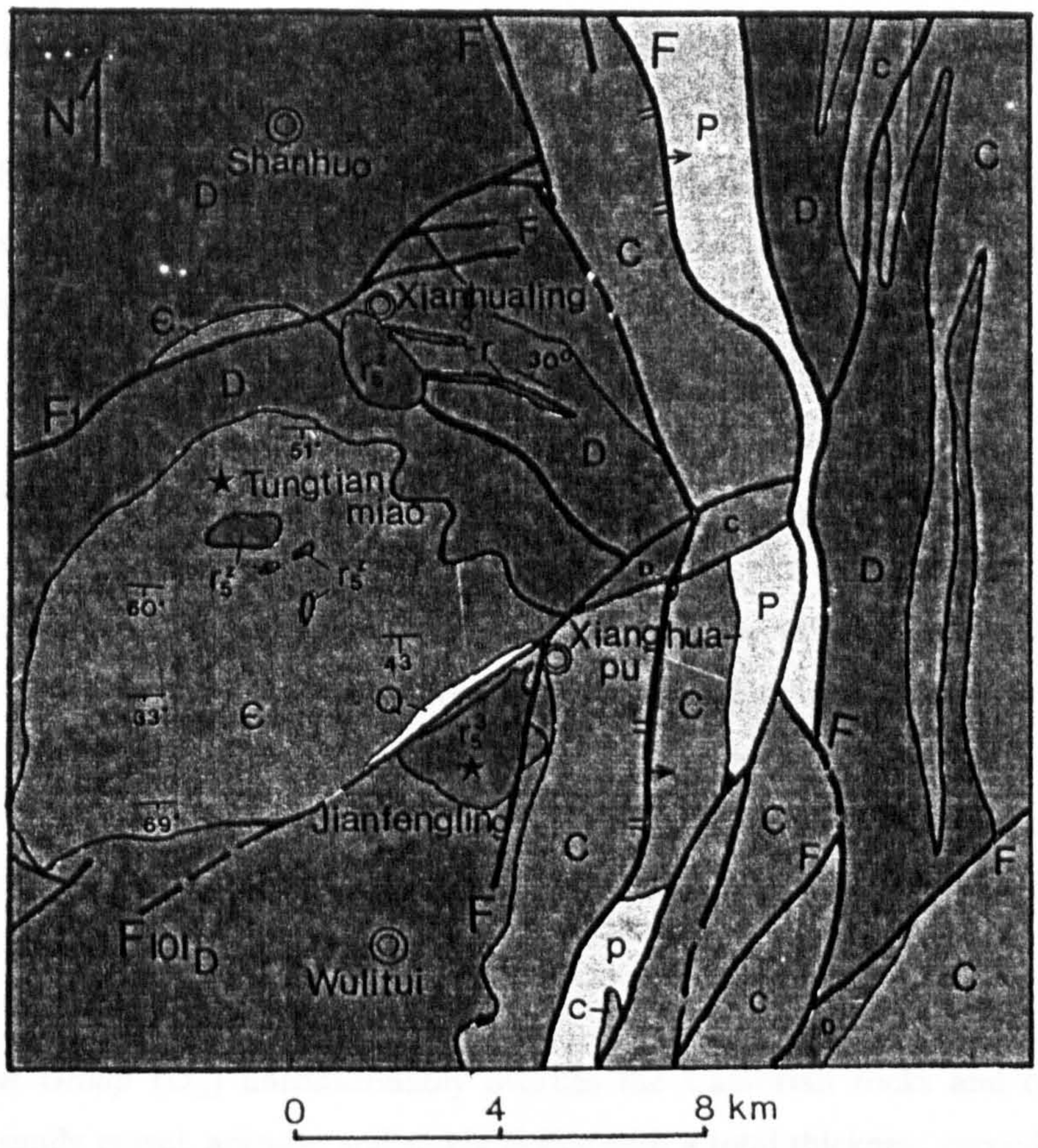

Legend

Q	Quarternary sediments	P	Permian
C	Carboniferous	D	Devonian
Є	Cambrian	γ	Granite
	Geological boundary		Fault

Fig. 2.5 Regional geological map of the Xianghualing orefield

(modified from Luo et al., 1981)

sandstones; the upper unit is dominantly of metamorphosed thin- to medium-bedded sandstones with intercalations of slates. The overall thickness of the Cambrian rocks exceeds 3500m.

Only rocks of the upper unit outcrop in the study area. They have variable strikes and dips (15-60° to the southeast and southwest), and are separated from the rocks of Devonian and Carboniferous ages by the F_{101} fault (see Appendix I).

Devonian and Carboniferous Systems

Overlying the Cambrian metasedimentary rocks with identical unconformity are the Lower Palaeozoic (Devonian and Carboniferous) sedimentary rocks, which are widely distributed over the whole region and constitute the main country rocks of both the granite intrusions and various types of mineralization. They consist of the middle Devonian Tiaomajian Group (D_{2t}) and Qiciqiao Group (D_{2q}), upper Devonian Shetianqiao Group (D_{3sh}), and Lower Carboniferous Menggongao Group (C_{1m}), Shitengci Group (C_{1sh}) and Ceshui Group (C_{1c}).

The *Tiaomajian Group* (D_{2t}) unconformably overlies the Cambrian rocks and comprises a basal conglomerate, sandy gravel, arkosite and sandy shales with a total thickness exceeding 1000 m.

The *Qiciqiao Group* (D_{2q}) and *Shetianqiao Group* (D_{3sh}) are mainly of thick limestone, crystalline dolomite with abundant foraminifera, carboniferous limestone with intercalations of calcareous shale, interbeddings of thick-bedded wormkalk and thin-bedded limestone, and dolomitic limestone with a total thickness of 800m. Because of both the granite intrusion and the intensive fracturation, most of the Shetianqiao Group is absent in the study area, the remainings occur along the eastern contact of the Jianfengling granite stock and have become skarn and marble due to the contact metasomatism and metamorphism.

The Lower Carboniferous *Menggongao Group* (C_{1m}) and *Shitangci Group* (C_{1sh}) comprise medium to thick bioclastic limestone, dolomitic striped limestone, thin carboniferous limestone and muddy limestone, thick limestone with chert strips, and carboniferous shales. The *Ceshui Group* (C_{1c}) is typified by the thin muddy siltstone, carboniferous and calcareous shales with intercalations of coal beds. The overall thickness of the Carboniferous rocks exceeds 500 m.

In the study area, the rocks of Devonian and Carboniferous age are monoclinal, strike north-south and

dip 20-45° to the east, and host both the Jianfengling granite and most of the mineralization.

2.2.3 Structural evolution

The importance of fracturing in the geological evolution of the Xianghualing region has long been recognised. No. 238 Geological Team (1958) was the early proponent of fracturing as a significant deformation process in the area. More recently, Huang (1985), Zhang & Xu (1989) and the Structure Group, Nanling Research Programme (1988) presented more detailed interpretation for the structural evolution of the region. It is now generally accepted that intensive fracturing not only controls the location and emplacement of the numerous granite intrusions, but also confines the distribution of the various types of mineralization (e.g. Zhang & Xu, 1989). Detailed structural work in the Xianghualing region (Zhang & Xue, 1989; this study) has led to the recognition of four major phases of fracturing: NE-SW, NW-SE, near N-S and near E-W (Fig. 2.5). These fractures were generated pre-, syn- and post-granite emplacement with multistage reactivation (Zhang & Xu, 1989).

NW-SE trending group

Faults trending NW (290-330°) and dipping 70-85° to the southeast are the earliest fractures in the region, and have been cross-cut by the faults of all other groups. The fault F_7, the main representative of this group, cuts through the centre of the orefield and extends over 30 km and changes its strike to the southwest (Fig. 2.5). It might be a deep-cutting fault and experienced multiphase reactivation (Zhang & Xu, 1989). In the study area, faults of this group, named F_{2S}, are the products of the latest phase and widely distributed within the Jianfengling granite stock and the country rocks. They were syn-dated the granite emplacement and cut all other three groups of faults. Within the granite stock, most of the these faults have left 20-80 cm wide open spaces (Plate 2.1) along which Sn, W, Be, Pb, Zn mineralised quartz veins with mica-rich greisen borders have been found, and the others have been filled with barren quartz veins.

NE-SW trending group

Faults of this group strike NE 30-50° and invariably dip SE, generally at 40-70° with their extensions reaching 15-20 km. The faults F_1 and F_{101} cut through the Xianghualing and the Xianghuapu area

respectively and these faults are the major fractures in the orefield and are multistage (Hunan Geol. Survey, 1962; Zhang & Xu, 1989).

The fault F_{101} is a reverse fault zone and extends over 17km northeastly with dips of 50-70° to the southeast. It cuts through the northern portion of the study area (see Fig. 3.2; Appendix I; Plate 2.1). This fault zone consists of several co-genetic faults distributing across a 20-100m wide zone. Slickensides clearly indicate the multistage activation history of the fault. A 10-50cm thick quartzite occurs along some part of the fault plane due to dynamic metamorphism. The northwest footwall block exposes the Cambrian metasedimentary rocks. Rocks in the southeastern hanging wall are the granite and Devonian and Carboniferous sediments. The age and active history of this fault zone are not known conclusively, but the occurrences of Sn, Pb and Zn mineralization within the fault zone suggest that it either pre-dated or was at least contemporaneous with the emplacement of the granite stock.

Near N-S trending group

This group comprises a series of left-lateral reverse faults mainly sited in the eastern part of the orefield. They strike NNW 330-355° in the north NNE 5-30° in the south, and invariably dip 20-85° to the east. The scale of these faults ranges from several metres to tens of kilometres (see Fig. 2.4).

In the study area, the faults of this group, named F_{4S} are hosted in the Devonian and Carboniferous sedimentary rocks and are located just east of the granite stock. They have been identified cross-cutting the F_{101} fault (Appendix I). They are interpreted to have developed from the branching fractures of the F_{101} fault and are the predominant faults controlling the distribution of the orebodies (Luo, 1981). The coexistence of fault gouge and breccia, consisting of dolomite and limestone fragments, in the faults suggests that these faults have undergone both extensional and thrust movements. According to the difference of in dips, these faults can be categorized into two subgroups. One consists of the steeply dipping faults which host the main fluorite-scheelite orebodies, the mineralization occurs predominantly in the heavily fractured footwall rocks. The other comprises gently dipping faults, developed parallel to beddings, and along which karst solution cavities have been formed. These cavities host the main galena-sphalerite orebodies. The dips of the two subgroups increase from 60-75° to 80-90° and from 20-30° to 40-50° respectively as the faults extend downwards.

Plate 2.1

Plate 2.1 Major fault zone F_{101} and other fractures within the granite

a. The F_{101} fault zone. Viewing direction: toward NE.

b & c. NW-trending fractures within intrusion B. Viewing direction: toward SSE.

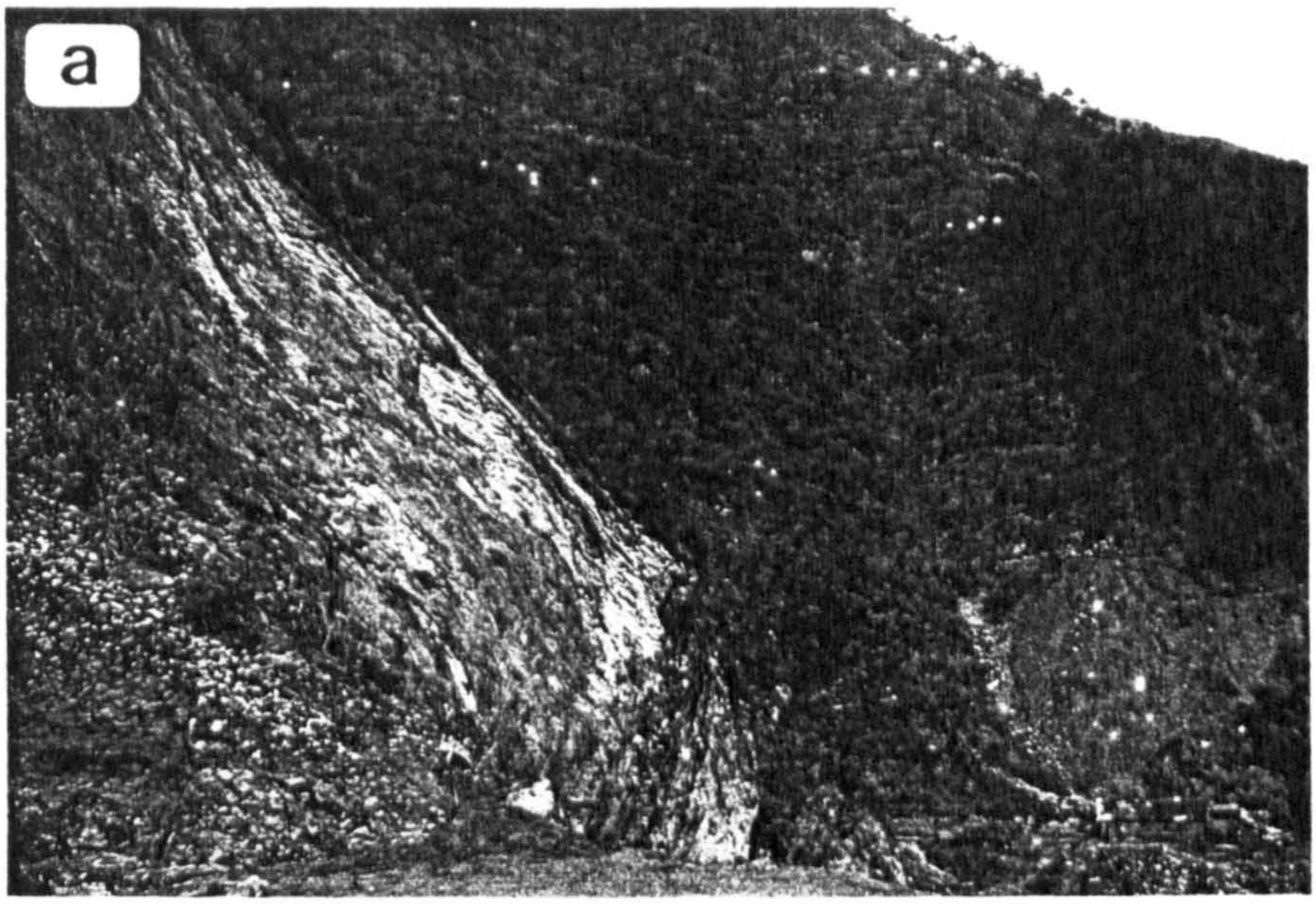
a

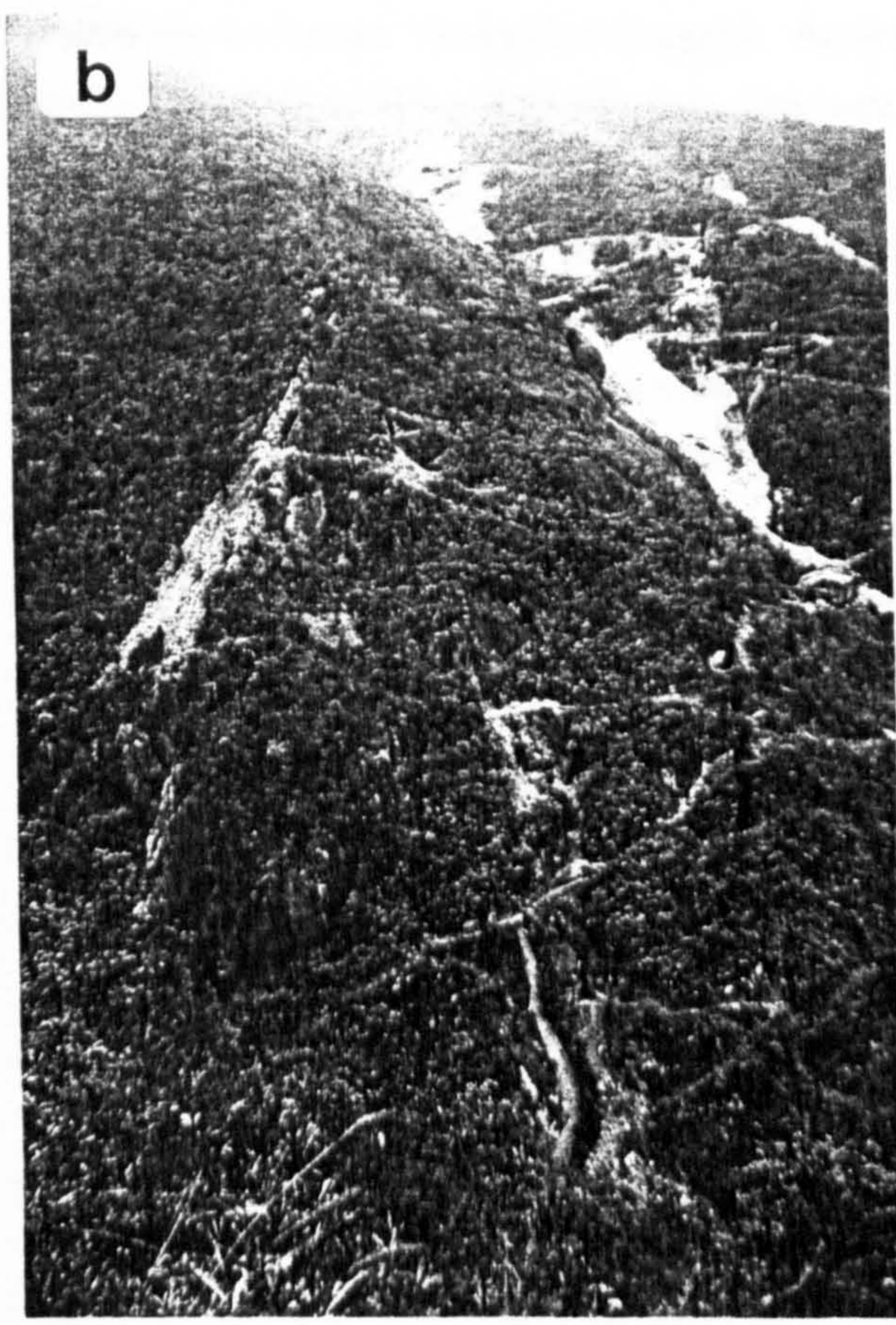
b

c

Near E-W trending group

The faults named F_{3S} (Appendix I) are a group of relatively small scale, right-lateral faults, generally striking E-W and dipping 55-85° to the south. They truncate the granite stock at their western limits and cross-cut other major faults in the study area. There are a few small Pb-Zn orebodies and granitic dykes hosted in these faults (such as the No. VI orebody of the Meishi deposit). The Jianfengling granite stock is located at the junction of these faults and the NE-trending fault (F_{101}).

2.2.4 Granite intrusions

A number of small granite bodies with area ranging from 0.0n km^2 to 4.4 km^2 are emplaced into a sequence of Cambrian metasedimentary rocks and Devonian and Carboniferous limestones and dolomites during the Yanshanian Orogeny. Among them, the Jianfengling stock (Xianghuapu area, 4.4 km^2) and the Laiciling stock (Xianghualing area, 2.2 km^2) are the largest. Both stocks are igneous complexes consisting of multistage intrusions (Zhang & Xue, 1989; this study). The poor exposure and strong alteration have limited detailed investigations for other small intrusions.

The Laiciling granite stock (also called Xianghualing stock), dated at 155 Ma (K-Ar age on biotite, Mo et al., 1980) and 117±1 - 157±9 Ma (Rb-Sr ages of whole rock, Zhang & Xu, 1989), consists of three intrusions: γ_5^{2-2} (157±9 Ma), γ_5^{2-3} and γ_5^{3} (117±1 Ma). All are biotite granites with main minerals of orthoclase (21-25 vol.%), albite (15-40 vol.%), quartz (20-45 vol.%) and biotite (5-20 vol.%), and minor minerals of topaz, zircon and allanite (Zhang & Xu, 1989). The granites are peraluminous and have high SiO_2, Na_2O+K_2O, Rb, Nb Ta, Y and Th, and low FeO, CaO, MnO, TiO_2, P_2O_5 and Sr contents. Compositions for major and selected trace elements are presented in Table 2.8. Chondrite-normalised REE patterns for the three intrusions are sub-parallel to each other and display pronounced negative Eu anomalies, and among these granites, the REEs decrease progressively in the later intrusions (Fig. 2.6). In the normalised geochemical patterns, all granites shale the similarity and show depletion in Ba, Sr, P, Ti, enrichment in all other elements (Fig. 2.7).

The Jianfengling stock comprises five intrusions which shale most of the characteristics of the Laiciling granites. It will be fully discussed in the later chapters.

Table 2.8 Compositions of the Laiciling granite (after Xue and Zhang, 1989)

Composition	γ_5^{2-2} (n=5)	γ_5^{2-3} (n=2)	γ_5^{3} (n=3)
SiO_2	69.37	69.43	67.66
TiO_2	0.04	0.04	0.03
Al_2O_3	16.36	16.32	17.46
Fe_2O_3	0.40	0.38	0.35
FeO	0.88	1.29	0.32
MnO	0.07	0.12	0.05
MgO	0.11	0.20	0.37
CaO	0.86	0.99	0.56
Na_2O	4.17	3.25	5.05
K_2O	5.46	4.73	6.03
P_2O_5	0.02	0.02	0.02
H_2O_+	1.17	1.21	1.17
H_2O_-	0.17	0.16	0.42
F	0.81	1.37	0.42
La	97	61	25
Ce	219	143	66
Pr	33	20	9
Nd	104	54	24
Sm	33	16	8
Eu	0.48	0.28	0.11
Gd	34	13	7
Tb	8	3	2
Dy	50	20	11
Ho	11	4	2
Y	258	78	38
Be	5	5	6
Pb	163	253	135
Zn	108	362	47
W	72	154	61
Sn	122	65	67
Nb	103	106	94
Ta	27	31	33

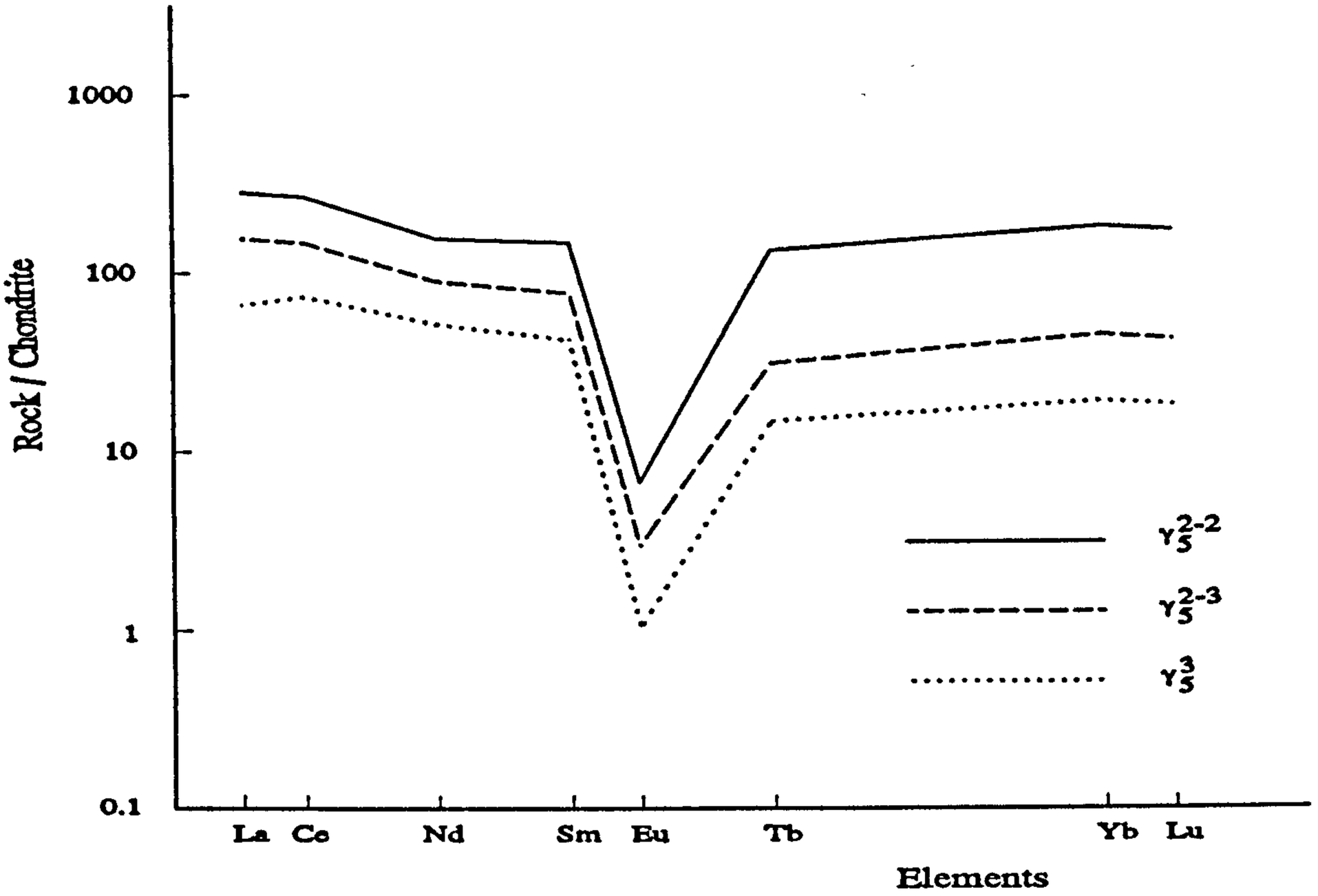

Fig. 2.6 REE distribution patterns of the Laiciling granites (after Zhang & Xu, 1989)

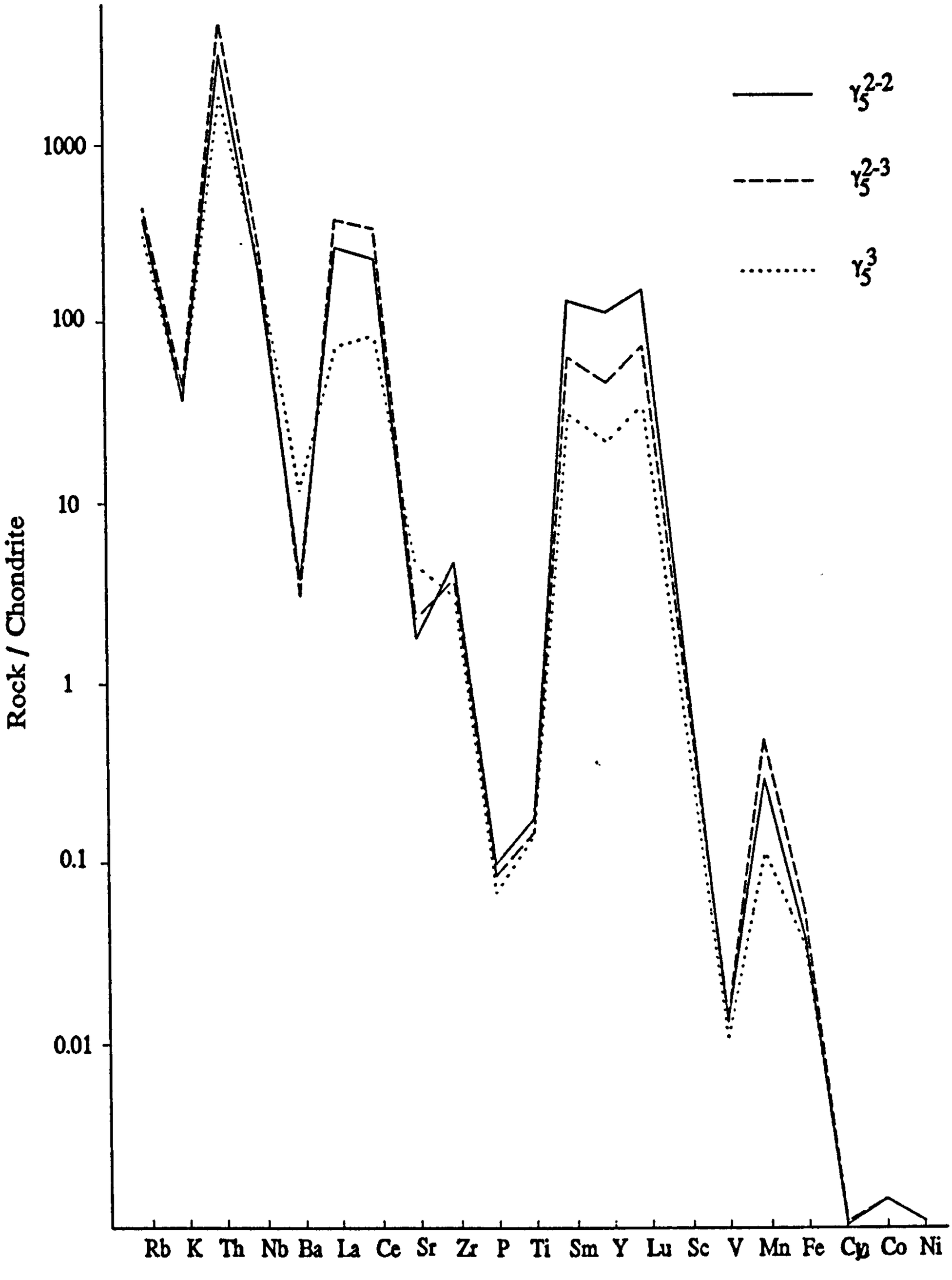

Fig. 2.7 Spidergram plot of trace elements from the Laiciling granites (after Zhang & Xu, 1989)

CHAPTER THREE

PETROLOGY OF THE JIANFENGLING GRANITES

CHAPTER THREE

PETROLOGY OF THE JIANFENGLING GRANITES

Contents

3.1 Introduction
3.2 Field relationships and general petrography of the granites of the Jianfengling stock
3.3 Petrography and mineralogy of the Jianfengling granites

3.1 INTRODUCTION

The Jianfengling granite complex is a well-exposed, small-scale, high-level intrusive stock. It occurs in the central northern part of the Nanling Ranges of Southeast China, which is well known for its wide distributions of granite intrusions. The stock has an late Jurassic-early Cretaceous age (No. 238 Geol. Team, 1974) and was emplaced in a sequence of Devonian and Carboniferous limestones and dolomites during the Yanshanian Orogeny (Mo *et al.*, 1980). The sedimentary country rocks locally form long, narrow roof-pendants that penetrate vertically into the granites (Plate 3.1a), thereby suggesting that the roof zone is presently exposed. The preservation of phase characteristic of the upper part of granitic intrusions, such as greisen and pegmatite zones, and the presence of local xenoliths of country rocks (Plate 3.1b), as observed near the granite-country rock contact in the 480 pit near the shaft also suggest a close proximity to the roof zone of the stock. The composite stock, previously known as "430 granite" (No. 238 Geol. Team, 1962, 1974), belongs to a series of granitic bodies exposed in the Xianghualing ore field, which is situated between two huge granite plutons, namely the Jiuyishan pluton in the southwest and the Jitianling pluton in the northeast, each of which occupies several thousands quare kilometres (Fig. 3.1). Gravity anomalies suggest that these intrusions in the Xianghualing area might connect with the Jitianling pluton at depth (Zhang & Xu, 1989; Yuang *et al.*, 1986).

Detailed field relationships and petrology of the Jianfengling granite stock are presented in this chapter. These are based on observations during field mapping at a scale of 1:10,000, which covers the whole Jianfengling stock and adjacent country rocks, and also on the examination of over two hundred thin and polished sections.

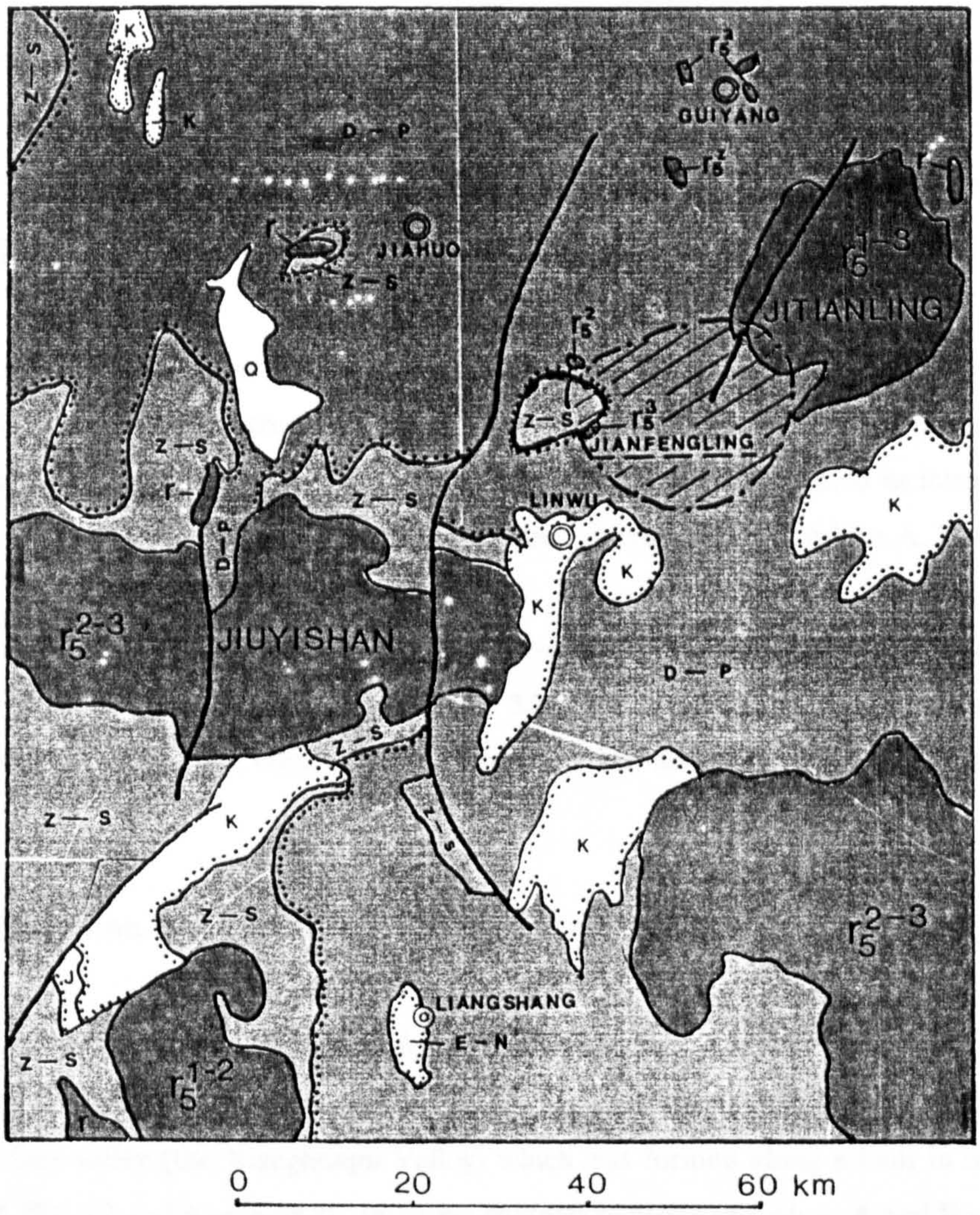

Legend

E-N	Eocene - Neocene	K	Cretaceous
D-P	Devonian - Permian	Z-S	Sinian (800-600 Ma) - Silurian

Granite emplaced during the Later Yangshan Orogeny (Cretaceous)

Granite emplaced during the Earlier Yangshan Orogeny (Jurassic)

Granite emplaced during the Indosinian Orogeny (Triassic)

Hidden granite body predicted by gravimetric and magnetic surveys

Geological boundary Fault

Fig. 3.1 Simplified geological map showing the distribution of granite intrusions in the Xianghualing region (modified from Yuang et al., 1986).

3.2 FIELD RELATIONSHIPS AND GENERAL PETROGRAPHY OF THE GRANITES OF THE JIANFENGLING STOCK

Evidence from the intrusive contacts shows the Jianfengling granite stock to be a polystage complex comprising five separate intrusions (Fig. 3.2, Appendix I). Referring to the order of intrusion and following the Chinese naming system[1] for granites, they have being named as intrusions $\gamma_5^{2\text{-}3A}$, $\gamma_5^{2\text{-}3B}$, $\gamma_5^{2\text{-}3C}$, $\gamma_5^{2\text{-}3D}$, and $\gamma_5^{2\text{-}3E}$, but hereinafter they will be referred to as intrusions A, B, C, D and E.

The granites of the Jianfengling stock are generally similar in terms of texture and grain size throughout the five intrusive phases (*e.g.* Plate 3.3a, b, c & d). However, in the terms of mineralogy and related mineralisation, these granites have their own distinctive characteristics (Table 3.1).

3.2.1 Intrusion A: medium-grained biotite granite

Drillhole data suggest that this intrusion is mainly hidden under the Jianfengling mountain which comprises intrusion B. There is a small, heavily weathered, xenolith-like, elongate outcrop exposed along a deep valley (the Xianghuapu Valley) which was formed along a fault in the east side of the stock (cf. Fig. 3.2 and Appendix I). Intrusive contacts between intrusions A and B and between A and D have been found in drill core and outcrop respectively. They are defined by 2-3 cm-wide discontinuous pegmatitic and/or chilled zones on the younger side and 1-5 cm-wide zones of contact metamorphism on the older side along the intrusive contact surfaces (Fig.3.3).

The granite of this intrusion is characterised by the presence of dense black biotite and a high content of pinkish K-feldspar. Estimates from the hand specimens indicate that this granite consists of quartz (15-30 vol.%), K-feldspar (20-45 vol.%), albite (10-25 vol.%, An 0-7), biotite (2-5 vol.%), and accessory minerals fluorite, topaz, zircon and monazite (total 1-2 vol.%).

---

[1] In this system, according to Yuan *et al.* (1986), γ_1 represents Sibaoan granites; γ_2 -- Jiningian granites (γ_2^1 -- Early Jiningian, γ_2^2 -- Late Jiningian, γ_2^3 -- Xuefengian); γ_3 -- Caledonian granites (γ_3^1 -- Early Caledonian, γ_3^2 -- Late Caledonian); γ_4 -- Hercynian granites (γ_4^1 -- Middle Hercynian, γ_4^2 -- Late Hercynian); γ_5 -- Indosinian and Yanshanian granites [γ_5^1 -- Indosinian, γ_5^2 -- Early Yanshanian ($\gamma_5^{2\text{-}1}$ -- first phase, $\gamma_5^{2\text{-}2}$ -- second phase, $\gamma_5^{2\text{-}3}$ -- third phase), γ_5^3 -- Late Yanshanian ($\gamma_5^{3\text{-}1}$ -- first phase, $\gamma_5^{3\text{-}2}$ -- second phase)]; γ_6 -- Himalayan granites.

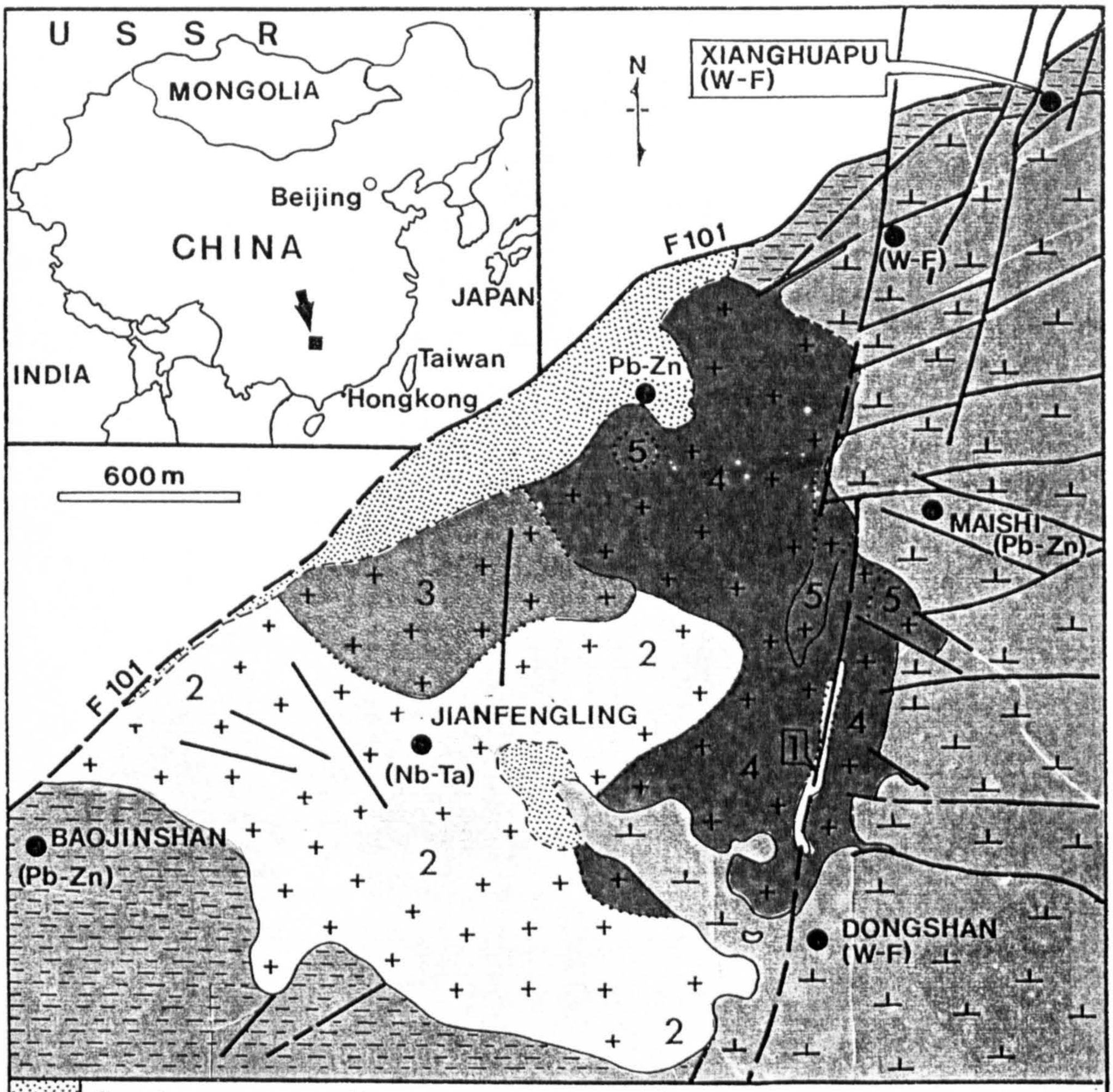

Fig. 3.2 Geological map of the Jianfengling complex, Hunan Province, P.R. China (only major ore deposits are show)

Plate 3.1

Plate 3.1 **Intrusive contacts between granite and country rock and between intrusions of different stages**

a. Marble xenolith within intrusion D, at the 480 pit near the shaft. Bar = 50cm, viewing direction: looking up to the roof.

b. Metamorphosed country rock (centre) penetrates into the granite (intrusion D) at the Wukuangling Hill (sampling location 142). Viewing direction: toward ESE.

c. Intrusive contact between country rock (left) and intrusion E (right) at the 480 pit near the shaft. Hammer length = 50cm, viewing direction: toward SSE.

d. Intrusive contact between intrusion D (bottom left) and metamorphosed country rock (top right). Viewing direction: toward SE.

e. Intrusive contact between intrusions B and C, shown by pegmatitic veins derived from the pegmatitic zone of intrusion C penetrating into intrusion B, near the top of the Jianfengling Mountain (sampling location 118). Viewing direction: toward SSW.

f. Intrusive contact between intrusions D and E, shown by feldspar crystals arranged perpendicular to the contact surface on the younger side (intrusion E, right). Photo taken in the 480 pit about 400m from the main entrance. Viewing direction: toward WNW.

g. Irregular shaped pegmatitic pod oriented along the intrusive contact of intrusions D (top) and E (bottom). Photo taken in the 480 pit near the shaft. Viewing direction: toward NNW.

h. Intrusive contact between intrusions D (top) and E (bottom) at the same location as g. The difference in grain size of the two intrusions is clearly evident. The pegmatitic pod (top left) comprises mainly quartz, feldspar, Li-mica and a few topaz crystals. Viewing direction: toward NNW.

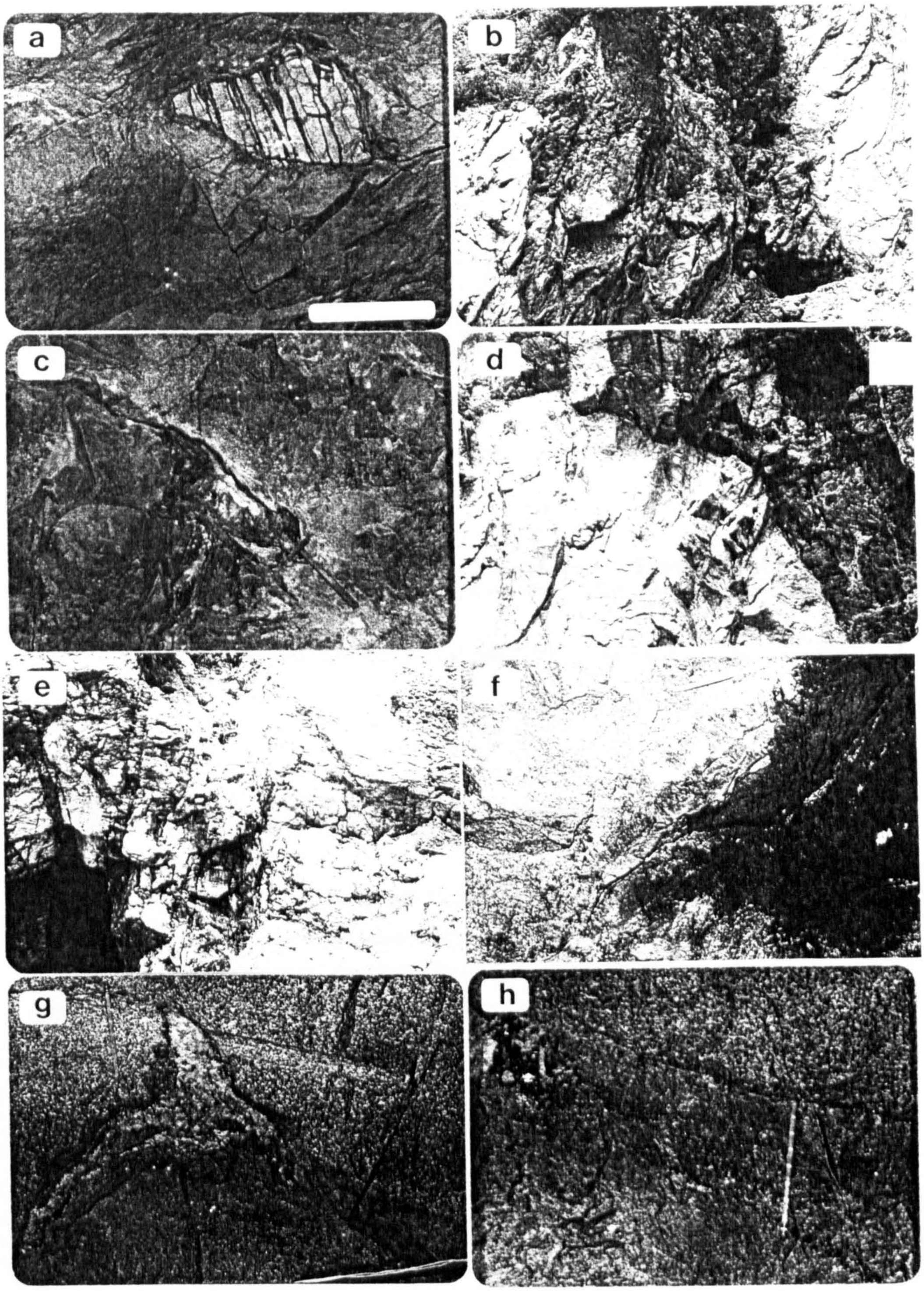
a
b
c
d
e
f
g
h

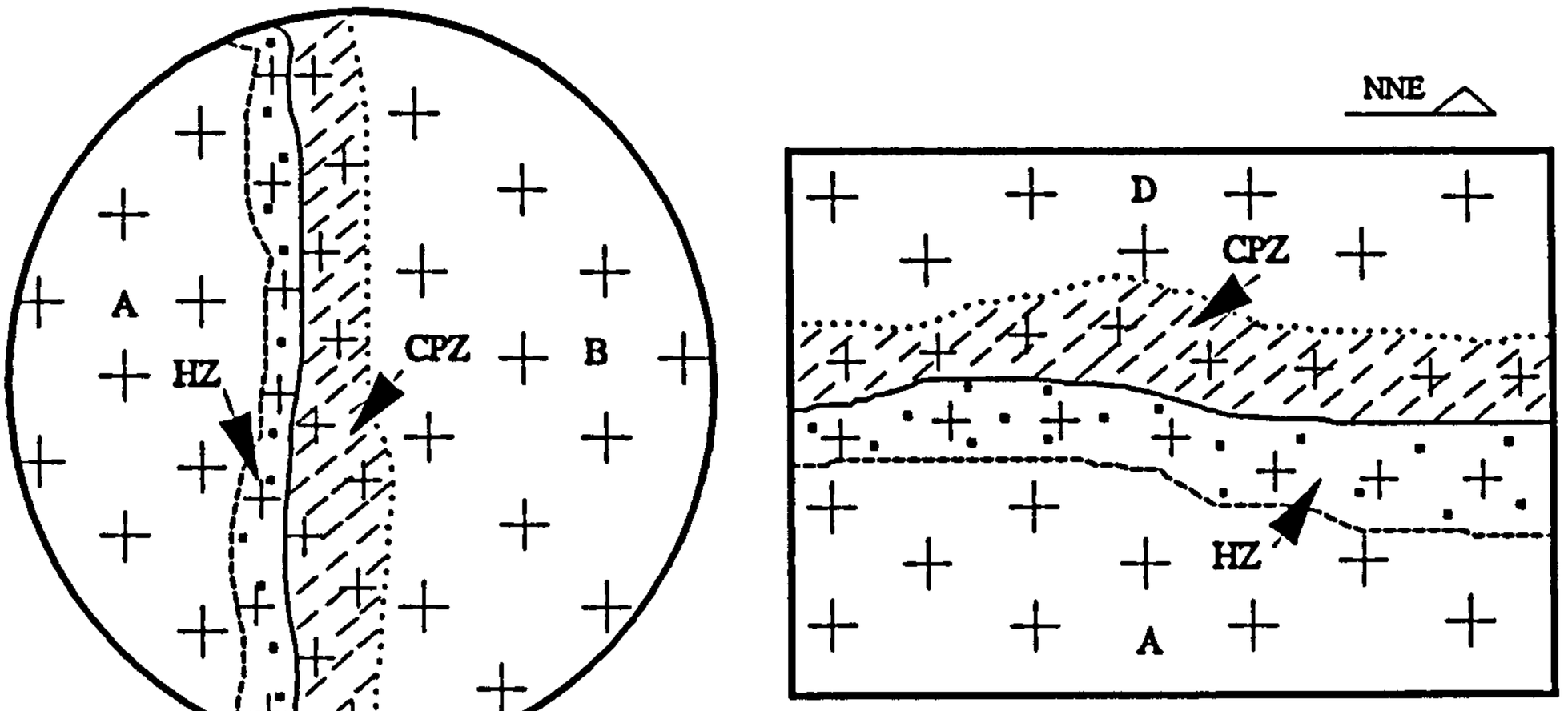

Fig.3.3 Sketches showing the intrusive contacts of intrusions A & B and intrusions A & D (a -- intrusive contact of A and B, drill core; b -- intrusive contact of A and D, vertical view, sampling location No. 124).

A=intrusion A, B=intrusion B, CPZ=chilling and/or pegmatitic zone(s), D=intrusion D, HZ=heated zone

3.2.2 Intrusions B & C: medium-grained zinnwaldite albite granite

Petrographically, these two intrusions are too similar to each other to be distinguished in the field, but they have been recognised as separate intrusions by the presence of an intrusive contact between them. The contact is best seen near the top of the Jianfengling mountain (sampling location No.118, see Appendix I). A pegmatitic zone, consisting of quartz, albite and zinnwaldite, occurs at the periphery of intrusion C, and the quartz veins derived from the pegmatitic zone have penetrated into intrusion B (Plate 3.1e). Intrusion B represents the largest component of the Jianfengling stock and forms the highest mountain peak in this area, whereas intrusion C is much smaller and forms a SW-NE-trending ridge northeast of intrusion B (see Appendix I). Typified by the presence of zinnwaldite and high contents of albite, both intrusions B and C share a similar appearance in the field and contain approximately 15-35 vol.% quartz, 20-45 vol.% albite, 15-30 vol.% alkali-feldspar, 5-15 vol.% zinnwaldite and sericite, and a small amount of zircon, monazite, fluorite, topaz, microlite, niobite, tantalite, galena and sphalerite.

The top of intrusion B has been strongly greisenised and Nb-Ta mineralisation has been found in the greisen (No. 228 Geol. Team, 1974). The greisen, consisting of quartz, Li-mica, topaz and ore minerals, and greisenised granite have a thickness of 30-200m and grade downwards into normal albite-granite. Tungsten, tin, and sometimes lead, zinc and beryllium mineralisation (which might be related to intrusion C) have been found along fractures (NW-trending faults), which are hosted by intrusions B and C and some of these cut the boundary of the two intrusions (see Appendix I).

3.2.3 Intrusion D: medium-grained biotite granite

This grey biotite granite has a crescent-shaped outcrop (Fig. 3.2 and Appendix I) and occurs in the eastern and northeastern parts of the composite Jianfengling stock and is a significant component of the stock. Due to the occurrence of the fluorite-scheelite mineralisation associated with this granite, the investigation of this intrusion has been identified as an important part of this study.

Several distinct zones are recognised in this intrusion and these are best seen at the top of Wukuongling Hill. An upper quartz shell passes into interlayered pegmatite and fine-grained granite, through greisen and greisenised granite, and eventually into the top of the inner (lower) granite (Fig. 3.4). The 5m-thick quartz shell comprises 99% quartz and a small amount of Li-mica. The regular growth zones indicate that the quartz shell actually comprises huge hexagonal quartz crystals (up to 300 cm in dimension, Plate 3.2i, j).

The underlying interlayered zone consists of several horizontal pegmatite layers and fine-grained granite layers and has a total thickness of 0.4-2m. The pegmatitic layers comprise Li-rich mica, quartz, topaz and feldspar and have a comb-structure which is defined by the parallel arrangement of Li-mica, quartz, topaz and feldspar crystals perpendicular to the two walls and by the occurrence of massive quartz and Li-mica occupying the central spaces between the two outer zones (Plate 3.2g, h). The greisen contains quartz, Li-mica and topaz.

These distinct zones differ slightly from place to place. At sample location No.144, a 10-20m-thick pegmatite shell covering the hill top has been found. It consists of quartz, Li-mica and a large quantity of topaz crystals. Some of the quartz shows clear growth zones (Plate 3.2i,j). The mica flakes can be as large as 10cm x 10cm. The topaz crystals form radial aggregates in the quartz and are generally vertical in aspect (Plate 3.2f). They occasionally reach a maximum length of about 90cm (Plate 3.2d).

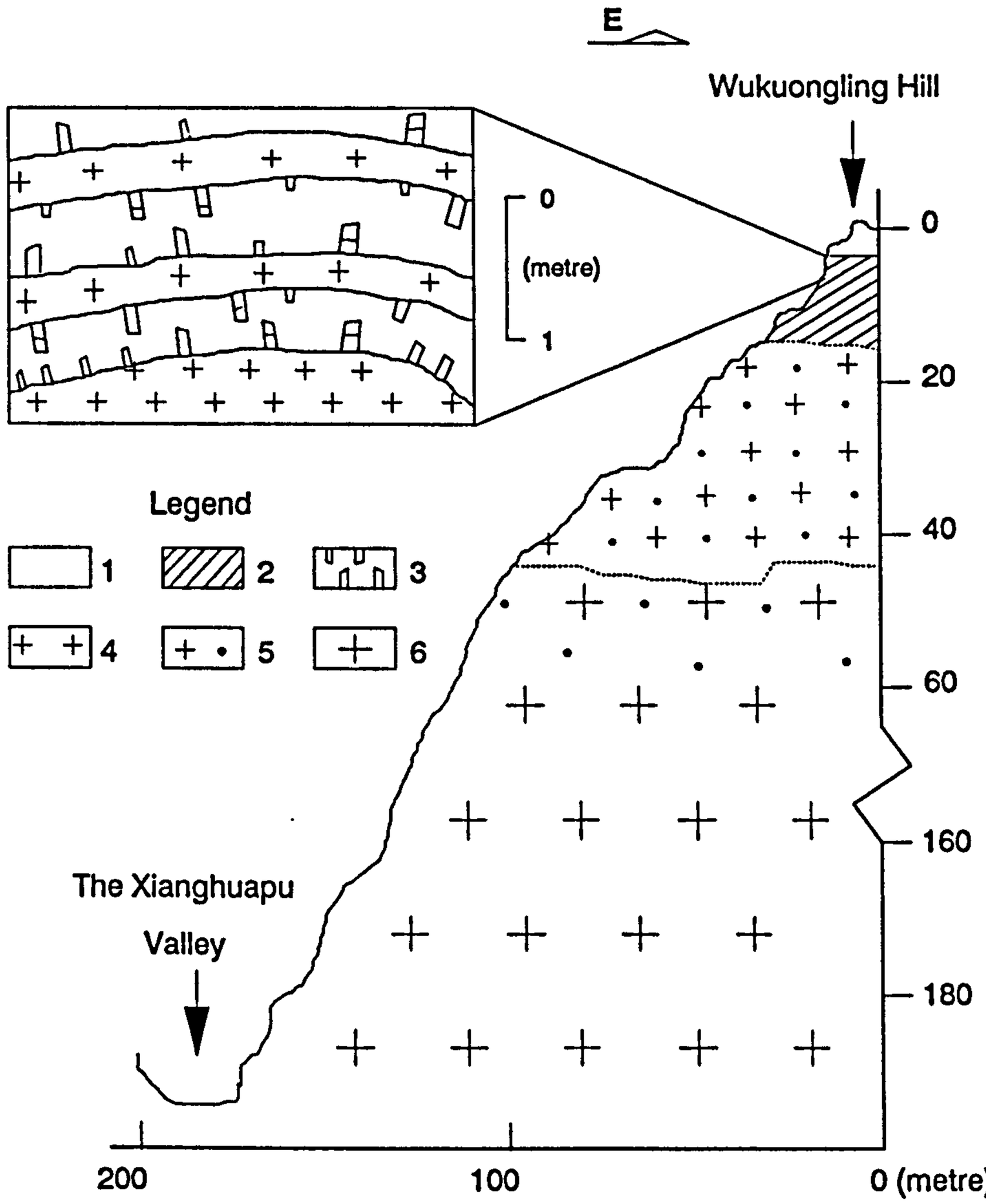

Fig. 3.4 Schematic cross section of Intrusion D at Wukuongling Hill

1 - Quartz shell; 2 - Pegmatite and fine-grained granite interlayers;
3 - Pegmatite; 4 - fine-grained granite; 5 - Greisen and greisenized granite;
6 - Normal granite

Some irregular pegmatitic pods have also been noted in the roof zone of intrusion D. They comprise quartz, albite and mica and have distinct boundaries with the host rocks (Plate 3.2a).

The main biotite granite contains 10-35 vol.% quartz, 15-35 vol.% K-feldspar, 10-40 vol.% albite and 4-5 vol.% minor minerals, namely biotite, sericite, topaz, fluorite, zircon and monazite.

Many fluorite-scheelite orebodies have been found and mined along the intrusion-country rock contact zone (Dongshan deposit) and in the country rocks adjacent to this intrusion (Xianghuapu deposit).

3.2.4 Intrusion E: medium- to fine-grained biotite granite

Most of this intrusion is concealed and is best observed underground in the northeast part of the area. Two small outcrops, extending over areas of approximately 750m x 120m and 220m x 300m respectively, are present adjacent to the hidden intrusion. They are mainly hosted by intrusion D and have only limited contact with the sedimentary country rocks (Appendix I).

A quartz shell, a pegmatitic zone, and a greisen sheet are evident in the top of the intrusion, features similar to those seen in intrusion D.

The quartz shell, consists of pure quartz, is 7m thick (Plate 3.2k) and is superimposed on the greisen. It extends laterally over 10-20m. The 2-3m-thick pegmatitic zone comprises coarse-grained quartz, mica, topaz, radial aggregates of acicular tremolite, galena, sphalerite, cassiterite and wolframite. Two types of greisen have been recognised. One contains equal quantities of Li-mica and quartz and covers the intrusion with a thickness varying from several metres to more than 50m. The grain-size is variable, especially in the eastern outcrop where Pb, Zn, Sn and W mineralization are frequently found within the greisen. The second occurs locally and consists mainly of Li-mica and small amounts of quartz, topaz and fluorite. The greisen sheet grades downwards into greisenised granite and into the normal granite in which abundant small pegmatitic pods are distributed throughout the roof zone. These lentoid pegmatitic pods are arranged vertically and are usually 20 to 50cm wide and 80-130cm long. They contain quartz, feldspars, mica and sometimes topaz, galena and sphalerite (Plate 3.2l,m,n). They are best observed in the quarry near the quartz shell (sampling locations no.101 & 120). One of the best exposed pegmatitic pods is described below.

The pegmatite pod hosted in the top of the granite is 50cm x 130cm in size and contains quartz, albite, K-feldspar (microperthite), biotite, galena and sphalerite (Plate 3.2l,m,n). Lateral zonation, parallel to the short axis of the elliptical pod, has been clearly identified. Outside the pod boundary, there is a 2-3cm-wide zone of fine-grained granite which passes gradually into the normal granite. A strong hydrothermal alteration is evident in this granite, most of the feldspars (Ab + Or) have been replaced by sericite and shows a skeletal texture. Inside the pod, a 10-15cm-wide feldspar (Ab + Or) zone occurs around the boundary and gradually changes into the core of quartz and a few feldspar crystals. Sulphide minerals, consisting of galena and sphalerite, are concentrated in the top of the pod.

Mineralogically, there is no difference between granites of intrusion D and intrusion E, but the distinct intrusive contacts clearly divide them into two separate intrusions. These contacts are best seen underground and occur as two types. One is shown by a 10-30cm-wide pegmatite zone on the younger side and a contact metamorphic zone on the older side (Plate 3.1f); the other is revealed by the occurrence of pegmatitic pods on the younger side (Plate 3.1g & h). These irregularly shaped pods are generally irregular in shape and oriented along the contact surfaces.

The granite of this intrusion contains 15-30 vol.% quartz, 20-35 vol.% alkali-feldspar, 15-40 vol.% albite and 5-10 vol.% minor minerals comprising biotite, sericite, fluorite, topaz, zircon and monazite, all exhibiting a medium grained equigranular texture. The main Pb-Zn mineralisation is spatially associated with this intrusion.

The characteristics of the five intrusions are summarized in Table 3.1. In brief, the five intrusions constituting the Jianfengling granite stock fall into two petrographic groups. One consists of intrusions B and C (Group I); the other comprises intrusions A, D and E (Group II). The granites of group I are characterised by the presence of zinnwaldite and a high content of albite, whereas the granites of group II are defined by the presence of biotite and by their high content of K-feldspar (microperthite). Although the granites in each group share many similarities, they can still be separated on the basis of their intrusive contacts and can also be distinguished by their different hydrothermal mineral associations.

Table 3.1 Characteristics of different intrusive phases of the Jianfengling granite complex

Intrusions	A	B	C	D	E
Name	Biotite-K-feldspar-granite	Zinnwaldite-albite-granite	Zinnwaldite-albite-granite	Biotite-granite	Biotite-granite
Colour	Pink-grey	White-grey	White-grey	Grey	Grey
Characteristics of roof zone	-	Strongly greisenised	Strongly greisenised	Tpz-Qz shell, Tpz-Qz-mica peg., Qz-Ab-peg. pods	Qz shell, Sulph.-Tpz-Qz-Ab peg. pods
Texture	Medium-coarse, inequigranular	Medium, inequigranular	Medium-fine, Inequigranular	Medium, granular	Medium, granular
Main minerals	Qz, K-flsp, Ab, Bi	Qz, Ab, K-flsp, Zinn	Qz, Ab, K-flsp, Zinn	Qz, K-flsp, Ab, Bi	Qz, K-flsp, Ab, Bi
Accessories	Monz, Tpz, Zicn, Fl	Fl, Tpz, Monz, Mit	Fl, Tpz, Monz, Mit	Monz, Tpz, Zicn, Fl	Monz, Tpz, Zicn, Fl
Mineralisation	-	Nb-Ta	Sn (Pb, Zn, W, Be)	W-F (Sn, Pb, Zn)	Pb-Zn (Sn As)

Ab = albite, Bi = biotite, Fl = fluorite, K-flsp = K-feldspar, Mit = microlite, Monz = monazite, Peg = pegmatite, Qz = quartz, Sulph = sulphides, Tpz = topaz, Zicn = zircon, Zinn = zinnwaldite

Plate 3.2

Plate 3.2 **Photographs showing the roof zone characteristics of the Jianfengling granites**

a. Pegmatitic pod within intrusion D (near sampling location 105). The pod consists mainly of quartz and feldspars.

b. Pegmatitic pod within intrusion D (sampling location 139). The pod consists of quartz, feldspars, Li-mica and topaz (centre of the pod, enclosed by Li-mica).

c. Irregular shaped pegmatitic pod at the contact of intrusions D and E. Photo taken in the 480 pit near the shaft.

d. Topaz crystals (up to 50cm in length) within pegmatite consisting of quartz, Li-mica and topaz on top of intrusion D. Sampling location 144.

e. Quartz-Li-mica-pegmatite vein intruded in fine-grained marginal phase of intrusion D. Sampling location 107.

f. Radial topaz aggregates in pegmatite on top of intrusion D at sampling location 144.

g. Interlayers of pegmatite and fine grained-granite (intrusion D). Photo taken at the Wukuangling Hill (sampling location 105).

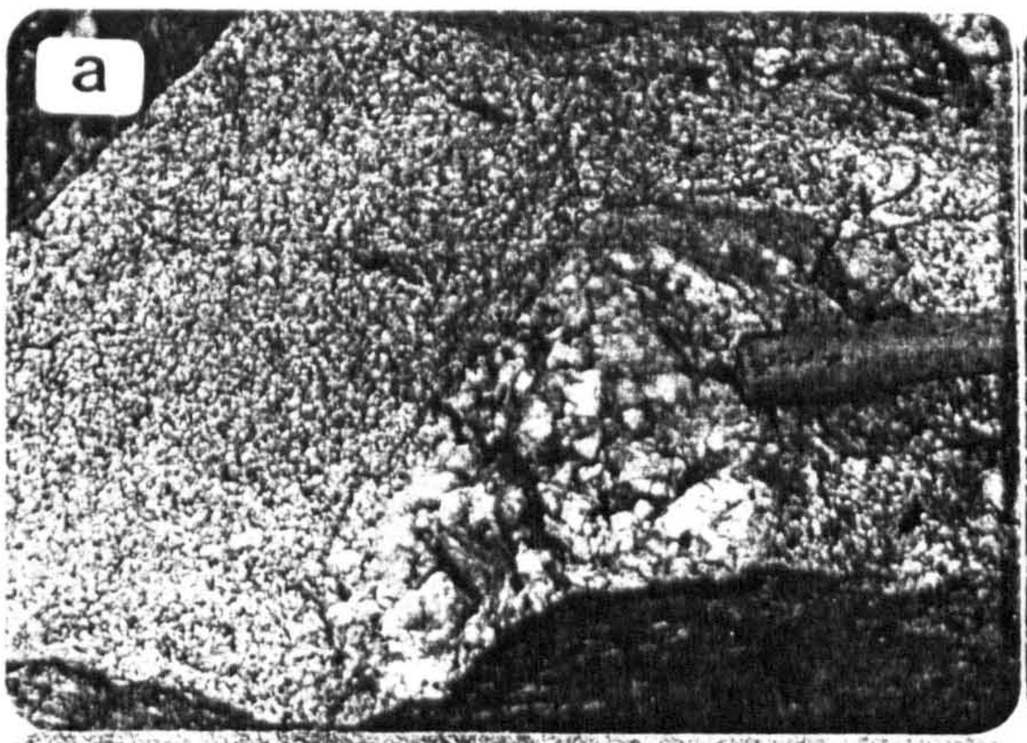
a

b

c

d

e

f

g

h

Plate 3.2 (continued)

Plate 3.2 **Photographs showing the roof zone characteristics of the Jianfengling granites (continued)**

i, j. Hexagonal quartz crystals (up to 2m in dimension) on top of the pegmatite zones of intrusion D. Photo taken at the Wukuangling Hill (sampling location 105).

k. Quartz shell (up to 7m thick) on top of intrusion E (sampling location 120).

l, m. Sulphide-containing pegmatitic pods within intrusion E (see text for detailed description). Photo taken at sampling location 101.

n. Topaz (centre) and sulphides (galena and sphalerite) within the pegmatitic pod of intrusion E (sampling location 101).

o. Li-mica-quartz pegmatitic pod within intrusion E (in the 480 pit near the shaft). Li-mica distributes along the margin of the pod.

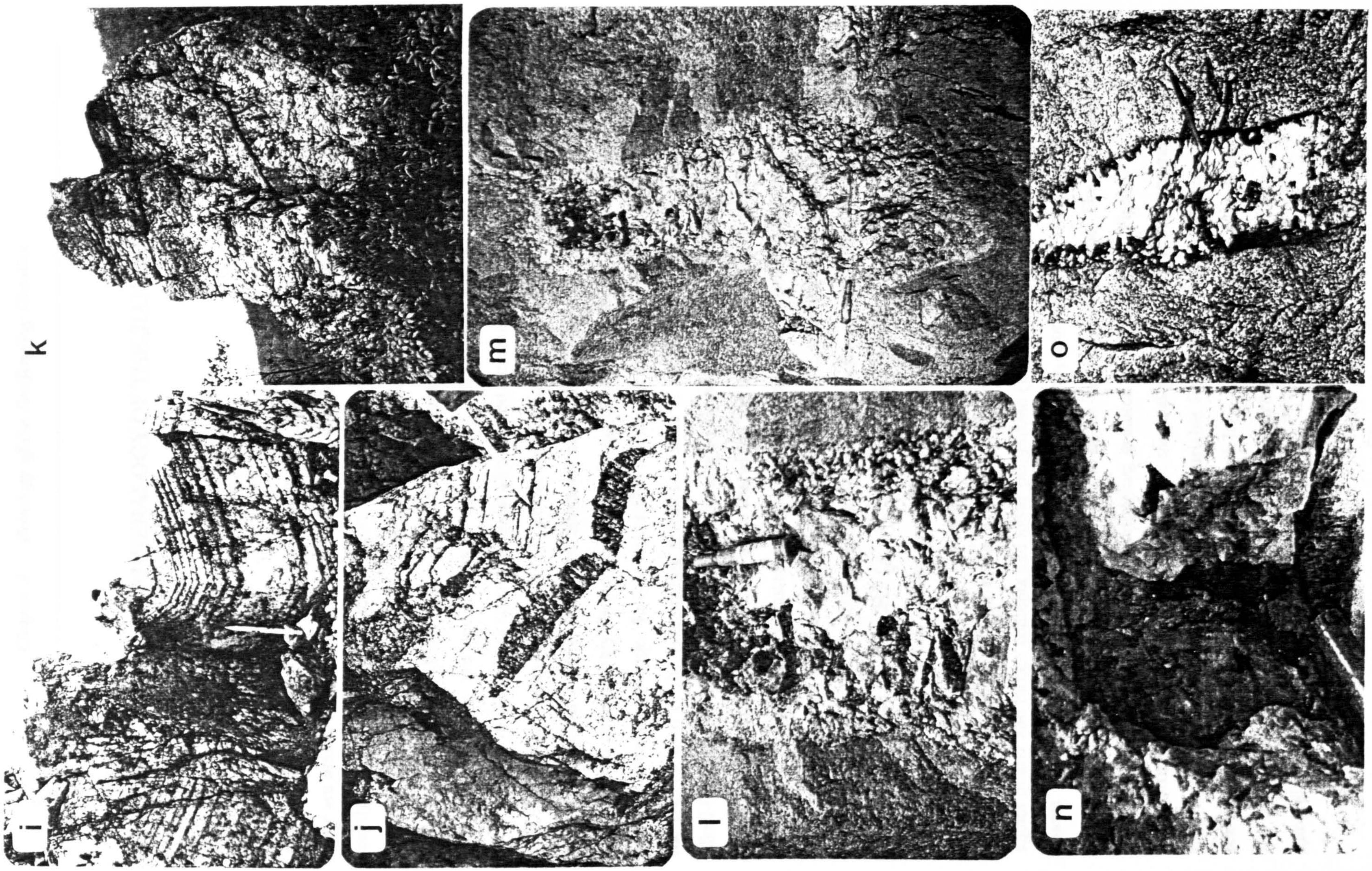
k
m
o
i
j
l
n

3.3 PETROGRAPHY AND MINERALOGY OF THE JIANFENGLING GRANITES

3.3.1 Introduction

As stated earlier, the granites of the Jianfengling stock are generally similar in texture and grain size. They are mainly medium-grained and equigranular with local porphyritic phases. These granites are mainly monzogranite with a small number plotting just within the syenogranite field on the basis of modal analyses (Table 3.2; Fig.3.5). It should be noted, however, that most of the plagioclase present in these rocks is pure albite. The largest extinction-angle measurements of the albite of these rocks indicate that they are mostly An_{0-5}, occasionally An_{5-10}, and rarely An_{10-15}. Non-standard semiquantitative SEM (back scatter) analysis also showed extremely low contents of calcium (less than 1 wt.%) in these albites (Section 3.3.3). In the classification system of Streckeisen (1976), plagioclase with An less than 5 wt.% should be allocated as alkali-feldspar (A). In practice, however, it is impossible to quantitatively distinguish albites of An_{0-5} from those having An greater than 5 wt.% using a conventional microscope. In this case, CIPW normative minerals (Cox *et al.* 1979) can be used for the classification of the Jianfengling granites. Albite is proportionally divided and distributed into alkali-feldspar (A) and plagioclase (P) according to Le Maitre (1976). Most of the samples plotted in the field of alkali-feldspar granite and a few within the left edge of the syenogranite field (Fig. 3.6). Therefore, the Jianfengling granites would be more correctly described as alkali-feldspar granites. The essential constituents with their average modal percentages (± standard deviation (1σ)), as determined from approximately 101,000 point-counts of 42 thin sections from the five intrusions, are quartz - 33.2 (± 6.7), plagioclase (albite) - 28.9 (± 4.7), K-feldspar (microperthite) - 28.9 (± 2.2), zinnwaldite - 4.3 (± 1.1), biotite - 1.4 (± 0.8) and topaz - 1.4 (± 1.2) for rocks of Group 1, and quartz - 36.7 (± 5.8), plagioclase (albite) - 26.2 (± 5.1), K-feldspar - 29.3 (± 5.9), biotite - 3.5 (± 1.7), zinnwaldite - 1.7 (± 1.2), and topaz - 1.0 (± 0.8) for rocks of Group 2. Compared with Group 1, rocks of Group 2 have higher quartz and biotite contents and lower plagioclase (albite) and zinnwaldite contents. Accessory phases , which include sericite, fluorite, andalusite, zircon, monazite and ore minerals (cassiterite, sulphides, oxides), account for less than 2 vol.% of the mineral constituents. The proportions of the major mineral constituents in the Jianfengling granites are illustrated in Figures 3.5 and 3.7 and demonstrate that, except for a few samples, the mineral proportions are fairly constant. Minerals of the Jianfengling granites are generally quite variable from idiomorphic to xenomorphic, the latter texture possibly resulting from the effects of both late- and post-magmatic alterations, especially for the rocks of Group 1, in which alteration is always stronger than in those of Group 2. The various mineral phases are considered below.

Table 3.2 Modal mineralogy of the Jianfengling granite stock

Sample	Points	Qz	Plag	K-flsp	Bi(zinnw)	Serit	Topaz	Others
CK3-1	2104	27.4	33.3	33.1	4.6	1.3	0.2	0.1
CK3-2	2243	29.1	21.4	38.3	6.9	4.0	0.3	
CK3-5	2357	30.0	32.3	34.1	1.3	2.1	0.2	
CK3-15	1869	47.0	29.8	18.7	2.9	1.6		
CK3-23	2500	31.4	38.2	26.1	2.6	0.7	0.8	0.2
CK3-24	2500	43.6	23.6	26.7	5.5	0.4	0.2	
CK3-25	2500	36.8	24.4	32.2	6.8	0.4	0.4	
CK3-27	2500	40.8	22.5	29.2	6.0	1.2	0.3	
CK3-28	2500	29.7	31.4	32.5	5.0	1.2	0.2	
CK3-31	2500	48.2	29.9	15.5	4.6	1.3	0.5	
CK3-32	2500	47.1	19.9	27.7	3.9	1.2	0.2	
CK6-1	1934	28.3	36.1	21.4	3.5	8.4	2.3	
CK6-2	2403	42.9	28.6	22.6	2.1	2.6	1.2	
125-3	2395	41.5	17.1	30.0	6.1	4.4	0.9	
125-5	2500	32.2	18.2	35.8	4.0	9.8		
131-1	2148	41.6	26.3	28.9	0.5	2.7		
131-2	2306	43.4	21.5	21.0	6.9	7.2		
AVG1		37.7	26.7	27.9	4.8	3.0	0.6	0.2
115-1	1943	27.9	31.4	31.7	6.5	1.9	0.3	0.3
127-2	2286	40.2	24.3	27.3	7.1	0.9	0.2	0.1
CK2-20	2500	28.7	35.4	25.3	4.8	1.4	3.7	0.7
AVG2		32.3	30.4	28.1	6.1	1.4	1.4	0.4
CK4-1	2306	40.5	24.1	29.5	3.8	1.1	0.1	0.9
CK4-3	2017	21.4	35.5	32.2	7.0	1.5	2.3	0.1
CK4-4	2500	37.0	25.2	28.1	6.2	1.4	1.5	0.6
CK4-5	2438	36.6	26.7	28.5	4.7	0.9	1.7	0.9
AVG3		33.9	27.9	29.6	5.4	1.2	1.4	0.6
95	2500	37.1	20.7	33.5	6.2	0.5	1.4	0.6
107-1	2500	38.3	27.2	17.0	10.4	2.0	2.5	2.6
107-7	2500	38.6	24.8	25.8	5.1	1.4	0.8	3.5
119-1	1593	33.2	30.7	32.8	3.0	0.3		
138-2	1814	32.9	18.6	39.2	7.1	2.1		0.1
138-8	2500	38.7	24.8	29.1	6.5	0.7		0.2
138-15	2500	37.8	25.6	31.9	4.0	0.1	0.6	
430-3	2500	35.4	24.9	34.7	4.3	0.2	0.4	0.1
430-5	2500	36.3	29.8	30.8	3.0			0.1
430-6	2500	39.7	20.3	32.6	5.5	0.4	1.4	0.1
86020	2500	31.3	34.6	26.6	5.5	1.2	0.7	0.1
86025	2415	35.4	27.8	28.9	3.1	1.4	3.1	0.3
AVG4		36.2	25.8	30.2	5.3	0.9	1.4	0.8
101-2	2500	26.2	24.2	41.1	7.3	1.4		
101-8	2500	43.7	48.3	1.4	6.6	0.1		
101-10	2500	35.6	28.5	31.8	3.4	0.7		
101-11	2500	31.8	25.9	34.1	5.3	2.3	0.6	
101-15	2500	39.8	25.7	25.9	6.1	1.6	0.9	
480-1	2500	42.3	21.5	27.0	6.8	0.2	2.2	
480-5	2500	34.3	27.8	28.2	6.9	0.9	1.8	0.1
AVG5		36.2	28.8	27.1	6.0	1.0	1.4	0.1

Qz = quartz, Plag = plagioclase, K-flsp = K-feldspar, Bi = biotite, Zinnw = zinnwaldite, Serit = sericite

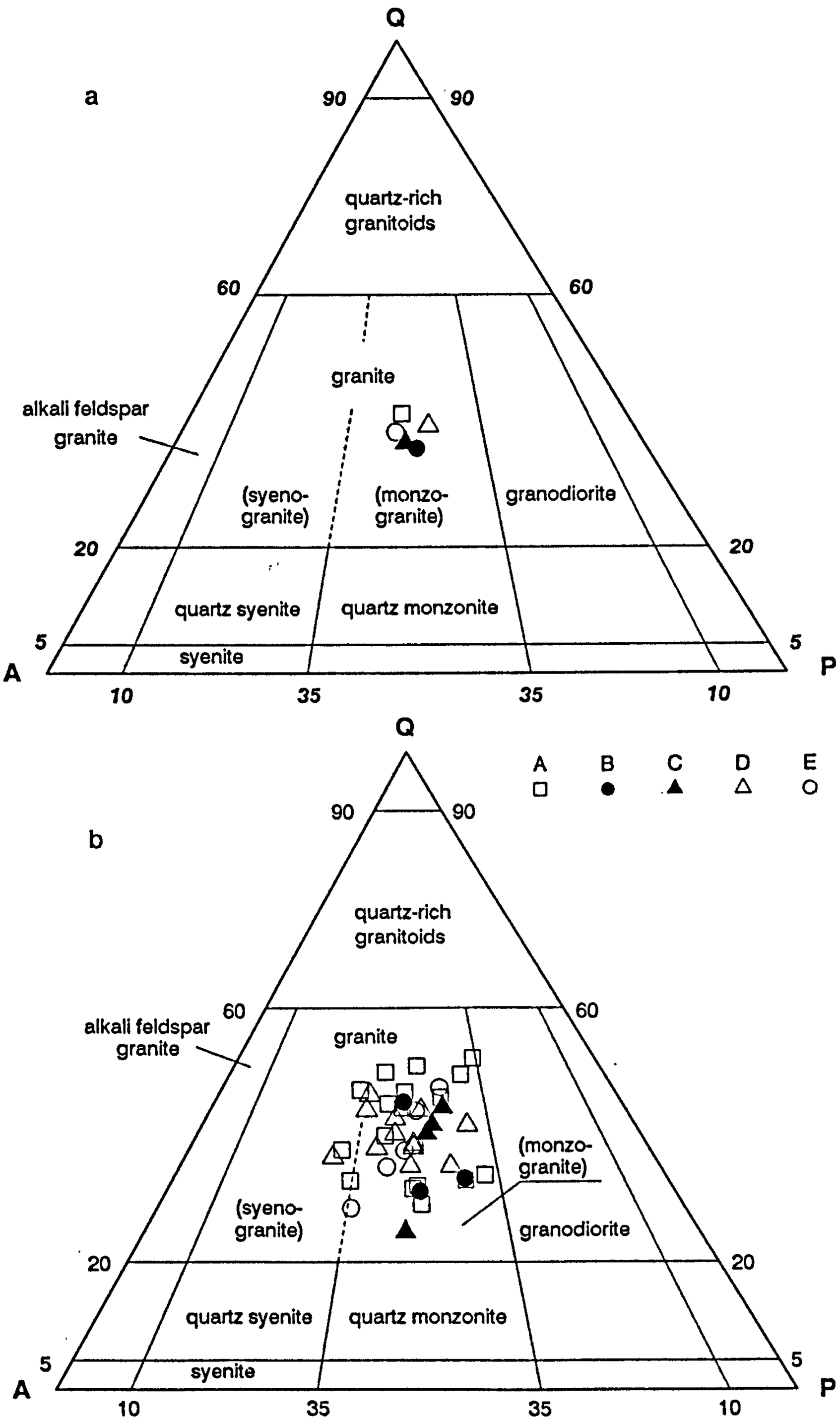

Fig. 3.5 Q (quartz) - A (alkali-feldspar) - P (plagioclase) diagrams for the Jianfengling granites (based on modal mineralogy)

a -- plot of averages of the five intrusive phases

b -- plot of the whole date set

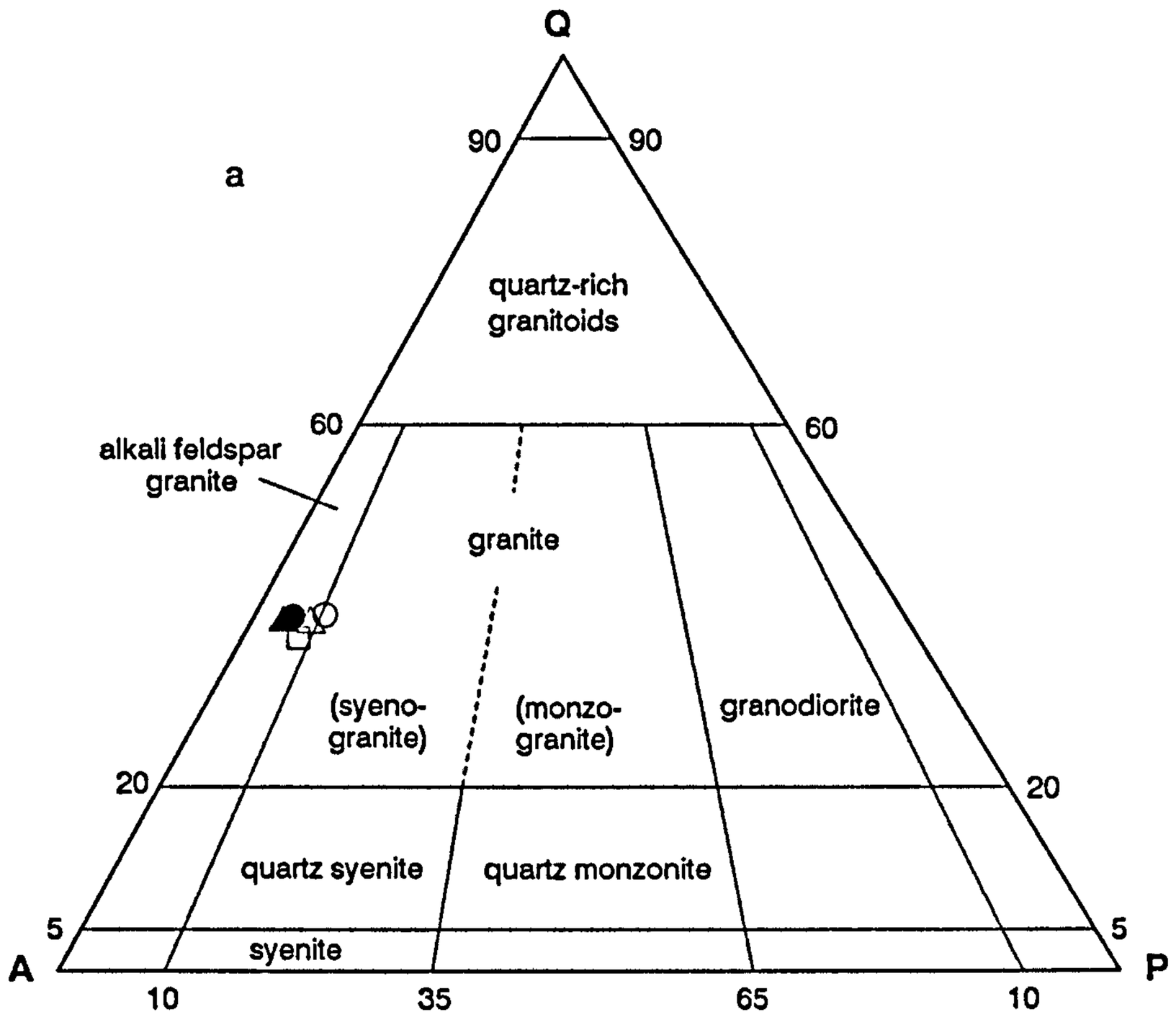

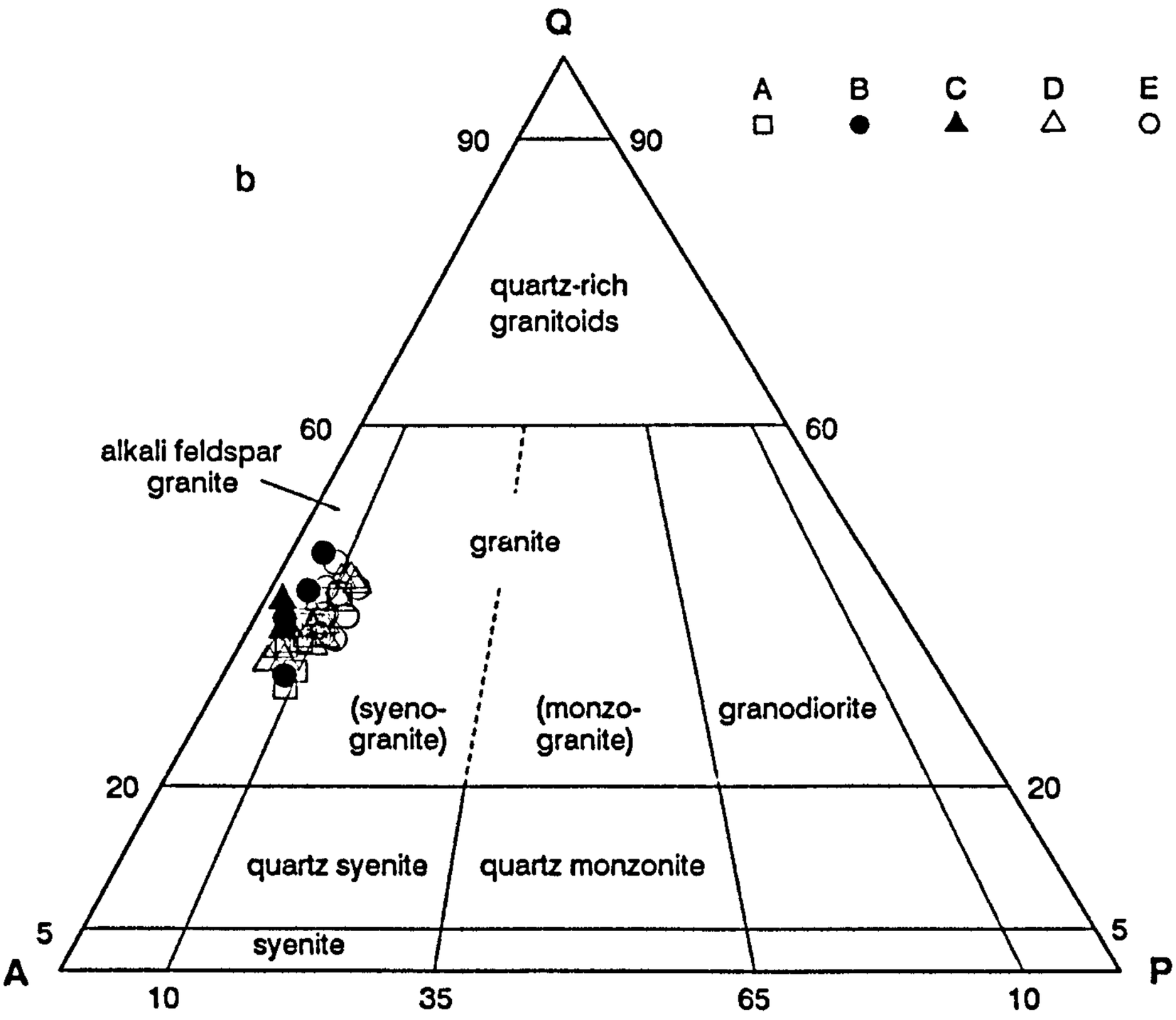

Fig. 3.6 Q (quartz) - A (alkali-feldspar) - P (plagioclase) diagrams for the Jianfengling granites (based on CIPW results, see text for deteiled explanation)

a -- plot of averages of the five intrusive phases

b -- plot of the whole date set

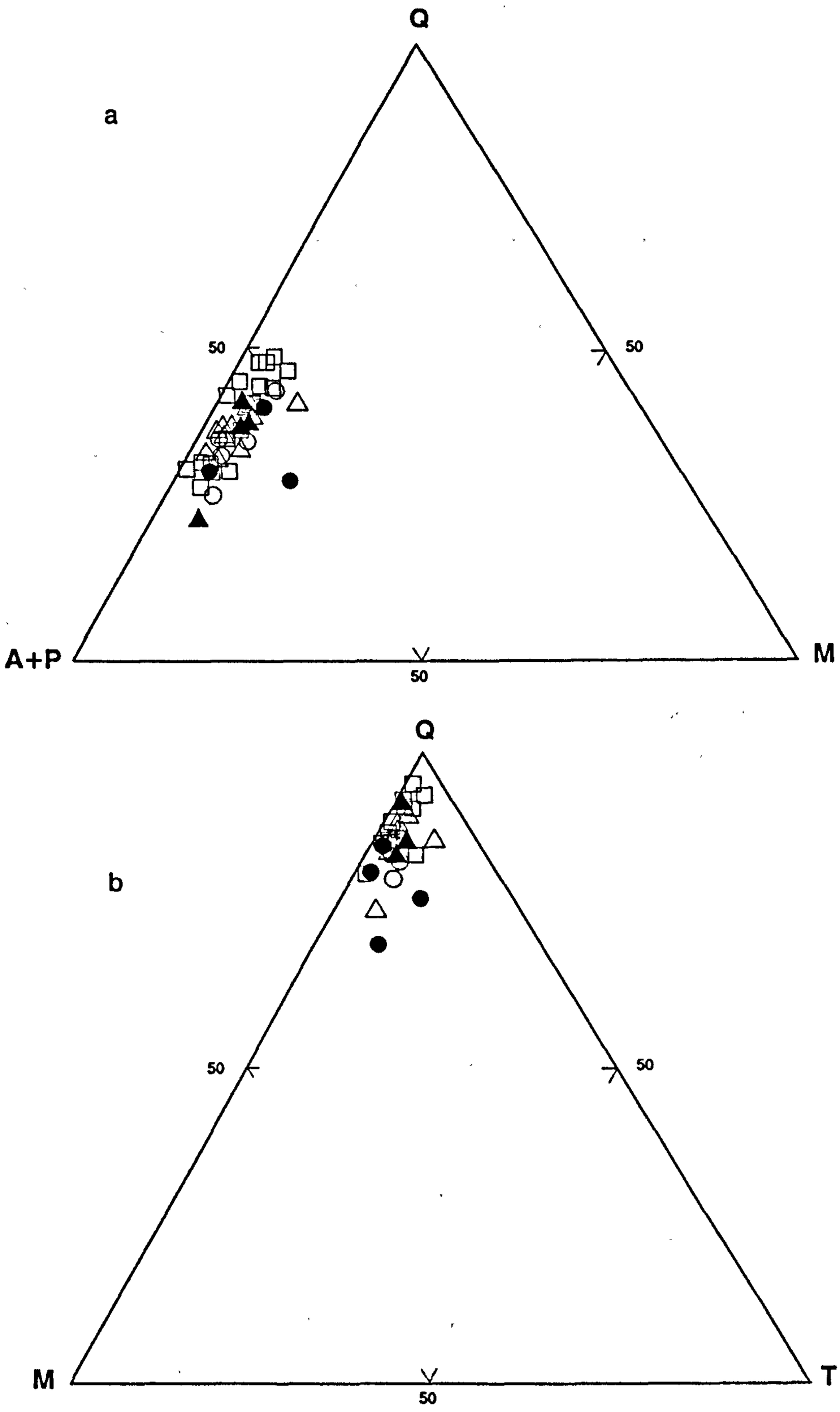

Fig. 3.7 Triangular plots showing results of point counting samples of the Jianfengling granites. Abbreviations: Q=quartz, A=alkali-feldspar, P=plagioclase, M=mica, T=topaz.

3.3.2 Quartz

In all the granites of the Jianfengling stock, granular quartz is present at 25-45 vol.%, reaching 40-60 vol.% in the aplite veins and more than 70 vol.% in the pegmatitic phases. The quartz is generally anhedral, but may also occur as equant grains having the habit of high-temperature quartz (Plate 3.3e). At least two stages of quartz have been identified. The earlier quartz usually occurs as small euhedral to subhedral grains exhibiting eutectic intergrowth with albite and topaz; small grains of albite and biotite have been observed within the quartz grains (Plate 3.3f). The later quartz appears mostly as large anhedral grains and it often contains numerous inclusions of albite, biotite, and topaz) (Plate 3.3g). A distinct texture, "*snowball texture*", produced by many small subhedral albite inclusions arranged concentrically along the growth planes of large quartz grains, has been noted in these granites (Plate 3.3h). This so-called "*snowball quartz*" is a common feature of sodic rare-metal granites. Geoscientists from the former Soviet Union correlate this with a metasomatic process (in Schwartz, 1992), whereas here it is considered to be a magmatic feature in agreement with Xu et al. (1987), Pollard (1988) and Schwartz (1992) and indicate coprecipitation from a magma of quartz + albite + K-feldspar + mica.

3.3.3 Plagioclase (albite)

Prismatic plagioclase laths (Plate 3.3i) are invariably subhedral to euhedral, vary from 0.1 to 0.5mm in width and 2 to 6mm in length and display albite and combined albite-Carlsbad twinning, very occasionally combined albite, Carlsbad and pericline twinning. No zonation has been noted, and sharp contacts with all other minerals have been observed (Plate 3.3j). The plagioclase frequently contains small inclusions of biotite, fluorite and topaz. It may also occur as subhedral laths occluded within K-feldspar and quartz (Plate 3.3k & l). Plagioclase inclusions within K-feldspar are mostly aligned in the same direction as the albite exsolution lamellae. There is no optical difference between the plagioclase of Group 1 and that of Group 2. The largest extinction-angle measurement of the plagioclases was carried out on more than forty samples in thin section revealing that the plagioclases are mostly albites with An commonly 0-6%, with some grains reaching 10-15%. Non-standard semiquantitative SEM (back scatter) analysis was performed on the plagioclases of thirteen samples from the Jianfengling granites; the whole data set is reported in Appendix IV and representative results are presented in Table 3.3 and plotted in Figure 3.8a. Almost all the plagioclases cluster between Ab_{100} and Ab_{95} $Or_{2.5}$ $An_{2.5}$ with those from Group 1 being relatively albitic.

Table 3.3 Representative compositions of plagioclase (albite)

	CK3-20					98-2				CH4-4			CK3-24		CK3-27		125-5		
	1*	2	6	9	11*	1	2	5	6*	1	3*	11	1	3	1	4*	1	3*	4
SiO2	67.90	66.71	67.34	68.73	68.79	68.32	67.38	66.37	67.93	67.83	66.39	67.29	67.28	69.03	67.73	69.17	67.82	66.94	65.72
Al2O3	20.83	19.87	19.92	19.14	19.73	19.65	19.72	19.62	19.83	18.93	20.67	21.05	21.31	20.24	21.17	19.96	20.05	19.87	21.04
FeO																	0.23		
MnO																			
MgO																	0.21		
CaO		0.12			0.12	0.22		0.20		0.15	0.10		0.12	0.25	0.25		0.17		0.31
K2O	0.17	0.23		0.11		0.17	0.41	0.46	0.15	0.34	0.31	0.42	0.23	0.12		0.26	0.28	0.14	
Na2O	11.10	13.07	12.73	12.01	11.36	11.64	12.48	13.35	12.09	12.75	12.52	11.24	11.06	10.36	10.85	10.61	11.24	13.05	12.93
structural formulae based on 8 oxygen atoms																			
Si	3.290	3.256	3.272	3.310	3.312	3.300	3.276	3.247	3.289	3.286	3.249	3.275	3.274	3.320	3.285	3.325	3.286	3.262	3.227
Al	0.595	0.571	0.570	0.543	0.560	0.559	0.565	0.566	0.566	0.540	0.596	0.604	0.611	0.574	0.605	0.565	0.572	0.571	0.609
Fe	0.000	0.000	0.000	0.000	0.000	0.000	0.000	0.000	0.000	0.000	0.000	0.000	0.000	0.000	0.000	0.000	0.009	0.000	0.000
Mn	0.000	0.000	0.000	0.000	0.000	0.000	0.000	0.000	0.000	0.000	0.000	0.000	0.000	0.000	0.000	0.000	0.000	0.000	0.000
Mg	0.000	0.000	0.000	0.000	0.000	0.000	0.000	0.000	0.000	0.000	0.000	0.000	0.000	0.000	0.000	0.000	0.015	0.000	0.000
Ca	0.000	0.006	0.000	0.000	0.006	0.011	0.000	0.010	0.000	0.008	0.005	0.000	0.006	0.013	0.013	0.000	0.009	0.000	0.016
K	0.011	0.014	0.000	0.007	0.000	0.010	0.025	0.029	0.009	0.021	0.019	0.026	0.014	0.007	0.000	0.016	0.017	0.009	0.000
Na	1.043	1.237	1.199	1.122	1.060	1.090	1.176	1.266	1.135	1.198	1.188	1.061	1.044	0.966	1.020	0.989	1.056	1.233	1.231
end-member feldspar, mole%																			
ab	99.0	98.4	100.0	99.4	99.4	98.0	97.9	97.0	99.2	97.7	98.0	97.6	98.1	97.9	98.7	98.4	97.6	99.3	98.7
or	1.0	1.1	0.0	0.6	0.0	0.9	2.1	2.2	0.8	1.7	1.6	2.4	1.3	0.7	0.0	1.6	1.6	0.7	0.0
an	0.0	0.5	0.0	0.0	0.6	1.0	0.0	0.8	0.0	0.6	0.4	0.0	0.6	1.3	1.3	0.0	0.8	0.0	1.3

	430-3			480-6			480-7			138-15				430-4				480-1			101-17	
	1	3	5*	2	3	4	1*	3	6	1	2	4	7	1	5*	8	9	1	4	5*	1	4*
SiO2	65.46	66.46	65.54	65.71	65.87	65.23	66.42	69.15	67.94	67.79	69.23	66.58	66.57	68.15	67.39	67.58	67.49	69.15	67.94	67.79	67.82	66.78
Al2O3	21.27	20.84	20.93	19.83	21.27	20.87	21.39	19.57	20.87	21.25	20.06	21.31	20.57	19.90	20.77	20.73	20.13	19.76	19.38	20.07	20.31	19.74
FeO			0.44			0.23								0.43								
MnO																						
MgO			0.67	0.26		0.43																
CaO	0.57	0.25		0.58	0.25	0.56		0.18	0.27	0.14		0.42	0.12	0.37	0.12	0.30		0.35	0.37		0.37	0.25
K2O	0.25			0.27	0.36		0.17	0.26		0.28	0.15	0.12			0.19	0.23	0.31		0.27		0.27	0.22
Na2O	12.45	12.44	12.42	13.35	12.25	12.68	12.02	10.84	10.92	10.54	10.56	11.57	12.74	11.14	11.53	11.16	12.07	10.74	12.04	12.15	11.23	13.01
structural formulae based on 8 oxygen atoms																						
Si	3.221	3.249	3.217	3.224	3.235	3.209	3.250	3.323	3.290	3.289	3.326	3.253	3.251	3.295	3.276	3.281	3.279	3.321	3.289	3.285	3.287	3.257
Al	0.617	0.600	0.605	0.573	0.615	0.605	0.617	0.554	0.596	0.607	0.568	0.614	0.592	0.567	0.595	0.593	0.576	0.559	0.553	0.573	0.580	0.567
Fe	0.000	0.000	0.018	0.000	0.000	0.009	0.000	0.000	0.000	0.000	0.000	0.000	0.000	0.017	0.000	0.000	0.000	0.000	0.000	0.000	0.000	0.000
Mn	0.000	0.000	0.000	0.000	0.000	0.000	0.000	0.000	0.000	0.000	0.000	0.000	0.000	0.000	0.000	0.000	0.000	0.000	0.000	0.000	0.000	0.000
Mg	0.000	0.000	0.049	0.019	0.000	0.032	0.000	0.000	0.000	0.000	0.000	0.000	0.000	0.000	0.000	0.000	0.000	0.000	0.000	0.000	0.000	0.000
Ca	0.030	0.013	0.000	0.030	0.013	0.030	0.000	0.009	0.014	0.007	0.000	0.022	0.006	0.019	0.006	0.016	0.000	0.018	0.019	0.000	0.019	0.013
K	0.016	0.000	0.000	0.017	0.023	0.000	0.011	0.016	0.000	0.017	0.009	0.007	0.000	0.000	0.012	0.014	0.019	0.000	0.017	0.000	0.017	0.014
Na	1.188	1.179	1.182	1.270	1.166	1.209	1.140	1.010	1.025	0.991	0.984	1.096	1.206	1.044	1.087	1.051	1.137	1.000	1.130	1.141	1.055	1.230
end-member feldspar, mole%																						
ab	96.3	98.9	100.0	96.4	97.0	97.6	99.1	97.6	98.7	97.6	99.1	97.4	99.5	98.2	98.4	97.2	98.3	98.2	96.9	100.0	96.7	97.9
or	1.3	0.0	0.0	1.3	1.9	0.0	0.9	1.5	0.0	1.7	0.9	0.7	0.0	0.0	1.1	1.3	1.7	0.0	1.4	0.0	1.5	1.1
an	2.4	1.1	0.0	2.3	1.1	2.4	0.0	0.9	1.3	0.7	0.0	2.0	0.5	1.8	0.6	1.4	0.0	1.8	1.6	0.0	1.8	1.0

* albite exsolution within K-keldspar

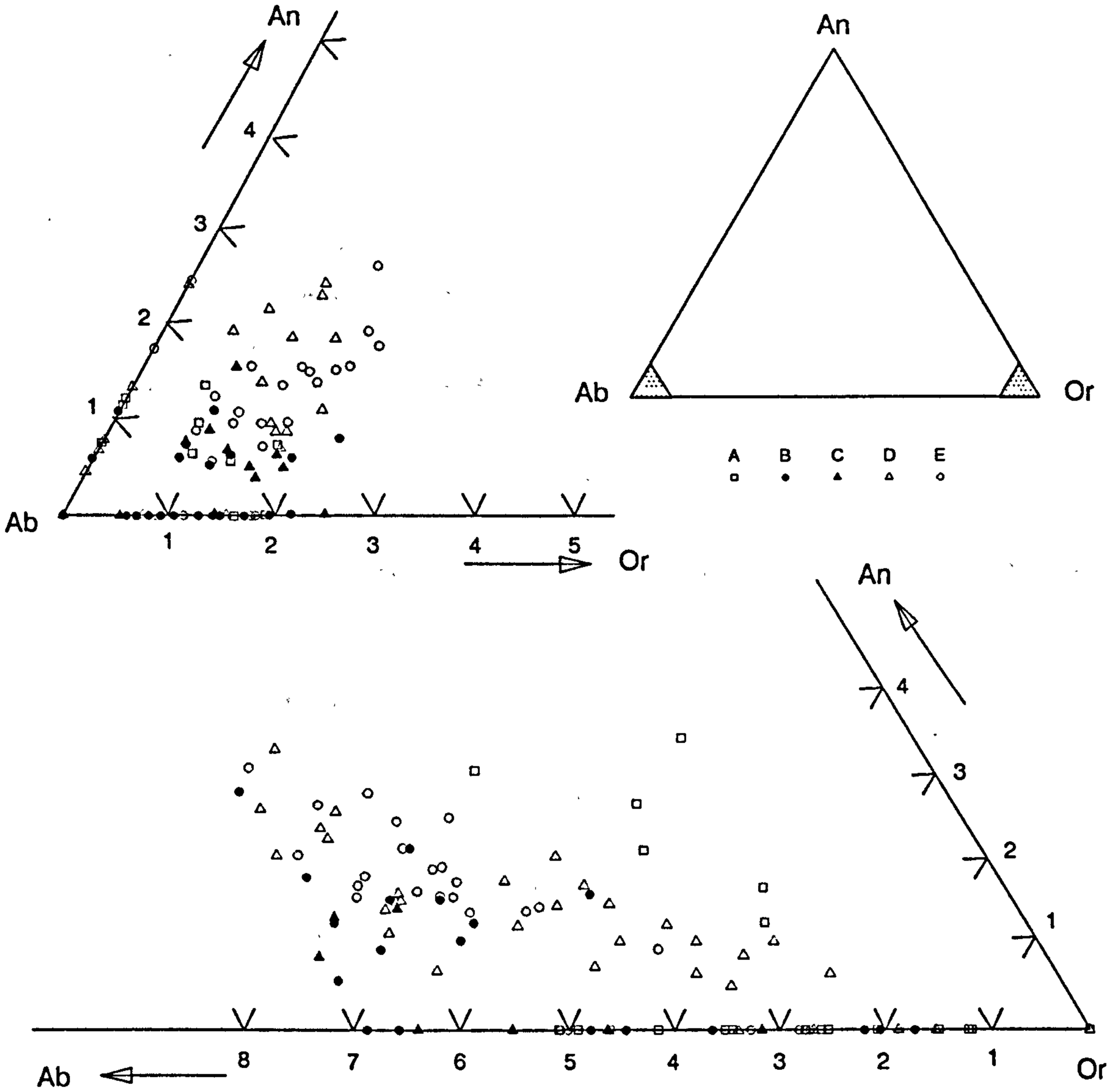

Fig. 3.8 Compositions of feldspars in the Jianfengling granites (based on semi-quantitative SEM analyses).

a -- plagioclase (albite). All analyses plot in the Ab corner. It is evidentthat plagioclases from Group 1 (B and C, filled circles and triangles) are relatively more albitic than those of Group 2 (A, D and E).

b -- K-feldspar. All analyses plot in the Or corner. No clear distinguishion exits between K-feldspars of Group 1 and those of Group 2.

3.3.4 K-feldspar

K-feldspar always forms the coarsest mineral phase in all these granite rocks, is generally subhedral to anhedral, and overgrows other minerals (Plate 3.3m), notably plagioclase, quartz, biotite and topaz. This K-feldspar appears late in the crystallisation sequence filling interstices or forming anhedral to poikilitic grains and possesses a microperthitic texture. Small, euhedral to subhedral grains of optically homogenous K-feldspar are also noted in some of the samples and they show sharp contacts with other minerals, such as biotite, plagioclase and quartz (Plate 3.3n, o & p), thus indicating a early crystallisation history. No twinning has been observed in the K-feldspar and so it is likely to have a monoclinic symmetry; consequently it is believed to be orthoclase-microperthite.

The orthoclase-microperthite from the Jianfengling granitic stock has been texturally classified according to the scheme proposed by Smith (1974). String-, film-, vein-, patch-, and plate-microperthites are present in these granites, among which the film-, vein-, and patch-microperthites are the most abundant. These different morphologies are discussed below.

String microperthite has been noted in only a few samples out of more than two hundred thin sections. *String albite* occurs as bodies of several hundred microns in length with rounded, elliptic or lenticular cross-section 10 to 5μm or less in diameter (Plate 3.3q). The string albite is regularly distributed in the orthoclase which shows no twinning.

Film albite is a very common feature of the granites, occurring in nearly all microperthites of every specimen examined. The films rarely exceed 10μm in thickness with variable length (Plate 3.3r). The density of the films varies from several strips to more than one hundred lines in 1mm across.

Vein albite presents in most of the microperthites from the Jianfengling granites. The veins are usually about 0.1mm across, but may reach several millimetres. Sometimes they form fairly continuous sheets cutting the orthoclase, but more usually they occur as irregular ribbons or bands. Rarely they run into different directions and occasionally form irregular intricate networks. The veins may grade into patches (Plate 3.3s). The vein albite usually amounts to about 5-30% of the total microperthite. However, in specimens containing abundant string albite the proportion may fall below 5% whilst in those specimen grading into patch microperthites it may rise to over 30%.Patch microperthite is very variable in texture.

Patch albite is usually twinned (albite-twinning) and aligned with those plagioclase inclusions (Plate 3.3t). Generally the contact between the orthoclase and albite is irregular though the patches tend to be elongated. The orthoclase is usually dominant and the albite forms coarse veins, but in a few cases, the albite is dominant and the orthoclase merely forms scattered islands.

Plate albite has been observed in only a few specimens. The plates of albite usually lie parallel to cleavage traces of (001) in the orthoclase-microperthite (Plate 3.3u).

The results of SEM analysis of the K-feldspar are presented in Appendix II and selected data in Table 3.4. All compositions plot at the Or corner on the An-Ab-Or diagram (Fig.3.8b). Compositions of the K-feldspar varies from Or_{100} to $Or_{90}Ab_7An_3$.

3.3.5 Other minerals

In the Jianfengling leucogranites, quartz and feldspars constitute 90% or more of the total mineral content. The remaining minerals are mica (biotite, zinnwaldite, sericite, and rarely muscovite), topaz, and accessory phases including fluorite, zircon, monazite, Nb-Ta oxides (niobite, tantalite, microlite), La-Ce fluorides, ore minerals (sphalerite, galena, pyrite, chalcopyrite, cassiterite), and surprisingly anorthite.

Detailed studies of micas from the Xianghualing area concerning its classification and nature were carried out by Huang and Du (1965) and Huang *et al.* (1979). Two types of mica, biotite and zinnwaldite, were recognised. In the rocks of Group 1 from the Jianfengling granite stock, greisenised phases, and pegmatites, mica is dominated by zinnwaldite, while that in rocks of Group 2 is mainly biotite. In practice, however, there is no way to distinguish these two types of mica optically or even through semiquantitative SEM analysis, because the differences between these two are the contents of lithium and fluorine[2]. As reported by Huang *et al.* (1979), following the sequence of normal granite through greisenised granite to greisen, the fluorine and lithium contents of the micas increase progressively, and the iron contents decline steadily.

---

[2] The ideal formulae for biotite and zinnwaldite are (Bailey, 1984):
biotite -- $K(Mg_{0.6\text{-}1.8},Fe_{2.4\text{-}1.2})(Si_3Al)O_{10}(OH,F)_2$
zinnwaldite -- $K[Fe^{2+}{}_{1.5\text{-}0.5}Li_{0.5\text{-}1.5}(Al, Fe^{3+})](Si_{3.5\text{-}2.5}Al_{0.5\text{-}1.5})O_{10}(F,OH)_2$

Table 3.4 Representative compositions of K-feldspar

	CK3-20					98-2			CH4-4			CK3-24					CK3-27			125-5	
	1*	3	4*	8	9	1	2*	8	1	2*	6	2	4*	5	6	2	4	8	9*	1	2
SiO2	62.73	62.52	63.24	62.79	62.39	64.38	63.57	63.48	63.92	63.46	62.93	65.90	65.92	65.17	65.38	65.43	62.15	65.09	64.82	64.92	65.27
Al2O3	20.84	19.95	18.62	20.53	20.47	18.73	20.04	18.55	19.42	19.82	20.32	20.67	19.97	20.04	20.17	17.81	19.59	18.75	19.21	19.73	20.07
FeO		0.18		0.26		0.24		0.24		0.38	0.20						0.45				
MgO				0.10		0.16											0.40				
CaO	0.23	0.30		0.51		0.10		0.20		0.15	0.25				0.30	0.64					0.51
K2O	15.62	16.37	17.89	15.09	16.73	15.62	15.86	16.78	15.93	15.43	15.57	5.58	14.10	14.29	13.78	15.87	17.01	16.03	15.84	14.92	13.73
Na2O	0.58	0.68	0.25	0.72	0.41	0.77	0.53	0.74	0.73	0.76	0.72	7.85		0.51	0.37	0.25	0.40	0.13	0.14	0.43	0.42
structural formulae based on 8 oxgen atoms																					
Si	3.245	3.243	3.273	3.242	3.242	3.286	3.271	3.272	3.281	3.265	3.250	3.270	3.327	3.307	3.300	3.320	3.232	3.314	3.306	3.304	3.305
Al	0.635	0.610	0.568	0.625	0.627	0.564	0.608	0.563	0.587	0.601	0.618	0.604	0.594	0.599	0.602	0.533	0.600	0.563	0.577	0.592	0.599
Fe	0.000	0.008	0.000	0.011	0.000	0.010	0.000	0.010	0.000	0.016	0.009	0.000	0.000	0.000	0.000	0.000	0.020	0.000	0.000	0.000	0.000
Mn	0.000	0.000	0.000	0.000	0.000	0.000	0.000	0.000	0.000	0.000	0.000	0.000	0.000	0.000	0.000	0.000	0.000	0.000	0.000	0.000	0.000
Mg	0.000	0.000	0.000	0.008	0.000	0.012	0.000	0.000	0.000	0.000	0.000	0.000	0.000	0.000	0.000	0.000	0.031	0.000	0.000	0.000	0.000
Ca	0.013	0.017	0.000	0.028	0.000	0.005	0.000	0.011	0.000	0.008	0.014	0.000	0.000	0.000	0.016	0.035	0.000	0.000	0.000	0.000	0.028
K	1.031	1.083	1.181	0.994	1.109	1.018	1.041	1.104	1.043	1.013	1.026	0.353	0.908	0.925	0.890	1.027	1.129	1.041	1.031	0.969	0.887
Na	0.058	0.068	0.025	0.072	0.041	0.076	0.053	0.074	0.073	0.076	0.072	0.755	0.000	0.050	0.036	0.025	0.040	0.013	0.014	0.042	0.041
end-member feldspar, mole%																					
ab	5.3	5.9	2.1	6.6	3.6	6.9	4.8	6.2	6.5	6.9	6.5	68.1	0.0	5.1	3.9	2.3	3.5	1.2	1.3	4.2	4.3
or	93.6	92.7	97.9	90.8	96.4	92.6	95.2	92.8	93.5	92.3	92.3	31.9	100.0	94.9	94.4	94.5	96.5	98.8	98.7	95.8	92.8
an	1.2	1.4	0.0	2.6	0.0	0.5	0.0	0.9	0.0	0.8	1.2	0.0	0.0	0.0	1.7	3.2	0.0	0.0	0.0	0.0	2.9

	430-3			430-6		480-7			138-15			430-4				480-1			101-17			
	1	2*	3	1	3	1	2	7*	1*	2	7	1*	3		10	1	3*	6	1	4*	5*	8
SiO2	64.28	64.15	63.53	65.22	63.48	62.53	63.73	64.52	63.17	63.58	63.95	63.73	64.34	63.72	63.16	63.18	62.53	65.13	62.37	62.82	63.22	63.71
Al2O3	19.68	19.35	20.03	19.64	18.73	19.93	19.04	18.51	18.72	18.22	19.06	19.52	17.14	19.13	19.77	17.94	20.35	17.83	19.75	20.33	19.37	18.36
FeO						0.35		0.20		0.13		0.10	0.25			0.40			0.10			0.16
MgO					0.27								0.24			0.20						0.20
CaO	0.20	0.16			0.46	0.49		0.29	0.14	0.36	0.27	0.18	0.63			0.58		0.47	0.28	0.34		0.52
K2O	15.41	16.01	16.44	14.80	16.34	16.02	17.01	16.04	17.55	17.13	16.04	16.06	16.63	16.84	16.49	17.02	16.81	16.02	16.88	15.93	16.83	16.34
Na2O	0.43	0.32		0.34	0.72	0.68	0.22	0.43	0.42	0.57	0.68	0.41	0.77	0.31	0.58	0.67	0.31	0.56	0.62	0.58	0.58	0.71
structural formulae based on 8 oxgen atoms																						
Si	3.288	3.288	3.274	3.311	3.265	3.240	3.282	3.298	3.268	3.276	3.281	3.276	3.290	3.280	3.262	3.261	3.247	3.313	3.241	3.249	3.266	3.272
Al	0.593	0.584	0.608	0.588	0.568	0.609	0.578	0.557	0.571	0.553	0.576	0.591	0.517	0.580	0.602	0.546	0.623	0.534	0.605	0.620	0.590	0.556
Fe	0.000	0.000	0.000	0.000	0.000	0.015	0.000	0.009	0.000	0.006	0.000	0.004	0.011	0.000	0.000	0.017	0.000	0.000	0.004	0.000	0.000	0.007
Mn	0.000	0.000	0.000	0.000	0.000	0.000	0.000	0.000	0.000	0.000	0.000	0.000	0.000	0.000	0.000	0.000	0.000	0.000	0.000	0.000	0.000	0.000
Mg	0.000	0.000	0.000	0.000	0.021	0.000	0.000	0.000	0.000	0.000	0.000	0.000	0.018	0.000	0.000	0.015	0.000	0.00	0.000	0.000	0.000	0.015
Ca	0.011	0.009	0.000	0.000	0.025	0.027	0.000	0.016	0.008	0.020	0.015	0.010	0.035	0.000	0.000	0.032	0.000	0.026	0.016	0.019	0.000	0.029
K	1.005	1.047	1.081	0.959	1.072	1.059	1.117	1.046	1.158	1.126	1.050	1.053	1.085	1.106	1.087	1.121	1.114	1.040	1.119	1.051	1.109	1.071
Na	0.043	0.032	0.000	0.033	0.072	0.068	0.022	0.043	0.042	0.057	0.068	0.041	0.076	0.031	0.058	0.067	0.031	0.055	0.062	0.058	0.058	0.071
end-member feldspar, mole%																						
ab	4.0	2.9	0.0	3.4	6.1	5.9	1.9	3.9	3.5	4.7	6.0	3.7	6.4	2.7	5.1	5.5	2.7	4.9	5.2	5.2	5.0	6.0
or	94.9	96.3	100.0	96.6	91.7	91.7	98.1	94.7	95.9	93.6	92.7	95.4	90.7	97.3	94.9	91.9	97.3	92.8	93.5	93.2	95.0	91.5
an	1.0	0.8	0.0	0.0	2.2	2.4	0.0	1.4	0.6	1.7	1.3	0.9	2.9	0.0	0.0	2.6	0.0	2.3	1.3	1.7	0.0	2.4

* analyses corresponde to those of albite exclusions

Biotite (zinnwaldite) occurs as subhedral, sometimes euhedral, grains, with inclusions of accessory minerals. It shares straight contacts with adjacent phases and is often overgrown by other minerals, notably quartz and K-feldspar (cf. Plates 3.3g, n). Results of SEM analyses are reported in Table 3.5 and Appendix IV. It is obvious that biotite from rocks of Group 2 has higher iron and magnesium contents than those from rocks of Group 1.

Topaz (Plate 3.3v, w) occurs in most samples but higher contents are evident in rocks of Group 1 (cf. Table 3.2). It is generally subhedral to anhedral, in many cases, filling the interstices, thus indicating that it was mainly a late phase of the crystallisation sequence. Euhedral grains have been noted in pegmatitic rocks. The topaz is most commonly fractured with sericite filling the fractures, although no structural modification has been observed in these specimens; the reason for this is not presently known. Inclusions in the topaz are rare, but biotite, feldspars, quartz, and La-Ce fluorides do occur. All indications are that most of the topaz represents a magmatic phase and not a later manifestation of hydrothermal activity.

Andalusite (Plate 3.3x) occurs as anhedral to subhedral grains in few samples. It encloses other minerals such as biotite, albite and quartz.

Anorthite was detected during the SEM studies (Table 3.6). It occurs as tiny anhedral inclusions, a few hundred microns across, in biotite, thus indicating its early formation in the crystallisation sequence. This might provide an explanation for the extremely low An content of the later plagioclase.

Table 3.5 Representative compositions of biotite

	CK3-20				98-2			CH4-4				CK3-24			CK3-27				125-5	
	1	4	5	8	1	4	6	1	4	7	8	1	3	4	2	4	5	1	2	4
SiO2	46.37	44.74	46.87	46.32	51.48	51.01	48.71	49.76	51.09	46.57	47.40	51.53	51.47	50.68	43.40	42.25	43.26	46.47	45.94	49.72
Al2O3	22.23	20.36	22.29	23.36	23.52	24.08	23.16	24.32	23.89	22.26	23.64	24.51	24.56	24.74	22.97	21.72	21.51	23.53	22.98	24.01
FeO*	18.63	20.62	20.16	19.47	14.53	13.65	14.91	13.56	14.18	18.09	17.78	14.40	14.41	14.37	21.63	22.77	23.48	17.44	18.05	15.93
K2O	10.76	10.76	9.78	9.11	9.52	9.24	10.22	9.84	9.04	10.23	9.32	9.56	9.32	9.49	10.80	10.03	10.03	9.79	9.84	9.24
MgO	0.10			0.10	0.12				0.17		0.13		0.25	0.46	0.60		0.36	0.64	0.59	0.46
MnO	1.61	1.68	0.90	1.24		1.55	1.62	0.92	0.79	1.36	1.36			0.25		1.52	1.13	1.42	1.50	
Na2O	0.30	1.66		0.40	0.83	0.47	1.38	1.60	0.84	1.49	0.37				0.60	1.46	0.22	0.70	0.93	0.65
CaO		0.18														0.23			0.17	
Σwt.%	100.00	100.00	100.00	100.00	100.00	100.00	100.00	100.00	100.00	100.00	100.00	100.00	100.01	99.99	100.00	99.98	99.99	99.99	100.00	100.01

	430-3			480-6			480-7		138-15			430-4			480-1			101-17		
	1	4	5	1	2	3	2	4	2	4	6	1	3	4	2	3	6	1	5	9	10
SiO2	48.18	48.77	47.50	50.59	48.34	47.48	45.26	45.64	49.38	48.48	51.06	49.87	44.76	49.34	46.34	47.40	47.36	48.43	50.04	46.37	45.72
Al2O3	25.48	25.43	25.70	24.38	24.29	24.16	22.64	21.30	21.21	22.18	24.26	23.49	21.92	23.82	22.54	23.16	21.93	22.72	24.85	21.42	22.06
FeO*	16.35	15.06	16.18	14.53	15.42	16.37	20.07	21.47	16.44	17.53	12.18	15.35	19.71	15.56	20.73	17.63	18.49	16.05	15.75	19.38	19.75
K2O	9.27	8.76	8.99	9.36	9.65	9.62	10.52	10.63	10.03	9.74	10.34	9.72	10.71	9.14	9.24	9.78	9.63	10.22	8.62	10.31	9.62
MgO		0.32		0.54	0.46	0.57	0.38	0.56	0.39	0.60	0.52	0.24	0.58	0.59	0.52	0.41	0.49		0.73	0.33	0.61
MnO	0.72	1.32	1.16	0.60	1.27	1.49	1.14	0.40	1.58	1.48	1.22	1.34	1.47	1.13	0.64	1.52	1.62	1.58		1.56	1.53
Na2O		0.36	0.47		0.56	0.32			0.97		0.42		0.65	0.42			0.47	0.92		0.46	0.70
CaO													0.20			0.10		0.10		0.18	
Σwt.%	100.00	100.02	100.00	100.00	99.99	100.01	100.01	100.00	100.00	100.01	100.00	100.01	100.00	100.00	100.01	100.00	99.99	100.02	99.99	100.01	99.99

Table 3.6 Compositions of anorthite inclusions in biotite

	480-6			CK3-27			
	1	2	3	1	2	3	4
SiO2	23.70	24.71	36.22	47.42	34.54	42.57	39.52
Al2O3	28.82	28.93	15.29	20.26	14.44	18.90	16.23
FeO	0.54	0.42	3.06	6.52	3.76	5.28	2.47
MnO	0.60	0.35	0.00	0.00	0.00	0.00	0.00
MgO	0.89	0.76	0.94	0.00	2.84	0.63	2.46
CaO	43.69	43.06	37.61	22.99	36.16	27.26	31.64
K2O	0.72	0.72	4.77	2.06	6.07	3.76	5.57
Na2O	1.03	1.05	2.11	0.97	2.20	1.61	2.11
structural formulae based 8 oxygen atoms							
Si	1.54	1.59	2.14	2.61	2.06	2.43	2.28
Al	1.10	1.10	0.53	0.66	0.51	0.63	0.55
Fe	0.03	0.02	0.15	0.30	0.19	0.25	0.12
Mn	0.03	0.02	0.00	0.00	0.00	0.00	0.00
Mg	0.09	0.07	0.08	0.00	0.25	0.05	0.21
Ca	3.03	2.97	2.38	1.36	2.31	1.66	1.96
K	0.06	0.06	0.36	0.14	0.46	0.27	0.41
Na	0.13	0.13	0.24	0.10	0.25	0.18	0.24
end-member feldspar, mole%							
ab	4.02	4.15	8.11	6.45	8.40	8.41	9.07
or	1.85	1.87	12.06	9.02	15.26	12.92	15.76
an	94.14	93.98	79.84	84.53	76.34	78.67	75.17

Plate 33

Plate 3.3 **Petrography and mineralogy the Jianfengling granites**

(All photomicrographs are taken under crossed nicols; adl = andalusite; bi = biotite, kf = k-feldspar, pl = plagioclase (albite), tz = topaz, qz = quartz)

a. Typical specimen of albite-zinnwaldite granite showing medium- to coarse-grained equigranular texture (locally porphyritic; sample 97-1).

b. Specimen of two-feldspar biotite granite showing medium-grained equigranular texture (sample 480-6).

c. Typical specimen of K-feldspar-biotite granite showing medium-grained equigranular texture (sample 101-15).

d. Photograph of specimen of biotite granite showing local alteration, a progressive transition from fresh granite (right) to altered granite (left) is evident (sample 107).

e. A typical microscopic view of the albite-zinnwaldite granite. Euhedral to subhedral quartz grains show straight contact with biotite, albite and topaz sample CK3-20). Bar = 0.50mm.

f. Photomicrograph showing the idiomorphic to hypidiomorphic granular texture (sample 480-4). Bar = 0.13mm.

g. Photomicrograph showing anhedral quartz overgrows biotite and albite. Bar = 0.20mm.

h. "Snowball texture" produced by numerous small subhedral to euhedral albite inclusions (white) arranged concentrically along the growth planes of a large subhedral quartz grain (dark background). Sample CK4-1. Bar = 0.50mm.

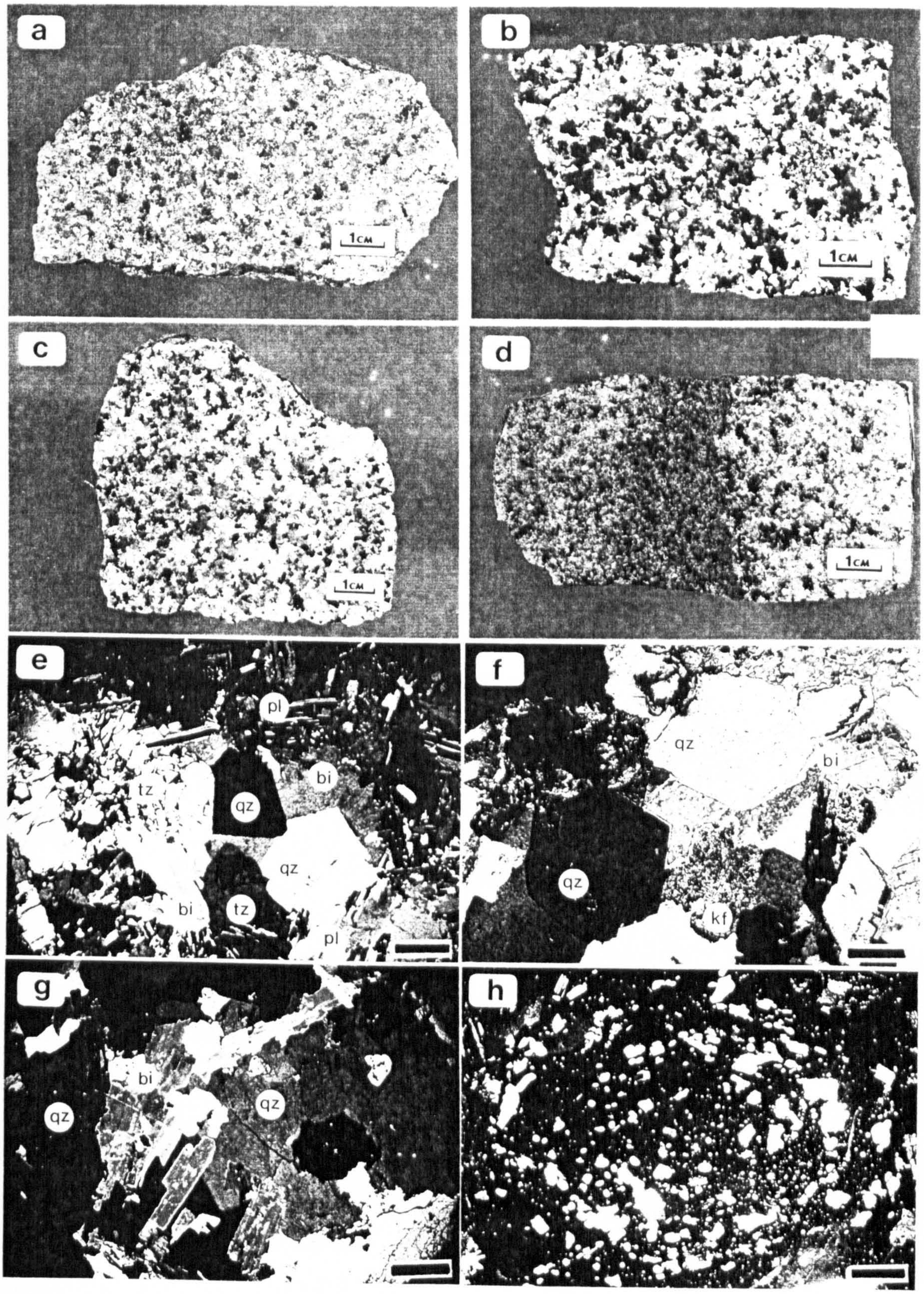
a
1cm
b
1cm
c
1cm
d
1cm
e
pl
bi
qz
tz
qz
bi
tz
pl
f
qz
bi
qz
kf
g
bi
qz
qz
h

Plate 3.3 (continued)

Plate 3.3 **Petrography and mineralogy of the Jianfengling granites (continued)**

i. Subhedral plagioclase (albite) lath displays albite twining (sample 86020). Bar = 0.13mm.

j. Plagioclase (albite) shares sharp contact with K-feldspar and quartz (sample 101-8). Bar = 0.50mm.

k. Small subhedral plagioclase grains (white) enclosed by K-feldspar. Note plagioclases are generally arranged in two directions. Sample 107-7. Bar = 0.25mm.

l. Plagioclase grains randomly enclosed within K-feldspar (sample 131-1). Bar = 0.25mm.

m. Late anhedral K-feldspar overgrows early euhedral to subhedral K-feldspar and plagioclase. Sample CK4-3. Bar = 0.50mm.

n. Euhedral K-feldspar enclosed by biotite and quartz (bottom centre), some alteration along contact is evident. Sample 480-5. Bar = 0.50mm.

o, p. Euhedral to subhedral K-feldspar grains show straight contact with biotite, quartz and plagioclase. Samples 480-6 and 125-2. Bars = 0.25mm and 0.50mm.

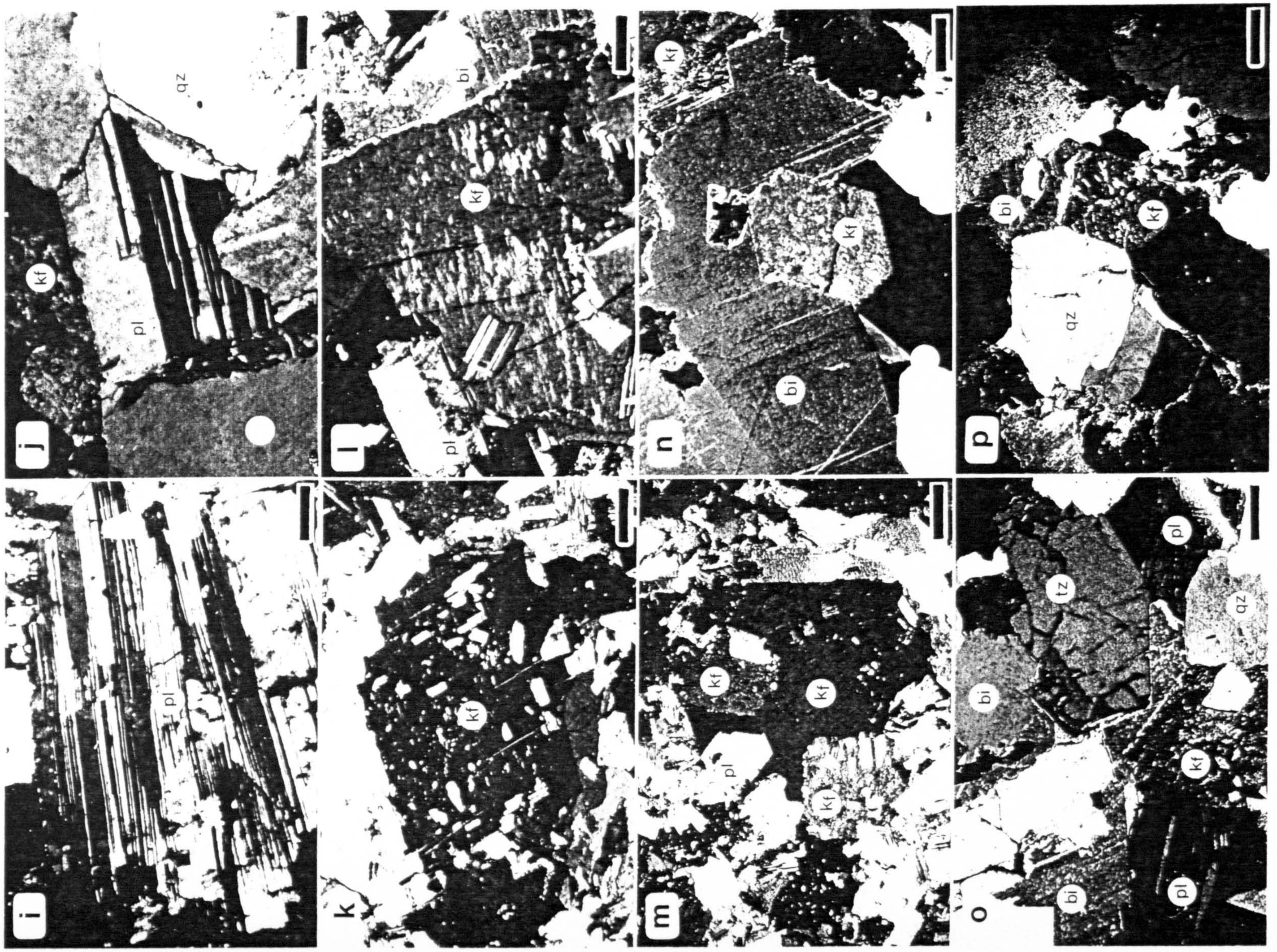
j
kf
pl
qz
l
pl
kf
bi
n
bi
kf
p
bi
kf
qz
i
pl
k
kf
m
pl
kf
kf
o
bi
bi
tz
kf
pl
pl
qz

Plate 3.3 (continued)

Plate 3.3 **Petrography and mineralogy of the Jianfengling granites (continued)**

q. Photomicrograph showing string albite (centre right) and film albite (centre left) within an orthoclase grain which displays albite twining. The string microperthite shows grey gritty texture. Sample CK3-25. Bar = 0.13mm.

r. Film microperthite. Films of albite distribute homogeneously in an orthoclase grain (centre). Sample 138-8. Bar = 0.25mm.

s. Vein microperthite. Irregular albite veins occur discontinuously in orthoclase. Some sericitisation of the microperthite is noticeable (top right). Sample 138-8. Bar= 0.25mm.

t. Patch microperthite. Irregular-shaped patches of albite show albitic twining and lie parallel to (001) plane. Sample 135-4. Bar = 0.25mm.

u. Plate microperthite. Albite twining of the albite plates is evident. Sample S-11. Bar = 0.25mm.

v. Subhedral topaz grains show straight contact with quartz and enclose albite and quartz. Sample 140-9. Bar = 0.50mm.

w. Anhedral topaz fills the interstial space between quartz and plagioclase. Sample 480-1. Bar = 0.50mm.

x. Anhedral andalusite partially encloses plagioclase and quartz. Sample 107-7. Bar = 0.50mm.

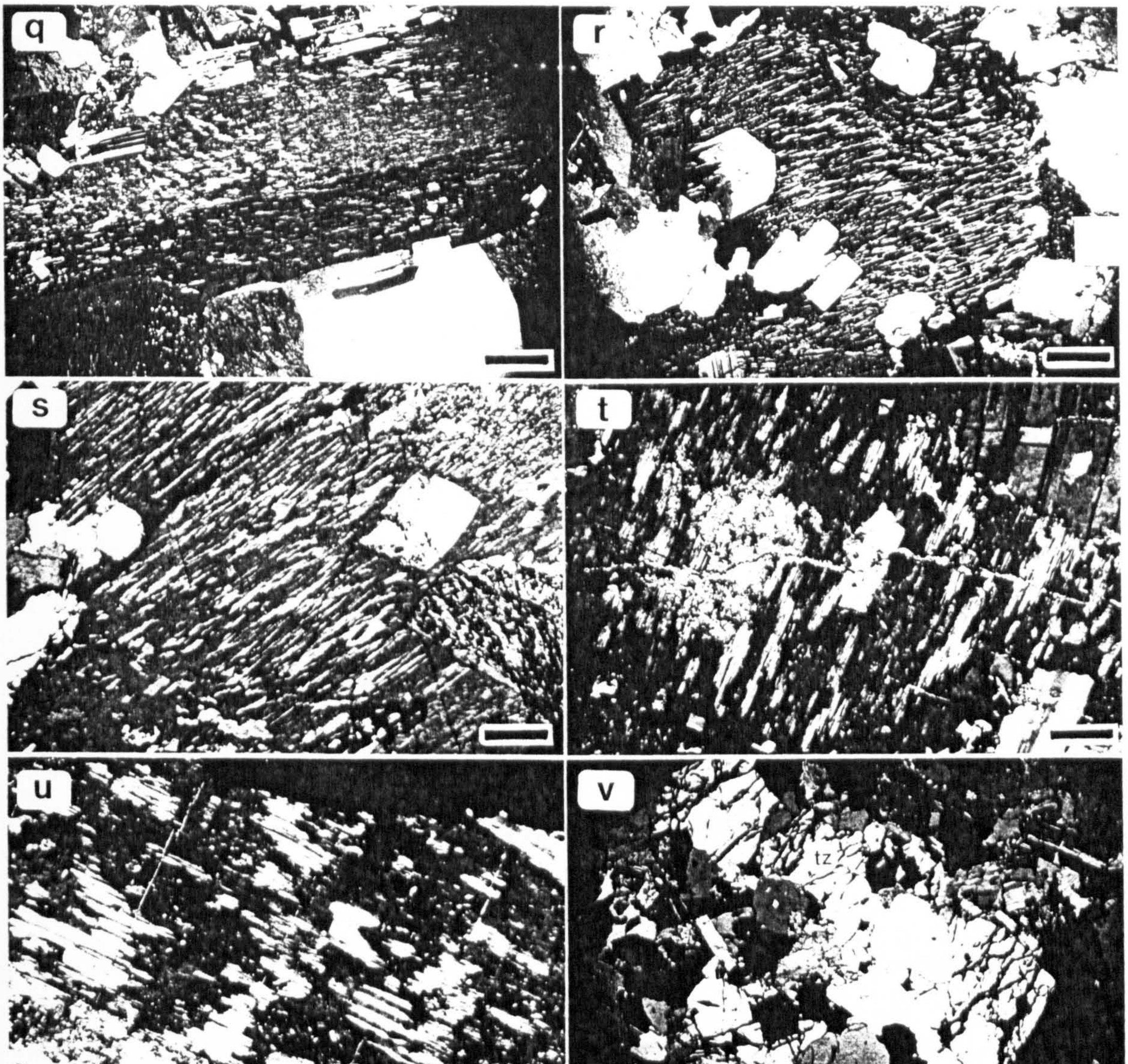
q
r
s
t
u
v
tz
tz
w
pl
qz
qz
tz
bi
x
adl
pl
qz

CHAPTER FOUR

GEOCHEMISTRY OF THE JIANFENGLING GRANITES

CHAPTER FOUR

GEOCHEMISTRY OF THE JIANFENGLING GRANITES

Contents

4.1 Introduction
4.2 Major and trace element geochemistry
4.3 Rare earth element geochemistry
4.4 Discussion

4.1 INTRODUCTION

Forty five representative samples, which were collected by drilling and blasting fresh out-crops, were chosen for major and trace-element chemical analyses. Sample selection was based on results of systematic geological mapping and detailed petrographic studies of more than 140 thin sections. Detailed sample preparation procedures are presented in Appendix III.

Powdered whole-rock samples were analyzed for major-elements (on fused glass discs) and a suite of trace-elements (Rb, Ba, Sr, Y, Zr, Nb, Th, U, W, Sn, Mo, Pb, Zn, Cu, Ni, Ga, As, Sb, Bi, V, Cr, La and Ce (on pressed powder pellets) using an automatic Philips X-ray fluorescence spectrometer (XRF) following the procedures developed by Croudace & Williams-Thorpe (1988) and Croudace & Gilligan (1990). Thirty of the same suite of samples were analyzed for rare-earth elements (REEs; La, Ce, Nd, Sm, Eu, Tb, Yb, Lu) and Th, U, Ta, Hf, Cs using instrumental neutron activation analysis (INAA) (Croudace *et al.*, 1980). Both XRF and INAA analyses were performed at the Department of Geology, University of Southampton. Atomic absorption spectrometry (AAS) was employed for Li analysis at the Department of Oceanography, University of Southampton. F analysis was carried out at the Department of Chemistry, University of Birmingham, using fast-neutron activation analysis following the procedures described by Croudace & Randle (1988) and Randle & Croudace (1989).

During all determinations both international and inter-laboratory reference samples were routinely included in with the Jianfengling granite samples. Precision for most elements was in the range 1-5%

Table 4.1 Whole-rock geochemistry of the Jianfengling granite stock

	A n=10		B n=4		C. n=3		D n=15		E n=11	
	x	σ	x	σ	x	σ	x	σ	x	σ
SiO_2	75.49	0.77	74.10	1.05	74.89	0.69	75.06	1.22	75.56	0.60
TiO_2	0.02	0.01	0.00	0.00	0.01	0.00	0.02	0.01	0.02	0.01
Al_2O_3	14.30	0.63	15.53	0.39	14.89	0.47	14.33	0.89	14.03	0.44
Fe_2O_3	0.90	0.18	0.74	0.15	0.79	0.08	1.38	0.32	1.32	0.26
MnO	0.08	0.01	0.13	0.01	0.16	0.01	0.09	0.03	0.08	0.02
MgO	0.05	0.01	0.13	0.06	0.04	0.00	0.08	0.03	0.10	0.06
CaO	0.46	0.12	0.34	0.06	0.21	0.05	0.47	0.13	0.61	0.11
Na_2O	3.80	0.65	3.46	0.73	3.65	0.28	3.71	0.60	3.47	0.58
K_2O	4.49	0.41	4.30	0.30	4.35	0.14	4.15	0.52	4.25	0.65
P_2O_5	0.00	0.00	0.01	0.00	0.01	0.00	0.01	0.00	0.00	0.00
F	0.97	0.19	1.36	0.12	1.29	0.15	1.23	0.34	1.09	0.22
-F=O	-0.41	-0.08	-0.55	-0.05	-0.54	-0.06	-0.52	-0.14	-0.46	-0.09
SUM	99.59		98.75		99.00		99.31		99.44	
LOI	0.81	0.15	1.15	0.18	0.93	0.04	0.93	0.17	1.07	0.14
Li	667	109	951	101	1176	51	865	264	858	154
Rb	1431	131	1908	185	2120	165	150	242	1494	151
Cs*	44.8	7.5	39.3	8.3	49.0	3.7	58.0	14.2	54.8	9.2
Sr	7	4	11	3	7	1	8	4	8	3
Ba	23	5	20	10	11	5	17	15	14	7
Y	72	37	12	16	30	14	88	55	121	30
Zr	59	19	35	5	45	12	66	19	75	12
Hf	4.5	1.3	4.4	0.4	5.5	1.2	5.1	1.0	5.7	1.9
Nb	58	7	49	11	59	1	59	6	61	9
Ta	26.6	7.1	63.8	27.8	55.8	2.7	31.7	10.6	26.5	5.5
Th	22	10	13	3	28	16	34	13	34	8
Th*	25	9	13	3	20	2	30	11	39	8
U	18	8	6	2	12	3	26	10	29	4
U*	19	5	14	2	17	2	27	10	31	4
Cr	6.5	2.7	33.5	46.3	9.7	9.2	48.8	78.9	30.5	41.0
V	0.3	0.6	0.0	0.0	0.0	0.0	0.6	1.1	0.1	0.2
Ni	11.9	5.3	9.4	3.4	12.5	4.4	9.1	2.7	11.6	4.2
Cu	3	2	22	33	5	4	2	1	3	2
Zn	52	38	376	169	233	193	73	33	283	436
Ga	34	3	46	4	42	4	34	4	34	2
Mo	2	3	4	4	1	1	4	8	1	1
W‡	42	18	26	20	16	2	79	37	115	130
Sn	78	38	160	52	176	2	80	67	143	138
Pb	94	135	188	58	162	142	75	94	52	22
As	4	10	139	137	50	53	6	14	6	11
Sb	0.0	0.0	0.3	0.5	7.3	9.9	0.0	0.0	2.1	4.4
Bi	0	1	7	8	22	31	10	20	2	4
C%	2.34	0.47	4.59	0.97	3.83	0.87	2.88	1.08	2.62	0.75
ASI	1.21	0.04	1.44	0.12	1.36	0.09	1.26	0.10	1.24	0.08

* denotes analysis of trace elements by INAA along with REE.
† W determined on samples grounded in a special hardened steel pot.
C%: percentage of normative (CIPW) corundum calculated on F-free basis.
ASI(=A/CNK): alumina saturation index (Zen, 1986), molecular ratio [Al2O3/(CaO+Na2O+K2O)].

relative depending on the element and its concentration (see Appendix III).

Results of the whole-rock analyses are reported in Appendix V (major- and trace-elements together with the normative minerals) and Appendix VI (rare-earth elements). The means and standard deviations (1σ) of the five intrusions of the Jianfengling stock are listed in Tables 4.1 and 4.2. The ranges and averages for all analyses are plotted on Figure 4.1. Comparison of the averages with other felsic igneous rocks which are characterised by an enrichment in F and LILE (large-ion-lithophile element) is presented in Table 4.3.

Table 4.2 Rare-earth element geochemistry of the Jianfengling granite stock

	A		B		C		D		E	
	n=10		n=4		n=3		n=10		n=6	
	x	σ	x	σ	x	σ	x	σ	x	σ
La*	27.5	9.5	9.4	10.0	16.0	7.6	33.2	13.3	38.3	6.8
La	29.0	8.5	8.5	6.4	15.6	6.4	33.8	13.1	48.4	8.2
Ce*	61.6	18.5	29.1	17.2	37.2	11.0	74.2	27.6	82.4	13.2
Ce	79.0	20.5	28.3	14.9	46.7	16.7	90.3	32.1	117.1	21.3
Nd	28.3	10.8	9.8	5.6	17.3	6.8	37.7	17.8	52.3	9.4
Sm	7.0	3.4	2.6	1.3	3.5	1.0	8.7	4.2	13.6	2.5
Eu	0.03	0.00	0.03	0.00	0.02	0.00	0.03	0.02	0.04	0.01
Tb	1.7	0.7	0.6	0.3	0.9	0.3	2.0	1.1	3.0	0.6
Yb	12.8	4.2	4.3	3.0	7.9	3.2	14.9	4.7	18.7	3.3
Lu	1.8	0.6	0.6	0.4	1.1	0.5	2.2	0.7	2.6	0.4

* denotes analysis by XRF; remainder determined by INAA.

Table 4.3 Comparative geochemistry of selected fluorine-rich felsic suites and Jianfengling granites

	1	2	3	4	5	6	7	8	9	10	11	12	13 (±STD)	14 (±STD)
SiO_2	71.10	73.27	73.90	72.32	73.30	70.86	74.43	76.09	75.06	73.81	73.39	73.39	74.44 (0.99)	75.33 (0.97)
TiO_2	0.06	0.02	0.06	0.02	0.12	-	0.02	0.02	0.01	0.26	0.26	0.28	0.01 (0.00)	0.02 (0.01)
Al_2O_3	16.11	15.04	13.10	15.63	13.89	15.98	14.46	12.64	13.46	12.40	13.43	13.45	15.26 (0.53)	14.23 (0.72)
Fe_2O_3	0.35	1.38[a]	1.43[a]			0.15	0.20	0.86[a]	0.79[a]	1.24	0.60	0.36	0.76[a] (0.13)	1.23[a] (0.34)
FeO	0.81			0.52[b]	0.89[b]	0.49	0.67			1.58	1.32	1.73		
MnO	0.07	0.04	0.06	0.06	0.10	0.22	0.03	0.10	0.09	0.06	0.05	0.04	0.15 (0.02)	0.08 (0.02)
MgO	0.09	0.03	0.08	0.02	0.02	0.13	0.02	0.05	0.05	0.20	0.55	0.58	0.09 (0.07)	0.08 (0.05)
CaO	0.59	0.49	1.27	0.23	0.26	0.52	0.27	0.45	0.30	0.75	1.73	1.28	0.29 (0.09)	0.51 (0.13)
Na_2O	3.73	3.65	4.33	4.10	4.07	5.87	3.98	3.91	4.25	4.07	3.33	2.81	3.54 (0.59)	3.66 (0.62)
K_2O	4.84	3.78	3.65	3.53	5.80	3.53	4.31	4.45	4.24	4.65	4.13	4.56	4.32 (0.24)	4.28 (0.55)
P_2O_5	0.50	0.48	0.00	0.58	-	0.09	0.15	0.01	0.00	0.04	0.07	0.14	0.01 (0.00)	0.01 (0.00)
F	1.22	0.77	1.10	1.30	0.16	2.05	0.59	0.15	0.98	-	-	-	1.30 (0.14)	1.11 (0.18)
Li	1254	464	80	3440	580	700[‡]	520	84	1015	-	-	-	1047 (139)	808 (217)
Rb	1218	890	1060	1160	480	1975	1106	-	1686	169	194	277	1999 (206)	1480 (192)
Cs	127	37	58	580	17	-	-	-	49	-	-	-	43 (8)	53 (13)
Sr	61	55	5	1.2	7	20	10	-	6	48	143	81	9 (3)	8 (3)
Ba	104	23	-[c]	1.7	-	-	16	-	329	352	510	388	16 (9)	18 (11)
Zr	46	30	120	25	-	-	29	63	60	528	144	136	39 (10)	67 (18)
Hf	3.1[•]	1	7.1	1.5	-	-	-	-	6.9	-	-	-	5 (1)	5 (1)
Nb	93	30	120	51	52	-	29	30.4	34	37	12	13	53 (9)	59 (8)
Ta	1.6[•]	13	25	24	-	-	-	16	16	-	-	-	60 (21)	29 (9)
Th	22	5	69	1.3	42	-	14	25.6	31	23	22	18	20 (13)	31 (12)
Ga	40	34	-	42.5[†]	-	-	36	-	-	24.6	16	17	44 (4)	34 (3)
W	20[••]	26	-	62[†]	26	13[‡]	12	-	26	-	-	-	22 (16)	80 (81)
Sn	127	181	-	155[†]	15	120[‡]	30	-	13	-	-	-	167 (40)	99 (95)
La	3	1.0	59	2.4	-	-	4	9.3	29	-	-	-	12 (10)	33 (11)
Ce	36	2.8	137	7.8	50	-	10	25.0	83	137	68	53	33 (15)	73 (23)
Y	10	4.3	135	5.6	58	-	31	154.9	82	75	34	33	20 (18)	94 (48)

1: Cornish topaz granite, SW England (10 analyses, Stone & Exley, 1986);
* data from Pearce *et al.* 1984;
** data from Alderton & Moore, 1981;
2: East Kemptville topaz-muscovite leucogranite, Nova Scotia (22 analyses, Kontak, 1990);
3: Spor Mountain topaz rhyolite, Utah (Christiansen *et al.*, 1984, sample SM-35, table 3);
4: Macusanite (rhyolite obsidian), Peru (London *et al.*, 1988);
† data from Pichavant *et al.*, 1988;
5: Glass inclusions in quartz phenocrysts of Taylor Creek Rhyolite, New Mexico (18 analyses, Webster & Duffield, 1991);
6: Ongonite, Mongolia (10 analyses, in Pichavant & Manning, 1984);
‡ data from Tischendorf, 1977;
7: Lottah alkali-feldspar granite, Blue Tier Batholith, NE Tasmania (3 analyses, Mackenzie *et al.*, 1988);
8: Xihuashan leucogranite, SE China (5 analyses, Maruéjol *et al.*, 1990);
9: The Pleasant Ridge zinnwaldite-topaz granite, Southern New Brunswick (Taylor, 1992, sample 82-4B, table 4);
10: A-type granite (148 analyses, Whalen *et al.*, 1987);
11: Felsic I-type granite (421 analyses, Whalen *et al.*, 1987);
12: Felsic S-type granite (205 analyses, Whalen *et al.*, 1987);
13: Average (± standard deviation) Group 1 of the Jianfengling granites (n=7);
14: Average (± standard deviation) Group 2 of the Jianfengling granites (n=36).

[a] total Fe as Fe_2O_3;
[b] total Fe as FeO.
[c] data not available;

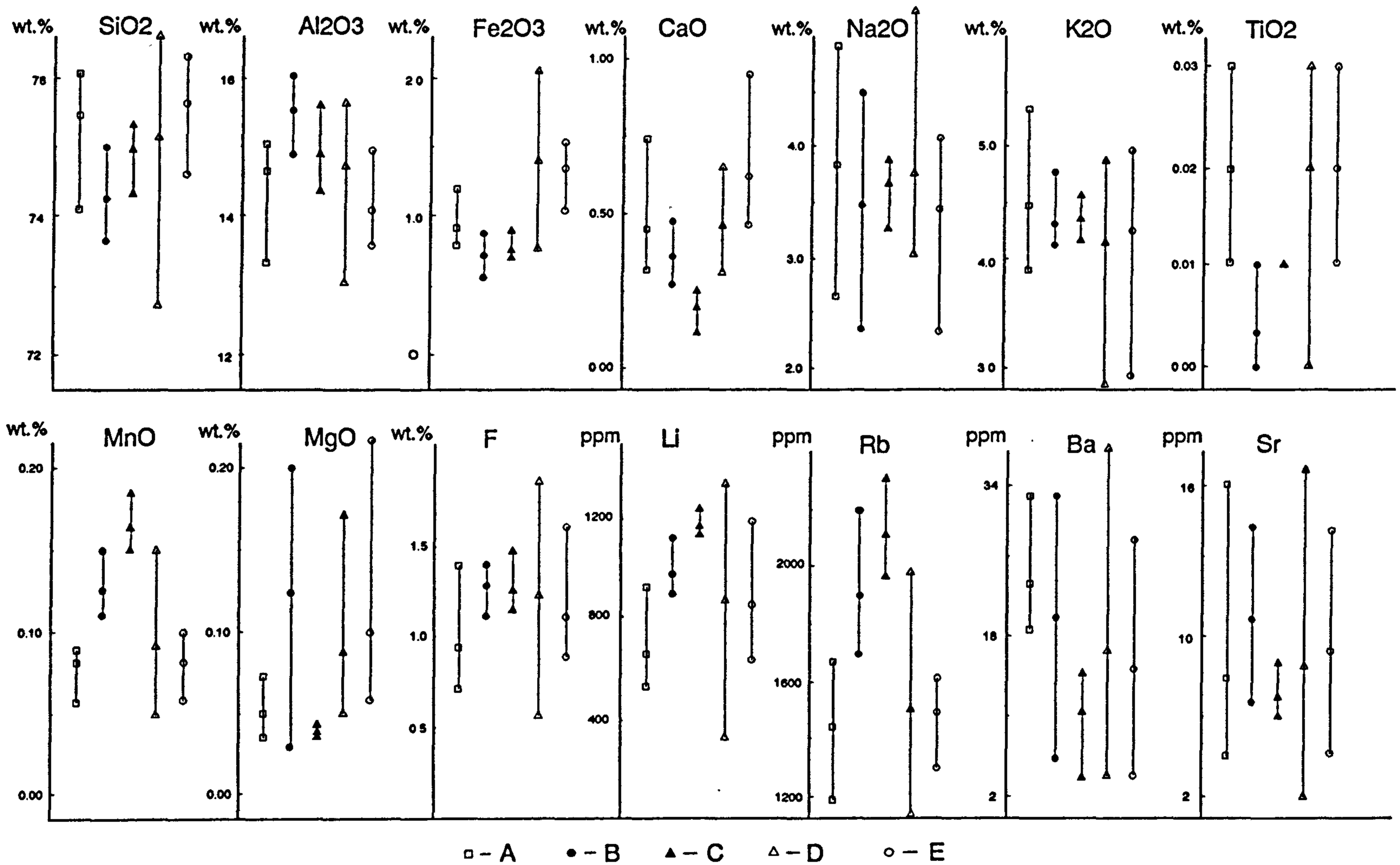

Fig. 4.1 Ranges and averages of major and trace element compositions of the Jianfengling granites

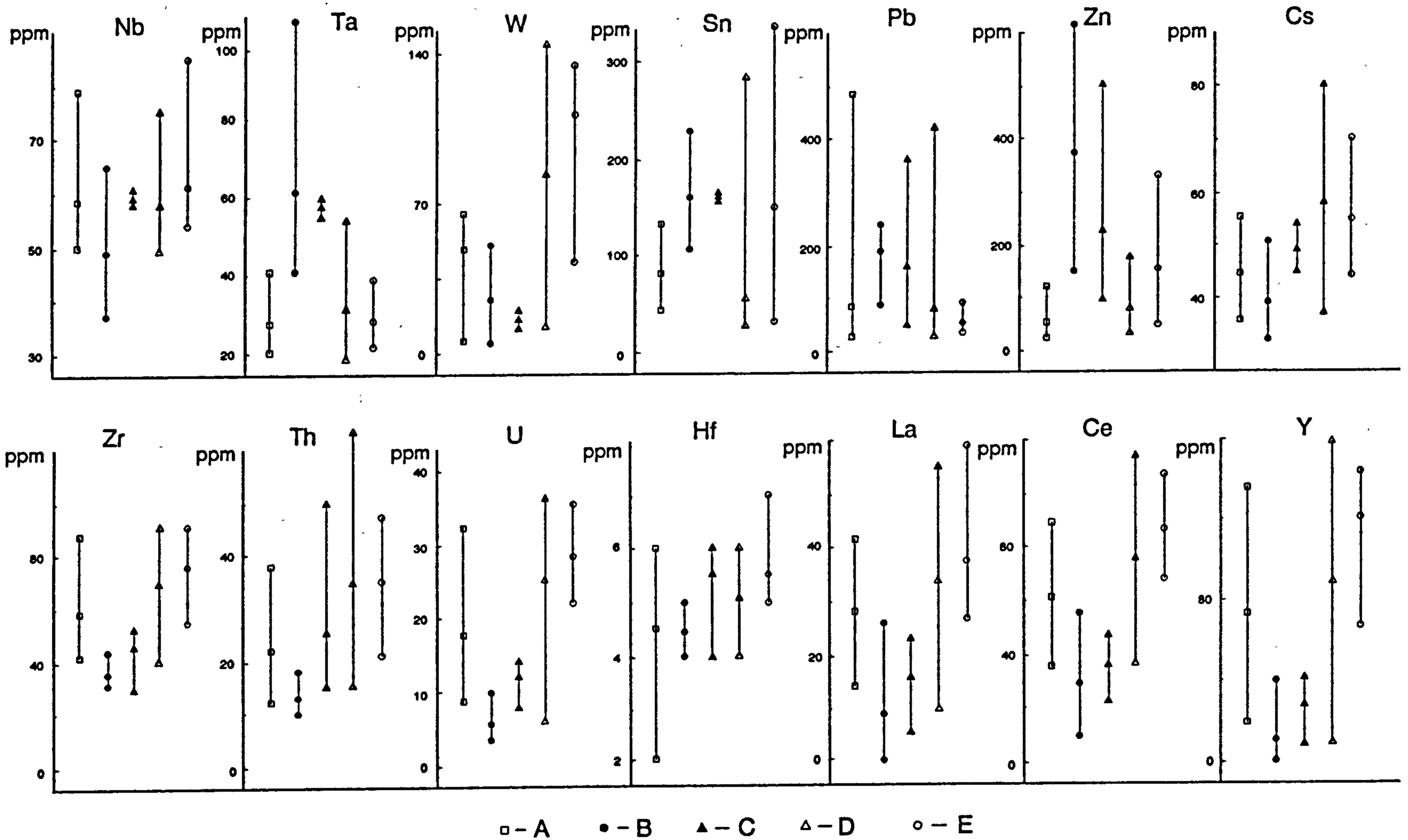

Fig. 4.1 (continued)

4.2 MAJOR AND TRACE-ELEMENT GEOCHEMISTRY

The petrological differences among the rocks of the Jianfengling granites provide a basis for separating these granites into two groups (see Chapter 3). As will be demonstrated below, the trace-element geochemistry can also effectively separate the biotite-bearing granite suite (Group 2) from the zinnwaldite-bearing albite granite suite (Group 1).

Samples of the Jianfengling granites have a very restricted range of major element compositions: they are all high silica (SiO_2 72.47-76.90 wt.%), slightly peraluminous (ASI[3]=1.07-1.54), fluorine-rich (F>0.84 wt.%) rocks, with low concentrations of TiO_2 (≤0.03 wt.%), MgO (≤0.15 wt.%), CaO (≤0.65 wt.%) and P_2O_5 (≤0.01 wt.%) relative to other types of granites (Table 4.3). Low TiO_2, MgO, CaO and P_2O_5 are reflected by the albitic nature of the plagioclase, the lithium-rich character of the mica (*i.e.* the presence of zinnwaldite), and the absence of apatite as a common accessory mineral (*cf.* Chapter 3). Alkali contents are high with (Na_2O+K_2O) values ranging from 6.96 to 8.62 wt.%; for most of the samples, like many common types of granite, the Jianfengling granites have K_2O in excess of Na_2O, with average molar K/Na ratios being 0.80 (±0.23).

Although major-element concentrations in the Jianfengling granites are fairly uniform, especially within each group, differences in the trace element geochemistry are still noticeable between the two groups. Rocks of Group 1 have higher Al_2O_3, MnO, F, Rb, Ta, and Sn, and lower SiO_2, total Fe_2O_3, CaO, Zr, Hf, and W concentrations relative to those of Group 2. The pertinent major- and trace-element compositions of these granites are represented in Harker variation diagrams in Figure 4.2. On diagrams of silica versus other major elements, samples from both groups are barely distinguishable; no noticeable correlation exists between these elements except Al_2O_3 and CaO. Al_2O_3 shows an inverse correlation with SiO_2, whereas CaO correlates positively with SiO_2. In both groups, there is a considerable variation in many of the trace-elements determined, emphasizing the relatively heterogeneous nature of the Jianfengling granites in terms of trace-element geochemistry. On most of those diagrams of silica versus trace elements (Fig. 4.2), samples of the two groups are noticeably separated, although some overlaps do exist; Zr, U, Y and REEs (represented by La) demonstrate a nearly linear increase with increasing silica, while Rb, Ta and Ga decrease with increasing silica. Sr, Y, Zr, U, La and Sm show positive correction with CaO content, while Rb and Ga decrease with increasing CaO.

[3] = A/CNK, alumina saturation index: molar $Al_2O_3/(CaO+Na_2O+K_2O)$ (Zen, 1986).

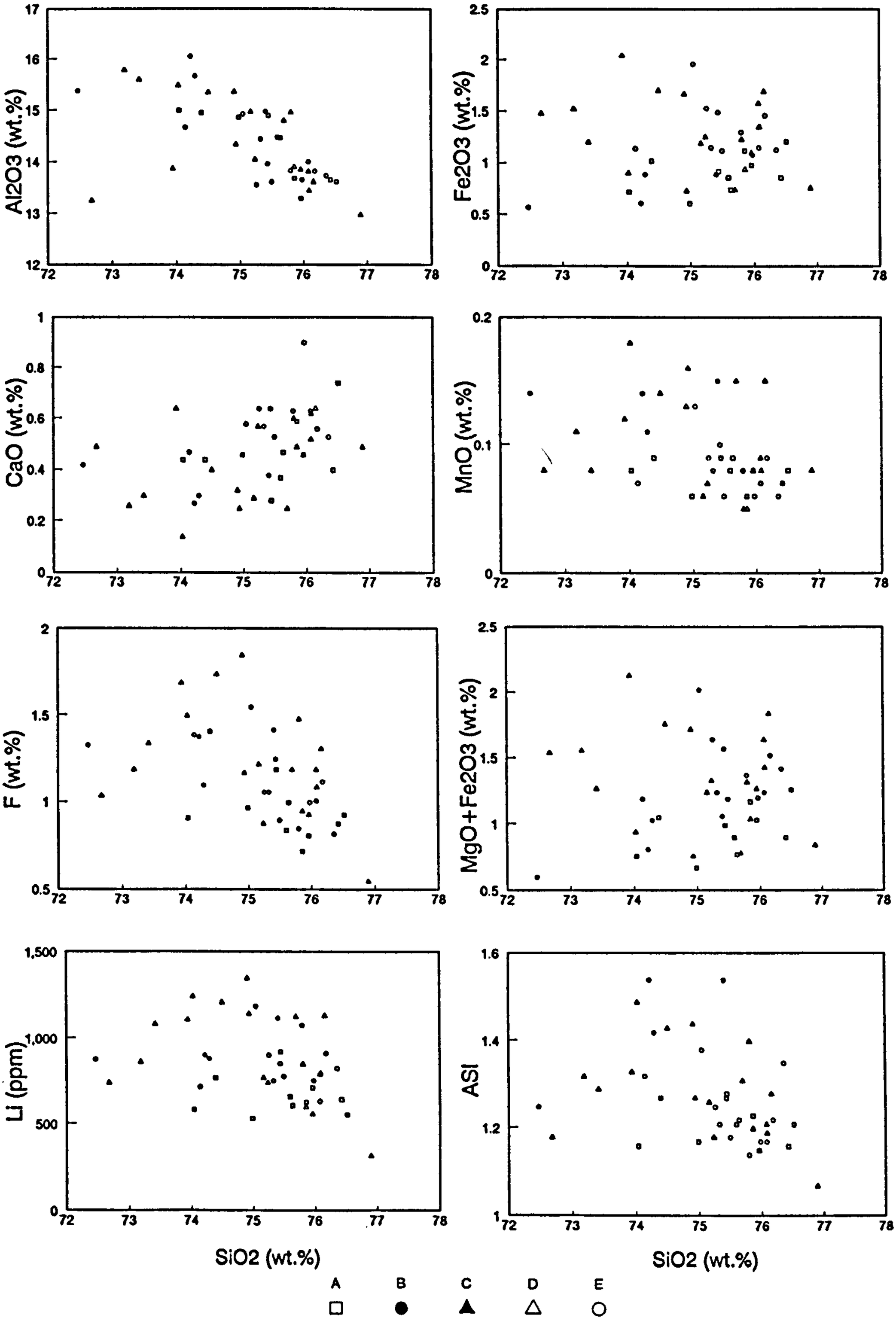

Fig. 4.2 Binary variation diagrams for some major and trace elements of the Jianfengling granites

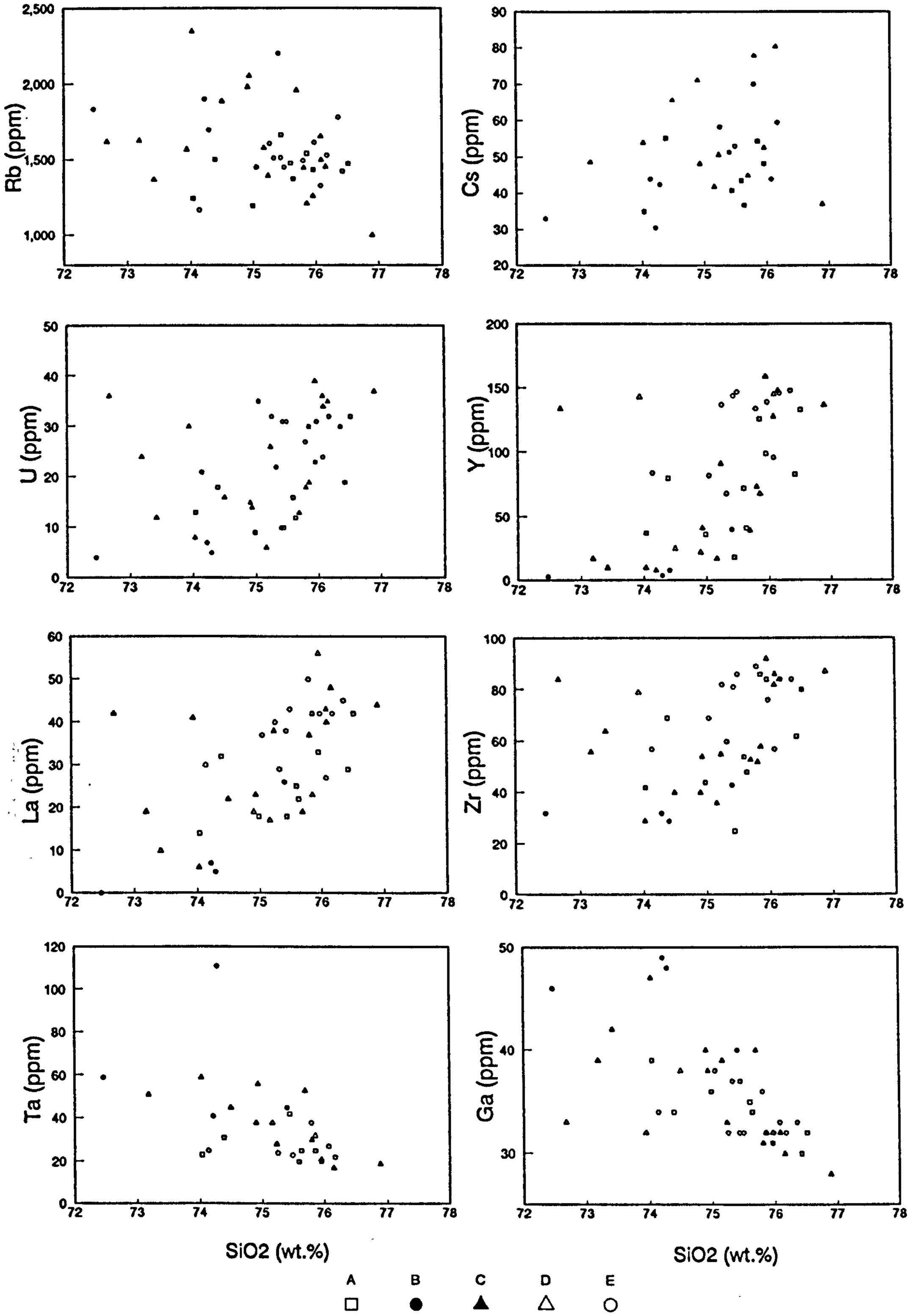

Fig. 4.2 (continued)

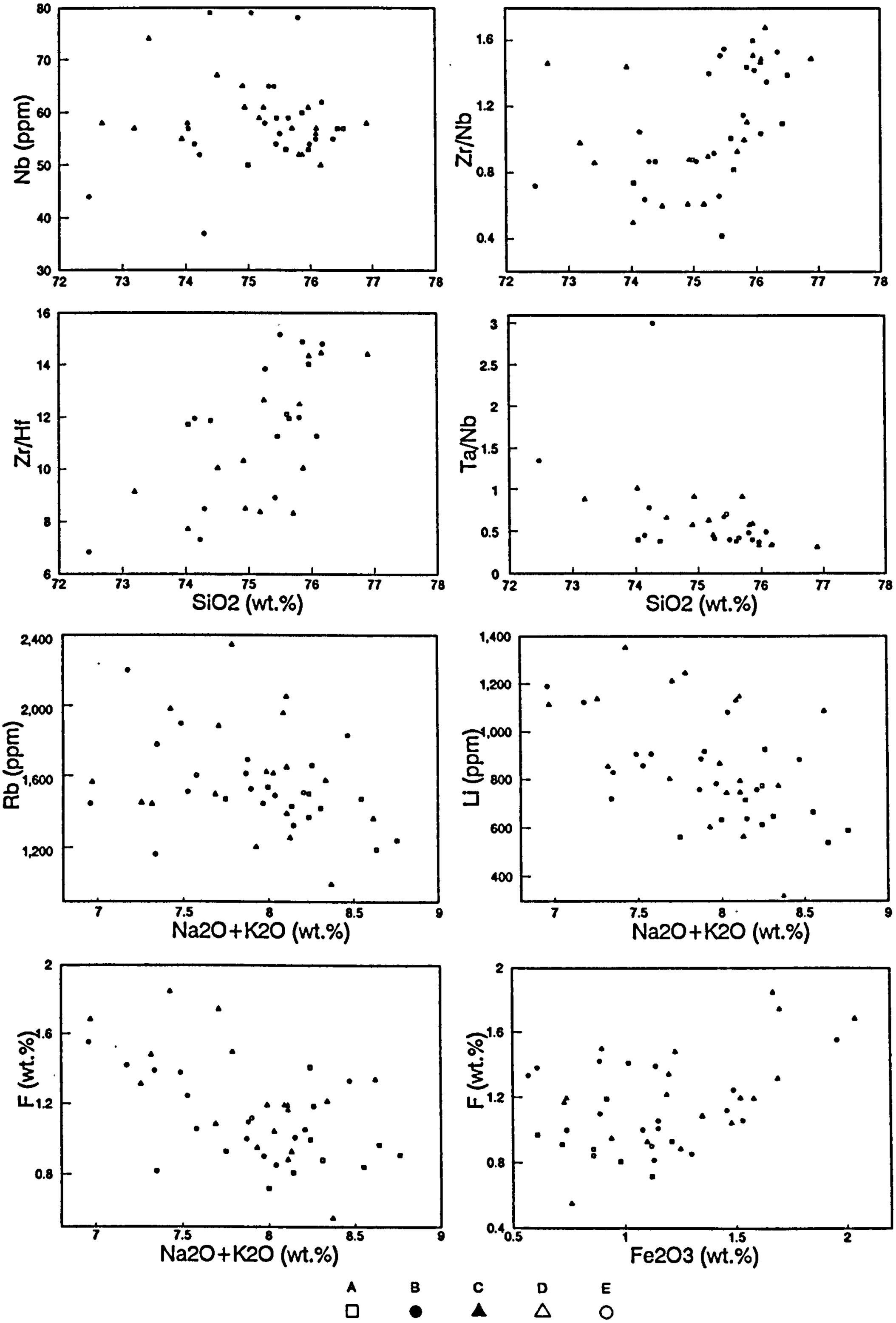

Fig. 4.2 (continued)

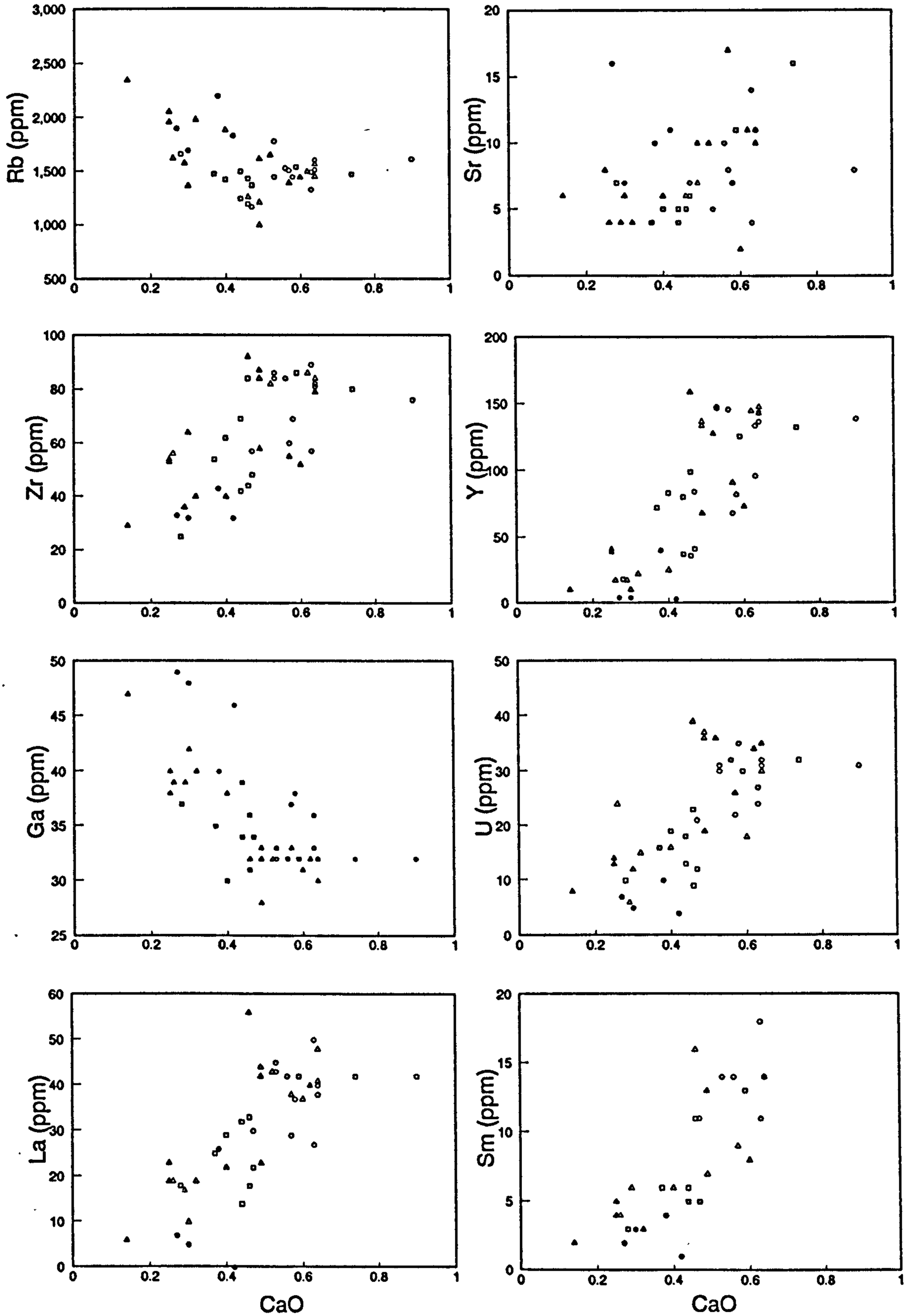

Fig. 4.2 (continued)

The major-element chemistry of the Jianfengling granites is generally comparable to those reported for Cornish topaz Li-mica granites (Stone & Exley, 1984; Manning & Pichavant, 1988), East Kemptville topaz-muscovite leucogranite (Kontak, 1990), Spor Mountain topaz rhyolites (Christiansen *et al.*, 1984), and Macusanite[2] of Peru (London *et al.*, 1988; Pichavant *et al.*, 1987, 1988), particularly the low Ti, Ca and Mg contents (Table 4.3). In both major and trace element chemistry, the Jianfengling granites compare closely to the so-called "low-P subtype topaz granite", particularly the Pleasant Ridge zinnwaldite topaz granites, New Brunswick (Taylor, 1992) (Table 4.3 and Fig.4.3). The total iron contents of Group 2 granites (1.23±0.34 wt.% in Fe_2O_3) are slightly higher than those of Group 1 (0.76±0.13 wt.% in Fe_2O_3), but are comparable with other types of felsic suites (Fig. 4.3). This relative iron enrichment of Group 1 can be attributed to the occurrence of iron-rich biotite. As expected , the redox state of the iron is mostly Fe^{2+} dominant, with FeO/Fe_2O_3 ratios averaging 2.88 ± 2.14, although a few sericitised samples have FeO/Fe_2O_3 ratios ranging from 0.83 to 1.0 (Zhang & Xu, 1990; Appendix VII). The depleted phosphorus contents are normal for felsic suites in general (*e.g.* Waston & Capobianco, 1981) and are consistent with the general variation trend of the Yanshanian granitic rocks in Southeast China (*e.g.* Guiyang Inst. Geochem., 1979; Tu *et al.*, 1980), but are not comparable to many chemically evolved S-type peraluminous igneous rocks, such as the Hercynian granites of Southwest England and the peraluminous rhyolites of the Andean Cordillera which may contain greater than 0.50 wt.% P_2O_5 (*cf.* London, 1992).

The variation in K_2O/Na_2O ratios, and therefore the normative Or/Ab ratios, is very small in both groups (Appendix V), although it appears that the rocks of Group 1 are more albitic than those of Group 2. The K_2O/Na_2O ratios of Group 1 and Group 2 granites range from 0.72 to 2.11 with the averages (± 1σ) being 1.27 (± 0.31) and 1.22 (± 0.35) respectively (Table 4.4). The apparent incompatability between the mineralogy and geochemistry may be attributed to the high Na_2O content of the K-feldspar (microperthite) in the Group 1 granites. Plots of Na_2O and K_2O versus SiO_2 show considerable scatter (Fig. 4.4) for both groups, probably as a result of late stage alteration (*i.e.* sericitisation). The slightly elevated Na concentration and the lower K_2O/Na_2O ratios are not uncommon for felsic igneous suites. Comparable enrichment of sodium is also found in other volatile-enriched felsic suites (*e.g.* Kovalenko, 1977; Kovalenko & Kovalenko, 1984; Manning,1982; Christiansen *et al.*, 1983, 1984, 1986, 1988; London *et al.*, 1988; Pichavant *et al.*, 1988), where it is generally considered to reflect the influence of dissolved volatile species (*i.e.* fluorine in this case) on

[2] Macusanite is named after the Pliocene non-hydrated obsidian glasses from Macusani, SE Peru (Pichavant *et al.*, 1987)

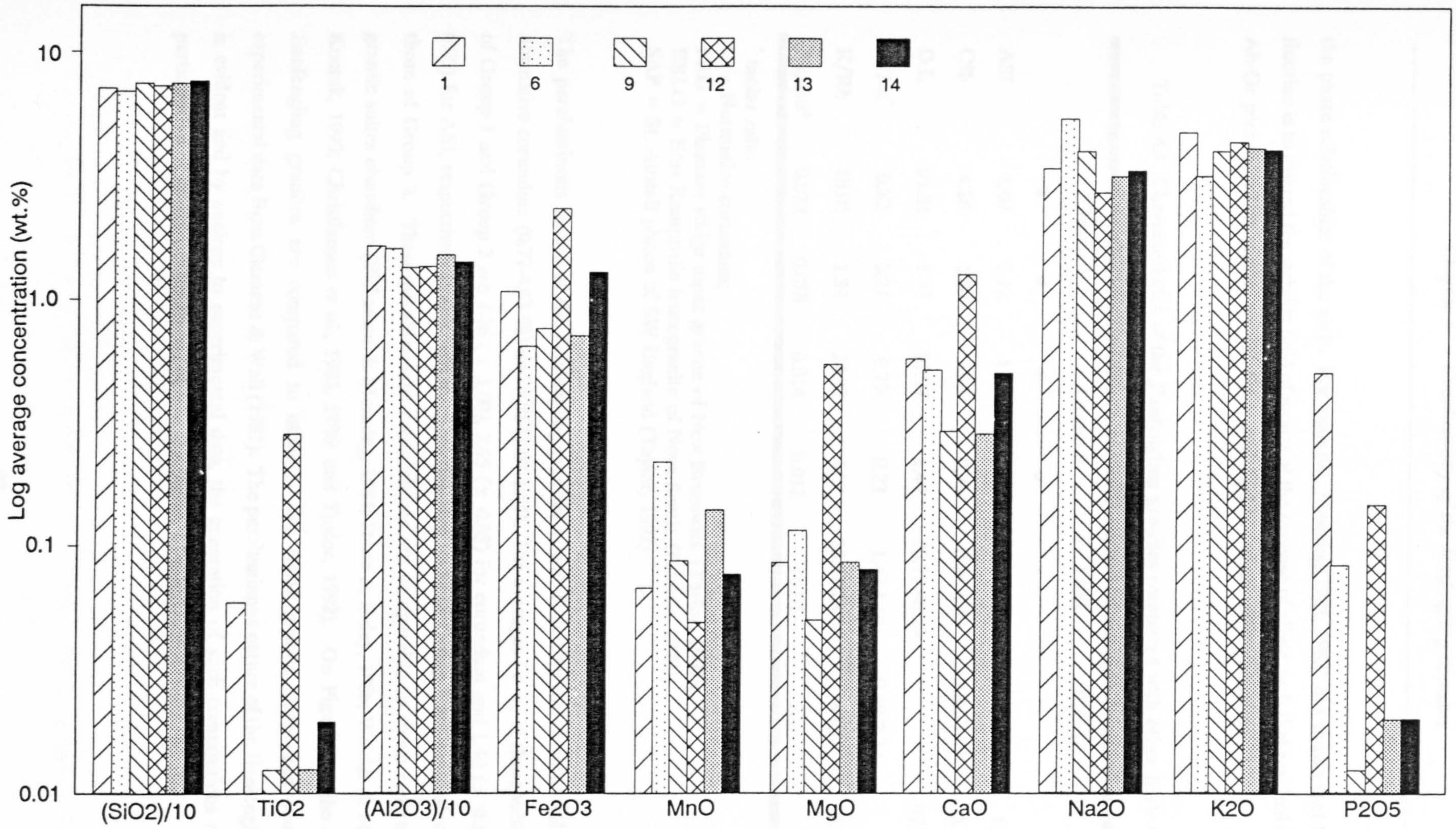

Fig. 4.3 Histograms of the average major-element abundances (in wt.%) of topaz granite of SW England (1), ongonite of Mongolia (6), zinnwaldite-topaz granite of New Brunswick (9), felsic S-type granite (12), and the Jianfengling granites (13, 14). Numbers correspond to those in Table 4.3

the phase relationships of the melt. For example, Manning(1981, 1982) has shown that the effect of fluorine is to expand the stability field of quartz at the expense of albite such that residual melts in Qz-Ab-Or pseudoternary system are relatively enriched in sodium over potassium.

Table 4.4 Characteristics of the Jianfengling granites compared with other felsic suites

	Group 1		Group 2		PRG	EKLG	SAP
	x	σ	x	σ			
ASI	1.40	0.12	1.24	0.09	1.08-1.12	1.13-1.84	1.22-1.42
C%	4.26	1.00	2.65	0.88	0.96-1.59	2.88-7.88	3.53-5.56
D.I.	91.81	1.35	91.97	1.49	95.77-96.29		97.27-97.86
K/Na*	0.82	0.21	0.79	0.23	1.42-1.63	0.48-2.20	
K/Rb	18.05	1.32	24.32	4.27	20.87-24.54	≈40	16.79-34.95
Eu/Eu*	0.032	0.018	0.014	0.012	<0.01	0.2	≈1

* molar ratio
C = Normative corundum;
PRG = Pleasant Ridge topaz granite of New Brunswick (Taylor, 1992);
EKLG = East Kemptville leucogranite of Nova Scotia (Kontak, 1990);
SAP = St. Austell pluton of SW England (Taylor, 1992)

The peraluminous nature of the Jianfengling granites is manifested by the elevated values of both normative corundum (0.77-4.63 %) and ASI (1.07-1.54). The averages (± σ) of these values for rocks of Group 1 and Group 2 are 4.26 (± 1.00), 2.65 (± 0.88) for corundum and 1.40 (± 0.12), 1.24 (± 0.09) for ASI, respectively (Table 4.4), emphasising that rocks of Group 1 are more aluminous than those of Group 2. These peraluminous compositions are comparable to those reported in topaz granite suites elsewhere (Pichavant & Manning, 1984; Stone & Exley, 1986; Weider & Martin, 1987; Kontak, 1990; Christiansen *et al.*, 1983, 1986; and Taylor, 1992). On Figure 4.5, the data of the Jianfengling granites are compared to other similar topaz granite suites and some relevant experimental data from Clemens & Wall (1981). The peraluminous nature of the Jianfengling granites is evident and by analogy to experimental data, the generation of such compositions requires the participation of strong peraluminous phases (*i.e.* topaz, Li-mica).

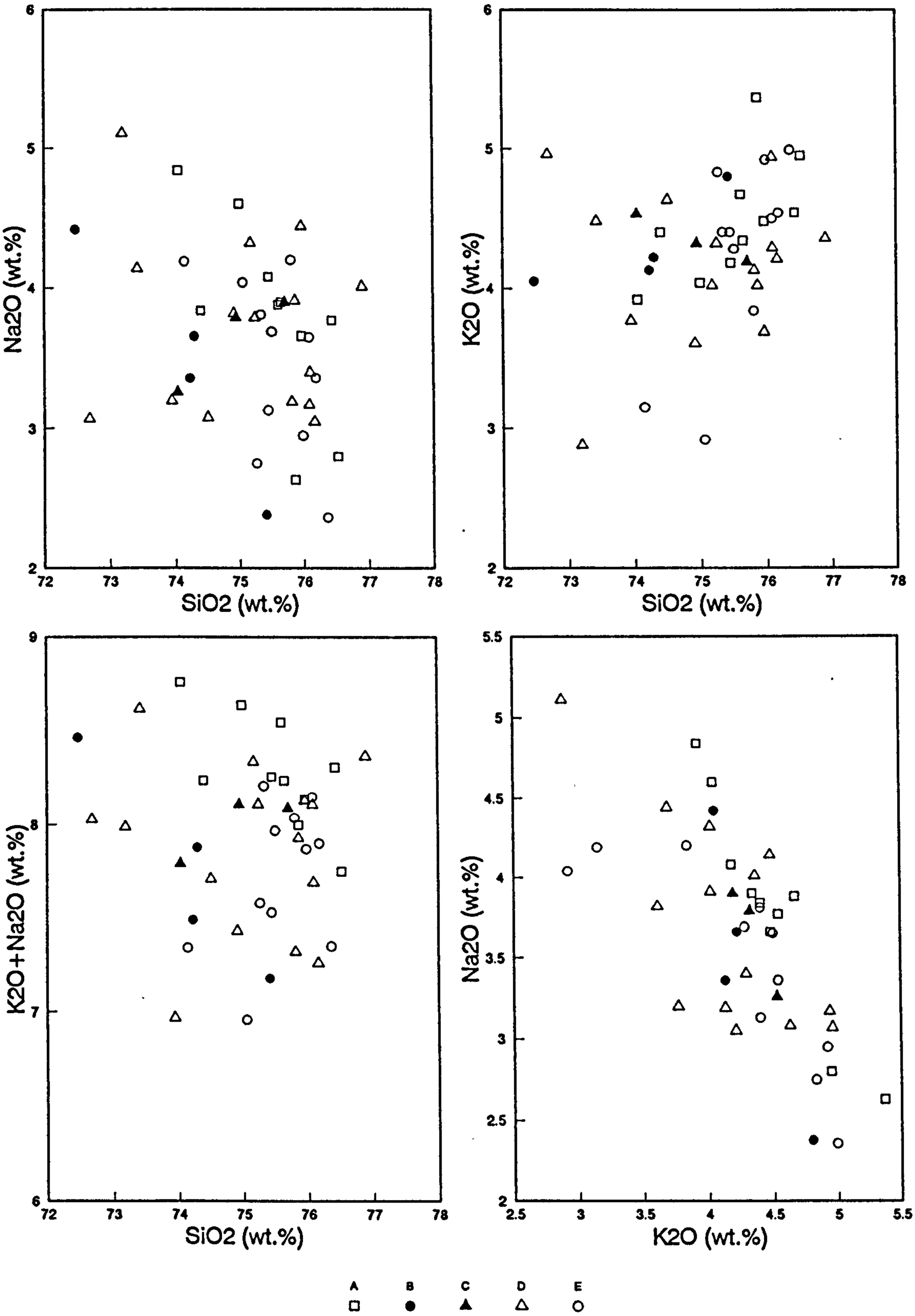

Fig. 4.4 SiO2, K2O and Na2O variation diagrams for the Jianfengling granites

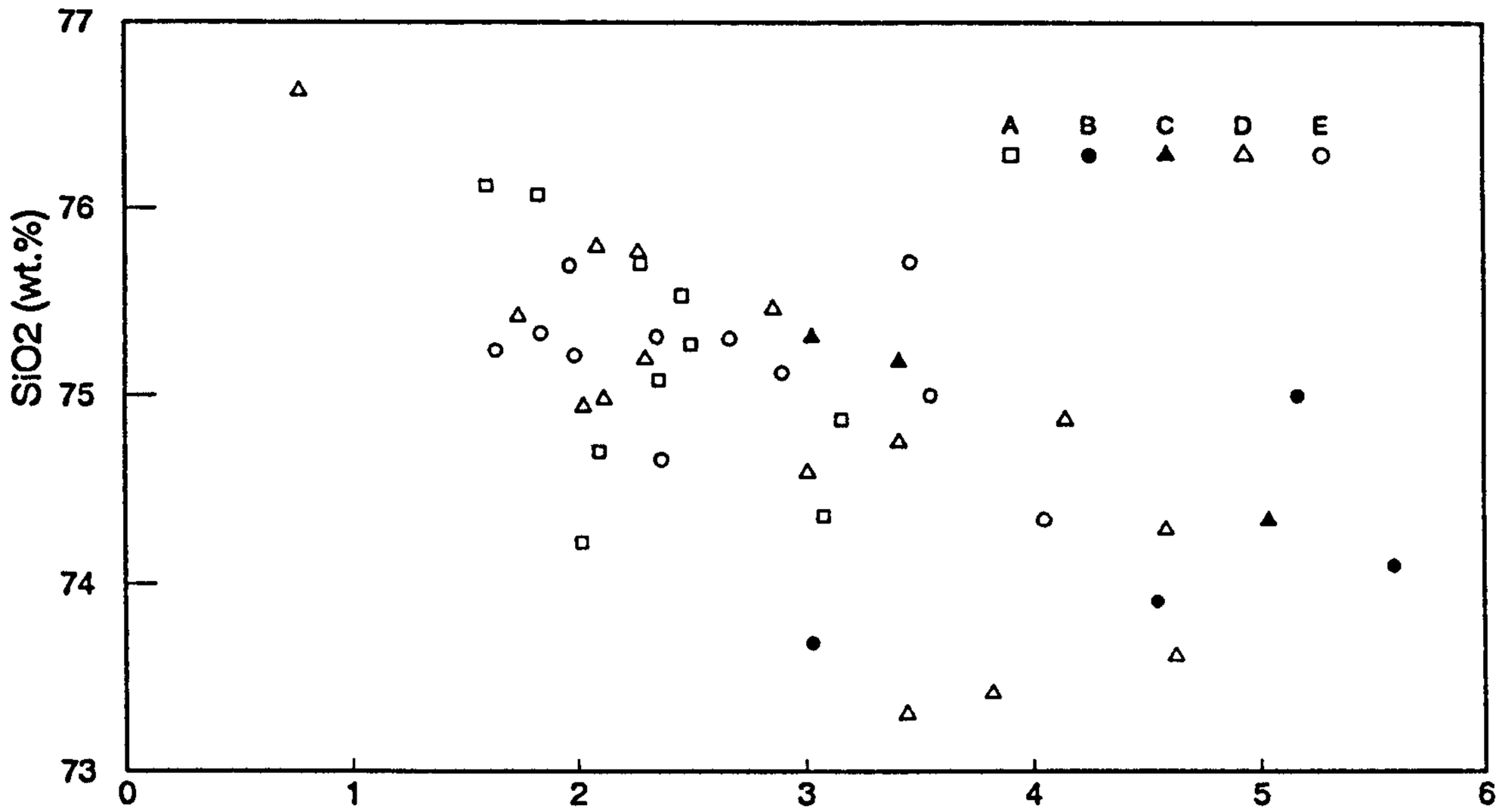

Fig. 4.5 Plot of SiO2 versus normative corundum for the Jianfengling granites compared to other felsic suites

(1) from Clemens and Wall, 1981;
(2) from Christiansen et al., 1983;
(3) from Pichavant et al., 1988.

A high fluorine content is one of the major characteristics of the Jianfengling granites. The averages (± σ) for the two groups are 1.30 (± 0.14) wt.% and 1.10 (± 0.18) wt.%, respectively, but there are considerable variations (between 1.10 to 2.75 wt.% and 0.71 to 1.85 wt.%, respectively), with the altered rocks having the highest fluorine contents (such as sample CK3-22, Appendix V). Compared to the abundance of fluorine in felsic suites in general (Bailey, 1977), the Jianfengling granites have similar concentrations to the zinnwaldite topaz granite of southern New Brunswick (Taylor, 1992), the topaz granite of SW England (Manning & Pichavant, 1988), ongonites of Mongolia (Kovalenko & Kovalenko, 1984), and Macusanite of Peru (Pichavant *et al.*, 1987, 1988; London *et al.*, 1988; Table 4.3 and Fig. 4.6). The enrichment of fluorine in highly evolved peraluminous felsic igneous rocks is generally considered to be due to the high fluorine affinity to the melt during late-stage differentiation (*cf.* Manning, 1981, 1982; Manning & Pichavant, 1983; Kovalenko, 1977; Weider & Martin, 1987; Webster, 1990; Webster *et al.*, 1987; Bailey, 1977; London, 1987, 1988; Kosals, 1976; Foley *et al.*, 1986; Dingwell, 1985; Dingwell & Scarfe, 1985). However, in this case, at least part of the fluorine enrichment might be attributed to late- and post-magmatic alteration, as sericitisation of feldspars and topaz is clearly evident in some of the samples determined.

The normative mineralogy of the Jianfengling granites is dominated by quartz, albite and orthoclase (with a combined total content over 90 vol.%), while anorthite is only 0.63-4.50 vol.%, and corundum and hypersthene account for 2-7 vol.%. These granites are compositionally similar to the haplogranite system (*cf.* Tuttle and Bowen, 1958). Comparison of the normative proportions of Q (quartz), Ab (albite) and Or (orthoclase) for the Jianfengling granites (Fig. 4.7a) to various polybaric cotectics in the H_2O- and F-bearing haplogranite systems is shown in Figure 4.7b. Although there is considerable scatter for the whole data set of the Jianfengling granites, the data form a rough trend parallel to the low-pressure cotectic at 0.5 kbar to 2 kbar for the haplogranite system (Luth, 1976). The averages of these granites plot near the 1 kbar cotectic of the F-rich system as determined by Manning (1981).

In view of the well-documented relationship between normative mineral composition and volatile content (*i.e.* F) in felsic igneous rocks, the fluorine contents of the Jianfengling granites are shown in Figure 4.6a. There appears to be no obvious correlation between proximity of samples to the albite apex of the triangular diagram and F contents, although the samples collectively define a trend towards the albite corner. Also shown in Figure 4.6b are other F-rich suites, *viz.* the Yichun lepidolite granite, SE China (Schwartz, 1992), the Macusanite glass, Peru (Pichavant *et al.* 1988), the Taylor Creek rhyolite, USA (Webster & Duffield, 1991), topaz rhyolites of the SW United States (Christiansen *et al.* 1984), ongonite of Mongolia (in Pichavant & Manning, 1984), Cornish topaz granite (Stone &

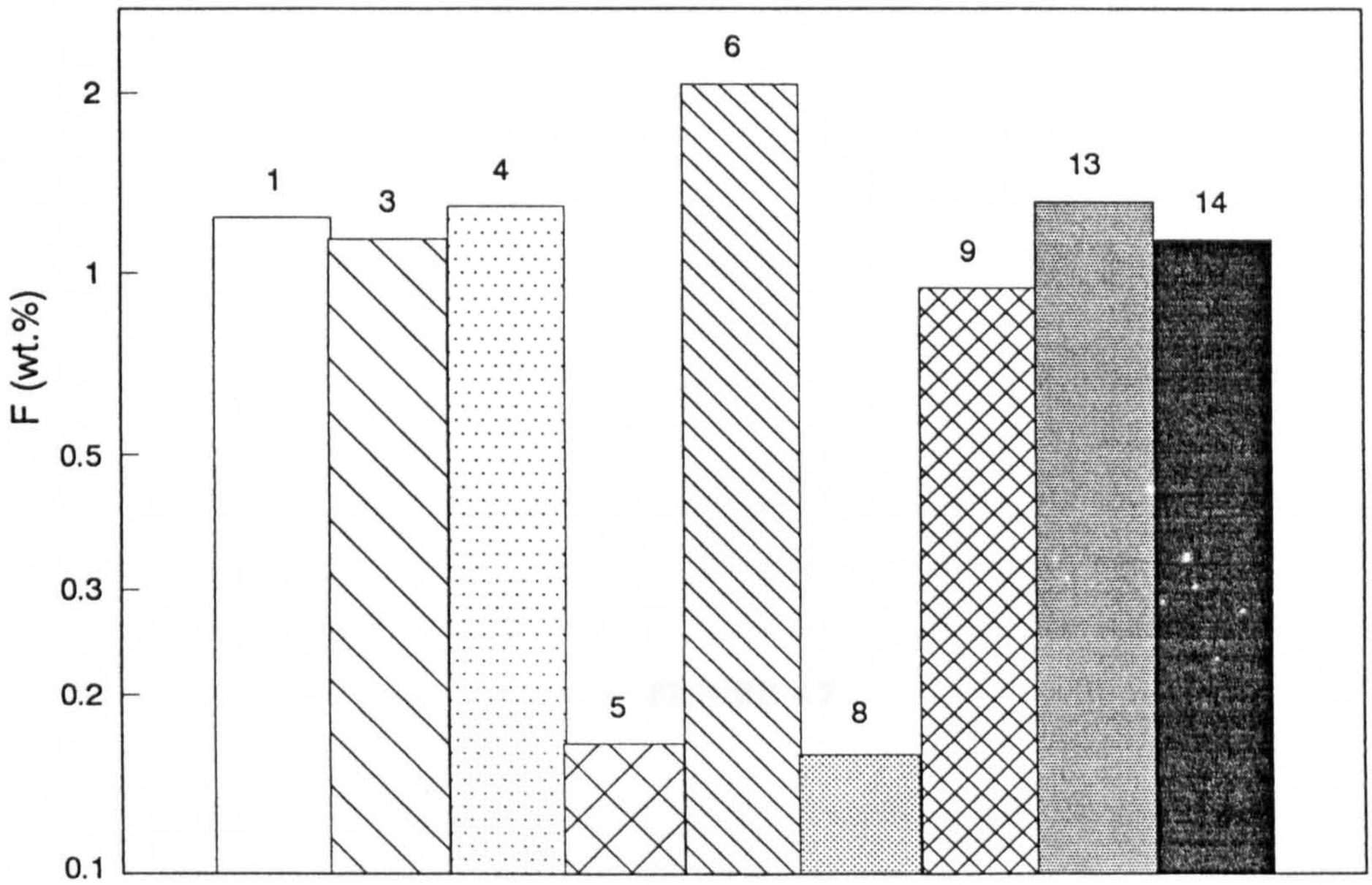

Fig. 4.6 Comparison of fluorine contents of Cornish topaz granite (1), topaz rhyolite (3), macusanite (4), glass inclusion in quartz phenocrysts of rhyolite (5), ongonite (6), Xihuashan leucogranite of SE China (8), zinnwaldite topaz granite of Canada (9), and the Jianfengling granites (Group 1 - 13, Group 2 - 14). Numbers correspond to those in Table 4.3.

Exley, 1984), and the East Kemptville leucogranite of Nova Scotia (Kontak, 1990). Although there is considerable variability among these suites, they do coincide roughly with the various cotectics at different pressures.

The Jianfengling granites are notably enriched in many of the trace-elements which are considered indicative of specialised granites (ongonites; *cf.* Tischendorf, 1977). By comparison with even the most highly fractionated samples of I- and S-type granites with similar contents of SiO_2 (*cf.* Whalen *et al.*, 1987), both groups of the Jianfengling granites contain elevated alkali metals (averages of Group 1 and Group 2 respectively, in ppm) Li (1047, 808), Rb (1999, 1480), Cs(43, 53) and high valence cations Y(20, 94), U(15, 26), Sn(167, 97), W(22, 80), Nb(53, 59), Ta(60, 29), and Ga(44, 34); conversely, they are depleted in Ba(16, 18), Sr(9, 8), Zr(39, 67), V (<5), and Ni(11, 11). Many of these enrichments and depletions are extreme: for example, using the mean abundances for the samples of intrusion A

FIGURE 4.7

Fig. 4.7 Normative Q (quartz) - A (alkali feldspar) - P (plagioclase) diagrams for the Jianfengling granites and other fluorine-rich felsic suites

a. QAP diagram for representative samples from the Jianfengling granites [numbers in brackets refer to wt.% F (*cf.* Appendix IV); * denotes samples with relatively stronger alteration]. In order to avoid overcrowding in the diagram, single samples have been chosen to represent groups of samples with similar QAP compositions.

b. QAP diagram comparing the field for the Jianfengling granites to other fluorine-rich felsic suites (sources of data given below) and experimentally determined cotectics for 1, 2 and 4 wt.% F at 1 kb (●, Manning, 1981) and F-free cotectics at 0.5, 1, 3 and 5 kb P_{H2O} (○, Luth, 1976).

Lepidolite granite, Yichun, SE China (Schwartz, 1992);

Macusanite glass, Peru (Pichavant *et al.*, 1987);

Ongonite, Mongolia (in Pichavant & Manning, 1984);

Topaz granite, SW England (Pichavant & Manning, 1984);

Taylor Creek rhyolite, USA (Webster & Duffield, 1991);

Topaz rhyolits, SW United States (Christiansen *et al.*, 1983);

Beauvoir leucogranite, France (Pichavant *et al.*, 1987);

East Kemptville topaz-muscovite leucogranite, Nova Scotia (Kontak, 1990).

a

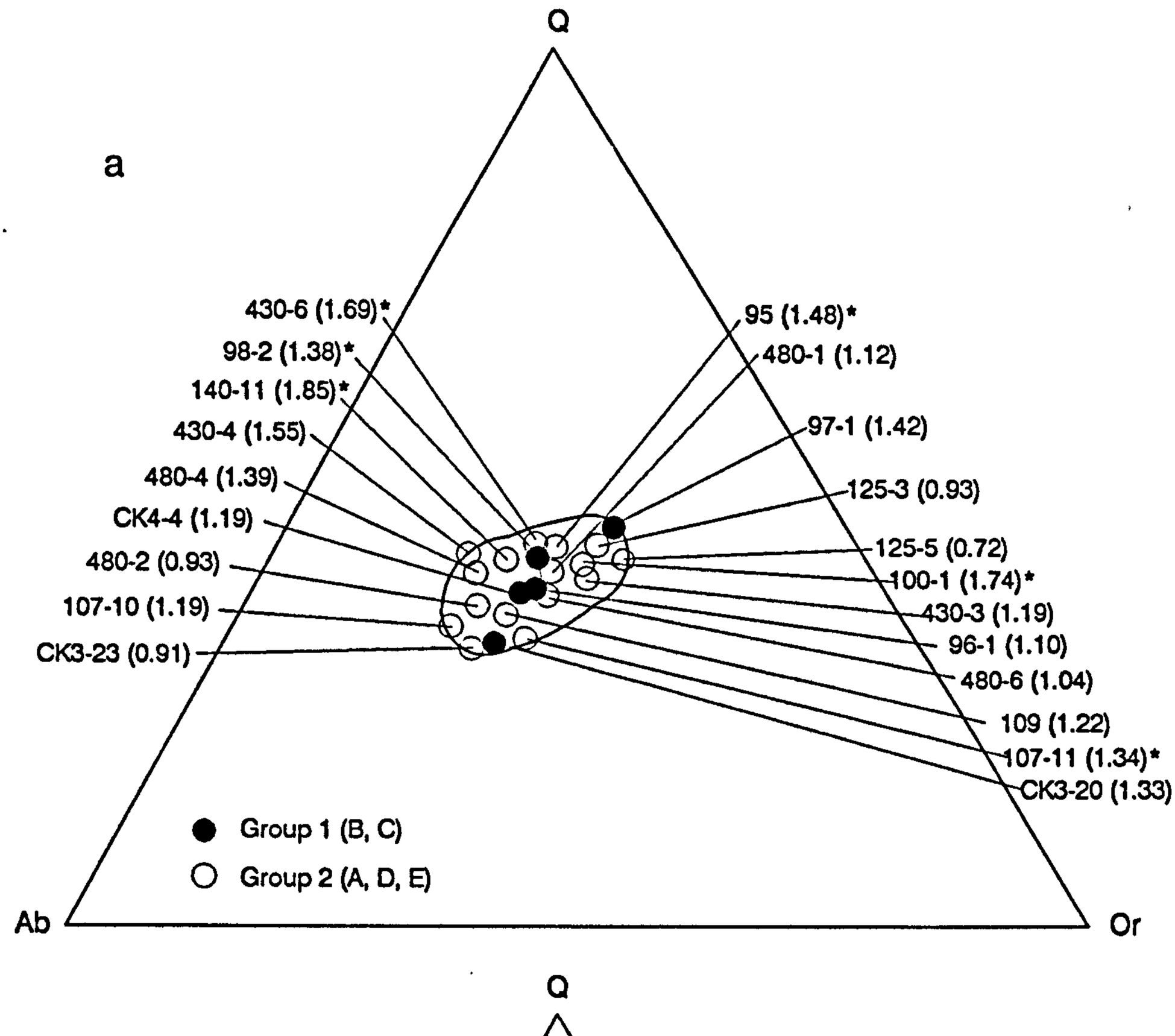
Q
430-6 (1.69)*
98-2 (1.38)*
140-11 (1.85)*
430-4 (1.55)
480-4 (1.39)
CK4-4 (1.19)
480-2 (0.93)
107-10 (1.19)
CK3-23 (0.91)
95 (1.48)*
480-1 (1.12)
97-1 (1.42)
125-3 (0.93)
125-5 (0.72)
100-1 (1.74)*
430-3 (1.19)
96-1 (1.10)
480-6 (1.04)
109 (1.22)
107-11 (1.34)*
CK3-20 (1.33)
Group 1 (B, C)
Group 2 (A, D, E)
Ab
Or

Q

b

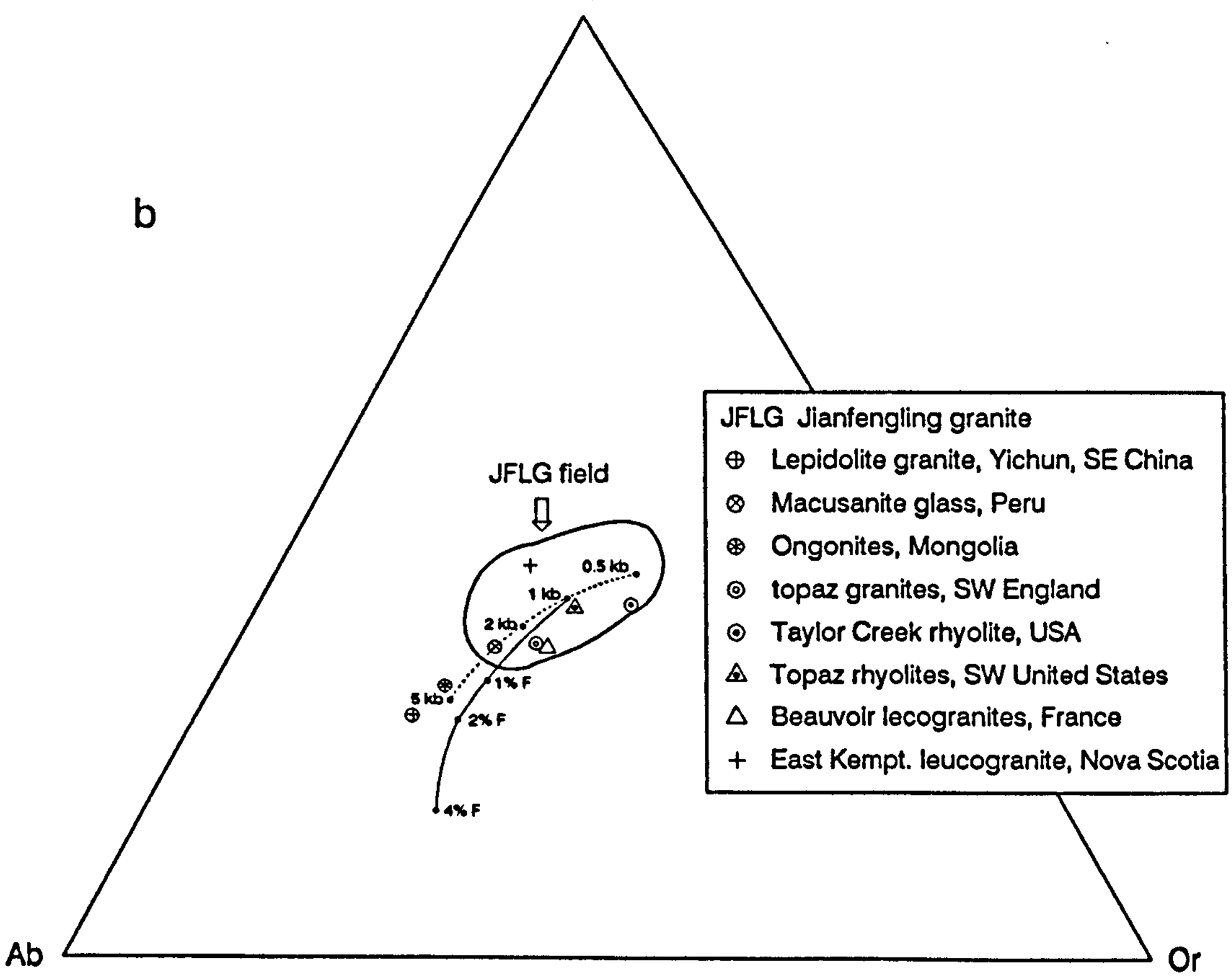
JFLG field
0.5 kb
1 kb
2 kb
5 kb
1% F
2% F
4% F
JFLG Jianfengling granite
⊕ Lepidolite granite, Yichun, SE China
⊗ Macusanite glass, Peru
⊛ Ongonites, Mongolia
⊙ topaz granites, SW England
⊙ Taylor Creek rhyolite, USA
△ Topaz rhyolites, SW United States
△ Beauvoir lecogranites, France
+ East Kempt. leucogranite, Nova Scotia
Ab
Or

of the Jianfengling granites in Table 4.1, the contents of Rb, Cs, Ta and Nb are from three to ten times as great as those of aluminous A-type granites, and the depletions in Ba, Sr and Zr are from eight to thirty times lower (comparative data from Collins *et al.*, 1982); the Rb, U, Nb and Ga concentrations are from three to five times greater than those of felsic S-type granites (comparative data from Whalen *et al.*, 1987). The enrichments and depletions of trace elements (plus F and P_2O_5) from both groups of the Jianfengling granites against the felsic S-type granites are illustrated in Figure 4.8. Various binary trace-element plots are presented in Figure 4.9 to show the relationship of the different elements. In these diagrams, most of the elements show linear correlations and two groups are distinguished.

Normalised geochemical patterns for the averages of both groups together with other comparable suites are given in Figure 4.10. Two normalising factors are chosen for different purposes. In Figure 4.10a, the averages of Group 2 are normalised to the averages of Group 1 to show the relative enrichment and depletion of trace-elements between the two groups, while the compositions of "Lower-Crust" (Taylor & McClennan, 1985) are used as normalising factors in Figure 4.10b, c, d, e & f. Together, Li-mica topaz granite of SW England (Stone & Exley, 1984) and topaz leucogranites of Nova Scotia (Kontak, 1990), the macusanite of Peru (London *et al.*, 1988) and the A-type and felsic I- and S-type granites are introduced for comparison. In these diagrams, the elements are listed in an approximate order of increasing incompatibility. It is clearly shown on these diagrams that, relative to Group 2, Group 1 is enriched in F, Li, Rb, Sr, Ta, Ga, and Sn, and is strongly depleted in Ba, W, La, Ce,and Y (Fig.4.10a); both groups have very similar trace elements patterns to the evolved granites from SW England and N America (Fig. 4.10b & c). All those granites are strongly enriched in F, Li, Rb, U, Nb, Ta, Cs, Sn, and W, and depleted in Ba, La, Ce, and Y. The evolved nature of the Jianfengling granites is also indicated by their very low K/Rb ratios (averaging 18 and 24 for Group 1 and Group 2 respectively; Table 4.4), approximating the pegmatite-hydrothermal field of Shaw (1968). In Figure 4.11, the trace elements Li and Rb are plotted against F in the classification diagrams of Taylor *et al.* (1985). These show that the Jianfengling granites compare favourably to the fields outlined for Li-mica granites and demonstrate the nature of extreme enrichment of Rb in these granites. On Rb-Nb and Ta-Nb variation diagrams (Fig. 4.12), the Jianfengling granites possess distinguishing features of the group of subvolcanic, fluorine-rich igneous rocks --- ongonites (*e.g.* Christiansen *et al.*, 1986).

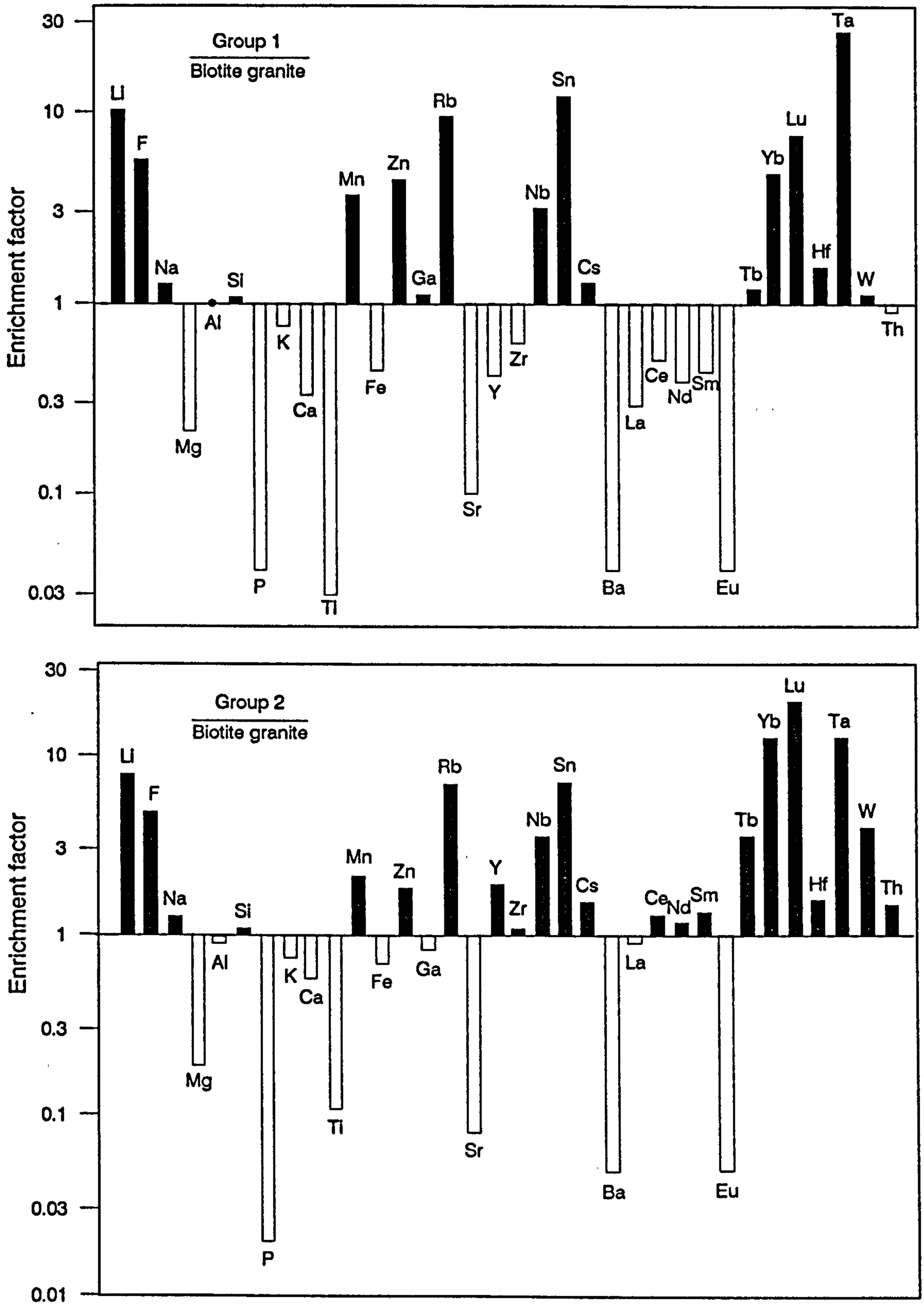

Fig. 4.8 Enrichment factors for 34 elements in the Jianfengling granites compared to a sample of biotite granite from SW England (Alderton et al., 1980; values for Y, Nb, Pb, Zn, Ga, Sn, Ba and Cs are from Stone & Exley, 1986; the value of W is from Alderton & Moore, 1981)

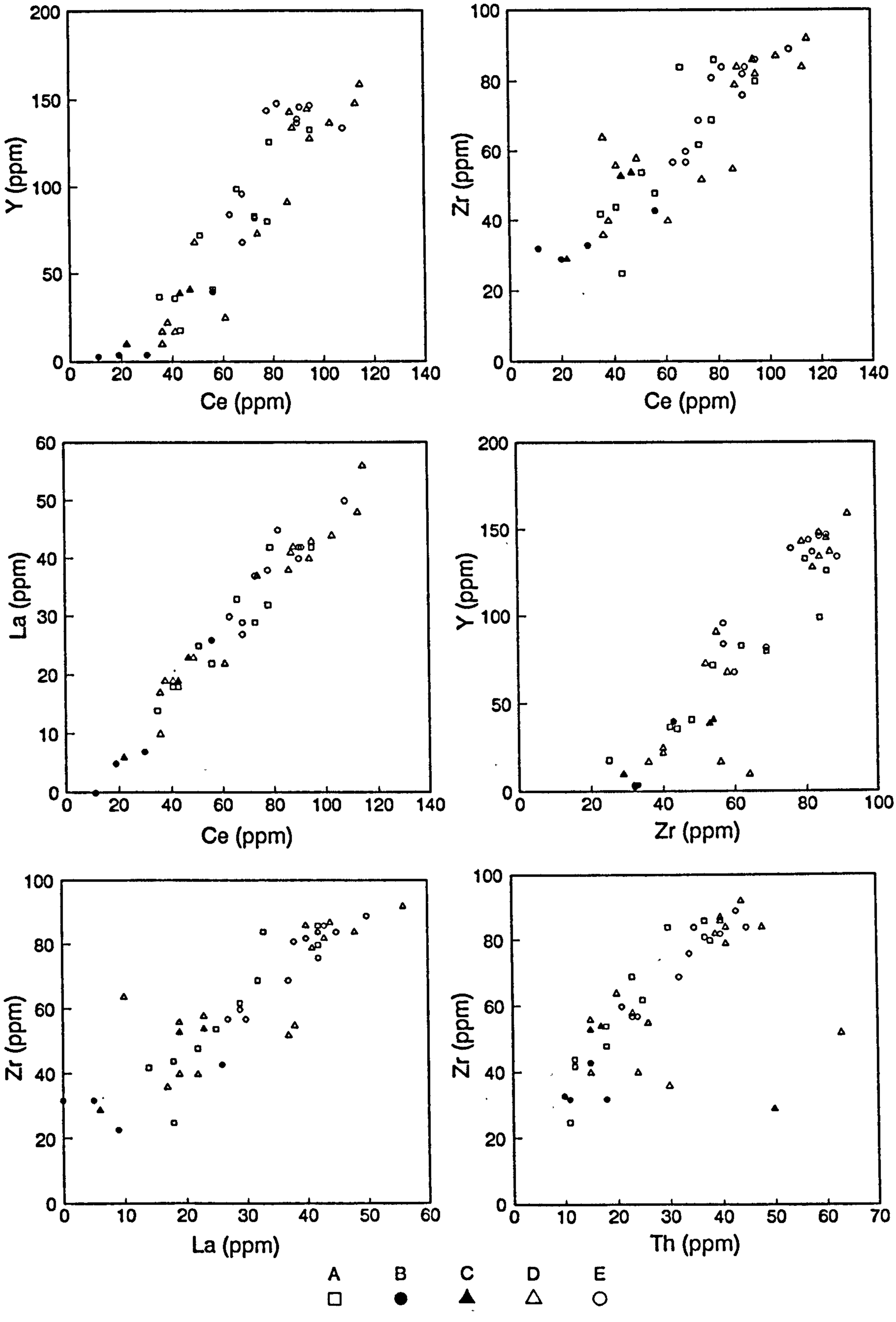

Fig. 4.9 Binary variation diagrams of imcompatible elements of the Jianfengling granites

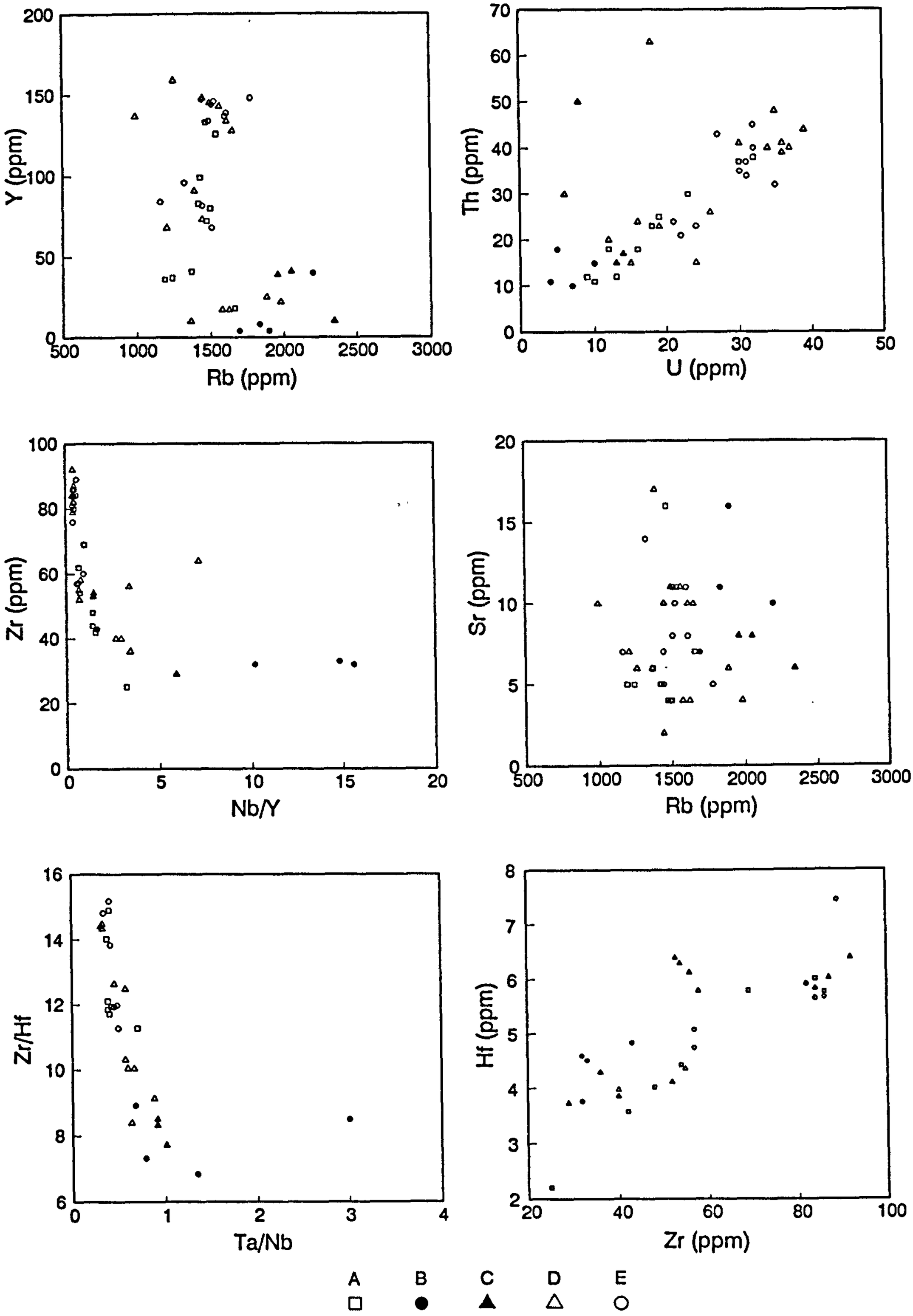

Fig. 4.9 (continued)

FIGURE 4.10

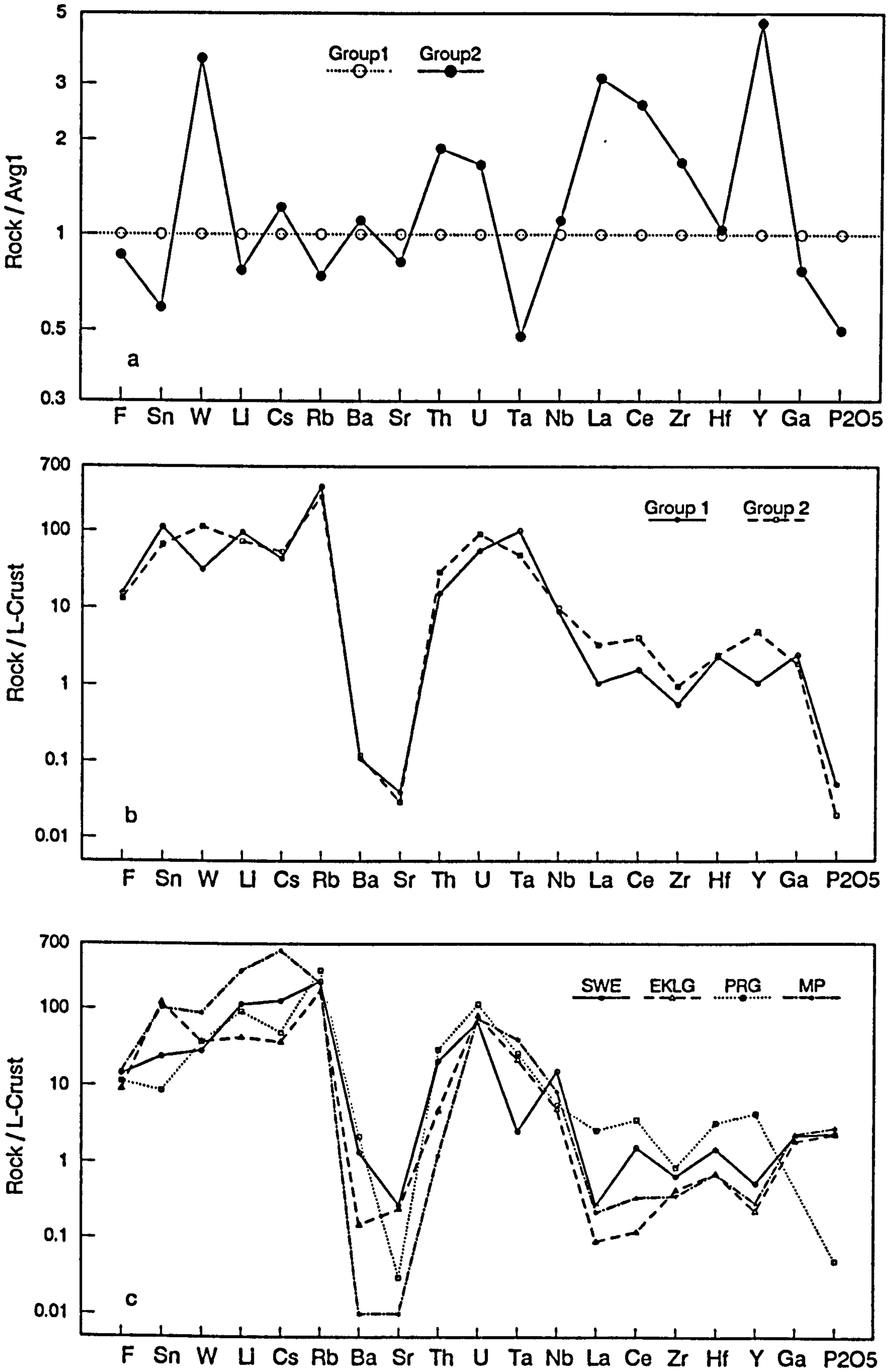
Group1
Group2
Rock / Avg1
5
3
2
1
0.5
0.3
a
F Sn W Li Cs Rb Ba Sr Th U Ta Nb La Ce Zr Hf Y Ga P2O5
Group 1
Group 2
Rock / L-Crust
700
100
10
1
0.1
0.01
b
F Sn W Li Cs Rb Ba Sr Th U Ta Nb La Ce Zr Hf Y Ga P2O5
SWE
EKLG
PRG
MP
Rock / L-Crust
700
100
10
1
0.1
0.01
c
F Sn W Li Cs Rb Ba Sr Th U Ta Nb La Ce Zr Hf Y Ga P2O5

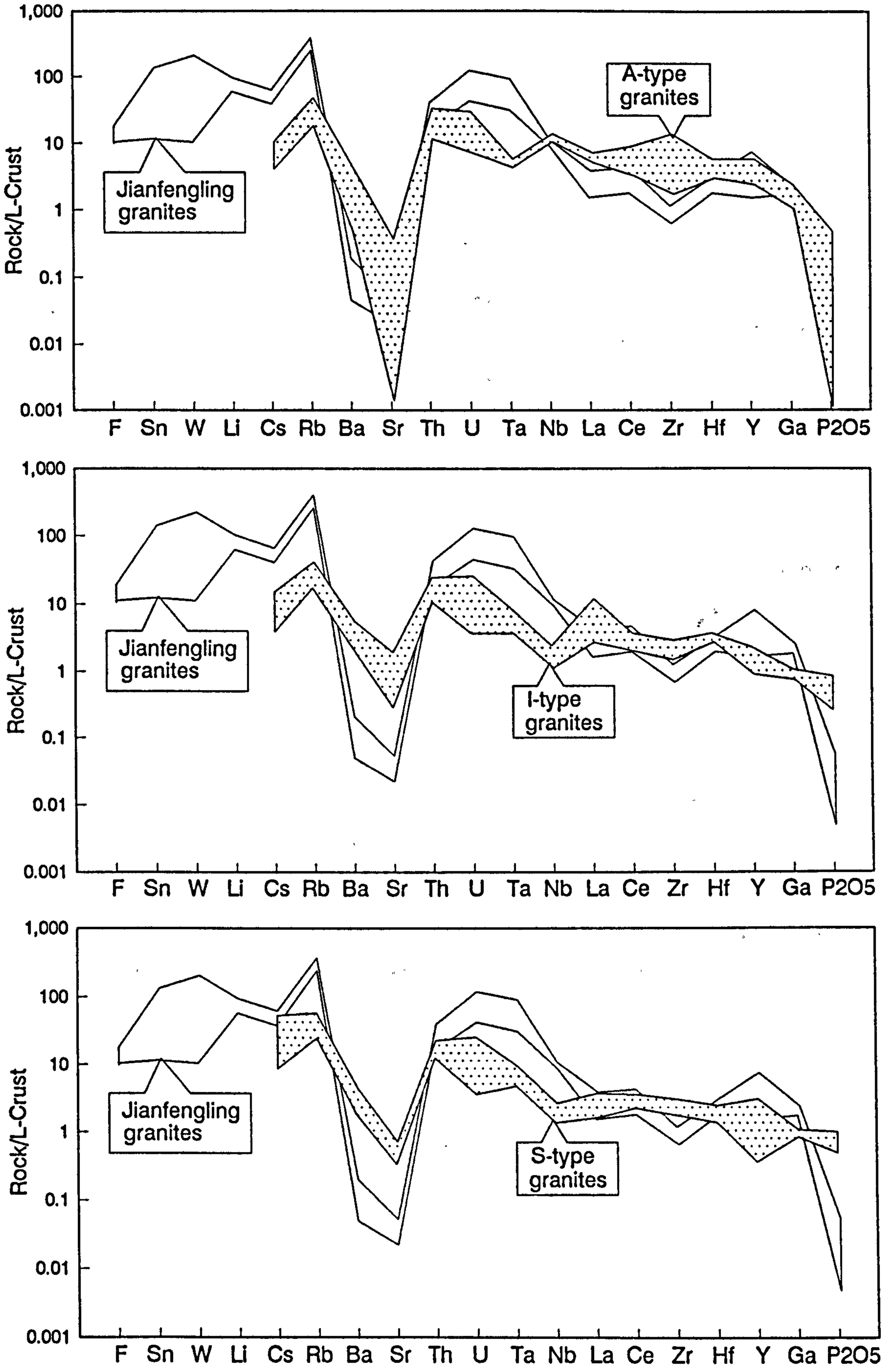
1,000
100
10
1
0.1
0.01
0.001
Rock/L-Crust
Jianfengling granites
A-type granites
I-type granites
S-type granites
F Sn W Li Cs Rb Ba Sr Th U Ta Nb La Ce Zr Hf Y Ga P2O5

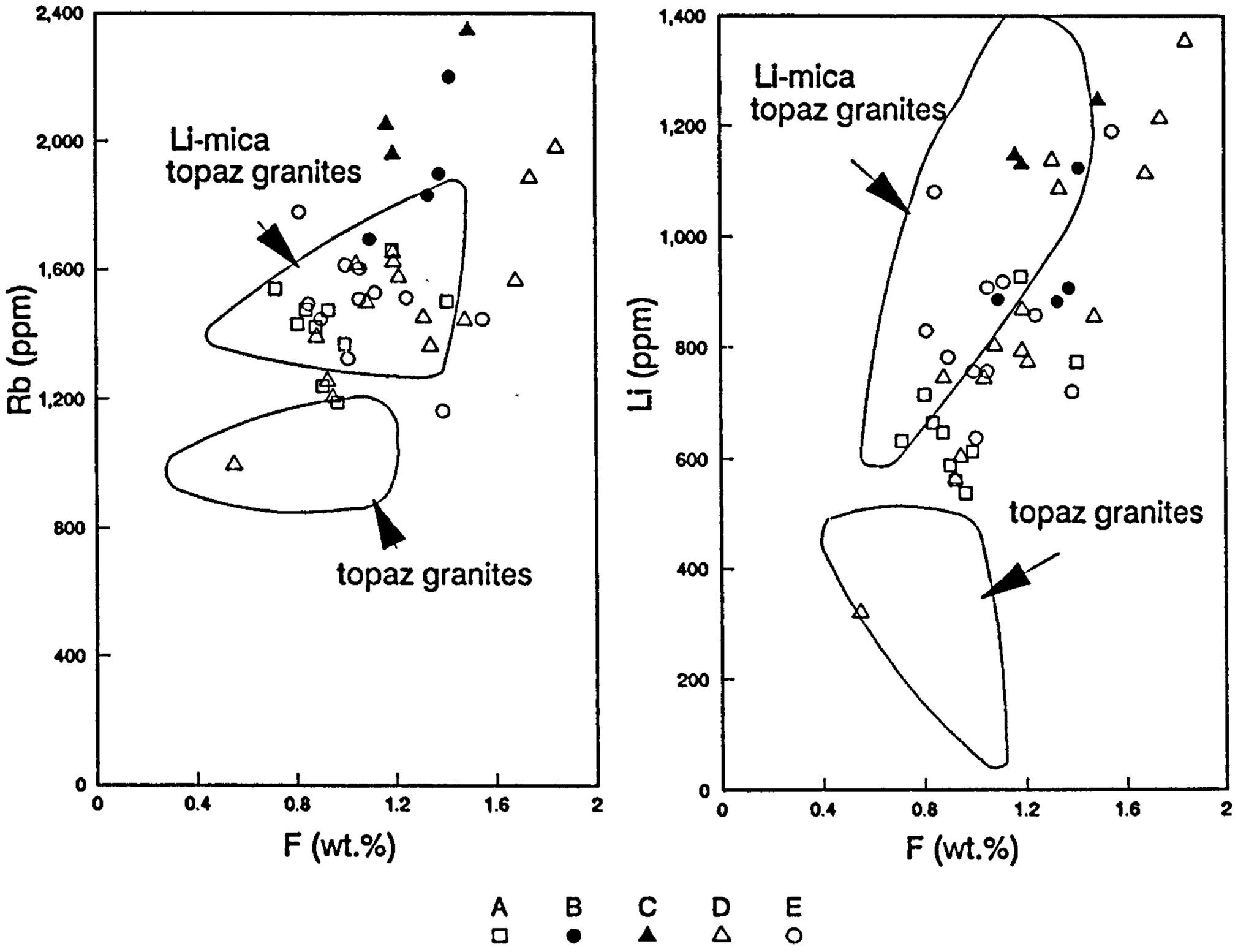

Fig. 4.11 Rb-F and Li-F variation diagrams for the Jianfengling granites. Fields for Li-mica granites and topaz granites are from Taylor et al. (1985)

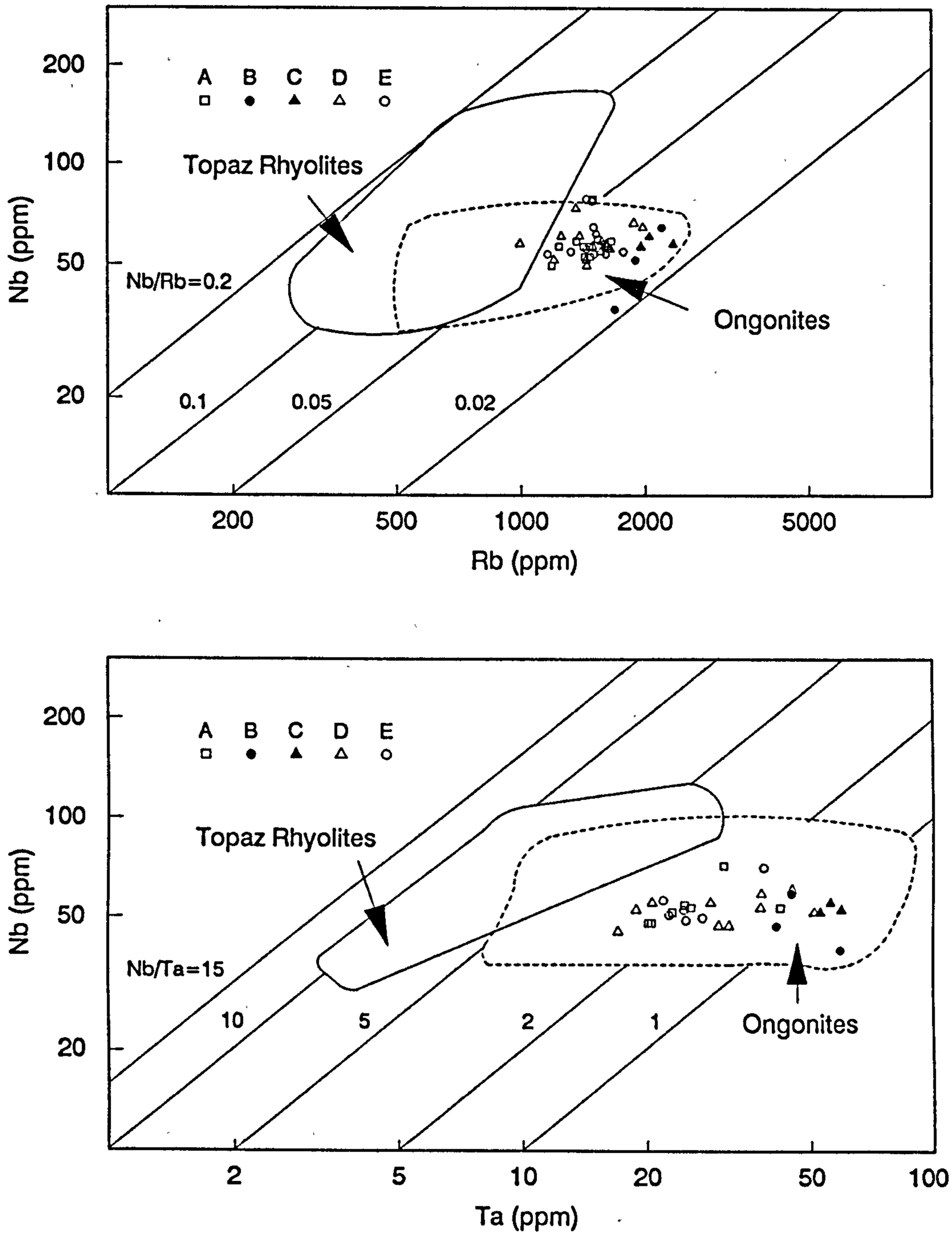

Fig. 4.12 Rb-Nb and Ta-Nb variation diagrams for the Jianfengling granites. Fields for topaz rhyolites and ongonites are from Christiansen et al. (1986)

4.3 RARE-EARTH ELEMENTS (REE) GEOCHEMISTRY

Rare-earth element (REE) data are presented in Appendix VI and Table 4.2, and chondrite-normalised patterns (Nakamura & Masuda, 1973) in Appendix VII and Figure 4.13. Total REE (Σ8REE) contents for the individual samples of the Jianfengling granites range from 32 to 122 ppm and from 93 to 347 ppm for Group 1 and Group 2 respectively. These values show considerable variations both within each group and between samples of the two groups. Generally, samples of Group 2 have much higher (3 to 10 times) REE concentrations (*cf.* Appendix VI). Compared to previous data presented by Zhang & Xu (1989) for samples from the Laiciling granites in the same ore field, the Jianfengling granites agree well; Group 2 is similar to the first stage ($\gamma_5^{2\text{-}2}$) of the Laiciling granites, and Group 1 corresponds to their final stage (γ_5^3).

The most notable feature of the REE data is the overall depletion of all the REEs in rocks of Group 1 relative to that of Group 2. Both groups exhibit sub-parallel, gullwing-shaped chondrite-normalized REE patterns, although clearly separated, suggesting a common genetic association. The average chondritic patterns for the Jianfengling granites are slightly fractionated [$(La/Yb)_N$ = 1.28 and 1.55 for Group 1 and Group 2 respectively], while stronger fractionation exists in LREEs [$(La/Sm)_N$ = 2.26 and 2.49, respectively]. These patterns have distinct deep negative Eu anomalies ($Eu/Eu^* < 0.07$). All the rare-earth elements, together with the total REEs, have a strong positive correlation with the CaO contents (Fig.4.14). According to Chen (1987), the main REEs carrier in the Jianfengling granites is biotite (the total REE content reaching 929 ppm); plagioclase (albite) and K-feldspar follow in declining order. Analytical SEM (with back scatter) revealed that REEs probably occur mainly as mineral accessory inclusions within the biotite. This may explain the differences of total REE contents between the two groups, as the biotite content in Group 1 is much less than in Group 2. It may also provide an explanation for the large variations of REE concentrations among samples within each group, as the contents of the accessory minerals in individual samples may vary considerably. The large negative Eu anomaly can be attributed to either the high degree of differentiation and/or metasomatic alteration. However, as shown by Corey & Chatterjee (1990), there is a strong positive correlation between the degree of K-feldspathisation and Eu enrichment. After detailed studies on samples of the Dartmoor granite, SW England, Ward *et al.* (1991) concluded that "*during pervasive sericitisation, chloritisation and tourmalinisation, REEs were mobilised over distance of centimetres only and into secondary alteration products, ... Whole-rock REE abundances were not affected.*"

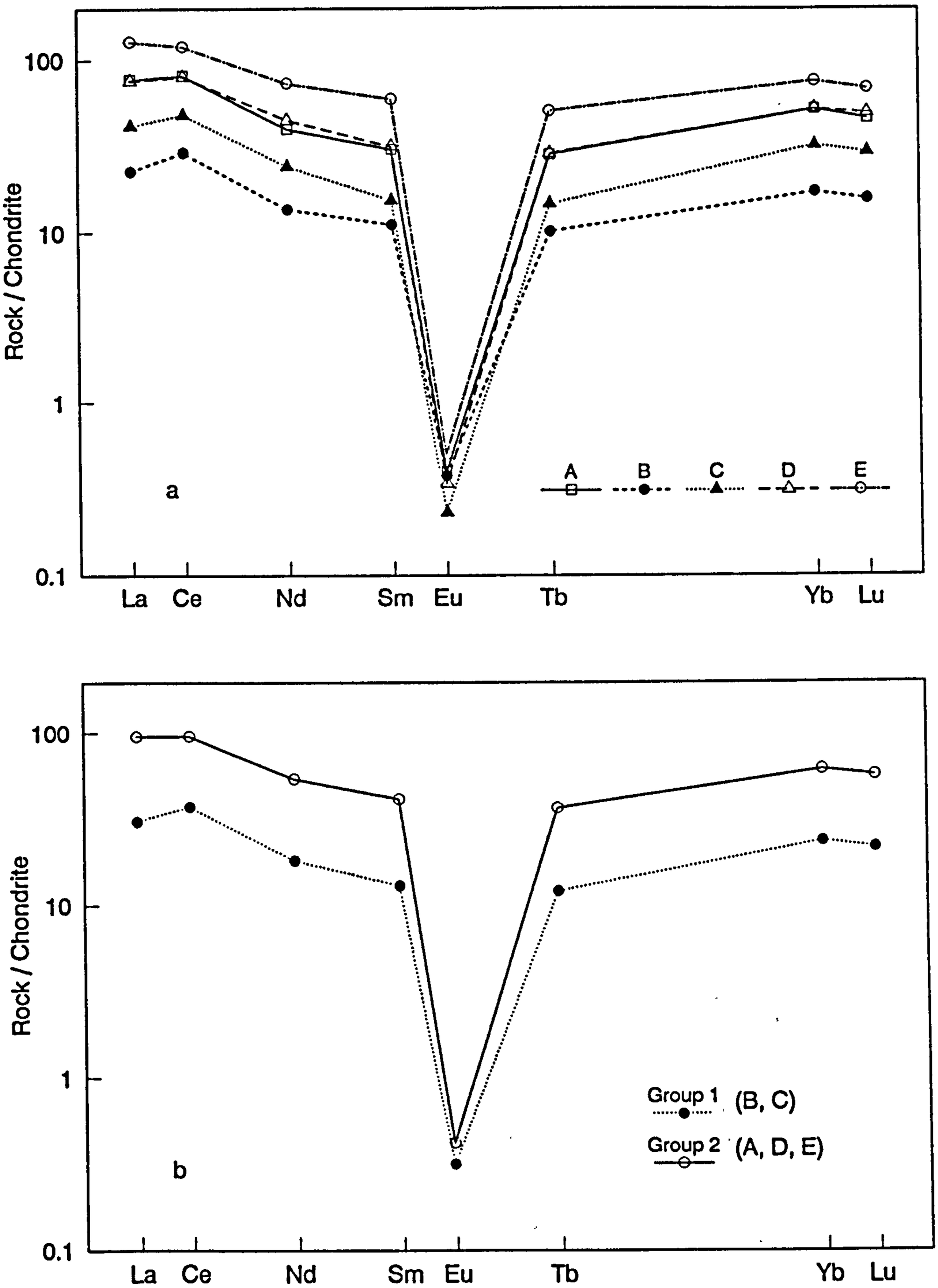

Fig.4.12 Chondrite-normalised REE patterns for the Jianfengling granites (data are obtained using INAA)

a - averages for the different intrusions

b - averages for the two groups

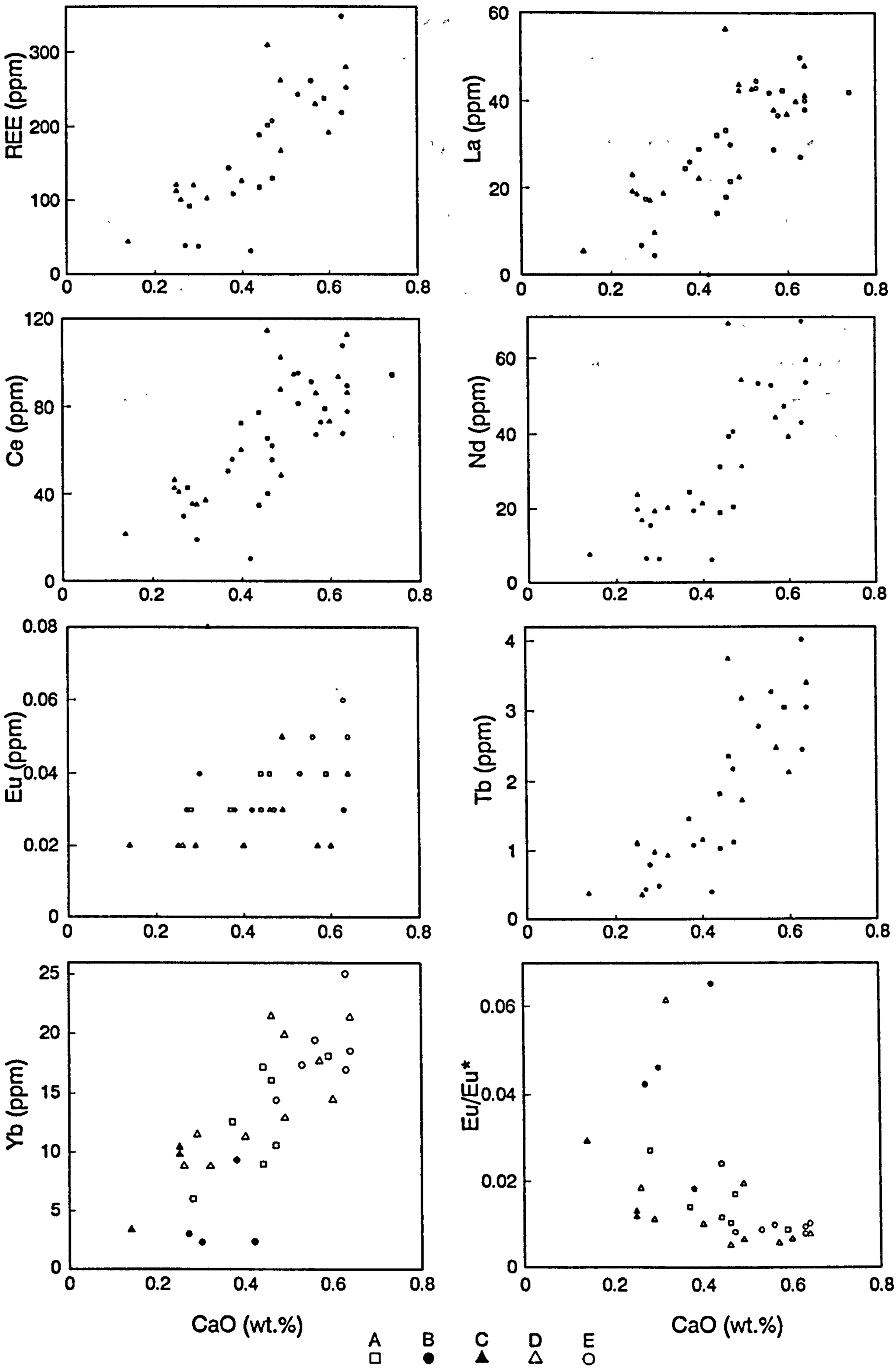

Fig. 4.14 Binary variation diagrams of REEs versus CaO

Comparisons of the REE data from the Jianfengling granites with other felsic F-rich suites are made in Figure 4.15. The following features are readily apparent from an inspection of these figures: (1) The REE patterns of the Jianfengling granites are similar to those of volatile-rich felsic volcanic rocks, particularly the topaz rhyolite (Christiansen *et al.*, 1984, 1986); (2) An overall depletion of REEs in the Jianfengling granites, especially the rocks of Group 1, compared to the topaz rhyolite, and an overall enrichment of REEs compared to the Macusani obsidian (Pichavant *et al.*, 1987) are clearly evident; (3) The Jianfengling granites compare closely with the "low-P" subtype topaz granite (the Pleasant Ridge zinnwaldite-topaz granite, southern New Brunswick; Taylor, 1992), but are markedly different from the "high-P" subtype topaz granite (the St Austell topaz granite, SW England; Taylor, 1992).

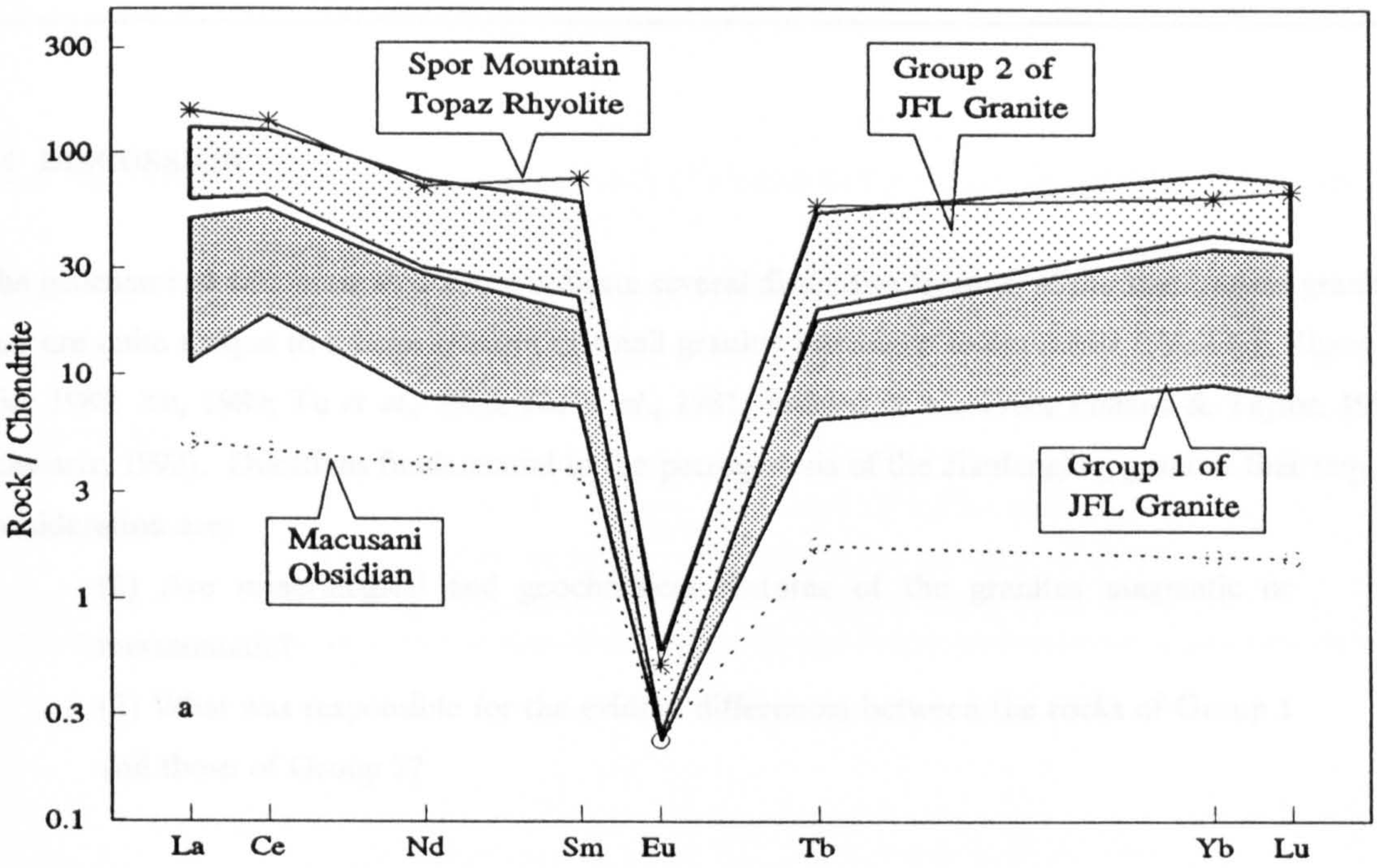

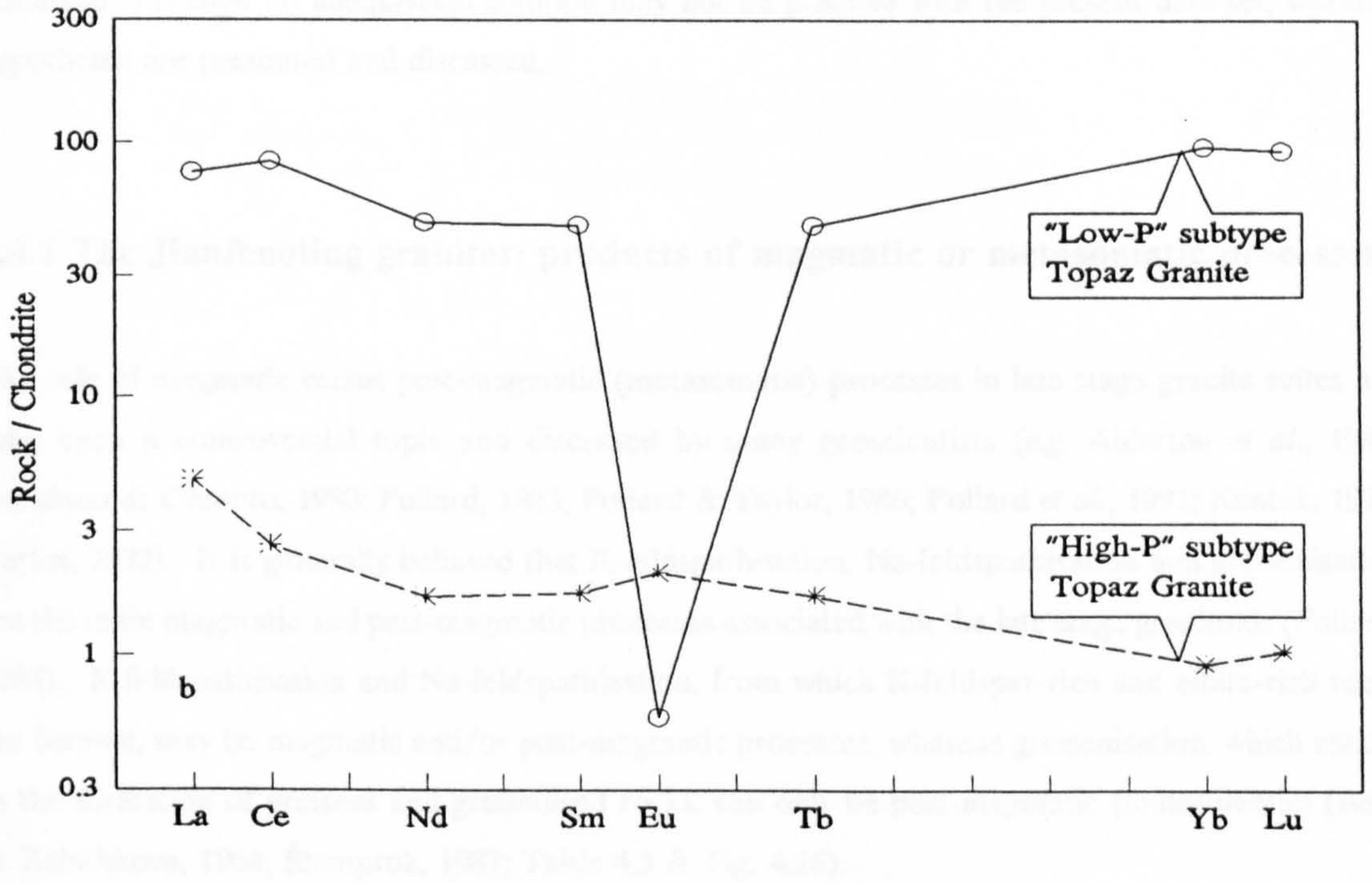

Fig. 4.15 Chondrite-normalised rare earth element patterns comparing the granites ($x \pm \sigma$) of both groups of the Jianfengling stock to the Spor Mountain topaz rhyolite (data from Christiansen *et al.*, 1986), the Macusani obsidian (data from Pichavant *et al.*, 1988), and the "low-P" and "high-P" topaz granites (data from Taylor, 1992).

4.4 DISCUSSION

The geochemical data presented above indicate several distinctive features of the Jianfengling granites that are quite unique to a large number of small granitic intrusions in Southeast China (*cf.* Zhang & Xia, 1988; Xu, 1989; Tu *et al.*, 1980; Xu *et al.*, 1981; Pollard et al., 1988; Pollard & Taylor, 1991; Schwartz, 1992). Questions fundamental to the petrogenesis of the Jianfengling granites that require consideration are:

(1) Are mineralogical and geochemical features of the granites magmatic or metasomatic?

(2) What was responsible for the evident differences between the rocks of Group 1 and those of Group 2?

In the following sections the geochemical implications relevant to these two questions are briefly discussed; although an unequivocal solution may not be possible with the present data set, working hypotheses are presented and discussed.

4.4.1 The Jianfengling granites: products of magmatic or metasomatic processes?

The role of magmatic versus post-magmatic (metasomatic) processes in late stage granite suites has long been a controversial topic and discussed by many geoscientists (*e.g.* Alderton *et al.*, 1980; Burnham & Ohmoto, 1980; Pollard, 1983; Pollard & Taylor, 1986; Pollard *et al.*, 1991; Kontak, 1990; Taylor, 1992). It is generally believed that K-feldspathisation, Na-feldspathisation and greisenisation are the main magmatic and post-magmatic processes associated with the late stage granitoids (Pollard, 1983). K-feldspathisation and Na-feldspathisation, from which K-feldspar-rich and albite-rich rocks are formed, may be magmatic and/or post-magmatic processes, whereas greisenisation, which results in the formation of greisens and greisenised rocks, can only be post-magmatic (metasomatic) (Beus & Zalashkova, 1964; Štemprok, 1987; Table 4.5 & Fig. 4.16).

Table 4.5 Major magmatic and post-magmatic processes and products in late stage granitoids (modified from Pollard, 1983)

Processes	Relative timing		Products
K-feldspathisation	magmatic	———	K-feldspar-rich granites and pegmatites.
	post-magmatic	———	Microclinisation, K-feldspar megacrysts.
Na-feldspathisation	magmatic	———	Albite granites, aplites, ongonites.
	post-magmatic	———	Albitised granites, albitites.
Greisenisation	post-magmatic	———	Greisens and greisenised rocks.

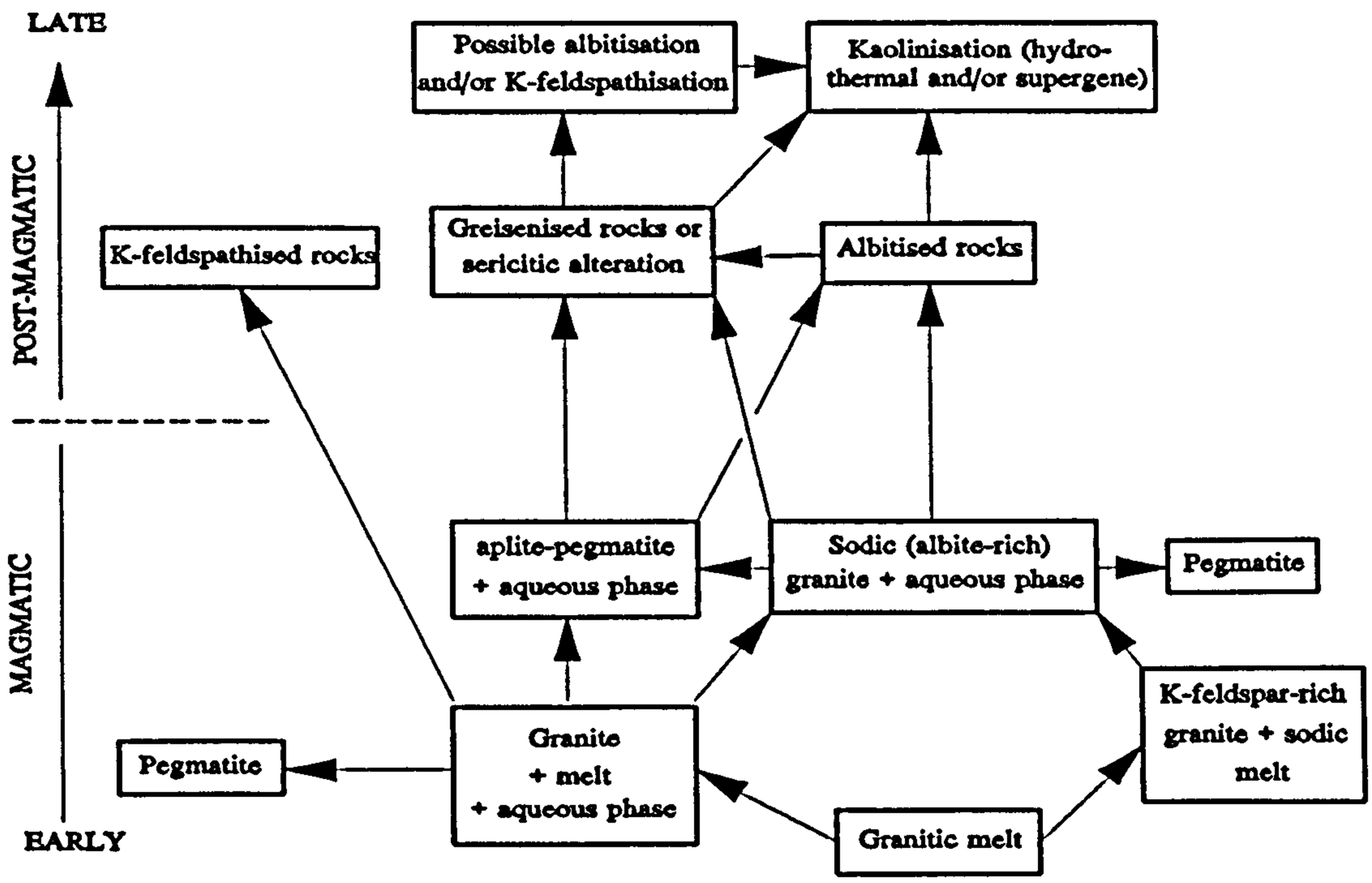

Fig. 4.16 Schematic model showing general timing of processes and succession of rocks produced during crystallisation of granitoids (modified from Pollard, 1983)

The effects of K-feldspathisation at the magmatic stage will depend largely on the concentration of fluorine, and perhaps lithium, in a melt and the amount of crystals produced in relation to the amount of residual melt. The presence of HF and LiO_2 in addition to water in a granitic system may lower

the first melting temperature to around 600°C (Wyllie & Tuttle, 1961, 1964). In the water-saturated Q-Ab-Qz system at 1 kb, the addition of fluorine causes the minimum normative composition to shift towards the albite apex (i.e. enlarge the quartz field) and the minimum temperature to be lowered significantly (630°C with 4 wt.% F; Manning, 1981, 1984). In a fractionating magmatic system, the increasing fluorine content in the residual melt thus requires this melt to become richer in sodium. This may be achieved in an undersaturated magma by crystallising K-feldspar (optically orthoclase or microcline) or K-rich feldspar and quartz, which may produce SiO_2- and K_2O-rich granitoids as precursors to more sodic, fluorine-rich granites. This process may be considered as K-feldspathisation at the magmatic stage. In general, owing to the large amount of crystallised material and the small volume of residual melt, this form of K-feldspathisation is barely recognized. The magmatic Na-feldspathisation is expressed by the crystallisation of sodium-rich melts, which may evolve by fractionation of less specialised magma owing to the increasing content of volatile components (chiefly fluorine). There is also growing evidence to suggest that granitic melts possess compositional gradients through the effects of convective circulation and internal diffusion (Hildreth, 1979). These gradients may result in the formation of roof zones enriched in sodium, fluorine, lithium and rare elements. In many highly evolved granites, the earliest post-magmatic alteration takes the form of the development of secondary K-feldspar. This may be revealed by the replacement of plagioclase by microcline and orthoclase and the partial replacement of ferromagnesian minerals by chlorite and/or sericite (*e.g.* Stone & Austin, 1961; Booth, 1968; Alderton *et al.*, 1980; Pollard *et al.*, 1991). This early post-magmatic K-feldspathisation may be produced when the melts become saturated in an aqueous phase which may migrate down a temperature gradient through already crystallised granite, where the lowering of the equilibrium K/Na ratio in the fluid will cause K to exchange for Na in the wallrocks (Lagache & Weisbrod, 1977). The replacement of plagioclase by K-feldspar indicates a removal of both sodium and calcium (Serebryakov, 1961), and the composition of the phases in equilibrium may be a function of the temperature and pressure (Holloway, 1987). At the post-magmatic stage, Na-feldspathisation (albitisation) is a common phenomenon in the development of late-stage granitoids and is most strongly developed in the apical zones of the final intrusive phase. This alteration may occur above the zone of K-feldspathisation and there may be a gradual transition between the two zones (Beus & Zalashkova, 1964).

Greisenisation, by definition, is "*a post-magmatic process which is related to the origin of high silica leucocratic granitoids*"; it "*acted on solid rocks without a significant participation of reaction in a liquid portion of the granite body*"; and in its course "*mineral changes occurred characterised by the decomposition of biotite and feldspars and remobilisation of silica and alumina in the rock*" (Štemprok,

1987). It is the main post-albitisation alteration related to rare element mineralisation associated with the late stage granitoids. This is not necessarily restricted to any particular zone, though its intensity is usually greatest in the apical portions of the final intrusive and the exocontact zone (Beus & Zalashkova, 1964; Štemprok, 1987). Minerals of biotite and feldspars are generally replaced by complex aggregates of micas, quartz, topaz and other fluorine minerals with a considerable impact on some elements such as W, Sn, Mo and Be.

Post-greisen alterations such as second phases of albitisation and K-feldspathisation, together with sericitisation, chloritisation and kaolinisation, are often recognized in the late stage granitoids (Exley, 1958; Beus & Zalashkova, 1964; Alderton *et al.*, 1980; Shwartz, 1990; Ward *et al.*, 1991). Late albitisation is expressed by late veins and replacements in which albite may replace topaz and micas. Late, relatively low-temperature K-feldspathisation is represented by the growth of new potassium feldspars and the recrystallisation of pre-existing potassium feldspar. One of the features of this late K-feldspathisation is the absence of perthite (Pollard, 1983). Sericitisation and chloritisation are characterised by the breakdown of feldspars, biotite and topaz to quartz, muscovite (or its fine-grained form "sericite") and chlorite (Rose & Burt, 1979; Alderton *et al.*, 1980). Kaolinisation is distinguished by the formation of clay minerals such as kaolinite and illite through low-temperature hydrothermal alteration and /or deep weathering (Alderton *et al.*, 1980; Pollard, 1983).

K-feldspathisation, Na-feldspathisation and greisenisation have been recorded in the Jianfengling granites. A large volume of K-feldspar-rich and albite-rich granites and greisens and greisenised rocks were produced by these processes (*cf.* Chapter 3). It is important to ascertain whether the main features observed in the Jianfengling granites are representative of a magma or are the products of metasomatism. Factors considered relevant to the argument are:

(1) the petrographic features and geochemistry of the granites;
(2) comparison with volcanic analogues and other fluorine-rich granitic suites with similar compositions; and
(3) experimental and thermodynamic considerations.

Assuming that the unusual petrographic and geochemical characteristics of the Jianfengling granites, such as the extreme enrichment of F, Li, Rb and Cs, and depletion of P_2O_5, Zr, Sr and Ba, were the results of a pervasive metasomatic alteration, then one might expect the following phenomena:

(1) a total replacement of feldspars and biotite by quartz and sericite, as the feldspars

and mica are unstable under hydrothermal conditions (Pollard 1983; Pollard & Taylor, 1986); and

(2) an extreme variation of the alkali components Na_2O and K_2O and correlations between these components and the so-called "mobile elements" such as F, Li, Rb, Cs, Sr and Ba (Schwartz, 1991).

As discussed in Chapter 3 and previous sections of this chapter, neither of these two aspects is relevant to the Jianfengling granites. Petrographic evidence has revealed that, for the majority of samples collected from the Jianfengling granites, the metasomatic effect is minor, with only a small amount of sericite and fluorite, which are usually the major products of metasomatism (Schwartz, 1991), being present in these rocks. For most of the samples determined here, the variations of Na_2O and K_2O are well within 2 wt.% (Appendix V). When Na_2O and K_2O are plotted against the mobile elements F, Li, Rb, Cs, Sr and Ba, there are no significant correlations evident (Fig. 4.17).

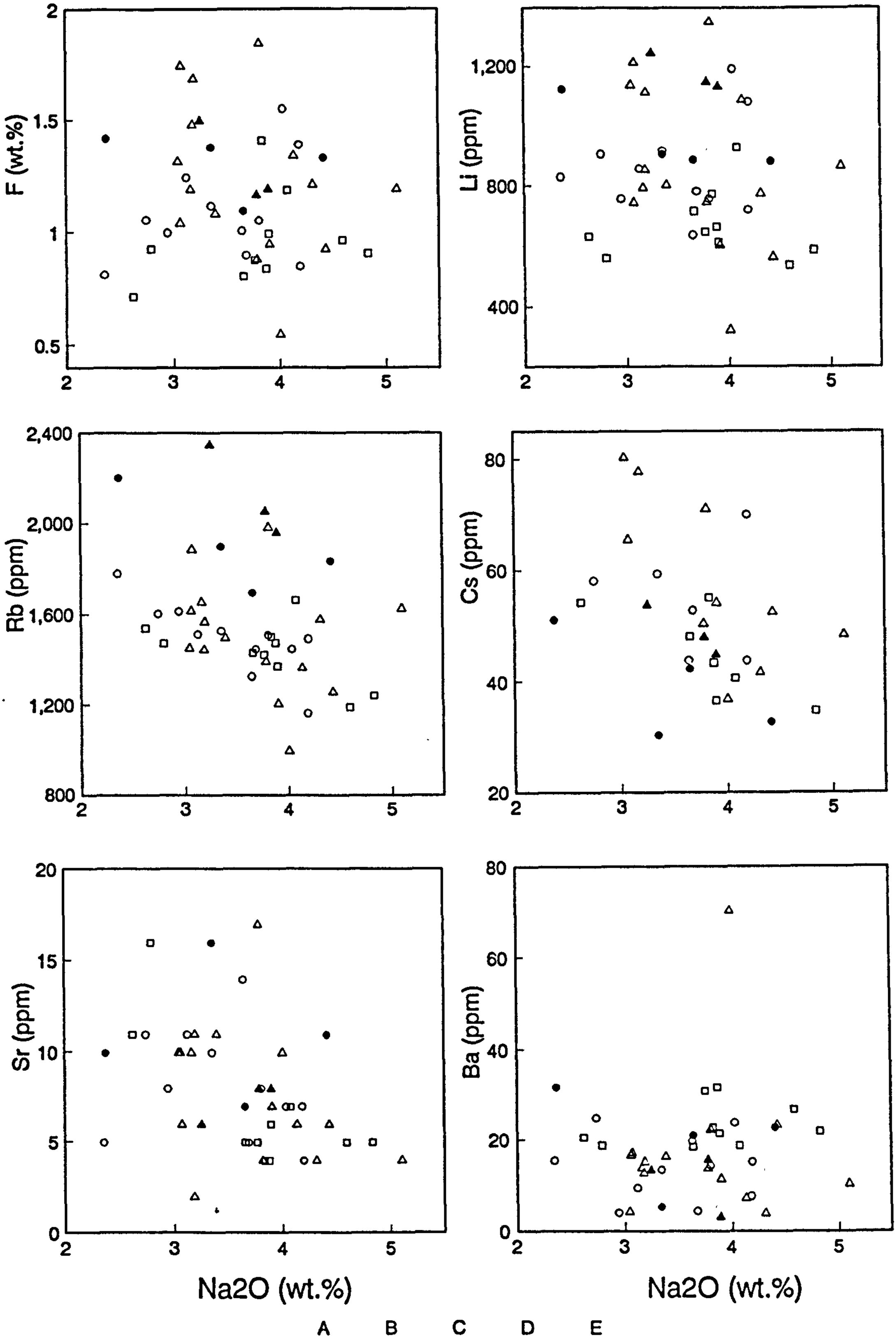

Fig. 4.17 Binary variation diagrams of selected mobile elements versus Na2O and K2O

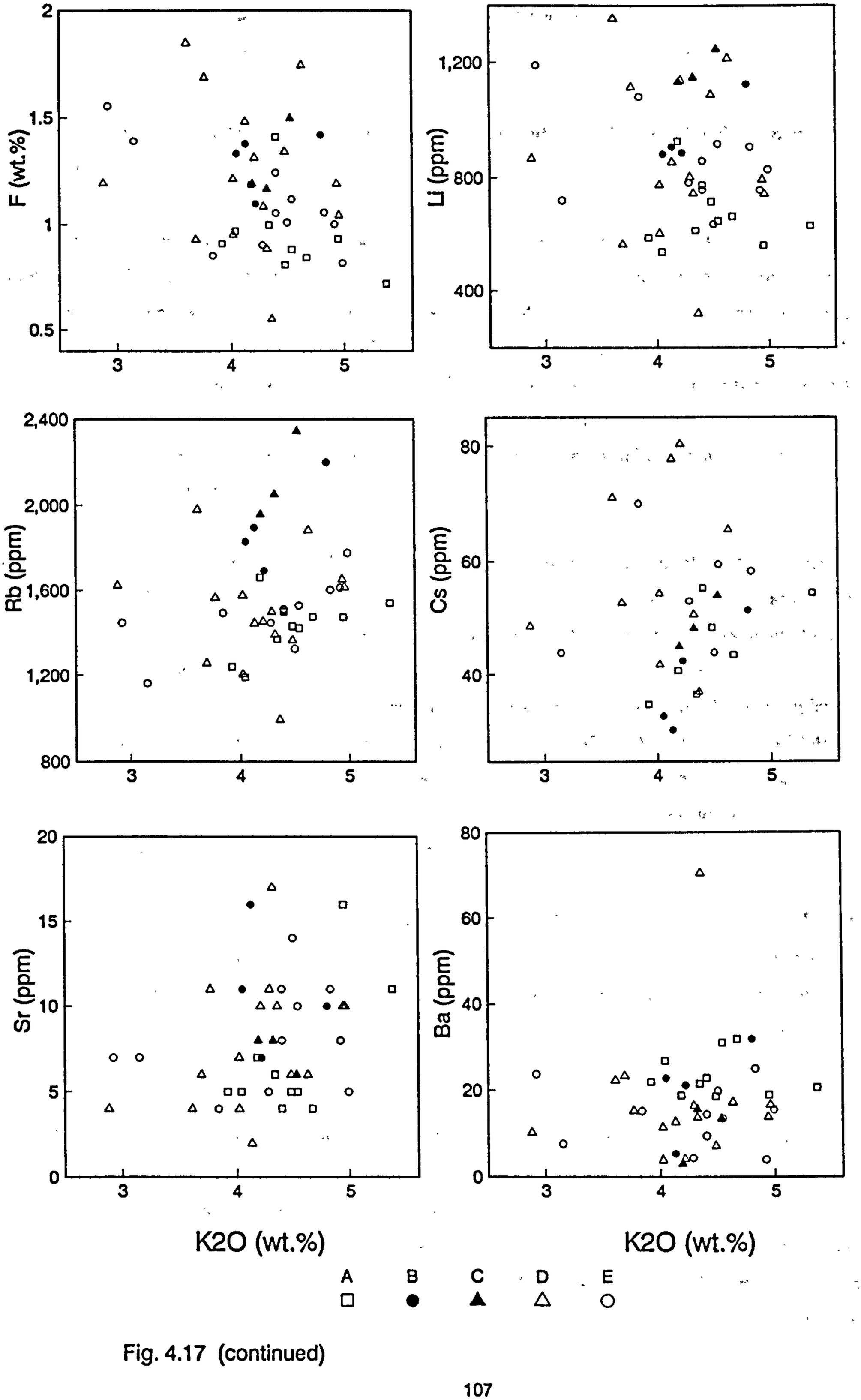

Fig. 4.17 (continued)

Geochemical arguments in favour of a dominantly magmatic control on the evolution the Jianfengling granites are summarised as follows:

(1) The major element compositions of the Jianfengling granites are comparable to those of other volatile-rich felsic suites (Table 4.3 and Fig. 4.3), and the normative mineralogy approximates minimum-melt compositions in the haplogranite system (Fig. 4.6b). Geochemical comparison of the Jianfengling granites to ongonites, macusanite, topaz rhyolites, and glass inclusions in Taylor Creek Rhyolite (Table 4.3) is particularly significant since these latter rocks are clearly of magmatic origin (*e.g.* Kovalenko & Kovalenko, 1984; Christiansen *et al.*, 1983, 1984, 1986; London, 1988; Webster & Duffield, 1991); hence the normative compositions of the Jianfengling granites are at least consistent with a magmatic parentage.

(2) Clustering of geochemical data with no obvious deviation toward alkali enrichment or depletion is considered to be best explained by magmatic rather than metasomatic origin (*e.g.* Pollard, 1983; Kontak, 1990). The variation of alkali compositions (Na_2O and K_2O) for most of the samples studied from the Jianfengling granites is small (within 2 wt.%) and K_2O is in excess over Na_2O. Samples which possess clear signs of metasomatic alteration (feldspars were replaced partially or completely by sericite) have either Na_2O in excess over K_2O (such as samples 480-2, 107-10, 109 and 430-4) or exhibit extreme depletion in Na_2O (less than 1 wt.%, sample $CK_{3\text{-}21}$; Appendix V). Thus, for the majority of the samples, even though minor amounts of re-equilibrium have occurred, changes are considered to have been isochemical. This may indicate a low fluid/rock ratio (Kontak, 1990).

(3) Examination of the behaviour of selected element pair correlations indicates uniformity of most of the data. For example, variation diagrams of CaO *vs.* trace elements and other major elements (*e.g.* Figs. 4.2 & 4.14) show generally smooth trends consistent with the variations expected for fractional crystallisation of a granitic melt (*e.g.* Mittlefehldt & Miller, 1983). On element pair plots of SiO_2 vs. other elements (Fig. 4.2), some discernible trends are also evident.

The alkaline and alkaline-earth elements are useful for delineating fractional crystallisation trends in granitic melts because their general partitioning behaviour in typical "granitic" minerals (*e.g.* the feldspars, biotite) is relatively well known (Hanson, 1978). In particular, Ba, Sr and Rb can be used to evaluate fractional crystallisation processes in granitic rocks (McCarthy & Hasty, 1976, McCarthy, 1978). Ba is concentrated in K-feldspar by factors of ~3-13, Sr is concentrated in feldspars by factors of 3-4, and Rb is slightly concentrated by biotite, muscovite, and perhaps K-feldspar, by 1-2 times the

melt concentration (*e.g.* Higuchi & Nagasawa, 1969; Long, 1978; Mittlefehldt & Miller, 1983). During fractional crystallisation of a granitic magma in which biotite and muscovite are normally less than 20%, plagioclase is more than 20%, and quartz and K-feldspar comprise most of the remainder of the crystallising assemblage, the bulk distribution coefficients for Ba and Sr will result in decreasing Ba and Sr and an increase in Rb. This trend is broadly observed in the Jianfengling granites, particularly for Rb. (Fig. 4.2).

(4) The rare earth element geochemistry of the Jianfengling granites shows consistent patterns that contrast markedly with the LREE-depleted, HREE-enriched chondrite patterns characteristic of greisenised lithologies (Chatterjee & Strong, 1984). Many studies have revealed that metasomatic processes tend to modify the REE chemistry of felsic rocks and cause irregular REE distributions (*e.g.* Alderton *et al.*, 1980; Taylor & Fryer, 1982, 1983; Corey & Chaterjee, 1990). Although the overall enrichments of REEs in the Jianfengling granites contrast sharply with those of Macusanite of Peru (Pichavant *et al.*, 1988; London *et al.*, 1988) and the St. Austell topaz granite of SW England (Hill & Manning, 1987; Manning & Hill, 1990; Taylor, 1992), their REE patterns compare extremely favourably to those of typical topaz rhyolites (Christiansen *et al.*, 1983, 1984, 1986), glass inclusions in the Taylor Creek Rhyolite (Webster & Duffield, 1991), and the Pleasant Ridge zinnwaldite-topaz granite (Taylor, 1992) (*cf.* Fig. 4.15), and are therefore consistent with a magmatic signature rather than being related to metasomatic phenomena (*e.g.* Higgins *et al.*, 1985; Chen, 1987; Zhu & Xu, 1989). The large negative Eu anomaly requires that much feldspar was involved in the mineral-melt equilibria during melting or crystallization (Cullers & Graf, 1984). Similarly, the low $(La/Lu)_N$ ratio requires the presence of one or more LREE-enriched accessory minerals during melting or crystallisation. Monazite, which occurs in trace amounts in samples of the Jianfengling granites, is the most likely host for the LREE (*cf.* Miller & Mittlefehldt, 1982; Mittlefehldt & Miller, 1983; Charoy, 1986; Congdon & Nash, 1991). Although it is not easy to assess the exact amount of monazite in the Jianfengling granites, it is safe to assume that there is enough monazite to account for all of LREE in these rocks since as little as 0.05 wt.% monazite is required to provide as much as 150 ppm LREE (Taylor, 1992).

Despite the fact that depletion of light rare-earth elements in felsic magma is relatively common (Miller & Mittlefehldt, 1982; Mittlefehldt & Miller, 1983), the high concentrations of the heaviest REE (up to 25 ppm Yb and 3.5 ppm Lu, Appendix VI) and very low $(La/Lu)_N$ ratios for the Jianfengling granites (Fig. 4.13) are unusual. Uraninite, which is often present as an accessory mineral in granitic rocks, is known to concentrate the HREE, specifically Yb and Lu (Fryer & Taylor, 1987), and is thus a possible host for these elements. The high content of U in these rocks may also indicate

the presence of uraninite. Other accessory minerals such as xenotime and thorite, in addition to Nb-Ta oxides, may also exist as the carriers of HREE (*e.g.* Haapala, 1977; Congdon & Nash, 1991).

Although the above features are considered to be consistent with a dominantly magmatic origin for the Jianfengling granites, the incoherent relationship between SiO_2 and K_2O, Na_2O (Fig. 4.4) indicates the effects of post-magmatic alteration of feldspars (*cf.* Manning & Hill, 1990). The elevated and erratic abundances of some elements (such as Bi, Pb, Zn, Sn, W, As, Sb; Appendix V) in a few samples may also indicate that some post-magmatic metasomatism occurred. The presence of an apical greisenised zone and marginal pegmatite clearly signals the existence of high-temperature hydrothermal fluids during the late stage of magma evolution. This exsolution of a fluid phase may have resulted in a marked redistribution of elements *via* melt-fluid partitioning in a limited zone at the upper contact of the granite (Pollard & Taylor, 1991).

Although it is difficult to ascertain the proportion of magmatic versus metasomatic contributions to such elevated concentrations, it is worthy to note that enrichment of some of these elements is found in ongonite of Mongolia (120 ppm ; Tischendorf, 1977), topaz rhyolite of USA (Christiansen *et al.*, 1983, 1984, 1986), and macusanite of Peru (96 ppm Zn, 69 ppm W, 203 ppm Sn, 325 ppm As; Pichavant *et al.*, 1987). Therefore, a certain degree of elemental enrichment in the Jianfengling granites can be attributed to magmatic processes, although it is also true that a metasomatic influence is recorded.

Petrological evidence in support of a magmatic origin:

Finally a consideration should be given to whether the assemblage of mineral phases of the Jianfengling granites is consistent with magmatic conditions. A number of recent experimental studies have been carried out on similar bulk compositions to that of the Jianfengling granites, and the results have demonstrated that topaz is a stable mineral in granitic melts over quite a large range of P and T condition (Anfilogov *et al.*, 1973; Kovalenko, 1977; Webster *et al.*, 1987, 1989). In addition, Naumove *et al.* (in Kontak, 1990) and Xia & Chen (1982) reported melt inclusions in topaz from ongonites of Mongolia and topaz granite of SE China, respectively, which proves a magmatic origin for the host, whereas Weidner & Martin (1987) have shown that, under water-saturated conditions, topaz, muscovite, and fluorite occur as magmatic minerals in accessory amounts together with plagioclase, K-feldspar, and quartz.

The foregoing discussions indicate that there is adequate reason to believe a predominantly magmatic origin for the Jianfengling granites. However, it is also evident that some degree of subsolidus modification did occur, since some of the plagioclase and K-feldspar clearly reflect hydrothermal alteration. For the most part, the geochemistry is considered to closely approximate a process of magmatic evolution.

4.4.2 The differences between the two groups of the Jianfengling granites: results of magmatism or metasomatism?

The evidence presented and discussed in the foregoing sections shows that the Jianfengling granites are the products of predominantly magmatic processes. It is also worth noting the existence of marked differences, both petrographically and geochemically, between rocks of Group 1 and Group 2. These differences have been discussed in detail in previous sections, but the salient points are reiterated here:

(1) mineralogically, rocks of Group 1 are enriched in albite and zinnwaldite, whereas rocks of Group 2 are enriched in K-feldspar and biotite;

(2) geochemically the rocks of Group 1, relative to those of Group 2, are enriched in Al_2O_3, MnO, F, Li, Rb, Sr, Pb, Zn, Sn, Ta, Ga and As, and depleted in SiO_2, Fe_2O_3, CaO, Cs, Ba, W, Th, U, Zr, Y and REEs.

One question that remains to be answered is what caused these differences: are they the results of magmatism or metasomatism or a combination of both? Do the rocks of these two groups represent two separate unrelated magmatic events and sources? The inseparable spatial association of Group 1 and Group 2 of the Jianfengling granite and the extremely comparability in their geochemistry have effectively ruled out the possibility that they came from two separate unrelated magmatic sources. A pervasive metasomatism in the sense of Pollard & Taylor (1986) and Taylor & Pollard (1988) is also ruled out during the formation of Group 1 rocks since most of the magmatic minerals and texture of the rocks still remain, although infiltration of late-stage fluids, probably *via* grain boundaries and microfractures, did occur and was ultimately responsible for, amongst other things, promoting re-equilibration of plagioclase to albite and unmixing of homogenous alkali feldspar to stable microperthite. If exceptionally large volumes of fluid had been involved in the formation of Group

UNIVERSITY OF SOUTHAMPTON LIBRARY

1 rocks, a whole scale transformation would have occurred. In contrast, where fluid focusing did occur and fluid/rock ratios were high, the rocks were converted to zoned greisens of markedly different modal mineralogy (quartz + topaz + mica + Nb-Ta oxides + sulphides) and geochemistry.

The magmatic evolution from the biotite granite (Group 2) to the zinnwaldite granite (Group 1) can be broadly explained by fractional crystallization. The depletion of some compatible elements or oxides were caused by the fractionation of plagioclase (CaO and Sr), K-feldspar (K_2O, Ba and Sr), biotite (TiO_2, Fe_2O_3, MnO and Ba), quartz (SiO_2); and accessory minerals such as monazite and uraninite (U, Th, Zr, Y, REEs). Conversely Al_2O_3, F, Li, Rb, Ta and Sn became enriched in the residual melt from which the zinnwaldite granite crystallised (Table 4.1 & Appendix V). The vapour-undersaturated melting experiments with Macusani obsidian (London *et al.*, 1989), which has a chemical composition similar to that of the Jianfengling granites, are in agreement with such a fractionation trend; e.g. at 65% crystallization, the order of decreasing C^* values (C_i residual melt / C_i starting glass) is F (2.25), Li (1.8), Rb (1.8), Ta (1.1), Na_2O (1.09), Al_2O_3 (1.07), SiO_2 (0.95), K_2O (0.79), Ba (0.5), CaO (0.45), Sr (0.2), and FeO (0.06).

The relationship between Na_2O, CaO, Sr and F is usually used in discussions of discriminating magmatic and metasomatic processes (Schwartz & Asbury, 1989; Schwartz, 1991, 1992). As has been shown by Schwartz & Asbury (1989) and Schwartz (1992), the strontium contents of hydrothermally albitised rocks are much higher than in the unaltered protolith; the same observation holds for calcium if there is enough fluorine present to fix it as fluorite (wt.% F/CaO≥0.68). Strontium released by hydrothermal destruction of plagioclase and/or K-feldspar and calcium released by the breakdown of plagioclase are readily fixed in albite and fluorite, respectively, which crystallized from the hydrothermal fluids. Strontium partitions strongly into albite which is in equilibrium with hydrothermal fluids [e.g. albite/fluid partition coefficients of ≥30 have been determined for strontium at 600°C and 1 Kb by Iiyama (1972, *in* Mittlefehldt & Miller, 1983)]. Hydrothermal albite and fluorite not only serve to stabilize strontium and calcium in the metasomatic rocks but they also act as scouring agents for strontium and calcium released from other types of alteration, such as muscovitisation (Schwartz, 1992), thereby increasing the strontium and calcium contents of the metasomatic rocks with respect to the unaltered protolith.

If the zinnwaldite granite (Group 1) of the Jianfengling Complex were to be derived by fluid interaction with the solidified biotite granite (Group 2), it should have much higher strontium and calcium concentrations than those of the biotite granite. However, the strontium concentrations of the

zinnwaldite granite are very much at the same level as those of the biotite granite; the calcium concentrations are much lower, although the fluorine concentrations are high enough to fix all calcium that would have become available by the hydrothermal breakdown of plagioclase in the biotite granite. In summary, the relationship between the zinnwaldite granite (Group 1) and biotite granite (Group 2) is characteristic of magmatic differentiation with fractionation of plagioclase causing depletion of the magma in CaO.

CHAPTER FIVE

MINERALISATION

CHAPTER FIVE

MINERALISATION

Content

5.1 General aspects of mineralisation in the Xianghuapu area

5.1.1 Types of mineralisation

5.1.2 Nb-Ta mineralisation

5.1.3 Sn-W (Pb, Zn) mineralisation

5.1.4 W-F (fluorite-scheelite) mineralisation

5.1.5 Pb-Zn mineralisation

5.2 Typical deposits

5.2.1 Meishi Pb-Zn deposit

5.2.2 Xianghuapu W-F (fluorite-scheelite) deposit

5.3 Summary

5.1 GENERAL ASPECTS OF MINERALISATION IN THE XIANGHUAPU AREA

5.1.1 Types of mineralisation

During the last 40 years, many types of mineralisation have been found both within the Jianfengling granite stock and the surrounding country-rock. These include Nb, Ta, Be, W, Sn, Pb, Zn, Ag and F (fluorite), and can be genetically categorised into two main groups: granite-type and lode-type. The granite-type hosted in greisen and pegmatite is syn-magmatic and/or late-magmatic in origin and includes Nb, Ta, Pb, Zn, and rarely W, Sn mineralisation. The lode-type is late- and post-magmatic in origin and consists of W, Sn, Be, F, Pb and Zn mineralisation. Hydrothermal alteration is the main mineralising process and limestone, metasandstone, and rarely granite are the main host-rocks. Massive (mainly for Pb-Zn and sometimes W-F), disseminated (for W-F, W-Sn, and some Pb-Zn) are the major forms of ore mineral association. The mineralisation in the Xianghuapu area occurs as four main associations: Nb-Ta, W-Sn, W-F, and Pb-Zn mineralisation. The main characteristics of these group are summarised in Table 5.1.

Table 5.1 Mineralisation types within and adjacent to the Jianfengling granite stock

Type	Host rock	Elements	Mineral assemblage	Size of deposit (tonnes ore)	Distance from the granite (metre)	Linked intrusion	Example
Nb-Ta	greisen	Nb, Ta	microlite, niobite, tantalite	$>10^6$	0	B	430 deposit
Sn-W	granite limestone metasandstone	Sn, W, Be, Pb, Zn	cassit, wolf, gal, sph, apy.	10^2-10^3	0 or 20-300	C (?)	
W-F	limestone dolomite	W, F, Pb, Zn	fl, qz, sch, cc, gal, sph, cpy.	$>10^6$	0-500	D	Dongshan, Xianghuapu
Pb-Zn	limestone dolomite	Pb, Zn, Sn, Fe, As, Ag	gal, sph, po, apy, py, freib, cassit, bourn	$>10^6$	10-500	E	Meishi, Baojingshan

apy = arsenopyrite, bourn = bournonite, cc = calcite, cassit = cassiterite, cpy = chalcopyrite, fl = fluorite, freib = freibergite, gal = galena, po = pyrrhotite, py = pyrite, qz = quartz, sch = scheelite, sph = sphalerite, wolf = wolframite.

5.1.2 Nb-Ta mineralisation

Nb-Ta mineralisation, named the 430 Nb-Ta deposit by the No. 238 Geological Team (1962, 1974), occurs in the greisen and greisenised granite covering the top of intrusion B with an extent of about 500m across and 20-150m in depth. Detailed exploration for this deposit was carried out by the No. 238 Geological Team between 1957 and 1974 (*op. cit.*).

The topaz-quartz greisen in which the Nb-Ta mineralisation is the richest is located on the top of Jianfengling Mountain. It consists of mainly quartz (about 90%), topaz and zinnwaldite and covers several hundred square metres to a depth of 2-3m. Microlite, niobite, tantalite, and Ti-Ta-niobite are the most abundant Nb-Ta minerals, accompanied by trace amounts of cassiterite, wolframite, monazite, zircon, weibyeite, La-Ce-fluorite, and xenotime. These minerals are disseminated throughout the roof zone of intrusion B. Their abundances decrease with increasing depth and weakening alteration (greisenisation, albitisation and K-feldspathisation; No. 238 Geol. Team, 1974). Microlite shows three different colours: black, dark brown and yellowish green. Its Nb-Ta contents ($Nb_2O_5+Ta_2O_5$) range from 62 wt.% to 80 wt.%. The Nb-Ta concentrations of selected minerals are given in Table 5.2.

Table 5.2 Nb and Ta concentrations in ore minerals

(summarised from No.238 Geol. Team, 1974)

	Nb_2O_5 (wt.%)	Ta_2O_5 (wt.%)
Microlite	12.50-28.30	45.78-62.50
Ta-niobite	40.10-50.40	16.62-32.50
Ti,Ta-niobite	2.70	11.80
Hf-zircon	0.13-0.21	0.10-0.19
Cassiterite	0.213-2.53	0.940-2.63
Wolframite	1.10-1.15	0.575-0.81

5.1.3 Sn-W (Be, Pb, Zn) mineralisation

A number of small cassiterite-sulphide (wolframite) deposits have been found in this area. According to their location and mineral assemblages, they have been classified into two groups. One occurs in quartz veins and mica-rich greisens developed along both sides of the quartz veins with widths varying for several centimetres to over one metre, typically 20-50cm. The quartz veins have been developed along the NW-SE-trending faults (F_{2S}) hosted within intrusions B and C (*cf.* section 2.2.3 and Plate 2.1). These quartz veins, with disseminated mineralisation, extend along strike from twenty to several hundred metres and have been mined recently, together with the greisens, by private individuals for cassiterite, wolframite, and occasionally for galena and sphalerite. Although coarse quartz pods rich in these minerals are found at the intersections of the faults, the greisens are the main host of economic minerals. The other group of deposit is localised in the country rocks of the Jianfengling stock and occur mainly in fissures within the F_{101} fault zone adjacent to the stock in the northeastern part of the Xianghuapu area. The mineralisation was formed by hydrothermal alteration. The shapes of orebodies follow the extent of these fissures and are much less regular than those described previously. Cassiterite, galena, sphalerite, pyrrhotite, pyrite, arsenopyrite and chalcopyrite are associated with the non-metallic minerals garnet, diopside, actinolite, calcite, dolomite, fluorite, chlorite and sericite.

Fine subhedral to anhedral granular cassiterite is the main economic minerals in this ore-type, its

content varying from 0.5 to 3 wt.%, with the highest value reportedly reaching 15 wt.%. Galena and sphalerite occur as anhedral grains disseminated in the ore, with a total content of 3-15 wt.% (personal communication with the miners).

5.1.4 W-F (fluorite-scheelite) mineralisation

Although a few small fluorite-scheelite deposits have been found in the contact zone of intrusion E and in its adjacent country-rocks, almost all significant fluorite-scheelite deposits discovered so far are present in the contact zone of intrusion D or in the adjacent country-rocks. More than ten separate fluorite-scheelite orebodies (10^3-10^6 tonnes in size) have been found and mined around the Jianfengling granite stock. All the orebodies are exclusively associated with the NNE-trending faults (F_{4S}) (Appendix I) and are hosted by the Devonian and Carboniferous limestones. These orebodies generally occur within several metres to 1000m from the intrusion and are located mainly in the eastern and northeastern parts of the Jianfengling stock, coinciding with the distribution of intrusion D. The Xianghuapu and Dongshan deposits are the two major fluorite-scheelite deposits in this area and consist of five and four separate orebodies, respectively. Fluorite, quartz, scheelite and calcite are the main minerals of the ores. The scheelite content in these ores is generally 0.5-5 wt.% and can reach as high as 30 wt.% in massive ores. The fluorite content ranges from 5 to 60 wt.%. Other minor phases include galena, sphalerite, and cassiterite (0.1-2 wt.%). The detailed mineralogy and petrography of the Xianghuapu deposit will be discussed in the next section.

5.1.5 Pb-Zn mineralisation

Pb-Zn mineralisation is a common feature of this area and has been exploited historically. It occurs in all the intrusions of the Jianfengling granite complex, although most of the mineable orebodies are exclusively associated with intrusions D and E. Based on the relations with the intrusions, mineral assemblages and their locations, three types of Pb-Zn mineralisation are noted: a) in zones of greisen and pegmatite; b) with the fluorite-scheelite ores; and c) massive sulphide lodes in carbonate host rocks.

The Pb-Zn mineralisation occurring in the greisen zones has been observed in three of the five intrusions. In intrusions A and B, fine-grained galena and sphalerite are disseminated throughout the

greisen zones (Plate 5.1a) which occupy limited areas (10-1000m^2) of the intrusions, they have normally not reached the grade for mining. In the top of the concealed body of intrusion E, the granite has been strongly greisenised and mineralised (Plate 5.1b). Disseminated galena, sphalerite and arsenopyrite are the dominant sulphides and are associated with trace amounts of chalcopyrite and pyrite. Most of the chalcopyrite occurs as veins and veinlets filling fractures within sphalerite and arsenopyrite (Plate 5.1c). Small inclusions (exsolutions) of chalcopyrite are also noticed along the edges of sphalerite grains (Plate 5.1d). The galena contains relatively high silver (0.20-0.47 wt.%), and the sphalerite contains high iron (10± wt.% Fe_2O_3), manganese (0.1-0.8 wt.%) and cadmium (1842-3000 ppm; Table 5.3) and appears black or dark brown in hand specimen.

Pb-Zn mineralisation associated with the fluorite-scheelite ores is mainly related to intrusion D. There is no apparent boundary between these two types of mineralization. Galena and sphalerite, accompanied by pyrrhotite, pyrite and chalcopyrite, occur either disseminated in altered country rocks or as massive aggregates in the NNE-trending faults zones as a later stage of fluorite-scheelite mineralization. The galena has a relatively lower silver content (0.02-0.2 wt.%). The sphalerite contains lower total iron (1.09-3.5 wt.%) and manganese (403-1106 ppm; Table 5.3) and appears as yellowish flakes.

The massive sulphide lode-type deposits are the most important Pb-Zn sources in this area. They are represented by the Meishi and Baojingshan deposits. Orebodies are mostly hosted in the gently dipping (20-40°E), NNE-trending faults (F_{4S}) and comprise massive galena, sphalerite, pyrrhotite, arsenopyrite, cassiterite and a small amount of chalcopyrite, pyrite, freibergite and bournonite. Sharp contacts are present between the orebodies and their Devonian and Carboniferous carbonate host rocks, and the grain size of the minerals changes from fine near the contact to coarse within the orebody. Detailed descriptions of the mineralogy of the Meishi deposit are given in the next section.

Table 5.3 Compositions of sphalerite and galena

Sample No.			101-5	104-14	DW-8	B324	S-1	III2'-2	M2-8	M3-8	M4-19	M4-31	M5-4	M5-5
ZnS	wt.%	Pb	0.25	0.18	4.00	5.25	0.53	0.08	4.38	4.38	14.00	5.88	3.13	5.63
		Zn	57.09	58.82	59.51	50.69	57.44	66.09	49.82	48.79	42.90	48.09	49.82	47.58
		S	31.96	31.84	31.85	31.15	32.72	32.77	31.15	32.36	28.88	31.60	32.55	32.56
		TFe	8.74	6.99	3.50	11.72	7.87	1.09	13.28	13.64	12.68	13.28	12.76	13.64
		Ag	0.0041	0.0013	0.0013	0.0190	0.0051	0.0011	0.0820	0.0670	0.1500	0.0660	0.0160	0.0840
		Cu	0.49	0.58	0.18	0.00	0.64	0.00	0.18	0.15	0.09	0.06	0.18	0.18
	ppm	Mn	2212	3394	1106	1313	2443	403	589	880	7735	1491	3839	1174
		Cd	2629	2349	1842	3000	2823	2870	2641	2610	2543	2289	2634	2366
		Ga	30	82	14	5.9	47	86	72	65	130	65	47	86
		Ge	0.3	0.3	0.3	0.7	1.7	15.0	0.3	0.3	0.3	0.3	0.3	0.3
		In	768	482	18	396	27	0.53	21	11	984	543	395	592
PbS	wt.%	Pb	85.52	85.10	82.80	85.41	86.03	83.98	85.08	84.46	84.92	85.45	85.29	
		Zn	0.24	0.72	2.07	0.41	0.14	0.76	0.28	0.67	0.57	0.22	0.16	
		S	13.66	13.74	14.59	13.79	13.62	14.34	13.99	13.71	14.03	13.82	14.03	
		Ag	0.22	0.02	0.12	0.05	0.05	0.25	0.2	0.47	0.26	0.22	0.22	
	ppm	Mn	36	26	14	64	38	28	74	170	58	54	16	
		Cd	85	50	280	51	143	146	210	174	75	160	83	
		Bi	285	10	4	5	1	1	1	1	2	2	1	
		Sb	300	70	325	255	120	830	740	870	1060	590	2000	
		Tl	390	3	4	11	3	28	65	190	100	89	53	

Plate 5.1

Plate 5.1 **Photographs and photomicrographs showing characteristics of Pb-Zn mineralisation in the Xianghuapu area**

a, b. Photographs showing disseminated Pb-Zn mineralisation in greisens on top of intrusions B and E, respectively.

c. Photomicrograph showing the distribution of chalcopyrite in fractures within arsenopyrite and sphalerite. Bar = 0.40mm.

d. Photomicrograph showing the distribution of chalcopyrite exsolutions along the edge of sphalerite grain. Bar = 0.20mm.

e, f. Photographs showing the sharp contacts between the galena-sphalerite ores and their country rocks (limestone). Bar = 2cm.

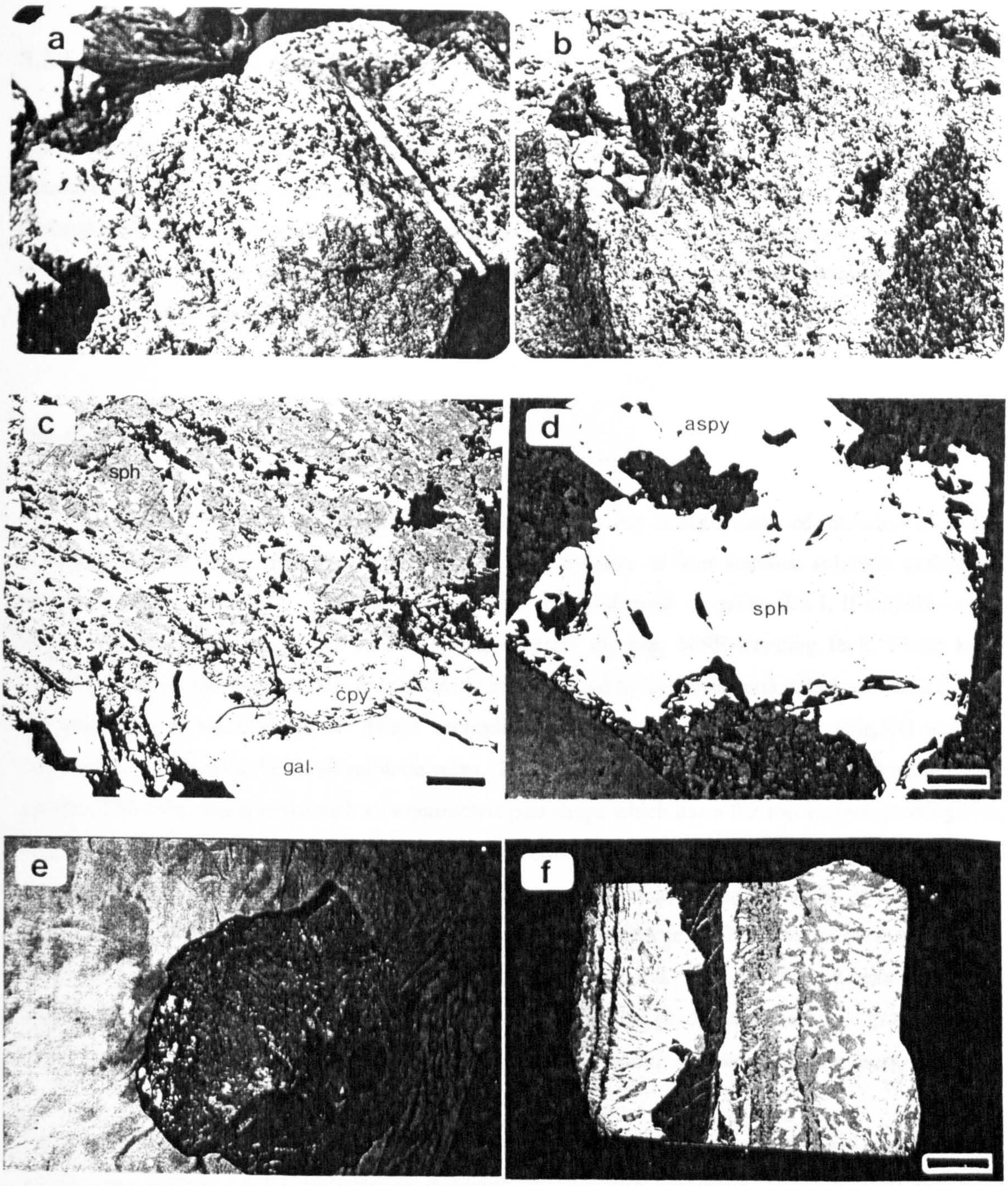
a
b
c
sph
cpy
gal
d
aspy
sph
e
f

5.2 TYPICAL DEPOSITS

5.2.1 Meishi Pb-Zn deposit

Up to the start of this study, they there has been neither geological research nor geological mining records, although other evidence for mining activities can be traced back over a decade. The discussion of deposit geology and ore mineralogy in the following sections is based solely on the result of two week's extensive underground mapping during the field work, personal communications with the miners, and subsequent laboratory studies.

Ore deposit geology

The Meishi Pb-Zn deposit is located 10-300m away from the contact zone of intrusion E in the northeast part of the Jianfengling granite stock, and consists of four massive sulphide orebodies, designated I, II, III and IV. The main components of this deposit --- orebodies I, II and III --- are hosted by karst solution cavities formed along a gently dipping, NNE-trending fault. These karst cavities could be the result of the limestones being replaced by hydrothermal solutions derived from the processes of mineralisation. These orebodies constitute en echelon lenses (Fig.5.1) and are connected to each other by small sulphide veins. Each orebody is about 30-45m wide, 0-8m thick, and extends 120-150m along strike with an asymmetric pod shape which has a flat top surface, striking N-S, dipping 26-45°E, and an uneven lower surface. Orebody III grades downward into sheet-like vein. Orebody IV is a small tablet confined to a steep EW-striking fault, dipping 68-75°S. It is 0-2m thick, 3-15m deep and 24-33m long. These four orebodies extend over a vertical interval of more than 150m. From 1984 to the end of 1989, orebodies I and II, and major parts of III and IV had been mined and more than one million metric tons of massive sulphide ore with a grade of sphalerite + galena varying from 5 to nearly 100 wt.% had been recovered (personal communication with the miners, 1990).

Distinct sharp contacts are present between the orebodies and their country rocks --- the Devonian argillaceous limestone and Carboniferous dolomite and dolomitic limestone. These contacts have been observed both megascopically and microscopically (Plate 5.1e & f). The ore displays apparent flow-foliation which is produced by mineral bands parallel to the boundaries of the orebodies (Zhang and Xu, 1989, p28) (Fig.5.2). Geodes and vughs have been found near the top surfaces (*op. cit.*). The grain size of minerals changes rapidly from fine near the contact boundary to coarse inside the

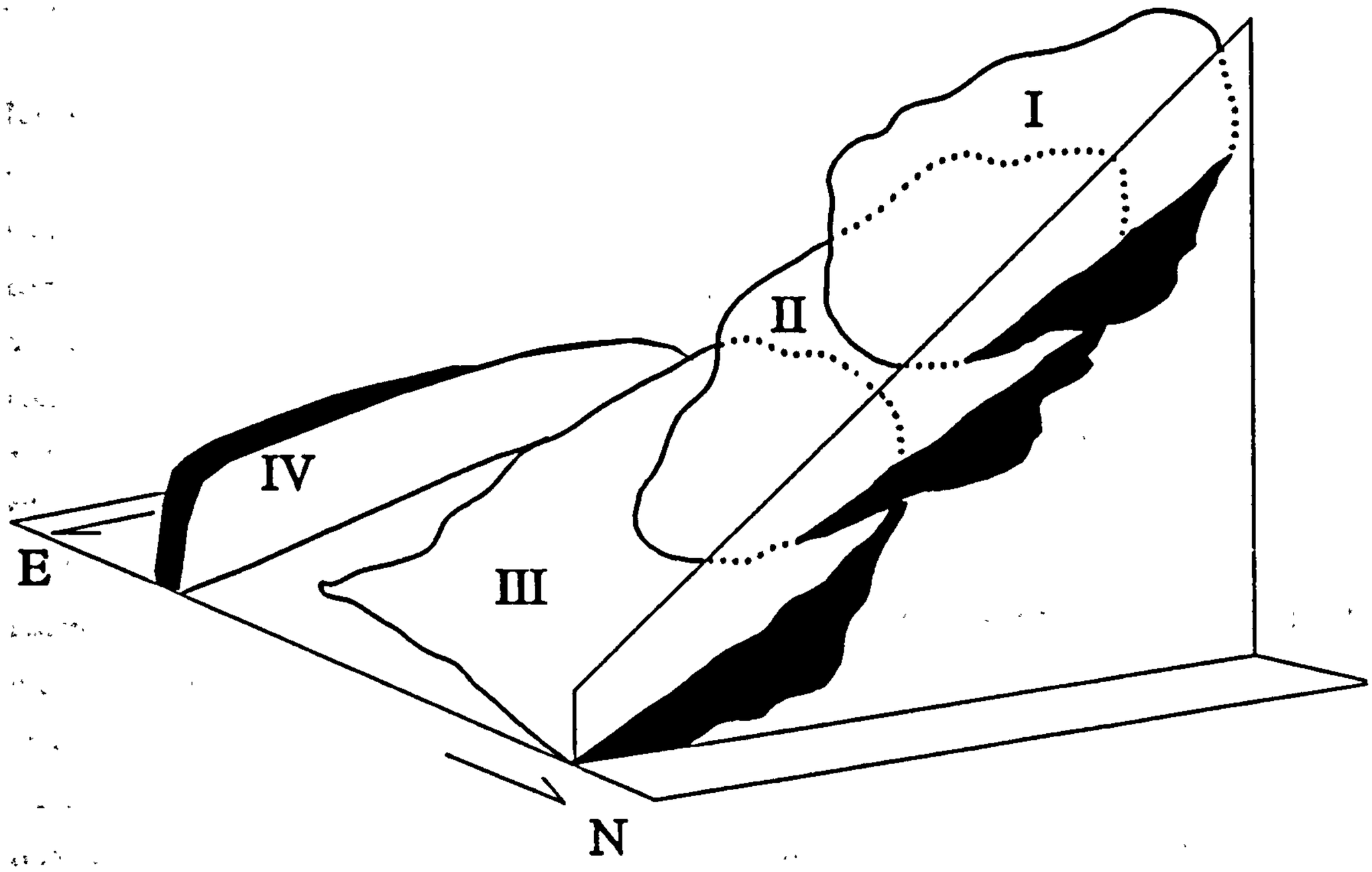

Fig. 5.1 A schematic diagram showing the distribution of four orebodies of the Meishi deposit

orebodies. Based on these field observations, Zhang and Xu (1989, p26) suggested an origin of ore minerals crystallising from a sulphide melt for this deposit. However, as it will be discussed later, the stable isotope studies reveal it to be a product of hydrothermal alteration and /or filling.

Various types of small veins and veinlets have been encountered in the fractured sedimentary wallrocks during the underground mapping. Quartz-sulphide (mainly arsenopyrite), mica-sulphide and pure calcite veins and veinlets are generally less than 20cm in width, a few tens of centimetres to a few metres in length and strike in different directions. The density of these veins and veinlets in the country rocks increases steadily as the mining activities go deeper (and also nearer to the granite intrusion). There is no apparent physical evidence suggesting genetic correlation between these veins and the Pb-Zn mineralisation. The distribution of these veins shows that they are more likely to be genetically related to the intrusion of the granite stock rather than the formation of mineralisation. Therefore the vein materials have not been chosen for further fluid inclusion and stable isotope studies.

Alteration of country rock

Razor-sharp contacts between the orebodies and their megascopically unaltered carbonate wallrocks are common in the Meishi deposit. Where alteration exists, it is generally confined to within a few centimetres to a few meters from the orebodies. Chloritisation and silicification are the most common forms of alteration. Extensive carbonate recrystallisation, presumably resulting mainly from the granite intrusion and partially from the mineralisation, is also found around these orebodies. It weakens gradually away from the granite intrusion and the orebodies.

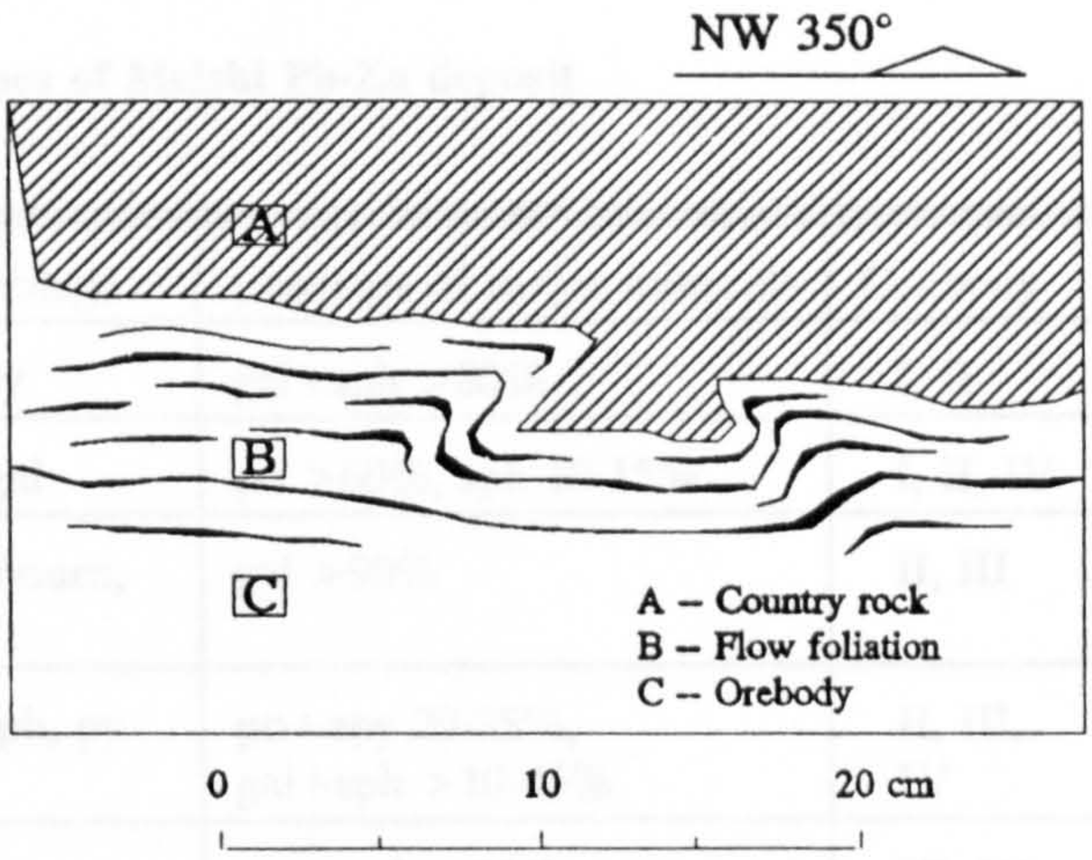

Fig. 5.2 Flow-foliation structure of the Meishi deposit
(modified from Zhang and Xu, 1989)

Ore mineralogy and paragenesis

Massive sulphide ores of the Meishi deposit have a consistent sulphide mineralogy but show significant variations in relative mineral abundances and assemblage. The principal sulphides are sphalerite, galena, pyrrhotite, arsenopyrite and pyrite. A small amount of chalcopyrite, freibergite and bournonite occur most commonly as inclusions within the main minerals. Cassiterite is also reported in some part of the deposit, reaching as high as 5 wt.% in ores of the deeper levels (personal communication with the miners, 1990). Based on the mineral assemblages and ore textures, six types of ores are recognized (Table 5.4). The galena-sphalerite-type ore occurs mainly in orebodies I and II, and the arsenopyrite-cassiterite-type ore occurs at the bottom of orebody III (personal communication with the miners, 1990). The different types of ores grade progressively from one to another.

Table 5.4 Ore types of Meishi Pb-Zn deposit

	Ore type	Mineral assemblage	Contents of major minerals	Orebody
1	gal-sph	gal, sph, po, py	gal+sph >80%	I, II
2	po-sph	po, sph, cpy, gal	po >60%, sph 10-15%	I, II, IV
3	gal	gal, sph, cpy, bourn, po	gal >90%	II, III
4	mixture	po, apy, gal, sph, py	po+apy 20-35%, gal+sph >10-45%	II, III, IV
5	apy-sph	apy, sph, gal, po, py, freib	apy+sph >65%	III, IV
6	apy-cassit	apy, cassit, gal, sph, po, cpy	apy >85%, cassit 1-5%	III

apy=arsenopyrite, bourn=bournonite, cassit=cassiterite, cpy=chalcopyrite, freib=freibergite, gal=galena, po=pyrrhotite, py=pyrite, sph=sphalerite.

There is a general lack of direct consistent evidence (such as cross-cutting veins) for the relative timing of mineralisation of these four orebodies, it is inferred that they were formed simultaneously through sequential mineral deposition. The paragenetic sequence and relative abundance of the ore minerals for each orebody is summarised in Fig.5.3. In addition to the overall sequential variation of ore types of the whole deposit, a general order of ore mineral deposition, starting with arsenopyrite, through pyrrhotite (pyrite), to galena and sphalerite, is clearly evident for each orebody.

Arsenopyrite (FeAsS) is generally the earliest sulphide mineral phase in the ore and occurs commonly as euhedral grains (Plate 5.2a) and is often fractured. It is the dominant sulphide mineral of the lower part of orebody III.

Two generations of **pyrite** (FeS_2) are recognised. The first generation, pyrite 1, is concentrated in orebody III and lower part of orebody II, and is often associated with the arsenopyrite and pyrrhotite. It occurs as euhedral grains and shares mutual interpenetrating grain boundaries with the arsenopyrite, indicating simultaneous crystallization. Later generations of base metal sulphides enclose and occasionally replace pyrite 1 along fractures (Plate 5.2b). The second generation, pyrite 2, often occurs as subhedral to anhedral grains and forms botryoidal rims of galena along its boundaries with the

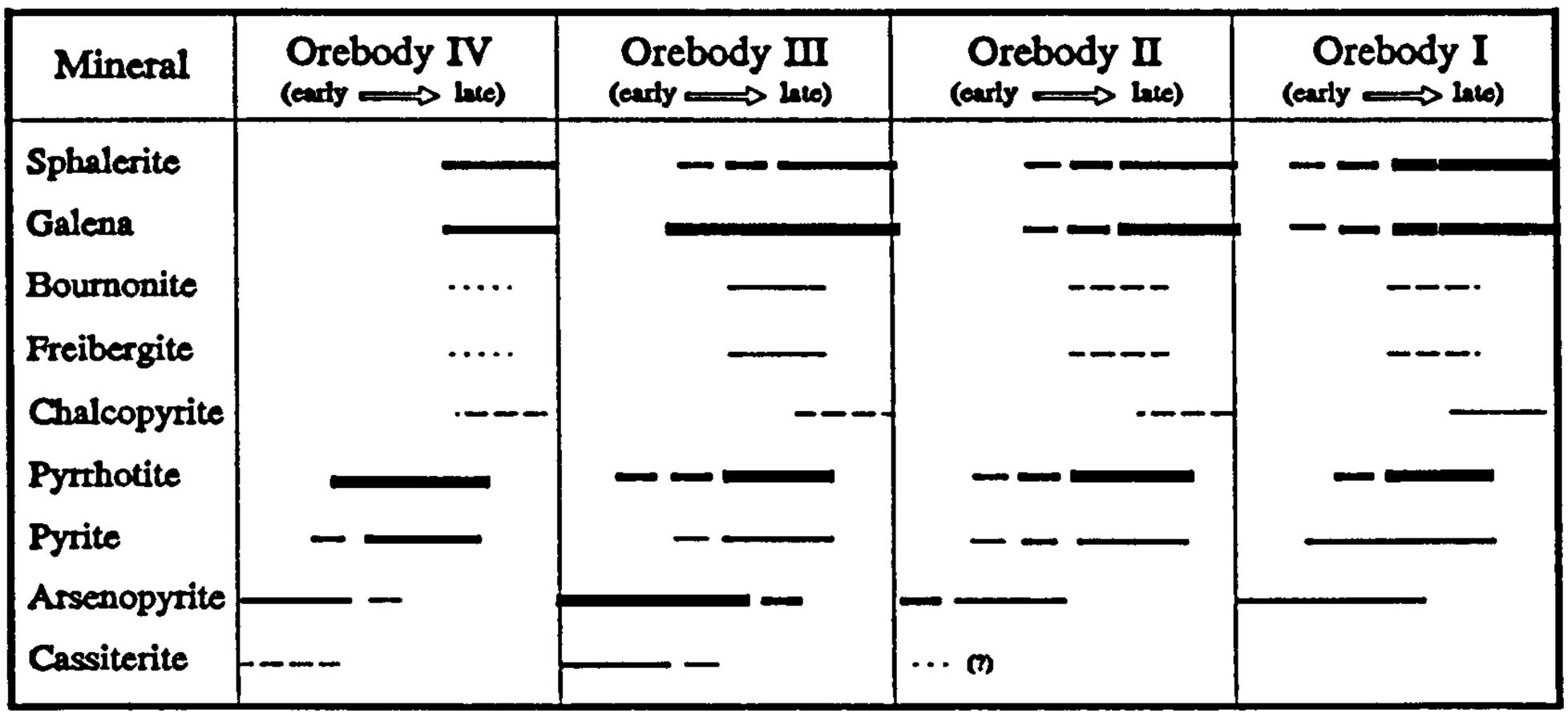

Fig. 5.3 Generalised paragenesis of the Meishi Pb-Zn deposit

pyrrhotite (Plate 5.3c).

Anhedral pyrrhotite ($Fe_{1-X}S$) is generally later than the arsenopyrite and pyrite 1, although mutual intergrowths between them do exist. It most commonly shows tree-branch and network textures with galena and sphalerite filling the open spaces (Plate 5.2d & e) and also appears as rounded or cigar shaped aggregates hosted in galena and sphalerite (Plate 5.2f & g).

Galena (PbS) and **sphalerite** (ZnS) are normally the later sulphide minerals. The mutual enclosure and replacement of these two minerals (Plate 5.2h & i) indicates their simultaneous precipitation. The galena contains minor inclusions of **pyrargyrite** (Ag_3SbS_3), **freibergite** [$(Ag,Cu)_{12}Sb_4S_{13}$], and **bournonite** ($PbCuSbS_3$). Sphalerite is generally riddled with inclusions of **chalcopyrite** ($CuFeS_2$) (Plate 5.2j) and subordinate pyrrhotite and galena.

Marcasite (FeS_2) is developed as a secondary mineral along fractures, which cross-cut other minerals and are filled with carbonate (calcite ?) and silicate (chlorite ?), and partially or entirely replaces pyrrhotite and pyrite (Plate 5.2k & l).

Plate 5.2

Plate 5.2 **Photomicrographs showing mineralogical characteristics of the Meishi Pb-Zn deposit**

(All photomicrographs were taken under plane-polarised light; aspy = arsenopyrite, gal = galena; mst = marcasite; po = pyrrhotite; py = pyrite; sph = sphalerite)

a. Sphalerite and pyrrhotite fill in interstice of arsenopyrite. Pyrrhotite partially replaced by marcasite. Bar = 0.40mm.

b. Early euhedral pyrite enclosed by galena and sphalerite. Bar = 0.20mm.

c. Subhedral to anhedral pyrite grains distribute along the contact of galena and pyrrhotite. Bar = 0.20mm.

d. Tree-branch texture. Subparallel pyrrhotite aggregates comprise the main framework, galena and sphalerite fill the open spaces. Bar = 0.40mm.

e. Network texture. Sphalerite and galena fill the open spaces left by interconnected pyrrhotite which forms the main frame of the network. Bar = 0.20mm.

f. Rounded pyrrhotite islands surrounded by galena. Bar = 0.20mm.

g. Cigar-shaped pyrrhotite aggregates hosted within galena. Bar = 0.20mm.

h. Galena replaces sphalerite evidenced by the remaining sphalerite islands within the galena. Bar = 0.20mm.

i. Chalcopyrite (yellow) and pyrrhotite (pink) inclusions within sphalerite. The chalcopyrite inclusions occur as rounded dots, whereas the pyrrhotite inclusions tend to form continuous lines. Bar = 0.10mm.

j. Galena replaces arsenopyrite evidenced by the remaining arsenopyrite skeleton within the galena. Bar = 0.20mm.

k, l. Marcasite replaces pyrrhotite and pyrite along fractures. Bar = 0.40mm.

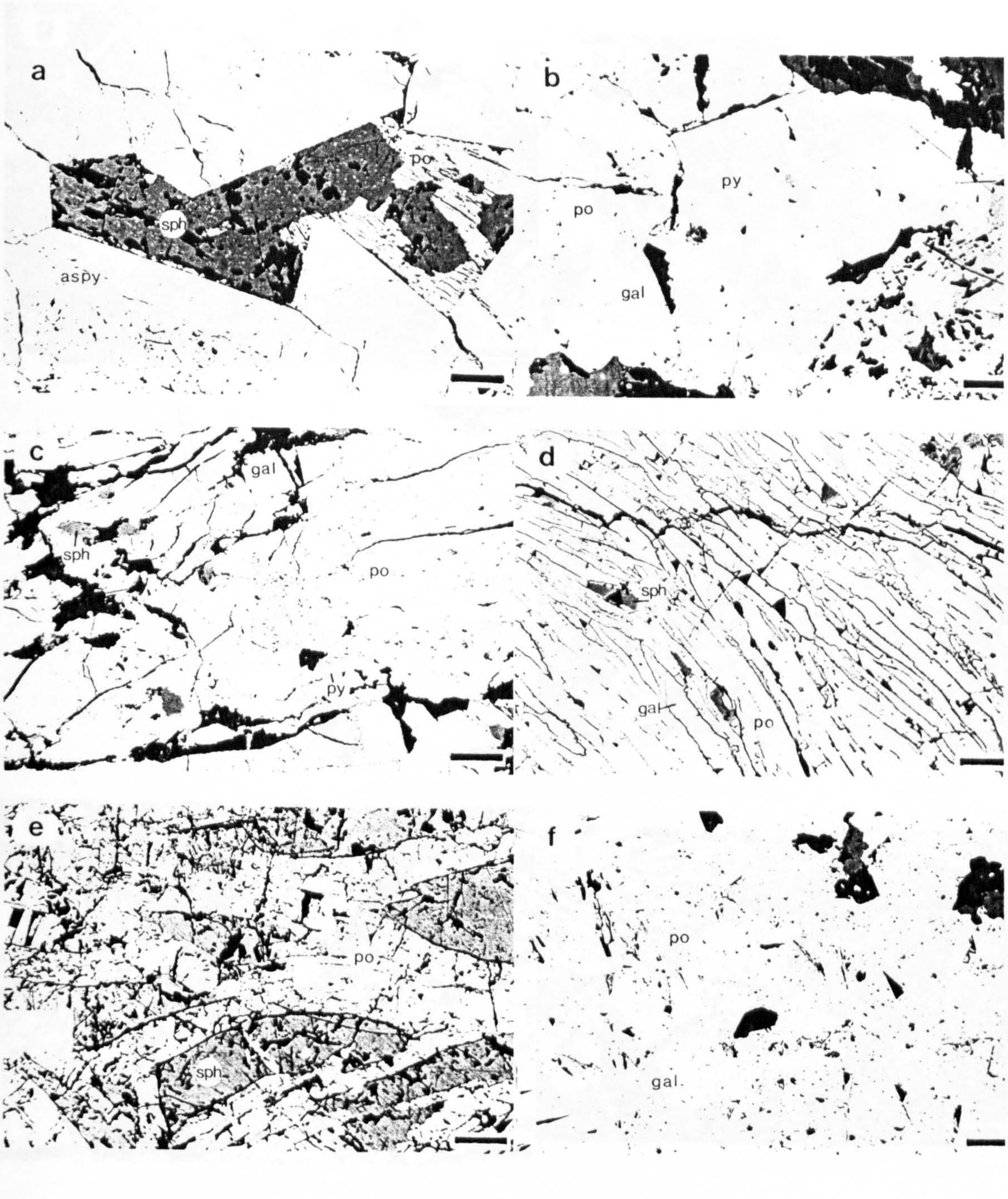
a
po
sph
aspy
b
py
po
gal
c
gal
sph
po
py
d
sph
gal
po
e
po
sph
f
po
gal

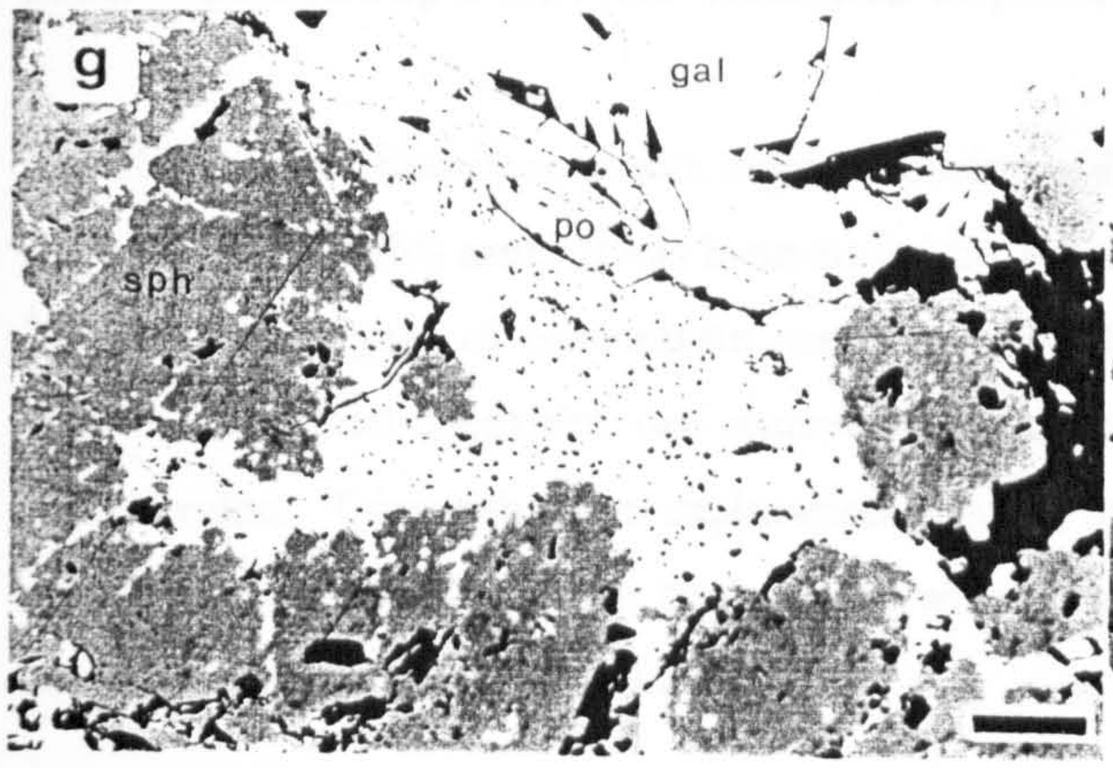
g
gal
po
sph

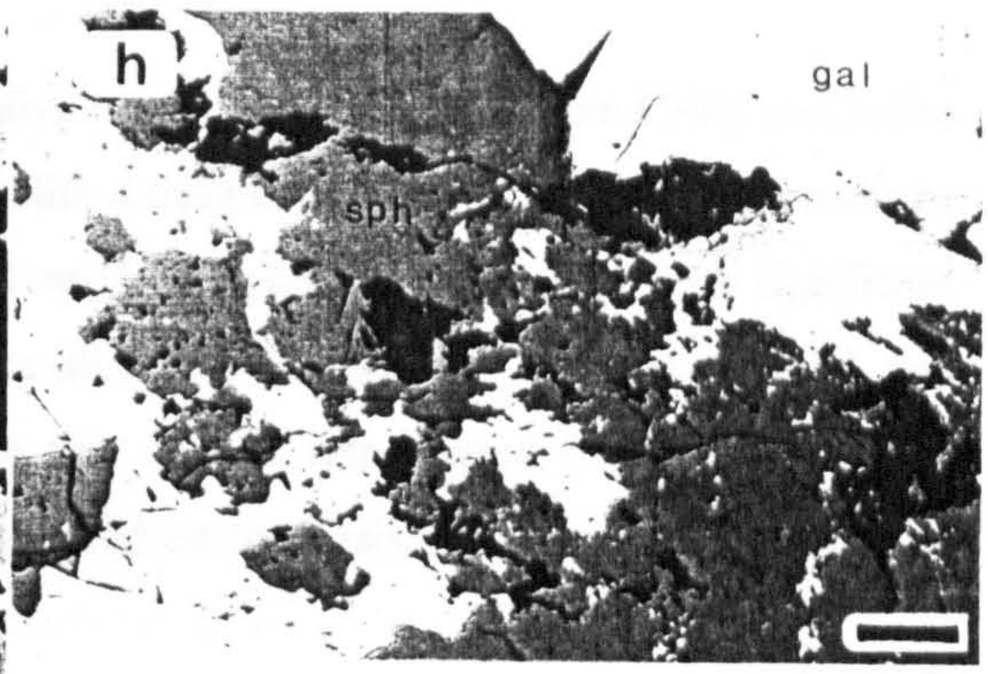
h
gal
sph

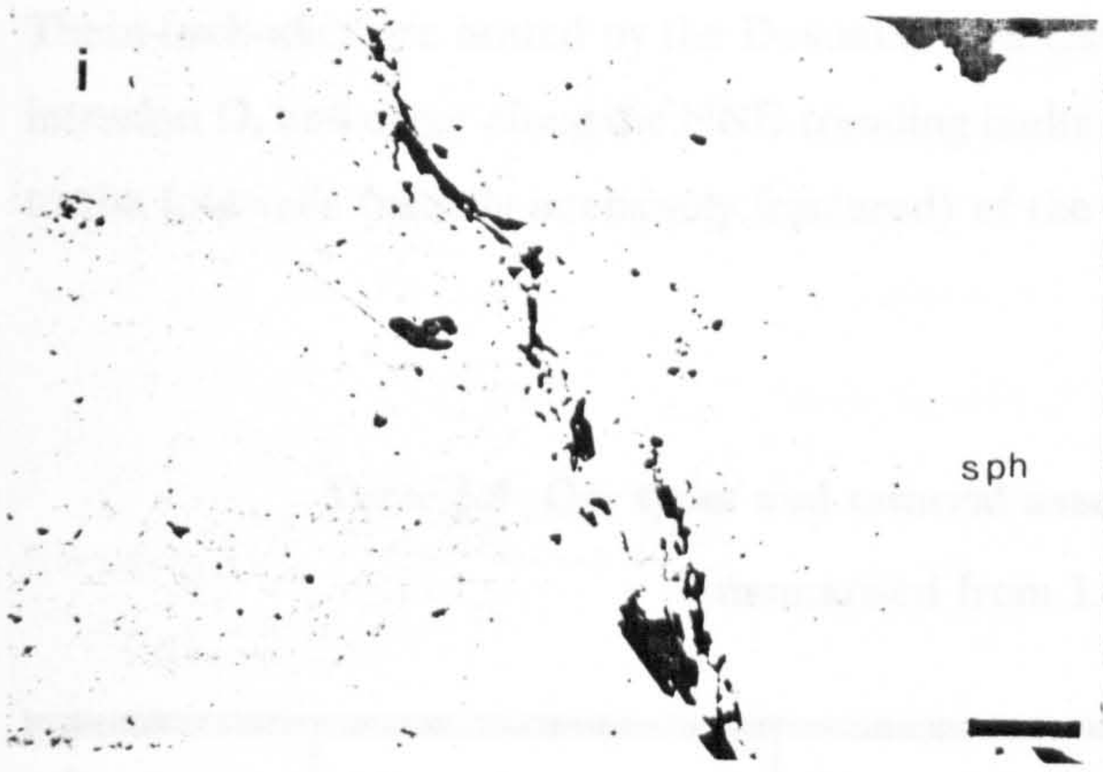
i
sph

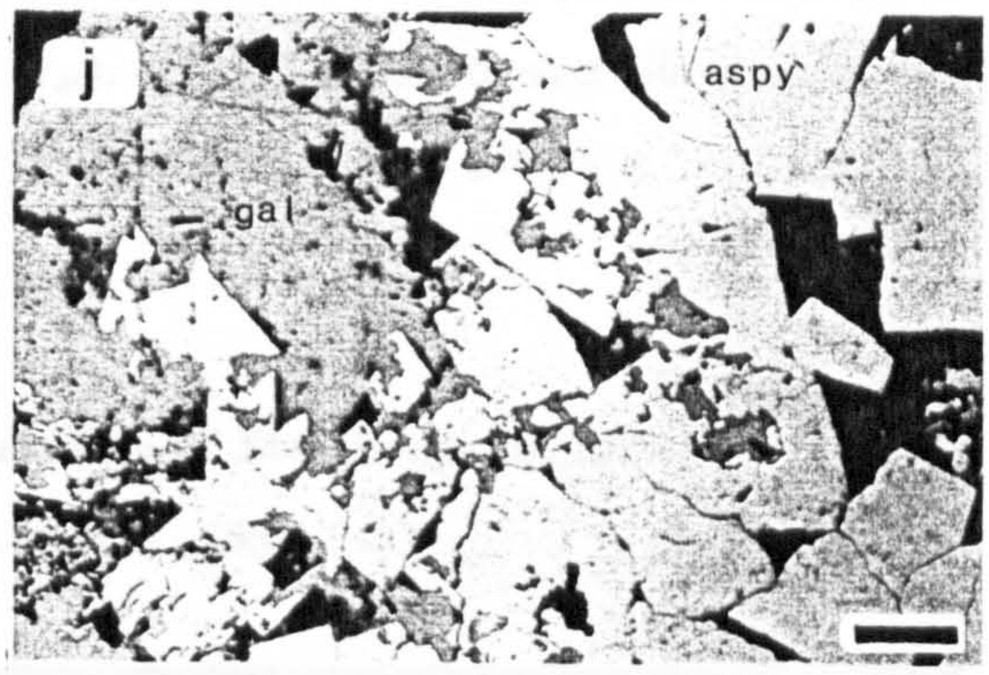
j
aspy
gal

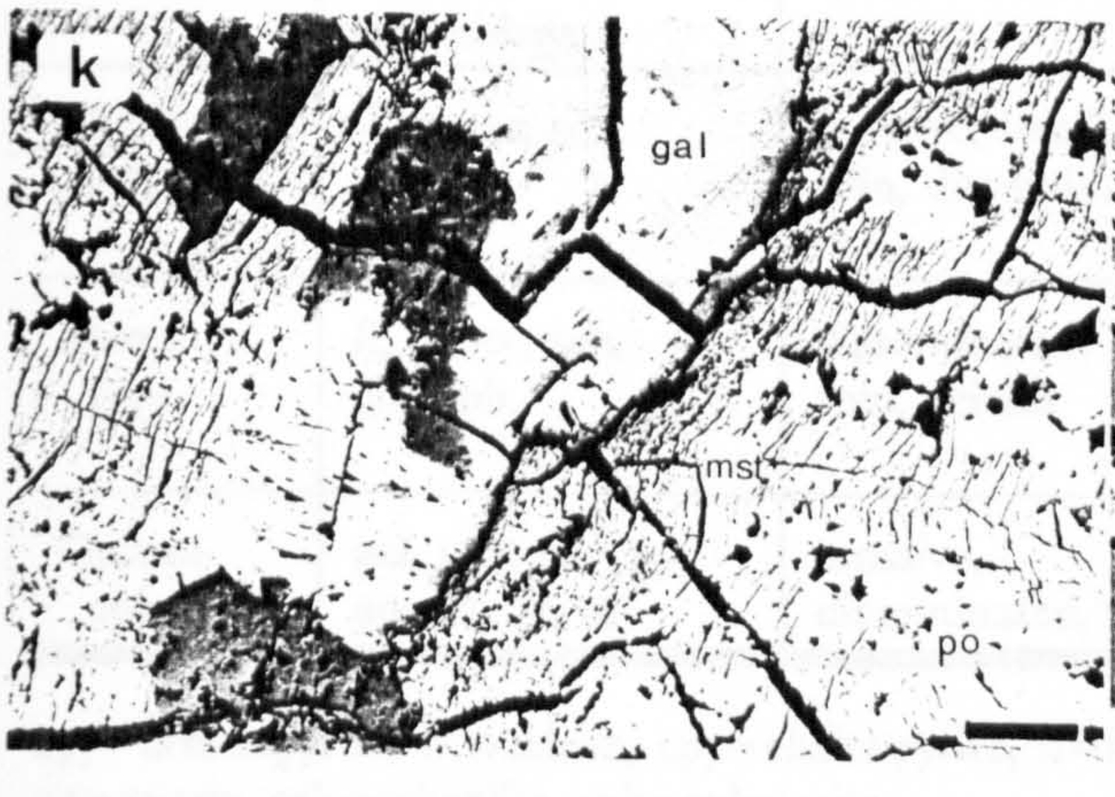
k
gal
mst
po

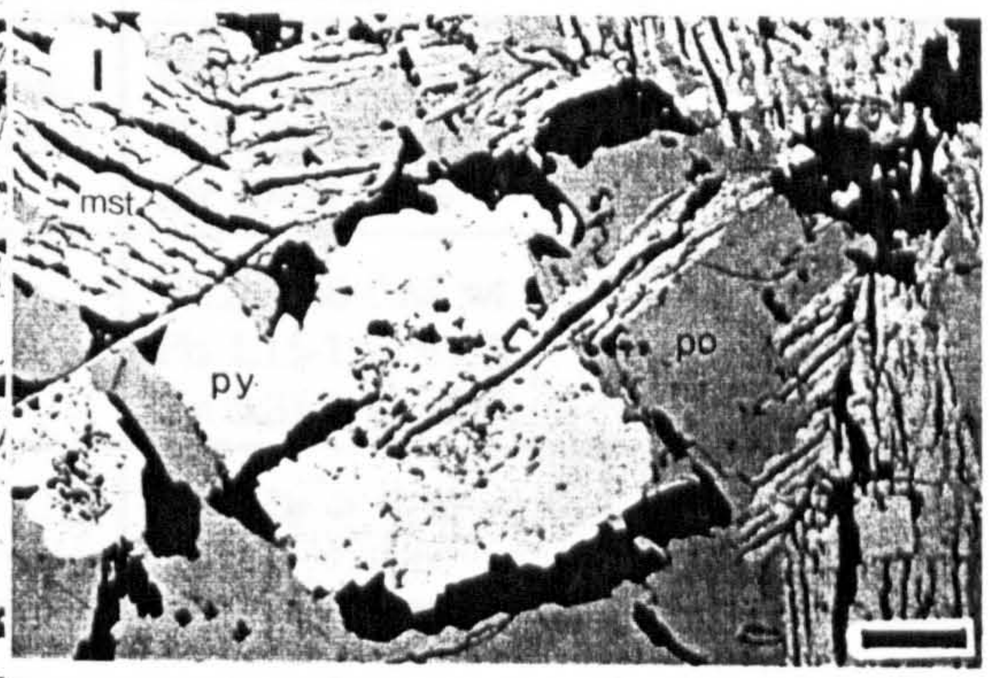
l
mst
py
po

5.2.2 Xianghuapu fluorite-scheelite deposit

The Xianghuapu fluorite-scheelite deposit consists of five orebodies (I, II, III, III' and 301) and is the largest deposit in this area. It has been mined for scheelite during the last three decades and produces 240-290 tonnes/year of concentrate containing 80-90 wt.% of scheelite. In addition, a significant amount of galena-sphalerite ore associated with the fluorite-scheelite ore has been mined and concentrated. Comprehensive exploration relating to this deposit was carried out by Luo and his colleagues in the 1970s. Three types of ore were recognised on the basis of mineral assemblage and ore textures (Luo et al.,1981; Table 5.5).

These orebodies are hosted by the Devonian and Carboniferous limestone and dolomite adjacent to intrusion D, and occur along the NNE-trending faults (F_{4S}). The mineralisation is confined exclusively to the footwalls (usually intensively fractured) of the faults and to the fault gouge.

Table 5.5 Ore types and mineral assemblage of Xianghuapu deposits
(summarised from Luo et al., 1981)

Ore type	Mineral assemblage	Ore texture	Contents of main components	Orebody
Fluorite-scheelite	fl, qz, cc, sch	massive, banding, vein, disseminated	WO_3 1-20.20 wt.%, CaF_2 20-60 wt.%, Qz 10-30 wt.%	I, II
Mixed type	fl, qz, cc, sch, gal, sph	disseminated, vein, veinlet	WO_3 0.66-0.88 wt.%, Pb 1.15-1.50 wt.%, Zn 0.81-1.12 wt.%	III, III'
Galena-sphalerite	gal, sph, py, cpy, apy, fl, qz, cc	massive, disseminated, vein	Pb+Zn > 8-10 wt.%	301

apy=arsenopyrite, cc=calcite, cpy=chalcopyrite, fl=fluorite, gal=galena, po=pyrrhotite, py=pyrite, qz=quartz, sch=scheelite, sph=sphalerite.

No. III orebody was suggested to consist of mixed ores with sphalerite and galena predominant (Luo et el., 1981). However, it was discovered to grade downwards into a large, extremely scheelite-rich

orebody during mining operations in the 1980s and subsequently became the main mining target of the Xianghuapu Mine. The content of scheelite varies from 1 wt.% to 20 wt.%, reaching 30 wt.% in places (Wu, J. H., 1986, personal communication). The ore is composed mainly of fluorite, quartz, scheelite, calcite, and shows massive and banded textures (Plate 5.3a, b & c). The massive ore is distributed in the orebody as irregular pods; the laminae of the banded ore are generally coincident with the bedding of the strata and often show an asymmetric comb structure (Plate 5.3d).

The growth habits, textures, and associations of the minerals comprising the ores allow the depositional history of the orebodies to be divided into three stages (Fig.5.4): (1) fluorite + quartz + scheelite + calcite; (2) sphalerite + galena + quartz; (3) calcite + quartz + fluorite + scheelite.

Mineral	Stage 1	Stage 2	Stage 3
Fluorite	▬▬▬	———	———
Quartz	▬▬▬	———	———
Scheelite	▬▬▬	———	— — —
Calcite	———	———	▬▬▬
Galena	— — —	▬▬▬	
Sphalerite	— — —	▬▬▬	
Chalcopyrite	— — —	———	
Arsenpyrite		———	
Pyrite		———	
Pyrrhotite	— — —	———	
Cassiterite	— — —	———	
Chlorite	— — —	———	———
Sericite	— — —	———	———

Fig. 5.4 Generalised paragenesis of the W-F mineralisation in the Xianghuapu deposit

STAGE 1: Fluorite + quartz + scheelite + calcite

Mineralisation in the Xianghuapu fluorite-scheelite deposit appears to begin with the precipitation of euhedral to subhedral, coarse-grained fluorite and quartz in which square-shaped scheelite grains are randomly distributed. The scheelite crystals in the massive ore can reach 2-3cm in size (Plate 5.3e) and occasionally show zonation (Plate 5.3f). Calcite always appears as a later mineral phase in this stage and occupies the central parts of the pods and veins. It replaces scheelite along fractures within the crystals (Plate 5.3g).

STAGE 2: Sphalerite + galena + quartz

The deposition of the stage 1 minerals was followed by the main episode of base metal sulphides, consisting mainly of sphalerite and galena accompanied by small amounts of chalcopyrite, pyrite, pyrrhotite and arsenopyrite. Galena encloses the stage 1 quartz and replaces pyrite and pyrrhotite. Sphalerite appears as yellowish flakes (Plate 5.3h). It replaces the earlier sulphide minerals (galena, pyrite and pyrrhotite) and contains only rare chalcopyrite inclusions. Chalcopyrite concentrates along the boundaries of other mineral phases. and also replaces these minerals. This sulphide ore generally occupies the upper parts of the orebodies, or occurs in the centre of the fluorite-quartz pods (Plate 5.3i).

STAGE 3: Calcite + quartz + fluorite + scheelite

Barren or weakly mineralized massive calcite bodies or veins are always associated with the orebodies. They are found either hosting fluorite-scheelite ore fragments (Plate 5.3l) or filling the spaces developed along the middle of the fluorite-quartz veins. The massive calcite shows two different colours: pink and white; there is no clear boundary between them and the reason for the colour difference is not yet known.

Plate 5.3

Plate 5.3 **Photographs showing petrographical characteristics of the Xianghuapu fluorite-scheelite deposit**

a, b, c. Photographs showing banded texture of the fluorite-scheelite ore.

d. Comb structure. Fluorite and quartz occupy both sides of the wall and calcite occurs in between. Scheelite grains distribute randomly within the vein.

e. Photograph showing scheelite crystals up to 4cm in dimension.

f. Single scheelite crystal within the matrix of fluorite. The crystal displays two growth zones.

g. Photograph showing light coloured (yellowish) sphalerite ore co-exists with W-F mineralised quartz pod.

h. Photograph showing galena aggregate within mineralised fluorite-calcite pod.

i. Photomicrograph showing an euhedral scheelite grain replaced partially by calcite. Bar = 0.50mm.

j. Photograph showing fragments of the W-F ore enclosed by later massive calcite.

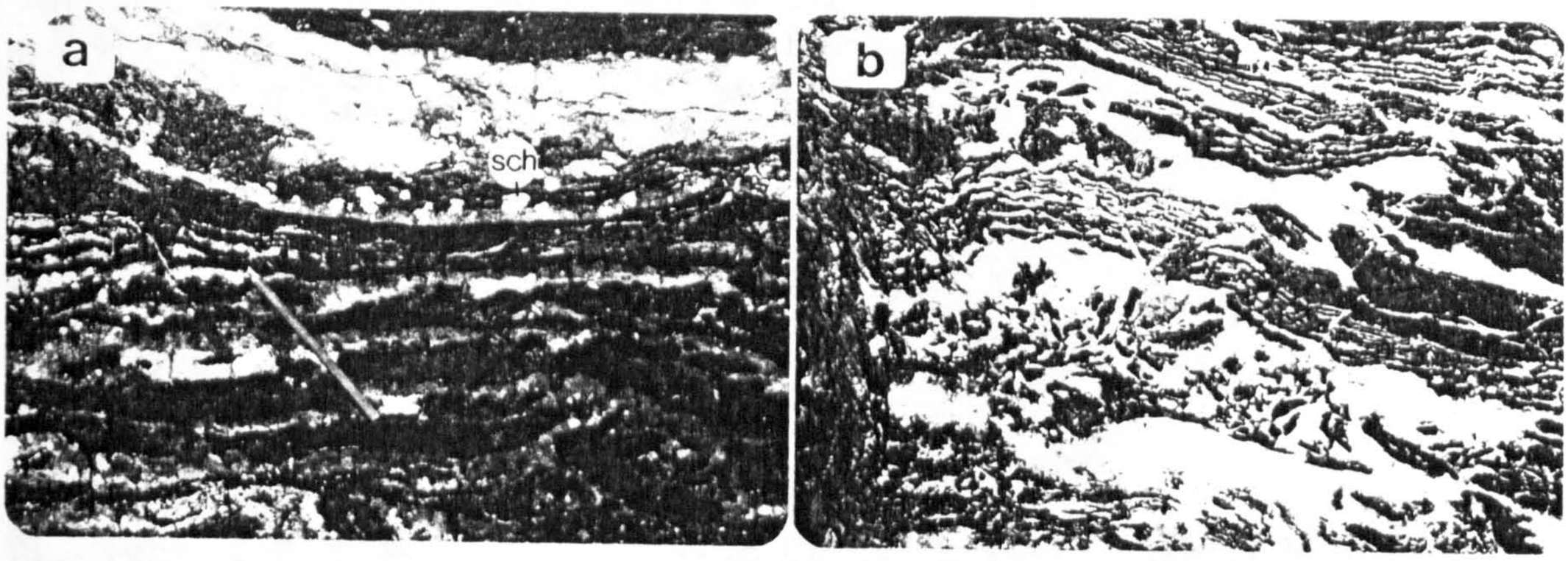
a
sch
b

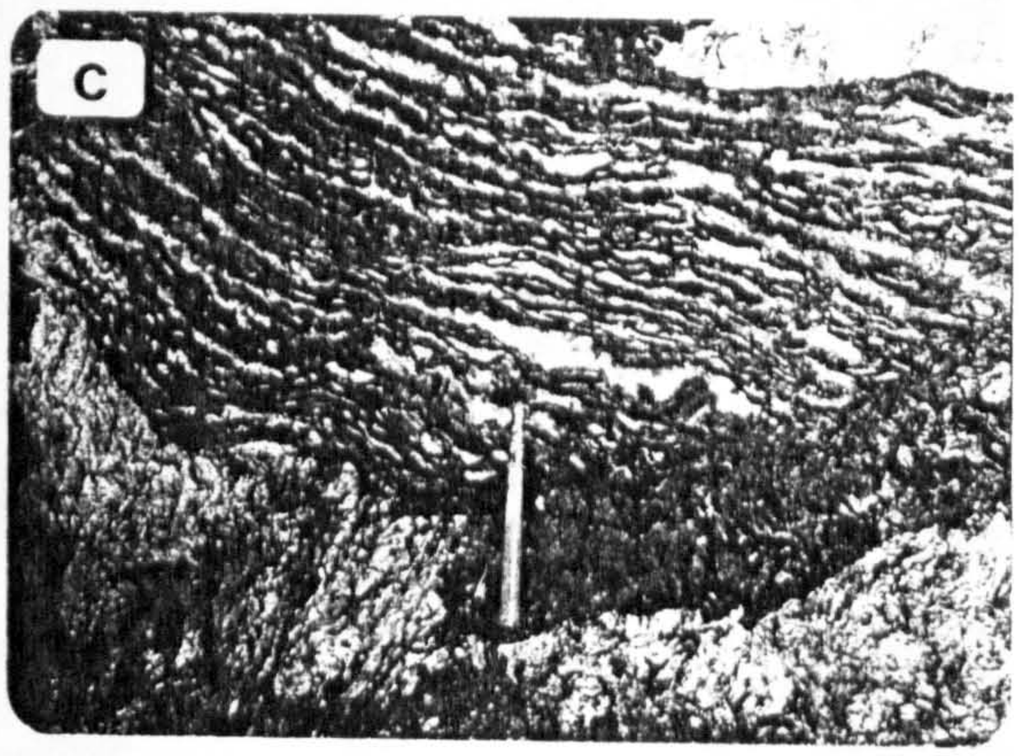
c

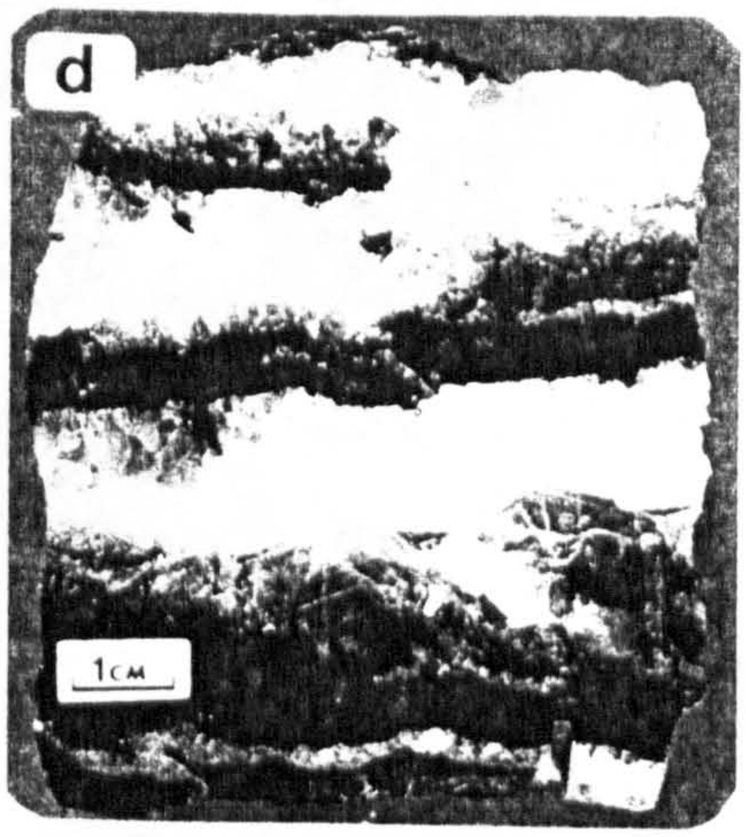
d
1cm

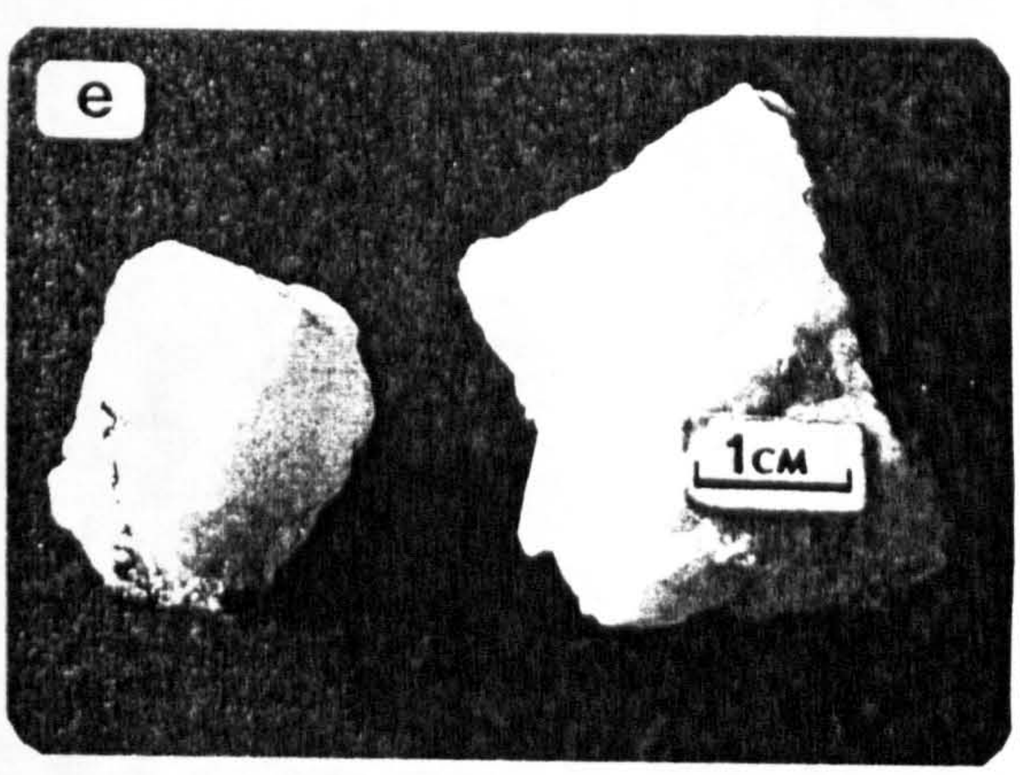
e
1cm

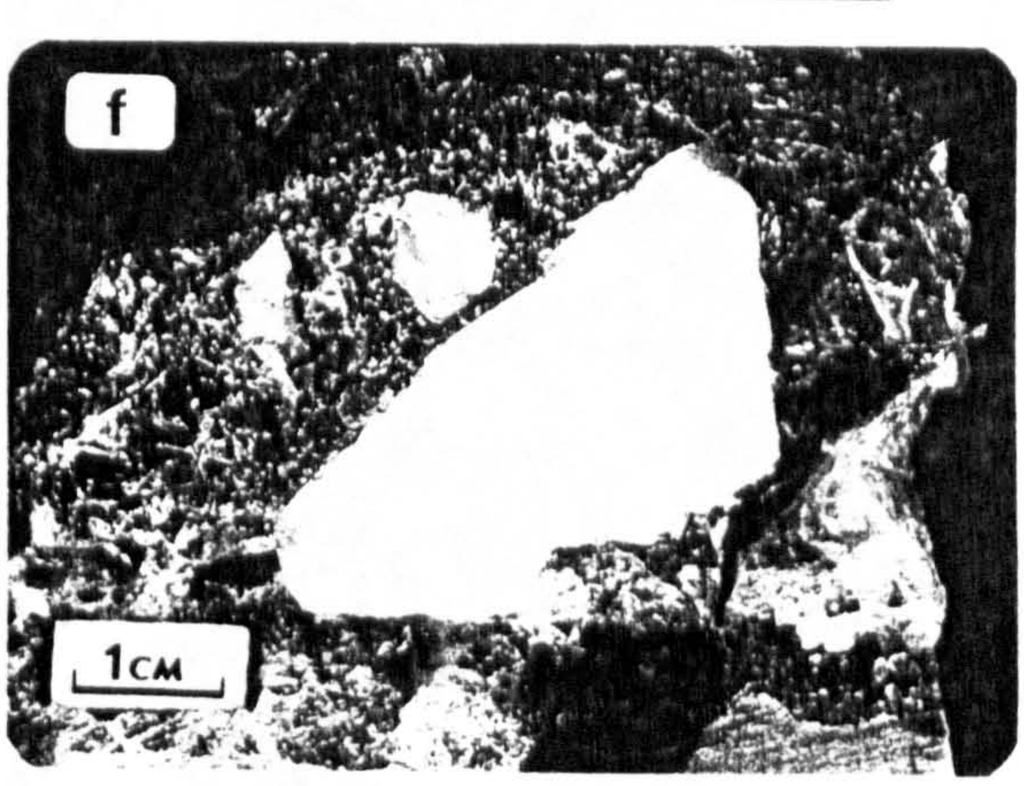
f
1cm

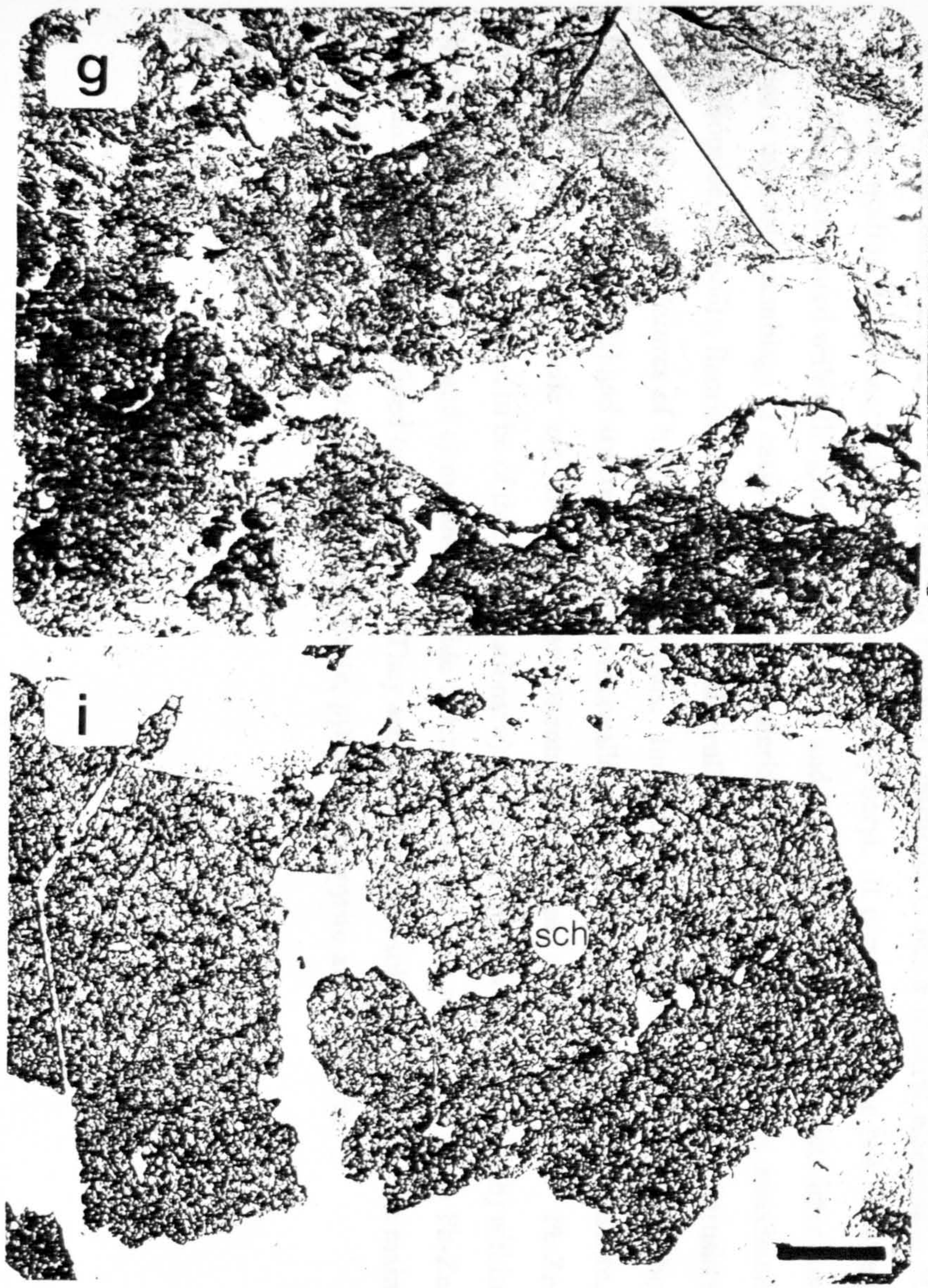
g

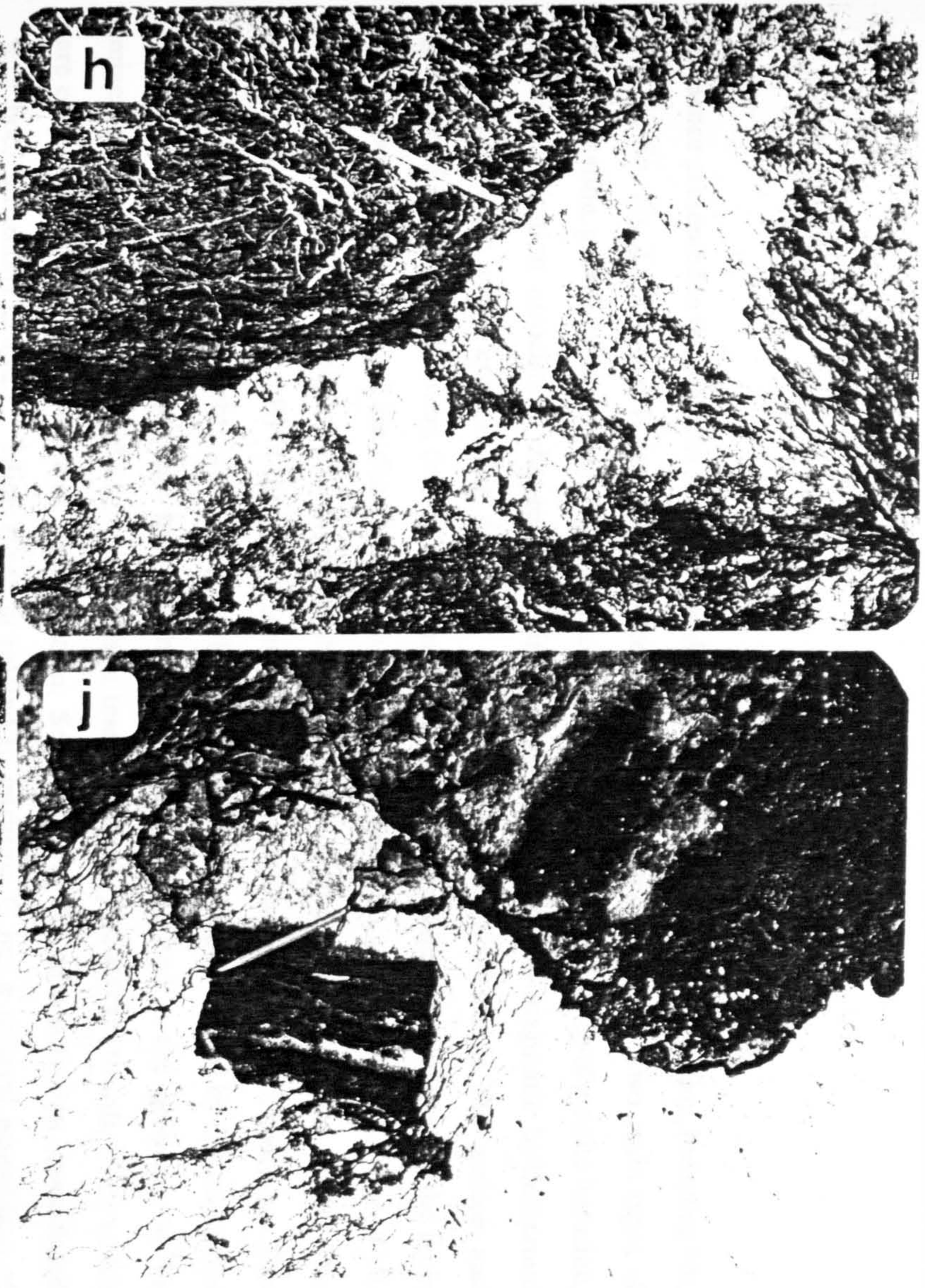
h

i
sch

j

5.3 SUMMARY

Evidence presented in the previous sections revealed that the polymetallic mineralisation, including Nb, Ta, W, Sn, Pb, Zn, Ag and F, is closely related to the Jianfengling granites. Two main types of mineralisation, granite-type and lode-type, are recognised. Following the sequence of granite intrusion, the mineralisation association changes accordingly. Late- and /or post-magmatic hydrothermal alteration is the main mineralising process. **Nb-Ta mineralisation** occurs in the greisen and greisenised granite which covers the top of intrusion B. Microlite, niobite and tantalite are the main Nb-Ta-bearing minerals and are disseminated throughout the greisen zone. The total content of Nb and Ta has a positive correlation with the strength of greisenisation (No. 238 Geol. Team., 1974). The associated granite (intrusion B) of the Nb-Ta mineralisation has the lowest Nb and Ta contents. This may suggest that these elements were extracted by a Li-, and F-rich (demonstrated by the existences of zinnwaldite and topaz) late-stage hydrothermal fluid and concentrated in the greisen. Nb-Ta minerals are often precipitated in Li-F-rich fluids at temperatures of 300-400°C (Kosals, 1976) which are consistent with the temperature of greisenisation. **Sn-W (Be, Pb, Zn) mineralisation** is associated with both intrusions C and E. Mineralisation related to intrusion C has a mineral assemblage of cassiterite, wolframite, galena, sphalerite, and occasionally beryl. It occurs along the NW-trending faults which are hosted within the granites (intrusions B and C). Mineralisation linked with intrusion E has a mineral assemblage of cassiterite, galena, sphalerite, arsenopyrite and pyrrhotite, associated with diopside, actinolite, fluorite and sericite. **W-F mineralisation** is confined dominantly to intrusion D and has general features of hydrothermal deposits. Individual orebodies are associated with the NNE-trending faults (F4s) and are confined to the footwalls of the faults and the fault gouge. Fluorite, scheelite, quartz and calcite are the main components of this type of mineralisation. **Pb-Zn mineralisation** is recognised to be of three associations: a) in zones of greisen and pegmatite; b) within the fluorite-scheelite ores; and c) massive sulphide lodes in carbonate host rocks. The main Pb-Zn orebodies are spatially confined to intrusion E. They are hosted in karst solution cavities with a main mineral assemblage of galena, sphalerite, pyrrhotite, pyrite, arsenopyrite and cassiterite.

CHAPTER SIX

FLUID INCLUSION AND STABLE ISOTOPE STUDIES

CHAPTER SIX

FLUID INCLUSION AND STABLE ISOTOPE STUDIES

Content

6.1 Fluid Inclusion Microthermometry

6.1.1 Introduction

6.1.2 Microthermometry

6.1.3 Summary

6.2 Stable Isotope Studies

6.2.1 Samples studied and analytical methods

6.2.2 Isotopic compositions of the granite-related rocks

6.2.3 Isotopic compositions of the W-F mineralisation

6.2.4 Sulphur isotope composition of Pb-Zn mineralisation

6.2.5 Discussion

6.1 FLUID INCLUSION MICROTHERMOMETRY

Fluid inclusions present in quartz and topaz from the pegmatitic rocks of the Jianfengling complex and in quartz and fluorite from the fluorite-scheelite ores (see Chapters 3 and 4) have been investigated microthermometrically in order primarily to characterise the fluids mobilised during the evolution of the granite intrusion and the associated mineralisation. The methodology is outlined briefly together with a discussion of limitations. The fluid data obtained are summarised in this chapter and are presented in full in Appendix IX. Discussions of fluid evolution, metal transport and ore deposition, based on the data reported in this chapter and previous chapters, are presented in Chapter 7.

6.1.1 Introduction

The significance of fluid inclusion studies in understanding and quantitatively modelling geological processes has been long recognized. But in recent years, the growth in interest has been rapid, with applications being found in extremely diverse branches of earth sciences. The fluid inclusion literature is vast, among which the texts and reference sources by Roedder (1984) and Shepherd *et al.* (1985) are particularly useful. Although at present there is a great deal of experimental and theoretical work being carried out in order to increase our understanding of multi-component fluid systems, a detailed account of the theoretical arguments employed in the interpretation of the thermometric data is beyond the scope of this study.

Among the methods used for fluid inclusion studies, thermometric analysis is the most popular technique. Not only can it be non-destructive, but is also it based on simple principles and requires relatively inexpensive equipment. The method involves the recognition and measurement of phase changes which take place in inclusions during heating or cooling. The P-V-T-X state of the fluids at the time of trapping can be derived by referring to simple fluid systems. However, the usefulness of this technique is limited by the fact that most natural systems are multi-component, so that the P-V-T-X estimates are only semi-quantitative at best. In such case, difficulty arises in interpretation of the thermometric data.

The main aim of this study has been to characterise the fluids generated during the evolution of the Jianfengling granites and the formation of the various types of mineralisation. The variables of major interest are the fluid composition (X), temperature (T) and pressure (P). These parameters are essential in modelling fluid evolution and the mobilisation, transportation and deposition of metals. An optical and thermometric fluid inclusion study forms an important part of this research programme. During the course of the investigation, fluid inclusions in more than 50 samples of granite-related rocks and ores have been studied in thin section under transmitted light, with 18 proving suitable (in terms of availability of inclusions, optical clarity and inclusion size) for thermometric analysis. Fluid inclusions have been analyzed thermometrically using 100-200μm thick, doubly-polished wafers and a Linkam THM 600 heating-freezing stage (for detailed sample preparation and stage operation procedures the reader is referred to Shepherd *et al.*, 1985). In total, about 500 inclusions have been investigated. The calibration method for the Linkam THM 600 heating-freezing stage is described by Wilkinson (1990, p.248-250).

6.1.2 Microthermometry

In the following sections, descriptions of the optical and thermometric characteristics of fluid inclusions from different sample groups are presented. For reasons of simplicity, samples from the pegmatitic rocks and ores of the fluorite-scheelite mineralisation are grouped separately, although there may be some overlap in terms of fluid inclusion characteristics. The classification of fluid inclusions is primarily based on their association with the rock and ore types. These inclusions are subsequently classified by their appearance at room temperature. Thus, two general types of fluid inclusions, P and O, have been defined. They represent inclusions from the pegmatitic rocks and from ores of the fluorite-scheelite mineralisation, respectively.

6.1.2.1 Fluid inclusions of the pegmatitic rocks

Optical characteristics

The term "pegmatitic rocks" here refers to pegmatites and rocks from the pegmatitic pods. Theoretically, minerals such as quartz, feldspars, topaz and micas, which are the main components of these rocks, could all be used for fluid inclusion study. Owing to availability and optical clarity, however, only quartz and topaz were chosen from the pegmatitic rocks for detailed microthermometric study. The recognition of primary and secondary inclusions is based on the criteria of Roedder (1984). Secondary trails are abundant in minerals from the pegmatitic rocks, especially quartz, and consist of inclusions, generally <1μm, the contents of which could not be ascertained. The quartz from the quartz shells of intrusions D and E has a near-opaque, milky appearance due to the presence of a large quantity of these tiny inclusions. Two main inclusion types may be distinguished both optically and thermometrically. Photomicrographs of typical thin section fields of views are show in Plate 6.1 and a summary of the main optical characteristics is presented in Table 6.1

Plate 6.1

Plate 6.1 **Photomicrographs showing characteristics of fluid inclusions in pegmatitic rocks and W-F ores.**

First page --- fluid inclusions in pegmatitic rocks:

a. Photomicrograph showing the distribution of two-phase (vapour-liquid) fluid inclusions in topaz from the pegmatites. Bar = 60μm.

b. Negative crystal-shaped inclusions in topaz of pegmatite. Bar = 60μm.

c, d. Irregularly shaped two-phase (vapour + liquid) fluid inclusions in quartz of pegmatites. Bar = 25μm.

e. One-phase (vapour ?) inclusion in quartz of pegmatites. Bar = 0.25μm.

f. Three-phase (vapour + liquid + halite) inclusion in quartz of pegmatites. Bar = 0.25μm.

g, h, i. Multiphase (vapour + liquid + unknown solid phase(s)) inclusions in quartz of pegmatites. The solid phases are generally birefringent and irregularly shaped. Bar = 0.25μm.

Second page --- fluid inclusions in the W-F ores:

j, k, m, n. Photomicrographs showing the distribution of two-phase (vapour + liquid) fluid inclusions in fluorite. Note the differences of the degree of fill of inclusions within the same field of view. Bar = 60μm for j, k and n, and 150μm for m.

l. One-phase (liquid ?) inclusions in fluorite. Bar = 60μm.

o, p, q, r. A series of photomicrographs showing the nature of extensive necking down of fluid inclusions in the later fluorite of the W-F ores. Bar = 60μm.

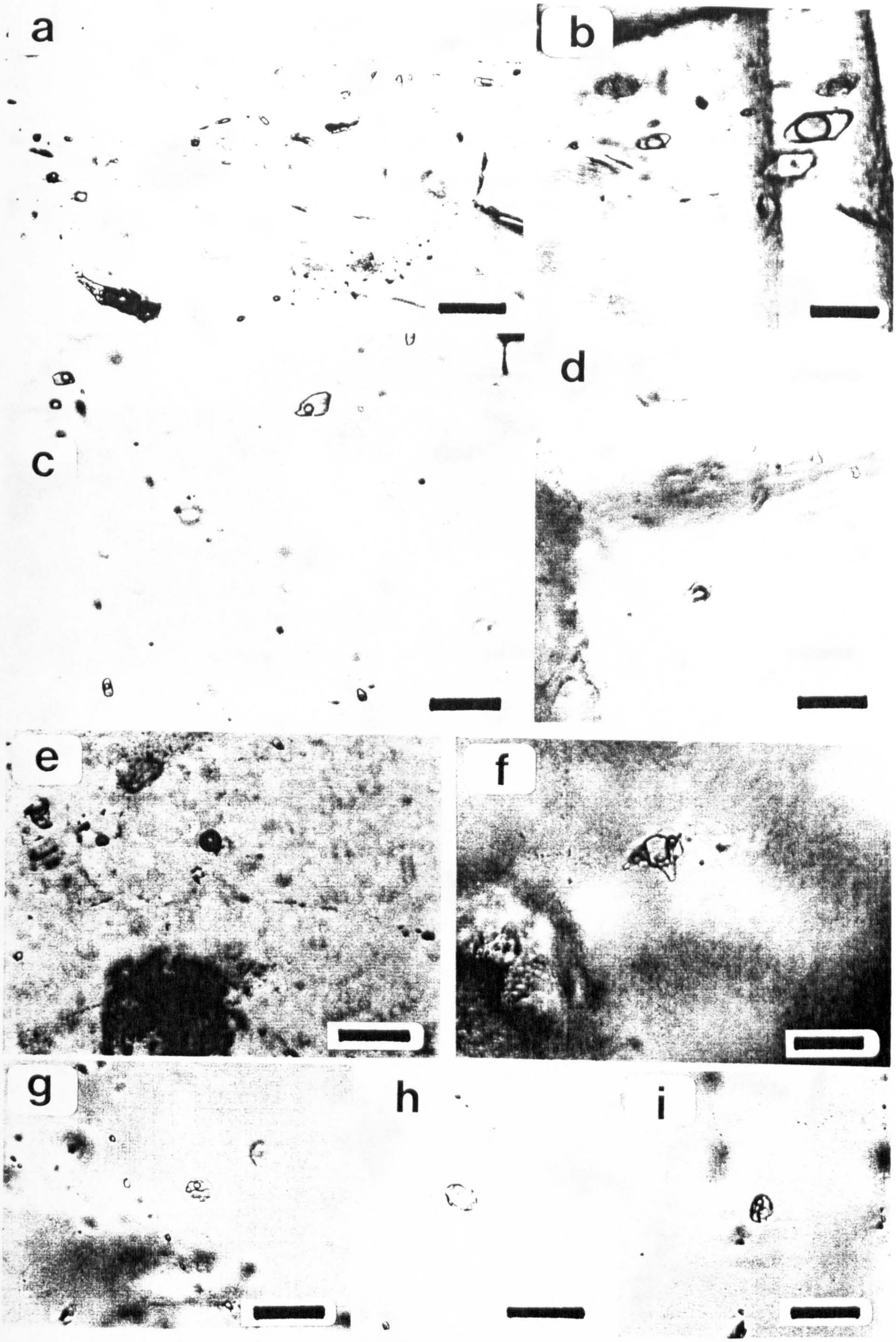
a
b
c
d
e
f
g
h
i

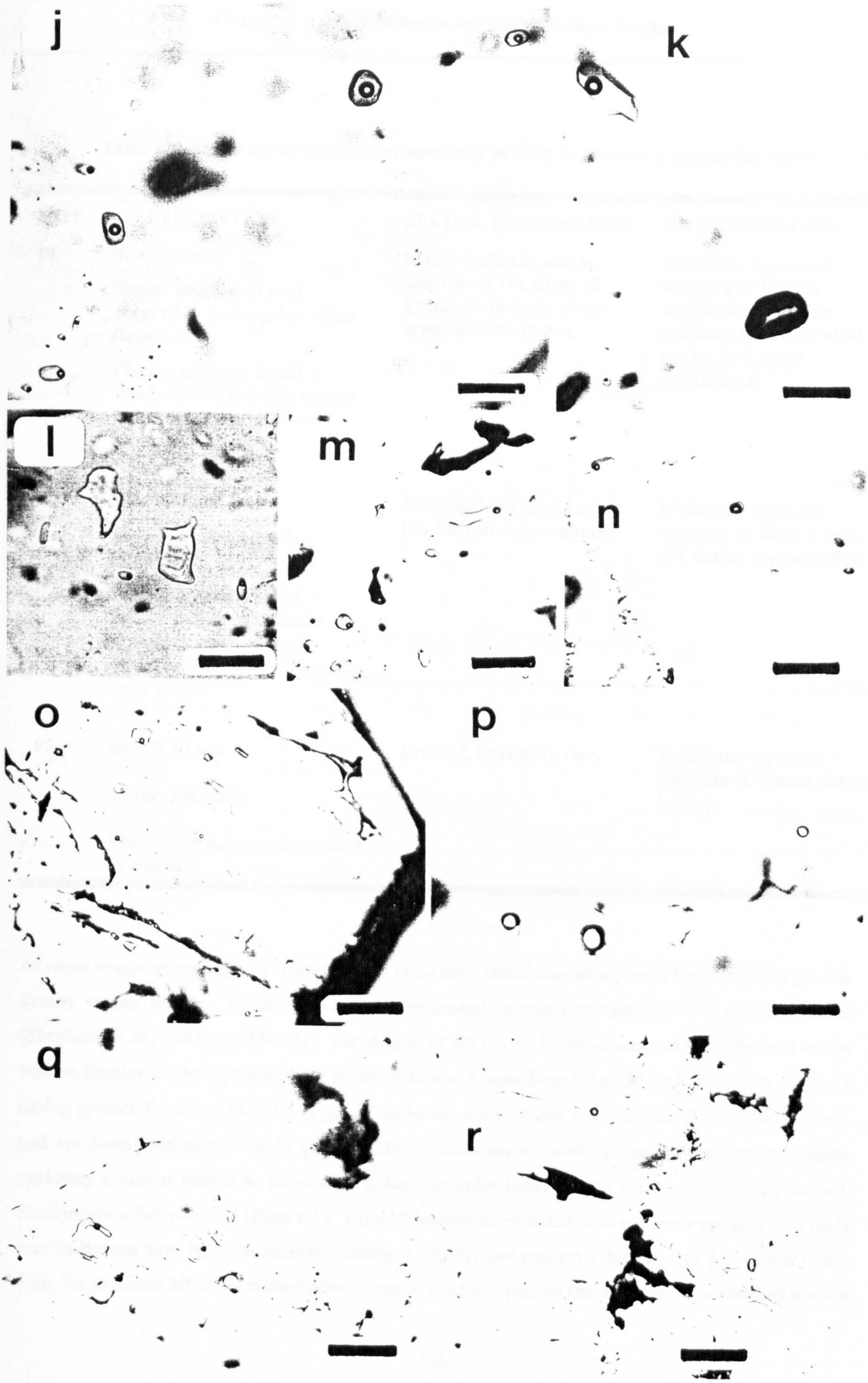
j
k
l
m
n
o
p
q
r

Table 6.1 Summary of optical characteristics of fluid inclusions in pegmatitic rocks

TYPE	DESCRIPTION	SPATIAL DISTRIBUTION	INTERPRETATION
P1	Size: 5-80μm. Shape: negative crystal, ellipsoidal, or irregular, often flattened. Phases: aqueous liquid + vapour (F=0.30-0.95); vapour phase may show different colours.	Mainly isolated; also in clusters on the edges of grains; or in trails along crystallisation planes.	Inclusions represent trapping of fluid in equilibrium with the granitic melt from which quartz and topaz crystallised.
P2	Size: 5-20μm. Shape: usually irregular, ellipsoidal. Phases: aqueous liquid + vapour + one cubic halite crystal, or one (or two) irregular shaped birefringent solid phases.	Exclusively isolated; only a few inclusions per sample.	Inclusions represent trapping of fluid ± melt (?) during crystallisation.
P3	Size: 5-10 μm. Shape: rounded. Phase: one vapour phase, dark in colour.	Isolated, extremely rare.	Inclusions represent trapping of vapour during boiling.

At room temperature, type P1 inclusions are two-phase containing an aqueous liquid enclosing a low density vapour bubble. Phase volumes were estimated by visual comparison with standard charts (Shepherd *et al.*, 1985, pp.255-256). The degree of fill (F) of P1 inclusions, which is defined as the volume fraction of the aqueous phase in the inclusion, ranges from 0.30-0.95 with inclusions in quartz having greater F values (Fig.6.1). Type P2 inclusion are rare and relatively small (less than 20μm), and are found exclusively within quartz. These inclusions are multi-phase with an aqueous liquid enclosing a vapour bubble in addition to either one cubic halite or one (or two) irregularly shaped, birefringent solids phase(s) (Plate 6.1). Type P3 inclusions, rounded in shape, are extremely rare (only four inclusions have been encountered during the study) and contain a dark vapour phase only (Plate 6.1). To avoid the effects of microfractures, especially for topaz, on the inclusion's contents, all studied

inclusions were selected as far from the fractures as possible.

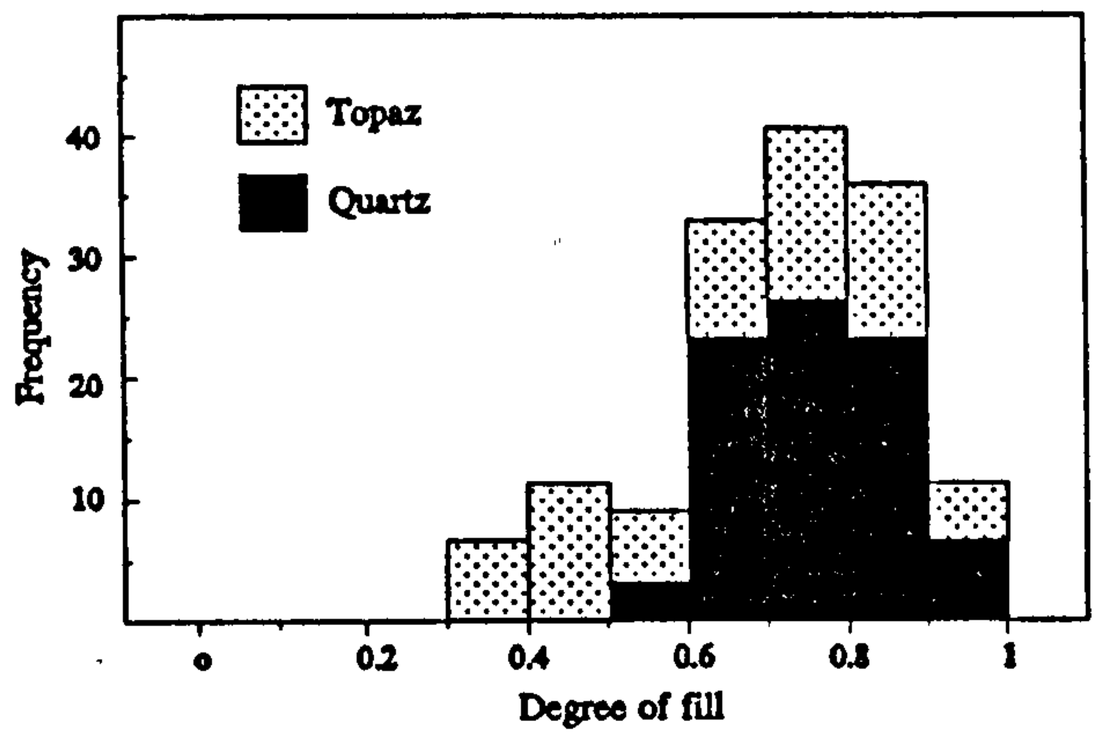

Fig. 6.1 Histogram of degree of fill (F) for the type P1 inclusions

Thermometric characteristics

Microthermometric data for fluid inclusions of the pegmatitic rocks are reported in Appendix IX. A summary of this information, in the form of temperature ranges for the phase changes observed, is presented in Table 6.2.

Table 6.2 Summary of P type inclusion thermometric data

TYPE	HOST MINERAL	Tm_{ice} (°C)	Ts (°C)	Tv (°C)	Th (°C)	S (wt.%)
P1	Quartz	-0.8 to -18.8			348 to 530	1.39 to 21.76
	Topaz	-0.8 to -7.6			360 to 540	1.39 to 11.23
P2	Quartz*		79.6 to 248.3		468 to 534	27.46 to 34.51
	Quartz**			350 to 510	~550†	

* quartz with halite, ** quartz without halite, † temperature at which inclusions decrepitate.

Fluid salinity estimates are usually made by referring the final ice melting temperature (Tm_{ice}) in the inclusions to the NaCl-H_2O system, using the data regression of Potter *et al.* (1978):

When S < 26.3 wt.%,

$$S(wt.\%) = -1.76958 \times T_{m_{ice}} - 0.042384 \times T^2_{m_{ice}} - 0.00052778 \times T^3_{m_{ice}}$$

When S ≥ 26.3 wt.%

$$S(wt.\%) = 26.218 + 0.0072 \times T_{m_{ice}} + 0.000106 \times T^2_{m_{ice}}$$

Such estimates neglect the effect of other solutes. However, several measurements of the first melting

(eutectic) temperature in the P1 inclusions of -18.9° to -28°C with the majority being -18.9° to -25.5°C indicate that NaCl is the dominant dissolved phase, but there may be some KCl, $FeCl_2$, and/or $MgCl_2$ present which would be needed to explain the lower temperatures. A salinity frequency histogram (Fig. 6.2) shows that the P1 inclusions are dominated by low to moderate salinities of 2-18 wt.% NaCl equivalent with the majority being 2-8 wt.%. No liquid or solid volatile phase or gas hydrate were observed on cooling to -180°C, indicating that H_2O is the major volatile component of the fluid.

As little is known of the properties of topaz as a host for fluid inclusions at high temperature, one inclusion was repeatedly run through its homogenisation point. If topaz stretched on heating, a progressive increase in Th_{V-L} would be expected (Roedder, 1984). Ten runs on a typical inclusion produced a mean Th of 496.7°C with STD (1σ) = 4.6°C. The small variation in these measurements is well within analytical error at these temperatures. Hence the topaz does not show significant stretch on heating to these temperatures.

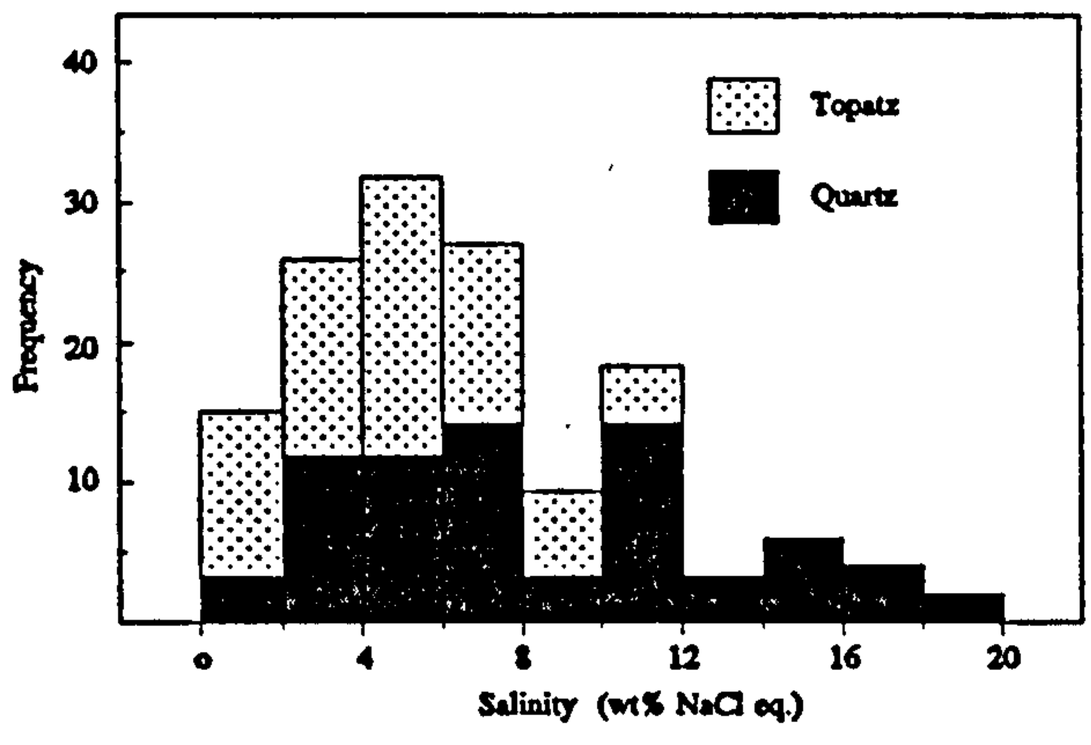

Fig. 6.2 Histogram of salinities for the P1 inclusions

Total homogenisation in the P1 inclusions (Table 6.2) occurs by either shrinkage and disappearance of the vapour bubble (mostly observed in quartz) or expansion of the vapour bubble or disappearance of the aqueous liquid phase (mainly noted in topaz) on heating. The former is usually referred to as homogenisation to the liquid phase (L), or homogenisation by vapour disappearance, whereas the latter is

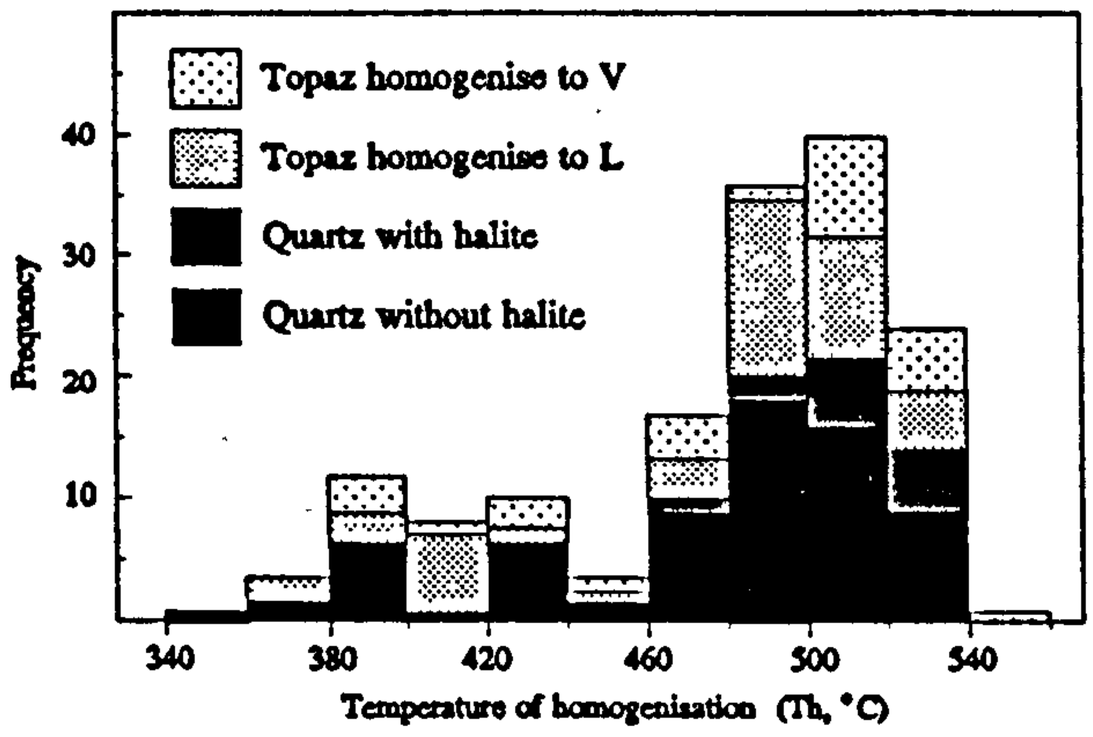

Fig. 6.3 Histogram of Th for the P1 and P2 inclusions

generally referred to as homogenisation to the vapour phase (V), or homogenisation by liquid disappearance. A homogenisation temperature (Th) frequency histogram (Fig. 6.3) shows a dominant population of 460°-540°C with a maximum at 480°-520°C and a less profound group peaking at 380°-440°C.

Eleven type P2 inclusions, containing solid phase(s) other than halite, have been encountered during the study. No total homogenisation temperature was obtained for these inclusions. The vapour bubble homogenises to the liquid phase at a temperature range of 350° to 510°C, while the solid phases remain unchanged until about 550°C at which most of these inclusions decrepitated. This may indicate that these solid phases might actually be captured minerals rather than daughter minerals crystallised after the trapping. Due to the small size of these inclusions, in addition to the interference from the solid phases, accurate determination of phase changes during freezing-heating is practically impossible. Thus, although a full range of physical and thermometric data have been recorded for these inclusions, the data are utilized only to complete the general survey of the various fluid inclusions types observed in the pegmatitic rocks. Little weight is placed upon any interpretation of this kind of type P2 inclusion data.

Fifteen type P2 inclusions containing a cubic halite crystal have been measured during the course of study. The halite crystals melt at temperatures of 79.6°-248.3°C, indicating a salinity range of 27 to 35 wt.% NaCl equivalent (Fig. 6.4), and total homogenisation temperatures of 460-530°C have been recorded for these inclusions (Fig. 6.3). Due to the reasons mentioned above, however, accurate determination of phase changes during freezing was not possible.

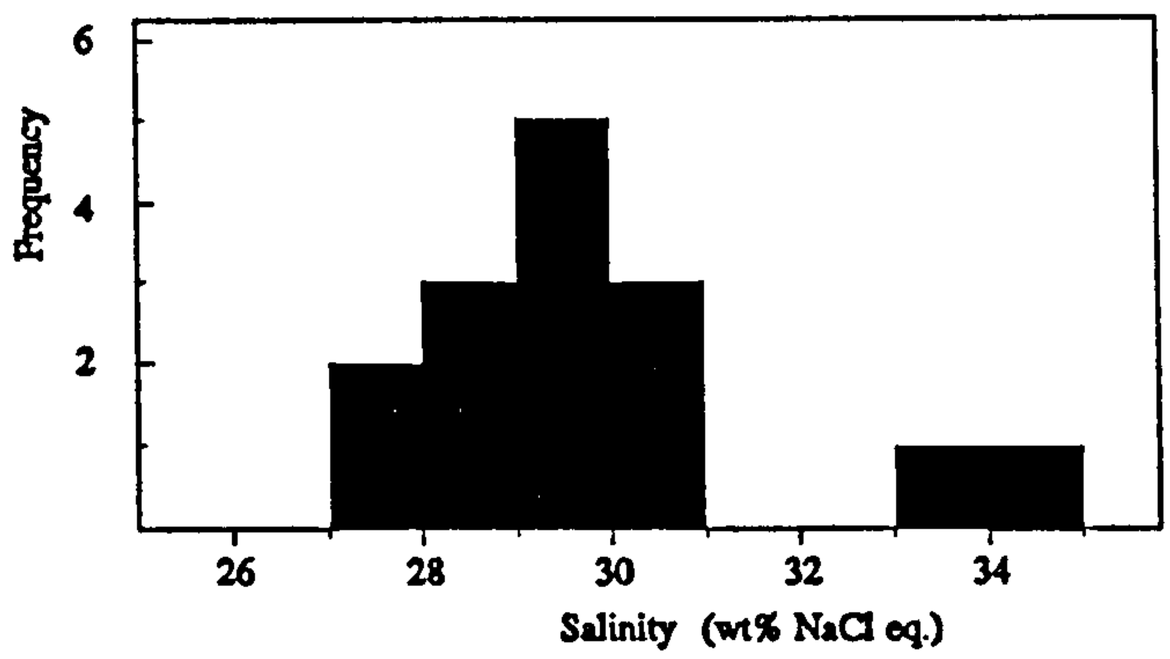

Fig. 6.4 Histogram of the salinity for the halite-containing P2 inclusions

6.1.2.2 Fluid inclusions of the fluorite-scheelite ores

Optical characteristics

Samples of the fluorite-scheelite ores studied for fluid inclusions are from the Xianghuapu deposit (orebody III) and the Dongshan deposit (orebody II). These ores consist mainly of quartz, fluorite, scheelite and calcite (see 5.2.2). Fluid inclusions are best preserved in quartz and fluorite, although small (<5μm) inclusions can also be observed in scheelite and calcite. Four main inclusion types may be defined on the basis of optical characteristics. Sketches of these four types of inclusions are presented in Figure 6.5 and photomicrographs of typical thin section views are shown in Plate 6.1. The main optical features of these inclusions are summarised in Table 6.3.

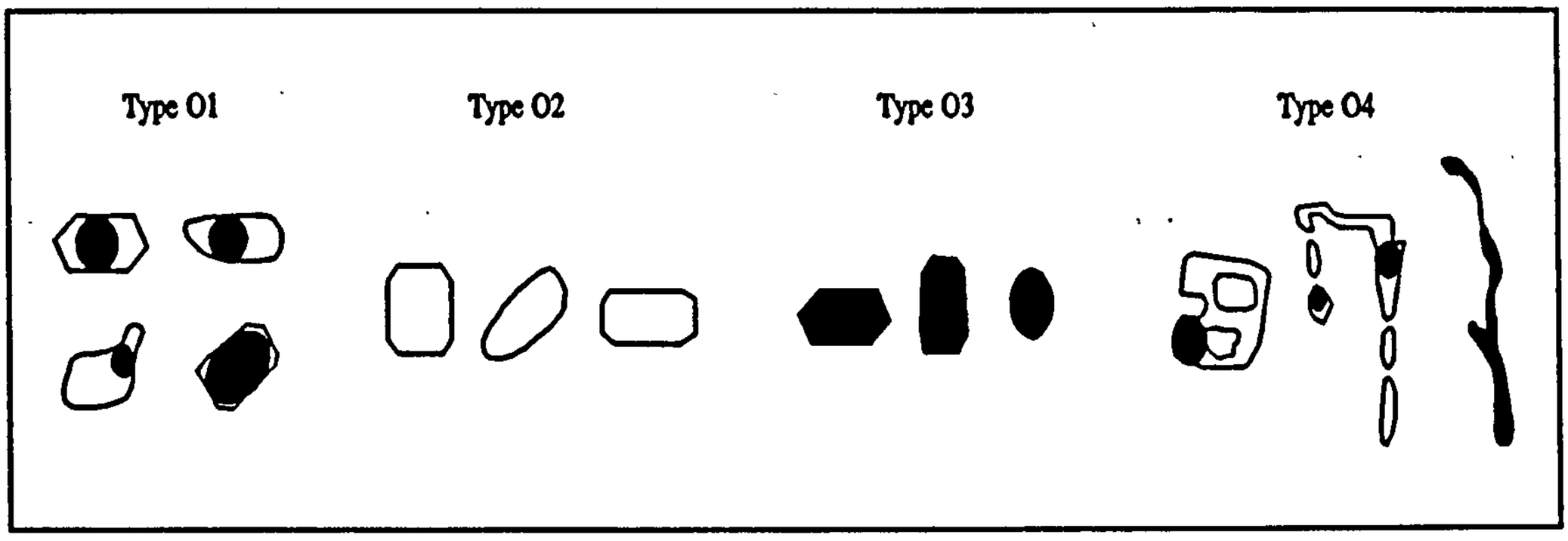

Fig. 6.5 Sketches showing the nature of the fluid inclusion types observed in the W-F ores.

Type O1 inclusions are by far the most abundant and are observed in both quartz and fluorite of all samples studied. These inclusions are two phase with variable degrees of fill (F=0.20-0.95, mostly 0.70-0.95; Fig. 6.6). Even within the same cluster of inclusions, the vapour may occupy from less than 30% to greater than 80% of an inclusion by volume. These inclusions occur mostly in trails crosscut by or truncating grain boundaries, also in clusters or isolated (Plate 6.1). Secondary type O1 inclusions are generally rounded or irregularly shaped and have greater F values (mostly over 0.95). They occur in trails along annealed fractures crosscutting grain boundaries and in clusters on the edge of grain. Type O2 (one liquid phase) and O3 (one vapour phase) inclusions are mostly of primary origin and are in close spatial association with type O1 inclusions in fluorite of most samples studied, but are absent in most of the quartz grains. Type O4 inclusions are rare in most of the samples but abundant

in a few of them (such as samples III_{4-3} and III_{4-5}). They are found exclusively in late stage fluorite and occur in clusters and trails within grain boundary. Due to extensive necking down, these inclusions possess extremely irregular shapes (Plate 6.1 and Fig. 6.5). The degree of fill for these inclusions is usually greater than 95% by volume (*i.e.* F≥0.95) or are free of any vapour bubble, but a few one-vapour phase inclusions have also been recorded. As many as ten inclusions with variable F values may be connected to each other by thin tubes. Such inclusions were interpreted by Roedder (1984, pp.64-65 and Figure 3-15) as pseudosecondary inclusions and "the process of necking down and isolation of these individual inclusions from the original layer of fluid filling an open cleavage crack must have taken place very little above Th and was subsequently arrested completely" (Roedder, 1984, p.65)

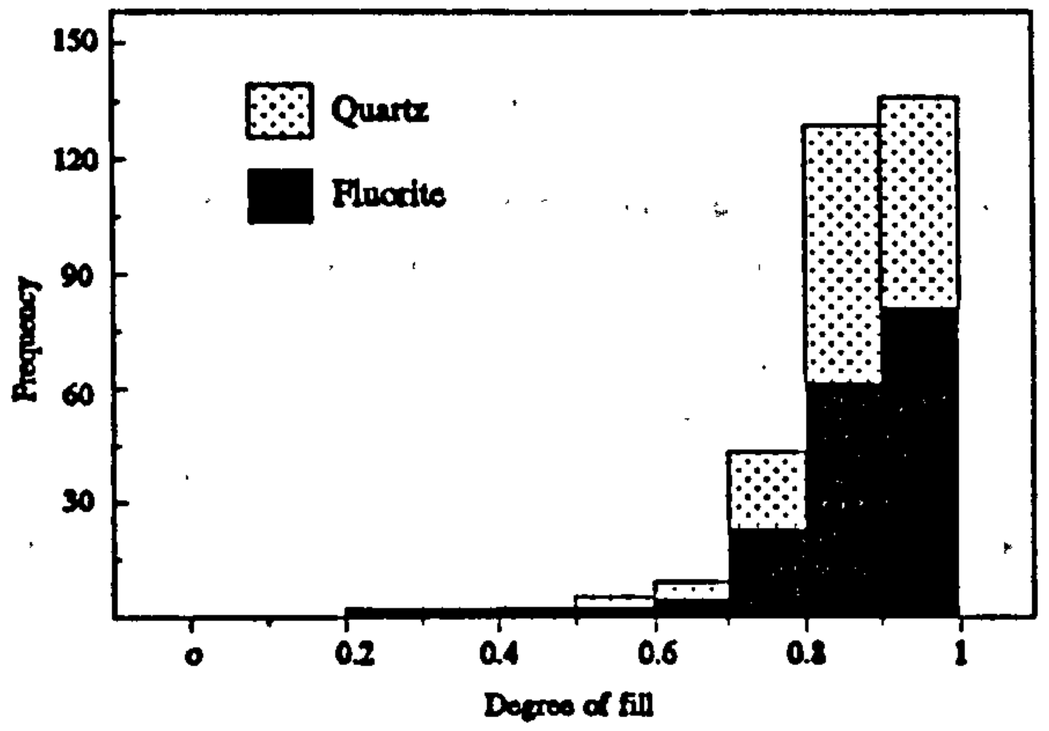

Fig. 6.6 Histogram of degree of fill (F) for the O1 inclusions

Table 6.3 Summary of optical characteristics of fluid inclusions in the W-F ores

TYPE	DESCRIPTION	SPATIAL DISTRIBUTION	INTERPRETATION
O1	Size: 5-80μm, may reach 200μm. Shape: negative crystal, ellipsoidal, or irregular. Phases: aqueous liquid + vapour (F=0.20-0.95).	Primary: isolated, clusters, or in trails along crystallisation planes. Secondary: trails crosscutting grain boundaries.	Primary inclusions represent trapping of mineralisation fluid. Secondary inclusions may represent trapping of late-stage fluid responsible for the formation of massive calcite
O2	Size: 5-80μm. Shape: negative crystal, ellipsoidal, or rounded. Phases: one aqueous phase.	Small numbers, closely associated with the O1 inclusions.	
O3	Size: 5-60μm. Shape: negative crystal, ellipsoidal, or rounded. Phase: one vapour phase, dark in colour.	Small numbers, closely associated with the O1 inclusions.	Inclusions represent trapping of vapour during boiling (?).
O4	Size: 10-100μm, may reach several hundred μm. Shape: extremely irregular Phase: aqueous + vapour, or one vapour phase.	Clusters, many inclusions connected to each by small tubes.	Inclusions represent the recrystallisation and necking down of large flat inclusions and are pseudosecondary origin.

Thermometric characteristics

Full microthermometric data for fluid inclusions of fluorite-scheelite ores may be found in Appendix IX and a summary is presented in Table 6.4.

Table 6.4 Summary of O type inclusion thermometric data

TYPE	HOST MINERAL	Tm_{ice} (°C)	Th (°C)	S (wt.% NaCl)
O1	Quartz	-0.4 to -7.8	109 to 356	0.70 to 11.47
	Fluorite	-0.2 to -14.4	108 to 338	0.35 to 18.27
O4	Fluorite	-0.2 to -5.1	83 to 238	0.35 to 7.99

A few measurements reveal that the initial melting of the type O1 inclusions, after cooling down to below -120°C and then reheating slowly, occurs between -50° and -19°C with most being -50° to -42°C (Appendix IX). This distribution clearly indicates the presence of solutes other than pure NaCl. The eutectic temperature of the H_2O-$CaCl_2$ system is -49.8°C and the ternary H_2O-NaCl-$CaCl_2$ eutectic occurs at -52°C (Shepherd *et al.*, 1985), suggesting $CaCl_2$ the most likely candidate for one of the other salts in the fluid. This is consistent with the geological observation, the presence of Ca in the fluid is confirmed by the formation of a large quantity of fluorite in the ores.

The ice in type O1 inclusions disappears between -0.4° and -7.8°C in quartz and -0.2° to -14.4°C in fluorite. The maximum frequency of final ice melting temperature is at -2°C for both minerals (Fig. 6.7a). The corresponding salinities range from 0.35 to 18.27 wt.% NaCl eq. with the maximum at 3 wt.% (Fig. 6.7b). Phase relationships in the system H_2O-NaCl-$CaCl_2$ indicate that inclusions with a final ice melting temperature of -14.4°C contain about 17 wt.% $CaCl_2$ with respect to total dissolved salts (Shepherd *et al.*, 1985, their Figure 6.7).

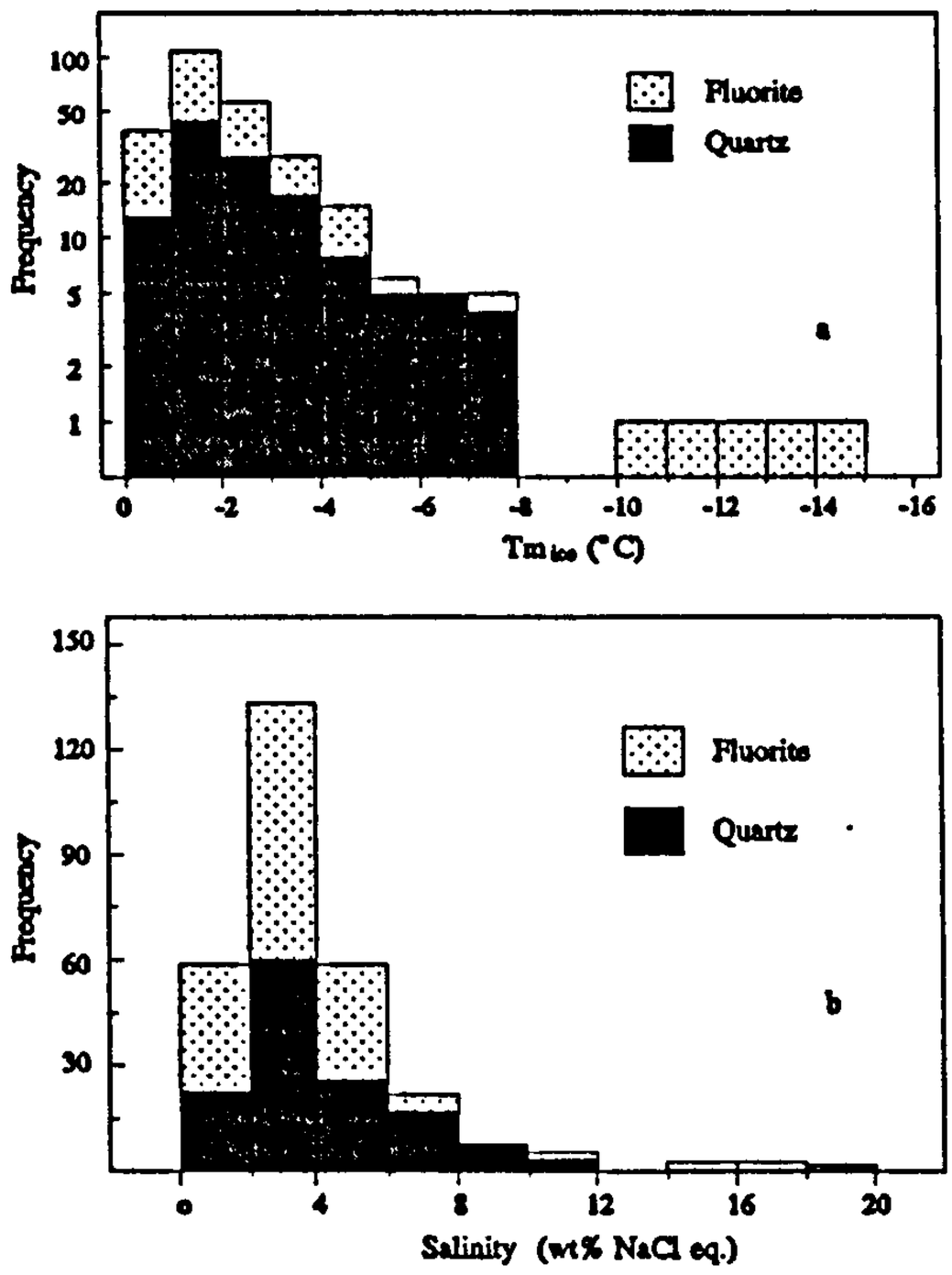

Fig. 6.7 Histograms of final ice-melting temperature (a) and salinity (b) for the O1 inclusions

Total homogenisation in the primary type O1 inclusions occurs in most cases by shrinkage and disappearance of the vapour bubble and occasionally by the expansion of the vapour bubble on heating at a temperature range of 100°-360°C. The data display two populations of 100°-220°C and 240°-340°C with the maxima at 140°-160°C and 260°-300°C, respectively (Fig. 6.8). It is also clear by inspecting this diagram that the homogenisation temperature of the quartz is generally higher than that of the fluorite, which is consistent with the results of paragenetic studies.

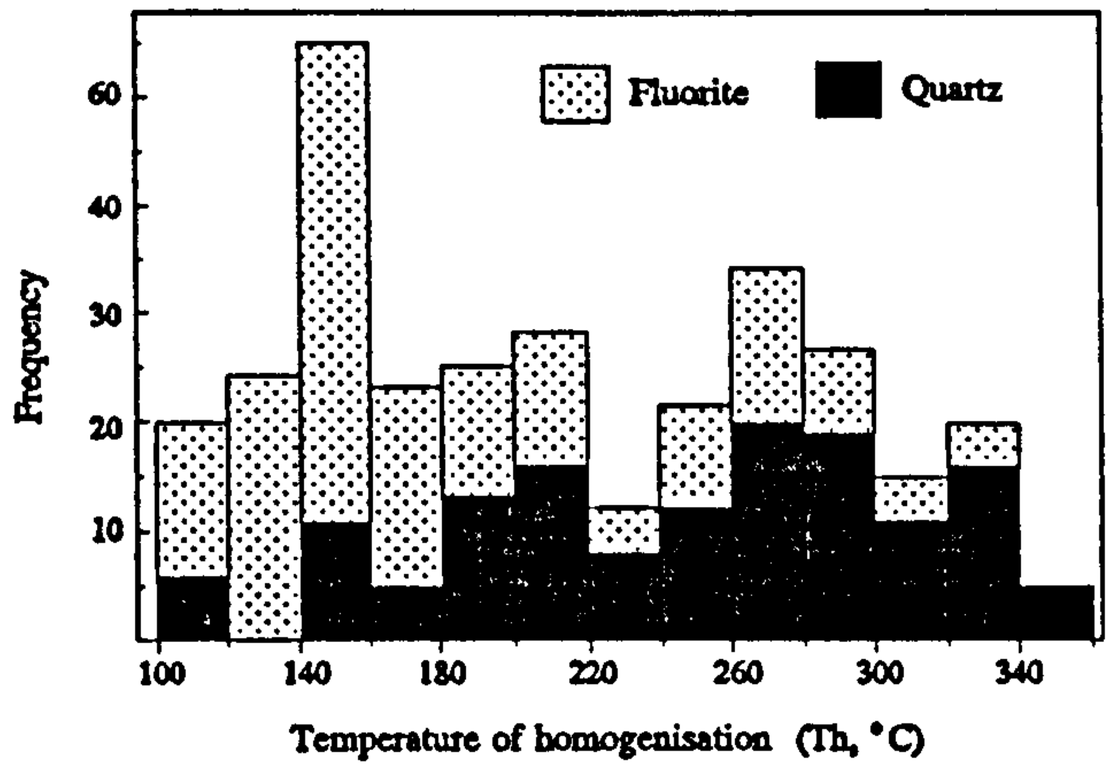

Fig. 6.8 Histogram of Th for the O1 inclusions

Due to the well known metastable melting behaviour of ice in the absence of vapour (*cf.* Roedder, 1984), the ice melting temperatures of the type O2 inclusions are erroneously high. It is not uncommon that these temperatures can be as high as +7.8°C. Hence no reliable data have been obtained for this type of inclusion. Upon cooling down to -196°C, no phase change has been evident for type O3 inclusions. It is believed that H_2O is the major component of the vapour, although its exact composition is not fully understood and the possibility of a small amount of CO_2 and other gas (such as CH_4) present in the vapour cannot exempted. In the case of type O4 inclusions, the necking down can seriously affect the validity of all measurements (Roedder, 1984). Thus the great variation of data for these inclusions (Appendix IX) also casts doubt on their significance.

6.1.2.3 Estimation of pressure and pressure corrections

The measured Th of each inclusion gives only a minimum value of the true trapping temperature (Tt) (Roedder, 1984). In order to calculate the Tt accurately, an estimate of the pressure of trapping is required. As in most hydrothermal ore deposits, in the absence of CO_2-bearing inclusions, the pressures under which aqueous liquids were trapped are difficult to determine. The existence, however, of coeval P-type inclusions with variable F values and contrasting salinities but similar homogenisation temperatures (homogenise to both liquid and vapour phases) indicates that boiling

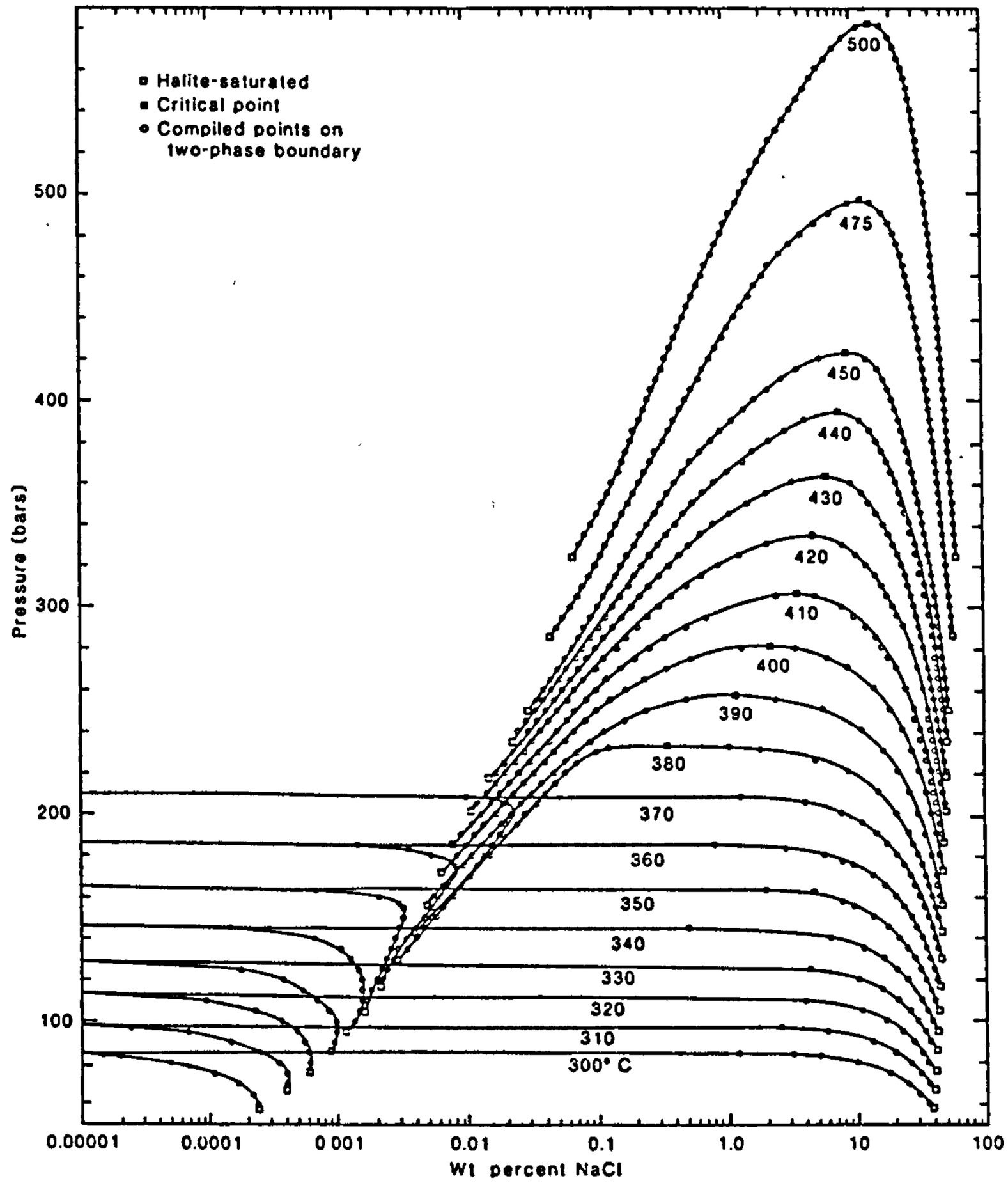

Fig. 6.9 Isotherms of the vapour-liquid region of NaCl-H_2O from 300° to 500°C (from Bischoff & Pitzer, 1989).

occurred during the crystallisation of quartz and topaz from the melt. Hence, no pressure correction is required for inclusions in the pegmatitic rocks, and the homogenisation temperature (Th=348°-540°, with the majority being 480°-520°C) should closely assemble the true trapping temperature (Roedder, 1984). As discussed by many researchers (Roedder & Bodnar, 1980; Roedder, 1984; Shepherd *et al.*, 1985), this type of inclusion is useful in estimating the pressure of fluid trapping. By employing the diagrams of Bischoff and Pitzer (1989), pressures of 440 to 560 bars are obtained for the pegmatite formation and fluid evolution (Fig. 6.9). These pressures are consistent with the crystallisation conditions of the subsolvus granites which, according to Martin and Bonin (1976) and Bonin (1986),

crystallise at pressures of ≤50 MPa (≈ 500 bar). Therefore, it is safe to assume that the Jianfengling granites were emplaced at, or less than, 500 bar, which confines the maximum pressure correction for the fluid inclusion temperatures of the W-F mineralisation in the Xianghuapu area. The maximum pressure correction required to estimate the temperature of entrapment of type O1 inclusions from their homogenisation temperatures is about 40°C for the low-temperature inclusions (mainly in fluorite) and 50°C for the high-temperature inclusions (mainly in quartz; estimated from P-V-T data in Potter and Brown, 1977). Using these corrections, it can be concluded that the low-salinity, high temperature aqueous fluid responsible for the deposition of quartz, scheelite and some fluorite was trapped between 280° and 410°C, and the low salinity, low temperature liquid responsible for the formation of fluorite, calcite and some quartz was trapped between 160° and 280°C.

6.1.3 SUMMARY

Three general types of fluid inclusions, two-phase type P1, three- or multiple-phase type P2 and one-phase type P3, have been recognised as being coeval with the formation of pegmatites in the Jianfengling granite. Type P1 NaCl-H_2O-bearing inclusions exhibit mainly low salinities of 3-8 wt.% NaCl eq. with a few moderate salinities of 10-20 wt.% NaCl eq.. Homogenisation of type P1 inclusions is achieved mostly between 440° and 540°C. Type P2 NaCl-H_2O-bearing inclusions contain one or two daughter minerals. Those containing halite as the daughter mineral exhibit high salinities of 27-35 wt.% NaCl eq. Total homogenisation obtained cluster between 460° and 530°C (Appendix IX). Microthermometric data indicate that type P1 and type P2 inclusions are products of boiling of a parent fluid with a salinity of approximately 10-15 wt.% NaCl eq. at 500 bar (Shepherd *et al.*, 1985, their Figure 6.25). Type P3 inclusions with only one vapour phase are extremely rare and no phase change has been recorded up on cooling down to -196°C.

Fluid inclusions in the W-F ores are dominantly two phase, liquid plus vapour. The majority of these NaCl-$CaCl_2$-H_2O-bearing inclusions have low salinities (1-7 wt.% NaCl eq.) but a few moderate salinity (10-19 wt.% NaCl eq.) inclusions, mainly in fluorite, have also been encountered. Total homogenisation of these inclusions occurred at two temperature ranges of 240°-340°C and 100°-220°C. After pressure correction, also in accordance with the paragenetic sequence of the mineralisation (*cf.* Chapter 5), temperatures of 350°, 320°C, 260° and 180°C are estimated to represent the deposition temperatures of quartz, scheelite, and fluorite, calcite, respectively.

6.2 STABLE ISOTOPE STUDIES

6.2.1 Samples studied and analytical methods

Following the detailed mineralogical and geochemical studies of the Jianfengling granites and their related varieties of mineralization, a total of 52 samples were chosen for stable isotope analyses. These samples include 14 quartzes from both granite-related rocks and ores of fluorite-scheelite mineralization, 6 calcite, 4 scheelite, 2 plagioclase, 3 biotite, 1 topaz and 11 pairs of galena + sphalerite. The sulphides (galena + sphalerite) have been analyzed for sulphur (S) and the others (quartz + scheelite + calcite) for both oxygen (O) and as appropriate hydrogen (H) and also carbon (C) for calcite. These minerals were separated by a combination of hand-picking and conventional magnetic and heavy liquid techniques (Zussman, 1977). Quartz samples were treated by boiling with 10% HNO_3 for 24 hours to remove any contamination. All separates have been checked under a binocular microscope and are believed to have been more than 98% pure.

Stable isotope analyses were performed at SURRC, East Kilbride, Scotland, using standard extraction and mass spectrometric techniques (McCrea, 1950; Bigeleisen *et al.*, 1952; Friedmann & Smith, 1958; Godfrey, 1962; Clayton & Mayeda, 1963; Robinson & Kusakabe, 1975; Borthwick & Harmon, 1982.). The analyses were completed by Dr. A. E. Fallick except for oxygen in seven quartz samples which were analyzed by myself under the supervision of Dr. Fallick. All analytical results are reported in standard δ notation, using per mil (‰) relative to Standard Mean Ocean Water (V-SMOW) for oxygen and hydrogen (Craig, 1961a & b; Hagemann *et al.*, 1970; Baertschi, 1976), to the belemnite Belemnitella americana from the PeeDee Formation (PDB) for carbon (Craig, 1957), and to Canyon Diablo troilite (CDT) for sulphur (Thode *et al.*, 1961). Analytical precisions are typically ±0.1 per mil for O and C, ±2 per mil for H and ±0.2 per mil or better for S.

6.2.2 Isotopic composition of the granite-related rocks

Seven quartz samples from the granite-related rocks, namely the pegmatitic pods and pegmatites, have been analyzed for oxygen (mineral) and hydrogen (fluid inclusion water) isotopes and the results are presented in Table 6.3. The $\delta^{18}O$ values of fluids in equilibrium with these minerals are calculated using the appropriate fractionation expressions given in Table 6.4.

Table 6.3 Oxygen, Hydrogen and Carbon isotope data (‰) from the Xianghuapu area

Sample No.	Mineral	Location	$\delta^{18}O$ (SMOW)	δD (SMOW)	$\delta^{13}C$ (PDB)	Calculated $\delta^{18}O_{H2O}$	T (°C)
101-5	Quartz	Pegmatitic pod, New Quarry	10.43	-79		8.14	500
101-6	Quartz	Pegmatitic pod, New Quarry	11.11			8.82	500
104	Quartz	Pegmatite zone, SL 104	13.03	-88		10.74	500
105	Quartz	Quartz shell, SL 105	11.03			8.74	500
118-3	Quartz	Pegmatite vein, SL 118	11.55			9.26	500
120-7	Quartz	Quartz shell, SL 120	10.90			8.61	500
143-3	Quartz	Topaz-quartz pegmatite, SL 143	11.20	-70		8.91	500
III_{3-4}	Quartz	Level 480, orebody III, XHPD	7.42	-88		3.28	350
III_{3-17}	Quartz	Level 480, orebody III, XHPD	8.18	-82		4.04	350
III_{3-18}	Quartz	Level 480, orebody III, XHPD	8.77			4.63	350
III_{4-2}	Quartz	Level 450, orebody III, XHPD	7.37			3.23	350
III_{4-3}	Quartz	Level 450, orebody III, XHPD	5.94			1.80	350
III_{4-5}	Quartz	Level 430, orebody III, XHPD	9.01			4.87	350
III_{4-6}	Quartz	Level 430, orebody III, XHPD	8.25			4.11	350
III_{3-17}	Scheelite	Level 480, orebody III, XHPD	-3.0			-1.08	320
III_{4-2}	Scheelite	Level 450, orebody III, XHPD	2.2			4.12	320
III_{4-3}	Scheelite	Level 450, orebody III, XHPD	-4.2			-2.28	320
III_{4-6}	Scheelite	Level 430, orebody III, XHPD	5.2			7.12	320
III_{3-14}	Calcite	Level 480, orebody III, XHPD	13.13		-0.58	2.47	180
III_{3-15}	Calcite*	Level 480, orebody III, XHPD	12.30		0.82	0.36	160
III_{3-18}	Calcite	Level 480, orebody III, XHPD	13.95		-0.18	3.29	180
III_{4-5}	Calcite	Level 430, orebody III, XHPD	12.95		-0.98	2.29	180
III_{4-6}	Calcite	Level 430, orebody III, XHPD	12.00		-1.31	1.34	180
390-6	Calcite*	Level 480, orebody III, XHPD	11.96		0.45	0.02	160

* Calcite from the later barren massive calcite. SL = Sample location, XHPD = Xianghuapu deposit (W-F).

Table 6.4 Stable isotope fractionation factors for oxygen

Fractionation	Fractionation coefficients[a]	T (°C)	Reference
Quartz - H_2O	A = 3.34 B = -3.31	250 - 500	Matsuhisa *et al.*, 1979
	A = 2.05 B = -1.14	500 - 800	
Scheelite - H_2O	A = 1.39 B = -5.87	200 - 500	Wesolowski & Ohmoto, 1986
Calcite - H_2O	A = 2.78 B = -2.89	0 - 500	O'Neil *et al.*, 1969

[a] where $\Delta_{a-b} = \delta_b - \delta_a \approx 1000 \ln\alpha_{a-b} = A(10^6 T^{-2}) + B$

Quartz samples from the pegmatitic pods and pegmatites from different locations do not show significant variations in $\delta^{18}O$ (Fig. 6.10). One sample from the greisen-pegmatite zone on top of intrusion E (No.104) has a slightly higher $\delta^{18}O$ (13.03‰), which could be due to isotopic exchange with an ^{18}O-rich fluid or lower precipitation temperature. The presence of skarn minerals (such as

tremolite) in this zone indicates that there had been some material exchange between the granite melt and the country rock (limestone), suggesting the former explanation is more likely.

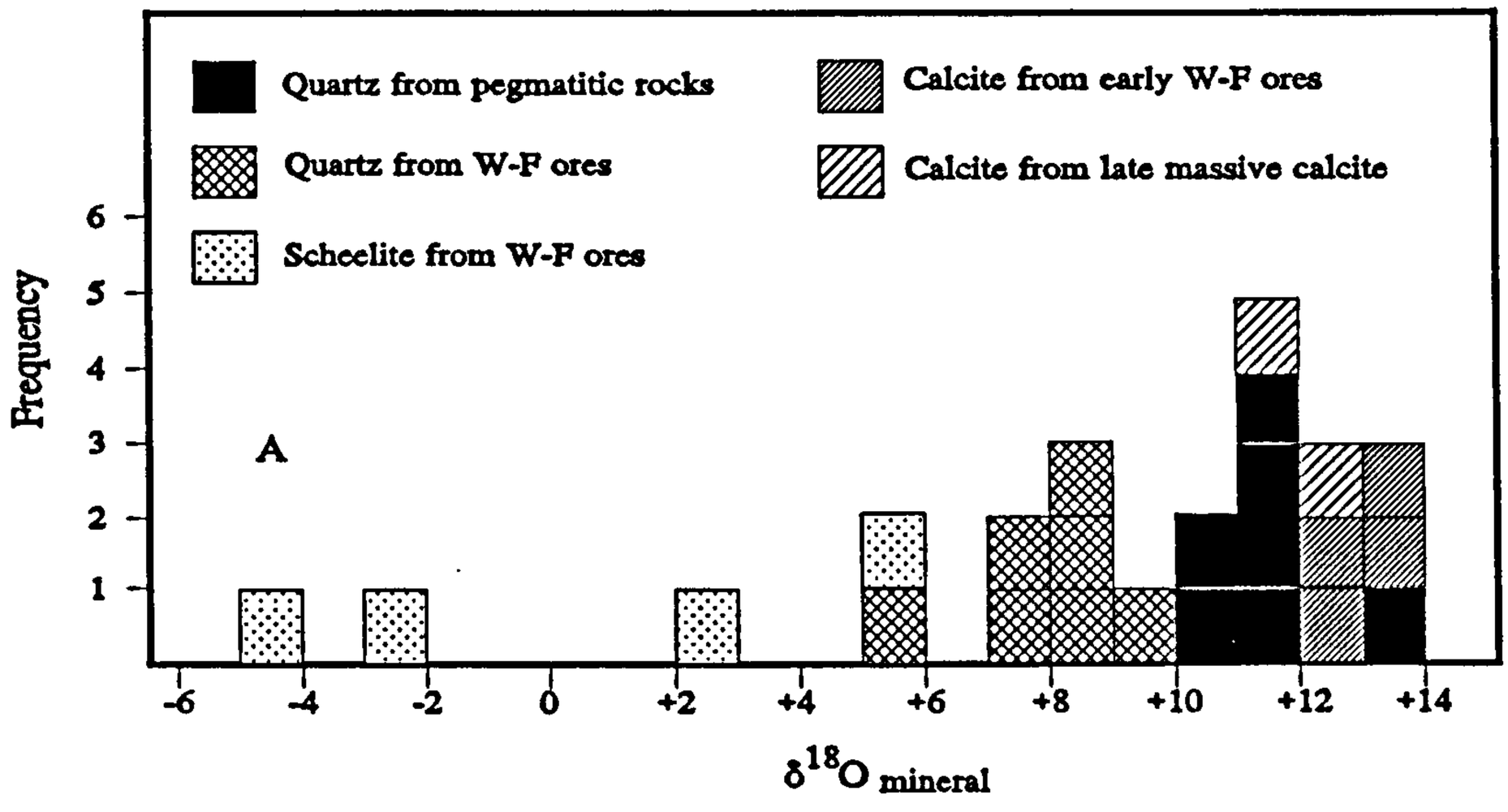

Fig. 6.10 Histograms of $\delta^{18}O$ values of minerals (A) and fluids (B) in equilibrium with these minerals in the Xianghuapu area

The $\delta^{18}O$ values of these quartz samples and δD values of their inclusion fluids are used to estimate the stable isotope compositions of primary magmatic fluids generated from the Jianfengling granites.

The calculated compositions of fluids in equilibrium with each sample are plotted in a conventional hydrogen versus oxygen isotope diagram (see Fig. 6.14) and will be discussed later. A temperature of 500°C is used in these calculations, consistent with the fluid inclusion temperatures of these rocks and a reasonable minimum solidus temperature for a F-rich granitic melt (Manning, 1982).

Fluid $\delta^{18}O$ values calculated using quartz range from 8.1‰ to 10.7‰ and δD values from -70‰ to -79‰ with averages of 9.0‰ and -76‰ respectively. For subsequent modelling, primary magmatic water from the Jianfengling granites is estimated to have had a $\delta^{18}O$ of 9.0 per mil and a δD of -76 per mil. This isotopic composition is consistent with the normal range of "primary magmatic water" (Fig. 6.13; $\delta^{18}O$ = 5.5-9.5 ‰, δD = -40 to -80‰, Sheppard, 1986).

6.2.3 Isotopic composition of the W-F mineralisation

Oxygen and hydrogen isotope compositions of minerals and fluids

Seven quartz, 4 scheelite and 6 calcite separates from different levels of orebody III of the Xianghuapu fluorite-scheelite deposit were analyzed for oxygen and hydrogen isotopes and the results are presented in Table 6.3 and Figure 6.10. The quartz and calcite separates possess narrow $\delta^{18}O$ ranges of 5.94 to 9.01 per mil and 11.96 to 13.95 per mil, respectively, while the scheelite separates show a relatively greater variation with a range of -4.2 to +5.2 per mil.

The oxygen isotope compositions of the fluids responsible for depositing the quartz, scheelite and calcite are calculated using the equations of Matsuhisa *et al.* (1979), Wesolowski & Ohmoto (1986) and O'Neil *et al.* (1969), respectively. Temperatures, resulting from fluid inclusion studies on quartz and fluorite the paragenesis studies of the mineralisation, of 350°C (for quartz), 320°C (for scheelite), 180°C and 160°C (for calcite) are used. The calculated $\delta^{18}O$ values of fluids fall into two distinct groups. Those of fluids in equilibrium with granitic rocks range from 8.14 to 10.74 per mil while fluids responsible for the W-F mineralisation have much lower $\delta^{18}O$ values of 1.80 to 4.63 per mil (Fig. 6.9). The δD values of fluid inclusion waters in quartz vary from -82 to -88 per mil. The combined $\delta^{18}O$ and δD results are plotted in Figure 6.13. The δD and $\delta^{18}O$ data are plotted in the "expected mixing trend" between meteoric water and the Jianfengling granitic fluids (discussed in detail in Section 6.2.5).

Carbon isotope compositions of calcite and fluids

The $\delta^{13}C$ values of calcite from the early stage W-F mineralisation (-1.31 to -0.18 per mil) are slightly different from values of calcite from the later massive calcite (0.45 to 0.85 per mil; Table 6.3 and Fig. 6.11), which could be attributed to either variable sources or different precipitation temperatures. However, the close paragenetic association between these two types of calcite (see Section 5.2.2 for detail) favours the latter explanation. In order to determine the source, the carbon isotopic composition of the hydrothermal fluid ($\delta^{13}C_{\Sigma C}$) should be known. The carbon isotopic composition of a hydrothermal mineral is controlled by the temperature at which it was precipitated, by the $\delta^{13}C$ value of the parent fluid, and by the relative abundance of carbon species (H_2CO_3, CO_2, HCO_3^-, CO_3^{2-}, CH_4) in the fluid, which in turn are controlled by temperature, fo_2, and pH of the solution (Ohmoto & Rye, 1979; Ohmoto, 1986). The isotopic composition ($\delta^{13}C_{\Sigma C}$) of hydrothermal fluids can be determined provided that isotopic equilibrium was achieved between the fluids and the carbonates and that the physico-chemical conditions (P, T, fo_2 and pH) are known.

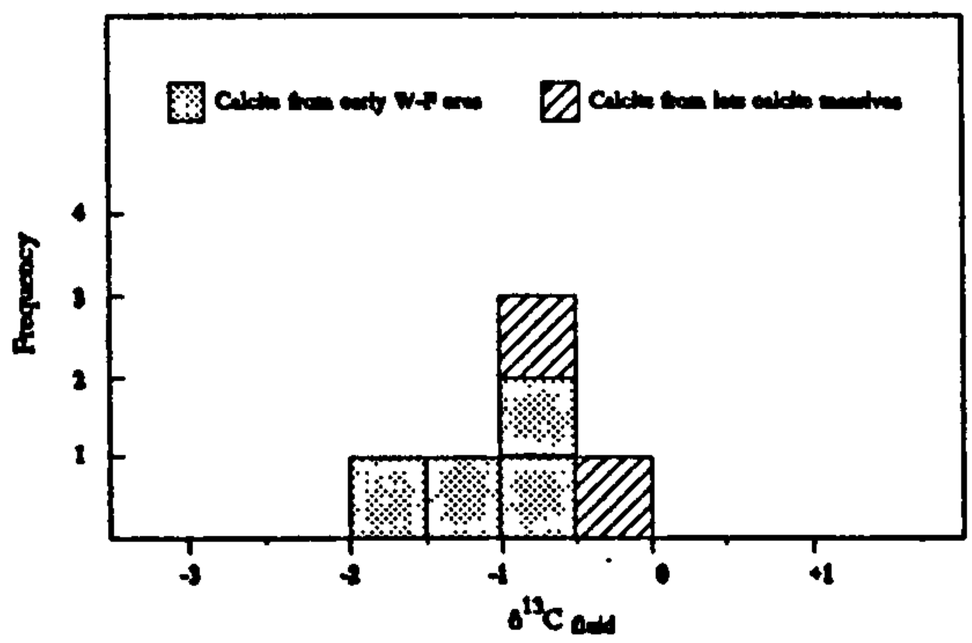

Fig. 6.11 Histogram of $\delta^{13}C$ values of calcite in the W-F ores

As defined by Ohmoto and Rye (1979), for an environment consisting of graphite-free, acid igneous rock associated with base metal mineralisation, the oxidation state is slightly above that of the QFM buffer (see Ohmoto & Rye, 1979, their Figure 10.7). For such an oxidation state, the dominant carbon species in hydrothermal fluids is CO_2 ($H_2CO_{3(approx.)} = CO_{2(aq)} + H_2CO_3 \approx CO_{2(aq)}$, as defined by Ohmoto and Rye (1979)); thus, the $\delta 13C_{\Sigma C}$ can be approximated by using the value for $H_2CO_{3(approx.)}$.

The paragenetic studyies have revealed that calcite in orebody III of the Xianghuapu deposit was generally formed later than quartz and fluorite (Section 5.2.2), thus the lower homogenisation temperatures (140°-200°C, Fig. 6.8) of fluorite should reasonably represent the calcite formation temperatures. Hence, temperatures of 180° and 160°C are used for the isotope equilibrium calculation.

The calculated $\delta^{13}C$ values, by using the data of Ohmoto and Rye (1979)[1], of the fluids responsible for the calcite precipitation range from -1.71 to -0.58 per mil for the early calcite (T=180°C) and -0.66 to -0.22 per mil for the late calcite (T=160°C) with the averages being -1.16 and -0.47 per mil respectively. These values suggest a common carbon source for these two types of calcite with a substantial contribution from the carbonate country rocks which are thought to have $\delta^{13}C$ values of 0±4‰ (Ohmoto & Rye, 1979).

6.2.4 Sulphur isotope composition of the Pb-Zn mineralisation

Isotopic compositions of mineral and fluids

Twelve pairs of galena and sphalerite from various locations in the Xianghuapu area were separated for sulphur isotope analysis. These samples represent different types of Pb-Zn mineralisation related to the Jianfengling granite stock. The results are reported in Table 6.5 and plotted in Fig. 6.12. The data display significant spatial variations in isotopic ratios in this area. Two distinctive groups are recognised:

--- Minerals from the lode-type Pb-Zn mineralisation --- the Meishi deposit --- possess negative values ranging from -1.9 to -6.9 per mil (sphalerite) and -5.5 to -9.6 per mil (galena).

--- Minerals from pegmatites, greisens and ores related to the W-F mineralisation show a relatively narrow range of positive values varying from 1.3 to 4.8 per mil (sphalerite) and 0.1 to 3.2 per mil (galena), although one pair from a deeply weathered greisen, S-4, had values of -0.6 and +12.6 per mil for sphalerite and galena respectively.

These spatial variations may be attributed to variable sulphur sources and/or different geological processes. In order to understand the geological processes and identify the source(s), it is necessary

---

[1] The formula used for calculating the isotopic fractionation between calcite and CO_2 is as follow:

$$\Delta_{Cc\text{-}CO_2} = \frac{A}{T^3} \times 10^8 + \frac{B}{T^2} \times 10^6 + \frac{C}{T} \times 10^3 + D$$

where A=-8.914, B=8.557, C=-18.11, D=8.27, T is the temperature in Kelvin (Ohmoto & Rye, 1979).

Table 6.5 Sulphur stable isotope data from the Xianghuapu area

Sample No.	Mineral	Description and location	$\delta^{34}S$ (CDT) (‰)	$\delta^{34}S_{H2S}$ (‰)	T (°C)
101-5	Sph	Massive sph & gal body within a pegmatitic pod	+4.8	+4.0*	500
101-5	Gal	in intrusion E. Sample location 101.	+3.2	+3.6*	
104-15	Sph	Disseminated in pegmatite zone in the top of	+2.1	+2.0	500
104-15	Gal	intrusion E. Sample location 104.	+1.1	+2.1	
S-1	Sph	Disseminated in greisen (fresh) zone in the top of	+1.3	+1.2	500
S-1	Gal	intrusion E. Shuanglian adit.	+0.2	+1.3	
S-4	Sph	Disseminated in greisen (deeply weathered) zone	+12.6		
S-4	Gal	in the top of intrusion E. Shuanglian adit.	-0.2		
III'_{2-2}	Sph	Sph & Gal vein, orebody III of Xianghuapu W-F	+1.9	+1.6	300
III'_{2-2}	Gal	deposit, level 480.	+0.9	+2.8	
D_{W-8}	Sph	Massive Sph & Gal aggregate within W-F ore of	+4.3	+4.0	300
D_{W-8}	Gal	Dongshan W-F deposit, level	+2.1	+4.0	
B_{324-1}	Sph	Massive Sph and Gal (+ Aspy, Py, Pyrr),	+1.8	+1.5	350
B_{324-1}	Gal	Baojingshan Pb-Zn deposit, level 324.	+0.1	+1.7	
M_{4-15}	Sph	Pyrr-sph ore, orebody II, level 4, Meishi Pb-Zn	-1.9	-1.5	250
M_{4-15}	Gal	deposit.	-5.5	-3.2	
M_{4-19}	Sph	Gal ore, orebody II, level 4, Meishi Pb-Zn	-3.9	-3.5	250
M_{4-19}	Gal	deposit.	-6.8	-4.5	
M_{4-31}	Sph	Gal-sph (+ Aspy, Pyrr) ore, ore body III, level 4,	-6.6	-6.2	250
M_{4-31}	Gal	Meishi Pb-Zn deposit.	-7.4	-5.1	
M_{5-4}	Sph	Massive galena and sphalerite pod in limestone	-4.3	-3.9	250
M_{5-4}	Gal	near by orebody III, level 5, Meishi deposit.	-7.9	-5.6	
M_{5-5}	Sph	Aspy-gal ore, orebody III, level 5, Meishi Pb-Zn	-6.9	-6.5	250
M_{5-5}	Gal	deposit.	-9.6	-7.3	

Aspy = arsenopyrite, Gal = galena, Py = Pyrite, Pyrr = pyrrhotite, Sph = sphalerite. * $\delta^{34}S_{HS^-}$ value

to know the sulphur isotope composition ($\delta^{34}S_{\Sigma S}$) of the hydrothermal fluids responsible for the deposition of these minerals.

The isotopic composition of sulphur, like carbon, in hydrothermal minerals is controlled by the temperature at which the minerals were precipitated, by the $\delta^{34}S$ value of the parent fluid, and by the relative abundances of sulphur species (H_2S, HS^-, S^{2-}, SO_4^{2-}, HSO_4^-, KSO_4^-, and $NaSO_4^-$) in the fluid, which in turn is controlled by physicochemical conditions such as T, P, fo_2, Eh and pH, of the solution (Ohmoto, 1972; Ohmoto & Rye, 1979; Ohmoto, 1986).

As discussed previously in Chapter 4, the Jianfengling granites have many similarities in terms of mineralogy and geochemistry to the "S-type" granites. According to experimental data on the solubility of sulphur in hydrous silicate melts, sulphur occurs in an S-type granitic melt predominantly as HS^- (Burnham, 1979; Ohmoto, 1986). If it is assumed that HS^- in a melt behaves isotopically in a similar

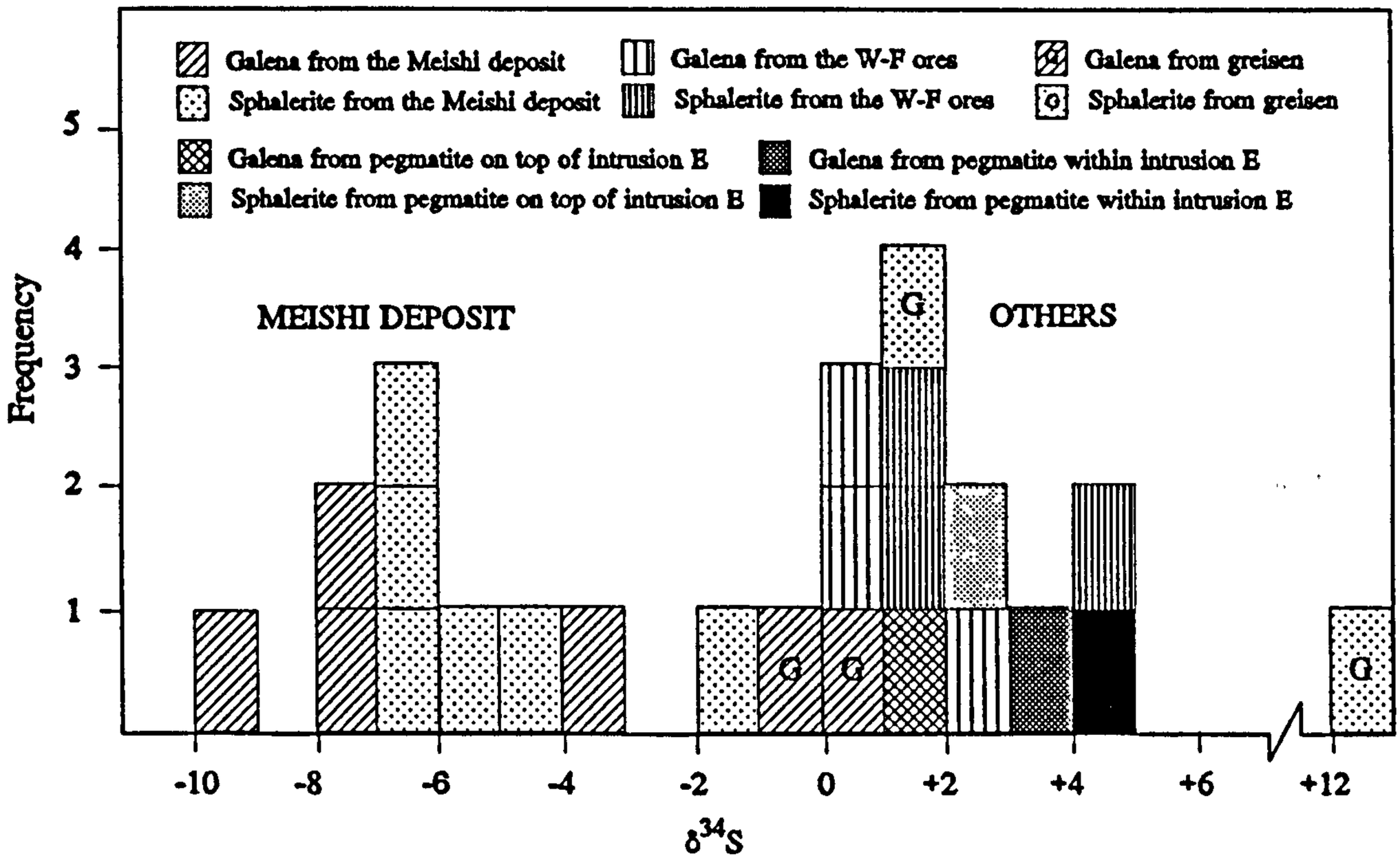

Fig. 6.12 Histogram of $\delta^{34}S$ values of sulphide minerals in the Xianghuapu area

manner to aqueous HS^-, the isotopic relationships among melt-crystal-fluids can be quantitatively evaluated from the equilibrium fractionation factors summarised by Ohmoto and Rye (1979, their Table 10-1). The equilibrium isotopic fractionation factor for sulphide-HS^- in hydrothermal systems in general is less than ±1 per mil (Ohmoto, 1972; Ohmoto & Rye, 1979; Ohmoto, 1986). For galena-HS^- and sphalerite-HS^-, the fractionation factors are smaller than ±0.9 and ±0.5 per mil respectively at 500°C or above (Ohmoto & Rye, 1979, Table 10-1). Hence for practical purposes we may assume that the $\delta^{34}S$ value of primary sulphide minerals is essentially identical to that of the sulphur in the melt. Thus the $\delta^{34}S$ compositions of galena and sphalerite from the pegmatitic pod within intrusion E (sample 101-5) should closely resemble that of the associated granite. Therefore, a value of 3.7 to 3.9 per mil is estimated for the $\delta^{34}S$ of the Jianfengling granite magma. This value is slightly higher than that of uncontaminated acidic igneous rocks (0 ± 3‰) proposed by Ohmoto & Rye (1979), but the difference is too small to be of any genetic significance.

Sulphur species that are quantitatively important in high temperature ($T \geq 400°C$) hydrothermal fluids are H_2S and SO_2 (Ohmoto & Rye, 1979). Therefore, the $\delta^{34}S$ value of the hydrothermal fluid ($\delta^{34}S_{fluid}$)

can be related to the $\delta^{34}S$ values of H_2S and SO_2 by approximation:

$$\begin{aligned}\delta^{34}S_{fluid} &= \delta^{34}S_{H_2S} \times X_{H_2S} + \delta^{34}S_{SO_2} \times X_{SO_2} \\ &= \delta^{34}S_{H_2S} + \Delta_{SO_2} \times \left(\frac{R}{1+R}\right)\end{aligned} \tag{6.1}$$

in which x_{H2S} is the mole fraction of H_2S with respect to the total sulphur content in the fluid (*i.e.* $x_{H2S} = m_{H2S} / (m_{H2S} + m_{SO2})$, R is the mole ratio of SO_2/H_2S and Δ_{SO2} is the equilibrium enrichment factor between SO_2 and H_2S (*i.e.* $\delta^{34}S_{SO2} - \delta^{34}S_{H2S}$).

When isotopic equilibrium is attained between sulphur in the fluid and sulphur in the melt, and because it is assumed that HS^- is the only sulphur species present in the melt, equation 6.1 can also be written as

$$\delta^{34}S_{fluid} = \delta^{34}S_{melt} - \Delta_{HS^-} + \Delta_{SO_2} \times \left(\frac{R}{1+R}\right) \tag{6.2}$$

in which Δ_{HS^-} is the equilibrium enrichment factor between HS^- and H_2S.

Because of the existence of significantly large isotopic fractionation factors between SO_2 and the reduced sulphur species (such as HS^- and H_2S) even at magmatic temperature (Ohmoto & Rye, 1979), equation 6.2 implies that $\delta^{34}S$ values of magmatic fluids can be quite different from that of silicate magmas, and that the deviation in $\delta^{34}S$ values is dependent on the SO_2/H_2S ratio in the fluid, on temperature, and on the relative masses of fluid and magma at the time of fluid separation. However, as discussed by Ohmoto & Rye (1979, their Figure 10.6), under realistic hydrothermal conditions (P_{fluid} = 0.5-3 kb, $x_{H2O} > 0.8$, $T < 850°C$, $fo_2 <$ QMF + 2 log units), H_2S is the dominant sulphur species in an aqueous fluid responsible for the formation of ore deposits. Hence, $\delta^{34}S_{\Sigma S}$ of the fluid is approximately equal to $\delta^{34}S_{H2S}$, *i.e.*

$$\delta^{34}S_{\Sigma S\,(magmatic\ fluid)} \approx \delta^{34}S_{H_2S\,(aq)} = \delta^{34}S_{sulphide} + \Delta_{sulphide\text{-}H_2S} \tag{6.3}$$

The calculated $\delta^{34}S$ values (using the compiled data of Ohmoto and Rye (1979)) of the fluids, from which the various phases of sphalerite and galena precipitated, range from -1.0 to +2.3 per mil. These values are identical to those of the Jianfengling granite magma, although minor differences are noticeable. The slight depletion of $\delta^{34}S$ in these fluids relative to the granitic magma may indicate a minor contribution of sulphur from the country rocks.

Sulphides from the Meishi deposit, which represents the massive lode-type Pb-Zn mineralisation, exhibit a considerable scatter of negative $\delta^{34}S$ values ranging from -1.9 to -9.6 per mil. The mineral assemblage (*i.e.* a large amount of pyrrhotite and lack of sulphates in the ores) suggests that H_2S was the dominant sulphur species in the fluid responsible for the precipitation of these sulphides (Ohmoto, 1986). Therefore, equation 6.3 can also applied here, and thus the $\delta^{34}S$ values of a fluid in equilibrium with these minerals are within a range of -1.7 to -10.7 per mil, suggesting a probable contribution from the Carboniferous limestone country rocks.

Isotopic equilibrium temperatures

The data in Table 6.5 and Figure 6.12 and from the above discussion indicate that the $\delta^{34}S$ values within each specimen behaved in accordance with the equilibrium fractionation sequence $\delta^{34}S_{Gal} < \delta^{34}S_{Sph}$. Thus, it is reasonably safe to assume that isotopic equilibrium between these two minerals had been reached. Calculations of isotope equilibrium temperature have revealed that the sulphides in the pegmatitic rocks were precipitated within a temperature range of 400°-580°C, which agrees well with the results of fluid inclusion studies, and those sulphides in the massive sulphide ores formed at 170°-500°C (Table 6.6, Fig. 6.13). Temperatures of 580°C and 300°C have been obtained for the Xianghuapu and Dongshan W-F mineralisation, respectively. The 300°C is in good agreement with the temperatures of fluid inclusion homogenisation, while the figure of 580°C is too high for this type of mineralisation and is well above the fluid inclusion homogenisation temperatures. This erroreous figure may be caused by some sort of disequlibrium between the mineral pair.

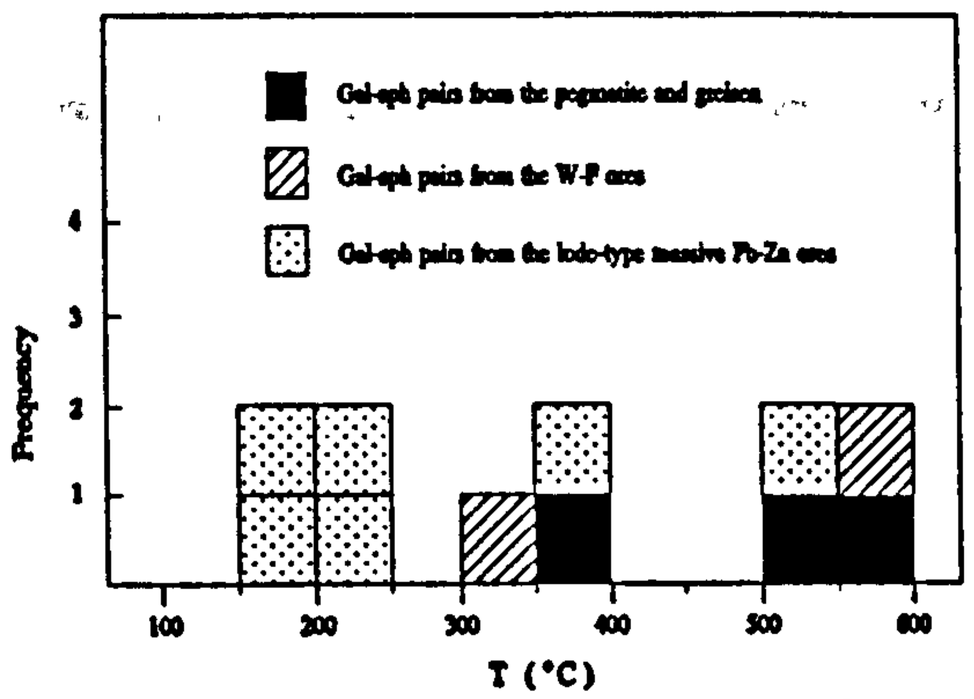

Fig. 6.13 Histogram of isotopic equilibrium fractionation temperatures (calculated for selected mineral pairs in Table 6.5)

Table 6.6 Isotopic equilibrium temperatures calculted from coexiting galena and sphalerite (gal-sph) according to Ohmoto and Rye (1979).

Sample	Location	Mineral pair	$\Delta^{34}_{gal\text{-}sph}S_{CDT}$ (‰)	T (°C)
101-5	Within pegmatitic pod	Gal-Sph	1.6	399
104-15	Pegmatite on top of intrusion E	"	1.0	577
S-1	Greisen on top of intrusion E	"	1.1	537
$III'_{2\text{-}2}$	Xianhguapu W-F ore	"	1.0	577
$D_{W\text{-}8}$	Dongshan W-F ore	"	2.2	300
$B_{324\text{-}1}$	Baojingshan Pb-Zn deposit	"	1.7	379
$M_{4\text{-}15}$	Meishi Pb-Zn deposit, orebody II	"	3.6	175
$M_{4\text{-}19}$	Meishi Pb-Zn deposit, orebody II	"	2.9	226
$M_{4\text{-}31}$	Meishi Pb-Zn deposit, orebody III	"	0.8	503
$M_{5\text{-}4}$	Meishi Pb-Zn deposit, orebody III	"	3.6	175
$M_{5\text{-}5}$	Meishi Pb-Zn deposit, orebody III	"	2.7	244

6.2.5 Discussion

The calculated $\delta^{18}O$ values of fluids in equilibrium with minerals from the W-F ores (quartz, 1.80 to 4.63 per mil; scheelite, -1.08 to 7.12 per mil; calcite, 0.02 to 3.29 per mil) are much lower than those of fluids in equilibrium with quartz from the granitic rocks (8.14 to 10.74 per mil; Table 6.3, Figs.6.14 & 6.15). This decrease of $\delta^{18}O_{H2O}$ values with time suggests a progressive increase of meteoric water in the Xianghuapu W-F hydrothermal system.

An alternative explanation of decreasing $\delta^{18}O_{H2O}$ values of tungsten-bearing hydrothermal fluids with respect to those of granitic fluids has been offered by Higgins and Kerrich (1982) and Higgins (1980). They proposed that the presence of large amount of CO_2 within a hydrothermal fluid could have a profound effect on the oxygen isotope composition of the aqueous component of the fluid (see also Blattner, 1985; Higgins & Kerrich, 1985). Oxygen isotope fractionation factors for CO_2-H_2O (Bottinga, 1968) show that CO_2 is preferentially enriched in ^{18}O. Thus H_2O in equilibrium with CO_2 will be depleted in ^{18}O, possibly leading to a misinterpretation of the contribution of meteoric water if CO_2 is a component of the hydrothermal fluid. However, fluid inclusion studies (see Section 6.1) have failed to report the present of any significant CO_2 in the fluids responsible for the mineralisation in this area. At a temperature of 350°C, the oxygen isotope fractionation between CO_2 and H_2O ($\Delta^{18}O$)

is approximately 11.2 per mil, and at 160°C is 18.5 per mil. If we assume that the CO_2 content in the fluid is less than 10 mole percent, the maximum negative shift in the $\delta^{18}O$ value of the fluid would be 2.1 per mil at 350°C and 3.5 per mil at 160°C. These shifts of 3.5 per mil or less in the $\delta^{18}O$ values of the aqueous fluids cannot adequately explain the measured near 10 per mil shifts in the $\delta^{18}O_{H2O}$ values over the 350° to 160°C temperature range in the Xianghuapu area (Table 6.3 and Fig. 6.14). Thus, it is believed that the decrease of $\delta^{18}O_{H2O}$ values with time represents the progressively increasing importance of meteoric water interaction in the Xianghuapu W-F hydrothermal system.

Fluid mixing is a well-documented phenomenon in different types of hydrothermal deposits (Shelton *et al.*, 1987; Sun & Eadington, 1987; Pollard *et al.*, 1991). The influence of meteoric water during later stages of mineralisation has been noted for various kinds of ore deposits and such a possibility exists also in the Xianghuapu area. In many cases, oxygen isotope data alone fail to determine the origin of the fluids because of possible extensive isotopic exchange with the country rocks. The oxygen and hydrogen isotope data can be combined to construct a δD and $\delta^{18}O$ plot for the fluids produced during the introduction of a granitic intrusion and subsequent evolution of the mineralisation in the Xianghuapu area (Fig. 6.14). Due to a lack of well-defined isotopic information for the meteoric water during the time of granite intrusion and mineralisation and only limited δD data for the mineralisation fluids, any such evaluation must be considered tentative. The measured δD values of inclusion fluids in quartz from the W-F ores fall within the range of magmatic fluids for the Jianfengling granites (JFL granitic water, Fig. 6.14). Based on paleogeographic reconstruction and relevant stable isotope studies, Fu *et al.* (1991) proposed an approximate δD of -130 per mil for meteoric waters in the Dachang tin orefield during the late Cretaceous. This tin orefield is located 500 km west of the Xianghuapu area along the same latitude and has a similar geological background (altitude, intrusion and country rocks) with the area studied. Based on this approach, a δD value of approximately -130 per mil has been assumed for the local meteoric water, which would have had a $\delta^{18}O$ value of -17.5 per mil (Craig, 1961b) at the time of mineralisation.

Figure 6.14 shows the distribution of measured δD and calculated $\delta^{18}O$ hydrothermal fluid compositions at Xianghuapu on a conventional hydrogen-oxygen diagram. The isotopic data for quartz from the granitic rocks define an area for the granitic fluids which is slightly shifted from that of the primary magmatic water (Taylor, 1974, 1979; Sheppard, 1986). The isotopic composition of the quartz from the W-F ores plotted outside the range of the Jianfengling granitic fluids towards more negative $\delta^{18}O$ values. These values are consistent with mixing of the granitic fluids with an unexchanged meteoric water (Shelton *et al.*, 1987; Sun & Eadington, 1987).

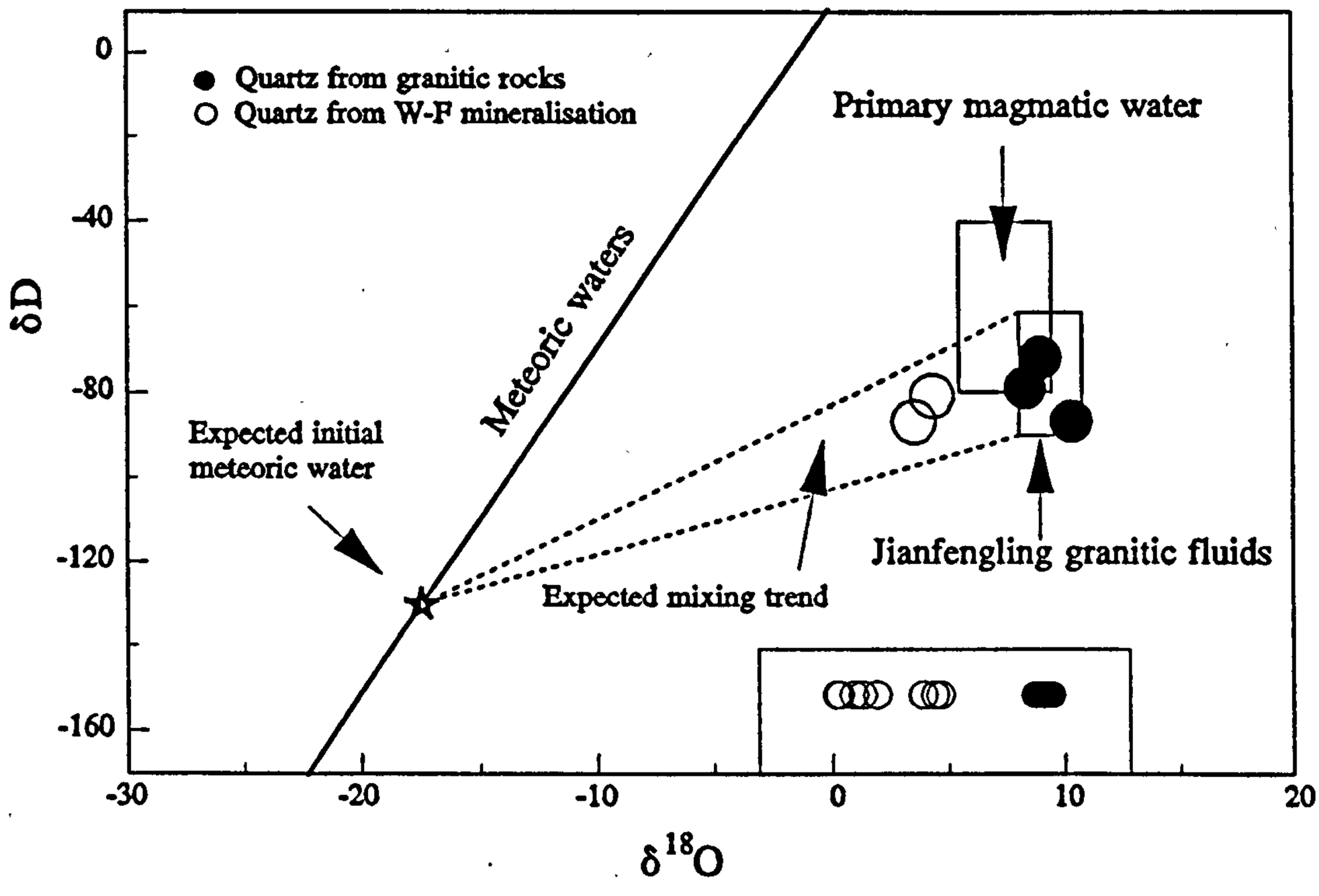

Fig. 6.14 δD vs $\delta^{18}O$ plot showing fluid in equilibrium with quartz from the Xianghuapu area. Field of primary magmatic water from Sheppard (1986). Inset: $\delta^{18}O$ data unconstrainted by δD.

The $\delta^{13}C_{\Sigma C}$ values, -0.47 to -1.71 per mil, of the fluids for the W-F mineralisation are 3 to 4 per mil less than commonly accepted magmatic $\delta^{13}C$ values of 5 ± 3 per mil (Ohmoto & Rye, 1979), a feature is also consistent with the mixing model. The calculated $\delta^{18}O_{H2O}$ values for quartz and calcite from the W-F mineralisation have similar narrow ranges of -0.25 to 2.58 per mil and 0.02 to 2.47 per mil respectively. A narrow range of $\delta^{13}C_{\Sigma C}$ values of -1.71 to -0.47 per mil, calculated from the calcite, is also noted. These results would suggest that these minerals were precipitated over a narrow range of mixing of the hydrothermal fluids despite large temperature differences.

Spatial variations in $\delta^{34}S_{H2S}$

The sulphur isotope ratios of galena and sphalerite in the Xianghuapu area indicate a progressive decrease in $\delta^{34}S_{H2S}$ ($\approx \delta^{34}S_{\Sigma S}$) values of the fluids from the granite towards the hydrothermal

mineralisation in the country rocks. According to Rye *et al.* (1974), spatial variation of $\delta^{34}S$ in hydrothermal sulphides may indicate different sources and/or physicochemical conditions (P, T, fo_2, Eh and pH). Two possible explanations for this phenomenon are either gradual addition of sulphur from an isotopically light source to an originally heavy magmatic sulphur or a progressive increase of oxygen fugacity in the fluid with isotopically heavy sulphur. At Xianghuapu it is not possible to use the mineral assemblages to tightly constrain the oxygen fugacity during the mineralisation. Nevertheless, the paragenetic studies show that the ores of the Meishi deposit, which have the lightest $\delta^{34}S$, contain a large quantity of arsenopyrite and pyrrhotite, minerals which are stable only at relatively low fo_2. Mineral assemblages with evidence for the highest oxidation states occur in the pegmatite and greisen systems, where pyrrhotite is absent, arsenopyrite is uncommon, and pyrite is the common sulphide. If the $\delta^{34}S$ values were controlled by fluid fo_2, then these pegmatite and greisen deposits should have the lightest, rather than the observed heaviest, $\delta^{34}S_{H2O}$ values. Consequently, depletion of ^{34}S through changing redox conditions is not a viable mechanism within the Xianghuapu area. As discussed in previous sections and also referred to Ohmoto (1972) and Ohmoto and Rye (1979), under magmatic and realistic hydrothermal conditions (P_{fluid} = 0.5-3 kb, $x_{H2O} > 0.8$, T < 850°C, fo_2 < QMF + 2 log units) the variation in $\delta^{34}S_{H2S}$ values of the fluid is within 1 per mil of the $\delta^{34}S_{\Sigma S}$ value. Hence at Xianghuapu the decrease in the $\delta^{34}S$ values of the fluids from the granite to the orebodies in the country rocks may be attributed to isotopic exchange reactions between the carbonaceous limestones and fluids derived from the granite and is unlikely to be due to changes in geochemical conditions.

A comparison of the sulphur isotope compositions of sulphides from the Xianghuapu area with those of minerals from other environments is presented in Figure 6.15. The variations of $\delta^{34}S$ in different systems of the Xianghuapu area are much smaller than is evident for other deposits, suggesting a relative uniform sulphur source for the granite, pegmatite, greisen, and W-F mineralisation. The incorporation of a sedimentary sulphur source for the Meishi Pb-Zn mineralisation is also reiterated.

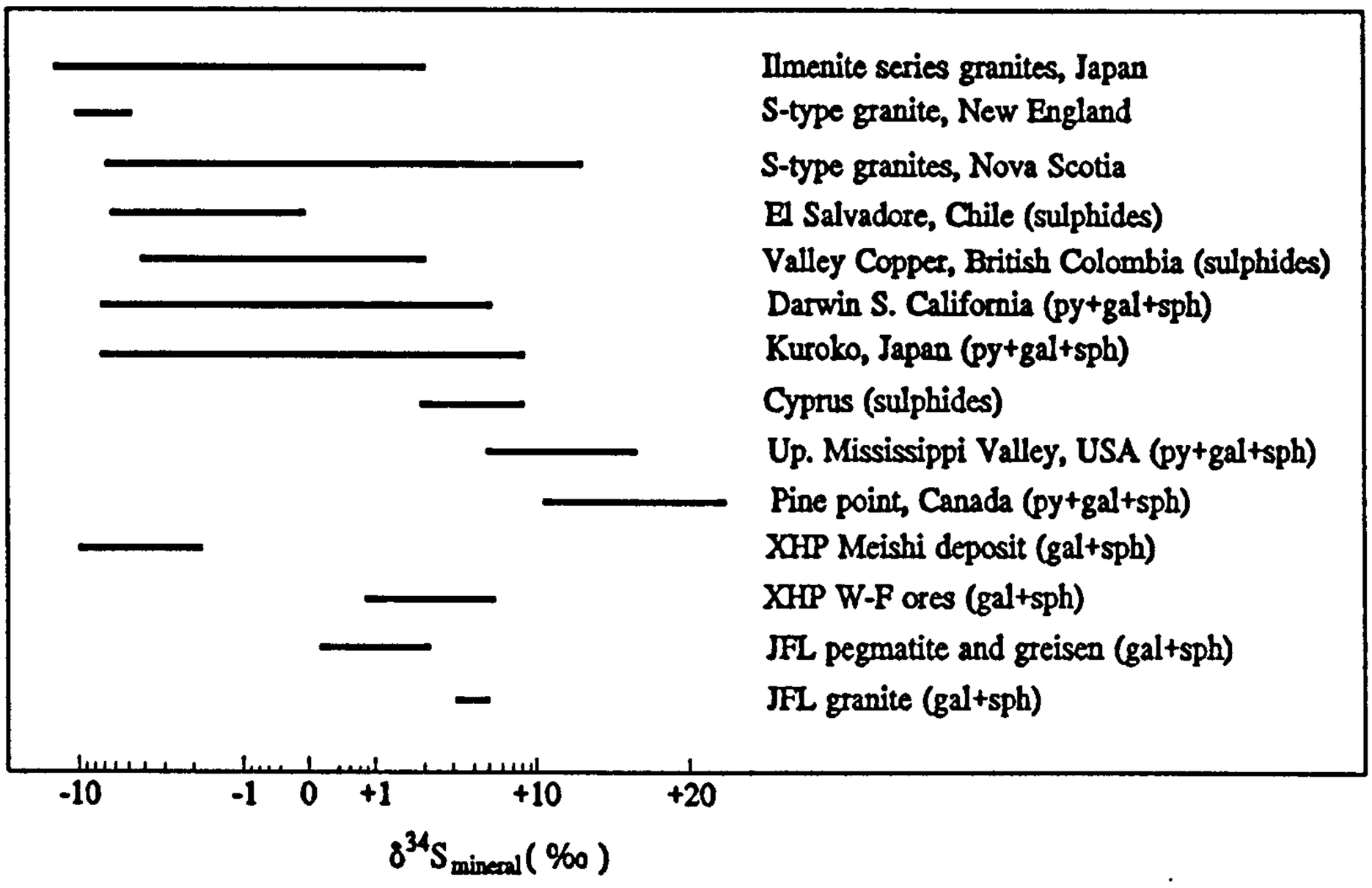

Fig. 6.15 Schematic comparison of sulphur istopic data of the Xianghuapu (XHP) area with ilmenite series (S-type) granites (Laouar et al., 1990), porphyry copper deposits (El Salvadore, Valley Copper; Ohmoto & Rye, 1979), stratiform massive sulphide deposits (Darwin, Kuroko, Cyprus; Rye & Ohmoto, 1974), and Mississippi Valley type deposits (Up. Mississippi Valley, Pine Point; Ohmoto & Rye, 1979).

CHAPTER SEVEN

DISCUSSION

CHAPTER SEVEN

DISCUSSION

Contents

7.1 Introduction
7.2 Petrogenesis of the Jianfengling granites
7.3 Origin of the pegmatitic rocks
7.4 The roles of volatile components
7.5 Fluid evolution
7.6 Mineralisation
7.7 Petrogenetic-metallogenetic model

7.1 INTRODUCTION

The main purpose of this chapter is to summarise and evaluate the results of the studies of the petrology and geochemistry of the Jianfengling granites and associated polymetallic mineralisation presented in the previous chapters. The petrogenesis of these granites is discussed and a number of parameters are constrained for the fluids evolved during the intrusion of the granites and mineralisation. The possible implication of these data for metal transport and deposition are also considered. Finally a petrogenetic-metallogenetic model for these intrusions and mineralisation is constructed.

7.2 PETROGENESIS OF THE JIANFENGLING GRANITES

The mineralogy and geochemistry of the Jianfengling granite complex have been discussed in detail in the previous chapters. The petrological evidence favours the hypothesis that the Jianfengling complex is a product of fractional crystallisation of a fluorine-rich melt originally generated through crustal anatexis. The derivation of these granites from a crustal reservoir requires an increase in isotherms such that melting can occur. Mechanisms for creating such a situation might include

frictional heating in a shear zone environment, transport of heat from the mantle *via* basaltic magmas, or crustal thickening during regional deformation concurrent with plate collision. The first suggestion was discussed by Strong and Hanmer (1981) in their treatment of the Britanny leucogranites. However, there is not sufficient reason to employ a similar model for the Jianfengling granites since there are more differences than similarities in both regional geology between these two areas and the granites themselves (Strong & Hanmer, 1981; this study). The second model was introduced by Kontak (1990) to explain the origin of the East Kemptville leucogranite of Nova Scotia, which is considered to have been generated by partial melting of a crustal reservoir as a result of input of heat from basaltic magma injected into the crust and then ascended to the surface through a crustal-scale structure. Whereas it may be appropriate for the East Kemptville leucogranite, there is no geological evidence to introduce this model here for the Jianfengling granites because of the apparent lack of large scale mafic igneous activity in this part of Southeast China to provide the necessary thermal component. The third model, which is analogous to that used explain the origin of the Himalayan leucogranites, described by Le Fort (1981, 1986, 1988), Le Fort *et al.* (1987) and Vidal *et al.* (1984), is consistent with the present status of knowledge of geology of the Southeast China terrane. The near-linear distribution of granitic intrusions parallel to the suture along which the Pacific plate subducts underneath the Eurasian plate has been recognised (Tu *et al.*, 1980). Crustal thickening, accompanied the subduction, would result in an upwelling of isotherms and subsequent crustal melting. For a detailed diagrammatic illustration of this model, the reader is referred to Feng *et al.* (1986, Figure 6) and Wilson (1989, Figure 8.2). Thus, the Jianfengling granite complex is considered to have been generated *via* partial melting of a crustal reservoir (sial zone) as a result of subduction. Ascent to a shallow level was facilitated by a deep-cut structure (F_{101} fault zone) and emplacement was confined to the intersection of several groups of faults as mentioned in previous chapters.

The rocks of the Jianfengling complex have mineralogical features that would normally identify them as "S-type" granites (*e.g.* Chappell & White, 1974; White *et al.*, 1986), but a detailed comparison with the Australian "S-type" granites (White & Chappell, 1988; White *et al.*, 1986) reveals differences that might have important petrogenetic implications. For example, the "AFM" mineralogy in the Jianfengling granites is characterised by biotite (zinnwaldite), with topaz and andalusite as typical subordinate phases. Most of the Australian "S-type " granites have an "AFM" mineralogy dominated by biotite-cordierite assemblages, although garnet and orthopyroxene are common. Topaz and andalusite are rarely observed. The evidence therefore points to source rocks which are less peraluminous and have lower F, Li and H_2O contents for the Australian "S-type" granites than for the Jianfengling granites.

Table 7.1 Comparison of the characteristic features of the Jianfengling granites to those of the two subtypes of topaz granites (Taylor, 1992)

	The Jianfengling granites	Low-P subtype	High-P subtype
Essential minerals	Quartz, K-feldspar, albite (An_{0-3}), biotite, zinnwaldite, and topaz.	Quartz, K-feldspar, albite (An_{0-5}), F-rich topaz, and lithian mica (mica compositions range from lithian siderophyllite through zinnwaldite to lepidolite).	
Accessory minerals	Monazite, andalusite, fluorite, Nb-Ta oxides, cassiterite, and sulphides.	Accessories common to both type include zircon niobian rutile, columbite-tantalite, cassiterite, and sulphides.	
		Phosphates are very rare: mainly monazite.	Abundant phosphates: apatite, monazite, amblygonite-montebrasite
Major elements	SiO_2 (72-77 wt.%), Al_2O_3 (13-16 wt.%) Na_2O (2.5-5.0 wt.%) K_2O (3.0-5.0 wt.%) Fe_2O_{3T} (0.5-2.0 wt.%) MgO (0.03-0.20 wt.%) CaO (0.14-0.90 wt.%) ASI = 1.07-1.54	Common features of both types are: the very low abundances of TiO_2 (<0.1 wt.%), MgO (<0.2 wt.%), and CaO (<0.5 wt.%); the low content of FeO^T (<1.0 wt.%); and the high concentrations of Na_2O (>4.0 wt.%) and high Na/K ratios (1.0-2.0, up to 3.6).	
		Higher SiO_2 (>73 wt.%), lower Al2O3 12-14.5 wt.%); weakly peraluminous (ASI=1.0-1.2).	Lower SiO_2 (68-73 wt.%), higher Al_2O_3 (14.5-20 wt.%); strongly peraluminous (ASI=1.2-1.5).
Phosphorus	P_2O_5 ≤0.01 wt.%	Low P_2O_5 (<0.10 wt.%)	High P_2O_5 (>0.40 wt.%)
Volatiles	F (0.71-2.75 wt.%) Cl (≤100 ppm)	Very high concentrations of F (>0.4 wt.%, up to 2.5 wt.%), and very low abundances of Cl (<250 ppm) and CO_2 (<0.2 wt.%).	
Minor and trace elements	High Li (300-1250 ppm), Rb (100-2350 ppm), Cs (30-80 ppm), Nb (35-80 ppm), Ta (20-110 ppm), W (5-120 ppm), Sn (30-290 ppm); low Sr, Ba, V, Cr, Ni, Mo, Cu, Sb.	Very high contents of the alkalis: Li (typically 250-2600 ppm, but up to 7500 ppm), Rb (800-2400 ppm, up to 4100 ppm), and Cs (20-150 ppm, up to 700 ppm); and the lithophile elements: Nb (30-120 ppm), Ta (10-60 ppm, up to 250 ppm), W (10-50 ppm), and Sn (10-300 ppm). Low to very low abundances of V, Cr, Co, Ni, Cu, Sr, Zr, Mo, and Ba.	
Rare earth elements, Y, and Th	ΣREE=30-350 ppm; gullwing-shaped REE patterns [$(La/Lu)_N$ =1.4-1.9] with deep negative Eu anomalies: (Eu/Eu^*)<0.01. High Y and Th	ΣREE=150-350 ppm; flat to gullwing-shaped REE patterns [$(La/Lu)_N$=0.6-1.5] with deep negative Eu anomalies: (Eu/Eu^*)<0.1. High Y (60-160 ppm) and moderate to high Th (20-50 ppm) contents.	ΣREE<10 ppm; slight enrichment of LREE [$(La/Lu)_N$>1.5]; moderate negative Eu anormalies: (Eu/Eu^*)<0.2. Low Y (<15 ppm), and low Th (<10 ppm) abundances.
Stable isotopes	Fluid in equilibrium with the pegmatitic quartz: δD=-70 to -88‰; $\delta^{18}O$=8.1-10.7‰.	Whole-rock δD compositions of both types vary over an extended range from -40 to -110‰.	
		Whole-rock $\delta^{18}O$ compositions are lower and range from 7.5 to *ca.* 10.0‰.	Whole-rock $\delta^{18}O$ compositions are higher and range from *ca.* 10.0 to 13.5‰.
Examples		Eurajoki, Finland; Pleasant Ridge, New Brunswick; Altenberg and Zinnwald, Germany; Kougarok, Alaska.	East Kemptville, Nova Scotia; St. Austell and Tregonning in SW England; Beauvoir, France; Yichun, SE China.

The unusual mineralogical character of the Jianfengling granites is reflected in their chemical composition, which is quite distinct from that of the most highly fractionated examples of I- and S-type granites and aluminous A-type granite (*cf.* Collins *et al.*, 1982; Whalen *et al.*, 1987; Sawka *et al.*, 1990). The Jianfengling granites are highly enriched in fluorine, the alkali metals (Li, Rb, Cs), and the lithophile elements (Nb, Ta, Sn, W), and have marked depletions of P, Ti, Fe, Mg, Ca, Sr and Ba (see Chapter 4 for details). These features are common also for topaz granites from other parts of the world, such as SW England, N America and SE Asia (Taylor, 1992). These topaz granites are thought to represent a group which "*can be distinguished from all other widely distributed types of granites by a variety of geochemical criteria, the most notable of which is their very high F content*" (Taylor, 1992, p913). Based on a comprehensive world-wide comparison, Taylor (1992) found a natural dichotomy within this unique group of F-rich felsic rocks, such that "low-P" and "high-P" subtypes of topaz granites can be distinguished (see Table 7.1). The Jianfengling granites are grouped into the "low-P" subtype based on the criteria used by Taylor (1992). A comparison of the basic characters of the Jianfengling granites to those of the two subtypes of Taylor is made in Table 7.1.

The Jianfengling granite stock (known as the 430 Granite in Chinese literature) was investigated thoroughly by geologists from the No. 238 Geology Team during the exploration of Nb-Ta mineralisation in the 1960s and 1970s. A model of "one-stage intrusion with seven differentiation and alteration zones" was proposed for the evolution of the Jianfengling stock (No. 238 Geol. Team, 1974; Fig. 7.1). In this model the granite stock was believed to be a product of one magmatic pulse and experienced extensive late-magmatic and post-magmatic modification. Seven zones were recognised on the basis of mineralogical assemblage and types of alteration. The main characteristics of these zones are summarised in Table 7.2.

However, the existence of intrusive contacts clearly indicates that the Jianfengling granite stock really comprises a complex of five intrusive phases. These five phases petrographically and geochemically fall into two groups and the intrusions of each group have their own distinct petrological and geochemical characteristics (Chapters 3 and 4). Hence a new petrogenetic model is needed to explain the evolution of the Jianfengling granite complex, and the detailed petrographical and geochemical investigations of this study allow the development of such a model.

It is unlikely that rocks of the two groups were generated from two different sources for the following reasons:

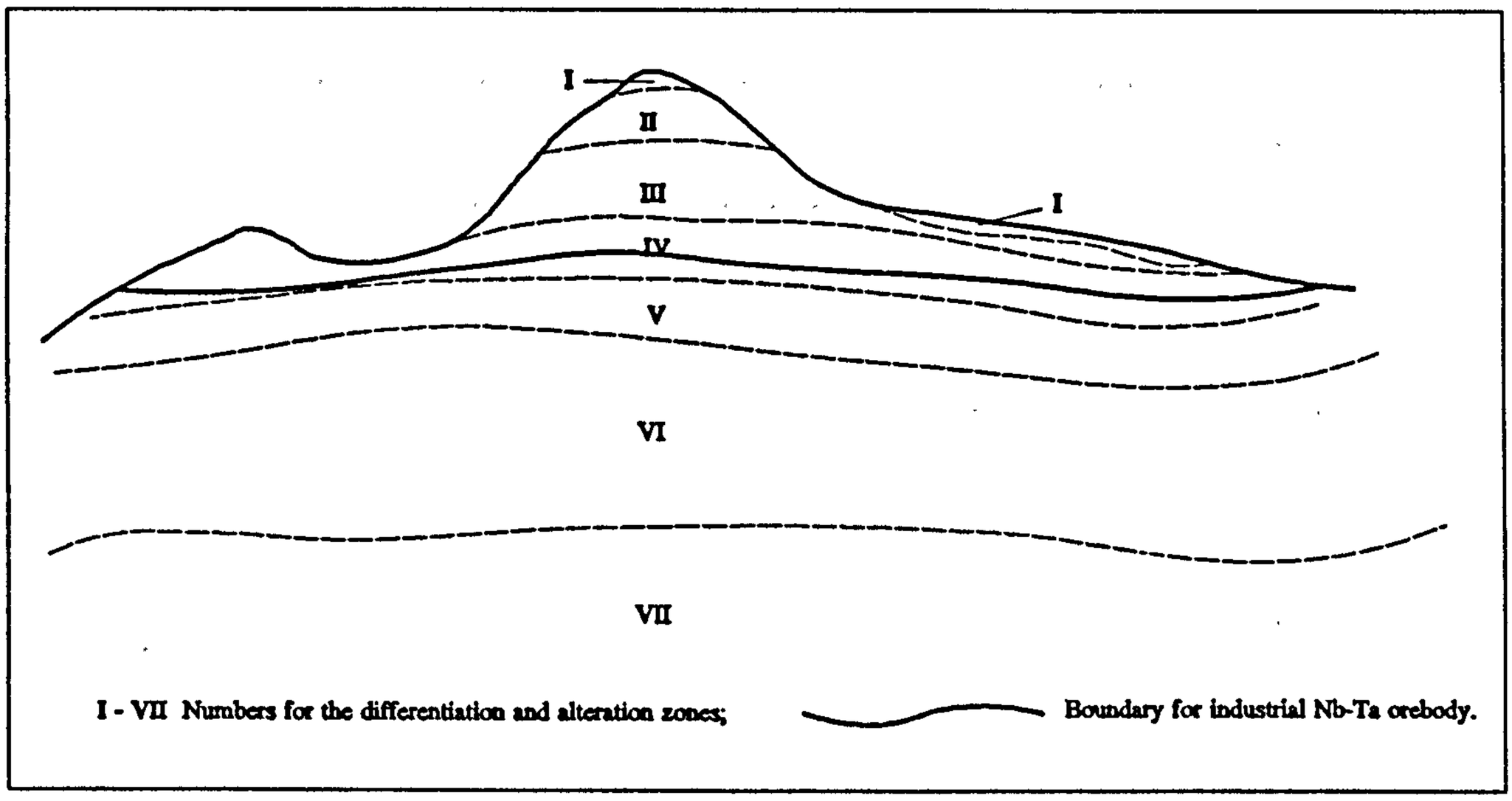

Fig. 7.1 Schematic profile of the Jianfengling granite stock proposed by the No. 238 Geological Team (1974); characteristics of each zone are listed in Table 7.2

(1) The intrusive contacts among the different phases are small scale, the pegmatitic and metamorphic zones along the contacts are only a few centimetres in width indicating a short time interval between two pulses.

(2) Despite the geochemical differences, the intrusions of both groups have an identical major element chemistry, and similar distribution patterns of trace elements, especially the REEs. These can only be explained by an internal evolution of magmas from a common magmatic chamber.

Table 7.2 Zonation characteristics of the Jianfengling granite (summarised from the No. 238 Geological Team, 1974).

Zone	Rock type	Grain size	Main minerals (vol%)	Accessories	
				Nb-Ta-bearing minerals	Others
I	Greisen	medium to fine (2 mm±)	Quartz (55-60), Li-mica (15-20), Sericite (5-10), Topaz 15-20	Microlite, niobite, tantalite	Zircon, fluorite, garnet
II	Strongly greisenised, albitised, and K-feldspathised granite	Fine (1-2 mm)	Microcline (10-15), Quartz (45-55), Li-bearing muscovite (10-15), Sericite (20-25), Topaz (3-5)	Microlite, niobite, tantalite	Cassiterite, fluorite, wolframite, zircon, manganite
III	Greisenised, albitised, and K-feldspathised granite	Fine (1 mm±)	Microcline (20-25), albite (20-25), Quartz (40-50), Li-bearing muscovite (3-5), Sericite (2-5), Topaz (1-3)	Microlite, niobite, tantalite	Fluorite, cassiterite, wolframite, sulphides
IV	Strongly albitised, weakly greisenised, and K-feldspathised granite	fine to medium (2-5 mm)	Microcline (20-25), albite (30-35), Quartz (35-45), Li-bearing muscovite (3-5), Topaz (1-3), Sericite (1-2)		
V	Strongly albitised, K-feldspathised granite	Medium, or fine to medium (<5 mm)	Microcline (15-20), albite (35-45), quartz (40-45), zinnwaldite (2-4)		
VI	Albitised, K-feldspathised granite	Medium (±5 mm)	Microcline (25-35), albite (20-30), quartz (35-40), zinnwaldite (2-5)		
VII	K-feldspathised biotite granite	Medium to course (≥5 mm)	Microcline (30-40), albite (20-50), quartz (35-40, Li-biotite (3-7)		

7.3 ORIGIN OF THE PEGMATITIC ROCKS

The pegmatitic units at the roof zones of the Jianfengling granite intrusions and at the contacts of the granites with the country rocks are similar to units found at the margins of many other granitic intrusives associated with rare metal mineralisation. Examples occur in Alaska (Puchner, 1986), Arizona (Schmitz & Burt, 1990), Tasmania (Groves & McCarthy, 1978), South Africa (von Gruenewaldt & Strydom, 1985), Germany and Czechoslovakia (Štemprok & Sulcek, 1969; Bauman, 1970), SW England (Badham, 1980), and other parts of SE China (Xia & Zhang, 1982; Zhang & Xia, 1988; and personal observations).

These contact or marginal pegmatites were first noted in the Erzgebirge mining region of eastern Europe, where they were called "*stockscheider*" (from German, literally "*stock separator*", in Schmitz & Burt, 1990). The *stockscheider* was interpreted as a late pegmatite emplaced in fissures formed due to contraction of the main stock on cooling (Baumann, 1970). Groves and McCarthy (1978) noted barren pegmatites overlying granite-hosted tin ore in Tasmania and South Africa and suggested that the pegmatites formed from an aqueous fluid that collected at the apex of the stocks. Similar ideas have been expressed by most of the authors cited above. Schmitz and Burt (1990) proposed that a pressure quench and loss of volatiles accounted for the formation of the pegmatite margin at the Black Peral mine, Arizona. The pressure quench was achieved by the opening of fissures at the top of the granite stock.

A theory of "liquid segregation" has been widely accepted by many workers from China and the former Soviet Union to explain the evolutions of some volatile and rare-metal-enriched granite stocks and associated pegmatites (Kosals, 1976; Wang, L.K. *et al.*, 1983, 1987, 1988; Xia & Zhang, 1982; Zhang & Xia, 1988; and many others). Experimental studies carried out by Wang L.K. *et al.* (1983, 1988) revealed that an originally homogeneous granite melt rich in F and Li could segregate into more than two immiscible liquid phases with contrasting compositions. The experiments were performed at 1 kb and 700-850°C by using a mixture of natural biotite granite, HF, NaF and pure H_2O.

The pegmatitic contacts of the Jianfengling granite stock are typically massive, but where indicators of crystal growth are present (as defined by Shannon *et al.*, 1982), these features indicate crystallisation directed from the contact inward toward the centre of the intrusive (*cf.* Plate 3.1f). This orientation suggests that the pegmatites cannot be late dykes that were emplaced along the contact. Most important of all, the presence of pegmatitic pods in the roof zones of the Jianfengling intrusions

provides direct evidence of phase segregation during the late-stages of the evolution of the granites. As discussed in Chapter 3, these pegmatitic pods have either an ellipsoidal shape with the long axis vertical or an irregular shape coincident with the intrusive contacts (see Plates 3.1). They are hosted within the granites and show sharp contacts with their hosts. There is no evidence of these pegmatitic pods intruding the granites. All these features suggest that these pegmatite melts were separated from the granite melts before or during the emplacement of the intrusives. The high concentrations of volatiles (F, Li, H_2O) caused the pegmatite melt to have a lower density and viscosity than its host granite melt; thus it migrated upwards toward the roof of the intrusion during the emplacement and kept an ellipsoidal shape until it reached the contact where it became ponded along the contact. The presence of F, Li, and H_2O could lower the liquidus and solidus of the pegmatite melt considerably (see next section for details). Therefore, it is reasonable to believe that the pegmatitic melt was still in a liquid state while the host granite melt was consolidating. During the crystallisation of minerals from the pegmatite melt, volatiles reacted with the surrounding granite and formed the alteration halos along the contact which are observed in the field.

The large crystal sizes of the pegmatite minerals indicate crystallisation in the presence of a low viscosity, presumably aqueous liquid (Jahns & Burnham, 1969). The melt that formed the marginal pegmatites and the pegmatitic pods of the Jianfengling intrusions therefore were probably saturated with volatiles during emplacement.

7.4 THE ROLE OF VOLATILE COMPONENTS

Both the extent and type of magmatic and hydrothermal processes in granitic systems are largely controlled by the relative abundances of volatile constituents. Volatiles such as H_2O, H_2S, CO_2, F, B, Li and Cl all undergo hydrolysis with O^{2-} and cause depolymerisation of the melt (Burnham, 1979; Dingwell, 1988). This change in melt structure due to depolymerisation results in

(1) a change in the order of crystallisation reflecting the greater entropy of the melt;
(2) changes in solid/melt and melt/liquid partition coefficients of elements because the stability of each element in these systems is altered;
(3) depression of both liquidus and solidus temperatures, a reduction of viscosity, and a resultant increase in diffusion rates.

The relative abundance of volatile components and how and when each is exsolved determines the extent of depolymerisation and diffusion, and ultimately the final compositions of the melt and aqueous fluid.

During the initial stages of crystallisation, the most profound effect of volatiles is to depress the liquidus and solidus. This allows the melt to undergo more extensive fractionation and, as long as the volatile phases remain dissolved in the melt, to ascend to shallow levels. Once a fluid phase (generally aqueous) exsolves from the melt, each volatile constituent is partitioned between the fluid and silicate phases. Because partition coefficients for different volatile constituents vary greatly, their relative abundances in the melt strongly influence subsequent melt properties, such as viscosity. Throughout the history of crystallisation and fluid evolution, the volatile content (both dissolved and exsolved) of the melt influences the phase equilibria and partitioning of elements among solid, melt and fluid phases, thereby affecting the order of crystallisation and hence the composition of the melt. This controls the availability of metals for ore genesis. Thus, the composition of the final melt and the nature of the fluid phases are influenced by (1) liquidus and solidus depression, (2) partitioning of volatiles, (3) effects of volatiles on phase equilibria, and (4) crystal-melt and melt-fluid partitioning of elements.

Liquidus and solidus depression

The effect of H_2O in lowering the liquidus and solidus of granitic melts has long been recognised (Tuttle & Bowen, 1958; Luth *et al.*, 1964; Luth, 1969, 1976; Steiner *et al.*, 1975; Whitney, 1988). Recent experimental work with hydrous granite melts shows that the solidus may be lowered by 100°C with an addition of F, B, Li, and perhaps P (Bailey, 1977; Manning, 1981, 1982; Manning & Pichavant, 1983, 1988; Martin, 1983; Pichavant, 1981, 1987; Pichavant & Manning, 1984; Dingwell, 1988; London *et al.*, 1993). Manning (1981) documented the persistency of melt at 550°C in a granitic system with 4 wt.% fluorine. The addition of several volatiles to melts with compositions near the granitic minimum could have additive effects and reduce the solidus to as low as 500°C at 1 kb (Henderson & Martin, 1985).

Extreme solidus depression in a F-rich melt was documented by Payette and Martin (1990) in their studies of melt or glass inclusions from the Topaz Mountain Rhyolite, USA. Melt inclusions in quartz commonly appear as negative crystals, that is, inclusions with shapes defined by crystal faces of the host mineral. In the Topaz Mountain Rhyolite, melt inclusions in primary phenocrysts of quartz occur in the form of hexagonal prisms with pyramidal terminations, an alpha-quartz habit. Thus, they concluded that the melt inclusions indicate quartz crystallisation below the quartz inversion temperature of 573°C, demonstrating extreme depression of the solidus temperature.

Fluid inclusions in topaz and quartz from the pegmatites of the Jianfengling stock show homogenisation temperatures of 480-530°C. Compared with the examples cited above, these temperatures should be reasonably close the solidus of the pegmatite melt which was extremely rich in fluorine (topaz content in the pegmatite can be as high as 60 wt.%) and lithium.

Partitioning of volatile components

The partitioning of volatiles between silicate melt and coexisting aqueous fluid has been extensively studied both experimentally and theoretically during the last 20 years or so (Kilinc & Burnham, 1972; Burnham & Ohmoto, 1980; London *et al.*, 1988; Webster & Holloway, 1988; Webster, 1990; Webster & Duffield, 1991; Holtz *et al.*, 1992). Most of these studies are related to the granitic system and volatiles such as H_2O, CO_2, S, F, Cl, Li and B have been investigated. Here, only investigations concerning F, Cl and S, which are thought to be important with respect to the evolution of melt and fluids and mineralisation in the studied area, are briefly reviewed in the following section.

The differing behaviour of F and Cl in the granite melt and associated aqueous fluid strongly

influences the distribution of metal-bearing species in the system. Critical experimental data on F and Cl partitioning presented by Webster and Holloway (1990) may be summarised as follows:

> D_{Cl}[2] ranges from 0.8 to 85; however under typical geological conditions, Cl partitions more strongly into aqueous fluids relative to F-bearing granitic melts. Cl partitions increasingly in favour of the fluid as F in the fluid and magma decrease and as temperature, pressure, H_2O content of the fluid, and Cl in the fluid and melt increase.

D_F ranges from 0.2 to >1.0; however, F is typically concentrated in granitic melts relative to coexisting aqueous fluids. F concentrates more strongly into the melt than the fluid as pressure and F in the system decreases, and as temperature and H_2O in the fluid increases, i.e.

$$D_F^{melt} \propto \frac{1}{P_{tot}}, \frac{1}{F_{tot}} \; ; \quad D_F^{melt} \propto T, P_{H_2O_{(fluid)}}$$

> The effects of increased F concentration in the system are to decrease melt viscosity, decrease both liquidus and solidus temperatures, and to increase cation and volatile diffusion rates, the thermal stability of hydrous phases, and the solubility of silicate melt in fluid phases.

> The effects of increased Cl concentration in the system are to increase the solubility of alkalis with respect to Al in the fluid and the partitioning of Pb, Zn, Cu, W, Mn, REE, Li, Rb, Cs, Nb, Y, Sr, and Ba from melt into fluid.

Webster and Holloway's (1990) experimental data support theoretical calculations by Candela and Holland (1984, 1986) that demonstrate that increased halogen concentrations in the melt may substantially increase the efficiency of metal removal from the melt by the magmatic aqueous phase. Both F and Cl depolymerise the silicate melt thus decreasing melt viscosity. Reduced viscosity results in high cation and volatile diffusion rates and may permit convection, thereby ensuring a close approach to equilibrium partitioning of metals between melt and fluid. F and Cl may become

[2] D = fluid (vapour)/melt partition coefficient

extremely enriched in granitic melt if H_2O, CaO, and ferromagnesian components are very low. If an aqueous phase is exsolved, Cl will be preferentially partitioned over F into the aqueous phase. F, however, will remain in the melt, depressing liquidus and solidus temperatures and preventing quenching.

Partitioning of sulphur, another important volatile component, is sensitive to oxygen fugacity (fo_2) and pressure because it is dissolved in hydrous melts principally as HS^- but exists in the aqueous phase as both H_2S and SO_2; H_2S is more soluble in the melt than SO_2 (Burnham, 1979). Under the fo_2 of a given phase assemblage, increasing pressure increases the proportion of H_2S to SO_2; hence the partition coefficient for sulphur ($\sum S_{fluid}/\sum S_{melt}$) is decreased. On the other hand, increasing fo_2 at a given pressure, for example by diffusive loss of hydrogen from the system, increases the proportion of SO_2; hence the partition coefficient for total sulphur is increased. These phenomena are of great importance to sulphide ore formation as they provide a mechanism for generating high concentrations of both sulphur and heavy metals in the magmatic aqueous phase.

Effects of volatiles on phase equilibria

The effects of F, B, and Li on phase equilibria in the synthetic granite system, Qz-Ab-Or, have been investigated by a number of workers (Manning, 1981; Martin, 1983; Pichavant, 1981, 1983, 1984, 1987) and can be compared with increasing P_{H2O} (Tuttle & Bowen, 1958; Luth *et al.*, 1964). Liquidus phase relationships for the system Qz-Ab-Or with added F, B and Li with excess H_2O are summarised in Figure 7.2. With increasing F and B contents, the minium of the system is shifted toward the albite apex, with expansion in the stability field of quartz. Conversely there is little change with added Li. Fluorine has also been observed to increase the thermal stability of biotite in a granite melt (Clemens, 1984). In every case, the addition of a volatile component reduces the minimum-melt temperatures (*cf.* Table 7.3) and, similarly, reduces the solidus temperature. This fluxing effect enables volatile-rich residual magmas to persist to low temperatures at high crystallisation levels.

So far, experimental studies have been carried out only on systems with single volatile species in addition to water. However, as discussed by Manning and Pichavant (1988), the addition of B (as B2O3) in the system Qz-Ab-Or with added F and H_2O would have an additive effect on the displacement of the minimum toward the Ab apex in addition to the lowering of liquidus and solidus temperatures. The addition of Li does not affect the quartz, alkali-feldspar field boundary for up to

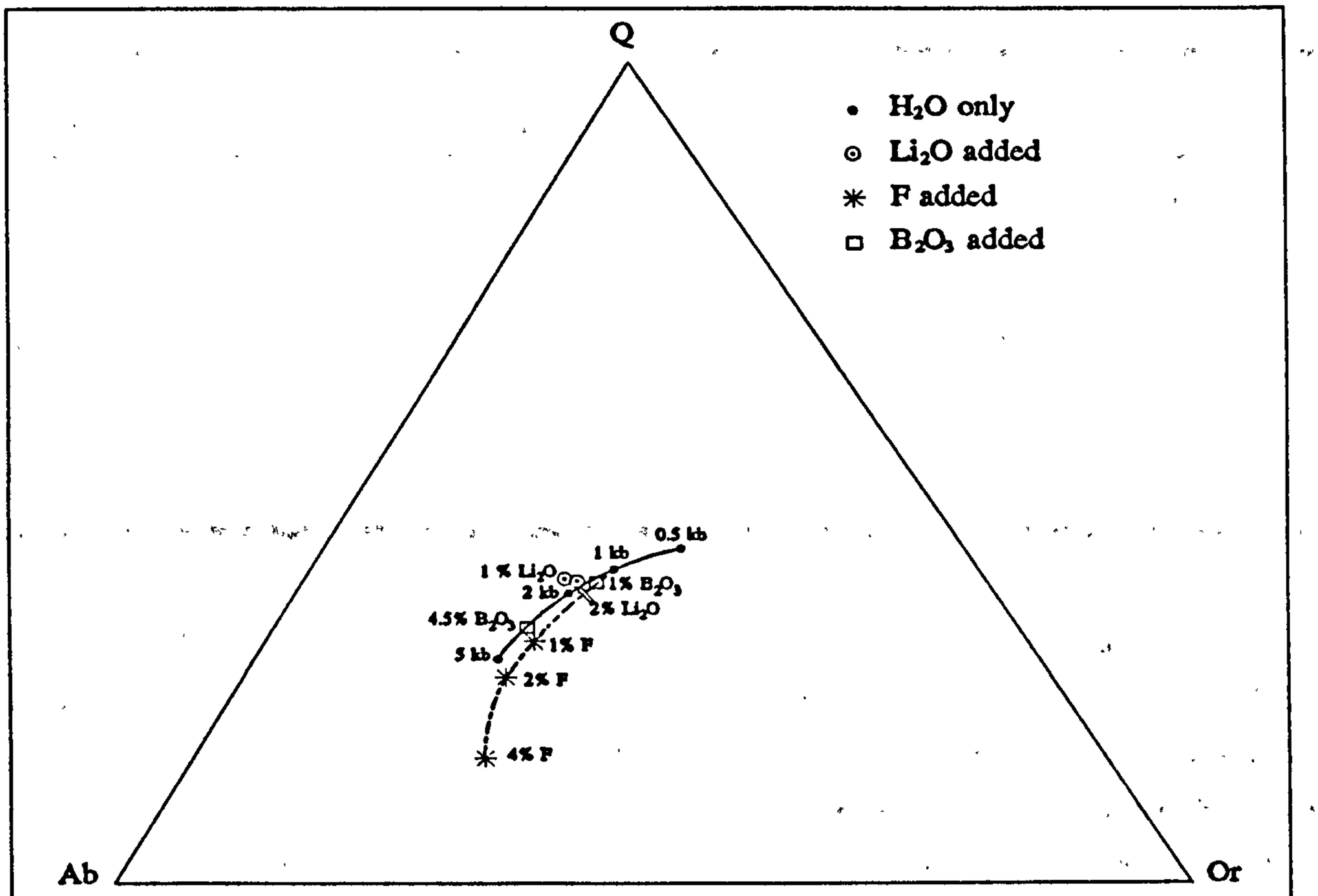

Fig. 7.2 Liquidus phase relationships in the system Qz-Ab-Or with excess water (Tuttle & Bowen, 1958) and with Li_2O, B_2O_3, and F added under water-saturated conditions (Manning, 1981; Martin, 1983; Pichavant, 1984).

2 wt.% Li_2O; with 4 wt.% Li_2O, petalite becomes a stable liquidus phase (Martin, 1983). For low concentrations of Li_2O, there appears to be no change in the proportion of the framework components of the melt, and Li is thought to be present as interstitial cations (Manning & Pichavant, 1988).

All of the added volatiles have a fluxing effect, reducing the temperatures of crystallisation and the viscosity of the magma (Dingwell, 1988), and facilitate the incorporation of molecular complexes of metals and other elements of economic interest.

The amount of H_2O in solution in granitic melts has a large influence upon phase relationships and

Table 7.3 Minimum compositions and temperatures for volatile-bearing melts in the water saturated system Qz-AB-Or, at 1 kb pressure

Volatile content	Qz	Ab	Or	T (°C)	Source
volatile-free	38	33	29	725	Tuttle and Bowen, 1958
1 wt.% F	29	45	26	690	Manning, 1981
2 wt.% F	25	50	25	670	Manning, 1981
4 wt.% F	15	58	27	630	Manning, 1981
1 wt.% Li_2O	37	42	21	700	Martin, 1983
2 wt.% Li_2O	36	41	23	675	Martin, 1983
1 wt.% B_2O_3	35	37	28	690	Pichavant, 1984
4.5 wt.% B_2O_3	31	46	23	630	Pichavant, 1984

the position of the cotectic curves in the system (Qz-Ab-Or-H_2O), as well as reducing solidus and liquidus temperatures. The experimental studies of Tuttle and Bowen (1958) and Luth *et al.* (1964) have shown that with increasing H_2O pressure (i.e. H_2O_{melt}) the stability field of quartz expands with displacement of the minimum and eutectic toward the albite corner (Fig. 7.2). However, the effects of either H_2O content of the melt (H_2O_{melt}) or pressure alone cannot be distinguished using these experimental results. Subsequent experimental data (Luth, 1969; Steiner et al., 1975; Boettcher et al., 1984) suggest that the effect of pressure and of H_2O_{melt} are different, and that it is principally the effect of pressure which result in the increase in the stability field of quartz. The relative importance of pressure and H_2O_{melt} may also change with pressure: at low pressures (< 3 kb) the effect of dissolved water may be predominant whereas at higher pressures the effect of pressure may be more important, because H_2O has less effect on phase relationships at higher pressures (the solidus curve in Qz-Ab-Or-H_2O does not show much reduction in temperature with increasing pressure above 3 kb P_{H2O}). It is also suggested that the displacement of the minima observed in the systems Qz-Ab-Or-F-H_2O and Qz-Ab-Or-B_2O_3-H_2O at 1 kb in H_2O-undersaturated conditions is not due to changes in the H_2O_{melt} associated with the addition of F and B_2O_3.

The available data show that the addition of F and Li to granitic melts has no significant effect on the solubility of H_2O at constant pressure (Manning, 1981; Martin, 1983), whereas this increases with increasing B content (Pichavant, 1981). Thus B-rich melts will therefore reach H_2O-saturation at a later stage of fractional crystallisation (or at a lower P_{total}) than volatile-free or F- and Li-rich melts. The presence of volatile components, such as CO_2, CH_4, Cl which do not readily disolve in a silicate magma, will favour the existence of an exsolved H_2O-poor fluid phase very early in the crystallisation

history (e.g. Holloway, 1976). The presence of these volatiless in the system will reduce f_{H2O} of the fluid and therefore will have an indirect effect on phase relationships, by reducing the melt H_2O-content.

Effects on vapour/melt partitioning of elements

Volatile components such as H_2O, CO_2, H_2S, F, B, Li, and Cl are both directly or indirectly involved in the incorporation, concentration and transport of metals (e.g. Sn, W, Nb, Ta, REE, Th, U, Cu, Pb, Zn) in granitic melts, and in the extraction of these metals from magmas into coexisting aqueous phases prior to mineralisation. As discussed in previous sections, a volatile enriched residual granitic melt may persist to a relatively low magmatic temperature, and may become enriched in incompatible (magmaphile) elements, especially metals of economic interest. If an aqueous fluid phase developed through exsolution, the partitioning behaviour of metals and complexing agents may vary as a function of volatile character and content. As Candela (1986) pointed out, our understanding of this process is still in its infancy, although a number of experimental studies have been carried out (Hards, 1976; Manning & Henderson, 1984; Candela & Holland, 1984; Candela, 1986; Keppler & Wyllie, 1991). Candela (1986) presented a quantitative model of vapour evolution in granitic system and summarised known vapour/melt partition coefficient for many elements. Considerable work remains, however, before a full understanding of this critically important step in the evolution of ore-bearing granites is achieved. A few examples showing the significance of volatiles on partitioning and vapour transport of elements in granitic systems are briefly outlined bellow:

Numerous studies have revealed that late-stage differentiation of highly evolved granites and rhyolites rich in F, Li, and/or B, Cl leads to extreme negative Eu anomalies, flattening of REE patterns, and commonly an enrichment of heavy REE sufficient to yield a gull-wing-shaped REE pattern (*e.g.* Christiansen *et al.*, 1983, 1984, 1986; Maruéjol *et al.*, 1990; Öhlander *et al.*, 1989; Schaltegger & Krähenbühl, 1990; Stein & Clark, 1990; Kontak, 1990; Taylor, 1992). In the Colorado Mineral Belt, for example, Late Cretaceous to Early Tertiary monzonites, quartz monzonites, and granodiorites display linear REE patterns with steep to moderately steep slopes and small to moderate Eu anomalies (Stein & Crock, 1990). Oligocene-Miocene granites and rhyolites have well developed gull-wing shaped REE patterns and show extreme Eu depletion. The distinctive patterns for the younger, highly evolved granites and rhyolites in the Colorado Mineral Belt are thought to be attributed to upper crustal crystal-melt and vapour-melt fractionation processes (*op. cit.*). Preferential solubility of heavy

REE over light REE in F-rich volatile phases (London & Herige, 1986; London *et al.*, 1987) supports the suggestion that vapour transport contributed to the pronounced gull-wing-shaped REE patterns. Extreme loss of Eu to the vapour phase has also been documented by Candela (1987).

Price *et al.* (1990) claimed that vapour phase crystallisation of an F-rich peraluminous magma produces extreme enrichment in incompatible elements in highly evolved rhyolites. REE patterns for peraluminous rhyolites of the Trans-Pecos region, Texas, are flat to slightly V-shaped, with light REE concentrations as much as several hundred times those of chondrite. High incompatible element concentrations cannot be accounted for by either magmatic assimilation or hydrothermal leaching of wall rock, and enrichment by crystal fractionation would require an unusual assemblage of minerals for which there is no evidence. Vapour phase transfer of incompatible elements, especially REE, is the most reasonable explanation.

The partitioning behaviour of Sn, W, Mo, Cu, Th, Pb, Zn in magmatic melt-vapour (fluid) systems has been investigated experimentally by many workers (Khitarov *et al.*, 1982; Candela & Holloway, 1984; Manning & Henderson, 1984; Taylor & Wall, 1984; Urabe, 1985; Webster *et al.*, 1989; Keppler & Wyllie, 1991) and the results are summarised in Table 7.4. The volatiles of principal interest are F and Cl; P may also be important as a transporting agent (Manning & Henderson, 1984), but its role in the Jianfengling granites is certainly limited as the concentrations of phosphate minerals in these rocks are extremely low.

Tin (Sn)

In Cl-bearing granitic melt-vapour systems, the tin partition coefficient (D_{Sn}) increases steadily with increasing chloride molality, while the effect of fluorine on D_{Sn} is not significant (Taylor & Wall, 1984; Keppler & Wyllie, 1991; Table 7.4). However, the D_{Sn} in both Cl- and F-bearing systems are significantly lower than 1 which means that tin cannot be easily extracted from a granitic melt by a chloride (or fluoride)-containing fluid, unless the concentration of the solution is greater than 2M for either halogen. It is considered that Sn is transported as Sn(II) chloride complexes for geologically reasonable oxygen fugacities and the tin-carrying capacity of high temperature chloride-rich fluids is in the order of 10^2 to 10^4 ppm (Taylor & Wall, 1984). Similar results have been obtained by Wilson and Eugster (1985) for submagmatic temperatures.

Table 7.4 Experimentally determined values for concentrations of W, Sn, Mo, Pb and Zn in granitic melts and co-existing aqueous fluids, and flui/melt partitioning coefficients (D)

(A) W - 800°C, 1 kb pressure

Complexing species		W (ppm) Vapour	W (ppm) Melt	D
H_2O		500	4400*	0.11
Na	0.5 M	4200	5000	0.84
	1.0 M	2700	5100	0.53
NaCl	0.5 M	5700	3910	1.5
	1.0 M	5100	2700	1.9
	2.0 M	6300	2500	2.6
	3.0 M	8700	2100	4.1
	3.4 M	6500	970	6.7
$Na(PO_4)_{1/3}$	0.5 M	5900	2900	2.0
	1.0 M	7100	2680	2.7
	2.0 M	6400	2700	2.4
$Na(CO_3)_{1/2}$	0.5 M	5400	2800	1.9
	1.0 M	3300	5600	0.59
	2.0 M	1900	5400	0.36
$NaB_4O_7)_{1/2}$	0.5 M	4300	4800	0.89

* glass contains WO_3 crystals

(B) Sn - 750°C, 2 kb pressure

Starting material	Fluid	Sn (ppm) Fluid	Sn (ppm) Glass	D
Haplogranitic gel + 1 wt.% Sn as SnO	H_2O	2.1	220	0.009
	1M HCl	280	3570	0.078
	1M HF	7.7	1900	0.004
Haplogranitic gel + 1 wt.% Sn as SnO + 0.5 wt.% Th as ThO_2	0.5M HCl	47	11300	0.004
	2M HCl	160	3010	0.052
	2M HF	5.5	3200	0.002
Haplogranitic gel + 1 wt.% Sn as SnO + 0.1 wt.% Th as ThO_2	1M HCl	450	7740	0.058
	1M HF	120	6200	0.020
	3M HF	13	720	0.017

(C) Mo - 750°C, 1.4 kb pressure

Complexing species		Mo (ppm) Vapour	Mo (ppm) Melt	D
Cl^-	0.05 M	133	40	3.3
	0.86 M	97	40	2.4
	2.1 M	29	11	2.6
	3.5 M	183	57	3.2
	4.6 M	76	32	2.4
4.6M Cl^- + F^-	0.6 M	97	44	2.2
	0.7 M	188	59	3.2
	0.8 M	166	68	2.4
	1.2 M	263	54	4.9
	1.7 M	342	120	2.8

(E) Cu - 750°C, 2 kb pressure

Starting material	Fluid	Cu (ppm) Fluid	Cu (ppm) Glass	D
Haplogranitic gel + 1 wt.% Cu as Cu_2O + 0.5 wt.% U as U_3O_8	H_2O	4.6	2.0	2.3
	0.5M HCl	600	9.9	61
	1M HCl	550	14	40
	1.5M HCl	1100	13	83
	1M HF	2.6	2.6	1.0
	2M HF	3.8	2.1	1.8
	3M HF	7.6	2.5	3.0
	4M HF	3.6	3.1	1.2
Pure haplogranitic, Cu-plated capsule	0.5M HCl	8300	470	18
Pure haplogranitic gel, 1 wt.% Cu as $Cu(NO_3)_3$ + 0.5 wt.% U as $(UO_2)(NO_3)_2$ in solution	0.5M HCl	310	23	13
Haplogranitic glass with 1 wt.% Cu as Cu_2O + 0.5 wt.% U as U_3O_8 dissolved in glass	0.5M HCl	470	7.8	60

(E) Pb - 800°C, 3.7 kb pressure

Solution	S/G ratio*	Pb (ppm) Fluid	Pb (ppm) Glass	D
1.0M HCl	0.46	172	27.7	6.21
	1.20	231	64.6	3.58
0.5 NaCl	0.49	13.0	72.0	0.181
	1.07	55.5	173	0.321
1.0 NaCl	0.99	190	61.0	3.11
2.0 NaCl	0.43	299	27.8	10.76
	1.05	271	34.7	7.81

* S/G ratio = initial solution/glass ratio.

Zn - 800°C, 3.7 kb pressure

Solution	S/G ratio*	Zn (ppm) Fluid	Zn (ppm) Glass	D
1.0M HCl	0.46	292	13.0	22.5
	1.20	253	36.0	7.03
0.5M NaCl	0.49	135	55.5	2.43
	1.07	156	86.3	1.81
1.0M NaCl	0.99	257	13.0	19.8
2.0M NaCl	0.43	343	11.5	29.83
	1.05	281	12.0	23.4

* S/G ratio = initial solution/glass ratio

Data for W are from Manning and Henderson (1984). Data for Sn and Cu are from Keppler and Wyllie (1991). Data for Mo are from Candela and Holland (1984). Data for Pb and Zn are from Urab (1985).

Tungsten (W)

The behaviour of tungsten in calcium-free granitic melt-vapour systems have been determined in the presence of a number of volatile species (F, Cl, P_2O_5, bornate and carbonate) as well as H_2O alone (Candela & Holloway, 1984; Manning & Henderson, 1984; Keppler & Wyllie, 1991; Table 7.4). At a given temperature and pressure (800°C and 1 kb), the behaviour of tungsten varies as a function of volatile character and concentration. With H_2O alone and F-rich melts and fluids, W partitions in favour of the melt, whereas with chloride and phosphate solutions W partitions strongly in favour of the aqueous phase. With carbonate and borate solutions, W partitioning is roughly equal between melt and vapour. With increasing fluoride and carbonate content of the fluid, W partitions increasingly in favour of the melt, whereas with increasing chloride content, W partitions increasingly in favour of the aqueous phase. There is little variation in W partitioning with increasing P content. The W solubilities in Cl or phosphate-bearing solutions are in excess of 10^3 to 10^4 ppm (Manning & Henderson, 1984)

Molybdenum (Mo)

The geochemistry of molybdenum resembles that of tungsten in many ways. Experimental studies have investigated the partitioning of molybdenum in the granitic melt-vapour systems in the presence of F, Cl and S (Candela & Holloway, 1984; Tingle & Fenn, 1984). Mo partitions in favour of the vapour (D_{Cl}=2.5 ± 1.6; Candela & Holloway, 1984) in Cl-bearing fluid systems irrespective of F and Cl concentrations, and it also partitions strongly into the vapour for S-bearing systems (Tingle & Fenn, 1984). The solubilities of Mo in high temperature (750°C) aqueous fluids exceed 10^2 ppm (Candela & Holloway, 1984).

Copper, lead and zinc (Cu, Pb, Zn)

Candela and Holland (1984) demonstrated that fluorine has no effect on the partitioning of copper, but D_{Cu} very strongly increases with increasing HCl concentration in the system. This was confirmed by the results of Keppler and Wyllie (1991). A similar partitioning behaviour was also noted for lead and zinc by Urabe (1985), who concluded that Pb and Zn partition strongly in favour the aqueous fluid phase when it is in equilibrium with an aluminous granitic magma.

Uranium and thorium (U, Th)

The partition coefficients of uranium and thorium are very low when H_2O is the only volatile present ($D_U < 0.002$ and $D_{Th} \approx 0.004$; Keppler & Wyllie, 1991). D_U increases strongly in the presence of HCl, HF or CO_2, while D_{Th} increases strongly only when fluorine (as HF) concentration increases, it does not increase in a system containing CO_2 or HCl (*op. cit.*).

Summary

The presence of volatiles such as Li and F in the quantities observed in the Jianfengling granites and pegmatites has considerable implications for their petrogenesis. Individually, each element has a significant effect on phase equilibria in the granite system, reducing liquidus and solidus temperatures, affecting minimum composition (Manning, 1981; Martin, 1983), and hence dictating the final compositions of the granites. The effect in combination is considered to be additive (Manning *et al.*, 1984). In addition to effects on the properties of the melts, volatiles also enhance the partitioning of elements between the melts and the associated aqueous fluids and lead to an associated enrichment of incompatible elements such as Rb, Sn, Nb, and Ta in the evolved granites.

Although the Jianfengling granites are not particularly enriched in Cl (~100ppm) and since Cl partitions strongly in favour of the aqueous fluid phase in equilibrium with a granitic melt (Kilinc & Burnham, 1972; Manning & Pichavant, 1988; Webster & Holloway, 1990), the Cl contents of the aqueous fluids derived from the Jianfengling granites could have been high enough to have had a significant effect on metal extraction and transport. Fluid inclusion studies show that boiling, which is thought to be essential for Cl to be enriched in magmatic-related fluids, occurred during the formation of the pegmatites. The fluid inclusion data also confirm that Cl^- is the major anion in the fluids in equilibrium with the pegmatites. According to Kilinc and Burnham (1972), an aqueous fluid in equilibrium with an NaCl-bearing melt contains 13-83 times more Cl than the melt, indicating that the melt needs contain only small concentrations of NaCl. Experimental studies (Eugster, 1985) reveal that fluids separated from such NaCl-bearing melts have high HCl fugacities as indicated by quench pH values of 1-2. A hydrolysis reaction such as the one shown below is probably involved (*op. cit.*):

$$2NaCl\,(melt) + H_2O\,(fluid) \rightarrow 2HCl\,(fluid) + Na_2O\,(melt) \qquad (7.1)$$

7.5 FLUID EVOLUTION

7.5.1 Extraction and transport of ore-forming metals

Extraction of ore-forming metals

Although the association of primary polymetallic deposits with acid magmatism is well established (Taylor, 1979; Ivanova & Naumov, 1985; Stone & Exley, 1985; Strong, 1986, 1988; Wills-Richards & Jackson, 1989; Jackson *et al.*, 1989). The mechanism of segregation and transport of ore-forming metals is still poorly understood. Nevertheless, recent experimental studies (Holland, 1972; Higgins, 1980; Rafal'skiy *et al.*, 1984; Jackson & Helgeson, 1985a,b; Urabe, 1985; Bourcier & Barnes, 1987; Wood & Vlassopoulos, 1989; Heinrich, 1990; Gibert *et al.*, 1992) have thrown some light on the understanding of this mechanism. Hypotheses proposed for element segregation from granitic melt in which ore-forming metals are transported in hydrothermal fluids are briefly outlined in the following section and their possible implications to mineralisation in the Xianghuapu area are also discussed.

A variety of processes are thought to be responsible for the pronounced enrichment of a large suite of elements of varied geochemical provenance, which include the alkali metals Na, Li, Rb, Cs, anions F, Cl, B, As, and ore-forming elements Nb, Ta, W, Sn, Mo, Cu, Pb and Zn, in the roof zones of polymetallic mineralisation-related granites. These include crystal-liquid equilibria, convection-driven thermogravimetric diffusion, fractionation between melt and aqueous fluid and exchange reactions between solids and aqueous fluids. Experimental studies have been confined largely to the crystal-liquid equilibria (Kilinc & Burnham, 1972; Manning, 1981; Pichavant, 1981, 1983) and to the determination of distribution constants of elements between granitic melts and coexisting aqueous fluids (Holland, 1972; Khitarov *et al.*, 1982; Candela & Holland, 1984; Manning & Henderson, 1984; Urabe, 1985; Webster *et al.*; 1989; Keppler & Wyllie, 1991). Convection-driven thermogravitational diffusion has been proposed to be an important mechanism for element enrichment in the roof of a magma chamber by Hildreth (1979) from analyses of sequential eruptions of the Bishop tuff, and similar conclusion have been reached by Mahood and Hildreth (1983). No experimental documentation of such a process has been offered, but support came from studies of silicate liquid structures and the concept of polymerisation control on trace element distribution (Waston, 1976; Ryerson & Hess, 1978). In particular, dissolved H_2O depolymerises siliceous melts by producing non-bridging oxygens and creating regions where those elements, which do not readily fit into the strongly

cross-linked framework of the melt because of size, charge or electronic structure, become enriched. These includes the anions F, Cl, B, the alkalis Li, Rb, Cs and the ore-forming elements such as Sn, W, Nb, Ta, Mo, As. Except for F, these are also elements which fractionate preferentially from the melt to an aqueous fluid, making it unlikely that the enrichment can be assigned to a single dominant mechanism.

Vesiculation, the exsolution of droplets of aqueous fluid from the melt is the most dramatic stage for element segregation and is an essential event for greisen and ore-bearing vein formation (Eugster & Wilson, 1985). Separation of a gas phase leads to hydrofracturing of the roof and flanks of the stock. These fracture systems may be the result of stresses produced during or soon after the emplacement of the intrusive and they would control the movement of hydrothermal fluids and subsequently host economically important vein deposits of W, Sn and many other metals (Jackson *et al.*, 1982).

Once a discrete fluid phase exsolves it is expelled by pressure build-up and the final fractionation mechanism, the leaching of ore-forming elements by exchange reactions with previously crystallised silicates and oxides, become operative (Eugster, 1985). The expelled fluids react not only with the previously crystallised granite but also the country rocks and it becomes difficult to distinguish ore-forming elements leached from the granite from those derived from the country rocks. Because of the consistent association of W, Sn, Nb, Ta ores with granites, the bulk of the W, Sn Nb, Ta, As, Li, and B is probably derived from the granitic melts, but a substantial portion of the Cu, Zn, Pb, Fe and S may well have been leached from the country rocks. In the Xianghuapu area, the contribution of Cu, Pb and Zn from the country rocks is thought to be minor for two reasons. Firstly, because the concentrations of these elements in the Jianfengling granites are high enough to provide resources for the mineralisation while those in the country rocks are very low (Zhang & Xu, 1989), and secondly because of an absence of extensive alteration in the country rocks which would be an inevitable result if a substantial amount of ore-forming elements had been leached by fluids from the granites. Further more, the observed depositional sequence cassiterite + arsenopyrite proceeding pyrrhotite + base metal sulphides in the Pb-Zn deposits in the Xianghuapu area is also consistent with the proposal of country rock playing minor role in providing metal resources. This depositional sequence is favoured by very low oxygen fugacity and may be attained during the chemical evolution and cooling of fluids of similar starting composition but with restricted opportunity for reacting with host rock redox buffers. This situation is likely to occur where fluids are channelled into narrow veins and pipes in rocks of very low permeability, where they deposited localised concentrations of hydrothermal minerals involving only limited wall-rock alteration (Heinrich and Eadington, 1986).

In summary, it is generally believed that Li, F, Cl and B are typically enriched in late stage liquids through fractional crystallisation, that these elements along with Rb, Cs, Sn, W, Nb, Ta, Mo, As, and others can also become enriched in the water-rich melt by thermogravitational diffusion, but that the most effective fractionation step, involving the halogens, Sn, W, Nb, Ta, as well as Cu, Pb, Zn and other ore-forming elements, is related to the separation of a supercritical aqueous fluid from the melt.

Transport of ore-forming metals

Tin (Sn)

A number of experimental studies and theoretical calculations concerning the existing forms of some ore-forming metals in hydrothermal fluids are available, the majority of which focus on tin and tungsten (Holland, 1972; Kosals, 1976; Foster, 1977; Taylor, 1979; Rafal'skisy *et al.*, 1984; Taylor and Wall, 1984; Eugster & Wilson, 1985; Jackson & Helgeson, 1985a,b; Bourcier & Barnes, 1987; Wood & Vlassopoulos, 1989; Bernard *et al.*, 1990; Heinrich, 1990; Gibert *et al.*, 1992). Thermodynamic data of Sn complexes at low to moderate temperatures (≤350°C) are well known, but there are few data available for higher temperatures (>350°C). Calculations of Jackson and Helgeson (1985a) show that in the absence of appreciable Cl and F concentrations, $[Sn(OH)_2]^{2+}$ and $[Sn(OH)_4]^0$ are the main Sn species in H_2O at 250°C and 2<pH<6.7. The relative stability of $[Sn(OH)_2]^{2+}$ increases dramatically at the expense of $[Sn(OH)_4]^0$ with increasing temperature from 250° to 350°C. In Cl- and F-bearing hydrothermal fluids, the concentrations of divalent Sn chloride complexes are several orders of magnitude greater than those of their fluoride and hydroxide counterparts. Meanwhile, the solubility of $[Sn(OH)_4]^0$ increases steadily with increasing F molality in the fluids at 300°C and pH=3-12 (Kosals, 1976). In high temperature (400°-600°C) chloride solutions, Sn^{2+} chloride complexes are also important, and the tin-carrying capacity of the solution is considered to be of the order of 10^2 to 10^4 ppm (Taylor & Wall, 1984). Consistent results have also been obtained by Eugster and Wilson (1985), who have demonstrated that divalent Sn chloride complexes predominate, and that up to 10^3 ppm Sn may be transported at 500°C, as a function of oxygen fugacity. Heinrich (1990) suggested that conditions of incomplete chemical buffering of the fluids by feldspathic host rocks are required to transport economic amounts of tin to an ore depositional environment at less than 400°C. Incomplete wallrock buffering will occur if the flow of hydrothermal fluid through a confined channel (such as a vein) is rapid relative to the kinetics controlling the interaction with fresh rocks (for example, the diffusion of aqueous components through an exhaustively altered vein selvage; Heinrich & Eadington,

1986; Holyland, 1987). The common association of fluoride minerals with cassiterite (the main mineral of tin mineralisation) and the development of topaz greisens in many tin deposits have led many workers to advocate high F fugacity and hence transport of Sn as Sn-fluoride complexes. Although the complexes $[SnF_2]^0$, $[SnF_3]^-$, $[SnF]^+$ are known to be stable, Kosals (1976) stated that the only possible form of tin being transported in high temperature hydrothermal fluids as a fluoride complex is $[SnF_X(OH)_{6-X}]^{2-}$, and Jackson and Helgeson (1985a) also concluded that fluoride complexing in hydrothermal solutions is negligible compared to chloride complexing, even in fluorite- or topaz-saturated magmatic fluids.

Tungsten (W)

The aqueous chemistry of tungsten is simplified by the fact that only W^{6+} is stable in most hydrothermal fluids; W^{5+} can only become important at very low oxygen fugacity which is not likely to be encountered, even in the presence of graphite (Wood & Vlassopoulos, 1989). Experimental results have revealed that $[H_2WO_4]^0$, $[HWO_4]^-$, and $[WO_4]^{2-}$ are the dominant tungsten aqueous species in H_2O-NaCl solutions at 500°C (Gibert *et al.*, 1992), and that W-chloride and W-fluoride complexes are not important in natural solutions (Kosals, 1976; Wood & Vlassopoulos, 1989). It is generally agreed that under hydrothermal conditions the monomeric species are dominant: $[WO_4]^{2-}$ in alkaline solutions, $[H_2WO_4]^0$ and $[HWO_4]^-$ in neutral and acidic solutions (Gibert *et al.*, 1992). Several authors have suggested the formation of Na-W complexes in concentrated NaCl solutions. In particular, Wood and Vlassopoulos (1989) have pointed out that $[NaHWO_4]^0$ or $[KHWO_4]^0$ are probably the most important species in concentrated solutions of NaOH, NaCl, or KCl. Although Bryzgalin (1986, quoted in Gibert *et al.*, 1992) has suggested the formation of $[WO_3Cl]^-$ in supercritical NaCl and KCl solutions, it is unlikely that W-Cl complexes would be dominant since, even at very low pH, positively charged tungsten species do not form (Gibert *et al.*, 1992). This has been confirmed by the measurement of crystalline WO_3 solubility in concentrated solutions of HCl (up to 5M) at 500°C and 1 kb (Wood & Vlassopoulos, 1989). The solubility of W in chloride-bearing fluids can be in excess of 10^3 to 10^4 ppm depending on temperature, pH and concentrations of chlorides in the solutions (Manning & Henderson, 1984; Rafal'skiy *et al.*, 1984). Foster (1977) investigated scheelite solubility in dilute KCl solutions (0.5M, 1M) where the molarity of the solution was buffered with the solid-phase assemblage quartz-feldspar-muscovite. The solubility of scheelite at 1 kb (100 MPa) increased almost exponentially from approximately 59 ppm at 300°C to more than 1000 ppm at 560°C indicating the possibility of mobilising tungsten in chloride-bearing hydrothermal solutions in economic concentrations. Foster *et al.* (1978) postulated that four main parameters control the transport and

deposition of tungsten, namely temperature, pH, fo_2/fs_2 and $\alpha Ca^{2+}/(\alpha Fe^{2+} + \alpha Mn^{2+})$. The solubility of scheelite is almost independent of temperature in the range of 100-300°C, while it is also independent of pH in the near-neutral range. The pH range in which this applies becomes narrower as the temperature arises, but it expands as the chloride concentration increases (Rafal'skiy *et al.*, 1984). The solubility increases as the pH falls in the acid range and as the pH increases in the alkaline range, but this can be hardly responsible for tungsten transport and deposition below 300°C (*op. cit.*). The solubility in alkaline media increases substantially only at pH>8 at 300°C and even greater values are required at lower temperatures. Therefore the migration capacity of tungsten is very low at temperatures below 300°C in solutions of low chloride concentration. A temperature of ~300°C is in most cases the lower limit for the deposition of scheelite from hydrothermal solutions (Rafal'skiy *et al.*, 1984).

Niobium and tantalum (Nb, Ta)

Literature concerning the transport of Nb and Ta is scarce and the main work was carried out in the former Soviet Union and summarised by Kosals (1976). Following are the main points outlined in his summary:

Among all Nb- and Ta-halogenide complexes, the fluoride complexes are the most stable species. The formation and solubilities of these complexes are related to the concentration of HF in solution. In high-HF fluids, $[H_2NbF_7]^0$ and $[H_2TaF_7]^0$ are dominant, otherwise $[(Nb, Ta)OF_5]^{2-}$, $[(Nb, Ta)OF_4]^-$, $[(Nb, Ta)O_2F_4]^{3-}$ and $[(Nb, Ta)O_2F_5]^{4-}$ become important. The solubilities of Nb and Ta are also closely related to temperature and the activities of Na and Li in the fluids. Decreasing temperature and increasing f_{Na} would cause Nb and Ta precipitation and at temperatures of 400°-300°C most of the Nb and Ta in the fluids would precipitate. The effect of Li on the solubilities of Nb is similar to that of Na, i.e. Nb precipitates when f_{Li} increases. However, in the presence of Li, the solubility of Ta increases with increasing temperatures (300°-500°C). This is considered to be the main reason causing the separation of Nb and Ta during the late-magmatic and post-magmatic processes.

Copper, lead and zinc (Cu, Pb, Zn)

Metal-sulphide and metal-chloride complexes are thought to be the major forms in which base metals (Cu, Pb and Zn) are transported in hydrothermal fluids associated with granitic melts (Barnes, 1979; Khitarov *et al.*, 1982; Bourcier & Barnes, 1987; Wood *et al.*, 1987). The dominant complexing ligands

among sulphur species are more likely to be HS^- or H_2S in hot, reducing hydrothermal solutions where equilibrium is favoured by time and high temperatures. Stronger complexing is caused by the bisulphide ionic field than by the dipole field of molecular H_2S. For this reason, it is in, or close to, the solubility field of HS^- that sulphide complexing is more likely to result in higher solubilities of the base metal sulphides (Barnes, 1979). On the other hand, as discussed by Barnes (1979), very alkaline solutions are required above approximately 300°C for HS^- to become a dominant species. Therefore, bisulphide complexes may be important to ore transport only at temperatures below roughly 350°C.

Among the bisulphide complexes of copper (Barnes, 1979; his Table 8-4), the dominant species change with increasing temperature from $[Cu(HS)_3]^{2-}$ to $[Cu(HS)_2]^-$, and then to $[Cu(HS)_2(H_2S)]^-$. The simple cuprous chloride complex, $[CuCl]^0$, is the dominant stoichiometry of copper-chloride complexes at all temperatures (Barnes, 1979). The relative stabilities of the chloride and bisulphide complexes of copper have been compared by Crerar and Barnes (1976). The general conclusion is that, for weakly alkaline solutions, CuCl predominates at 250°-350°C up to $\Sigma S = 0.1$ to 1, but that bisulphide complexes become relatively more important at temperatures below 250°C. Because of the increased stability of the chloride complex at temperatures above 250°C, the concentration of copper, as CuCl, in the solutions may easily reach several thousand ppm (Barnes, 1979).

At temperatures less than 300°C, the dominant zinc chloride species in the range 0.5-5.0M total chloride (Cl_{tot}) of most solutions are $[ZnCl_3]^-$ and $[ZnCl_4]^{2-}$, whereas the neutral complex $[ZnCl_2]^0$ is dominant at temperatures above 300°C (Bourcier & Barnes, 1987). This trend is consistent with both the known dominance of neutral metal complex species in high temperature-low density solutions (Frank, 1969, as quoted in Bourcier and Barnes, 1987) and the shift from $[ZnCl_4]^{2-}$ toward $[ZnCl_2]^0$ with increasing temperature (Schultz, 1974, as quoted by Barnes, 1979). The only zinc hydroxide complex that is present in significant amount is $[Zn(OH)]^+$, and it is only important at a very low chloride molality (Bourcier & Barnes, 1987). For near-neutral ore solutions having HS^- concentrations of 0.01 to 0.1m, the dominant zinc bisulphide complex at low temperature (less than 300°C) is $[Zn(HS)_3]^-$, which changes to $[Zn(HS)_2]^0$ with increasing temperature. $[Zn(HS)(OH)]^0$ may be the dominant aqueous zinc species in near-neutral pH solutions of low total sulphur (less than 0.001M HS^-), but it will never contribute more than about 0.1 ppm Zn in solutions in equilibrium with sphalerite and is therefore not important as an ore transporting agent. (Barnes, 1979). For any case in which significant zinc is present in an ore solution as bisulphide complexes, it will be present as $[Zn(HS)_3]^-$ and $[Zn(HS)_2]^0$. In NaCl-H_2S solutions, zinc bisulphide complexes are dominant over the chloride complexes at temperatures up to about 200°C, whereas at temperatures above 200°C the chloride

complexes become predominant (Bourcier & Barnes, 1987). Calculations of Holland (1972) have suggested that rather ordinary concentrations (a few tens ppm) of zinc are sufficient to yield economically significant zinc concentrations in hydrothermal solutions derived from granitic melts.

Few data are available for lead complexing with sulphide and chloride at temperatures above 300°C. At 300°C, $[Pb(HS)_2H_2S]^0$ is the dominant sulphide species in neutral to acidic solutions at $\Sigma S<1.0$ (Barnes, 1979). Experiments carried out by Barnes (1979) have shown that PbS solubility increases with increasing ΣS, P_{H2S}, and especially temperature, reaching a maximum concentration of just 47 ppm at 300°C, $P_{H2S}=75$ atm and 0.5M NaHS. Therefore, lead sulphide complexes are not sufficiently stable to form low temperature, hydrothermal deposits, as also concluded by Hamnan and Anderson (1978). Lead chloride complexes stable at 200°-300°C are $[PbCl]^+$, $[PbCl_2]^0$, $[PbCl_3]^-$, and $[PbCl_4]^{2-}$, only $[PbCl_2]^0$ and $[PbCl4]^{2-}$ are significant with increasing temperatures (Barnes, 1979).

7.5.2 Segregation and concentration of mineralising fluids

The close association of the polymetallic mineralisation with the Jianfengling granites in the Xianghuapu area has been shown to be related to mineralising fluids that originated from the evolving granite melts. Judging from the large number of deposits occurring in the area and the small size of the Jianfengling stock, it would be likely that the aqueous fluids separated from the crystallising granites and pegmatites at a very late stage. Such a late stage vapour separation during the crystallisation of the granites and pegmatites could, according to Whitney (1975), occur over a very narrow temperature interval, just above the solidus of the melt. The generation of an aqueous phase during such a late stage in the crystallisation history from a highly fractionated interstitial liquid would generate a very high-Cl fluid, which in turn would lead to the very effective removal of several metallic species from the silicate melt (Holland, 1972).

The Jianfengling granites, as discussed in Chapter 3, were emplaced at a shallow level and into an environment pre-heated by the emplacement and crystallisation of two granite plutons, the Jiuyishan complex and the Jitianling complex. Thus, the cooling of the stock was probably very slow. On the other hand, high contents of F and Li would have reduced the solidus and liquidus temperatures of the melts and prolonged the crystallisation history. Consequently there would be more time for the aqueous fluids to extract metallic cations from the melts and the incompatible element-enriched aqueous phases would have sufficient time to percolate upward through the interstices of the minerals,

because of their lower densities and the possible aid of a process of filter pressing of the interstitial granitic liquid, to higher levels in the stock. By this way the apical portions of the intrusions became gradually enriched in late aqueous phases. Upward movements of these phases are thought to have occurred along channel ways, the positions of which were probably determined by a combination of: incipient fracturing in the virtually consolidated roof zones of the intrusions and differential streaming of fluids, generally in an upward direction. These metallic cation-enriched aqueous fluids would cause extensive alteration such as albitisation and greisenisation in the apical zones of the intrusions and might also eventually migrate into the country rocks along fractures developed before or during the intrusion of the stock and to form economic deposits.

7.6 MINERALISATION

7.6.1 Origin of fluids

***Pegmatite fluids*:** Fluids associated with the evolution of the Jianfengling granites and the formation of the pegmatites are represented by the primary fluid inclusions in topaz and quartz from the pegmatites. The inferred stable isotope compositions ($\delta^{18}O$ and D) of these fluids imply a predominantly magmatic fluid source. The fluids are of relatively high temperature (Tt=350°-530°C) and low to moderate salinities (S from <5 to 35 wt.% NaCl eq.) with NaCl being the dominant solute. The fluid of moderate salinity was mainly the result of boiling during the formation of the pegmatites, although it could also be possible for a primary magmatic fluid of an appropriate salinity (up to 15 molal total chloride) to have originated by direct separation of an aqueous phase from the magma during continued crystallisation of the Jianfengling granites (the second boiling of Burnham, 1979). However, as the Cl contents in Jianfengling granites are relatively low (less than 0.1 wt.%), a minimum D_{Cl} of 260 to 350 would be required to produce a coexisting aqueous fluid with 26 to 35 wt.% NaCl (10-15 molal Cl). Recent experimental data (Webster & Holloway, 1988, 1990; Malinin *et al.*, 1989; Shinohara *et al.*, 1989), however, show the D_{Cl} for granitic melts is unlikely to exceed 85 at a geological reasonable pressure and temperature, and thus boiling during pegmatite growth is the preferred explanation for the moderate salinities.

Fluids of W-F mineralisation: Fluids responsible for the fluorite-scheelite mineralisation were of low to moderate temperature (Tt=180°-400°C) and salinity (S=1-19 wt.% NaCl eq., mostly less than 7 wt.%) with NaCl and $CaCl_2$ being the main solutes. The stable isotope compositions ($\delta^{18}O$, δD, $\delta^{34}S$ and $\delta^{13}C$) of these fluids also suggest a mixed fluid source (Chapter 6). These characteristics suggest that they may represent a portion of originally NaCl-dominant magmatic fluids which became $CaCl_2$ enriched as a result of mixing with a meteoric water of low salinity and reacting with the wallrocks during its migration through fractures. Thus, based upon the information available from fluid inclusion and stable isotopes, the fluids responsible for the W-F mineralisation in the Xianghuapu area are interpreted to represent a somewhat diluted, chemically- exchanged successor to the predominantly magmatic fluid derived from the evolution of the Jianfengling granites, inferred to be from intrusion D.

7.6.2 Deposition of ore metals and formation of various types of deposits in the Xianghuapu area

The deposition of ore metals from a hydrothermal fluid can be achieved when the fluid becomes saturated with these metals. The main parameters affecting this are:

1) cooling,
2) depressurisation,
3) decrease in the activities of the complex-forming ligands,
4) increase in the activities of the ore mineral-forming anions or cations such as S^{2-}, O^{2-}, and Ca^{2+}.
5) mixing with a second solution.

Reactions with these effects may be homogenous or heterogenous and involve either loss of gases or, more commonly, reaction with host rocks. In every case, however, metal-bearing complexes are converted into oxide and sulphide minerals, liberating HCl or H^+ in the processes.

Formation of the greisen-type Nb-Ta mineralisation: Nb-Ta mineralisation, as discussed in Chapter 5, occurs in the greisen and greisenised granite which covers the top of intrusion B. Microlite, niobite and tantalite are the main Nb-Ta-bearing minerals and occur disseminated throughout the greisen zone. The total content of Nb and Ta increases steadily from deep to shallow levels and has a positive correlation with the intensity of the greisenisation (No. 238 Geol. Team, 1974). This could be the result of two different processes: fractionation and metasomatism, the effects of which could be additive. Fractionation may play an important role in concentrating ore metals in the residual melt which eventually crystallises, together with the ore minerals, and forms the top part of the intrusion.

During the early stage of crystallisation of a F- and Li-rich melt, the ore metals rarely crystallise as separate minerals, the majority of them form complexes with alkali metals and volatiles (*e.g.* $[Na_2(Nb,Ta)F_7]$ and $[K_2(Nb,Ta)F_7]$) and stay in the volatile-rich residual melt. Only a small proportion of these metals enter, in the form of isomorphism, into rock-forming minerals such as biotite (zinnwaldite) and feldspars. As discussed in previous sections, the volatiles, especially F and Li, not only lower the liquidus and solidus temperatures, hence prolonging the crystallisation history, but also enhance the distribution of ore metals between the melt and the associated fluids. During the process of fractionation, F tends to remain in the residual melt, and therefore the F content in the melt is increased compared to the initial melt. Nb and Ta have a strong tendency to form stable fluoride complexes and then remain in the melt until the final moment of crystallisation. Thus, the residual

melt becomes increasingly enriched in volatiles and ore metals due to the change in the relative amounts of rock-forming minerals crystallising from the residual melt (less micas and more quartz and feldspars). The capacity of the ore metals entering these minerals as isomorphism is also reduced. All these would result in the crystallisation of ore minerals from the residual melt together with the rock-forming minerals (quartz and feldspars) and increase the Nb and Ta contents in the top part of the intrusion.

During the evolution of a volatile-rich magma like the Jianfengling granite melt, an aqueous fluid phase would certainly develop at a late stage of crystallisation and accumulate in the top of the magma chamber. This fluid is capable of not only extracting ore metals from the magma and crystallised rocks and carrying them to the site of deposition, but also causing extensive alteration (albitisation, K-feldspathisation and greisenisation). Upon cooling, the ore-metals carried by the fluid would precipitate to form ore minerals such as microlite, niobite and tantalite. These minerals often precipitate from F-Li-rich fluids at temperatures of 300°-400°C (Kosals, 1976) which are consistent with the temperatures of greisenisation reported by many workers (Shepherd *et al.*, 1977; Jackson *et al.*, 1978; Witt, 1988).

Formation of the W-Sn deposits: W-Sn (Be, Pb, Zn) mineralisation is spatially associated with both intrusions C and E (probably intrusion B as well). Mineralisation related to intrusion C occurs along the NW-trending fractures hosted within the granite (intrusions B & C) and has an ore mineral assemblage of cassiterite, wolframite, galena, sphalerite, and beryl, which are disseminated in quartz veins and greisens developed along both sides of the veins. Mineralisation linked with intrusion E is localised in the country rocks of the intrusion and occurs in fissures within the F_{101} fault zone. It has a mineral assemblage of cassiterite, galena, sphalerite, arsenopyrite and pyrrhotite with associated diopside, actinolite, fluorite and sericite. The fluids responsible for the formation of these deposits were most likely to be originated from the evolution of the Jianfengling granites, analogous to many other tin deposits in the world (*e.g.* Taylor, 1979; Jackson *et al.*, 1989), although some involvement of meteoric water could not be ruled out entirely. Ore-forming elements such as Sn, W, Pb, Zn, and Be carried by these fluids could precipitate as the result of cooling, decreasing in pressure and/or reaction with the country rocks.

The chemical evolution of a single-phase magmatic fluid on its cooling and depressurisation path from the source to the ore deposit can be considered in terms of two limiting cases (Heinrich, 1990): cooling of the fluid in equilibrium contact with excess granitic source rock (i.e., rock-buffered evolution), and

cooling in isolation from reactive host rocks, such that fluid speciation is controlled entirely by equilibration among aqueous species and possibly congruent precipitation of minerals (i.e., fluid-buffered evolution). These two extremes, in contrast to any intermediate cases of partial rock reaction, lead to an equilibrium state of the fluid at any P and T of a depositional site. Neither process may be realised in nature, but the condition of rock-buffered evolution is probably approached by cooling of an igneous fluid in contact with its source granite or immediate adjacent country rocks, and will typically involve a 10- to 100-fold excess of rock over fluid by weight (Burnham, 1979). The fluid-buffered evolution can be achieved by quenching of a fluid or any other physical process of fluid focusing, such that the amount of fluid relative to reactive wallrock is sufficiently high to dominate the equilibrium mineralogy of the rock, without significant modification of the fluid composition by rock interaction.

The deposition of cassiterite could be exemplified by the following reactions (Heinrich, 1990):

$$[SnCl_x]^{2-x} + 2H_2O \rightleftharpoons SnO_2 + 2H^+ + XCl^- + H_2 \quad (7.2)$$

$$SnCl_2 + 3(Na,K)AlSi_3O_8 + 2H_2O \rightleftharpoons SnO_2 + KAl_3Si_3O10(OH)_2 + SiO_2 + 2NaCl + 2H_2 \quad (7.3)$$

$$SnCl_2 + 3KFe_3AlSi_3O_{10}(OH)_2 + 2H_2O \rightleftharpoons SnO_2 + KAl_3Si_3O10(OH)_2 + SiO_2 + 3Fe_3O_4 + 2KCl + 4H_2 \quad (7.4)$$

$$SnCl_2 + CaCO_3 + H_2O \rightleftharpoons SnO_2 + CaCl_2 + CO_2 + H_2 \quad (7.5)$$

$$3SnCl_2 + H_3AsO_3 + 2FeCl_2 + 2H_2S \rightleftharpoons 3SnO_2 + 2FeAsS + 10HCl \quad (7.6)$$

Precipitation of cassiterite from a reduced acid solution is favoured by oxidation (H_2 consumption) or acid neutralisation (Pabalan, 1986, as quoted in Heinrich, 1990). This can be achieved by the fluids reacting with crystallised granite rocks. H_2 is used in the reduction of a ferric silicate component, e.g. oxybiotite to biotite:

$$KFe_2^{2+}Fe^{3+}AlSi_3O_{10}(OOH) + 0.5H_2 \rightleftharpoons KFe_3^{2+}AlSi_3O_{10}(OH)_2 \quad (7.7)$$

or by more complex Fe^{3+}-Fe^{2+} reactions involving Ti minerals (Wones, 1981). Acidity is consumed by hydrolysis of feldspars to hydrous silicates (muscovite) (Heinrich, 1990):

$$3KAlSi_3O_8 + 2HCl \rightleftharpoons KAl_3Si_3O_{10}(OH)_2 + 6SiO_2 + 2KCl \quad (7.8)$$

$$3NaAlSi_3O_8 + 2HCl + KCl \rightleftharpoons KAl_3Si_3O_{10}(OH)_2 + 6SiO_2 + 3NaCl \quad (7.9)$$

Reduction and acid neutralisation both promote reactions (7.2-7.6), and under rock-buffered conditions 99% of the initial Sn content of the fluid will be precipitated at temperatures above 400°C (Heinrich, 1990). After cooling, low concentrations of cassiterite will be dispersed through a large volume of altered granite. In the absence of rock-buffering, the high initial concentrations of $HCl + H^+$ and of H_2 in the fluids will be maintained throughout cooling and so cassiterite will not precipitate as the reactions (7.2-7.6) are counteracted by increasing hydrogen ion concentration and a constant high H_2 concentration. Based on experimental studies, Heinrich (1990) concluded that "*neither simple quenching of a tin-rich ore fluid, nor in situ cooling of a magmatic fluid in contact with an excess of quartz of feldspathic rock, is likely to form an economic tin deposit at the typical temperature range of 300° to 400°C recorded by fluid inclusion studies. .... High concentrations of tin can be transported by a saline fluid to any low-temperature site provided that the fluid is prevented from chemical interaction with feldspathic rocks during parts of its cooling history*".

Wolframite deposition, like that of cassiterite, liberates acid (H^+ or HCl) (Eugster, 1985):

$$H_2WO_4 + FeCl_2 \rightleftharpoons FeWO_4 + 2HCl \quad (7.10)$$

but this is outweighed by a steep increase in the calculated equilibrium constant of reaction (7.10) with falling temperature. Wolframite precipitation occur over a relatively narrow cooling interval of about 50°C, with or without rock interaction (Jaireth *et al.*, 1990, as quoted in Heinrich, 1990).

Observations on the contrasting distributions of cassiterite and wolframite in the Xianghuapu area may be easily explained by the different chemical behaviour of tin and tungsten outlined above. Cassiterite predominates over wolframite in greisens developed along the quartz veins and in skarns formed along fissures within the F_{101} fault zone (dispersed fluid flow with intensive rock contact). Under these environments the rock-buffering conditions were likely maintained. Wolframite occurs only in minor quantities within thick quartz veins (focused fluid flow with restricted wall rock contact) under which the fluid-buffering conditions were probably the case.

Formation of the W-F deposits: W-F mineralisation is associated predominantly with intrusion D and has a mineral assemblage of fluorite, scheelite, quartz and calcite. Individual orebodies occur along

the NNE-trending faults (F_4) and are confined to the fractured footwalls and the fault selvage. The formation of these W-F deposits depends on (1) high-temperature magmatic processes leading to generation of high W concentrations in the fluids (fluid/melt partitioning and/or subsolidus leaching; Campbell *et al.*, 1984), (2) physical processes of cooling a sufficient quantity of fluid within a restricted space, and (3) reaction of relatively Ca- and Fe-poor fluids with calcareous wallrocks. The most important factor in the formation of the W-F deposits in the Xianghuapu area is the presence of a rather unusual granite stock. Its initial tungsten (and other rare metals) content was determined by partial melting processes in an evolved stock, but the partitioning of metals (especially W) into residual melts was promoted by high volatile contents. High levels of F and Li in the magma increased water solubility in the residual melt. Large volumes of potential magmatic fluid were therefore available for the late-stage extraction of metals from the melt. It is worth repeating that a high total content of volatile components (F, Li, H_2O) could reduce the liquidus and solidus temperatures and prolong the crystallisation history. In addition, a high total content of radioactive elements might also generate sufficient heat to extend primary crystallisation to long after initial emplacement. Thus, all these would extend the window of opportunity within which magmatically derived metal-enriched fluids could be released. It is postulated that metals were extracted from the melt on exsolution of an aqueous phase and that these fluids migrated along fractures into the calcareous country rocks adjacent to the intrusion and mixed with meteoric water circulating within the fault zones. Owing to shearing nature of these steep-dipping fractures, a layer of poor permeability selvage was developed along the fault surfaces. The ore metal-carrying fluids were prevented from migrating further by the selvage and accumulated within the fault zones and highly fractured footwall rocks. Deposition of ore minerals probably occurred within the zone of fluid mixing, dilution, and rapid cooling. Because of the presence of carbonate country rocks , tungsten precipitated as scheelite rather than wolframite. This can be accounted for either by a precipitation or an exchange reaction (Eugster & Wilson, 1985):

$$H_2WO_4 + CaCO_3 \rightleftharpoons CaWO_4 + H_2CO_3 \qquad (7.11)$$

$$FeWO_4 + CaCl_2 \rightleftharpoons CaWO_4 + FeCl_2 \qquad (7.12)$$

The absence of wolframite in the fluorite-scheelite ores in the Xianghualing area indicates that $\alpha_{Fe^{2+}}$ in the fluid was very low and hence the effect of the exchange reaction was minimum. The deposition temperatures of 300-350°C for the scheelite in this area, obtained from fluid inclusion studies (Section 6.1.2.2), are consistent with the experimental results of Rafal'skiy *et al.* (1984). They concluded that *"scheelite may be formed under neutral circumstances by solutions cooling over the range of 400-300°C, by interactions of the solutions with country rocks rich in calcium at temperature below 400-350°C, and*

on account of pH change, in any case, the deposition of scheelite should in the main be completed by 300°C."

Formation of the Pb-Zn deposits: Pb-Zn mineralisation in the Xianghuapu area can be genetically categorised into two groups: granite-type and lode-type. The granite-type is hosted in pegmatite and greisen and is syn-magmatic and/or late-magmatic in origin, whereas the lode-type occurs in fault zones within the carbonate country rocks and is late- and post-magmatic in origin. The fluids responsible for the granite-type Pb-Zn mineralisation were derived from the evolution of the Jianfengling granites with little involvement of meteoric water, while the fluids for the lode-type Pb-Zn mineralisation were probably to be a mixture of magmatic and meteoric waters as evident by their stable isotope compositions (Section 6.2).

As discussed in previous sections, chloride and sulphide complexes are the major forms by which base metals (Pb, Zn, Cu, Fe) are transported in hydrothermal fluids. Deposition of the base metal sulphide minerals (sphalerite, galena, pyrite, chalcopyrite and pyrrhotite) from chloride- and sulphide-complexed metals, Me^{2+}, in weakly acidic solutions can be expressed by following reactions (Burnham, 1979):

$$MeCl_2 + H_2S \rightarrow MeS + 2H^+ + 2Cl^- \quad (7.13)$$

$$Me(HS)_3^- \rightarrow MeS + HS^- + H_2S \quad (7.14)$$

Reaction (7.13) is written not in terms of HS^- or S^{2-} but in terms of H_2S, because it is the predominant sulphide species at low temperature and at a pH below neutral as well as in mildly alkaline solutions at temperatures above approximately 300°C (Barnes, 1979). This reaction shows that either the degree of saturation or the extent of deposition of the sulphides will increase as a consequence of the following processes:

1) Increased H_2S concentration (in terms of α_{S^-}) due to, for example, sulphate reduction, reaction from organics, or mixing with sulphide solutions.

2) Increased pH caused by either reaction with carbonates or feldspars or boiling off acid gases.

3) Decreased chloride concentration (α_{Cl^-}), resulting from dilution by circulating meteoric waters or caused by reactions adding strong Cl^--ion-pairing cations like Ca^{2+}.

4) Decreased temperature.

Clearly, for reaction (7.14), any processes that reduce the product (α_{HS^-}, $\alpha_{H_2S\,(aq)}$) will either increase the degree of saturation in the sulphide complex or cause deposition. Also a decrease in temperature or pressure, especially where boiling takes place, may cause deposition.

Sulphide precipitation in granitic rocks, as in the pegmatite and greisen of the Jianfengling granites, can be represented by (Heinrich & Eadington, 1986)

$$ZnCl_2 + 3KAlSi_3O_8 + H_2S \rightleftharpoons ZnS + KAl_3Si_3O10(OH)_2 + 6SiO_2 + 2KCl \quad (7.15)$$

or by

$$ZnCl_2 + 3KFe_3AlSi_3O_{10}(OH)_2 + 10H_2S \rightleftharpoons ZnS + 9FeS + KAl_3Si_3O10(OH)_2 + SiO_2 + 2KCl + 12H_2O \quad (7.16)$$

and in carbonate rocks , as the lode-type Pb-Zn mineralisation in the Xianghuapu area, can be represented by (*op. cit.*)

$$ZnCl_2 + CaCO_3 + H_2S \rightleftharpoons ZnS + CaCl_2 + H_2CO_3 \quad (7.17)$$

Similar reactions can be formulated for galena, pyrite, pyrrhotite and chalcopyrite. In every case, a neutralisation reaction is involved, which consumes the HCl or H^+ produced by the sulphide precipitation, represented by reaction (7.13). These acidic solutions could easily dissolve the limestone country rocks and cause karstification.

7.6 PETROGENETIC-METALLOGENETIC MODEL

On the basis of petrological and geochemical observations and the foregone discussions, the following model for the petrogenesis and metallogenesis of the Jianfengling granites and the associated mineralisation can be proposed.

Lower crustal anatexis focused along a linear discontinuity in the region of Southeast China and led to the generation of a large amount of granitoid magma and the formation of numerous granitic plutons, in response to the subduction of the Pacific plate underneath the Eurasian plate. This resulted in the intrusion of two major plutons (the Jiuyishan Complex and the Jitianling Complex) and a number of small intrusions of Jurassic-early Cretaceous age. The emplacement of the Jianfengling granite stock was slightly latter than that of the two major plutons (No. 238 Geol. Team, 1974; Yuan *et al.*, 1986). Ascent of the Jianfengling granite melt to a shallow level was facilitated by the activation of the F_{101} fault zone and the emplacement was confined to intersection of several groups of faults. As the melt was emplaced into an environment pre-heated by the intrusion and crystallisation of the Jiuyishan and Jitianling Complexes, the cooling of the stock was probably very slow. Once the granitic melt ascended to a shallow level, the melt at the top part of the magma chamber started to solidify and form a carapace, while the melt underneath the carapace remained in a liquid state. A lower temperature magma subchamber formed and the melt inside became more and more sodic owing to the increasingly important role of fluorine during the fractional crystallisation. This residual melt then re-intruded the solidified carapace to be emplaced in the roof zone of the stock. The pulse cycle of the re-intrusion probably occured several times before the complete solidification of the stock. The lowering of solidus temperature because of the presence of volatiles (particularly fluorine) and lithium permitted an extended period of crystallisation and allowed the exsolved aqueous phases to collect in the apical portion of the intrusions. Owing to the increase in the relative contents of fluorine and other volatiles, the residual melt became more and more volatile-saturated and liquid segregation started to take place. As a result, patches of pegmatitic melt formed and migrated upwards toward the roof zone until their ascent was halted by the more completely solidified magma and eventually crystallised to form the pegmatitic pods.

As the pulse-intrusion progressed, aqueous fluids separated from the crystallising granites and pegmatites at a late stage and percolated upward through the intrusions to extract a large quantity of metals. Cooling of these intrusions was probably very slow, owing to the pre-heated environment and to the high contents of volatiles (*i.e.* F) and lithium which would depress the solidus and liquidus

temperatures of the melts and prolong the crystallisation history (albeit over a narrow temperature interval). Consequently the aqueous fluids had more time to extract metalls from the melts and to percolate through the interstices of the intrusives and reach the apical portion of the intrusions without causing too much alteration during their ascent. These fluids reacted with the crystallised materials and carbonate country rocks along the contacts and formed greisens at the roof zone of the intrusions and skarns along the contacts. Nb-Ta mineralisation and some of the W-F mineralisation were probably formed during this stage. Some evolved magmatic fluids migrated away from the Jianfengling granites along pre-existing fractures and deposited scheelite, fluorite, cassiterite and sulphide minerals at various locations by reacting with limestone and mixing with meteoric water.

CHAPTER EIGHT

CONCLUSIONS

CHAPTER EIGHT

CONCLUSIONS

The current study concerning the mineralogy and geochemistry of the late Jurassic-early Cretaceous Jianfengling granite stock and associated polymetallic mineralisation reveal the following important features:

Granitoids:

1) The stock is a multiple intrusive complex consisting of five intrusions (A, B, C, D and E) which show evident intrusive contacts.

2) The rocks are fluorine-rich, high-silica, peraluminous granites with extremely elevated contents of F, Li, Rb, Cs and ore-forming elements such as Nb, Ta, W, Sn. These granites have mineralogical and chemical compositions that identify them as "S-type" granites (*i.e.* they are derived from a meta-sedimentary protolith). They may also be grouped into the "low-P (phosphorus)" subtype of topaz granites based on the criteria used by Taylor (1992). They are also examples of subsolvus granite (Tuttle and Bowen, 1958; Taylor, 1992) in which two discrete feldspars exist, *i.e.* albitic plagioclase and K-feldspar. These granites represent products of pulse intrusion and crystallisation from a highly evolved, volatile (*i.e.* fluorine) and lithium-rich felsic melt.

3) The intrusions appear, in their upper portions, to be composed entirely of alkali feldspar granite with essential quartz, K-feldspar, albite (An_{0-6}), lithium mica (lithium biotite, zinnwaldite), and topaz.

4) The evident intrusive contacts between the granites and their country-rocks shows the Jianfengling stock to have a magmatic origin rather than being a result of granitisation or migmatisation proposed by some previous workers. The petrographic data for these granites are consistent with a magmatic origin for the bulk of the albite, topaz and lithium mica. Textural relations support the early crystallisation of these minerals, and the subsequent inclusion of these minerals in later quartz and K-

feldspar. Such a mineral paragenesis is comparable to the sequence of crystallisation recorded at pressures of 1 to 2 kbar in the experiments of Weidner and Martin (1987).

5) The major and trace element chemistry of the granites is also consistent with a magmatic origin (see Chapter 4 for details). The enrichment of SiO_2, F, Li, Rb, Cs, and ore-forming elements such as Nb, Ta, W and Sn is interpreted as the result of fractional crystallisation, although some contribution from metasomatism cannot be ruled out.

6) The petrological and geochemical differences among the rocks of the Jianfengling granites provide a basis for separating these granites into two groups. Group 1, the zinnwaldite-bearing albite granite suite, consists of intrusions B and C and Group 2; the biotite-bearing granite suite, comprises intrusions A, D and E. Mineralogically rocks of Group 1 are more albitic than those of Group 2. Zinnwaldite is the main ferromagnesian mineral in group 1, while in Group 2 biotite is dominant. Chemically, rocks of Group 1 have higher Al_2O_3, MnO, F, Li, Rb, Ta, and Sn, lower SiO_2, total Fe_2O_3, CaO, Zr, Hf, W, and REEs concentrations relative to those of Group 2.

7) The Jianfengling granites share some similarities with other fluorine-rich felsic suites, including topaz granites, which are characterised by elevated contents of F, Li, Rb, Cs, Nb and Ta, and depletion in Ca, Mg, Mn, Ti, Ba, Co, Ni, Sc and V. However, the Jianfengling granites are extremely enriched in F, Li, Rb, Cs, Nb, Ta, W, Sn and U, even by comparing to the most highly fractionated examples of I-, S- and A-type granites.

Pegmatoids:

8) Pegmatites and pegmatitic pods associated with the Jianfengling granites, especially intrusions D and E, are considered to be the result of "liquid segregation". During the late stages of the evolution of the granites, volatiles (particularly fluorine) and lithium became more and more concentrated in the residual melt. When this concentration reached a certain level, phase segregation started to take place in the residual melt. The separated pegmatitic melt rich in volatiles and ore-forming

elements migrated upwards toward the roof zone of the intrusion until it was halted by the solidified granite.

9) Both $\delta^{18}O$ and δD values of quartz from the pegmatitic rocks have narrow ranges, from 10.4 to 13.0‰ and from -70 to -88‰ respectively, features indicative of a predominantly magmatic fluid source.

10) Fluids associated with the pegmatitic rocks are of relatively high temperature (Th=350°-530°C) and low to moderate salinities (S from <5 to 27-35 wt.% NaCl eq.) with NaCl being the dominant solute. The fluid of moderate salinity was mainly the result of boiling during the formation of the pegmatites.

Mineralisation:

11) Multiple phases of mineralisation occur both within the intrusions and in the adjacent country rocks. These different types of mineralisation are mainly related to the various intrusions and the following associations are noted:

i) Nb-Ta mineralisation --- intrusion B

ii) Sn (W, Pb, Zn) mineralisation --- intrusions C and E

iii) W-F mineralisation --- intrusion D

iv) Pb-Zn mineralisation --- intrusion E

12) The distribution and shapes of the orebodies are controlled by faults and by the contact zones of the granites and their wall rocks. Mineralisation occurs mainly along these faults and the contact zones.

13) Nb-Ta mineralisation occurs in the greisen and greisenised granite which covers the top of intrusion B. Microlite, niobite and tantalite are the main Nb-Ta-bearing minerals and disseminated throughout the greisen zone. These minerals could have crystallised directly from the residual melt and/or precipitated from a fluid derived during the evolution of the melt.

14) Sn (W, Pb, Zn) mineralisation associated with intrusion C is distributed along fractures developed within intrusions B and C. Ore minerals, mainly cassiterite, wolframite, galena, sphalerite and beryl, are disseminated in quartz veins filling these

fractures and in greisens developed along the quartz veins.

15) Sn (Pb, Zn) mineralisation spatially linked to intrusion E occurs mainly in fissures within the NE-trending F_{101} fault zone and has a mineral assemblage of cassiterite, galena, sphalerite, arsenopyrite, pyrite, diopside, actinolite, fluorite and sericite. The deposition of these minerals results from the reaction of fluid derived from the granite with the fractured country rock.

16) W-F (fluorite-scheelite) deposits are associated predominantly with intrusion D with a mineral assemblage of quartz, fluorite, scheelite and calcite. Individual orebodies occur along the NNE-trending faults and are confined to the fractured footwalls the fault selvage. Mixing of magmatic fluids with meteoric water was probably the major cause of mineral deposition.

17) Fluids responsible for the formation of the W-F deposits were of low to moderate temperature (Th = 180°-350°C) and salinities (S = 1-19 wt.% NaCl eq., mostly less than 7 wt.%) with NaCl and $CaCl_2$ being the main solutes. Stable isotope ($\delta^{18}O$, δD, $\delta^{13}C$ and $\delta^{34}S$) compositions of these fluids suggest a mixed fluid source for these deposits. The fluid represents a diluted, chemically-exchanged successor to the predominantly magmatic fluid derived from the evolution of the Jianfengling granites.

18) The granite-type Pb-Zn mineralisation hosted in pegmatites and greisens is syn-magmatic and/or late-magmatic in origin. The fluids responsible for this type of mineralisation were derived from the evolution of the Jianfengling granites with little involvement of meteoric water. The $\delta^{34}S$ values of these fluids are identical to those of magmatic sulphur.

19) Orebodies of the lode-type Pb-Zn deposits are exclusively localised in the NNE-trending fault zones. A depositional sequence of (cassiterite) + arsenopyrite preceding pyrrhotite + base metal sulphides have been noted in the main Pb-Zn deposits of the Xianghualing area. The main metal resources were supplied by the Jianfengling granites, although some of the sulphur might be provided by the country rocks.

REFERENCES

ALDERTON, D.H.M., PEARCE, J.A. & POTTS, P.J., 1980. Rare earth element mobility during granite alteration: evidence from Southwest England. *Earth Planet. Sci. Lett.*, 49, 149-165.

ALDERTON, D.H.M. & MOORE, F., 1981. New determinations of tin and tungsten in granites from Southwest England. *Mineral. Mag.*, 44, 354-356.

ANFILOGOV, V.N., GLYUK, D.S. & TRUFANOVA, L.G., 1973. Phase relation in the interaction between granite and sodium fluoride at water vapour pressure of 1000 kg/cm^3. *Geochem. Int.*, 10 (1), 30-33.

BADHAM, J.P.N., 1980. Late magmatic phenomena in the Cornish Batholith: useful field guides for tin mineralisation. *in* EDWARDS, R.A. (ed), Research into the geology and geomorphology of SW England. *Ussher Soc. Proc.* 5 (1), 44-53.

BAERTSCHI, P., 1976. Absolute ^{18}O content of standard mean ocean water. *Earth Planet. Sci. Lett.*, 31, 341-344.

BAILEY, 1977. Fluorine in granitic rocks and melts: a review. *Chem. Geol.*, 19, 1-42.

BARNES, H.L., 1979. Solubilities of ore minerals. *in* BARNES, H.L. (ed), Geochemistry of hydrothermal deposits. *John Wiley & Sons*, 405-460.

BAUMANN, L., 1970. Tin deposits of the Erzgebirge. *Inst. Mining Metall. Trans.*, 79, B68-B75.

BEUS, A.A. & ZALASHKAVA, N.Y., 1964. Post-magmatic high temperature metasomatic processes in granitic rocks. *Int. Geol. Rev.*, 6, 668-681.

BIGELEISEN, J., PERLMAN, M.L. & PROSSER, H.C., 1952. Conversion of hydrogenetic materials to hydrogen for isotope analysis. *Anal. Chem.*, 27, 1356-1357.

BISCHOFF, J.L., 1991. Densities of liquids and vapours in boiling NaCl-H_2O solutions: a PVTX summary from 300°-500°C. *Am. J. Sci.*, 291, 309-338.

BISCHOFF, J.L. & ROSENBAUER, R.J., 1986. The system NaCl-H_2O: Relations of vapour-liquid near the critical temperature of water and of vapour-liquid-halite from 300° to 500°C. *Geochim. Cosmochim. Acta*, 50, 1437-1444.

BISCHOFF, J.L. & PITZER, K.S., 1989. Liquid-vapour relations for the system NaCl-H_2O: summary of the P-T-X surface from 300°-500°C. *Am. J. Sci.*, 289, 217-248.

BLATTNER, P., 1985. Isotope shift data and the natural evolution of geothermal system. *Chem. Geol.*, 49 (1-3), 187-203.

BODNAR, R.J., BURNHAM, C.W. & STERNER, S.M., 1985. Synthetic fluid inclusions in natural quartz. III. Determination of phase equilibrium properties in the system H2O-NaCl to 1000°C and 1500 bars. *Geochim. Cosmochim. Acta*, 49, 1861-1863.

BOETTCHER, A., GUO, Q., BOHLEN, S. & HANSON, B., 1984. Melting in feldspar-bearing systems to high pressures and the structures of aluminosilicate liquids. *Geology*, 12, 202-204.

BONIN, B., 1986. Ring complex granites and anorogenic magmatism. *Elsevier.*

BOOTH, B., 1968. Petrogenetic significance of alkali feldspar megacrysts and their inclusions in Cornubian granites. *Nature*, 217, 1036-1038.

BORTHWICK, J. & HARMON, R.S., 1982. A note regarding ClF_3 as an alterative to BrF_3 for oxygen isotope analysis. *Geochim. Cosmochim. Acta*, 46, 1665-1668.

BOTTINGA, Y., 1968. Calculation of fractionation factors for carbon and oxygen isotopic exchange in the system calcite-carbon dioxide-water. *J. Phys. Chem.*, 72, 800-808.

BOTTINGA, Y. & JOVAY, M., 1973. Comments on stable isotope geothermometry: the system quartz-water. *Earth Planet. Sci. Lett.*, 20, 251-265.

BOTTINGA, Y. & JOVAY, M., 1975. Oxygen isotope partitioning among the minerals in igneous and metamorphic rocks. *Rev. Geophys. Space Phys.*, 13, 401-418.

BOURCIER, W.L. & BARNES, H.L., 1987. Ore solubility -- VII. stabilities of chloride and bisulphide complexes of zinc to 350°C. *Econ. Geol.*, 82, 1839-1863.

BURNHAM, C.W., 1979. Magmas and hydrothermal fluids. *in* BARNES, H.L. (ed) "Geochemistry of hydrothermal ore deposits (second edition)", *John Wiley & Sons*, 71-136.

CANDELA, P.A., 1986. The evolution of aqueous vapour from silicate melts: effects on oxygen fugacity. *Geochim. Cosmochim. Acta*, 50, 1205-1211.

CANDELA, P.A., 1987. Theoretical constraints on the chemistry of the magmatic aqueous phase. *Geol. Soc. Am. Abstr. Prog.*, 19, 610.

CANDELA, P.A. & HOLLAND, H.D., 1984. The partitioning of copper and molybdenum between silicate melts and aqueous fluids. *Geochim. Cosmochim. Acta*, 48, 473-480.

CANDELA, P.A. & HOLLAND, H.D., 1986. A mass transfer model for copper and molybdenum in magmatic hydrothermal system: the origin of porphyry-type ore deposits. *Econ. Geol.*, 81, 1-19.

CHAMPBELL, A.R., 1987. A sulphur isotopic study of the Sam Cristobal tungsten-base metal mine, Peru. *Mineral. Deposita*, 22, 42-46.

CHAPPELL, B.W. & WHITE, A.J.R., 1974. Two contrasting granite types. *Pacific Geology*, 8, 173-174.

CHAROY, B., 1986. The genesis of the Cornubian Batholith (south-west England): the example of the Carnmenellis Pluton. *J. Petrol.*, 27, 571-604.

CHATTERJEE, A.K. & STRONG, D.F., 1984. Rare-earth and other element variation in greisens and granites associated with East Kemptville tin deposit, Nova Scotia, Canada. *Inst. Mining Metall. Trans.*, 93, B59-B70.

CHEN, Y.C., 1983. The metallogenetic series of the rare-earth, rare-metal and nonferrous metal deposits related to the Yanshanian granites in South China. *Mineral Deposits*, 2(2), 15-24 (in Chinese with English abstract).

CHEN, D.Q., 1987. The genesis and characteristics of REE geochemistry of the Xianghualing granites. *Bull. Inst. Mineral. Deposits*, No.2, 62-74 (in Chinese with English abstract).

CHENG, Y.Q., 1986. Magmatic rocks and magmatism in China. *in* Yang, z.y., Cheng, Y.Q. & Wang, H.Z. (eds), Geology of China, *Clarence Press, Oxford*, 189-229.

CHRISTIANSEN, E.H., BIKUN, J.V., SHIERIDAN, M.F. & BURT, D.M., 1984. Geochemical evolution of topaz rhyolites from the Thomas Range and Spor Mountain, Utah. *Am. Mineral.*, 69, 223-236.

CHRISTIANSEN, E.H. & LEE, D.E., 1986. Fluorine and chlorine in granitoids from the Basin and Range Province, western United States. *Econ. Geol.*, 81, 1484-1494.

CHRISTIANSEN, E.H., SHIERIDAN, M.F. & BURT, D.M., 1986. The geology and geochemistry of Cenozoic topaz rhyolites from the western United States. *Am. Geol. Soc. Spec. Pap.*, 82p.

CHRISTIANSEN, E.H., BURT, D.M., SHIERIDAN, M.F. & WILSON, R.T., 1983. The petrogenesis of topaz rhyolites from western United States. *Contrib. Mineral. Petrol.*, 83, 16-30.

CHRISTIANSEN, E.H., STUCKLESS, J.S., FUNKHOUSER-MAROLF, M.J. & HOWELL, K.H., 1988. Petrogenesis of rare-metal granites from depleted crustal sources: an example from the Cenozoic of western Utah, U.S.A. *in* TAYLOR, R.P. AND STRONG, D. (eds.) "Recent Advances in the Geology of Granite-Related Mineral Deposits", *Can. Inst. of Mining Metall.*, 39, 307-321.

CLAYTON, R.N. & MAYEDA, T.K., 1963. The use of bromine pentafluoride in the extraction of oxygen from oxides and silicates for isotopic analysis. *Geochim. Cosmochim. Acta*, 27, 43-52.

CLEMENS, J.D. & WALL, V.J., 1981. Origin and crystallisation of some peraluminous (S-type) granitic magmas. *Can. Mineral.*, 19, 111-131.

CLEMENS, J.D., 1984. Origin of A-type granites --- experimental constraints. *Geol. Soc. Am. Prog. Abstr.*, 16, 473.

COLLINS, P.L.F., 1981. The geology and genesis of the Cleveland tin deposit, western Tasmania: Fluid inclusion and stable isotope studies. *Econ. Geol.*, 76, 365-392.

COLLINS, W.J., BEAMS, S.D., WHITE, A.J.R. & CHAPPELL, B.W., 1982. Nature and origin of A-type granites with particular reference to southeastern Australia. *Contrib. Mineral. Petrol.*, 80, 189-200.

CONGDON, R.D. & NASH, W.P., 1991. Eruptive pegmatite magma: rhyolite of the Honeycomb Hills, Utah. *Am. Mineral.*, 76, 1261-1278.

COREY, M.C. & CHATTERJEE, A.K., 1990. Characteristics of REE and other trace element in response to successive and superimposed metasomatism within a portion of the South Mountain Batholith, Nova Scotia, Canada. *Chem. Geol.*, 85, 265-285.

COX, K.G., BELL, J.D. & PANKHURST, R.J., 1979. The interpretation of igneous rocks. *George Allen and Unwin*, 450p.

CRAIG, H., 1957. Isotopic standards for carbon and oxygen and correction factors for mass-spectrometric analysis of carbon dioxide. *Geochim. Cosmochim. Acta*, 12, 133-149.

CRAIG, H., 1961a. Standards for reporting concentrations of deuterium and oxygen 18 in natural water. *Science*, 133, 1833-1834.

CRAIG, H., 1961b. Isotopic variations in nature waters. *Science*, 133, 1702-1703.

CRERAR, D.A. & BARNES, H.L., 1976. Ore solubility V. Solubility of chalcopyrite and chalcocite assemblages in hydrothermal solution at 200-350°C. *Econ. Geol.*, 71, 772-794.

CROUDACE, I.W. & GILLIGAN, J.M., 1990. Versatile and accurate trace element determinations in iron-rich and other geological samples using X-ray fluorescence analysis. *X-ray Spectrometry*, 19, 117-123.

CROUDACE, I.W., JORON, J.L., JAFFREZIC, H., MEYER, G. & TREUIL, M., 1982. Neutron activation analysis of seven B.C.S. certified reference materials of geological interest. *Geostandards Newsletter*, 6 (2), 233-239.

CROUDACE, I.W. & RANDLE, K., 1988. A rapid non-destructive method of fluorine determination using fast-neutron activation analysis. *Chem. Geol.*, 67, 165-170.

CROUDACE, I.W. & WILLIAMS-THORPE, O., 1988. A low dilution, wavelength-dispersive X-ray fluorescence procedure for the analysis of archaeological rock artifacts. *Archaeometry*, 30 (2), 227-236.

CULLERS, R.L. & GRAF, J.L., 1984. Rare earth elements in igneous rocks of the continental crust: intermediate to silicic rocks -- ore genesis. *in* HENDERSON, P. (ed), Rare element geochemistry. *Elsevier, London*, 275-316.

DEPARTMENT OF GEOLOGY, NANJING UNIVERSITY, 1980. Investigations on the time and spatial distribution of the granitic rocks in Southeast China: their petrographic evolution, petrogenetic types, and metallogenetic relations. *J. Nanjing Univ.*, Spec. Issue on Geology (in Chinese).

DEPARTMENT OF GEOLOGY, NANJING UNIVERSITY, 1981. Granitoids of different ages and their metallogenetic relations in South China. *Science Press, Beijing* (in Chinese).

DEPARTMENT OF GEOLOGY, NANJING UNIVERSITY, 1972. Granitic rocks of different periods in southeastern China and their genetic relation to certain metallic mineral deposits. *Scientia Sinica* (in Chinese),

DINGWELL, D.B., 1988. The structure and properties of fluorine-rich magmas: a review of experimental studies. *in* TAYLOR, R.P. & STRONG, D.F. (eds) "Recent advances in the geology of granite-related mineral deposit", *Can. Inst. Min. Metall. Spec.*, 39, 1-12.

DINGWELL, D.B. & SCARFE, C.M., 1985. Chemical diffusion of fluorine in melts in the system Na_2O-Al_2O_3-SiO_2. *Earth Planet. Sci. Lett.*, 73, 377-384.

DU, S.H. & HUANG, Y.H., 1979. Xianghualingite --- a new type of magmatic rock. *in* "Symposium of international geological exchange", 3, *Geol. Press*, 45-60 (in Chinese).

EUGSTER, H.P. & WILSON, G.A., 1985. Transport and deposition of ore-forming elements in hydrothermal systems associated with granites. *in* High heat production (HHP) granites, hydrothermal circulation and ore genesis, *Inst. Min. Metall.*, 87-98.

EUGSTER, H.P., 1985. Granites and hydrothermal deposits: a geochemical framework. *Mineral. Mag.*, 49, 7-23.

EXLEY, C.S., 1958. The petrology of the St. Austell granite [abs]. Conf. Geol. Geomorph. SW England Abs. Pr., 19-20.

FENG, Z.W., XIA, W.H., ZHANG, J.T. & CHEN, Z.Y., 1986. The formation mechanism of multiple-remelting type granites in southern China. *Earth Sci. – J. Wuhan Coll. Geol.*, **11** (1), 41-49.

FOLEY, S.F., 1986. The effect of fluorine on phase relationships in the system $KAlSiO_4$-Mg_2SiO_4-SiO_2 at 28 kb and the solution mechanism of fluorine in silicate melts. *Contrib. Petrol. Mineral.*, 93, 46-55.

FOSTER, R.P., 1977. Solubility of scheelite in hydrothermal chloride solution. *Chem. Geol.*, 20, 27-43.

FRIEDMAN, I. & SMITH, R.L., 1958. The deuterium content of water in some volcanic glasses. *Geochim. Cosmochim. Acta*, 15, 218-228.

FRYER, B.J. & TAYLOR, R.P., 1987. Rare earth element distributions in uraninites: implications for ore genesis. *Chem. Geol.*, 63, 101-108.

FU, M., CHANGKAKOTI, A., KROUSE, H.R., GRAY, J. & KWAK, T.A.P., 1991. An oxygen, hydrogen, sulphur, and carbon isotope study of carbonate-replacement (skarn) tin deposits of the Dachang tin field, China. *Econ. Geol.*, 86, 1683-1703.

GIBERT, F., MOINE, B., SCHOTT, J. & DANDURAND, J-L., 1992. Modelling of the transport and deposition of tungsten in the scheelite calc-silicate gneisses of the Montagne Noire, France. *Contrib. Mineral. Petrol.*, 112, 371-384.

GLYUK, D.S., TRUFANOVA, L.G. & BAZAROVA, S.B., 1981. Phase relations in the granite-H_2O-LiF system at 100 Kg/cm^2. *Geochem. Int.*, 17 (5), 35-48.

GODFREY, J.D., 1962. The deuterium content of hydrous minerals from the East-Central Sirrea Nevada and Yosemite National Park. *Geochim. Cosmochim. Acta*, 26, 1215-1245.

GROVES, D.I. & McCARTHY, T.S., 1978. Fractional crystallisation and the origin of tin deposits in granitoids. *Mineral. Deposita*, 13, 11-26.

GUIYANG INSTITUTE OF GEOCHEMISTRY, 1979. Geochemistry of the granitoids in South China. *Science Press, Beijing* (in Chinese).

HAAPALA, I., 1977. Petrograpgy and geochemistry of the Eurajoki stock, a rapakivi granite complex with greisen-type mineralisation in southwest Finland. *Bull. Geol. Surv. Finland*, 286.

HAGEMANN, R., NIEF, G. & ROTH, E., 1970. Absolute isotopic scale for deuterium analysis of natural waters: Absolute D/H ratio for SMOW. *Tellus*, 22, 712-715.

HANSON, G.N., 1978. The application of trace elements to the petrogenesis of igneous rocks of granitic composition. *Contrib. Mineral, Petrol.*, 38, 26-43.

HARDS, N.J., 1976. Distribution of elements between the fluid phase and silicate melt phase of granites and nepheline sysenites. *NERC Rept. Progress in Experi. Geol.*, 3, 88-90.

HARRIS, N.B.W., 1981. The role of fluorine and chlorine in the petrogenesis of a peralkaline complex from Saudi Arabia. *Chem. Geol.*, 31, 303-310.

HEINRICH, C.A., 1990. The chemistry of hydrothermal tin (-tungsten) ore deposition. *Econ. Geol.*, 85. 457-481.

HEINRICH, C.A. & EADINGTON, P.J., 1986. Thermodynamic predictions of the hydrothermal chemistry of arsenic, and their significance for the paragenetic sequence of some cassiterite-arsenopyrite-base metal sulphide deposits. *Econ. Geol.*, 81, 511-529.

HIGGINS, N. & KERRICH, R., 1982. Progressive ^{18}O depletion during CO_2 separation from a carbon dioxide-rich hydrothermal fluid: evidence from the Grey River tungsten deposit, Newfoundland. *Can. J. Earth Sci.*, 19. 2247-2257.

HIGGINS, N.C., 1980. Fluid inclusion evidence for the transport of tungsten by carbonate complexes in hydrothermal solutions. *Can. J. Earth Sci.*, 17, 823-830.

HIGGINS. N.C., SOLOMON, M. & VARNE, R., 1985. The genesis of the Blue Tier Batholith, northern Tasmania, Australia. *Lithos*, 18, 129-149.

HIGUCHI, H. & NAGASAWA, H., 1969. Partition of trace elements between rock-forming minerals and the host volcanic rocks. *Earth Sci. Planet. Lett.*, 7, 281-287.

HILDRETH, W.H., 1979. The Bishop Tuff: evidence for the origin of compositional zonation in silicic magma chambers. *Geol. Soc. Am. Spec. Pap.*, 180, 43-75.

HOLLAND, H.D., 1956. The chemical composition of vein minerals and the nature of ore forming fluids. *Econ. Geol.*, 51, 781-797.

HOLLAND, H.D., 1972. Granites, solutions and base metal deposits. *Econ. Geol.*, 67, 281-301.

HOLLOWAY, J.R., 1976. Fluids in the evolution of granitic magmas --- consequences of finite CO_2 solubility. *Geol. Soc. Am. Bull.*, 87, 1513-1518.

HOLLOWAY, J.R., 1987. Igneous fluids. *in* CARMICHAEL, I.S.E. & EUGSTER, H.P. (eds) "Thermodynamic modelling of geological materials: minerals, fluids and melts", *Reviews in Mineralogy*, 17, 211-234.

HOLTZ, F., PICHAVANT, M., BARBEY, P. & JOHANNES, W., 1992. Effects of H_2O on liquidus phase relations in the haplogranite system at 2 and 5 kbar. *Am. Mineral.*, 77, 1223-1241.

HOLYLAND, P.W., 1987. Dynamic modelling at the Renison tin mine [abs.]. *Pacific Rim Congress '87*, Gold Coast, Australia, Ext. Abs. 189-193.

HU, Y.J., HAN, X.G., ZHENG, R.F., TONG, Q.M., HUANG, R.M., GONG, M.Y. & WANG, S.M., 1980. The ore-formation regularities and prospecting for Pb-Zn ore deposits in Southern Hunan Province. *in* XU, K.Q. and TU G.C. (eds) "Geology of Granites and Their Metallogenetic Relations" -- Proceedings of the International Symposium, hold at Nanjing University, Nanjing, China, Oct. 26-30, 1982. *Science Press, Beijing*, 125-136.

HUANG, Y.H., 1985. Variation in the contents of some elements along the F4 fault in Xianghualing area. *Geotectonica et Metallogenia*, 9 (4), 289-308, (in Chinese with English abstract).

HUANG, Y.H. & DU, S.H., 1979. The characteristics of mineral assemblages of Xianghualing area. *in* Symposium of international geological exchange, 3, *Geol. Press*, 74-93.

HUANG, Y.H., ZHOU, X.Z. & DU, S.H., 1979. A further discussion on micas from the greisenised granite and related "ribbon rocks" tactite at Xianghualing. *in* Symposium of international geological exchange, 3, *Geol. Press*, 156-182.

HUNAN GEOLOGICAL SURVEY, 1962. Comprehensive exploration report on geology of Guiyang area, Hunan Province (G-49-82-B) (with maps). *Internal report* (in Chinese).

IVANOVA, G.F., 1969. Conditions of concentration of tungsten during greisenisation. *Geochem. Int.*, 6, 12-21.

IVANOVA, G.F. & NAUMOV, V.B. 1985. Geochemical inter-relations of rare-metal ore mineralisation with granites. *in* High heat production (HHP) granites, hydrothermal circulation and ore genesis, *Inst. Min. Metall.*, 155-162.

JACKSON, N.J., HALLIDAY, A.N., SHEPPARD, S.M.F. & MITCHELL, J.G., 1982. Hydrothermal activity in the St. Just Mining District, Cornwall, England. *in* EVANS, A.M. (ed), Metallisation associated with acid magmatism. *John Wiley & Sons*, 137-179.

JACKSON, K.J. & HELGESON, H.C., 1985. Chemical and thermodynamic constraints on the hydrothermal transport and deposition of tin: I. Calculation of the solubility of cassiterite at high pressures and temperatures. *Geochim. Cosmochim. Acta*, 49, 1-22.

JACKSON, K.J. & HELGESON, H.C., 1985. Chemical and thermodynamic constraints on the hydrothermal transport and deposition of tin: II. Interpretation of phase relations in the southwest Asian tin belt. *Econ. Geol.*, 80, 1365-1378.

JACKSON, N.J., MOORE, J.M. & RANKIN, A.H., 1977. Fluid inclusions and mineralization at Cligga Head, Cornwall, England. *J. Geol. Soc. London*, 134, 343-349.

JAHNS, R.H. & BURNHAM, C.W., 1969. Experimental studies of pegmatite genesis: I. A model for the derivation and crystallisation of granitic pegmatites. *Econ. Geol.*, 64, 843-864.

KELLY, W.C. & RYE, R.O., 1979. Geology fluid inclusion and stable isotope studies of the tin and tungsten deposits of Panasqueira, Portugal. *Economic Geology*, 74, 1721-1822.

KELLY, W.C. & TURNEAURE, F.S., 1970. Mineralogy, paragenesis and geometry of the tin and tungsten deposits of the eastern Andes, Bolivia. *Economic Geology*, 65, 609-680.

KEPPLER, H. & WYLLIE, P.J., 1992. Partitioning of Cu, Sn, Mo, W, U, and Th between melt and aqueous fluid in the system haplogranite-H_2O-HCl and haplogranite-H_2O-HF. *Contrib. Mineral. Petrol.*, 109, 139-150.

KERR, P.F., 1959. Optical mineralogy. *McGraw-Hill Book Company*, 442p.

KHITAROV, N.I., MALININ, S.P., LEBEDEV, Y.B. & SHIBAYEVA, N.P., 1982. The distribution of Zn, Cu, Pb, and Mo between a fluid phase and a silicate melt of granitic composition at high temperatures and pressures. *Geochem. Int.*, 19(4), 123-136.

KILINC, I.A. & BURNHAM, C.W., 1972. Partitioning of chloride between a silicate melt and coexisting aqueous phase from 2 to 8 kbar. *Econ. Geol.*, 67, 231-235.

KNIGHT, C.L. & BODNAR, R.J., 1989. Synthetic fluid inclusions: IX. Critical PVTX properties of

NaCl-H_2O solutions. *Geochim. Cosmochim. Acta*, 53, 3-8.

KONTAK, J.D., 1991. The East Kemptville topaz-muscovite leucogranite, Nova Scotia, II. Mineral geochemistry. *Can. Mineral.*, 29, 37-60.

KONTAK, J.D., 1990. The East Kemptville topaz-muscovite leucogranite, Nova Scotia, I. Geological setting and whole rock geochemistry. *Can. Mineral.*, 28, 787-825.

KOSALS, R.A., 1976. Geochemical characteristics of rare elements in granitic melts and fluids. *Geol. Press*, 199p, (in Chinese, translated from Russian).

KOVALENKO, V.I. & KOVALENKO, N.I., 1984. Problems of the origin, ore-bearing and evolution of rare-metal granitoids. *Phys. Earth Planet. Interiors*, 35, 51-62.

KOVALENKO, N.I., 1977. The reactions between granite and aqueous hydrofluoric acid in relation to the origin of fluorine-bearing granites. *Geochem. Int.*, 14 (2), 108-118.

LAGACHE, M. & WEISHROD, A., 1977. The system: two alkali feldspars-KCl-NaCl-H_2O at moderate to high temperatures and low pressures. *Contrib. Mineral. Petrol.*, 62, 77-101.

LANDIS, G.P. & RYE, R.O., 1974. Geologic, fluid inclusion and stable isotope studies of the Pasto Bueno tungsten-base metal ore deposit, northern Peru. *Economic Geology*, 69, 1025-1059.

LAYNE, G.D. & SPOONER, E.T.C., 1991. The JC tin skarn deposit, southern Yukon Territory: I. Geology, paragenesis, and fluid inclusion microthermometry. *Economic Geology*, 86, 29-47.

LAYNE, G.D., LONGSTAFFE, F.J. & SPOONER, E.T.C., 1991. The JC tin skarn deposit, southern Yukon Territory: II. A carbon, oxygen, hydrogen, and sulphur stable isotope study. *Economic Geology*, 86, 48-65.

LE BAS, M.J. & STRECKEISEN, A.L., 1991. The IUGS systematics of igneous rocks. *J. Geol. Soc. London*, 148, 825-833.

LE FORT, P., 1981. Manaslu leucogranite: a collision signature of the Himalaya, a model for its genesis and emplacement. *in* "Granites and rhyolites, JGR." *Jour. Geophy. Res.* B 86 (11), 10545-10568.

LE FORT, P., 1986. Metamorphism and magmatism during the Himalaya collision. *in* COWARD, M.P. (ed) "Collision tectonics", *Geol. Soc. Spec. Publ.*, 19, 159-172.

LE FORT, P., CUNNEY, M., DENIEL, C., FRANCE-LANORD, C., SHEPPARD, S.M.F., UPRETI, B.N. & VIDAL,P., 1987. Crustal generation of the Himalayan leucogranites. *in* GUPTA, H.K. (ed), Deep seated processes in collision zones. *Tectonophysics*, 134 (1-3), 39-57.

LE MAITRE, R.W., 1976. Some problems of the projection of chemical data into mineralogical classifications. *Contrib. Mineral. Petrol.*, 56, 181-189.

LEHMANN, B., ISHIHARA, S., MICHEL, H., MILLER, J., RAPELA, C., SANCHEZ, A., TISTL, M. & WINKDMANN, L., 1990. The Bolivian tin province and regional tin distribution in the central Andes: a reassessment. *Economic Geology,* 85, 1044-1058.

LIU, J.Y. & SHEN, J.L., 1984. The metallogenetic complex of Yangchuling porphyry tungsten (molybdenum) deposit --- A genetic and evolutionary model of transitional type granitoids.

in XU, K.Q. and TU G.C. (eds) "Geology of Granites and Their Metallogenetic Relations" -- Proceedings of the International Symposium, hold at Nanjing University, Nanjing, China, Oct. 26-30, 1982. *Science Press, Beijing*, 329-346.

LONDON, D., HERVIG, R.L. & MORGAN VI, G.B., 1988. Melt-vapour solubilities and elemental partitioning in peraluminous granite-pegmatite systems: experimental results with Macusani glass at 200 MPa. *Contrib. Mineral. Petrol.*, 99, 360-373.

LONDON, D. MORGAN, G.B. VI, & HERIGE, R.L., 1987. Element partitioning and fractionation trends in volatile- and LILE-rich rhyolite. *EOS Trans. Geophys. Union*, 68, 450.

LONDON, D., 1992. Phosphorus in S-type magmas: The P_2O_5 content of feldspars from peraluminous granites, pegmatites, and rhyolites. *Am. Mineral.*, 77, 126-145.

LONDON, D., MORGAN, G.B. VI & LERVIG, R.L., 1989. Vapour-undersaturated experiments with Macusani glass + H_2O at 200 MPa, and the internal differentiation of granitic pegmatites. *Contrib. Mineral. Petrol.*, 102, 1-17.

LONDON, D. & HERIGE, R.L., 1986. Trace element partitioning in the system macusanite-H_2O at 200 MPa (H_2O). *EOS Trans. Geophys. Union*, 67, 1258.

LONG, P.E., 1978. Experimental determination of partition coefficients for Rb, Sr and Ba between alkali feldspar and silicate liquid. *Geochim. Cosmochim. Acta*, 42, 833-846.

LUO, X.Z., WANG, Z.R. & LUO, X.G., 1988. Research on the silver minerals in Xianghualing tin orefield, Hunan. *J. Central-South Inst. Mining Metall., Spec.* 2, 42-46 (in Chinese).

LUTH, W.C., 1969. The systems $NaAlSi_3O_8$-SiO_2 and $KAlSi_3O_8$-SiO_2 to 20 kb and the relationships between H_2O content, P_{H2O} and P_{total} in granitic magma. *Am. J. Sci.*, 267-A, 325-341.

LUTH, W.C., 1976. Granitic rocks. *in* BAILEY, D.K. & MacDONALD (eds) "The evolution of the crystalline rocks", *Academic Press, London*, 335-417.

LUTH, W.C., JAHN, R.H. & TUTTLE, O.F., 1964. The granite system at pressures of 4 to 10 kb. *J. Geophys. Res.*, 69, 759-773.

MaCKENZIE, D.E., BLACK, L.P. & SUN, S.S., 1988. Origin of alkali-feldspar granites: A example from the Poimena granite, northeastern Tasmania, Australia. *Geochim. Cosmochim. Acta*, 52, 2507-2524.

MAHOOD, G. & HILDRETH, W.H., 1989. Large partition coefficients for trace elements in high silica rhyolites. *Geochim. Cosmochim. Acta*, 47, 11-30.

MALININ, S.D., KRAVCHUK, I.F. AND DELBOVE, F., 1989. Chloride distribution between phases in hydrated and dry chloride-aluminosilicate melt systems as a function of phase composition. *Geochem. Int.*, 26, 32-48.

MANNING, D.A.C., 1981. The effect of fluorine on liquidus phase relationships in the system Qz-Ab-Or with excess water at 1 kb. *Contrib. Mineral. Petrol.*, 76, 206-215.

MANNING, D.A.C., 1982. An experimental study of fluorine on the crystallisation of granitic melts. *in* EVANS, A.M. (ed) "Metallisation associated with acid magmatism", *John Wiley & Sons*,

191-203.

MANNING D.A.C. & PICHAVANT, M., 1983. The role of fluorine and boron in the generation of granitic melts. *in* ALDERTON, D.P. & GRIBBLE, C.D. (eds.) "Migmatites, Melting and Metamorphism", *Shiva*, 94-109.

MANNING D.A.C. & HILL, P.I., 1990. The petrogenetic and metallogenetic significance of topaz granite from the S.W. England orefield. *in* STEIN, H.J. & HANNAH, J.L. (eds), Ore-bearing granite systems. *Geol. Soc. Am. Spec. Pap.*, 246, 51-69.

MANNING, D.A.C. & PICHAVANT, M., 1988. Volatiles and their bearing on the behaviour of metals in granitic systems. *In* TAYLOR, R.P. and STRONG, D.F. (eds) "Recent Advances in the Geology of Granite Related Mineral Deposits", *Can. Inst. Metall., Spec.*, 39, 13-24.

MARTIN, J.S., 1983. An experimental study of the effects of lithium on the granite system. *Proc. Ussher Soc.*, 5, 417-420.

MARTIN, R.F. & BONIN, B., 1976. Water and magma genesis: the association hypersolvus granite - -- subsolvs granite. *Can. Mineral.*, 14 (3), 228-237.

MARUÉJOL, P., CUNEY, M. & TURPIN, L., 1990. Magmatic and hydrothermal REE fractionation in the Xihuashan granites (SE China). *Contrib. Mineral. Petrol.*, 104, 668-680.

MATSUHISA, Y., GOLDSMITH, J.R. & CLAYTON, R.N., 1979. Oxygen isotope fractionation in the system quartz-albite-anorthite-water. *Geochim. Cosmochim. Acta*, 43, 1131-1140.

McCARTHY, T.S. & HASTY, R.A., 1976. Trace element distribution patterns and their relationship to the crystallisation of granitic melts. *Geochim. Cosmochim. Acta*, 40, 1351-1358.

McCARTHY, T.S., 1978. On the relationship between cumulus mineralogy and trace and alkali element chemistry in an Archean granite from the Barberton region, South Africa. *Geochim. Cosmochim. Acta*, 42, 21-26.

McCRAE, J.M., 1950. On the isotope chemistry of carbonates and paleotemperature scale. *J. Chem. Phys.*, 18, 849-857.

MILLER, C.F. & MITTLEFEHLDT, D.W., 1982. depletion of light rare earth elements in felsic magmas. *Geology*, 10, 129-133.

MITTLEFEHLDT, D.W. & MILLER, C.F., 1983. Geochemistry of the Sweetwater Wash Pluton, California: implications for "anomalous" trace element behaviour during differentiation of felsic magmas. *Geochim. Cosmochim. Acta*, 47, 109-124.

MO, Z.S. YE, B.D., PAN, W.Z., WANG, S.N., ZHANG, J.L., GAO, B.Z., LIU, J.Q. & LIU, W.Z., 1980. Geology of the granites in the Nanling Ranges. *Geological Press, Beijing* (in Chinese).

NAKAMURA, N. & MASUDA, A., 1973. Chondrites with peculiar rare earth patters. *Earth Planet. Sci. Lett.*, 19, 429-437.

NAUMOVE, V.B. & IVANOVA, G.F., 1981. Association between rare-metal mineralization and acid magmatism based on a study of mineral inclusion. *International Geology Review*, 23(5), 591-598.

NO. 238 GEOL. TEAM, 1958. Geology of the Xianghualing polymetallic orefield. *Internal Report* (in Chinese).

NO. 238 GEOL. TEAM, 1962. Preliminary exploration report on Nb-Ta mineralization related to the 430 granite stock. *Internal Report* (in Chinese)

NO. 238 GEOL. TEAM, 1974. The detailed exploration report on Nb-Ta mineralization related to the 430 granite stock. *Internal Report* (in Chinese).

O'NEIL, J.R., CLAYTON, R.N. & MAYEDA, T.K., 1969. Oxygen isotope fractionation in divalent metal carbonates. *J. Chem. Phys.*, **51**, 5547-5558.

OAKES, C.S., BODNAR, R.J. & SIMONSON, J.M., 1990. The system NaCl-$CaCl_2$-H_2O: I. The ice liquidus at 1 atm and total pressure. *Geochim. Cosmochim. Acta*, **54**, 603-610.

OHMOTO, H., 1972. Systematics of sulphur and carbon isotopes in hydrothermal ore deposits. *Econ. Geol.*, **67**, 551-578.

OHMOTO, H., 1986. Stable isotope geochemistry of ore deposits. *in* VALLEY, J.W., TAYLOR, Jr. H.P. & O'NEIL, J.R. (eds) "Stable isotopes in high temperature geological processes" *Reviews in Mineralogy*, **16**, 491-559.

OHMOTO, H. & RYE, R.O., 1979. Isotopes of sulphur and carbon. *in* BARNES, H.L. (ed) "Geochemistry of hydrothermal ore deposits (second edition)", *John Wiley & Sons*, 509-567.

ÖHLANDER, B., BILLSTRÖM, K. & HÅLENIUS, E., 1989. Behaviour of rare earth elements in highly evolved granitic systems: evidence from Proterozoic molybdenite mineralised aplites and associated granites in norther Sweden. *Lithos*, **23**, 267-280.

PATTERSON, D.J., OHMOTO, H. & SOLOMON, M., 1981. Geologic setting and genesis of the cassiterite-sulphide mineralisation at Rension Bell, western Tasmania. *Econ. Geol.*, **76**, 393-438.

PAYETTE, C. & MARTIN, R.F., 1990. Melt inclusions in the quartz phenocrysts of rhyolites from Topaz and Keg Mountains, Thomas Range, Utah. *in* STEIN, H.J. & HANNAH, J.L. (eds) "Ore-bearing granite systems: petrogenesis and mineralising processes", *Geol. Soc. Am. Spec.*, **246**, 89-102.

PICHAVANT, M., 1981. An experimental study of the effect of boron on a water saturated aplogranite at 1 kbar vapour pressure. *Contrib. Mineral. Petrol.*, **76** (4), 430-439.

PICHAVANT, M., 1983. Melt-fluid interaction deduced from studies of silicate B_2O_3-H_2O systems at 1 kbar. *Bull. Mineral.*, **106**, 201-211.

PICHAVANT, M., KONTAK, D.J., BRIQUEU, L., HERRERA, J.V. & CLARK, A.H., 1988. The Miocene-Pliocene Macusani volcanics, Se Peru, II. Geochemistry and origin of a felsic peraluminous magma. *Contrib. Mineral. Petrol.*, **100**, 325-338.

PICHAVANT, M. & MANNING, D.A.C., 1984. Petrogenesis of tourmaline granites and topaz granites: the contribution of experimental data. *Phys. Earth Plant. Interior*, **35**, 31-50.

POLLARD, P.J., 1983. Magmatic and post-magmatic processes in the formation of rocks associated

with rare-element deposits. *Trans. Inst. Min. Metall. (Sect. B)*, 92, B1-B9.

POLLARD, P.J., 1988. Mineralogical and geochemical features of rare-metal granites. *in* "The 5th Int. Symp. Tin/Tungsten Granites in SE Asia and Western Pacific", IGCP Project 220, Oct. 17-19, 1988, *Shimane University, Matsue, Japan*, 131-133.

POLLARD, P.J., ANDREW, A.S. & TAYLOR, R.G., 1991. Fluid inclusion and stable isotope evidence for interaction between granites and magmatic hydrothermal fluids during formation of disseminated and Pipe-style mineralisation at Zaaiplaats Tin Mine. *Econ. Geol.*, 86, 121-141.

POLLARD, P.J. & TAYLOR R.G., 1986. Progressive evolution of alteration and tin mineralisation: controls by interstitial permeability and fracture-related tapping of magmatic fluid reservoirs in tin granites. *Econ. Geol.*, 81, 1795-1800.

POLLARD, P.J., TAYLOR, R.G., TAYLOR, R.P. & GROVES, D.I., 1991. Petrographic and geochemical evolution of pervasively altered Bushveld granites at Zaaiplaats Tin Mine. *Econ. Geol.*, 86, 1401-1433.

POLLARD, P.J. & TAYLOR R.P., 1991. Petrogenetic and metallogenetic implications of the occurrence of topaz Li-mica granite at the Yichun Ta-Nb-Li mine, Jiangxi Province, South China. *in* PAGEL, M. and LEROY, J.L. (eds) "Source, Transport and Deposition of Metals" -- Proceedings of the 25th SGA anniversary meeting, Nancy, France, Aug.30-Sept.3, 1991. *A.A. Balkema*, 789-791.

POTTER, R.W.II & BROWN, D.L., 1977. The volumetric properties of aqueous sodium chloride solutions from 0° to 500°C at pressures up to 200 bars based on a regression of available data in the literature. *U.S. Geol. Surv. Bull.*, 1421c.

POTTER, R.W.II, CLYNNE, M.A. & BROWN, D.L., 1978. Freezing point depression of aqueous sodium chloride solutions. *Econ. Geol.*, 73, 284-285.

PRICE, J.G., RUBIN, J.N., HENRY, C.D., PINKSTON, T.L., TWEEDY, S.W. & KOPPENAAL, D.W., 1990. Rare metal enriched peraluminous rhyolites in a continental arc, Sierra Blance area, Tran-Pecos Texas: chemical modification by vapour phase crystallisation. *in* STEIN, H.J. & HANNAH, J.L. (eds) "Ore-bearing granite systems: petrogenesis and mineralising processes", *Geol. Soc. Am. Spec.*, 246, 103-120.

PUCHNER, C.C., 1986. Geology, alteration, and mineralisation of the Kougarok Sn deposit, Seward Peninsula, Alaska. *Econ. Geol.*, 81, 1775-1794.

RAFAL'SKIY, R.P., 1984. Tungsten migration and scheelite deposition under hydrothermal deposition conditions. *Geochim. Int.*, 21 (5), 1-13.

RANDLE, K. & CROUDACE, I.W., 1989. Rapid non-destructive determination of fluorine in seventy-one geological and other reference samples using fast-neutron activation analysis. *Geostandards Newsletter*, 13 (1), 69-73.

RIBEIRO, L., 1987. Petrogenesis of early Palaeozoic peralkaline rhyolites from the Macedo de

Cavaleiros (NE Portugal). *Geologische Rundschau*, 76 (1), 147-168.

ROBISON, B.W. & KUSAKABE, M., 1975. Quantitative preparation of sulphur dioxide for $^{34}S/^{32}S$ from sulphides by combustion with cuprous oxide. *Anal. Chem.*, 47, 1179-1181.

ROEDDER, E., 1984. Fluid inclusions. *Reviews in Mineralogy*, 12, 644p.

ROEDDER, E. & BODNAR, R.J., 1980. Geological pressure determinations from fluid inclusion studies. *Ann. Rev. Earth Planet. Sci.*, 8, 263-301.

ROSE, A.W. &BURT, D.M., 1979. Hydrothermal alteration. *in* BARNES, H.L. (ed) "Geochemistry of hydrothermal ore deposits (second edition)", *John Wiley & Sons*, 173-235.

RYE, R.O., HALL, W.E. & OHMOTO. H., 1974. Carbon, hydrogen, oxygen and sulphur isotope study of the Darvin lead-silver-zinc deposit, southern California. *Econ. Geol.*, 69 (4), 468-481.

RYERSON, F.J. & HESS, P.C., 1978. Implications of liquid-liquid distribution coefficients to mineral-liquid partitioning. *Geochim. Cosmochim. Acta*, 42, 921-932.

SALVI, S. & WILLIAMS-JONES, A.E., 1990. The role of hydrothermal processes in the granite hosted Zr, Y, REE deposit at Strange Lake, Qucbec/Labrador: Evidence from fluid inclusion. *Geochim. Cosmochim. Acta*, 54, 2403-2418.

SAWKA, W.N., HEIZLER, M.T., KISTLER, R.W. & CHAPPELL, B.W., 1990. Geochemistry of fractionated I-, and S-type granites from the tin-tungsten province of western Tasmania. *in* STEIN, H.J. & HANNAH, J.L. (eds), Ore- bearing granite systems. *Geol. Soc. Am. Spec. Pap.*, 246, 161-179.

SCHALTEGGER, U. & KRÄHENBÜHL, U., 1990. Heavy rare earth element enrichment in granites of the Aar Massif (Central Alps, Switzerland). *Chem. Geol.*, 89, 49-63.

SCHMITZ, C. & BURT, D.M., 1990. The Black Pearl Mine, Arizona: wolframite veins and stockscheidor pegmatite related to an albitic stock. *in* STEIN, H.J. & HANNAH, J.L. (eds) "Ore-bearing granite systems: petrogenesis and mineralising processes", *Geol. Soc. Am. Spec.*, 246, 221-231.

SCHWARTZ, M.O., 1991. Geochemical criteria for distinguishing magmatic and metasomatic albite-enrichment in granitoids. *in* PAGEL, M. and LEROY, J.L. (eds) "Source, Transport and Deposition of Metals" -- Proceedings of the 25th SGA anniversary metting, Nancy, France, Aug.30-Sept.3, 1991. *A.A. Balkema*, 811-814.

SCHWARTZ, M.O., 1992. Geochemical criteria for distinguishing magmatic and metasomatic albite enrichment in granitoids --- examples from the Ta-Li granite Yichun (China) and the Sn-W deposit Tikus (Indonesia). *Mineral. Deposita.*, 27, 101-108.

SEREBRYAKOV, V.A., 1961. Autometasomatic alteration of granitoids and association of tin mineralisation with the zone of sodium-potassium metasomatism. *Int. Geol. Rev.*, 3, 100-113.

SHANNON, J.R., WALKER, B.M., CARTEN, R.B. & GERAGHTY, E., 1982. Unidirectional solidification textures and their significance in determine relative ages of intrusions at the Henderson Mine, Colorado. *Geology*, 10, 293-297.

SHELTON, K.L., TAYLOR, R.P. & SO, C.S., 1987. Stable isotope studies of the Dae Hwa tungsten-molybdenum mine, Republic of Korea: evidence of progressive meteoric water interaction in a tungsten-bearing hydrothermal system. *Econ. Geol.*, 82, 43-52.

SHEPHERD, T.J., RANKIN, A.H. & ALDERTON, D.H.M., 1985. A practical guide to fluid inclusion studies. *Blackie & Sons, London*, 235p.

SHEPPARD, S.M.F., 1986. Characteristics and isotopic variations in natural waters. *in* VALLEY, J.W., TAYLOR, Jr. H.P. & O'NEIL, J.R. (eds) "Stable isotopes in high temperature geological processes" *Reviews in Mineralogy*, 16, 165-183.

SHINOHARA, H., IIYAMA, J.T. AND MATSUO, S., 1989. Partition of chlorine compounds between silicate melt and hydrothermal solutions: I. Partition of NaCl-KCl. *Geochim. Cosmochim. Acta*, 53, 2617-1630.

SMITH, J.V., 1974a. Feldspar minerals. vol. 1: Crystal structure and physical properties. *Heidelberg: Springer-Verlag*, 627p.

SMITH, J.V., 1974b. Feldspar minerals. vol. 2: Chemical and textural properties. *Heidelberg: Springer-Verlag*, 690p.

STEIN, H.J. & CROCK, J.G., 1990. Late Cretaceous-Tertiary magmatism in the Colorado Mineral Belt: rare earth elements and samarium-neodymium isotopic studies. *in* ANDERSON, J.L. (ed) "The nature of origin of Cordilleran magmatism", *Geol. Soc. Am. Mem.*, 174, 195-224.

STEINER, J.C., JAHNS, R.H. & LUTH, W.C., 1975. Crystallisation of alkali feldspar and quartz in the haplogranite system $NaAlSi_3O_8$-$KAlSi_3O_8$-SiO_2-H_2O at 4 kb. *Geol. Soc. Am. Bull.*, 86, 83-98.

ŠTEMPROK, M. & SULČEK, Z., 1969. Geochemical profile through an ore-bearing lithium granite. *Econ. Geol.*, 64, 392-404.

STONE, M. & AUSTIN, W.G.C., 1961. The metasomatic origin of the potash feldspar megcryststs in the granites of southwest England. *J. Geol.*, 69, 464-472.

STONE, M. & EXLEY, C.S. 1984. High heat production granites of Southwest England and their associated mineralisation: a review. *Trans. Miner. Metall.*, B25-B36.

STONE, M. & EXLEY, C.S., 1985. High heat production granites of southwest England and their associated mineralisation: a review. *in* "High heat production (HHP) granites, hydrothermal circulation and ore genesis", *Inst. Min. Metall.*, 571-593.

STRECKEISEN, A.L., 1976. To each plutonic rock its proper name. *Earth Sci. Rev.*, 12, 1-33.

STRONG, D.F., 1980. granitoid rocks and associated mineral deposits of eastern Canada and western Europe. *in* STRANGWAY, D.W. (ed), The continental crust and its mineral deposits. *Geol. Soc. Can. Spec. Pap.*, 20, 741-769.

STRONG, D.F., 1988. A review and model for granite-related mineral deposits. *in* TAYLOR, R.P. and STRONG, D.F. (eds) "Recent advances in the geology of granite-related mineral deposits". *Can. Inst. Min. Metall. Spec.*, 39, 424-445.

STRUCTURE RESEARCH GROUP, NANLING PROGRAMME 1988. Research into the regional structural characteristics and their controls on rock-formation and mineralization. *Geol. Press* (in Chinese with English abstract)

SUN, S., LI, J.L., CHEN, H.H., PENG, H.P., HSÜ, K.J. & SHELTON, J.W., 1989. Mesozoic and Cenozoic sedimentary history of South China. *AAPG*, 73, 1247-1269.

SUN, S.S. & EADINGTON, P.J., 1987. Oxygen isotope evidence for the mixing of magmatic and meteoric waters during tin mineralisation in the Mole Granite, New South Wales, Australia. *Econ. Geol.*, 82, 43-52.

TAYLOR, J.R. & WALL, V.J. 1984. The mobilisation of tin from granitoid magmas. *27th IGC*, IV (9), 474.

TAYLOR, R.G., 1979. Geology of tin deposits. *Elsevier*, 534p.

TAYLOR, R.G. & POLLARD, P.J., 1988. Pervasive hydrothermal alteration in tin-bearing granites and implications for the evolution of ore-bearing magmatic fluids. *in* TAYLOR, R.P. and STRONG, D.F. (eds) "Recent Advances in the Geology of Granite Related Mineral Deposits", *Can. Inst. Metall., Spec.*, 39, 86-95.

TAYLOR, R.P., 1992. Petrological and geochemical characteristics of the Pleasant Ridge zinnwaldite-topaz granite, southern New Brunswick, and comparisons with other topaz-bearing felsic rocks. *Can. Mineral.*, 30, 895-921.

TAYLOR, R.P. & FRYER, B.J., 1982. Rare earth element geochemistry as an aid to interpreting hydrothermal ore deposits. *in* EVANS, A.M. (ed), Metallisation associated with acid magmatism. 6. *John Wiley & Sons*, Chichester, England, 357-365.

TAYLOR, R.P. & FRYER, B.J., 1983. Rare earth element lithogeochemistry of granitoid mineral deposits. *Can. Inst. Min. Metall.*, 76, 74-84.

TAYLOR, S.R. & McCLENNAN, S.M., 1985. The continental Crust: its composition and evolution. *Blackwell Scientific Publications*, 312p.

THORDE, H.G., MONSTER, J. & DUNFORD, H.B., 1961. Sulphur isotope geochemistry. *Geochim. Cosmochim. Acta*, 25, 150-174.

TINGLE, T.N. & FENN, P.M., 1984. Transport and concentration of molybdenum in granite and molybdenite system: effects of fluorine and sulphur. *Geology*, 12, 156-158.

TISCHENDORF, G., 1977. Geochemical and petrographical characteristics of silicic magmatic rocks associated with rare element mineralisation. *in* ŠTEMPROK, M., BURNOL, I. and TISCHENDORF, G. (eds) "Mineralisation Associated with Acid Magmatism", Volume 2. *Geol. Survey Prague*, 41-98.

TU, G.C., WANG, L.K. & YU, X.Y., 1980. Genesis of granitic rocks and related mineralisation in South China. *in* Ishihara, S. & Takanouchi, S. (eds) "Granitic magmatism and related mineralisation", *Mining Geol.*, Spec. Issue No.8, 189-196.

TUTTLE, O.F. & BOWEN, N.L., 1958. Origin of granite in the light of experimental studies in the

system $NaAlSi_3O_8$-$KAlSi_3O_8$-SiO_2-H_2O. *Geol. Soc. Am. Mem.*, 74, 153p.

URABE, T., 1985. Aluminous granite as a source magma of hydrothermal ore deposits: a experimental study. *Econ. Geol.*, 80, 148-157.

VIDAL, P., COCERIE, A. & LE FORT, P., 1982. Geochemical investigations of the origin of the Manaslu leucogranite (Himalaya, Nepal). *Geochim. Cosmochim. Acta*, 46, 2279-2292.

VON GRUENEWALDT, G. & STRYDOM, J.H., 1985. Geochemical distribution patterns surrounding tin-bearing pipes and the origin of the mineralising fluids at Zaaplaats tin mine, Potgietersrus District. *Econ. Geol.*, 80, 1201-1211.

WANG, C.S., FOSTER, R.P., CROUDACE, I.W. XIA, W.H. & ZHANG, J.T., 1991. Multiphase metalliferous mineralisation associated with the Mesozoic Jianfengling granite complex, Hunan Province, P.R. China. *in* PAGEL, M. and LEROY, J.L. (eds) "Source, Transport and Deposition of Metals" -- Proceedings of the 25th SGA anniversary metting, Nancy, France, Aug.30-Sept.3, 1991. *A.A. Balkema*, 833-837.

WANG, H.Z., 1978. On the subdivision of the stratigraphic provinces of China. *Acta Strat. Sinica*, 2 (2), 81-104 (in Chinese with English abstract).

WANG, H.Z., 1981. Geotectonic units of China from the viewpoint of mobilism. *Earth Sciences -- J. Wuhan coll. Geol.*, (1), 42-66 (in Chinese with English abstract)

WANG, H.Z., 1986. Introduction to the stratigraphy of China. *in* Yang, Z.Y., Cheng, Y.Q. & Wang, H.Z. (eds): The geology of China, *Clarence Press, Oxford*, 11-15.

WANG, X.C., 1945. Geological report on tin and arsenic mineralisation in Xianghualing area, Hunan Province. *Internal report* (in Chinese).

WASTON, E.B., 1976. Two liquid partition coefficients: experimental data and geochemical implications. *Contrib. Mineral. Petrol.*, 56, 119-134.

WEBSTER, J.D., 1990. Portioning of F between H_2O and CO_2 fluids and topaz rhyolite melt -- implication for mineralizing magmatic hydrothermal fluids in F-rich granitic systems. *Contrib. Mineral. Petrol.*, 104, 428-438.

WEBSTER, J.D. & DUFFIELD, W.A., 1991. Volatiles and lithosphile elements in Taylor Creek Rhyolite: constraints from glass inclusion analysis. *Am. Mineral.*, 76, 1628-1645.

WEBSTER, J.D. & HOLLOWAY, J.R., 1988. Experimental constraints on the partitioning of Cl between topaz rhyolite melt and H_2O and H_2O + CO_2 fluids: new indications for granitic differentiation and ore deposition. *Geochim. Cosmochim. Acta*, 52, 2091-2105.

WEBSTER, J.D., HOLLOWAY, J.R. & HERVIG, R.L., 1987. Phase equilibria of a Be, U and F-riched vitrophyre from Spor Mountain, Utah. *Geochim. Cosmochim. Acta*, 51, 389-402.

WEBSTER, J.D., HOLLOWAY, J.R. & HERIGE, R.L., 1989. Partitioning of lithosphile trace elements between H_2O and H_2O + CO_2 fluids and topaz rhyolite melt. *Econ. Geol.*, 84, 116-134.

WEI, L., 1915. Geological report on tin mineralisation in Xianghualing area, Hunan Province.

Internal report (in Chinese).

WEIDNER, J.R. & MARTIN, R.F., 1987. Phase equilibria of a fluorine-rich leucogranite from the St. Austell pluton, Cornwall. *Geochim. Cosmochim. Acta*, **51**, 1591-1597.

WESOLOWSKI, D. & OHMOTO, H., 1986. Calculated oxygen isotope fractionation factors between water and the minerals scheelite and powellite. *Econ. Geol.*, **81**, 471-477.

WHALEN, J.B., CURRIE, K.L. & CHAPPELL, B.W., 1987. A-type granites: geochemical characteristics, discrimination and petrogenesis. *Contrib. Mineral. Petrol.*, **95**, 407-419.

WHITE, A.J.R. & CHAPPELL, B.W., 1988. Some supracrustal (S-type) granites of the Lachlan Fold Belt. *Trans. Royal Soc. Edinb.: Earth Sci.*, **79**, 71-86.

WHITE, A.J.R., CLEMENS, J.D., HOLLOWAY, J.R., SILVER,L.T., CHAPPELL, B.W. & WALL, V.J. 1986. S-type granites and their probable absence in southeastern North America. *Geology*, **15**, 115-118.

WHITNEY, J.A., 1975. Vapour generation in a quartz monzonite magma: a systematic model with application to porphyry copper deposits. *Econ. Geol.*, **70**, 346-358.

WILKINSON, J.J., 1990. The origin and evolution of Hercynian crustal fluids, South Cornwall, England. Ph.D thesis, University of Southampton, Southampton, U.K. 336p.

WILSON, G.A. & EUGSTER, H.P., 1984. Cassiterite solubility and tin chloride speciation in supercritical solutions. *Geol. Soc. Am. Abstr. Prog.*, **16**, 696.

WILSON, M., 1989. Igneous petrology -- a global tectonic approach. *Unwin Hyman*, 466p.

WITT, W.K., 1988. Evolution of the high-temperature hydrothermal fluids associated with greisenisation and feldspathic alteration of a tin-mineralisation granite, Northeast Queensland. *Econ. Geol.*, **83**, 310-334.

WOOD, S.A., CRERAR, D.A. & BORCSIK, M.P., 1987. Solubility of the assemblage pyrite-pyrrhotite-magnetite-sphalerite-galena-gold-stibnite-bismuthinite-argentite-molybdnite in H_2O-NaCl-CO_2 solutions from 200-350°C. *Econ. Geol.*, **82**, 1864-1887.

WOOD, S.A. & VLASSOPOULOS, D., 1989. Experimental determination of the hydrothermal solubility and speciation of tungsten at 500°C and 1 kbar. *Geochim. Cosmochim. Acta*, **53**, 303-312.

WYLLIE, P.J. & TUTTLE, O.F., 1961. Experimental investigation of silicate systems containing two volatile components. II. The effects of NH_3 and HF, in addition to H_2O on the melting temperatures of albite and granite. *Am. J. Sci.*, **262**, 128-143.

WYLLIE, P.J. & TUTTLE, O.F., 1964. Experimental investigation of silicate systems containing two volatile components. III. The effects of SO_3, P_2O_5, HCl and Li_2O, in addition to H_2O on the melting temperatures of albite and granite. *Am. J. Sci.*, **262**, 930-939.

XIA, W.H. & CHEN, Z.Y., 1984. The discovery of melt inclusions in topaz and quartz and its significance to genesis of Nb-Ta granites in southern China. *Earth Sci. — J. Wuhan Coll. Geol.*, **25** (2), 79-83 (in Chinese with English abstract).

XIA, W.H., ZHANG, J.T., FANG, Z.W. & CHEN, Z.Y., 1989. On the mechanism of rock-formation and mineralisation of rare-metal granites in Nanling area, South China. *China University of Geosciences Press, Wuhan* (in Chinese with English abstract).

XU, K.Q., ZHU, J.C., & XU, J.C., 1987. Geological environment and geochemical differences of W, Sn, Nb/Ta-bearing granites and related mineral deposits in South China. *Report on the 4th Int. Symp. IGCP Project 220 (abstr.), Oct. 21-26, 1987, Guilin, China*, 194-197.

XU, Q.D., 1989. Genesis and geological significance of feldspars in Limu granite, Guangxi. *Minerals and Rocks*, 9 (1), 15-25 (in Chinese with English abstract).

YAN, M.Z., WU, Y.L. & LI, C.Y., 1980. Metallogenetic systems in Southeast China and their mineralisation. *in* Ishihara, S. & Takanouchi, S. (eds) "Granitic Magmatism and Related Mineralisation", *Mining Geol. Spec.*, No.8, 215-221.

YUAN, K.R., WANG, Y.M., YANG, X.Y. & LIU, J.Y., 1986. Hidden granites and exploration of deep ore deposits. *Science Press, Beijing* (in Chinese with English abstract).

ZEN, E-AN., 1986. Aluminum enrichment in silicate melts by fractional crystallisation: some mineralogic and petrographic constraints. *J. Petrol.*, 27, 1095-1117.

ZEN, E-AN., 1988. Phase relations of peraluminous granitic rocks and their petrogenetic implications. *Ann. Rev. Earth Planet. Sci.*, 16, 21-51.

ZHANG, J.T. & XIA, W.H., 1988. Topaz-alkali feldspar granite and its ore deposits. *Geosci. Techn. Inform.*, 7 (4), 77-84 (in Chinese with English abstract).

ZHANG, Z.M., LIOU, J.G. & COLEMAN, R.G., 1984. An outline of the plate tectonics of China. *Geol. Soc. Am. Bull.*, 95, 295-312.

ZHOU, L.W., 1982. The relationships of REE, Nb, Ta, mineralisation and potash feldspar- and alkaline feldspar-granites. *Geol. Prosp.*, 12, 12-15 (in Chinese).

ZHU, J.C. & XU, S.J., 1989. REE patterns tin and tungsten-bearing granites in South China and their petrogenetic implications. *Mineral Deposits*, 8 (3), 21-31 (in Chinese with English abstract).

ZUSSMAN, J., 1977. Physical methods in determinative mineralogy. 2nd edition, Academic Press, London, 720p.

APPENDICES

APPENDIX I

GEOLOGICAL MAP OF XIANGHUAPU, HUNAN PROVINCE, P. R. CHINA

(in the pocket)

APPENDIX II. LIST OF SAMPLES USED IN THIS STUDY

1. Granitic rocks

Intrusion	Sample	Location on the map	Description
A	CK3-23	Sampling location CK3	Medium-grained biotite granite
	CK3-24	"	"
	CK3-25	"	"
	CK3-27	"	"
	CK3-28	"	"
	CK3-29	"	"
	CK3-31	"	"
	CK3-32	"	"
	125-3	Sampling location 125	Medium- to coarse-grained biotite granite
	125-5	"	"
B	CK3-20	Sampling location CK3	Medium-grained albite granite
	CK3-21	"	slightly altered albite granite
	CK3-22	"	strongly altered albite granite
	96-1	Sampling location 96	Medium-grained to slightly porphyritic
	97-1	Sampling location 97	albite granite
	98-2	Sampling location 98	"
C	CK4-3	Sampling location CK4	Fine- to medium-grained albite granite
	CK4-4	"	"
	CK4-5	"	"
D	430-1	Level 430, Xianghuapu	Medium-grained biotite granite
	430-3	deposit	"
	430-5	"	"
	430-6	"	"
	480-2	Level 480, Xianghuapu	"
	480-6	deposit	"
	95	Sampling location 95	"
	100-1	Sampling location 100	"
	107-10	Sampling location 107	"
	107-11	"	"
	109	Sampling location 109	"
	138-15	Sampling location 138	"
	138-16	"	"
	140-11	"	"
	86028	Level 480, XHP deposit	"
E	430-2	Level 430, XHP deposit	Fine-grained biotite granite
	430-4	"	Medium-grained biotite granite
	480-1	Level 480, XHP deposit	"
	480-3	"	"
	480-4	"	Fine-grained biotite granite
	480-5	"	"
	101-9	Sampling location 101	Medium-grained biotite granite
	101-15	"	"
	101-16	"	"
	101-17	"	"
	86045	level 480, XHP deposit	"

2. Pegmatitic rocks

Sample	Location	Description
101-5	Sampling location 101, within	Pegmatite containing sulphides
101-6	the pegmatitic pod	Pegmatite containing topaz
104	Sampling location 104	Pegmatite, intrusion D
105	Sampling location 105	Quartz shell, intrusion D
118-3	Sampling location 118	Pegmatite vein, intrusion B
120-7	Sampling location 120	Quartz shell, intrusion E
143-3	Sampling location 143	Quartz-topaz pegmatite, intrusion D

3. Fluorite-scheelite ores

Sample	Location	Description
III_{3-4}	Level 480, orebody III, XHPD	Massive fluorite-scheelite ore
III_{3-14}	"	Massive calcite
III_{3-15}	"	"
III_{3-17}	"	"
III_{3-18}	"	"
III_{4-2}	Level 450, orebody III, XHPD	"
III_{4-3}	"	"
III_{4-5}	Level 430, orebody III, XHPD	"
III_{4-6}	"	"
390-6	Level 480, orebody III, XHPD	Massive calcite

4. Galena-sphalerite ores

Sample	Location	Description
101-5	Sampling location 101	Massive Gal + Sph in pegmatitic pod
104-15	Sampling location 104	Disseminated in pegmatite zone, intrusion E
S-1	Shuanglian adit	Disseminated in greisen zone, intrusion E
S-4	"	"
III'_{2-2}	Level 480, orebody III, XHPD	Sph + Gal vein, level 480, orebody III, XHPD
D_{W-8}	Orebody II, Dongshan deposit	Massive Gal + Sph in W-F ore, Dongshan
B_{324-1}	Level 324, Baojingshan deposit	Massive sulphide lode, Baojinshan deposit
M_{4-15}	orebody II, level 4, Meishi deposit	Massive sulphide lode, Meishi deposit
M_{4-19}	"	"
M_{4-31}	orebody II, level 4, Meishi deposit	"
M_{5-4}	Level 5, Meishi deposit	Massive sulphide pod, Meishi deposit
M_{5-5}	"	"

PAGE NUMBERING AS ORIGINAL

APPENDIX III

SAMPLE PREPARATION AND XRF ANALYSIS TECHNIQUE

In order to investigate the major and trace element compositions of the different intrusions and establish the relationship between the various forms of mineralisation and their wall-rocks, 75 samples which comprise 50 granite rocks and 25 wall-rocks have been carefully selected from the 250 samples collected from the five different intrusions and the country rocks related to the various types of mineralisation. The procedures of preparing the samples for the geochemical analyses are described below, the whole data sets of the analyses are presented in Appendices V and VI.

These samples were first cut by a Cu-Co alloy saw in the Department of Geology. About 1/4 to 1/3 of each sample was kept as hand specimen, and three chips of size 2cm x 3cm were reserved for making thin, polished and fluid inclusion sections. After being crushed into small fragments with a steel jaw crusher, each sample was randomly divided into two equal portions. One was ground into 200 mesh powder with a tungsten-carbide mill and the other was ground by a hardened steel mill. These procedures were carried out to minimise contaminations of tungsten and iron from these mills. The tungsten-carbide-mill-ground samples were used for major-element determinations and the steel-mill-ground samples were taken for trace-element analyses.

Pellets were made for trace element analyses by mixing 10-15 grams of the steel-mill-ground powder from each sample with 10-15 drops of PVA binding liquid and compressing the mixture under 10-15 atm. in a liquid-pressure pumper. Then, these pellets were marked, dried, bagged, and ready to be analyzed.

The procedures for making beads for major element analyses are briefly outlined as follow:

About 5 grams of the tungsten-carbide-mill ground powder from each sample were first dried at 110°C for 2-3 hours in an oven to remove the absorbing water contained in the powder.

After being cooled for 5-10 minutes in a desiccator, the powder was then transferred into a clean silica crucible and weighed precisely. The crucible was then placed in a furnace pre-set at 1000°C for 6 hours to remove all volatile components (such as H2O, Cl, F and B). The ignited powder was transferred into a desiccator after being cooled in air for 5-8 minutes and was accurately reweighed when it was cooled down to room temperature. The difference of these two weights was recorded as the loss of ignition (LOI).

The ignited powder was mixed in a platinum dish with cool, pre-ignited 100B flux, which makes the

melting more easily and quickly, in a ratio of 1:5. The platinum dish containing the mixture was placed in a high temperature furnace pre-set at 1200°C for 10-15 minutes. In order to get a homogeneous bead, the melt was swirled periodically. It was then poured into a platinum mould while in the furnace. The mould was carefully removed from the furnace and transferred to a position where cooling was assisted by a jet of air. Finally, a satisfactory bead was produced.

The beads and pellets were used for the major and trace element analyses respectively. These analyses were carried out on the Philips 1400 X-ray fluorescence spectrometer (XRF) in this Department. 13 major elements and 27 trace elements for each sample have been analyzed.

APPENDIX IV

SEM (Or, Ab, Bi) DATA SET

1 Plagioclase (albite)

			wt%							formulae based on 8 oxygen atoms							end-member		
			SiO2	Al2O3	FeO	MgO	CaO	K2O	Na2O	Si	Al	Fe	Mg	Ca	K	Na	ab	or	an
Group 1	CK3-20	1	67.90	20.83				0.17	11.10	3.29	0.59	0.00	0.00	0.00	0.01	1.04	99.0	1.0	0.0
		2	66.71	19.87			0.12	0.23	13.07	3.26	0.57	0.00	0.00	0.01	0.01	1.24	98.4	1.1	0.5
		3	66.47	21.41				0.31	11.80	3.25	0.62	0.00	0.00	0.00	0.02	1.12	98.3	1.7	0.0
		4	66.13	21.03				0.25	12.60	3.24	0.61	0.00	0.00	0.00	0.02	1.20	98.7	1.3	0.0
		5	66.72	21.05				0.13	12.10	3.26	0.61	0.00	0.00	0.00	0.01	1.15	99.3	0.7	0.0
		6	67.34	19.92					12.73	3.27	0.57	0.00	0.00	0.00	0.00	1.20	100.0	0.0	0.0
		7	69.05	18.73				0.17	12.05	3.32	0.53	0.00	0.00	0.00	0.01	1.12	99.1	0.9	0.0
		8	67.27	18.67			0.16	0.38	13.51	3.27	0.53	0.00	0.00	0.01	0.02	1.27	97.6	1.8	0.6
		9	68.73	19.14				0.11	12.01	3.31	0.54	0.00	0.00	0.00	0.01	1.12	99.4	0.6	0.0
		10	67.14	20.42				0.14	12.30	3.27	0.59	0.00	0.00	0.00	0.01	1.16	99.3	0.7	0.0
		11	68.79	19.73			0.12		11.36	3.31	0.56	0.00	0.00	0.01	0.00	1.06	99.4	0.0	0.6
		12	69.03	19.32				0.19	11.46	3.32	0.55	0.00	0.00	0.00	0.01	1.07	98.9	1.1	0.0
	98-2	1	68.32	19.65			0.22	0.17	11.64	3.30	0.56	0.00	0.00	0.01	0.01	1.09	98.0	0.9	1.0
		2	67.38	19.72				0.41	12.48	3.28	0.56	0.00	0.00	0.00	0.03	1.18	97.9	2.1	0.0
		3	69.49	19.03				0.26	11.23	3.33	0.54	0.00	0.00	0.00	0.02	1.04	98.5	1.5	0.0
		4	67.88	18.97				0.37	12.78	3.29	0.54	0.00	0.00	0.00	0.02	1.20	98.1	1.9	0.0
		5	66.37	19.62			0.20	0.46	13.35	3.25	0.57	0.00	0.00	0.01	0.03	1.27	97.0	2.2	0.8
		6	67.93	19.83				0.15	12.09	3.29	0.57	0.00	0.00	0.00	0.01	1.14	99.2	0.8	0.0
		7	67.15	20.71			0.13	0.14	11.87	3.27	0.59	0.00	0.00	0.01	0.01	1.12	98.6	0.8	0.6
		8	68.57	18.94				0.16	12.34	3.31	0.54	0.00	0.00	0.00	0.01	1.15	99.2	0.8	0.0
	CK4-4	1	67.83	18.93			0.15	0.34	12.75	3.29	0.54	0.00	0.00	0.01	0.02	1.20	97.7	1.7	0.6
		2	68.94	18.94			0.34	0.16	11.62	3.32	0.54	0.00	0.00	0.02	0.01	1.08	97.5	0.9	1.6
		3	66.39	20.67			0.10	0.31	12.52	3.25	0.60	0.00	0.00	0.00	0.02	1.19	98.0	1.6	0.4
		4	68.73	19.74				0.11	11.42	3.31	0.56	0.00	0.00	0.00	0.01	1.07	99.4	0.6	0.0
		5	66.91	20.32			0.16	0.23	12.38	3.26	0.58	0.00	0.00	0.01	0.01	1.17	98.1	1.2	0.7
		6	66.58	21.73			0.16	0.14	11.39	3.25	0.63	0.00	0.00	0.01	0.01	1.08	98.4	0.8	0.8
		7	67.79	19.92				0.26	12.03	3.29	0.57	0.00	0.00	0.00	0.02	1.13	98.6	1.4	0.0
		8	67.28	19.95			0.21	0.18	12.38	3.27	0.57	0.00	0.00	0.01	0.01	1.17	98.1	0.9	0.9
		9	68.17	18.72			0.12	0.36	12.63	3.30	0.59	0.00	0.00	0.01	0.02	1.18	97.7	1.8	0.5
		10	69.02	18.94			0.10	0.27	11.68	3.32	0.54	0.00	0.00	0.01	0.02	1.09	98.0	1.5	0.5
		11	67.29	21.05				0.42	11.24	3.28	0.60	0.00	0.00	0.00	0.03	1.06	97.6	2.4	0.0
Group 2	CK3-24	1	67.28	21.31			0.12	0.23	11.06	3.27	0.61	0.00	0.00	0.01	0.01	1.04	98.1	1.3	0.6
		2	68.09	20.94	0.15		0.14	0.15	10.53	3.30	0.60	0.01	0.00	0.01	0.01	0.99	98.4	0.9	0.7
		3	69.03	20.24			0.25	0.12	10.36	3.32	0.57	0.00	0.00	0.01	0.01	0.97	97.9	0.7	1.3
		4	67.93	21.03		0.18	0.24		10.62	3.29	0.60	0.00	0.01	0.01	0.00	1.00	98.8	0.0	1.2
	CK3-27	1	67.73	21.17			0.25		10.85	3.28	0.61	0.00	0.00	0.01	0.00	1.02	98.7	0.0	1.3
		2	68.58	20.41				0.32	10.69	3.31	0.58	0.00	0.00	0.00	0.02	1.00	98.1	1.9	0.0
		3	67.99	21.00				0.32	10.69	3.29	0.60	0.00	0.00	0.00	0.02	1.00	98.1	1.9	0.0
		4	69.17	19.96				0.26	10.61	3.32	0.57	0.00	0.00	0.00	0.02	0.99	98.4	1.6	0.0
		5	67.22	20.36	0.85		0.21	0.14	11.22	3.27	0.58	0.03	0.00	0.01	0.01	1.06	98.2	0.8	1.0
	125-5	1	67.82	20.05	0.23	0.21	0.17	0.28	11.24	3.29	0.57	0.01	0.02	0.01	0.02	1.06	97.6	1.6	0.8
		2	66.46	20.10	0.47	0.36		0.18	12.43	3.25	0.58	0.02	0.03	0.00	0.01	1.18	99.1	0.9	0.0
		3	66.94	19.87				0.14	13.05	3.26	0.57	0.00	0.00	0.00	0.01	1.23	99.3	0.7	0.0
		4	65.72	21.04			0.31		12.93	3.23	0.61	0.00	0.00	0.02	0.00	1.23	98.7	0.0	1.3
		5	65.77	20.46	0.56		0.19		13.02	3.23	0.59	0.02	0.00	0.01	0.00	1.24	99.2	0.0	0.8

			SiO2	Al2O3	FeO	MgO	CaO	K2O	Na2O	Si	Al	Fe	Mg	Ca	K	Na	ab	or	an
Group 2	430-3	1	65.46	21.27			0.57	0.25	12.45	3.22	0.62	0.00	0.00	0.03	0.02	1.19	96.3	1.3	2.4
		2	66.87	21.29			0.16		11.68	3.26	0.61	0.00	0.00	0.01	0.00	1.10	99.2	0.0	0.8
		3	66.46	20.84			0.25		12.44	3.25	0.60	0.00	0.00	0.01	0.00	1.18	98.9	0.0	1.1
		4	65.39	21.38			0.17		13.05	3.22	0.62	0.00	0.00	0.01	0.00	1.25	99.3	0.0	0.7
		5	65.54	20.93	0.44	0.67			12.42	3.22	0.61	0.02	0.05	0.00	0.00	1.18	100.0	0.0	0.0
		6	66.13	20.45			0.23	0.31	12.88	3.24	0.59	0.00	0.00	0.01	0.02	1.22	97.5	1.5	1.0
	480-6	1	66.90	20.13		0.37	0.51	0.16	11.93	3.26	0.58	0.00	0.03	0.03	0.01	1.13	96.9	0.9	2.3
		2	65.71	19.83		0.26	0.58	0.27	13.35	3.22	0.57	0.00	0.02	0.03	0.02	1.27	96.4	1.3	2.3
		3	65.87	21.27			0.25	0.36	12.25	3.23	0.62	0.00	0.00	0.01	0.02	1.17	97.0	1.9	1.1
		4	65.23	20.87	0.23	0.43	0.56		12.68	3.21	0.60	0.01	0.03	0.03	0.00	1.21	97.6	0.0	2.4
	480-7	1	66.42	21.39				0.17	12.02	3.25	0.62	0.00	0.00	0.00	0.01	1.14	99.1	0.9	0.0
		2	66.64	20.48				0.31	12.57	3.26	0.59	0.00	0.00	0.00	0.02	1.19	98.4	1.6	0.0
		3	69.15	19.57			0.18	0.26	10.84	3.32	0.55	0.00	0.00	0.01	0.02	1.01	97.6	1.5	0.9
		4	68.77	19.94			0.23		11.06	3.31	0.57	0.00	0.00	0.01	0.00	1.03	98.9	0.0	1.1
		5	68.13	21.03			0.28	0.19	10.37	3.30	0.60	0.00	0.00	0.01	0.01	0.97	97.4	1.2	1.5
		6	67.94	20.87			0.27		10.92	3.29	0.60	0.00	0.00	0.01	0.00	1.03	98.7	0.0	1.3
	138-15	1	67.79	21.25			0.14	0.28	10.54	3.29	0.61	0.00	0.00	0.01	0.02	0.99	97.6	1.7	0.7
		2	69.23	20.06				0.15	10.56	3.33	0.57	0.00	0.00	0.00	0.01	0.98	99.1	0.9	0.0
		3	67.32	20.94			0.39	0.21	11.14	3.27	0.60	0.00	0.00	0.02	0.01	1.05	96.9	1.2	1.9
		4	66.58	21.31			0.42	0.12	11.57	3.25	0.61	0.00	0.00	0.02	0.01	1.10	97.4	0.7	2.0
		5	65.49	21.27			0.40	0.37	12.46	3.22	0.62	0.00	0.00	0.02	0.02	1.19	96.4	1.9	1.7
		6	65.88	20.92				0.13	13.07	3.23	0.61	0.00	0.00	0.00	0.01	1.24	99.3	0.7	0.0
		7	66.57	20.57			0.12		12.74	3.25	0.59	0.00	0.00	0.01	0.00	1.21	99.5	0.0	0.5
		8	66.93	20.13			0.21	0.32	12.41	3.26	0.58	0.00	0.00	0.01	0.02	1.17	97.4	1.7	0.9
	430-4	1	68.15	19.90	0.43		0.37		11.14	3.30	0.57	0.02	0.00	0.02	0.00	1.04	98.2	0.0	1.8
		2	69.57	19.21		0.53	0.29		10.41	3.33	0.54	0.00	0.04	0.01	0.00	0.97	98.5	0.0	1.5
		3	67.13	21.09			0.15	0.26	11.37	3.27	0.61	0.00	0.00	0.01	0.02	1.07	97.8	1.5	0.7
		4	66.94	21.87	0.48		0.47		10.24	3.26	0.63	0.02	0.00	0.02	0.00	0.97	97.5	0.0	2.5
		5	67.39	20.77			0.12	0.19	11.53	3.28	0.59	0.00	0.00	0.01	0.01	1.09	98.4	1.1	0.6
		6	68.23	21.41			0.17	0.13	10.05	3.30	0.61	0.00	0.00	0.01	0.01	0.94	98.2	0.8	0.9
		7	67.92	21.19		0.21		0.17	10.51	3.29	0.60	0.00	0.02	0.00	0.01	0.99	98.9	1.1	0.0
		8	67.58	20.73			0.30	0.23	11.16	3.28	0.59	0.00	0.00	0.02	0.01	1.05	97.2	1.3	1.4
		9	67.49	20.13				0.31	12.07	3.28	0.58	0.00	0.00	0.00	0.02	1.14	98.3	1.7	0.0
		10	66.88	21.08			0.33	0.27	11.44	3.26	0.61	0.00	0.00	0.02	0.02	1.08	96.9	1.5	1.5
		11	67.27	20.98			0.34	0.18	11.23	3.27	0.60	0.00	0.00	0.02	0.01	1.06	97.3	1.0	1.6
	480-1	1	69.15	19.76			0.35		10.74	3.32	0.56	0.00	0.00	0.02	0.00	1.00	98.2	0.0	1.8
		2	68.77	19.45			0.41	0.33	11.04	3.31	0.55	0.00	0.00	0.02	0.02	1.03	96.1	1.9	2.0
		3	68.13	19.89			0.18	0.22	11.58	3.30	0.57	0.00	0.00	0.01	0.01	1.09	97.9	1.2	0.8
		4	67.94	19.38			0.37	0.27	12.04	3.29	0.55	0.00	0.00	0.02	0.02	1.13	96.9	1.4	1.6
		5	67.79	20.07					12.15	3.28	0.57	0.00	0.00	0.00	0.00	1.14	100.0	0.0	0.0
		6	69.23	19.74			0.21	0.19	10.63	3.33	0.56	0.00	0.00	0.01	0.01	0.99	97.8	1.1	1.1
	101-17	1	67.82	20.31			0.37	0.27	11.23	3.29	0.58	0.00	0.00	0.02	0.02	1.06	96.7	1.5	1.8
		2	67.58	20.70			0.40	0.28	11.03	3.28	0.59	0.00	0.00	0.02	0.02	1.04	96.5	1.6	1.9
		3	65.94	20.94			0.63	0.30	12.19	3.23	0.61	0.00	0.00	0.03	0.02	1.16	95.7	1.5	2.7
		4	66.78	19.74			0.25	0.22	13.01	3.26	0.57	0.00	0.00	0.01	0.01	1.23	97.9	1.1	1.0
		5	65.97	21.07			0.22	0.31	12.43	3.24	0.61	0.00	0.00	0.01	0.02	1.18	97.4	1.6	1.0
		6	65.93	21.42			0.22	0.26	12.17	3.24	0.62	0.00	0.00	0.01	0.02	1.16	97.7	1.4	1.0
		7	68.35	19.71			0.39	0.37	11.18	3.30	0.56	0.00	0.00	0.02	0.02	1.05	96.1	2.1	1.9
		8	68.57	19.82			0.30	0.29	11.02	3.31	0.56	0.00	0.00	0.02	0.02	1.03	96.9	1.7	1.5
		9	67.73	21.07				0.13	11.07	3.29	0.60	0.00	0.00	0.00	0.01	1.04	99.2	0.8	0.0

2 K-feldspar

			wt%							formulae based on 8 oxygen atoms							end-member		
			SiO2	Al2O3	FeO	MgO	CaO	K2O	Na2O	Si	Al	Fe	Mg	Ca	K	Na	ab	or	an
Group 1	CK3-20	1	62.73	20.84			0.23	15.62	0.58	3.24	0.64	0.00	0.00	0.01	1.03	0.06	5.3	93.6	1.2
		2	64.53	18.93			0.21	15.72	0.61	3.30	0.57	0.00	0.00	0.01	1.02	0.06	5.5	93.4	1.1
		3	62.52	19.95	0.18		0.30	16.37	0.68	3.24	0.61	0.01	0.00	0.02	1.08	0.07	5.9	92.7	1.4
		4	63.24	18.62				17.89	0.25	3.27	0.57	0.00	0.00	0.00	1.18	0.03	2.1	97.9	0.0
		5	64.13	18.79			0.30	16.33	0.46	3.29	0.57	0.00	0.00	0.02	1.07	0.05	4.1	94.5	1.5
		6	65.37	17.74	0.25		0.41	15.63	0.60	3.32	0.53	0.01	0.00	0.02	1.01	0.06	5.4	92.6	2.0
		7	63.14	18.88		0.10	0.30	16.92	0.66	3.26	0.57	0.00	0.01	0.02	1.12	0.07	5.5	93.1	1.4
		8	62.79	20.53	0.26	0.10	0.51	15.09	0.72	3.24	0.62	0.01	0.01	0.03	0.99	0.07	6.6	90.8	2.6
		9	62.39	20.47				16.73	0.41	3.24	0.63	0.00	0.00	0.00	1.11	0.04	3.6	96.4	0.0
		10	63.82	19.04				16.88	0.26	3.28	0.58	0.00	0.00	0.00	1.11	0.03	2.3	97.7	0.0
		11	65.27	17.82	0.12		0.34	15.71	0.74	3.32	0.53	0.00	0.00	0.02	1.02	0.07	6.6	91.8	1.7
	98-2	1	64.38	18.73	0.24	0.16	0.10	15.62	0.77	3.29	0.56	0.01	0.01	0.01	1.02	0.08	6.9	92.6	0.5
		2	63.57	20.04				15.86	0.53	3.27	0.61	0.00	0.00	0.00	1.04	0.05	4.8	95.2	0.0
		3	64.51	19.72				15.04	0.73	3.29	0.59	0.00	0.00	0.00	0.98	0.07	6.9	93.1	0.0
		4	64.28	19.83				15.71	0.18	3.29	0.60	0.00	0.00	0.00	1.03	0.02	1.7	98.3	0.0
		5	64.12	18.79	0.18	0.13		16.03	0.75	3.29	0.57	0.01	0.01	0.00	1.05	0.07	6.6	93.4	0.0
		6	65.17	17.82				16.52	0.50	3.32	0.53	0.00	0.00	0.00	1.07	0.05	4.4	95.6	0.0
		7	63.47	18.08	0.27	0.20	0.26	16.94	0.78	3.27	0.55	0.01	0.02	0.01	1.11	0.08	6.5	92.4	1.2
		8	63.48	18.55	0.24		0.20	16.78	0.74	3.27	0.56	0.01	0.00	0.01	1.10	0.07	6.2	92.9	0.9
	CK4-4	1	63.92	19.42				15.93	0.73	3.28	0.59	0.00	0.00	0.00	1.04	0.07	6.5	93.5	0.0
		2	63.46	19.82	0.38		0.15	15.43	0.76	3.26	0.60	0.02	0.00	0.01	1.01	0.08	6.9	92.3	0.8
		3	64.53	18.37				16.74	0.36	3.30	0.55	0.00	0.00	0.00	1.09	0.04	3.2	96.8	0.0
		4	63.92	18.06				17.47	0.55	3.29	0.55	0.00	0.00	0.00	1.15	0.05	4.6	95.4	0.0
		5	64.27	17.93			0.28	16.82	0.70	3.29	0.54	0.00	0.00	0.02	1.10	0.07	5.9	92.8	1.3
		6	62.93	20.32	0.20		0.25	15.57	0.72	3.25	0.62	0.01	0.00	0.01	1.03	0.07	6.5	92.3	1.2
		7	64.52	18.65				16.03	0.80	3.30	0.56	0.00	0.00	0.00	1.05	0.08	7.1	93.0	0.0
		8	63.94	18.84				16.58	0.64	3.28	0.57	0.00	0.00	0.00	1.09	0.06	5.5	94.5	0.0
Group 2	CK3-24	1	65.23	20.41				14.36		3.31	0.61	0.00	0.00	0.00	0.93	0.00	0.0	100.0	0.0
		2	65.90	20.67				5.58	7.85	3.27	0.60	0.00	0.00	0.00	0.35	0.76	68.1	31.9	0.0
		3	65.34	20.31				14.11	0.24	3.31	0.61	0.00	0.00	0.00	0.91	0.02	2.5	97.5	0.0
		4	65.92	19.97				14.10		3.33	0.59	0.00	0.00	0.00	0.91	0.00	0.0	100.0	0.0
		5	65.17	20.04				14.29	0.51	3.31	0.60	0.00	0.00	0.00	0.93	0.05	5.1	94.9	0.0
		6	65.38	20.17			0.30	13.78	0.37	3.31	0.60	0.00	0.00	0.02	0.89	0.04	3.9	94.4	1.7
		7	65.29	20.36				14.03	0.32	3.31	0.61	0.00	0.00	0.00	0.91	0.03	3.4	96.7	0.0
	CK3-27	1	63.36	18.48			0.27	17.59	0.30	3.27	0.56	0.00	0.00	0.01	1.16	0.03	2.5	96.3	1.2
		2	65.43	17.81			0.64	15.87	0.25	3.32	0.53	0.00	0.00	0.03	1.03	0.02	2.3	94.5	3.2
		3	62.28	19.55	0.71	0.41		16.88	0.17	3.24	0.60	0.03	0.03	0.00	1.12	0.02	1.5	98.5	0.0
		4	62.15	19.59	0.45	0.40		17.01	0.40	3.23	0.60	0.00	0.03	0.00	1.13	0.04	3.5	96.6	0.0
		5	62.93	19.43	0.15	0.32	0.41	16.39	0.37	3.25	0.59	0.00	0.02	0.02	1.08	0.04	3.3	94.8	2.0
		6	64.72	17.94	0.15		0.52	16.33	0.34	3.30	0.54	0.01	0.0	0.03	1.06	0.03	3.0	94.5	2.5
		7	65.14	18.63				15.94	0.29	3.32	0.56	0.00	0.00	0.00	1.03	0.03	2.7	97.3	0.0
		8	65.09	18.75				16.03	0.13	3.31	0.56	0.00	0.00	0.00	1.04	0.01	1.2	98.8	0.0
		9	64.82	19.21				15.84	0.14	3.31	0.58	0.00	0.00	0.00	1.03	0.01	1.3	98.7	0.0
	125-5	1	64.92	19.73				14.92	0.43	3.30	0.59	0.00	0.00	0.00	0.97	0.04	4.2	95.8	0.0
		2	65.27	20.07			0.51	13.73	0.42	3.30	0.60	0.00	0.00	0.03	0.89	0.04	4.3	92.8	2.9
		3	64.78	20.52				14.25	0.45	3.30	0.62	0.00	0.00	0.00	0.93	0.04	4.6	95.4	0.0
		4	63.92	19.74	0.12			15.69	0.53	3.28	0.60	0.01	0.00	0.00	1.03	0.05	4.9	95.1	0.0
		5	62.96	19.91				16.83	0.30	3.26	0.61	0.00	0.00	0.00	1.11	0.03	2.6	97.4	0.0
		6	64.23	19.72				15.83	0.22	3.29	0.60	0.00	0.00	0.00	1.03	0.02	2.1	97.9	0.0

			SiO2	Al2O3	FeO	MgO	CaO	K2O	Na2O	Si	Al	Fe	Mg	Ca	K	Na	ab	or	an
Group 2	430-3	1	64.28	19.68			0.20	15.41	0.43	3.29	0.59	0.00	0.00	0.01	1.01	0.04	4.0	94.9	1.0
		2	64.15	19.35			0.16	16.01	0.32	3.29	0.58	0.00	0.00	0.01	1.05	0.03	2.9	96.3	0.8
		3	63.53	20.03				16.44		3.27	0.61	0.00	0.00	0.00	1.08	0.00	0.0	100.0	0.0
		4	62.72	19.63			0.21	17.03	0.41	3.25	0.60	0.00	0.00	0.01	1.13	0.04	3.5	95.5	1.0
		5	62.64	19.82			0.14	16.71	0.69	3.25	0.61	0.00	0.00	0.01	1.11	0.07	5.9	93.5	0.7
		6	62.13	19.92	0.22		0.16	17.05	0.52	3.24	0.61	0.01	0.00	0.01	1.13	0.05	4.4	94.9	0.8
		7	64.47	19.36				16.01	0.16	3.30	0.58	0.00	0.00	0.00	1.04	0.02	1.5	98.5	0.0
		8	63.44	19.21			0.40	16.48	0.47	3.27	0.58	0.00	0.00	0.02	1.08	0.05	4.1	94.0	1.9
		9	64.09	18.96			0.43	15.83	0.69	3.28	0.57	0.00	0.00	0.02	1.03	0.07	6.1	91.8	2.1
		10	63.82	18.97			0.21	16.62	0.38	3.28	0.57	0.00	0.00	0.01	1.09	0.04	3.3	95.7	1.0
	430-6	1	65.22	19.64				14.80	0.34	3.31	0.59	0.00	0.00	0.00	0.96	0.03	3.4	96.6	0.0
		2	64.27	18.92	0.11		0.23	15.79	0.68	3.29	0.57	0.00	0.00	0.01	1.03	0.07	6.1	92.8	1.1
		3	63.48	18.73		0.27	0.46	16.34	0.72	3.27	0.57	0.00	0.02	0.03	1.07	0.07	6.1	91.7	2.2
		4	63.97	19.03			0.33	16.22	0.45	3.28	0.58	0.00	0.00	0.02	1.06	0.04	4.0	94.4	1.6
		5	62.36	19.85	0.14		0.12	17.27	0.26	3.24	0.61	0.01	0.00	0.01	1.15	0.03	2.2	97.2	0.6
		6	63.73	19.37	0.27	0.26	0.37	15.26	0.74	3.27	0.59	0.01	0.02	0.02	1.00	0.07	6.7	91.4	1.9
		7	64.58	17.82	0.24		0.30	16.54	0.52	3.30	0.54	0.01	0.00	0.02	1.08	0.05	4.5	94.1	1.4
		8	63.85	18.41			0.25	17.09	0.41	3.28	0.56	0.00	0.00	0.01	1.12	0.04	3.5	95.4	1.2
	480-7	1	62.53	19.93	0.35		0.49	16.02	0.68	3.24	0.61	0.02	0.00	0.03	1.06	0.07	5.9	91.7	2.4
		2	63.73	19.04				17.01	0.22	3.28	0.58	0.00	0.00	0.00	1.12	0.02	1.9	98.1	0.0
		3	64.21	17.73	0.14		0.30	16.92	0.71	3.29	0.54	0.01	0.00	0.02	1.11	0.07	5.9	92.7	1.4
		4	64.53	17.93		0.16	0.32	16.38	0.67	3.30	0.54	0.00	0.01	0.02	1.07	0.07	5.8	92.7	1.5
		5	64.90	18.02	0.15	0.30	0.49	15.41	0.73	3.30	0.54	0.01	0.02	0.03	1.00	0.07	6.6	91.0	2.4
		6	63.34	19.01				17.33	0.32	3.27	0.58	0.00	0.00	0.00	1.14	0.03	2.7	97.3	0.0
		7	64.52	18.51	0.20		0.29	16.04	0.43	3.30	0.56	0.01	0.00	0.02	1.05	0.04	3.9	94.7	1.4
	138-15	1	63.17	18.72			0.14	17.55	0.42	3.27	0.57	0.00	0.00	0.01	1.16	0.04	3.5	95.9	0.6
		2	63.58	18.22	0.13		0.36	17.13	0.57	3.28	0.55	0.01	0.00	0.02	1.13	0.06	4.7	93.6	1.7
		3	63.89	18.03			0.11	17.59	0.38	3.29	0.55	0.00	0.00	0.01	1.16	0.04	3.2	96.3	0.5
		4	64.74	17.92			0.29	16.38	0.67	3.30	0.54	0.00	0.00	0.02	1.07	0.07	5.8	92.9	1.4
		5	64.43	17.82			0.23	16.94	0.58	3.30	0.54	0.00	0.00	0.01	1.11	0.06	4.9	94.0	1.1
		6	63.28	19.05	0.16	0.23	0.65	15.93	0.70	3.26	0.58	0.01	0.02	0.04	1.05	0.07	6.1	90.8	3.1
		7	63.95	19.06			0.27	16.04	0.68	3.28	0.58	0.00	0.00	0.01	1.05	0.07	6.0	92.7	1.3
	430-4	1	63.73	19.52	0.10		0.18	16.06	0.41	3.28	0.59	0.0	0.00	0.01	1.05	0.04	3.7	95.4	0.9
		2	64.77	17.55	0.15		0.35	16.46	0.72	3.31	0.53	0.01	0.00	0.02	1.07	0.07	6.1	92.2	1.7
		3	64.34	17.14	0.25	0.24	0.63	16.63	0.77	3.29	0.52	0.01	0.02	0.03	1.09	0.08	6.4	90.7	2.9
		4	62.28	19.20	0.20		0.26	17.46	0.59	3.24	0.59	0.01	0.00	0.01	1.16	0.06	4.8	94.0	1.2
		5	63.72	19.13				16.84	0.31	3.28	0.58	0.0	0.00	0.00	1.11	0.03	2.7	97.3	0.0
		6	63.47	18.73			0.42	16.72	0.66	3.27	0.57	0.00	0.00	0.02	1.10	0.07	5.6	92.5	2.0
		7	63.27	18.92	0.45	0.20	0.48	16.05	0.62	3.26	0.57	0.02	0.02	0.03	1.05	0.06	5.4	92.3	2.3
		8	62.78	20.30	0.35		0.37	15.62	0.58	3.25	0.62	0.02	0.00	0.02	1.03	0.06	5.2	92.9	1.9
		9	62.92	20.17		0.24	0.30	15.68	0.69	3.25	0.61	0.00	0.02	0.02	1.03	0.07	6.2	92.3	1.5
		10	63.16	19.77				16.49	0.58	3.26	0.60	0.00	0.00	0.00	1.09	0.06	5.1	94.9	0.0
		11	65.23	17.63				16.82	0.32	3.32	0.53	0.00	0.00	0.00	1.09	0.03	2.8	97.2	0.0
	480-1	1	63.18	17.94	0.40	0.20	0.58	17.02	0.67	3.26	0.55	0.02	0.02	0.03	1.12	0.07	5.5	91.9	2.6
		2	62.15	20.14	0.22		0.28	16.68	0.53	3.23	0.62	0.01	0.00	0.02	1.11	0.05	4.6	94.1	1.3
		3	62.53	20.35				16.81	0.31	3.25	0.62	0.00	0.00	0.00	1.11	0.03	2.7	97.3	0.0
		4	63.52	19.51		0.10	0.30	15.94	0.63	3.27	0.59	0.00	0.01	0.02	1.05	0.06	5.6	93.0	1.5
		5	64.64	19.32				15.68	0.35	3.30	0.58	0.00	0.00	0.00	1.02	0.03	3.3	96.7	0.0
		6	65.13	17.83			0.47	16.02	0.56	3.31	0.53	0.00	0.00	0.03	1.04	0.06	4.9	92.8	2.3
	101-17	1	62.37	19.75	0.10		0.28	16.88	0.62	3.24	0.60	0.00	0.00	0.02	1.12	0.06	5.2	93.5	1.3
		2	64.44	18.85			0.36	15.77	0.58	3.29	0.57	0.00	0.00	0.02	1.03	0.06	5.2	93.0	1.8
		3	64.39	18.72			0.30	15.97	0.61	3.29	0.56	0.00	0.00	0.02	1.04	0.06	5.4	93.1	1.5
		4	62.82	20.33			0.34	15.93	0.58	3.25	0.62	0.00	0.00	0.02	1.05	0.06	5.2	93.2	1.7
		5	63.22	19.37				16.83	0.58	3.27	0.59	0.00	0.00	0.00	1.11	0.06	5.0	95.0	0.0
		6	62.27	19.97	0.10		0.31	16.72	0.63	3.24	0.61	0.00	0.00	0.02	1.11	0.06	5.3	93.2	1.5
		7	63.38	18.71	0.24		0.41	16.48	0.78	3.27	0.57	0.01	0.00	0.02	1.08	0.08	6.6	91.5	1.9
		8	63.71	18.36	0.16	0.20	0.52	16.34	0.71	3.27	0.56	0.01	0.02	0.03	1.07	0.07	6.0	91.5	2.5
		9	65.18	17.92	0.17		0.35	15.71	0.67	3.31	0.54	0.01	0.00	0.02	1.02	0.07	6.0	92.3	1.7

3 Mica

			SiO2	Al2O3	FeO	K2O	MgO	MnO	Na2O	CaO	SUM
Group 1	CK3-20	1	46.37	22.23	18.63	10.76	0.10	1.61	0.30		100.00
		2	51.29	24.35	14.62	9.59		0.15			100.00
		3	48.28	23.22	16.43	10.48		1.32	0.12	0.15	100.00
		4	44.74	20.36	20.62	10.76		1.68	1.66	0.18	100.00
		5	46.87	22.29	20.16	9.78		0.90			100.00
		6	48.38	23.16	18.07	9.49		0.90			100.00
		7	47.95	22.94	17.93	9.18		1.44	0.56		100.00
		8	46.32	23.36	19.47	9.11	0.10	1.24	0.40		100.00
		9	48.28	20.84	18.38	10.12		1.58	0.80		100.00
		10	46.78	21.47	18.73	10.74		1.49	0.67	0.12	100.00
		11	50.04	22.31	16.05	9.83		0.64	1.12		99.99
	98-2	1	51.48	23.52	14.53	9.52	0.12		0.83		100.00
		2	51.76	22.71	13.94	9.83		1.04	0.72		100.00
		3	51.83	24.07	12.78	9.36		1.52	0.44		100.00
		4	51.01	24.08	13.65	9.24		1.55	0.47		100.00
		5	50.21	23.85	14.22	9.93	0.10	0.43	1.26		100.00
		6	48.71	23.16	14.91	10.22		1.62	1.38		100.00
	CK4-4	1	49.76	24.32	13.56	9.84		0.92	1.60		100.00
		2	47.91	23.72	15.28	10.08		1.48	1.53		100.00
		3	51.64	24.18	13.07	9.75		0.92	0.44		100.00
		4	51.09	23.89	14.18	9.04	0.17	0.79	0.84		100.00
		5	49.02	22.96	15.73	9.62		1.47	1.20		100.00
		6	47.85	22.40	16.35	10.56		1.27	1.57		100.00
		7	46.57	22.26	18.09	10.23		1.36	1.49		100.00
		8	47.40	23.64	17.78	9.32	0.13	1.36	0.37		100.00
Group 2	CK3-24	1	51.53	24.51	14.40	9.56					100.00
		2	50.22	25.29	14.83	9.65					99.99
		3	51.47	24.56	14.41	9.32	0.25				100.01
		4	50.68	24.74	14.37	9.49	0.46	0.25			99.99
		5	51.59	24.61	14.33	9.49					100.02
	CK3-27	1	45.34	21.94	21.91	10.82					100.01
		2	43.40	22.97	21.63	10.80	0.60		0.60		100.00
		3	44.79	21.01	22.93	10.60			0.67		100.00
		4	42.25	21.72	22.77	10.03		1.52	1.46	0.23	99.98
		5	43.26	21.51	23.48	10.03	0.36	1.13	0.22		99.99
	125-5	1	46.47	23.53	17.44	9.79	0.64	1.42	0.70		99.99
		2	45.94	22.98	18.05	9.84	0.59	1.50	0.93	0.17	100.00
		3	47.82	23.85	16.57	9.58		1.47	0.70		99.99
		4	49.72	24.01	15.93	9.24	0.46		0.65		100.01
		5	50.34	24.07	16.18	9.42					100.01

			SiO2	Al2O3	FeO	K2O	MgO	MnO	Na2O	CaO	SUM
Group 2	430-3	1	48.18	25.48	16.35	9.27		0.72			100.00
		2	51.90	26.32	11.73	9.51		0.54			100.00
		3	50.06	23.72	14.71	9.92		1.59			100.00
		4	48.77	25.43	15.06	8.76	0.32	1.32	0.36		100.02
		5	47.50	25.70	16.18	8.99		1.16	0.47		100.00
		6	47.76	24.48	15.45	9.68		1.27	1.35		99.99
	480-6	1	50.59	24.38	14.53	9.36	0.54	0.60			100.00
		2	48.34	24.29	15.42	9.65	0.46	1.27	0.56		99.99
		3	47.48	24.16	16.37	9.62	0.57	1.49	0.32		100.01
		4	46.73	24.04	16.82	9.58	0.53	1.34	0.95		99.99
	480-7	1	47.11	24.26	19.36	9.29					100.02
		2	45.26	22.64	20.07	10.52	0.38	1.14			100.01
		3	46.71	22.47	20.93	9.74	0.15				100.00
		4	45.64	21.30	21.47	10.63	0.56	0.40			100.00
	138-15	1	47.41	22.52	20.38	9.70					100.01
		2	49.38	21.21	16.44	10.03	0.39	1.58	0.97		100.00
		3	50.14	24.53	15.05	9.26		1.02			100.00
		4	48.48	22.18	17.53	9.74	0.60	1.48			100.01
		5	51.70	24.65	12.93	9.88	0.41	0.45			100.02
		6	51.06	24.26	12.18	10.34	0.52	1.22	0.42		100.00
	430-4	1	49.87	23.49	15.35	9.72	0.24	1.34			100.01
		2	46.13	22.72	19.82	10.37		0.95			99.99
		3	44.76	21.92	19.71	10.71	0.58	1.47	0.65	0.20	100.00
		4	49.34	23.82	15.56	9.14	0.59	1.13	0.42		100.00
		5	50.58	25.63	13.58	9.76	0.45				100.00
		6	46.77	24.21	18.36	9.26	0.24	1.05		0.11	100.00
		7	47.68	22.09	17.73	10.65	0.53	1.32			100.00
	480-1	1	49.57	24.26	16.38	9.32	0.46				99.99
		2	46.34	22.54	20.73	9.24	0.52	0.64			100.01
		3	47.40	23.16	17.63	9.78	0.41	1.52		0.10	100.00
		4	44.57	21.07	21.24	10.38	0.62	1.41	0.72		100.01
		5	43.75	22.57	20.48	10.80	0.51	1.38	0.50		99.99
		6	47.36	21.93	18.49	9.63	0.49	1.62	0.47		99.99
	101-17	1	48.43	22.72	16.05	10.22		1.58	0.92	0.10	100.02
		2	47.94	22.56	15.87	10.49	0.71	1.60	0.83		100.00
		3	47.83	22.73	16.83	9.81	0.62	1.54	0.66		100.02
		4	48.72	23.28	15.88	9.74	0.56	1.42	0.40		100.00
		5	50.04	24.85	15.75	8.62	0.73				99.99
		6	47.18	22.01	17.13	10.73	0.44	1.62	0.90		100.01
		7	50.19	23.85	14.39	9.82	0.36	1.39			100.00
		8	50.31	25.08	14.46	9.17	0.63	0.26		0.10	100.01
		9	46.37	21.42	19.38	10.31	0.33	1.56	0.46	0.18	100.01
		10	45.72	22.06	19.75	9.62	0.61	1.53	0.70		99.99

APPENDIX V

XRF and INAA data set

	Group 1								
	CK3-20	CK3-21	CK3-22	96-1	97-1	98-2	CK4-3	CK4-4	CK4-5
SiO2	72.47	77.30	74.41	74.29	75.41	74.22	74.03	75.70	74.94
TiO2	0.00	0.01	0.01	0.00	0.01	0.00	0.01	0.01	0.01
Al2O3	15.39	14.16	16.09	15.68	14.99	16.06	15.50	14.81	14.35
Fe2O3	0.57	1.13	2.09	0.89	0.89	0.61	0.90	0.74	0.73
MnO	0.14	0.24	0.25	0.11	0.15	0.14	0.18	0.15	0.16
MgO	0.03	0.09	0.09	0.14	0.17	0.20	0.04	0.04	0.03
CaO	0.42	0.55	0.45	0.30	0.38	0.27	0.14	0.25	0.25
Na2O	4.42	0.28	2.52	3.66	2.38	3.36	3.26	3.90	3.79
K2O	4.05	6.13	2.38	4.22	4.80	4.13	4.53	4.19	4.32
P2O5	0.01	0.01	0.01	0.01	0.01	0.01	0.01	0.01	0.01
F	1.33	1.69	2.75	1.10	1.42	1.38	1.50	1.19	1.17
-F=O	-0.56	-0.71	-1.16	-0.46	-0.60	-0.58	-0.63	-0.50	-0.49
SUM	98.27	100.88	99.90	99.94	100.02	99.80	99.47	100.49	99.28
LOI	0.86	1.56	1.92	1.21	1.34	1.17	0.98	0.89	0.92
CIPW compositions calculated on F-free basis									
Q	30.56			35.51	41.52	37.72	37.20	35.88	35.69
Ab	38.06			30.79	20.04	28.33	27.66	32.73	32.23
Or	24.33			24.80	28.23	24.33	26.87	24.57	25.63
An	2.07			1.42	1.82	1.27	0.63	1.17	1.17
Hy	0.68			1.12	1.28	1.16	0.98	0.82	0.79
C	3.03			4.55	5.17	5.60	5.04	3.41	3.03
Mt	0.39			0.58	0.57	0.39	0.60	0.48	0.49
Il	0.00			0.00	0.02	0.00	0.02	0.02	0.02
Ap	0.02			0.02	0.02	0.02	0.02	0.02	0.02
SUM	99.15			98.80	98.67	98.83	99.01	99.11	99.07
Li	883	1555	2176	887	1125	907	1247	1132	1148
Rb	1834	2827	1835	1696	2202	1900	2347	1960	2053
Cs*	32.9			42.4	51.3	30.5	53.9	44.9	48.1
Sr	11	16	10	7	10	16	6	8	8
Ba	23	16	10	21	32	6	14	3	16
Y	3	11	8	4	40	4	10	39	41
Zr	32	23	29	32	43	33	29	53	54
Hf*	4.6			3.8	4.8	4.5	3.7	6.4	6.3
Nb	44	44	32	37	65	52	58	57	61
Ta*	58.9			110.6	44.6	41.1	59.1	52.5	55.6
Th	11	14	16	18	15	10	50	15	17
Th*	10			11	19	13	23	19	20
U	4	3	12	5	10	7	8	13	14
U*	15			16	15	12	14	18	19
Cr	6.3	288.0	4.9	6.7	7.1	113.7	22.8	3.4	3.0
V	0.0	0.7	0.0	0.0	0.0	0.0	0.0	0.0	0.0
Ni	6.3	14.2	7.7	6.1	14.1	11.1	10.0	18.7	8.9
Cu	2	12	5	3	80	5	10	3	1
Zn	423	1771	153	307	618	155	506	95	97
Ga	46	37	43	48	40	49	47	40	38
Mo	0	13	4	2	2	11	2	0	0
W	8	215	101	5	40	52	13	19	17
Sn	115	210	125	107	186	232	174	174	179
Pb	230	312	77	188	241	94	362	47	78
As	0	155	161	49	151	356	125	15	10
Sb	0.0	0.0	0.0	1.2	0.1	0.0	21.4	0.0	0.6
Bi	8	6	10	21	0	0	65	0	0

* denots analyses by INAA

Group 2

	CK3-23	CK3-24	CK3-25	CK3-27	CK3-28	CK3-29	CK3-31	CK3-32	125-3	125-5	430-1	430-3
SiO2	74.04	75.96	76.43	75.64	74.99	74.39	75.45	75.60	76.52	75.86	75.24	76.08
TiO2	0.01	0.03	0.02	0.01	0.01	0.02	0.01	0.01	0.03	0.03	0.02	0.03
Al2O3	15.01	13.30	13.66	14.48	14.88	14.96	14.91	14.49	13.62	13.69	14.05	13.82
Fe2O3	0.72	0.98	0.86	0.74	0.61	1.02	0.92	0.86	1.21	1.12	1.25	1.58
MnO	0.08	0.08	0.07	0.09	0.06	0.09	0.09	0.08	0.08	0.06	0.07	0.09
MgO	0.04	0.05	0.04	0.03	0.06	0.03	0.07	0.04	0.05	0.05	0.08	0.06
CaO	0.44	0.46	0.40	0.47	0.46	0.44	0.28	0.37	0.74	0.59	0.57	0.52
Na2O	4.84	3.66	3.77	3.90	4.60	3.84	4.08	3.88	2.80	2.63	3.79	3.17
K2O	3.92	4.48	4.54	4.34	4.04	4.40	4.18	4.67	4.95	5.37	4.32	4.94
P2O5	0.00	0.00	0.01	0.00	0.00	0.00	0.01	0.00	0.00	0.00	0.01	0.00
F	0.91	0.81	0.88	1.00	0.97	1.41	1.19	0.84	0.93	0.72	0.88	1.19
-F=O	-0.38	-0.34	-0.37	-0.42	-0.41	-0.59	-0.50	-0.35	-0.39	-0.30	-0.37	-0.50
SUM	99.63	99.47	100.31	100.28	100.26	100.02	100.69	100.49	100.54	99.82	99.91	100.99
LOI	0.66	0.79	0.68	0.78	0.68	0.92	0.77	0.69	1.08	1.04	0.95	0.88
CIPW compositions calculated on F-free basis												
Q	29.74	36.32	35.82	34.87	31.42	34.11	34.46	33.82	38.83	38.17	34.85	36.65
Ab	41.03	31.04	31.72	32.82	38.74	31.97	34.26	32.57	23.43	22.16	31.97	26.47
Or	23.21	26.52	26.69	25.51	23.74	26.10	24.51	27.40	28.94	31.59	25.39	28.82
An	2.18	2.28	1.92	2.33	2.28	2.23	1.32	1.84	3.62	2.93	2.76	2.53
Hy	0.65	0.64	0.71	0.68	0.59	0.86	0.88	0.73	0.99	0.87	1.07	1.24
C	2.02	1.60	1.83	2.50	2.10	3.08	3.16	2.36	2.28	2.46	2.12	2.30
Mt	0.49	0.65	0.58	0.49	0.42	0.68	0.61	0.58	0.78	0.74	0.83	1.03
Il	0.02	0.06	0.04	0.02	0.02	0.04	0.02	0.02	0.06	0.06	0.04	0.06
Ap	0.00	0.00	0.02	0.00	0.00	0.00	0.02	0.00	0.00	0.00	0.02	0.00
SUM	99.34	99.11	99.33	99.22	99.32	99.08	99.24	99.31	98.93	98.97	99.06	99.11
Li	589	716	648	614	539	774	927	665	562	633	746	794
Rb	1242	1432	1423	1371	1192	1502	1663	1476	1474	1541	1393	1654
Cs*	34.9	48.3		36.7		55.2	40.7	43.5		54.4	50.6	
Sr	5	5	5	6	5	4	7	4	16	11	17	10
Ba	22	19	31	22	27	23	19	32	19	21	14	14
Y	37	99	83	41	36	80	18	72	133	126	91	128
Zr	42	84	62	48	44	69	25	54	80	86	55	82
Hf*	3.6	6.0		4.0		5.8	2.2	4.4		5.8	4.4	
Nb	57	53	57	59	50	79	59	53	57	60	61	56
Ta*	23.0	20.1		25.5		30.6	42.0	20.5		24.6	28.4	
Th	12	30	25	18	12	23	11	18	38	37	26	39
Th*	15	34		21		26	14	21		40	30	
U	13	23	19	12	9	18	10	16	32	30	26	36
U*	19	23		12		22	13	18		28	27	
Cr	4.9	6.8	7.3	5.6	8.7	13.1	6.6	6.0	3.7	2.7	227.9	6.6
V	2.0	0.5	0.0	0.0	0.0	0.0	0.0	0.0	0.0	0.0	0.0	0.0
Ni	6.7	7.3	11.7	9.8	5.9	23.9	10.7	18.7	11.3	12.8	9.5	8.9
Cu	1	0	3	4	2	6	6	3	3	3	3	3
Zn	23	30	27	38	19	34	123	28	120	83	53	58
Ga	39	31	30	34	36	34	37	35	32	32	33	32
Mo	1	0	0	3	0	0	1	0	12	0	1	2
W	21	42	49	29	23	66	14	52	59	62	82	69
Sn	34	41	93	49	49	117	36	136	107	119	154	62
Pb	63	31	39	100	41	25	30	26	492	89	50	41
As	2	1	0	1	0	1	34	0	0	0	0	0
Sb	0.0	0.0	0.0	0.0	0.0	0.0	0.0	0.0	0.0	0.0	0.0	0.0
Bi	0	0	0	0	0	0	0	0	2	0	0	0

Group 2 (continued)

	430-5	430-6	480-2	480-6	95	100-1	107-10	107-11	109	138-15	138-16	140-11
SiO2	76.90	73.94	75.96	72.68	75.81	74.50	73.19	73.42	75.17	76.09	75.86	74.91
TiO2	0.03	0.03	0.03	0.03	0.02	0.01	0.00	0.00	0.01	0.03	0.02	0.01
Al2O3	12.98	13.88	13.86	13.25	14.97	15.36	15.79	15.61	14.98	13.45	13.91	15.37
Fe2O3	0.76	2.04	1.10	1.48	1.23	1.70	1.52	1.20	1.19	1.35	0.94	1.67
MnO	0.08	0.12	0.08	0.08	0.05	0.14	0.11	0.08	0.06	0.08	0.05	0.13
MgO	0.08	0.09	0.17	0.06	0.09	0.06	0.04	0.07	0.05	0.08	0.10	0.05
CaO	0.49	0.64	0.46	0.49	0.60	0.40	0.26	0.30	0.29	0.62	0.49	0.32
Na2O	4.01	3.20	4.44	3.07	3.19	3.08	5.11	4.14	4.32	3.40	3.91	3.82
K2O	4.36	3.77	3.69	4.96	4.13	4.63	2.88	4.48	4.02	4.29	4.02	3.61
P2O5	0.01	0.00	0.01	0.01	0.01	0.01	0.00	0.01	0.01	0.01	0.01	0.01
F	0.55	1.69	0.93	1.04	1.48	1.74	1.19	1.34	1.22	1.09	0.95	1.85
-F=O	-0.23	-0.71	-0.39	-0.44	-0.62	-0.73	-0.50	-0.56	-0.51	-0.46	-0.40	-0.78
SUM	100.02	98.68	100.34	96.70	100.96	100.91	99.59	100.09	100.80	100.03	99.85	100.97
LOI	0.65	1.22	0.91	0.91	1.15	1.06	0.79	0.84	0.67	1.00	0.83	0.92
CIPW compositions calculated on F-free basis												
Q	35.36	39.16	34.23	35.41	39.19	36.71	31.46	31.09	33.42	37.90	36.29	37.23
Ab	33.83	27.32	37.30	26.73	26.64	25.54	43.31	34.93	36.20	28.67	32.99	32.05
Or	25.69	22.50	21.61	30.18	24.09	27.52	17.07	26.40	23.56	25.22	23.68	21.14
An	2.36	3.22	2.22	2.46	2.86	1.92	1.29	1.42	1.37	3.01	2.36	1.52
Hy	0.74	1.81	1.19	1.17	1.09	1.49	1.26	1.04	0.92	1.16	0.89	1.46
C	0.77	3.41	1.74	2.03	4.14	4.63	3.82	3.44	3.01	2.09	2.27	4.59
Mt	0.52	1.29	0.73	1.03	0.77	1.10	1.00	0.81	0.80	0.87	0.62	1.06
Il	0.06	0.06	0.06	0.06	0.04	0.02	0.00	0.00	0.02	0.06	0.04	0.02
Ap	0.02	0.00	0.02	0.02	0.02	0.02	0.00	0.02	0.02	0.02	0.02	0.02
SUM	99.36	98.77	99.10	99.09	98.85	98.96	99.20	99.16	99.33	99.00	99.17	99.09
Li	321	1114	565	745	855	1214	867	1087	775	803	604	1354
Rb	998	1567	1258	1617	1445	1886	1625	1365	1578	1499	1207	1982
Cs*	37.0		52.6		77.9	65.6	48.6		41.8		54.3	71.1
Sr	10	11	6	10	2	6	4	6	4	11	7	4
Ba	71	15	23	17	13	17	10	7	4	17	12	22
Y	137	143	159	134	73	25	17	10	17	145	68	22
Zr	87	79	92	84	52	40	56	64	36	86	58	40
Hf*	6.0		6.4		4.1	4.0	6.1		4.3		5.8	3.9
Nb	58	55	61	58	52	67	57	74	59	57	52	65
Ta*	18.8		20.5		29.8	44.7	50.8		37.6		31.6	37.7
Th	40	41	44	41	63	24	15	20	30	40	23	15
Th*	45		47		27	20	19		18		32	18
U	37	30	39	36	18	16	24	12	6	34	19	15
U*	37		43		22	21	24		9		27	21
Cr	29.2	8.7	236.1	3.2	8.9	49.3	3.3	3.6	7.0	133.3	7.3	5.8
V	0.0	2.1	3.6	0.0	0.0	0.0	0.0	0.0	2.1	0.0	0.0	0.0
Ni	7.6	10.0	17.8	9.1	7.6	10.2	9.0	6.5	7.6	10.3	5.4	9.5
Cu	2	3	3	2	3	3	3	1	2	1	0	3
Zn	57	73	59	104	54	94	66	73	47	63	31	85
Ga	28	32	32	33	31	38	39	42	39	32	32	40
Mo	0	0	1	0	0	1	0	1	11	4	0	33
W	21	137	57	83	47	122	38	85	88	111	68	147
Sn	7	72	28	61	31	84	91	57	28	129	73	287
Pb	66	31	46	60	50	81	57	38	47	58	48	28
As	0	0	0	0	0	23	20	3	0	0	0	0
Sb	0.0	0.0	0.0	0.0	0.0	0.0	0.0	0.0	0.0	0.0	0.0	0.0
Bi	0	8	0	0	80	15	0	0	29	4	0	0

Group 2 (continued)

	86028	430-2	430-4	480-1	480-3	480-4	480-5	101-9	101-15	101-16	101-17	86045
SiO2	76.16	76.08	75.05	76.18	75.33	74.14	75.44	76.36	75.50	75.98	75.80	75.26
TiO2	0.03	0.01	0.02	0.03	0.01	0.01	0.03	0.03	0.03	0.03	0.03	0.03
Al2O3	13.62	14.01	14.94	13.83	14.45	14.68	13.97	13.74	13.62	13.66	13.84	13.56
Fe2O3	1.69	1.15	1.96	1.46	1.15	1.14	1.49	1.13	1.12	1.08	1.30	1.53
MnO	0.15	0.07	0.13	0.09	0.08	0.07	0.10	0.06	0.06	0.06	0.08	0.09
MgO	0.15	0.09	0.06	0.06	0.09	0.05	0.08	0.29	0.07	0.12	0.07	0.11
CaO	0.64	0.63	0.58	0.56	0.57	0.47	0.64	0.53	0.53	0.90	0.63	0.64
Na2O	3.05	3.65	4.04	3.36	3.81	4.19	3.13	2.36	3.69	2.95	4.20	2.75
K2O	4.21	4.50	2.92	4.54	4.40	3.15	4.40	4.99	4.28	4.92	3.84	4.83
P2O5	0.00	0.01	0.00	0.00	0.01	0.00	0.01	0.00	0.00	0.00	0.01	0.01
F	1.31	1.01	1.55	1.12	1.06	1.39	1.25	0.82	0.90	1.00	0.85	1.06
-F=O	-0.55	-0.42	-0.65	-0.47	-0.44	-0.58	-0.52	-0.34	-0.38	-0.42	-0.36	-0.44
SUM	100.46	100.79	100.60	100.75	100.51	98.71	100.02	99.97	99.42	100.28	100.29	99.41
LOI	1.22	0.94	1.25	1.04	0.98	0.96	1.13	1.35	0.85	1.15	0.94	1.14
CIPW compositions calculated on F-free basis												
Q	39.77	35.40	38.00	37.10	34.30	36.66	38.27	41.24	36.19	37.27	34.59	38.83
Ab	25.54	30.54	33.83	28.08	31.97	35.86	26.39	19.79	31.30	24.70	35.27	23.26
Or	24.62	26.28	17.06	26.51	25.75	18.84	25.86	29.23	25.33	28.82	22.50	28.52
An	3.12	3.01	2.83	2.73	2.76	2.38	3.11	2.63	2.63	4.41	3.06	3.11
Hy	1.73	1.05	1.74	1.18	1.07	0.99	1.30	1.53	0.94	1.05	1.07	1.39
C	2.86	1.99	4.05	2.35	2.37	3.55	2.90	3.46	1.97	1.84	1.64	2.67
Mt	1.06	0.76	1.19	0.94	0.76	0.74	0.96	0.71	0.74	0.70	0.86	0.99
Il	0.06	0.02	0.04	0.06	0.02	0.02	0.06	0.06	0.06	0.06	0.06	0.06
Ap	0.00	0.02	0.00	0.00	0.02	0.00	0.02	0.00	0.00	0.00	0.02	0.02
SUM	98.77	99.06	98.74	98.96	99.02	99.04	98.87	98.66	99.15	98.84	99.07	98.85
Li	1138	638	1191	918	758	721	858	830	783	758	1081	908
Rb	1453	1327	1448	1530	1510	1165	1514	1780	1448	1615	1494	1605
Cs*	80.4	43.9		59.5		43.9			52.9		70.1	58.3
Sr	10	14	7	10	8	7	11	5	5	8	4	11
Ba	4	20	24	14	15	8	10	16	5	4	15	25
Y	148	96	82	146	68	84	144	148	147	139	134	137
Zr	84	57	69	84	60	57	81	84	86	76	89	82
Hf*	5.8	5.1		5.6		4.8			5.7		7.4	5.9
Nb	50	55	79	62	65	54	54	55	56	54	78	58
Ta*	17.0	27.2		21.8		24.8			22.6		38.1	24.5
Th	48	23	32	45	21	24	37	35	37	34	43	40
Th*	47	29		45		27			40		50	42
U	35	24	35	32	22	21	31	30	31	31	27	32
U*	38	31		35		24			30		30	35
Cr	1.8	5.3	100.7	3.1	7.7	121.4	5.5	57.5	5.5	11.8	3.2	13.4
V	1.5	0.0	0.0	0.0	0.0	0.0	0.0	0.1	0.0	0.0	0.0	0.8
Ni	7.5	6.8	8.7	15.8	11.0	11.4	8.0	17.2	11.1	7.7	20.4	9.1
Cu	2	0	1	3	2	8	4	3	1	4	2	2
Zn	178	48	68	68	107	1628	314	227	66	337	74	177
Ga	30	33	38	32	37	34	32	33	32	32	36	32
Mo	0	0	1	2	0	2	0	0	0	0	0	4
W	32	63	515	109	61	121	62	46	52	44	56	134
Sn	34	32	517	270	164	20	177	61	50	66	78	137
Pb	424	48	44	42	46	18	44	91	57	97	52	30
As	50	0	0	0	0	3	25	0	0	0	2	34
Sb	0.0	0.0	0.3	0.0	0.0	0.0	11.4	0.0	0.0	0.0	0.0	11.7
Bi	16	0	12	5	0	0	0	0	0	0	0	0

APPENDIX VI. RARE-EARTH ELEMENT GEOCHEMISTRY OF THE JIANFENGLING GRANITE STOCK

		La*	La	Ce*	Ce	Nd	Sm	Eu	Tb	Yb	Lu
Group 1	96-1	4.5	4.9	19.4	20.9	6.56	2.72	0.04	0.48	2.33	0.32
	97-1	26.1	19.6	56.3	54.1	19.55	4.49	0.03	1.08	9.39	1.32
	98-2	6.8	5.6	30.2	20.6	6.69	2.08	0.03	0.43	3.03	0.44
	CK3-20	0.0	4.1	10.6	17.7	6.29	0.92	0.03	0.39	2.37	0.36
	CK4-3	5.5	6.5	21.8	23.2	7.86	2.18	0.02	0.37	3.37	0.45
	CK4-4	19.3	19.5	43.1	56.9	19.93	4.72	0.02	1.10	9.84	1.40
	CK4-5	23.1	20.7	46.8	60.2	23.96	3.73	0.02	1.12	10.44	1.53
Group 2	CK3-23	14.2	21.6	35.3	61.8	19.05	4.78	0.04	1.03	9.04	1.20
	CK3-24	33.3	35.9	65.9	94.9	39.46	11.43	0.04	2.36	16.12	2.26
	CK3-27	21.6	24.4	56.0	67.7	20.58	4.98	0.03	1.12	10.62	1.43
	CK3-29	32.2	34.3	77.6	95.7	31.37	6.49	0.03	1.82	17.22	2.42
	CK3-31	17.5	16.8	43.3	49.6	15.67	2.79	0.03	0.79	6.05	0.84
	CK3-32	24.6	27.3	50.8	71.5	24.50	5.61	0.03	1.46	12.64	1.69
	125-5	42.4	43.0	79.4	111.8	47.51	12.59	0.04	3.05	18.15	2.54
	430-1	37.9	42.0	86.3	112.4	44.55	9.23	0.02	2.48	17.74	2.69
	430-5	43.8	46.5	102.5	122.9	54.42	12.56	0.03	3.18	19.90	2.98
	480-2	56.4	54.3	114.6	140.6	69.38	16.47	0.03	3.74	21.48	3.15
	86028	40.0	49.5	112.8	128.7	59.71	14.35	0.04	3.40	21.42	3.17
	95	36.9	35.8	73.5	90.9	39.42	8.00	0.02	2.13	14.50	2.13
	100-1	22.3	21.3	60.5	63.7	21.60	6.06	0.02	1.16	11.33	1.69
	107-10	18.7	17.5	41.2	51.9	17.05	4.42	0.02	0.35	8.84	1.35
	109	17.2	21.6	35.9	60.0	19.45	5.74	0.02	0.98	11.55	1.78
	138-16	22.6	31.3	49.0	82.0	31.47	6.94	0.05	1.73	12.93	1.79
	140-11	18.9	18.3	37.6	50.2	20.36	3.29	0.08	0.93	8.83	1.21
	430-2	27.2	41.9	68.2	101.6	43.07	10.92	0.03	2.45	17.03	2.39
	480-1	41.9	48.1	91.4	121.5	52.99	14.25	0.05	3.27	19.48	2.63
	480-4	30.0	38.3	62.5	99.8	40.78	10.84	0.03	2.18	14.44	2.06
	86045	40.1	47.9	89.7	113.4	53.68	14.07	0.05	3.05	18.59	2.59
	101-15	43.0	49.5	95.4	104.3	53.49	13.54	0.04	2.78	17.40	2.64
	101-17	49.9	64.6	107.8	161.8	70.02	18.18	0.06	4.02	25.06	3.50

* denotes analysis by XRF

APPENDIX VII. MAJOR-ELEMENT GEOCHEMISTRY OF THE JIANFENGLING GRANITE STOCK (wet-chemical analyses)

	Group 1				Group 2						
	115-2	116-1	117-3	CK4-1	CK3-6	CK3-7	CK3-13	107-5	119-2	138-7	138-13
SiO_2	73.36	73.63	70.87	72.69	74.35	75.62	73.39	72.34	73.42	74.42	73.81
TiO_2	0.01	0.01	0.01	0.01	0.01	0.04	0.02	0.01	0.01	0.04	0.04
Al_2O_3	14.85	15.42	16.47	15.58	14.01	12.94	14.84	15.68	14.67	13.59	13.88
Fe_2O_3	0.23	0.29	0.30	0.28	0.23	0.50	0.46	0.40	0.43	0.40	0.54
FeO	0.60	0.27	0.34	0.60	0.60	0.48	0.80	0.70	1.05	0.96	1.63
MnO	0.12	0.09	0.08	0.14	0.06	0.07	0.10	0.07	0.08	0.08	0.15
MgO	0.05	0.06	0.05	0.01	0.02	0.05	0.02	0.04	0.01	0.06	0.00
CaO	0.48	0.27	0.28	0.19	0.42	0.59	0.35	0.76	0.19	0.50	0.46
Na_2O	3.71	3.90	5.32	4.33	3.92	3.87	4.06	4.27	4.20	3.55	3.26
K_2O	4.04	4.31	4.15	4.09	4.96	4.57	3.91	3.67	4.37	4.60	3.46
H_2O^+	0.96	0.73	0.90	0.75	0.73	0.72	0.93	1.13	0.78	0.81	0.85
H_2O^-	0.10	0.29	0.21	0.08	0.10	0.03	0.03	0.14	0.08	0.00	0.03
F	1.48	1.15	0.79	1.59	0.95	0.70	1.48	1.91	0.45	1.26	2.20
-F=O	-0.62	-0.48	-0.33	-0.67	-0.40	-0.29	-0.62	-0.80	-0.19	-0.53	-0.92
SUM	99.27	99.65	99.23	99.59	99.86	99.86	99.74	100.18	99.47	99.74	99.36

	Group 2 (continued)										
	142-8	142-10	142-11	86030	101-7	101-8	101-10	101-11	136-4	136-9	86053	116-7
SiO_2	73.49	75.22	72.66	73.15	74.90	75.54	74.39	75.06	71.72	73.31	73.23	73.95
TiO_2	0.02	0.01	0.02	0.02	0.02	0.02	0.02	0.03	0.02	0.01	0.01	0.01
Al_2O_3	14.54	13.73	14.30	13.86	13.92	13.09	13.53	13.23	14.30	14.07	13.76	14.37
Fe_2O_3	0.64	0.58	0.64	0.56	0.45	0.17	0.24	0.32	0.44	0.40	0.49	0.25
FeO	0.57	0.19	2.38	0.76	0.76	1.91	0.91	0.93	1.27	1.12	2.65	0.72
MnO	0.06	0.05	0.17	0.08	0.08	0.11	0.06	0.06	0.09	0.06	0.20	0.14
MgO	0.06	0.40	0.09	0.14	0.15	0.05	0.17	0.04	0.33	0.03	0.09	0.05
CaO	0.85	0.52	0.97	1.07	0.43	0.82	0.44	0.53	1.61	0.56	1.09	0.32
Na_2O	2.64	3.70	0.69	4.05	4.51	4.31	3.18	3.72	2.03	3.97	0.08	3.28
K_2O	5.05	3.76	3.12	3.71	2.77	1.48	4.77	4.49	4.63	4.18	3.92	4.07
H_2O^+	1.33	1.59	2.30	1.11	1.10	1.22	1.08	0.83	1.73	0.88	2.06	1.26
H_2O^-	0.03	0.22	0.12	0.20	0.11	0.10	0.20	0.10	0.33	0.14	0.16	0.20
F	1.46	0.58	3.10	1.59	0.78	1.79	0.80	1.14	1.71	1.18	2.20	1.14
-F=O	-0.61	-0.24	-1.30	-0.67	-0.33	-0.75	-0.34	-0.48	-0.72	-0.50	-0.92	-0.48
SUM	100.10	100.09	99.14	99.43	99.54	99.76	99.25	99.90	99.16	99.27	98.86	99.08

APPENDIX VIII

CHONDRITE-NORMALISED REE PATTERNS FOR INDIVIDUAL SAMPLES

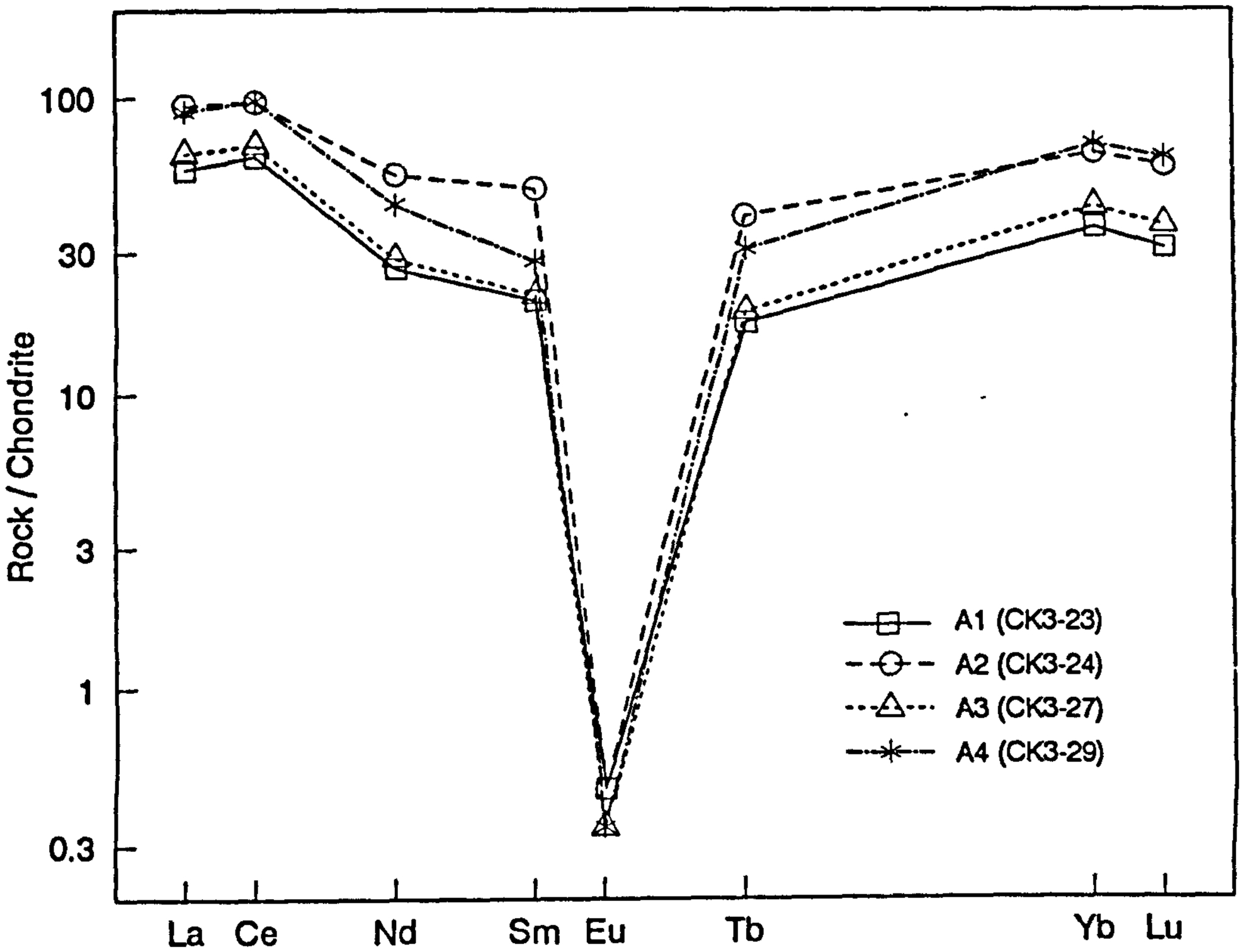
100
30
10
3
1
0.3
Rock / Chondrite
La
Ce
Nd
Sm
Eu
Tb
Yb
Lu
A1 (CK3-23)
A2 (CK3-24)
A3 (CK3-27)
A4 (CK3-29)

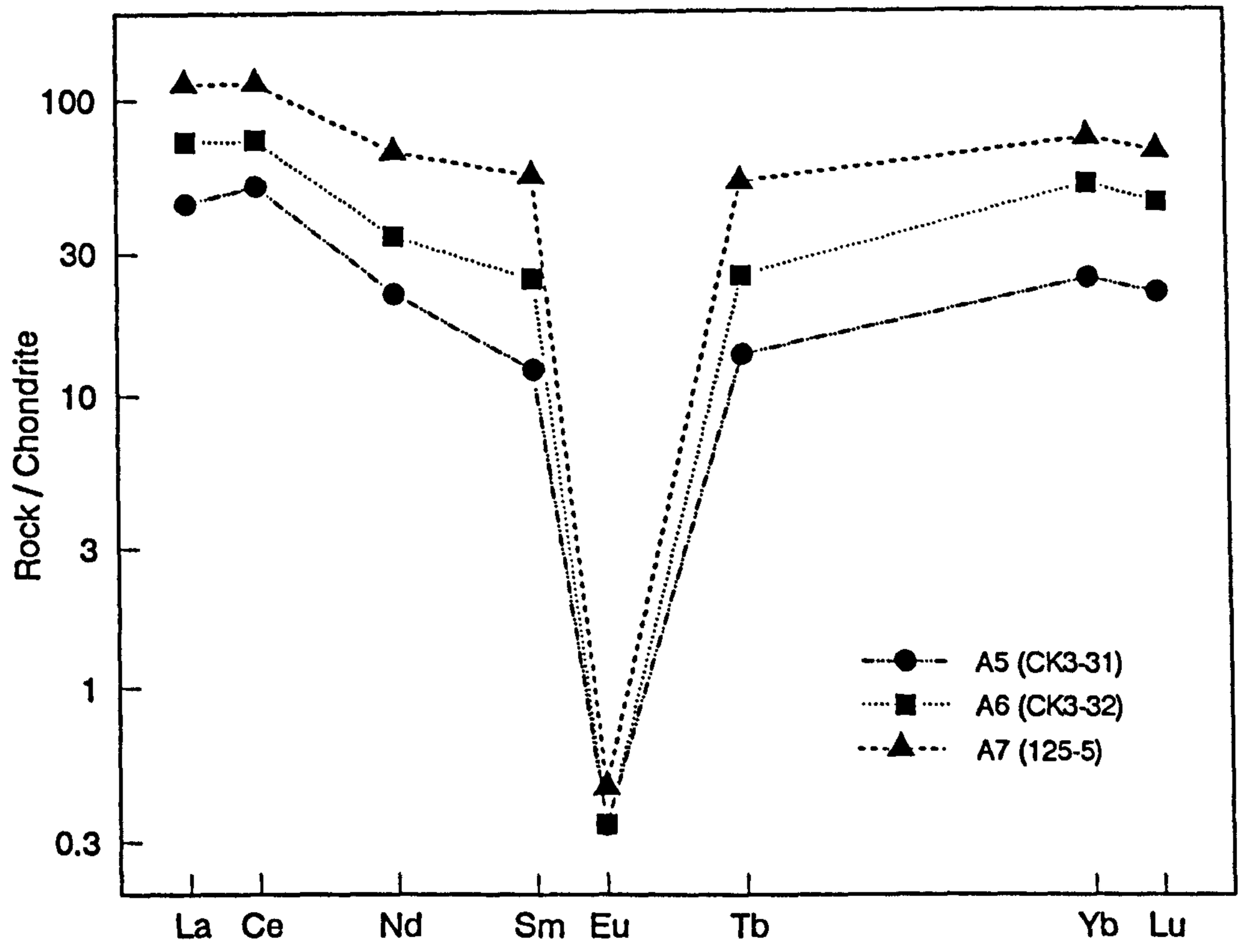
100
30
10
3
1
0.3
Rock / Chondrite
La
Ce
Nd
Sm
Eu
Tb
Yb
Lu
A5 (CK3-31)
A6 (CK3-32)
A7 (125-5)

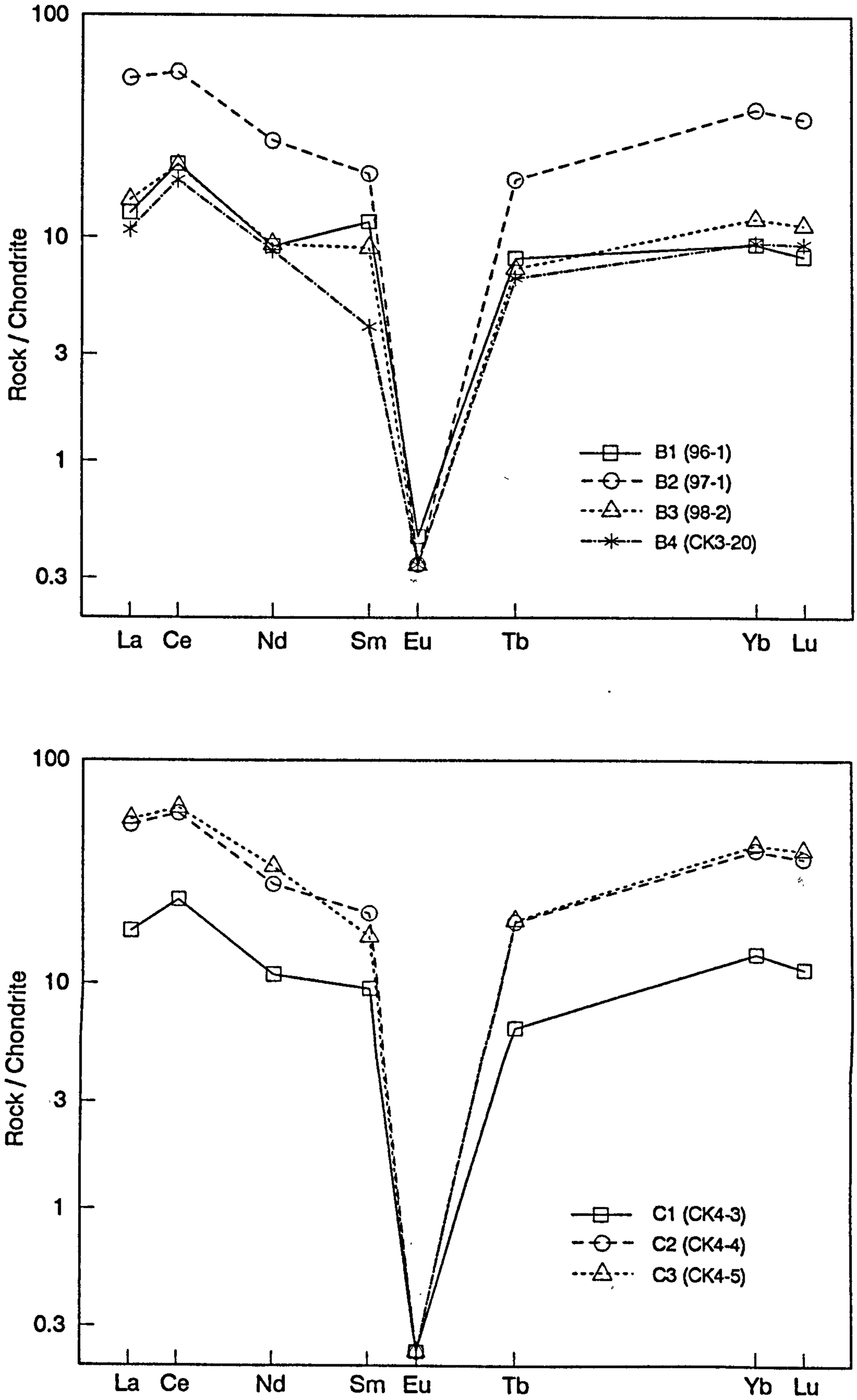
100
10
3
1
0.3
Rock / Chondrite
La
Ce
Nd
Sm
Eu
Tb
Yb
Lu
B1 (96-1)
B2 (97-1)
B3 (98-2)
B4 (CK3-20)
C1 (CK4-3)
C2 (CK4-4)
C3 (CK4-5)

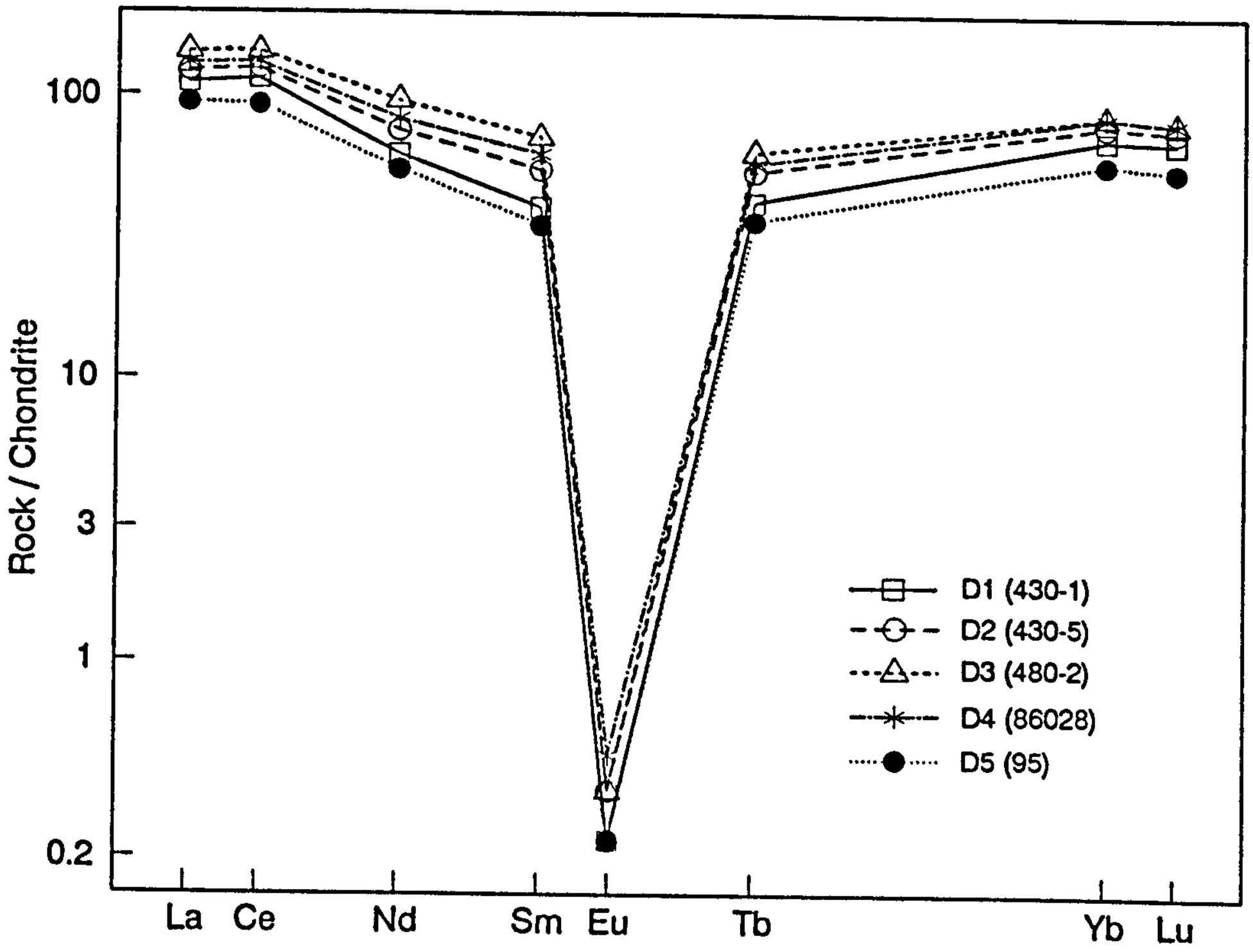
100
10
3
1
0.2
Rock / Chondrite
La
Ce
Nd
Sm
Eu
Tb
Yb
Lu
D1 (430-1)
D2 (430-5)
D3 (480-2)
D4 (86028)
D5 (95)

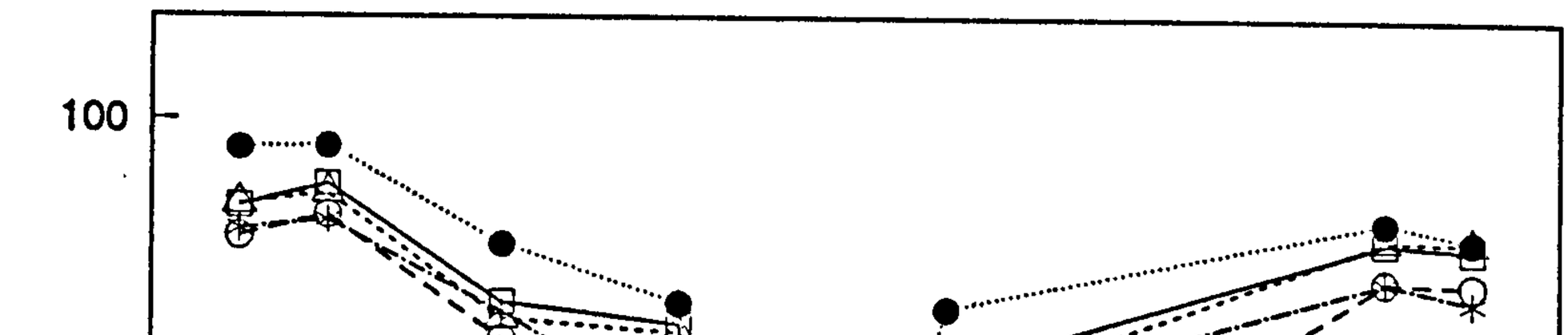
100
10
3
1
0.2
Rock / Chondrite
La
Ce
Nd
Sm
Eu
Tb
Yb
Lu
D6 (100-1)
D7 (107-10)
D8 (109)
D9 (138-16))
D10 (140-11)

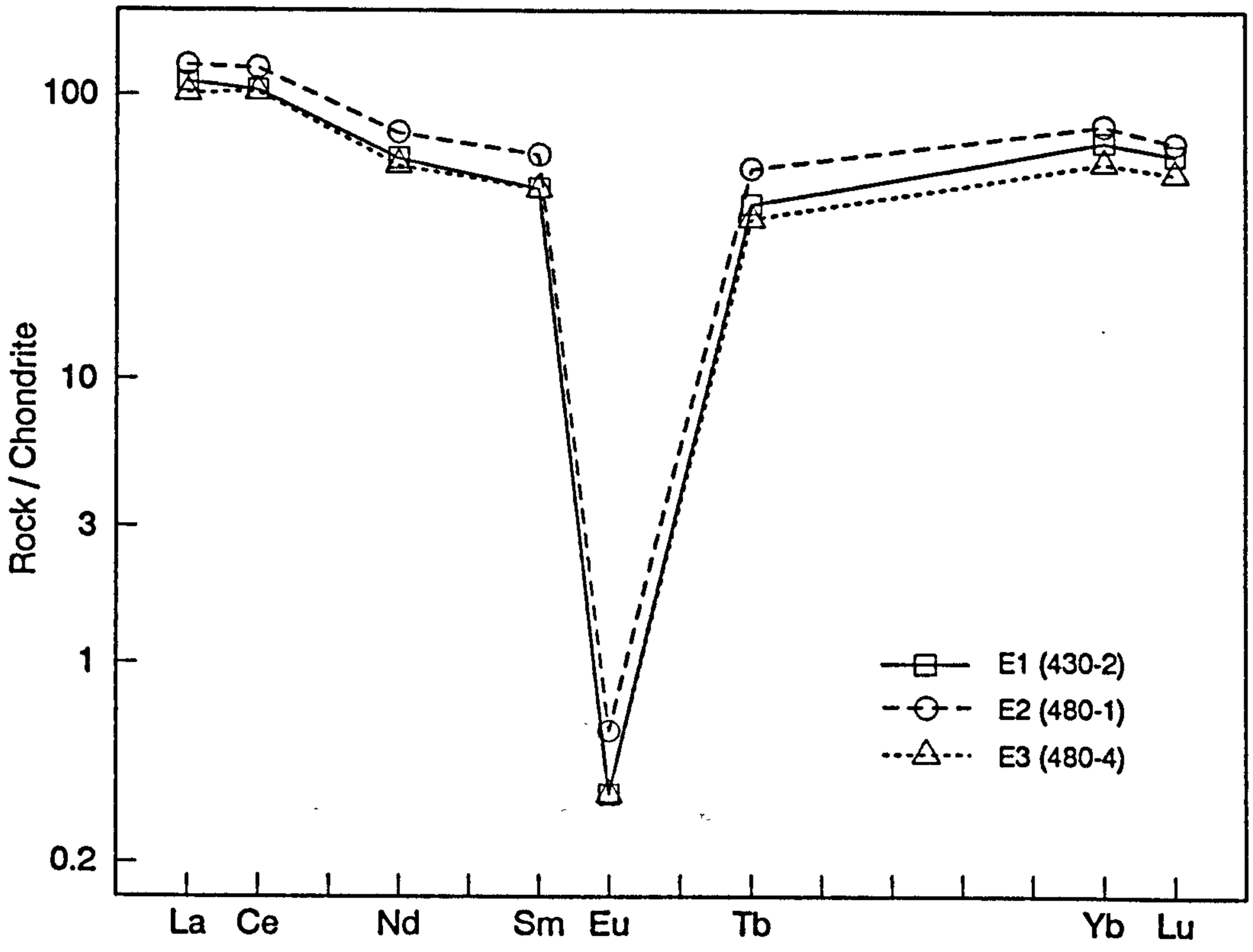
100
10
3
1
0.2
Rock / Chondrite
La
Ce
Nd
Sm
Eu
Tb
Yb
Lu
E1 (430-2)
E2 (480-1)
E3 (480-4)

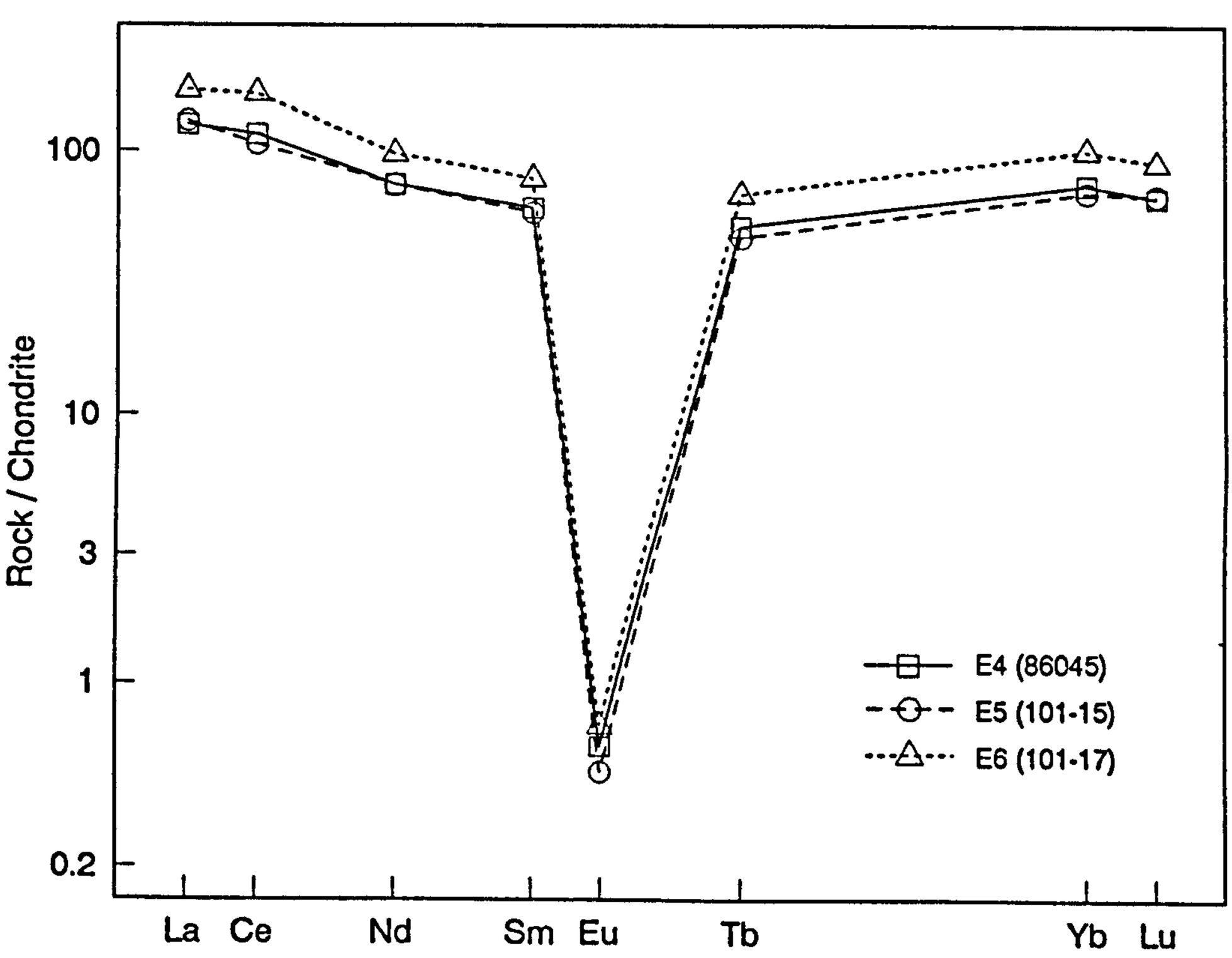
100
10
3
1
0.2
Rock / Chondrite
La
Ce
Nd
Sm
Eu
Tb
Yb
Lu
E4 (86045)
E5 (101-15)
E6 (101-17)

APPENDIX IX

FLUID INCLUSION DATA SET

1. FLUID INCLUSION DATA OF THE PEGMATITIC ROCKS

Sample	HM	Size (μm)	F	Origin	Tfm	Tm_{ice}	Ts_{NaCl}	S	Th	to	D
101-6	Quartz	10	0.7	P		-7.2		10.74	508.7	L	
"	"	15	0.65	P		-15.6		19.29	530.9	L	0.64
"	"	12	0.85	P		-4.7		7.44	484.2	L	
"	"	25	0.9	P		-1.9		3.21	479.6	L	
"	"	24	0.8	P	-18.9	-2.1		3,53	488.2	L	
"	"	40	0.75	P		-2.8		4.63	491.7	L	
"	"	15	0.65	P		-3.9		6.29	508.7	L	
"	"	5	0.9	P		-1.1		1.90	449.3	L	
"	"	10	0.85	P		-2.9		4.79	473.8	L	
"	"	24	0.7	P		-5.6		8.67	489.4	L	
"	"	14	0.7	P		-5.8		8.94	490.7	L	
"	"	35	0.65	P	-19.6	-6.7		10.11	508.4	L	
"	"	10	0.5	P		-18.8		21.76	529.6	V	0.60
"	"	15	0.6	P		-7.4		10.99	509.3	V	0.59
"	"	20	0.75	P		-7.5		11.11	489.7	L	
"	"	15	0.7	P		-6.8		10.24	496.1	L	
"	"	30	0.65	P	-21.2	-12.2		16.24	509.7	L	
"	"	15	0.65	P		-13.1		17.09	512.3	L	
"	"	14	0.7	P		-10.8		14.83	509.1	L	
"	"	12	0.8	P		-11.0		15.04	500.8	L	
"	"	15	0.85	P		-8.1		11.83	474.1	L	
"	"	22	0.75	P		-6.9		10.37	493.0	L	
"	"	25	0.9	P		-3.2		5.25	488.1	L	
"	"	5	0.85	P		-2.1		3.53	493.2	L	
"	"	5	0.75	P		-4.7		7.44	504.5	L	
"	"	8	0.95	P		-0.8		1.39	421.6	L	
"	"	6	0.9	P				170.1	30.51	483.0	L	0.76
"	"	10	0.85	P				136.2	29.16	490.7	L	0.75
"	"	15	0.6	P				248.3	34.54	508.4	L	
"	"	15	0.65	P				142.7	29.40	503.7	L	0.76
"	"	10	0.75	P				118.1	28.55	501.3	L	0.74
"	"	12	0.65	P				125.3	28.78	526.4	L	0.74
"	"	15	0.6	P				158.7	30.03	534.0	L	0.72
"	Topaz	40	0.7	P	-26.4	-2.7			4.48	483.8	L	
"	"	45	0.75	P	-25.9	-3.4			5.55	4480.1	L	
"	"	15	0.65	P		-2.2			3.69	396.1	L	
"	"	25	0.6	P		-0.9			1.56	479.3	V	
"	"	30	0.55	P	-23.9	-0.8			1.39	501.7	V	
"	"	24	0.5	P		-1.0			1.73	540.2	V	
"	"	30	0.45	P		-3.4			5.55	538.4	V	
"	"	45	0.4	P	-25.1	-3.7			5.99	509.1	V	
"	"	55	0.35	P	-24.7	-2.9			4.79	387.4	V	
"	"	32	0.3	P		-1.8			3.05	399.1	V	
"	"	25	0.45	P		-3.1			5.09	408.6	V	
"	"	60	0.65	P		-3.0			4.94	508.4	L	
"	"	15	0.7	P		-3.4			5.55	521.2	L	
"	"	50	0.8	P	-22.9	-3.3			5.40	487.9	L	
"	"	5	0.85	P		-2.6			4.32	501.7	L	
"	"	20	0.85	P		-2.4			4.01	507.4	L	
"	"	12	0.85	P		-2.8			4.63	500.9	L	

Sample	HM	Size (μm)	F	Origin	Tfm	Tm_{ice}	TsNaCl	S	Th	to	D
101-6	Topaz	25	0.8	P	-27.0	-7.1		10.62	491.0	L	
"	"	28	0.75	P	-26.4	-6.4		9.73	508.1	L	
"	"	15	0.9	P		-3.7		5.99	410.7	L	
"	"	22	0.85	P	-19.5	-3.4		5.55	483.7	L	
"	"	20	0.8	P		-2.9		4.79	488.1	L	
"	"	15	0.75	P		-5.1		7.99	499.3	L	
"	"	15	0.65	P		-6.8		10.24	524.0	L	
"	"	5	0.9	P		-3.0		4.94	403.8	L	
"	"	15	0.75	P		-1.9		3.21	471.4	L	
"	"	14	0.75	P		-6.1		9.34	480.3	L	
"	"	12	0.7	P		-7.0		10.49	499.1	L	
101-12	Quartz	5	0.85	P		-5.1		7.99	437.6	L	
"	"	10	0.55	P		-11.6		10.65	528.7	V	
"	"	18	0.65	P		-10.7		14.73	506.4	L	
"	"	20	0.7	P	-28.0	-9.2		13.10	472.1	L	
"	"	10	0.75	P		-8.1		11.83	468.5	L	
"	"	6	0.85	PS		-3.9		6.29	443.6	L	
"	"	15	0.95	PS		-1.0		1.73	378.5	L	
"	"	14	0.75	PS		-1.3		2.23	396.0	L	
"	"	12	0.7	PS		-4.6		7.29	368.4	L	
"	"	15	0.85	PS		-3.7		5.99	390.3	L	
"	"	25	0.7	P	-25.4	-4.2		6.72	427.6	L	
"	"	25	0.95	P	-23.8	-0.9		1.56	380.1	L	
"	"	5	0.85	P		-1.8		3.05	394.6	L	
"	"	5	0.85	P		-2.1		3.53	426.5	L	
"	"	10	0.95	P		-2.0		3.37	348.5	L	
"	"	8	0.9	P		-1.7		2.89	390.1	L	
"	"	10	0.75	P			136.7	29.18	467.6	L	0.75
"	"	12	0.65	P			144.8	29.48	521.7	L	0.76
"	"	12	0.6	P			151.2	29.73	522.6	L	0.74
"	"	15	0.75	P			139.6	29.29	508.4	L	0.75
"	"	10	0.65	P			160.7	30.11	530.6	L	0.73
"	"	5	0.8	P			224.1	33.15	504.3	L	0.77
"	Topaz	25	0.75	P	-19.6	-1.8		3.05	500.3	L	
"	"	15	0.9	P		-0.9		1.56	440.1	L	
"	"	35	0.65	P	-23.4	-3.8		6.14	524.0	L	
"	"	18	0.65	P		-4.1		6.58	510.8	V	
"	"	20	0.55	P		-5.6		8.67	479.0	V	
"	"	10	0.45	P		-0.8		1.39	508.4	V	
"	"	15	0.5	P		-0.4		0.71	511.0	V	
"	"	40	0.45	P	-21.5	-1.0		1.73	527.5	V	
"	"	36	0.35	P		-0.5		0.87	530.0	V	
"	"	30	0.4	P	-19.7	-1.1		1.99	508.4	V	
"	"	28	0.45	P		-2.0		3.37	500.1	V	
"	"	24	0.65	P		-4.9		7.72	497.0	V	
"	"	12	0.75	P		-5.6		8.67	408.6	L	
"	"	12	0.85	P		-3.7		5.99	411.7	L	
"	"	25	0.9	P	-23.8	-0.9		1.56	401.3	L	
"	"	20	0.85	P		-2.1		3.53	427.1	L	
"	"	12	0.8	P		-3.4		5.55	409.1	L	
"	"	15	0.9	P		-2.9		4.79	387.5	L	
"	"	15	0.95	P		-0.8		1.39	360.1	L	
"	"	18	0.95	P		-0.7		1.22	369.3	L	

Sample	HM	Size (μm)	F	Origin	Tfm	Tm_{ice}	TsNaCl	S	Th	to	D
104-7	Quartz	16	0.6	P		-11.6		15.65	531.7	L	
"	"	5	0.85	P		-7.8		11.47	471.3	L	
"	"	12	0.95	PS		-1.3		2.23	386.1	L	
"	"	14	0.9	PS		-3.7		5.99	394.2	L	
"	"	30	0.85	PS		-4.1		6.58	428.0	L	
"	"	5	0.65	P		-10.2		14.20	508.4	L	
"	"	10	0.85	P		-7.6		11.23	500.9	L	
"	"	6	0.7	P		-8.4		12.19	493.0	L	
"	"	15	0.8	P		-7.1		10.62	471.6	L	
"	"	14	0.75	P		-7.2		10.74	493.8	L	
"	"	10	0.75	P		-8.3		10.07	490.1	L	
"	"	14	0.6	P		-12.8		16.81	521.7	L	0.56
"	"	5	0.55	P		-14.6		18.44	530.4	L	0.60
"	"	10	0.7	P		-7.7		11.35	507.2	L	
"	"	20	0.8	P		-6.5		9.86	494.7	L	
"	"	10	0.75	P		-3.0		4.94	498.6	L	
"	"	20	0.65	P		-2.9		4.79	521.7	L	
"	"	12	0.9	P		-1.7		2.89	476.0	L	
"	"	5	0.65	P		-4.2		6.72	521.3	L	
"	"	5	0.85	P		-3.9		6.29	501.7	L	
"	"	5	0.8	P		-3.2		5.25	508.4	L	
"	"	5	0.7	P		-4.8		7.58	520.6	L	
"	"	6	0.75	P		-5.0		7.85	479.0	L	
"	"	5	0.75	P		-4.7		7.44	483.4	L	
"	"	6	0.85	P		-3.2		5.25	423.6	L	
"	"	8	0.65	P		-8.9		12.76	488.7	L	
"	"	5	0.8	P		-3.1		5.09	435.2	L	
"	"	8	0.85	P		-1.8		3.05	410.7	L	
"	"	10	0.65	P		-3.4		5.55	494.5	L	
"	"	12	0.6	P		-13.7		17.64	520.2	L	
"	"	10	0.7	P		-4.3		6.87	501.6	L	
"	"	8	0.75	P			79.6	27.46	491.8	L	0.75
"	"	5	0.65	P			101.2	28.03	503.4	L	0.74
111-1	Topaz	5	0.45	P					438.9	V	
"	"	6	0.35	P					521.0	V	
"	"	6	0.4	P		-7.6		11.23	532.4	V	
"	"	12	0.3	P		-6.1		9.34	460.3	V	
"	"	15	0.35	P		-3.8		6.14	508.1	V	
"	"	25	0.4	P		-2.2		3.69	478.4	V	
"	"	20	0.3	P		-5.0		7.85	433.5	V	
"	"	40	0.45	P					453.4	V	
"	"	35	0.75	P		-1.9		3.21	483.6	L	
"	"	40	0.9	P		-2.2		3.69	475.3	L	
"	"	25	0.85	P		-2.6		4.32	491.6	L	
"	"	30	0.75	P		-2.1		3.53	499.1	L	
"	"	15	0.75	P		-1.7		2.89	507.4	L	
"	"	10	0.6	P		-1.5		2.56	521.0	V	
"	"	8	0.65	P		-1.9		3.21	517.5	V	
"	"	20	0.8	P		-4.4		7.01	501.8	L	
"	"	12	0.75	P		-5.1		7.99	511.8	L	
"	"	15	0.65	P		-6.3		9.60	491.0	L	
"	"	25	0.9	P		-1.7		2.89	474.6	L	
"	"	22	0.8	P		-3.0		4.94	521.9	L	

Results of ten runs on the same inclusion

Sample	HM	Size (μm)	F	Origin	Tfm	Tm_{ice}	S	Th	to
101-6	Topaz	65	0.65	P	-19.5	-3.1	5.09	495.8	L
								493.3	L
								498.6	L
								501.7	L
								492.8	L
								503.5	L
								500.3	L
								490.7	L
								492.1	L
								502.9	L

χ = 496.7°C, 1σ = 4.6°C

1. FLUID INCLUSION DATA OF THE FLUORITE-SCHEELITE ORES

Sample	HM	Size (μm)	F	Origin	Tfm	Tm_{ice}	S	Th	to	D
III_{3-3}	Quartz	25	0.75	P		-2.8	4.63	345.2	L	0.752
"	"	40	0.85	P		-3.1	5.09	328.4	L	0.796
"	"	15	0.95	PS		-2.9	4.63	169.6	L	0.982
"	"	25	0.9	PS		-1.8	3.05	201.7	L	0.934
"	"	30	0.8	PS		-2.3	3.85	268.3	L	0.864
"	"	45	0.85	PS	-50.3	-2.1	3.53	260.1	L	0.860
"	"	15	0.95	PS				201.3	L	
"	"	15	0.9	P		-0.8	1.39	217.6	L	0.902
"	"	10	0.75	P		-3.7	5.99	322.1	L	0.796
"	"	24	0.9	P		-3.0	4.94	230.7	L	0.926
"	"	20	0.8	P		-2.7	4.48	248.3	L	0.896
"	"	45	0.85	P	-49.1	-3.1	5.09	238.5	L	0.901
"	"	10	0.9	P		-2.4	4.01	200.7	L	0.943
"	"	15	0.9	P		-2.3	3.85	209.1	L	0.934
"	"	30	0.95	P				148.7	L	
"	"	20	0.8	P		-1.8	3.05	294.0	L	0.807
"	"	30	0.85	P		-1.7	2.89	288.6	L	0.821
"	"	15	0.75	P		-3.8	6.14	328.4	L	0.851
"	"	40	0.7	P		-3.7	5.99	340.5	L	0.749
"	"	15	0.8	P		-3.1	5.09	321.4	L	0.790
"	"	25	0.85	P		-3.0	4.94	309.6	L	0.828
"	"	22	0.95	P				118.4	L	
"	"	25	0.9	P		-0.9	1.56	196.7	L	0.916
"	"	55	0.75	P		-2.7	4.48	208.1	L	0.952
"	"	50	0.85	P		-2.4	4.01	268.9	L	0.871
"	"	18	0.95	P		-0.4	0.70	257.7	L	0.858
"	"	40	0.9	P	-39.6	-1.6	2.72	283.0	L	0.825
"	"	60	0.85	P	-42.0	-1.9	3.21	290.9	L	0.821
"	Fluorite	65	0.85	P	-46.4	-3.2	5.25	132.8	L	1.007
"	"	15	0.95	P	-46.8	-3.1	5.09	142.4	L	0.998
"	"	15	0.85	P		-0.8	1.39	116.8	L	0.996
"	"	20	0.95	P				279.1	L	
"	"	55	0.9	P		-1.0	1.73	114.4	L	0.998
"	"	40	0.9	P		-3.3	5.40	141.3	L	0.984
"	"	60	0.95	P	-46.7	-3.6	5.85	127.7	L	1.020
"	"	55	0.85	P		-2.4	4.01	132.1	L	1.010
"	"	20	0.9	P				133.8	L	
"	"	30	0.85	P				136.7	L	
"	"	24	0.95	P				134.5	L	
"	"	20	0.85	P				184.1	L	
"	"	40	0.9	P	-45.1			118.3	L	
"	"	45	0.85	P		-1.4	2.40	171.4	L	0.957
"	"	30	0.95	P				114.1	L	
"	"	25	0.85	P				109.0	L	
"	"	40	0.85	P		-3.0	4.94	147.1	L	0.994
"	"	15	0.9	P				132.5	L	
"	"	10	0.85	P				177.3	L	
"	"	35	0.95	P		-2.8	4.63	118.7	L	1.019
"	"	20	0.95	P				114.7	L	
"	"	55	0.85	P				154.5	L	

Sample	HM	Size (μm)	F	Origin	Tfm	Tm_{ice}	S	Th	to	D
III_{3-14}	Quartz	25	0.9	P		-1.3	2.23	271.6	L	0.834
"	"	20	0.85	P		-2.0	3.37	294.3	L	0.816
"	"	20	0.95	P		-0.8	1.39	118.7	L	0.988
"	"	35	0.8	P	-39.0	-3.8	6.14	198.0	L	0.960
"	"	22	0.85	P		-3.4	5.55	199.3	L	0.952
"	"	45	0.7	P	-38.8	-5.8	8.94	248.2	L	0.933
"	"	15	0.65	P		-6.1	9.34	340.6	L	0.795
"	"	5	0.9	P		-3.0	4.94	201.7	L	0.952
"	"	15	0.8	P		-3.8	6.14	238.1	L	0.930
"	"	15	0.75	P		-2.7	4.48	309.5	L	0.828
"	"	20	0.85	P		-2.9	4.63	301.6	L	0.828
"	"	35	0.9	P	-44.8	-1.1	1.90	211.8	L	0.913
"	"	10	0.55	P		-7.0	10.49	356.2	L	0.817
"	"	15	0.65	P		-6.5	9.86	344.7	L	0.806
"	"	30	0.9	P		-2.0	3.37	209.1	L	0.934
"	"	10	0.7	P		-4.9	7.72	298.3	L	0.839
"	"	10	0.65	P		-5.1	7.99	344.1	L	0.761
"	"	15	0.9	P		-2.3	3.85	280.5	L	0.854
"	"	24	0.85	P		-3.0	4.94	291.0	L	0.834
"	"	15	0.8	P		-2.9	4.79	301.4	L	0.828
"	"	15	0.9	P		-1.8	3.05	220.3	L	0.907
"	Fluorite	25	0.7	P		-1.6	2.72	285.5	L	0.826
"	"	15	0.9	P		-1.9	3.21	183.1	L	0.957
"	"	40	0.8	P		-1.8	3.05	297.1	L	0.807
"	"	15	0.9	P				147.7	L	
"	"	25	0.9	P				117.8	L	
"	"	20	0.9	P				188.1	L	
"	"	10	0.85	P		-2.0	3.37	136.6	L	0.984
"	"	30	0.9	P		-0.8	1.39	245.7	L	0.858
"	"	45	0.85	P		-1.9	3.21	284.5	L	0.844
"	"	15	0.9	P		-0.7	1.22	151.6	L	0.962
"	"	70	0.7	P		-0.7	1.22	230.1	L	0.888
"	"	10	0.9	P		-0.7	1.22	172.3	L	0.940
"	"	15	0.75	P				228.1	L	
"	"	45	0.7	P				209.4	L	
"	"	60	0.8	P	-43.7			188.7	L	
"	"	65	0.9	P	-46.1			132.7	L	
"	"	25	0.9	P				130.6	L	
"	"	10	0.95	PS				131.2	L	
"	"	20	0.9	PS		-0.9	1.56	132.8	L	0.971
"	"	30	0.9	PS				130.7	L	
"	"	15	0.9	PS		-2.0	3.37	130.6	L	0.988
"	"	15	0.9	PS				131.9	L	
"	"	10	0.85	PS		-2.1	3.53	132.6	L	0.992
"	"	15	0.95	PS				132.8	L	
"	"	5	0.95	PS				132.4	L	
"	"	15	0.85	PS		-2.5	4.17	208.1	L	0.952
"	"	10	0.85	PS		-2.9	4.79	211.0	L	0.938
"	"	55	0.8	P	-44.8	-3.8	6.14	238.4	L	0.925
"	"	20	0.8	P		-4.0	6.43	250.6	L	0.906
"	"	12	0.9	P		-1.7	2.89	201.3	L	0.934
"	"	8	0.9	P		-1.8	3.05	200.1	L	0.934
"	"	40	0.75	P		-4.6	7.29	271.0	L	0.732

Sample	HM	Size (μm)	F	Origin	Tfm	Tm_{ice}	S	Th	to	D
III_{3-18}	Quartz	10	0.9	P		-3.8	6.14	287.6	L	0.857
"	"	20	0.9	P		-6.4	9.73	241.0	L	0.933
"	"	25	0.8	P		-5.4	8.40	269.7	L	0.903
"	"	15	0.95	P		-2.1	3.53	119.2	L	0.996
"	"	20	0.85	P		-1.8	3.03	271.4	L	0.844
"	"	45	0.75	P	-49.7	-7.0	10.49	301.1	L	0.889
"	"	10	0.8	P		-6.1	9.34	291.7	L	0.869
"	"	15	0.95	P		-0.9	1.56	140.3	L	0.962
"	"	15	0.9	P		-1.2	2.06	167.5	L	0.977
"	"	12	0.9	P		-1.4	2.40	166.1	L	0.982
"	"	14	0.9	P	47.8	-2.0	3.37	150.3	L	0.978
"	"	45	0.85	P		-3.8	6.14	209.4	L	0.969
"	"	5	0.95	P		-3.6	5.85	154.7	L	0.994
"	"	15	0.85	P		-4.6	7.29	294.4	L	0.849
"	"	20	0.8	P		-4.1	6.58	308.3	L	0.840
"	"	20	0.8	P		-4.0	6.43	328.5	L	0.801
"	"	10	0.9	P				270.1	L	
"	"	15	0.95	P				140.5	L	
"	"	24	0.75	P		-7.1	10.62	338.9	L	0.836
"	"	15	0.85	P		-6.3	9.64	331.0	L	0.834
"	"	15	0.8	P		-5.6	8.67	324.7	L	0.830
"	"	25	0.9	PS	50.3	-4.4	7.01	243.0	L	0.915
"	"	20	0.95	PS	49.8	-3.7	5.99	119.8	L	1.020
"	"	5	0.85	P		-4.1	6.58	183.7	L	0.987
"	"	6	0.9	P				208.4	L	
"	"	5	0.95	PS				109.0	L	
"	"	6	0.9	P				194.7	L	
"	"	10	0.75	P		-5.6	8.67	284.1	L	0.903
"	"	15	0.8	P		-7.8	11.47	325.6	L	0.855
"	"	15	0.75	P		-4.0	6.43	340.0	L	0.772
"	Fluorite	10	0.75	P	-19.2	-1.4	2.40	273.2	L	0.844
"	"	12	0.65	P		-1.6	2.72	262.6	L	0.877
"	"	15	0.85	P		-2.1	3.53	184.1	L	0.957
"	"	45	0.75	P		-1.5	2.56	178.5	L	0.957
"	"	60	0.9	P		-1.5	2.56	175.3	L	0.957
"	"	55	0.65	P	-19.5	-1.1	1.90	338.5	L	0.736
"	"	20	0.95	P	-43.5	-2.4	4.01	148.6	L	0.986
"	"	30	0.9	P	-36.0	-2.4	4.01	157.9	L	0.986
"	"	24	0.9	P	-19.5	-1.4	2.40	176.3	L	0.957
"	"	30	0.9	P	-19.7	-1.7	2.89	162.7	L	0.961
"	"	45	0.9	P	-34.1	-0.8	1.39	145.4	L	0.962
"	"	35	0.9	P	-34.4	-1.3	2.22	163.2	L	0.968
"	"	40	0.95	PS	-34.7	-0.3	0.53	151.0	L	0.962
"	"	25	0.85	PS	-33.0	-1.0	1.73	262.7	V	0.841
"	"	24	0.9	PS				202.4	L	
"	"	15	0.75	PS				265.0	V	
"	"	10	0.85	PS				170.3	L	
"	"	55	0.8	P				168.1	L	
"	"	20	0.85	P	-43.5	-1.7	2.89	159.8	L	0.968
"	"	12	0.85	P		-1.8	3.05	159.7	L	0.968
"	"	50	0.95	PS		-2.5	4.17	155.9	L	0.994
"	"	45	0.9	P	-47.9	-2.5	4.17	156.1	L	0.994
"	"	35	0.2	P	-53.0	-14.4	18.28	439.1	V	0.760

Sample	HM	Size (μm)	F	Origin	Tfm	Tm_{ice}	S	Th	to	D
III_{3-18}	Fluorite	15	0.9	P	-45.4	-2.3	3.85	184.6	L	0.957
"	"	20	0.95	P	-45.6	-1.7	2.89	154.3	L	0.978
"	"	35	0.75	P		-1.8	3.05	155.1	L	0.978
"	"	35	0.85	P		-1.9	3.21	163.8	L	0.968
"	"	20	0.85	P		-1.9	3.21	156.8	L	0.968
"	"	45	0.95	P		-1.0	1.73	155.2	L	0.962
"	"	15	0.75	P		-4.7	7.44	178.0	L	0.991
"	"	15	0.9	P				147.7	L	0.976
"	"	15	0.95	P		-0.9	1.56	141.3	L	0.962
"	"	12	0.75	P				204.9	L	
"	"	20	0.85	P		-0.9	1.56	142.1	L	0.962
"	"	45	0.75	P				150.0	L	
"	"	10	0.9	P				143.2	L	
"	"	15	0.9	P		-2.3	3.85	143.1	L	0.984
"	"	30	0.9	P		-2.3	3.85	149.9	L	0.984
"	"	20	0.9	P		-2.3	3.85	153.7	L	0.984
"	"	30	0.8	P	-45.7	-2.6	4.32	289.8	L	0.856
"	"	15	0.8	P		-0.9	1.56	156.6	L	0.962
"	"	24	0.85	P		-2.2	3.69	143.3	L	0.978
"	"	15	0.85	P	-49.6	-1.4	2.40	148.7	L	0.972
"	"	25	0.9	P	-49.8	-2.0	3.37	258.2	L	0.871
"	"	25	0.9	P		-0.6	1.05	129.9	L	0.982
"	"	30	0.8	P		-0.8	1.39	147.5	L	0.962
"	"	55	0.8	P		-0.9	1.56	139.7	L	0.962
"	"	50	0.8	P				158.1	L	
"	"	45	0.8	P	-45.2	-2.1	3.53	264.8	L	0.877
"	"	40	0.85	P	-49.4	-1.3	2.23	249.1	L	0.868
"	"	60	0.8	P		-1.3	2.23	150.2	L	0.968
"	"	15	0.8	P				155.3	L	
"	"	15	0.9	P				156.3	L	
"	"	45	0.9	P				150.7	L	
"	"	10	0.9	P		-1.2	2.06	152.7	L	0.868
"	"	15	0.9	P				154.5	L	
"	"	45	0.85	P	-49.8	-1.6	2.72	163.7	L	0.968
"	"	60	0.85	P		-1.6	2.72	157.9	L	0.968
"	"	55	0.85	P		-1.5	2.56	156.9	L	0.968
"	"	25	0.85	P		-1.4	2.40	148.2	L	0.968
"	"	30	0.75	P				164.4	L	
"	"	24	0.8	P		-1.4	2.40	154.5	L	0.968
"	"	20	0.85	P		-1.1	1.90	154.6	L	0.969
"	"	40	0.75	P		-1.5	2.56	156.8	L	0.968
"	"	45	0.9	P		-1.6	2.72	153.8	L	0.967
"	"	30	0.9	P		-1.5	2.56	141.0	L	0.968
"	"	25	0.9	P	-47.0	-2.1	3.53	256.0	L	0.877
"	"	40	0.9	P		-2.7	4.48	283.7	L	0.846
"	"	15	0.9	P		-1.8	3.05	171.2	L	0.957
"	"	10	0.8	P		-1.1	1.90	301.8	L	0.797
"	"	55	0.75	P		-3.4	5.55	321.5	L	0.790
"	"	20	0.8	P		-2.0	3.37	284.0	L	0.844
"	"	35	0.75	P		-1.7	2.89	322.1	L	0.768
"	"	50	0.9	P		-1.8	3.05	256.3	L	0.877
"	"	45	0.9	P		-1.9	3.21	208.7	L	0.934
"	"	35	0.9	P		-0.7	1.22	143.0	L	0.962

Sample	HM	Size (μm)	F	Origin	Tfm	Tm_{ice}	S	Th	to	D
III_{4-3}	Quartz	25	0.85	P	-48.8	-0.8	1.39	272.0	L	0.824
"	"	20	0.85	P	-48.7			312.0	L	
"	"	35	0.9	P		-1.2	2.06	283.7	L	0.821
"	"	25	0.7	P	-50.1	-2.5	4.17	278.5	L	0.859
"	"	24	0.9	P		-2.7	4.48	190.4	L	0.952
"	"	45	0.9	P		-2.1	3.53	144.2	L	0.978
"	"	10	0.85	P		-1.8	3.05	225.7	L	0.907
"	"	15	0.85	P		-1.2	2.06	167.1	L	0.960
"	"	15	0.85	P		-1.1	1.90	194.2	L	0.916
"	"	12	0.85	P		-1.4	2.40	195.3	L	0.934
"	"	20	0.85	P		-1.7	2.89	313.9	L	0.807
"	"	35	0.85	P		-1.8	3.05	321.6	L	0.768
"	"	10	0.85	P		-1.3	2.23	320.1	L	0.757
"	"	15	0.9	P		-1.0	1.73	190.6	L	0.916
"	"	30	0.8	P		-0.7	1.22	242.5	L	0.858
"	"	20	0.85	P		-1.5	2.56	253.6	L	0.877
"	"	30	0.85	P		-1.8	3.05	261.9	L	0.861
"	"	15	0.8	P		-2.0	3.37	264.5	L	0.860
"	"	24	0.75	P		-1.1	1.90	253.1	L	0.868
"	"	15	0.75	P		-0.9	1.56	266.3	L	0.824
"	"	25	0.8	P		-0.8	1.39	261.3	L	0.824
"	"	55	0.9	P		-1.0	1.73	149.4	L	0.962
"	"	30	0.85	P		-1.3	2.23	217.9	L	0.922
"	"	65	0.9	P		-1.1	1.90	155.6	L	0.970
"	"	50	0.9	P		-1.5	2.56	202.0	L	0.934
"	"	45	0.95	P		-1.4	2.40	185.1	L	0.946
"	Fluorite	40	0.9	PS		-0.7	1.22	171.0	L	0.957
"	"	60	0.95	PS		-0.4		110.3	L	
"	"	65	0.8	PS		-1.7	2.89	160.1	L	0.968
"	"	15	0.85	PS		-1.1	0.70	158.0	L	0.962
"	"	15	0.95	PS		-1.8	3.05	124.5	L	0.996
"	"	10	0.85	PS		-1.5	2.56	189.8	L	0.962
"	"	55	0.8	P		-1.3	2.23	203.1	L	0.934
"	"	45	0.8	P		-2.1	3.53	225.3	L	0.907
"	"	40	0.95	P		-1.9	3.21	108.3	L	1.011
"	"	50	0.95	P		-1.8	3.05	194.7	L	0.934
"	"	25	0.85	P		-2.0	3.37	208.1	L	0.926
"	"	30	0.95	P		-2.1	3.53	199.1	L	0.940
III_{4-5}	Quartz	15	0.9	P		-3.0	4.94	279.0	L	0.864
"	"	30	0.9	P		-1.8	3.09	288.4	L	0.826
"	"	15	0.8	P		-2.9	4.79	321.0	L	0.790
"	"	5	0.75	P		-32.8	6.14	333.8	L	0.802
"	"	10	0.85	P		-1.0	1.73	291.6	L	0.805
"	"	25	0.85	P		-4.1	6.58	298.7	L	0.849
"	"	10	0.8	P		-5.0	7.85	320.5	L	0.812
"	"	5	0.85	P		-4.7	7.44	308.7	L	0.849
"	Fluorite	30	0.95	P		-1.4	2.40	115.8	L	1.004
"	"	50	0.75	P				248.1	L	
"	"	20	0.95	P		-0.6	1.05	148.2	L	0.994
"	"	10	0.95	P		-1.1	1.90	181.5	L	0.937
"	"	50	0.9	P				148.5	L	
"	"	45	0.85	P		-1.2	2.06	154.4	L	0.970
"	"	35	0.85	P		-1.1	1.90	162.5	L	0.960

Sample	HM	Size (μm)	F	Origin	Tfm	Tm_{ice}	S	Th	to	D
III_{4-5}	Fluorite	25	0.8	P				255.9	L	
"	"	20	0.85	P				273.1	L	
"	"	25	0.75	P				271.4	L	
"	"	35	0.85	P				265.3	L	
"	"	25	0.85	P				243.4	L	
DW-8	Quartz	15	0.9	P		-2.5	4.17	152.1	L	0.994
"	"	5	0.9	P		-2.3	3.85	231.9	L	0.914
"	"	5	0.9	P		-2.3	3.85	236.0	L	0.914
"	"	10	0.9	P		-1.7	2.89	196.5	L	0.934
"	"	20	0.8	P		-1.5	2.56	217.5	L	0.922
"	"	15	0.85	P		-2.0	3.37	241.4	L	0.877
"	"	5	0.85	P		-2.9	4.79	252.2	L	0.896
"	"	10	0.9	P		-1.9	3.21	149.3	L	0.978
"	"	15	0.8	P		-1.3	2.23	280.8	L	0.826
"	"	20	0.8	P		-2.2	3.69	282.5	L	0.826
"	"	20	0.8	P		-1.9	2.56	319.2	L	0.768
"	"	30	0.8	P		-0.9	1.56	278.9	L	0.824
"	"	15	0.85	P		-1.3	2.23	267.5	L	0.861
"	"	10	0.75	P		-0.9	1.56	273.4	L	0.824
"	"	15	0.7	P		-0.8	1.39	271.0	L	0.824
"	"	15	0.85	P		-0.5	0.87	261.9	L	0.811
"	"	25	0.9	P		-1.4	2.40	306.1	L	0.801
"	"	20	0.85	P		-1.2	2.06	268.4	L	0.862
"	"	5	0.9	P		-1.3	2.23	259.3	L	0.877
"	"	6	0.8	P		-1.9	3.21	185.3	L	0.846
"	"	5	0.85	P		-1.5	2.56	185.7	L	0.857
"	"	8	0.95	P		-1.1	1.90	149.4	L	0.970
"	"	10	0.85	P		-1.0	1.73	234.3	L	0.888
"	"	15	0.9	P		-1.0	1.73	162.0	L	0.962
"	"	15	0.75	P				206.0	L	
"	"	15	0.85	P				257.5	L	
"	"	10	0.75	P				217.6	L	
"	"	15	0.85	P		-2.1	3.53	281.7	L	0.826
"	"	40	0.85	P	-19.8	-1.9	3.21	324.1	L	0.768
"	Fluorite	60	0.95	PS	-44.0	-0.7	1.22	117.6	L	0.988
"	"	65	0.95	PS	-48.3	-0.9	1.56	120.3	L	0.976
"	"	25	0.9	PS		-1.0	1.73	135.8	L	0.962
"	"	30	0.95	PS		-0.2	0.35	109.6	L	1.007
"	"	24	0.9	PS		-1.8	3.05	120.7	L	0.966
"	"	20	0.95	PS		-0.9	1.56	118.4	L	0.988
"	"	40	0.9	PS		-1.7	2.89	201.6	L	0.934
"	"	45	0.85	P		-2.8	4.63	267.3	L	0.880
"	"	30	0.5	P		-11.6	15.65	308.4	L	0.895
"	"	25	0.65	P		-7.0	10.49	294.0	L	0.889
"	"	40	0.45	P		-12.2	16.24	326.6	L	0.915
"	"	15	0.3	P		-13.1	17.09	318.9	L	0.921
"	"	10	0.4	P		-10.3	14.31	308.7	L	0.927
"	"	55	0.65	P	-50.1	-3.8	6.14	298.1	L	0.849
"	"	20	0.95	P		-0.9	1.56	180.6	L	0.925
"	"	10	0.75	P		-4.2	6.72	275.4	L	0.884
"	"	50	0.7	P	-48.8	-4.7	7.44	281.0	L	0.867
"	"	45	0.85	P		-2.9	4.79	244.7	L	0.896
"	"	35	0.75	P		-3.5	5.70	278.4	L	0.876

GEOLOGICAL MAP OF XIANGHUAPU HUNAN PROVINCE, P. R. CHINA

WANG, C-S(1990) BASED IN PART ON LUO,S-G et al.(1981)

300 200 100 0 100 200 300 400 500 600 700 METRES

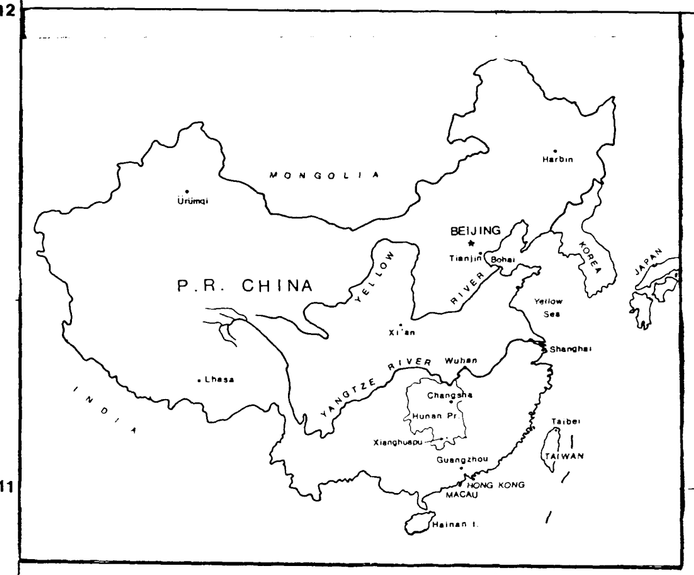

LEGEND

- Q — Quaternary sedments
- P_2l — Upper Permian Leping Group: sandstone, carbonaceous shale
- P_1q — Low Permian Qixia Group: limestone and dolomite
- C_1z — L Carboniferous Zimenjiao Group: dolomite with minor chert
- C_1sh — L Carboniferous shitangci Group: chert-coral - bearing limestone and dolomite
- D_3sh — U Devonian Shetianjiao Group: limestone, dolomite, marble, and skarns
- D_1l — L Devonian Lianhuashan Group: quartz arenite, slate
- Mb — Marble
- Gr — Greisenized granite
- To-Qz — Quartz and topaz
- r_5^{3-D} — Fourth stage granite
- r_5^{3-B} — Second stage granite
- r_π — Porphyritic granite vein
- Geological boundary, definite and inferred
- Fq — Fracture filled with quartz
- F — Fault
- Pb-Zn — Pb - Zn mineralization
- Nb-Ta — Nb - Ta mineralization
- P_2c — Upper Permian Changxing Group: argillaceous limestone and calcareous shale
- P_2d — Upper Permian Dangchong Group: Mn-Fe - bearing chert
- $C_{2+3}h$ — M + U Carboniferous Hutian Group: limestone and dolomite
- C_1c — L Carboniferous Zeshui Group: coal - bearing carbonaceous shale
- C_1m — L Carboniferous Menggongao Group: argillaceous crinoidal limestone, dolomite with minor chert
- D_2j — M Devonian Jicijiao Group: carbonaceous limestone, argillaceous limestone and bryazoan-bearing dolomite
- Є — Cambrian: quartzite, slate
- Sk — Skarns
- Qz — Quartz
- r_5^{3-E} — Fifth stage granite
- r_5^{3-C} — Third stage granite
- r_5^{3-A} — First stage granite
- Underground outcroup of fifth stage granite
- Boundary of different granitic phases, definite and inferred
- F_{401} — Fault and identification number
- 105 — Sample location
- W-F — W - F mineralization